ORNL/TM-2021/2046

Post-Closure Nuclear Criticality Safety Evaluations for Disposition of Criticality Control Overpacks at the Waste Isolation Pilot Plant

Bret D. Brickner
Riley Cumberland
Richard Reed
Alex Lang

February 2022

Approved for public release.
Distribution is unlimited.

OAK RIDGE National Laboratory

ORNL IS MANAGED BY UT-BATTELLE LLC FOR THE US DEPARTMENT OF ENERGY

ORNL/TM-2021/2046

Nuclear Energy and Fuel Cycle Division

POST-CLOSURE NUCLEAR CRITICALITY SAFETY EVALUATIONS FOR DISPOSITION OF CRITICALITY CONTROL OVERPACKS AT THE WASTE ISOLATION PILOT PLANT

Bret D. Brickner
Riley Cumberland
Richard Reed
Alex Lang

February 2022

Prepared by
OAK RIDGE NATIONAL LABORATORY
Oak Ridge, TN 37831-6283
managed by
UT-BATTELLE, LLC
for the
US DEPARTMENT OF ENERGY
under contract DE-AC05-00OR22725

This page is intentionally blank

CONTENTS

LIST OF FIGURES

APPENDIX A: LIST OF FIGURES

APPENDIX B: LIST OF FIGURES

APPENDIX C: LIST OF FIGURES

APPENDIX D: LIST OF FIGURES

APPENDIX E: LIST OF FIGURES

APPENDIX F: LIST OF FIGURES

APPENDIX G: LIST OF FIGURES

APPENDIX H: LIST OF FIGURES

APPENDIX I: LIST OF FIGURES

APPENDIX J: LIST OF FIGURES

APPENDIX K: LIST OF FIGURES

APPENDIX L: LIST OF FIGURES

APPENDIX M: LIST OF FIGURES

APPENDIX N: LIST OF FIGURES

APPENDIX O: LIST OF FIGURES

LIST OF TABLES

APPENDIX A: LIST OF TABLES

APPENDIX B: LIST OF TABLES

APPENDIX C: LIST OF TABLES

APPENDIX D: LIST OF TABLES

APPENDIX E: LIST OF TABLES

APPENDIX F: LIST OF TABLES

APPENDIX H: LIST OF TABLES

APPENDIX I: LIST OF TABLES

APPENDIX J: LIST OF TABLES

APPENDIX K: LIST OF TABLES

APPENDIX L: LIST OF TABLES

APPENDIX M: LIST OF TABLES

APPENDIX N: LIST OF TABLES

APPENDIX O: LIST OF TABLES

This page is intentionally blank

ABBREVIATIONS

ANS	American Nuclear Society
ANSI	American National Standards Institute
CBFO	Carlsbad Field Office
CCC	criticality control container
CCO	criticality control overpack
CFR	US Code of Federal Regulations
CH	contact-handled
DOE	US Department of Energy
EALF	energy of average lethargy causing fission
ENDF	Evaluated Nuclear Data File
EPA	US Environmental Protection Agency
ERDA	Energy Research and Development Administration
FEP	feature, event, and process
FGE	fissile gram equivalent
MCNP	Monte Carlo N-Particle code
MOX	mixed oxide
MT	metric ton
NEA	Nuclear Energy Agency
NEFCD	Nuclear Energy and Fuel Cycle Division
NWP	Nuclear Waste Partnership LLC
ORNL	Oak Ridge National Laboratory
POC OR POP	pipe overpack container
SAR	safety analysis report
SBMS	Systems-Based Management System
SNL	Sandia National Laboratories
SRS	Savanah River Site
TRU	transuranic
TRUPACT	TRU Package Transporter
WAC	waste acceptance criteria
WIPP	Waste Isolation Pilot Plant

This page is intentionally blank

ACKNOWLEDGMENTS

This work would not have been possible without the excellent communication and collaboration within the of the extended multi-laboratory technical team: Ron Livingston (Omega Technical Services), Paul Shoemaker (SNL), Benjamin Reedlunn (SNL), Robert Rechard (SNL), Brad Day (WIPP), Steve Wagner (SNL) and Ross Kirkes (SNL). Special thanks to Brad and Ben for never shying away from asking the hard questions. The authors are also grateful for the engagement, support, and excellent feedback provided by Rose Montgomery (ORNL), Rose Rainey (ORNL), Kathy Jones (ORNL), and Molly Smith (ORNL).

This page is intentionally blank

EXECUTIVE SUMMARY

The Waste Isolation Pilot Plant (WIPP) is a geological repository in southern New Mexico that provides for disposal of transuranic (TRU) wastes from atomic energy defense activities. The Sandia National Laboratories (Sandia) Report, *Consideration of Nuclear Criticality When Disposing of Transuranic Waste at the Waste Isolation Pilot Plant* [1], addresses nuclear criticality safety based on the projected inventory characteristics for the initial compliance certification application of WIPP in 1996 [1]. As the inventory, waste forms, and disposal package designs change, revised or new analyses are necessary to demonstrate acceptability for these configurations within the WIPP safety basis [2] and compliance with 10,000-year post-closure standards of the US Environmental Protection Agency (EPA). Saylor and Scaglione evaluated criticality control overpacks (CCOs) in 2017 [3] based on conservative assumptions for post-closure repository structural conditions with resulting effects on containers and container spacing,

The Saylor and Scaglione evaluation of CCOs addressed a single waste configuration that represents the Surplus Plutonium Disposition Program's dilute and dispose waste form and composition. This initial CCO study demonstrated that 50 grams of boron carbide (B_4C) per CCO is sufficient to ensure post-closure criticality safety based on a well-mixed waste composition, and Oak Ridge National Laboratory (ORNL) subsequently determined that this amount of B_4C does not require constraints on moisture or plastic present as moderator [29]. The Saylor and Scaglione [3] analysis conservatively assumes repository room closure that eliminates all space between fissile gram equivalent (FGE) ^{239}Pu masses. The close-packed array was selected based on limited availability of repository salt creep modeling results at that time. In 2019, Brickner [4] provided additional evaluations for pipe overpack containers (POCs), building on the conservative basis provided by Saylor and Scaglione. Brickner's 2019 analysis made use of new geomechanical data for post-closure spacing that rely on advances in repository modeling as documented in the work by Reedlunn and Bean [7].

This current CCO evaluation for generic waste materials expands on earlier work performed at ORNL and includes evaluation of CCOs across a much broader range of possible waste compositions and geometries. This evaluation is intended to provide input for the required feature, event and process (FEP) screening to determine if post-closure criticality must be included as an event in the 10,000-year regulatory evaluation. As such, the approach to modeling post-closure criticality presented in this report has been coordinated with the Sandia team responsible for FEP screening. The resulting analysis supports disposition of fissile materials in the CCO containing up to 380 FGE ^{239}Pu and expands conditions acceptable for disposal of fissile material in CCOs [6]. This evaluation builds on the methodology of Saylor and Scaglione [3] and Brickner [4], using the most recently available geomechanical data for CCO spacing under salt creep compaction scenarios provided by Reedlunn and Bean [8]. The broad range of fissile material configurations analyzed in this report are intended to account for configurations that may occur during the post-closure disposal time period, and it also includes waste configurations that are not physically possible to support analysis of conditions that influence neutron fluence.

Given the mechanical deformation resulting from room collapse per the recent analysis of Reedlunn and Bean [8], the extent of compaction in a room is significantly less than that used in the initial ORNL bounding evaluation performed by Saylor and Scaglione [3]. Consequently, the results of this analysis support addition of other options for TRU waste disposal in CCOs that do not include B_4C, as the results indicate strong dependence on the size of the waste form (as calculated from mass of materials present in the fissile region) and the amount of moderator from hydrogen-bearing materials within the waste form. Results of this analysis are presented in $H/^{239}Pu$ curves that are used for FEP screening to evaluate the effective neutron multiplication factor (k_{eff}) for disposal of CCO payload containers within the WIPP repository. These $H/^{239}Pu$ curves are used to evaluate rooms filled with CCOs and provide the neutron multiplication as a function of various system parameters for the CCOs at the maximum authorized FGE ^{239}Pu loading

of 380 g. Without B_4C, subcriticality is shown to be highly dependent upon (1) the mass of H in the fissile region of the waste form, (2) the mass of nonfissile, non-H materials within the waste form, and (3) the assumed final geometry of the waste form resulting from post-closure conditions.

Parametric evaluations were performed to facilitate analysis of the limits for moderator (i.e., the maximum mass limit of H containing materials) and the benefits of including nonfissile filler materials that may be present in the waste (i.e., a minimum mass limit). The parametric variations reported herein demonstrate that 380 FGE ^{239}Pu may be safely dispositioned using the CCO without requiring the use of B_4C, given the appropriate constraints on water and plastic as long as the assumptions provided as the basis of the safety evaluation are maintained (i.e. well mixed system). This generic approach accounts for the range of parameters allowed for transport to WIPP in the CCO [9], which is also sufficient to demonstrate the k_{eff} associated with disposal of dilute surplus Pu in CCOs. Therefore, this analysis supports the disposal of any waste form that complies with the CCO payload characteristics credited in the FEP evaluation and correspondingly specified in the WIPP waste acceptance criteria (WAC) [5].

This analysis was divided into three sets of calculations. The first set provides evaluation of regular, uniformly compacted arrays in a three-high stack of spheres or cylinders, with an equivalent spacing based on Sandia geomechanical compaction results. The first set includes two different spacing evaluations, both with waste forms stacked directly on top of one another. The second set of calculations supports evaluation of an irregular, nonuniformly compacted array with spacing determined by results from Sandia geomechanical modeling. These data include evaluation for the upper and lower horizons of the WIPP repository. The third dataset analyzes the effect of splitting the TRU waste into smaller handling containers within the CCO. In total, more than 20 parameters were evaluated using approximately 28,800 combinations per calculation set (155,520 total combinations) to assess the impact on k_{eff}. The complete list of results for these datasets is included in Addendum 1.

Table E.S-1 provides the most restrictive moderator mass that may be present in the generic waste forms when utilizing maximum fissile loading, beryllium content based on transportation limits, and the constraints from the safety evaluation using irregular, nonuniformly compacted array results from set-2 calculations. This ensures a conservative assessment of k_{eff} without B_4C present in the waste composition with an array spacing based on geomechanical modeling presented in set-2. Thus, Table ES-1 provides limits for the system to remain subcritical for an irregular array of waste a conservative assumption that waste obtains a spherical geometry postulated as a result of post-closure changes in the material geometry. The table illustrates the ability to increase moderator content when inorganic, non-hydrogenous filler materials are included in the waste to increase the size of the fissile region (i.e., dilution of the fissile material contents with filler material). The set two results include many other conservatisms necessary to support a rigorous safety analysis when allowing for potential uncertainties in the post-closure WIPP environment.

Results from sets one and three provide additional valuable insights into the factors influencing post-closure criticality, and they support continuity with prior analysis to inform the FEP screening for improbability of WIPP post-closure criticality. Based on evaluations of set two data, three components of the waste form content should be considered when prescribing disposal limits. The three controlling parameters for criticality safety evaluation of CCO waste forms—assuming maximum fissile mass and Be contents—include mass of hydrogenous moderator (water plus plastic), mass of non-hydrogenous filler material, and mass of B_4C. Note that the mass of B_4C is provided for comparison purposes based on work performed by Saylor and Scaglione [3] and support reduction in the quantity of B_4C required for fissile material discarded in the CCO. Other conditions that are subcritical and that support FEP screening can be ascertained using the data provided in the present report.

Table E.S-1. Example of possible post-closure criticality safety mass limits for waste content in CCOs to maintain a subcritical limit of 1.0 for spheres with a thick steel pipe reflector.

Option[1]	B_4C[2]	Hydrogenous content[3]	Miscellaneous filler[4]
	(g)	(g)	(g)
A	≥10	<3,900	—
B	—	<1,690	—
C	—	<1,880	≥2,000

1. To maintain a subcritical limit of 1.0 for CCOs subject to long-term emplacement at WIPP, waste packaged in each CCO shall adhere to the limits specified under Options A, B, or C.
2. The B_4C shall be well mixed with the ^{239}Pu FGE and remain so during transportation, storage, and handling operations. The B_4C mass is based on the natural abundance of ^{10}B (i.e., 19.9 ^{wt}% ^{10}B). The B_4C mass requirement shall apply to (a) each criticality control container (CCC) that contains directly loaded TRU waste with ^{239}Pu FGE, or (b) any convenience containers used to load a CCC that contain ^{239}Pu FGE. For example, if a CCC is directly loaded with TRU waste containing ^{239}Pu FGE and also loaded with two cans containing ^{239}Pu FGE, the directly-loaded TRU waste in the CCC and each can in the CCC shall include at least 10-g of well mixed B_4C.
3. Mass of hydrogenous content shall include mass of any organic material (e.g., mass of plastic, cellulose, foam) and mass of water associated with any inorganic material (e.g., mass of adsorbed water on zeolite, water of hydration in concrete and clay, or water in hydrate such as hydrated metal ion).
4. Only the non-hydrogenous portion of the miscellaneous filler mass that is well mixed with the ^{239}Pu FGE mass shall meet the miscellaneous filler mass requirement. The miscellaneous filler shall remain well mixed with ^{239}Pu FGE during transportation, storage, and handling operations. If several convenience containers are used to load a CCC, then each convenience container shall independently meet the miscellaneous filler criteria.
5. The values of mass of hydrogenous content for Option A, B and C, and the mass of miscellaneous filler for Option C, are selected as an example using the spheres with thick steel pipes as reflectors in the nonuniform array models. The value of hydrogenous content for Option A can be seen in Figure 6.58, for Option B it can be seen in Table 6.5 (rounded) and for both the hydrogenous content and miscellaneous filler for Option C it can be interpolated from the results presented in Table 6.5 or utilizing the raw data (see Addendum 1).
6. FGE should only include fissile isotopes, but the fissile material does not have to be uniformly mixed with the waste form or have a specific geometric size or shape.
7. It is allowable to utilize a separate Option for individual CCOs since each Option is based on the same maximum reactivity subcritical limit.

This page is intentionally blank

1. INTRODUCTION AND PURPOSE

The Waste Isolation Pilot Plant (WIPP) provides for safe permanent disposal of government-owned transuranic (TRU) and TRU mixed wastes. Receipt and disposal of waste at the WIPP site began in March of 1999. The Sandia Report, *Consideration of Nuclear Criticality When Disposing of Transuranic Waste at the Waste Isolation Pilot Plant* [1], addresses potential nuclear criticality safety issues based on the projected inventory characteristics known at the time of its 2,000 publication date [1]. As the inventory, waste forms, and disposal package designs have changed, new analyses have been performed to address any potential effects to the performance assessment. More recent evaluations have considered post-closure effects on container spacing. In 2017, Saylor and Scaglione [3] evaluated criticality control overpacks (CCOs) and pipe overpack containers (POCs), and in 2019, Brickner [4] evaluated POCs. The evaluation presented in this document provides additional information for CCOs containing 380 fissile gram equivalent (FGE) ^{239}Pu to provide a generic analysis that was specifically performed to support the use of CCOs for the disposal of materials in addition to dilute surplus Pu in CCOs [6].

The current WAC for CCO waste forms with 380 FGE ^{239}Pu is supported by the 2017 analysis of Saylor and Scaglione [3], which determined that 50 g B_4C per (CCO) was sufficient to preclude criticality. The Saylor and Scaglione [3] analysis assumes that all space between FGE masses is eliminated due to salt creep. Brickner's 2019 analysis [4] made use of geomechanical analysis data for post-closure spacing from Sandia National Laboratories (SNL) as documented by Reedlunn and Bean in 2019 [7]; Brickner developed a methodology for using the data [4] to demonstrate that no restrictions (waste acceptance limits) were required for 200 FGE ^{239}Pu in POCs.

This analysis builds on the post-closure criticality safety methodology developed by Saylor, Scaglione [3], and Brickner [4], using the most recently available (2020) geomechanical data for CCO spacing under salt creep compaction scenarios as provided by Reedlunn and Bean [8]. The main objective of this evaluation is to determine the k_{eff} of disposed CCOs loaded with 380 FGE ^{239}Pu as a function of moderator content for various parametric combinations of reflector, non-hydrogenous filler, waste form shape and spacing configurations related to room compaction scenarios. The upper edge of the envelope of the curves representing plausible configurations could inform the FEP process for various CCO contents. The results of the analysis provide a full range of k_{eff} vs. moderator curves to evaluate the k_{eff} effect of the most important system parameters for the CCO's allowable payload per the CCO *TRUPACT-II Safety Analysis Report* [9], and sufficient information to demonstrate k_{eff} associated with disposal of dilute surplus Pu in CCOs [10].

While the waste stream for the disposal of dilute surplus Pu in CCOs is not specifically addressed, the results remain applicable because the dilute surplus Pu is shipped in the CCO and must meet the CCO *TRUPACT-II Safety Analysis Report* [9] limits. To avoid specifying allowable waste forms, the analysis herein examines the potential for criticality in CCOs containing generic waste forms. This approach requires a more general analysis using criticality conditions that are based primarily on CCO transportation limits.

To certify the compliance[1] of a geologic repository for radioactive waste, the US Environmental Protection Agency (EPA) requires estimates of the range of future behavior through models that capture the disposal system's essential FEPs. At the WIPP, it may be possible for sufficient fissile mass and concentration to cause a self-sustained neutron chain reaction—or *criticality*. In the past, concern about *criticality* in TRU waste has been low because of the low fissile mass limits in contact-handled containers, the neutronic isolation associated with the disposal of remote-handled containers, and the natural tendency of fissile solute to disperse after release from degraded containers. This low concern is

[1] Much of the discussion in this section is directly from Rechard [11].

still valid for the majority of TRU waste disposed at WIPP. However, waste destined for WIPP has expanded to include TRU waste disposed in CCOs with larger fissile mass limits per transportation cask. Hence, the likelihood of assembling a critical mass and concentration of CCOs in WIPP after its closure is being reevaluated.

The EPA uses a probabilistic approach to evaluation of criticality that has previously been applied to WIPP as part of prior FEP screening [1], [14], [15], [30]. Because EPA does not designate post-closure criticality for special consideration, the post-closure criticality potential is evaluated within the probabilistic regulatory framework for disposal as defined by EPA in 40 CFR 191 [12], [13].

Section 2 discuses quality assurance specifications and describes the process used to develop this report. The software used to perform these calculations is described in Section 3. Direct inputs that were used in the development of this technical product are documented in Section 4. Section 5 describes the assumptions used in the absence of direct confirming data or evidence to perform the modeling and analyses documented herein. A description of the different analyses performed is provided in Section 6, as well as the systems, processes, and phenomena considered to assess criticality potential over the WIPP post-closure period.

This report documents a large, complicated analysis, and thus some key terms, concepts, and assumptions are listed as follows for technical clarification purposes.

1. Emplacement and Compaction

   The CCOs are placed in the repository at time = 0 during emplacement. The geometry of the emplaced configuration is technically equivalent to the transport condition with respect to the physical configuration and arrangement of the various CCO components.

   The CCOs are at the final resting location after room closure at a time between 0 and 10,000 years after compaction. The geometry of the compacted configuration is variable, and the material composition and arrangement of the various CCO components is variable.

2. Waste Form

   The mass/volume of anything placed within the CCC. This does not include the CCC pipe itself at emplacement. However, the waste form always includes the FGE and moderator and may also include the filler, Be, and/or B_4C at emplacement. It may also include other materials present in the repository after compaction (e.g., packaging materials).

3. FGE

   The mass of fissile isotopes. It does not include any other elements, such as O, which may be chemically bound. Therefore, the calculation of the FGE should only include fissile isotopes. It does not have to be uniformly mixed with the waste form or have a specific geometric shape or size.

4. Waste Form Moderator

   The H-bearing compounds in the CCC represented as either pure water or polyethylene (CH_2). This includes water, polyethylene, the moisture content of inorganic materials (e.g., cement) and materials of unknown organic content (should be conservatively considered to be water or plastic). Organics are typically excluded from the CCO based on other WIPP operational constraints. It is always assumed to be uniformly mixed with the waste form.

5. Waste Form Moderator Mass

   Mass of water or polyethylene in the CCC. It always includes the mass of every H-bearing molecule within the CCC and uniformly mixed with the waste form. Therefore, the calculation of the moderator mass at emplacement should include the total mass of all H-bearing molecules within the CCC as the equivalent mass of water or plastic. Only the moisture content of an inorganic materials (e.g., cement) is included as part of the moderator, not the full mass of the materials. Materials of unknown organic content should be represented as plastic in evaluating moderator content. Organics are typically excluded from the CCO based on other WIPP operational constraints.

6. Filler Material

   Any material placed within the CCC that is non-fissile and inorganic may be considered as filler, Beryllium metal and compounds are excluded as a special reflector material. Filler material is always assumed to be uniformly mixed with the fissile material during transportation, handling and emplacement.

7. Filler Material Mass

   The total mass of filler material compounds within the CCC that is credited toward a filler mass limit at emplacement. It does not include the mass of H-bearing compounds, FGE, or special reflector materials at emplacement.

   For a filler material that contains moisture or releases water vapor during thermal decomposition, the filler mass calculation should exclude the mass loss associated with the water. For example, concrete present in as filler may include 20% water yet appear dry. This water must be included in the waste form moderator mass calculation. However, the balance of dry cement ingredients associated with concrete (e.g., gravel and sand) may be included as part of the filler mass.

   Any additional material that could be characterized as a *filler material* and that is not being credited toward a filler mass is not required to be uniformly mixed with the waste form.

8. Be Mass

   The total mass of special reflector material (modeled as Be) that is uniformly mixed with the waste form in the CCC at emplacement. It is always assumed to be uniformly mixed with the waste form.

9. B_4C Mass

   The total mass of neutron absorber material that is uniformly mixed with the waste form at emplacement. Therefore, the calculation of the waste form neutron absorber material mass must include the neutron absorption cross section equivalent of B_4C. It is always assumed to be small particles (e.g., less than 3.3 mm diameter or 6 mesh) and uniformly mixed with the waste form.

10. Reflector

    In this evaluation, the term *interstitial reflector*, or *discrete reflector*, is used to describe materials physically external to the waste form, and the term *waste form* is used to describe anything placed inside the CCC prior to emplacement.

This page is intentionally blank

2. QUALITY ASSURANCE

This report was prepared in accordance with Oak Ridge National Laboratory (ORNL) procedures meeting DOE Order 414.1D, Admin Change 1, *Quality Assurance*. Procedures, policies, and guidelines can be found in the *Publications and Other Scientific Communications* subject area of the ORNL Standards-Based Management System (SBMS) under the Integrated Performance Management system.

This page is intentionally blank

3. SOFTWARE AND CALCULATIONS

The calculations for this investigation were predominately performed using the SCALE code system (ORNL 2016 [16]), version 6.2.3. The Criticality Safety Analysis Sequences (CSAS) with KENO-VI (CSAS6) were used to calculate neutron multiplications factors (k_{eff} values). The sequences have different geometry packages, but the solutions they provide are statistically identical.

All cases were performed with Evaluated Nuclear Data File (ENDF)/B-VII.1 cross section data in the 252-group library. CENTRM was used to provide problem-dependent multigroup cross section processing on the Remus or Artemis computer cluster. Remus and Artemis are maintained under the configuration control of ORNL's Fusion and Fission Energy and Science Division staff.

All calculations were run with sufficient numbers of neutron histories (generations, neutrons per generation, and generations skipped) to yield converged results that passed the appropriate statistical checks. The plots showing k_{eff} by generation and k_{eff} by generation skipped provided in the output files showed that the k_{eff} eigenvalue was essentially flat for all active generations for all cases. Fission source convergence was verified using the Shannon entropy tests or other means. The results are reported as k_{eff}.

Sampler [see Section 6.7 of the SCALE Manual] is referred to as a *super-sequence* within SCALE because it wraps around other sequences (e.g., CSAS) and perturbs inputs. Sampler has two modes: (1) uncertainty quantification via random sampling, and (2) parametric analysis via sweeping through parameter space. In this work, the second option was used extensively to explore parameter space for moderator mass, along with many other variables impacting system reactivity. These additional variables include the size and geometry of the waste form, constituents, and spacing. Sampler creates entire SCALE inputs—in this case CSAS6 inputs—with each combination of variable parameters, thus allowing for a single input to generate a large number of SCALE inputs covering the entire desired space. Further discussion of similar analyses using the Sampler parametric capability for nuclear criticality analyses is presented in Marshall et al. [27].

As with any computer code/calculation used for safety analysis and assessment, the ability of the calculation methodology to prove a configuration to be subcritical is realized through a validation process. This safety analysis utilized SCALE with TSNUAMI sequence (see Appendix H) for validation.

The SCALE MAVRIC sequence was used to perform neutron transport calculations. MAVRIC accelerates convergence of Monte Carlo transport calculations using variance reduction techniques. The MAVRIC results were successfully compared to experimental measurements that tested photon and neutron transmission through various shielding materials [32]. Therefore, MAVRIC is appropriate for modeling highly attenuating shielding. SCALE 6.2 development practices follow various quality standards, enabling compliance with American Society of Mechanical Engineers (ASME) Nuclear Quality Assurance (NQA)-1 [33].

This page is intentionally blank

4. DEVELOPMENT OF ANALYSIS INPUTS AND DATA

In this section, the physical system being modeled is first considered from a repository-wide perspective, then focusing down to waste form level. The general characteristics of the WIPP CCO configuration are outlined in this subsection, beginning with a large drift-scale description, and narrowing in scale to a description of the waste form itself. Then the data supporting values for parameter sweeps are identified and discussed. Finally, an overview of the layout for the system models is provided.

This work is focused on ^{239}Pu from atomic energy defense activities in general and surplus weapons Pu in particular, rather than fissile uranium. Pu was modeled as PuO_2 instead of metallic Pu or Pu with water of hydration or hydroxyl groups (i.e., $PuO_2(OH)_2{\cdot}H_2O$ or $Pu(OH)_4$). For highly enriched ^{239}Pu, the mineral form only influences criticality limits when the mixture is severely under moderated [11].

The CCO FGE loading is set at the transportation maximum limit of 380 FGE ^{239}Pu. During a transportation accident, a CCO is designed to maintain fissile separation, so each CCO in a shipment can be at the maximum 380 FGE ^{239}Pu , which is not the case for other TRU waste containers except for the similar POC. Although some TRU waste containers, such as the standard waste box and the 55-, 85-, and 100-gallon drums, slightly increase the transportation maximum mass limit if the ^{240}Pu mass is specified, the CCO is fixed at 380 FGE ^{239}Pu in all cases [11].

Other isotopes mixed with ^{239}Pu, such as ^{240}Pu, have an important influence on criticality. Therefore, the transportation limit is actually set at 380 FGE ^{239}Pu rather than ^{239}Pu. The ^{239}Pu FGE is the mass of ^{239}Pu plus a factor for other fissionable masses: specifically, $0.113{\cdot}^{238}$Pu, $0.0225{\cdot}^{240}$Pu, $2.25{\cdot}^{241}$Pu, $0.0075{\cdot}^{242}$Pu, $0.9{\cdot}^{233}$U, $0.643{\cdot}^{235}$U, $0.015{\cdot}^{237}$Np, $0.0187{\cdot}^{241}$Am, $34.6{\cdot}^{242m}$Am, $0.0129{\cdot}^{243}$Am, $15{\cdot}^{245}$Cm, $0.5{\cdot}^{247}$Cm, $45{\cdot}^{245}$Cf, and $90{\cdot}^{251}$Cf [11]. In general, the contact-handled TRU waste disposed at WIPP is typically only 90% enriched in ^{239}Pu, and remote-handled TRU waste is typically only 78% enriched. However, some of the surplus weapons Pu may have higher enrichment (>95%). In this work the waste form is modeled as 100% ^{239}Pu to accommodate this possibility. This assumption adds conservatism, but it avoids requiring that the waste form composition be defined precisely for the criticality analysis [10].

4.1 QUALITATIVE CHARACTERISTICS OF THE WIPP CCO CONFIGURATION

Determination of whether a fissile region or an assembly of fissile regions is critical depends upon the fissile region neutron generation rate and interaction of neutrons with matter within and outside the fissile regions. For a finite heterogenous system[2], this depends upon the individual package configuration and its contents:

(1) The type of fissile material,

(2) The fissile mass,

(3) Mass of other materials intermingled in the fissile material region,

(4) Mass of materials in the non-fissile regions,

(5) The shape and distribution of the materials in the fissile and non-fissile regions

[2] The WIPP system is considered a heterogenous system of packages. The neutron generation rate of a homogenous system depends on the fissile material concentration.

and the array of packages with the facility and distribution and concentration of materials within the array:

(1) Mass of materials between, above, and below individual packages

(2) The overall distribution and concentration of the materials, and

(3) The location and contents of other packages disposed within the same drift at WIPP (not covered in this analysis)

Because of the robust capability of geologic disposal in general and the WIPP salt repository in particular, characteristics of waste packages important to criticality are primarily based on technical constraints for transportation as specified in the WAC [5]. That is, the transportation mass limits in the CCO *TRUPACT-II Safety Analysis Report* [9] on waste packages set the primary boundary conditions for modeling potential criticality at WIPP: if the waste can be shipped, it can be disposed if the social-political agreements in the *WIPP Land Withdrawal Act* are met [21]).

4.1.1 General Description of WIPP Drift Configuration

The WIPP underground disposal repository consists of multiple salt panels mined from the Salado formation, a series of salt beds that are 2,000 feet thick. A typical underground panel includes several rooms, each of which is approximately 33 feet wide by 13 feet high by 300 feet long [11].

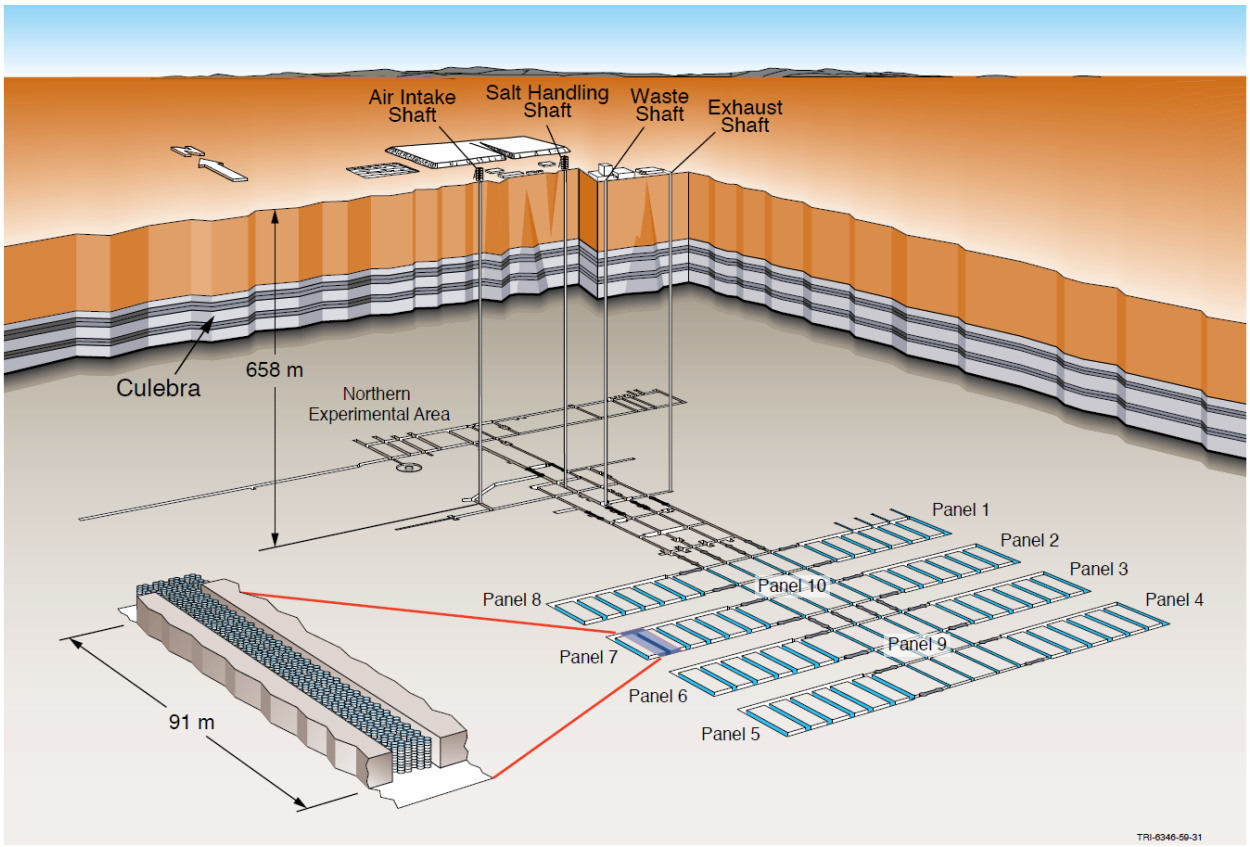

Figure 4.1. Schematic of WIPP repository, used with permission from Rechard [11].

The area shown in Figure 4.1 represents the boundaries for both the geomechanical and criticality analysis models. Panels cross-connect via drifts, as shown in Figure 4.2. The cross-connect drifts are not included in either the geomechanical analysis or the criticality analysis because it is assumed that they do not change the results. For the criticality analysis, the array models neglect the cross-connects on either end because the area of interest is in the center, where compaction is greatest, and where neutrons have the lowest chance of escaping in the horizontal direction due to the large number CCOs in that direction. Furthermore, since the major compaction effects are oriented vertically and horizontally along the shortest horizontal dimension of the room, the reactivity effect of the cross-connects is insignificant to the effect in the center of the room. However, future work could investigate the effect using results from alternative compaction models which include the cross-connects when those models are available.

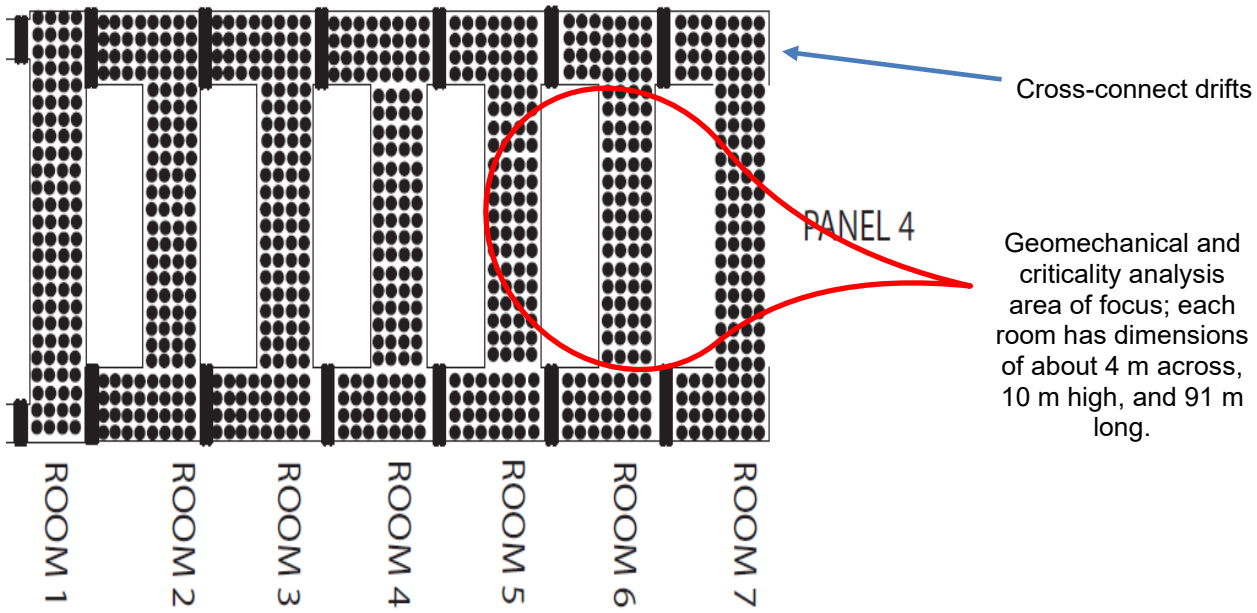

Figure 4.2. Diagram showing cross-drifts, used with permission [18].

The emplaced configuration of the waste form consists of 7-packs of COCs stacked no more than three high in a closely packed hexagonal array. MgO Supersacks are placed on top of the stacks of waste containers for approximately every other stack. A representative photograph showing how a room is loaded at WIPP is provided in Figure 4.3.

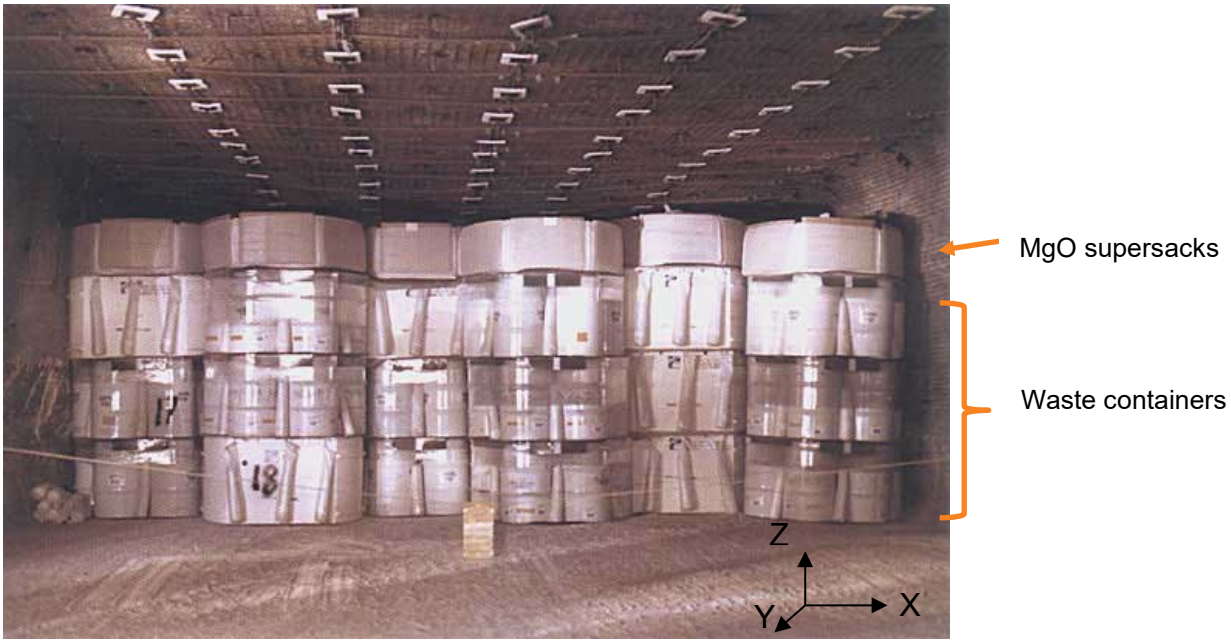

Figure 4.3. Photograph of WIPP room loaded with waste containers, used with permission from Saylor and Scaglione [3].

The WIPP panel rooms were modeled as single-room models surrounded by an infinite salt reflector [3,4]. The three-high hexagonal stacks of containers with MgO Supersacks have been modeled within the single-room model as individual containers in a conservatively tight fitting triangular-pitched array[3] filling the room space (approximately 7,000 containers), with MgO either as a thick reflector above the array [3] or intermixed uniformly with the salt between the packages [4].

4.1.2 Overview of CCO Configuration

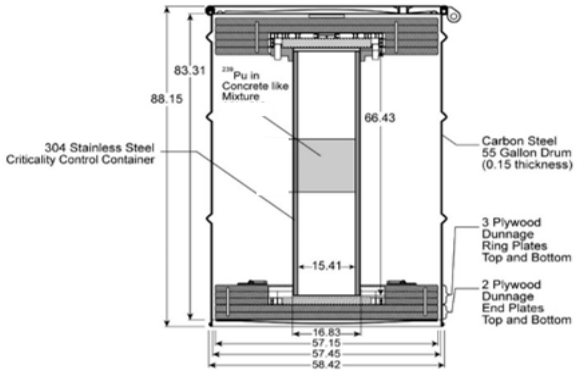

Figure 4.4. Criticality control container (CCC), and criticality control overpack (CCO), used with permission from Rechard [11].

[3] Triangular-pitched arrays are more closely packed than hexagonally-pitched arrays and are therefore conservative because the fissile masses are closer together.

Based on the CCC information presented in Figure 4.4, the thickness of the CCC pipe wall is modeled as 0.7112 cm, which is a measurement used specifically in the models as a discrete reflector. Reflector geometry is discussed in more detail in Section 4.2.2. Previous analyses by Saylor, Scaglione [3], and Brickner [4] evaluated the impact of the plywood (as cellulose) and other container material remnants. The results of those analyses show that the reactivity effect of interstitial mixing of the CCO materials between the waste forms with the salt and MgO is inconsequential. Therefore, the compaction of plywood around the waste forms is better evaluated by using the discrete reflector models in this analysis.[4]

The material composition of the waste form is based on a combination of the TRUPACT-II safety analysis report (SAR) limits [9], which is the approach used by Saylor and Scaglione [3] to evaluate the surplus Pu waste form. Waste form materials and geometry are discussed in more detail in Sections 4.1.3 and 4.2.3.

The WIPP repository may be subject to various types of geologic, environmental, and material degradation, as well as biological transmutation processes, over the regulatory timeframe. Because the final amount and configuration of any emplaced materials cannot be known, care is taken to avoid an approach which attempts to credit any specific amount of material either as a waste form or as reflector. Instead, known compositions and quantities at emplacement are used to establish the most likely material compositions and configurations post-emplacement. This information is then used to evaluate system k_{eff} under various scenarios, and a conservative and bounding approach is then taken with materials and geometry to account for the unknown nature of the repository over 10,000 years.

In this evaluation, the term *interstitial reflector*, or *discrete reflector*, is used to describe compositions physically external to the waste form, and the term *waste form* is used to describe anything placed inside the CCC prior to emplacement.

During the initial post-closure timeframe, the waste form will retain its original geometry. For example, the surplus Pu waste form is placed within the CCC in what is termed a *can-bag-can* configuration [20] (Figure 4.5).

[4] Specifically the polyethylene discrete reflector is a surrogate and bounding for materials like cellulose.

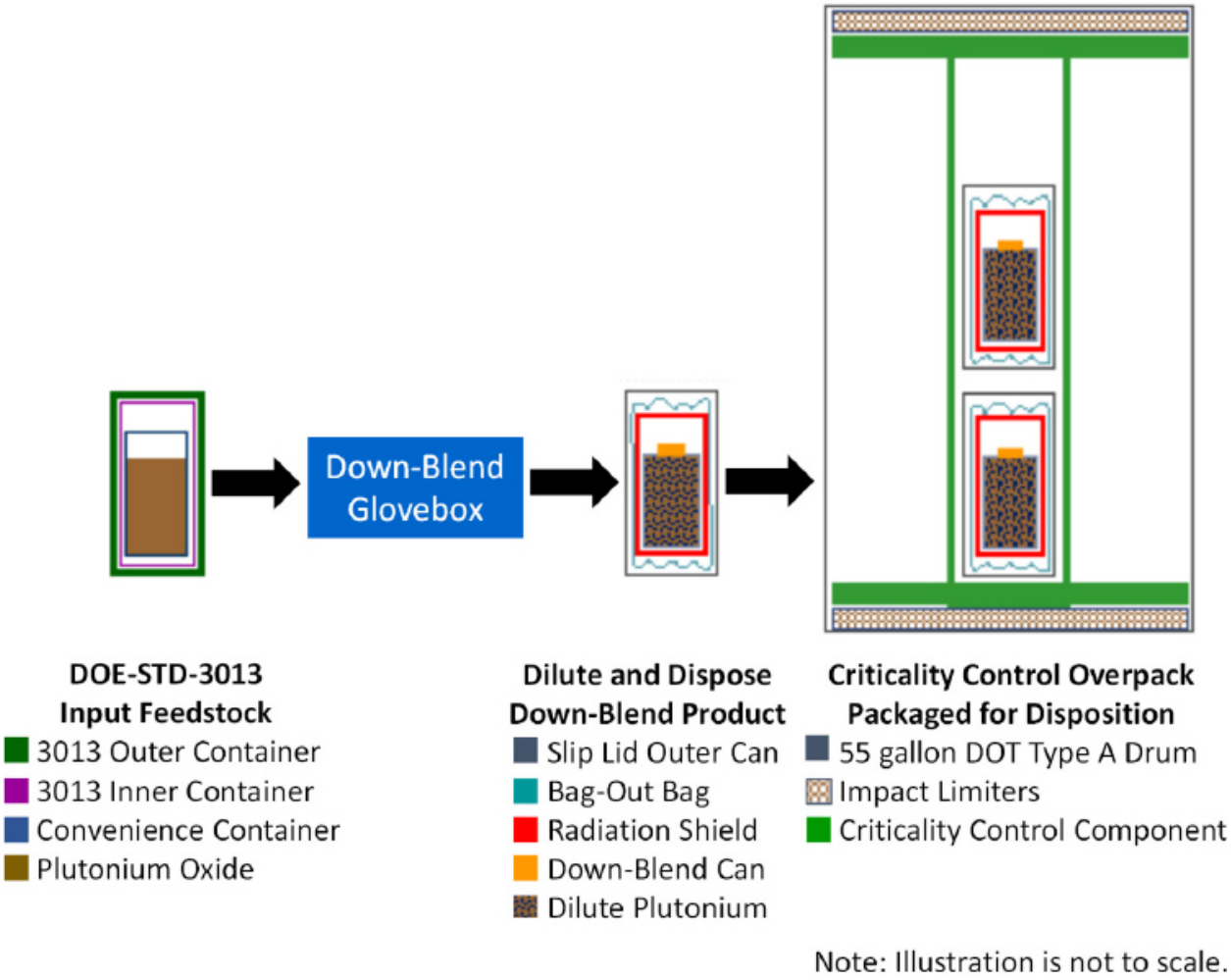

Figure 4.5. Diagram of the surplus Pu can-bag-can process, used with permission [21].

The can-bag-can configuration illustrated in the center of Figure 4-5 contains the waste form within a single can, which is wrapped in plastic and then placed in another can. The entire configuration is then placed in a CCC, and sometimes these are stacked two high (right image in Figure 4-5). The slip lid outer can and down-blend cans are referred to in this work as *convenience cans* and are modeled as a uniformly mixed mass (Section 4.2.3). At emplacement, this configuration illustrates how the waste form may be surrounded by layers of material that can act as a discrete reflector. Additionally, in the two-per-CCC configuration, the materials between the waste forms may act to thermalize neutrons as they pass from one can, through these materials, and into the adjacent waste form. This moderation by interstitial material could increase total system k_{eff} when compared to a case in which an interstitial material has reduced moderating power.

The materials physically external to the waste form inside the inner can may compact around the waste form during salt intrusion and room compaction. During the later stages of the repository timeframe, the materials which were once discrete external reflectors could degrade and migrate within the waste form, mixing with the waste form and becoming some unknown configuration. Therefore, variations of known (steel from the pipe or can) and conservative (graphite) materials are used as filler in the KENO cases constituting this study.

The scenarios requiring evaluation involve (1) the steel from the CCC and from the convenience can that is used to directly hold the waste forms and (2) how that material impacts k_{eff} either as a discrete reflector (initial emplacement), as a material mixed within the waste form (long timeframes), or both together (intermediate timeframes). Likewise, other scenarios to be considered involve (1) the polyethylene from the convenience can's bag-out bag or from other external sources such as other package designs, and (2) how that polyethylene material impacts k_{eff} either as a discrete reflector (initial emplacement), as a material mixed within the waste form (long timeframes), or both together (intermediate timeframes). Furthermore, these two material types being considered should also be considered coincidently. The masses of the stainless steel from the CCC or convenience can types of containers and polyethylene considered in this calculation sufficiently bound any realistic amount anticipated to be present.

For the initial post-emplacement timeframe, the full CCC wall thickness of stainless-steel material surrounding the waste form, as well as the waste form containers themselves, are known to be present. The known thickness of the CCC is sufficient to determine the effect that a thick discrete reflector has on k_{eff}. Like the surplus Pu can-bag-can configuration, under compaction, the wall thicknesses of the CCC and waste form containers are likely to be reduced by the pressures of salt intrusion during room closure. Therefore, the discrete reflector's thickness is alternatively set to be very thin so that the k_{eff} trend associated with the thin discrete reflector thickness can be compared to a thick discrete reflector with a thickness of 0.7112[5] cm.

4.1.3 Waste Form Geometry and Composition Representative of the CCO in the WIPP Drift

As a generic analysis, the evaluation considers parametric variations on both waste form geometry (i.e., cylinders and spheres) and materials (i.e., amounts and compositions). The inclusion of both cylinders and spheres provides additional information for the FEP screening process that can be used to determine the potential k_{eff} of the system as a function of time, especially for waste forms where either geometry is especially appropriate. This is particularly applicable for the CCC because it is cylindrical in shape and is constructed from steel. The CCC is not expected to change its shape for some significant period of time after disposal and it may not decompose at all unless the system chemistry changes significantly. If it does decompose, a sphere may be more appropriate due to the uncertainty associated with the shape over the passage of time. Under flooding and post-flooding (dryout) conditions, the CCC geometry may no longer be cohesive or contiguous, and the material composition may have changed as a result of oxidation or other processes. The introduction of brine interstitially into the system dramatically reduces reactivity [4]. Migration of materials subsequent to dryout and during that process all but preclude any ideal spherical shape.

4.2 SELECTION OF PARAMETERS TO CHARACTERIZE CCO SYSTEMS AT WIPP

The methodology contains sets of evaluations that include (1) cases with masses of pure water or polyethylene uniformly mixed with the waste form in part to account for long timeframes, (2) pure stainless steel homogeneously mixed with the waste form from the CCC or waste form containers like the surplus Pu can-bag-can material to account for very long timeframes, and (3) combinations of those two to represent intermediate timeframes. Polyethylene as a discrete reflector is treated in the same manner, so it is important to evaluate the reactivity effect of the bag in the surplus Pu type of can-bag-can scenario, as well as other external sources of plastics which may migrate around the waste forms.

Approaching the evaluation in this manner also allows for evaluation of waste form containers like the surplus Pu can-bag-can configuration in its emplaced geometry, with the can walls considered discretely, and with those materials uniformly mixed with the waste form or neglected. This is an important

[5] Additional thicker discrete reflector thicknesses are evaluated in Appendix O.

component of the evaluation, because the initial geometry of waste forms like the surplus Pu can-bag-can configurations are known to be cylindrical in geometry, and the radius of the cylindrical geometry waste form has a significant effect on k_{eff}. Therefore, the acceptability of the waste form could be determined by the geometry using, for example, the inner radius of the inner can in the surplus Pu can-bag-can configuration, to define the waste form radius. The results from such an analysis could be used to demonstrate an acceptable FEP screening for the early repository timeframes. In this scenario, any material associated with the can-bag-can from the surplus Pu can-bag-configuration may be used or neglected as uniformly mixed with the waste form, or it could be evaluated as part of the discrete reflector. Specifically, the sets of results representing the desired configuration are used. Flexibility is therefore also allowed in the calculations with the CCC pipe wall thickness as a discrete reflector to be considered as part of the waste form if that is deemed appropriate for waste form processing. Additionally, providing such a range of results and possible ways to interpret those results allows for alternative waste form situations to be evaluated as acceptable. For example, Saylor and Scaglione [3] provide calculations to show the acceptability of having 1 in 7 CCOs with no B_4C. An alternative approach using the results in this report would be to show that due to the unique geometry and materials inherent in the surplus Pu waste form, no B_4C is required to be subcritical. While some requirement for B_4C in the surplus Pu waste form may exist [5] for various reasons, situations in which CCOs are not required to utilize B_4C could be evaluated as acceptable based on the results herein.

The WIPP Project uses administrative controls for (1) safely moving TRU waste within the WIPP facility, (2) positioning TRU waste containers in the disposal room, (3) placing the MgO engineered barrier, and (4) recording the emplacement location of TRU containers for auditing and potential retrieval. The administrative controls on positioning TRU packages relate to the stability of waste package types when they are stacked on top of each other to promote operational safety. For example, 4-packs of 85-gallon drums can only be stacked on top of each other or placed on the top tiers of other container stacks. The proximity of various types of packages to each other is not specified (e.g., any number of CCOs can be placed next to each other in a room). Placing administrative controls on CCO proximity could complicate CCO disposal if a large campaign of CCOs must be stored while waiting for other waste streams to be shipped in order to mix them within a disposal room. Therefore, the criticality analysis evaluates the possibility of a room filled entirely with CCOs during the post-closure period [11].

4.2.1 CCO Spacing and Centroid Location Data

Location of the CCOs in the post-closure configuration is a key factor when evaluating post-closure criticality. Table 4.1 shows a summary of the array spacings evaluated. Set-1 and set-3 are assumed to be uniform array cases. Set-1 has one waste form per CCO. Because three CCOs are stacked, this results in three waste forms stacked on top of each other with no spacing aside from the discrete reflectors. Set-3 evaluates a variant configuration having two waste forms per CCO. This results in set-3 consisting of six waste forms stacked on top of each other with no spacing aside from discrete reflectors. Set-2 is a nonuniform case using best-estimate data for locations of waste forms after 1,000 years from Reedlunn and Bean [8], so the waste forms are typically not in direct contact.

Table 4.1. Evaluated array spacings

Case	Description	Location of results
set-1	Uniform array with three-high spheres and cylinders, with the most conservative spacing based on the SNL compaction data. Waste forms are stacked directly on top of each other.	Appendix A Addendum 1
set-1a	Uniform array with three-high spheres and cylinders, with an alternative spacing based on the SNL compaction data. Waste forms are stacked directly on top of each other.	Appendix B Addendum 1
set-2	Nonuniform array with spacing based on SNL compaction data. Two sets are included: one set for the upper horizon (uh), and one set for the lower horizon (lh).	Appendix C Addendum 1 Appendix D Addendum 1
set-3	Uniform array with six-high spheres and cylinders, with the most conservative spacing based on the SNL compaction data. FGE limited to 180 per waste form. Waste forms are stacked directly on top of each other.	Appendix F Addendum 1
set-3a	Uniform array with six-high spheres and cylinders, with an alternative spacing based on the SNL compaction data. FGE limited to 180 per waste form. Waste forms are stacked directly on top of each other.	Appendix I Addendum 1

4.2.1.1 Uniform arrays

The parametric evaluations based on the uniform arrays use a horizontal, center-to-center spacing which conservatively bounds the reduction of the horizontal pitch based on the greatest overall room closure for the upper and lower horizons. The use of tightly packed, triangular pitched arrays filling a large single room is expected to be modeled on a scale large enough to preclude some other combination of room and cross-drift configuration being more reactive. For both uniform and nonuniform arrays, the portion of the model external to the panel is an infinite salt reflector that mimics the WIPP repository geology.

Two sets of cases are evaluated with the three-high model: set-1 and set-1a. The purpose of set-1a is to evaluate the reactivity effect of the spacing. The only difference between these two sets is the distance between waste forms in the x-direction (as shown in Figure 4.3), where set-1a has an increase in spacing. The SNL data used to determine the spacing for both sets are presented in Table 4.3 below.

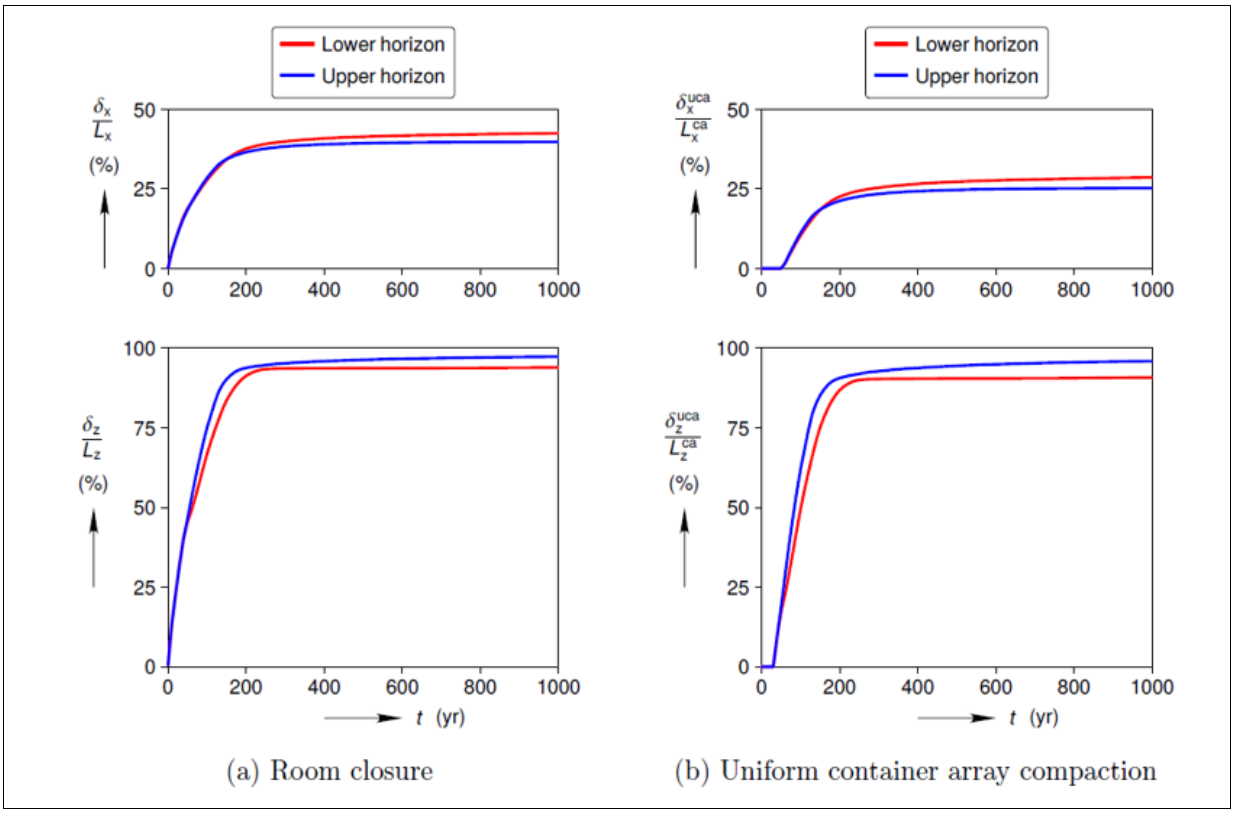

Figure 4.6. Representation of the SNL compaction data used with permission from Reedlunn [25].

The data presented in Figure 4.6 above show that there are two ways to view the compaction of the room with CCOs where the top diagram represents the x direction closure and the bottom diagram represents the z direction closure. The first factor assumes that the compaction of the array is proportional to the overall room closure (see also Figure 4.7 and Table 4.2), as opposed to the compaction of the uniform array of containers only. Sets 1 and 3 assume that the x-direction compaction is proportional to room closure, which provides a high estimate of the level of compaction. The second approach (an assumption used for the x direction in Sets 1a and 3a) does not penalize the value with the gaps in the room where the ingress of the salt simply fills in the space that is not used during emplacement. The room closure values used in set-1 serve as a value for spacing, which conservatively bounds the SNL data for both upper horizon and lower horizon for overall room closure (i.e., including the closure of the empty space). The other approach is to consider how the containers themselves are compacted. In other words: the approach of sets 1a and 3a assume that for the x direction, only space is removed within the confines of the containers during compaction. Note that for both methods, the models are constructed such that each waste form is stacked on top of the one below with zero space at the point where they touch in the z-direction, and although there is little to no compaction in the y-direction, a value of 10% compaction is used. A summary of these approaches for using the SNL data is shown in Table 4.2 below.

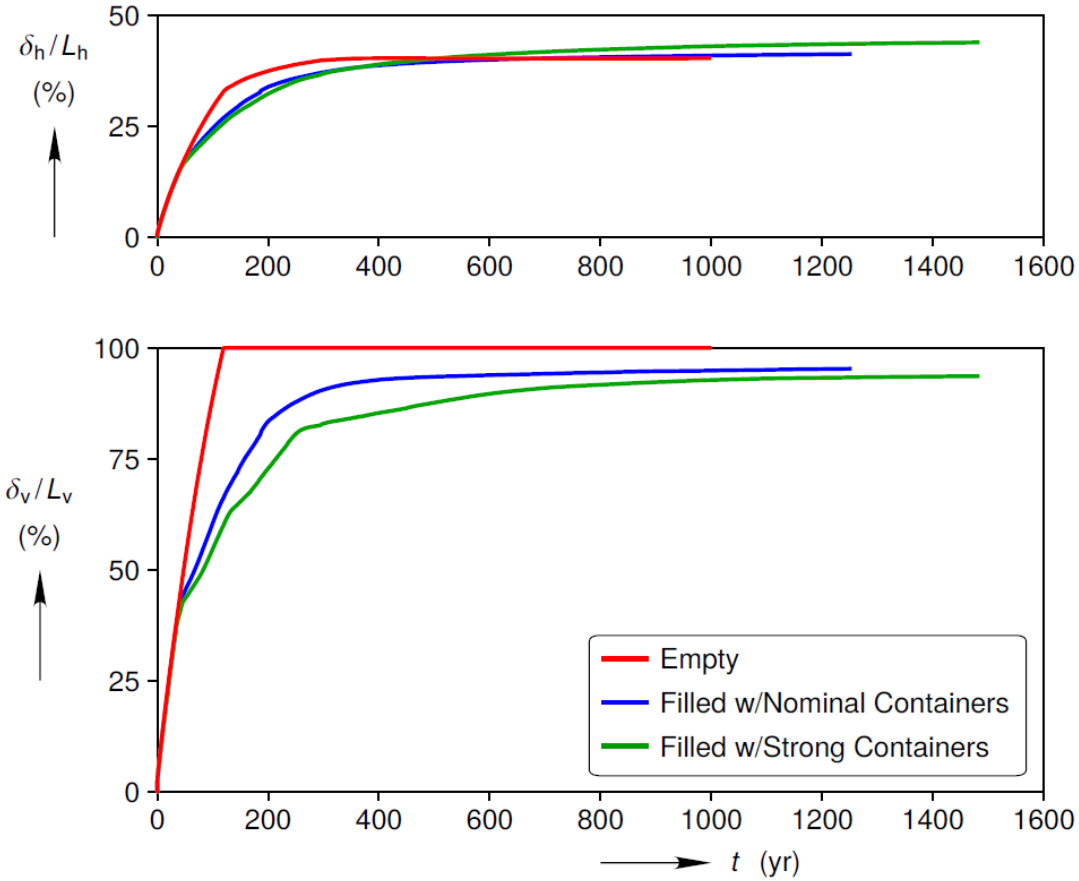

Figure 4.7. Illustration of the room closure in the vertical and horizonal directions, used with permission [8].

Table 4.2. Comparison of the SNL closure data used for uniform arrays

Horizon (at 1,000 years)	Horizontal room closure (%)	Vertical room closure (%)	Horizontal uniform container array compaction (%)	Vertical uniform container array compaction (%)
Upper	39.77	97.32	25.25	95.94
Lower	42.45	93.94	28.58	90.81
Empty room (maximum horizon)	44.5%	—	—	—

The SNL data were used to select values for x-direction pitch reduction. These values provide the level of conservatism desired in the results. For set-1, the purpose of the case is to bound all analysis results in the range of interest. For a best-estimate approach, the set-1a value is used as shown in Table 4.3 below. These pitch reduction factors are used to reduce the assumed triangular pitch spacing from the CCO's 57.45 cm diameter shown in Figure 4.4.

Table 4.3. Horizonal closure percentage used for x-direction spacing reductions

Case	Horizonal pitch reduction %	Basis for closure percentage
set-1	50	Spacing reductions that include empty room space closing
set-1a	25	Spacing reductions that include CCO compaction only
set-3	50	Spacing reductions that include empty room space closing
set-3a	25	Spacing reductions that include CCO compaction only

4.2.1.2 Nonuniform arrays

The parametric evaluations with nonuniform arrays use the CCO centroid locations data from Reedlunn and Bean [8] for the upper and lower horizons. The difference between the two horizons is illustrated in Figure 4.8. Panels mined on the lower horizon have different stratigraphy from those carved on the upper horizon, so room compaction may proceed differently. The methodology to use geomechanical post-closure data was developed by Brickner [4]. This previous analysis evaluating POCs used earlier results from Reedlunn and Bean [7]. The parametric evaluation of the CCOs documented herein uses the most recent simulations from Reedlunn and Bean [8], in which CCO post-compaction behavior data are used to evaluate the lower and upper horizon scenarios.

The Reedlunn and Bean [8] analysis used the CCO center-to-center pitch information (outer diameter in Figure 4.4) as an initial condition in two ways: (1) as a uniform orthogonal reduction in the pitch between containers for the uniform arrays, and (2), as the location of container centroids post compaction in nonuniform arrays. Model spacing is discussed in more detail in Section 4.1.

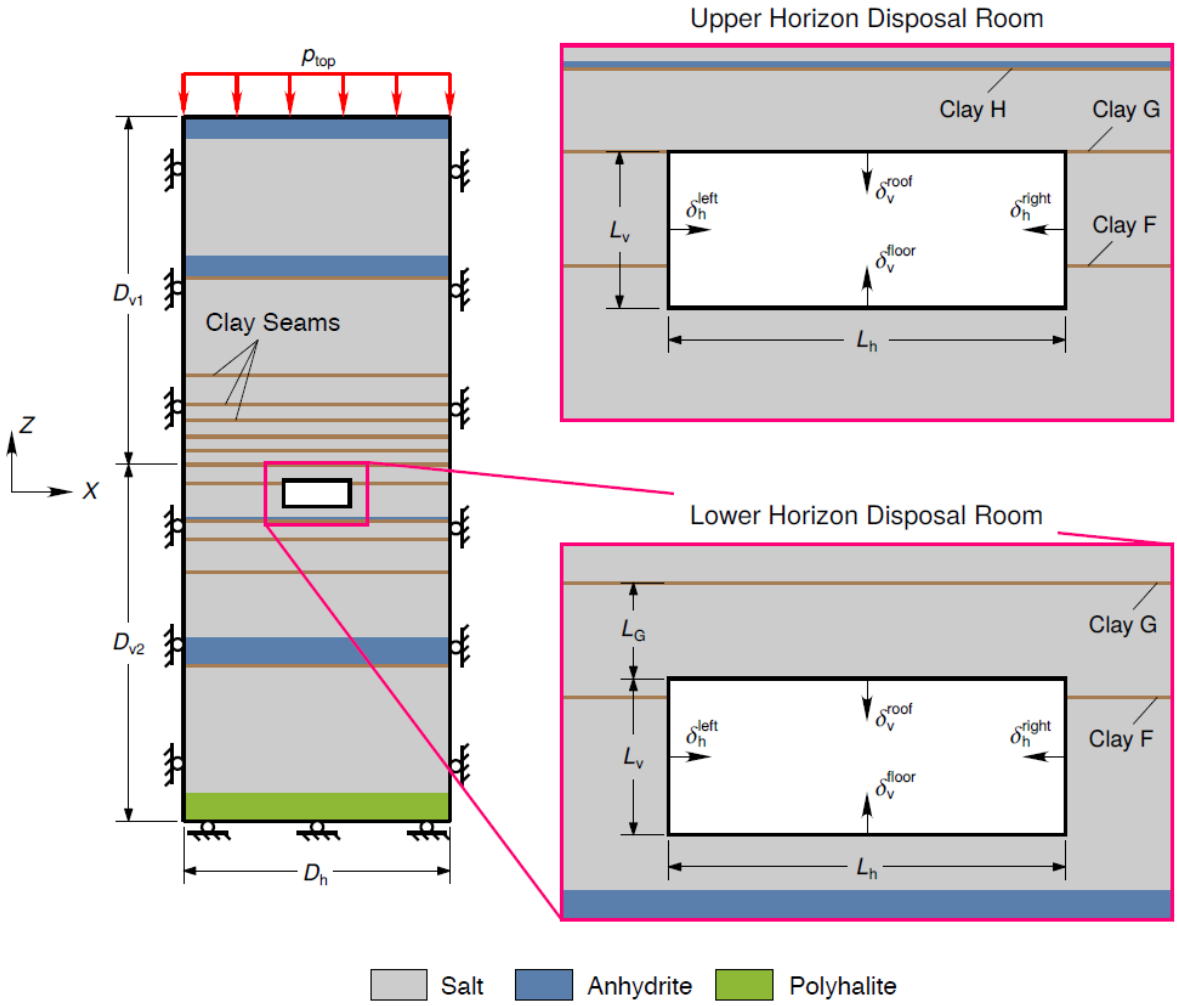

Figure 4.8. Illustration of the lower and upper horizons at WIPP used with permission from Reedlunn and Bean [8].

Although the post-closure compaction behavior between the lower and upper horizons is similar [8], the centroid compaction data from Reedlunn and Bean [8] is used in two separate sets of nonuniform array models to evaluate the potential impact on criticality because the data are available, and it allows for comparison of the ways that geologic variations may impact k_{eff}.

Figure 4.9 below provides an illustration of the nonuniform array compaction simulation data from Reedlunn and Bean [8], and Table 4.4 provides the centroid-specific locations derived by SNL using a weighted center of mass average. The 153 CCOs occupy a space much smaller than a full panel, so the front and back have reflective boundary conditions to approximate the room as being infinitely long. Thus, neutrons leaving the boundary are re-introduced, resulting in the front and back dimension appearing infinite in extent, thus bounding the length of the full panel.

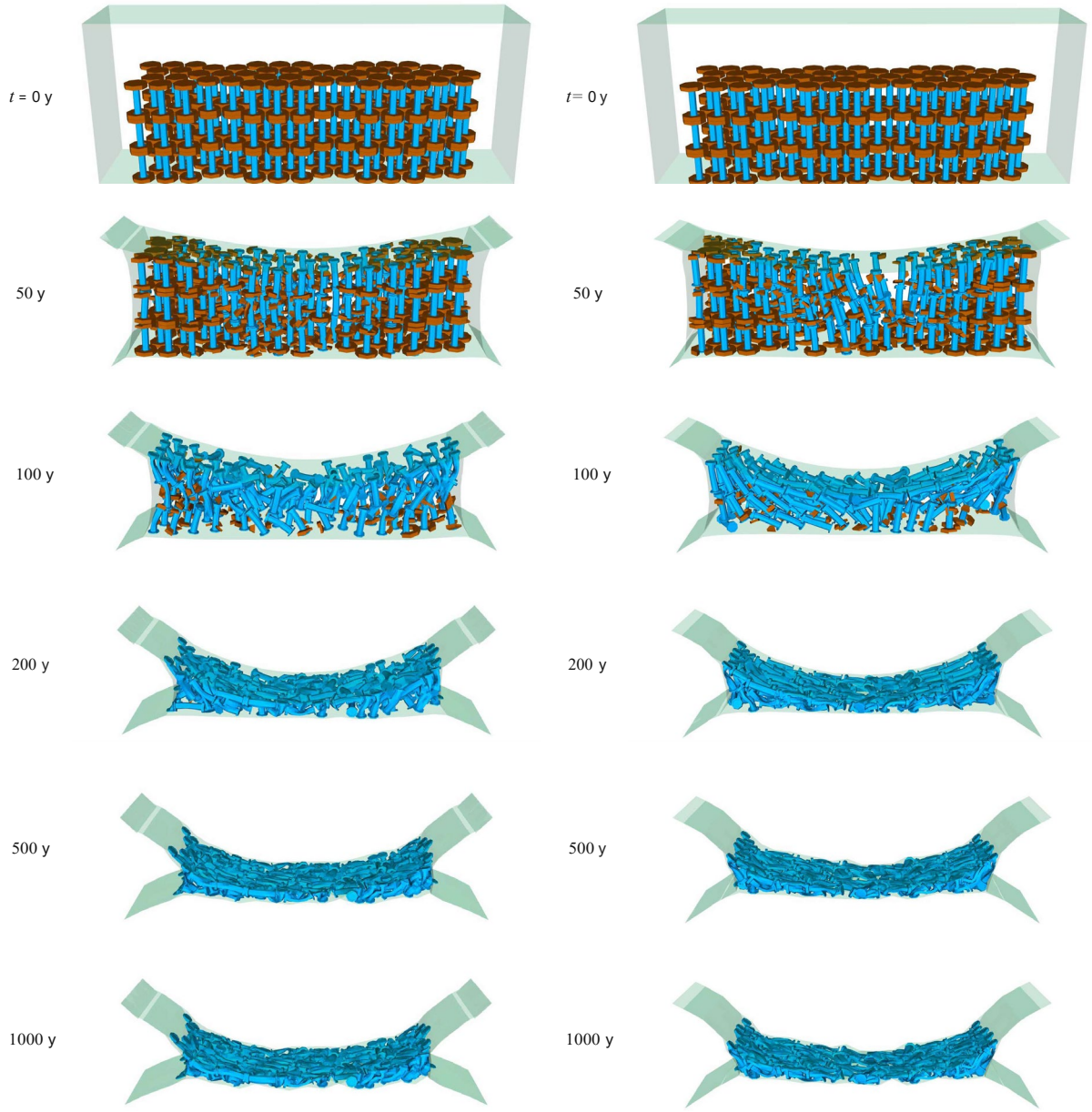

Figure 4.9. Salt compaction of CCOs in WIPP disposal room: (a) lower strata horizon in southern portion of repository, and (b) upper strata horizon in northern portion of repository, used with permission [11].

Table 4.4. Reedlunn and Bean [8][6] compaction study of centroid locations (in cm) for upper and lower horizons

Centroid	Lower horizon			Upper horizon		
	x-coordinate	y-coordinate	z-coordinate	x-coordinate	y-coordinate	z-coordinate
1	-195.6072	-8.5814	-566.9087	-213.4896	-2.0576	-284.4357
2	-168.3766	38.4815	-551.902	-163.8594	-20.9648	-300.5868
3	-206.4903	68.5531	-568.2877	-187.2823	47.4028	-298.7615
4	-232.1483	48.1034	-537.9253	-225.6460	60.1507	-300.7980
5	-211.7788	-27.3806	-549.6381	-232.8352	8.4008	-286.8479
6	-189.8944	-64.4194	-529.0411	-218.9769	-60.0147	-295.0244
7	-187.1205	-6.4709	-549.6133	-191.5388	-72.1002	-291.3473
8	102.0811	-29.7449	-552.5645	137.3855	20.8934	-300.5575
9	174.8612	-47.1992	-538.3002	184.3125	18.9962	-292.9760
10	127.9292	26.2153	-550.6479	169.3188	64.0558	-297.1980
11	24.2554	27.7693	-567.3369	87.8555	43.2948	-308.5008
12	9.6590	38.3789	-563.5939	23.8535	13.5799	-311.4196
13	24.5192	-68.4402	-562.3103	101.8339	-64.3174	-302.3304
14	99.7466	-82.1888	-555.3967	142.7472	-40.0338	-297.0448
15	252.7654	10.0135	-548.1866	257.5228	-43.9402	-292.7001
16	282.4657	-35.1615	-538.2288	288.9069	-3.1321	-296.7938
17	282.5897	93.3085	-536.9157	281.6632	69.4535	-287.4882
18	278.5696	51.3496	-509.8827	271.7254	38.1149	-286.9477
19	225.9322	37.0264	-527.9882	236.5810	-16.8224	-292.4982
20	273.4185	-63.8927	-518.9328	246.1724	-76.1062	-298.3139
21	276.9387	-88.4429	-542.0559	269.1834	-67.0046	-300.5688
22	-163.4146	3.6923	-554.6168	-146.6181	-4.9767	-306.9386
23	-123.7791	2.3381	-558.0016	-101.9203	-35.8322	-312.8182
24	-171.4336	49.8568	-558.1559	-120.5979	40.8157	-312.6055
25	-213.1447	26.1211	-547.1646	-157.1704	64.5581	-311.4320
26	-242.8409	-1.6661	-563.6853	-170.6807	3.5146	-308.9558
27	-202.9402	-57.4155	-555.2846	-131.5732	-50.6890	-310.5286
28	-135.2804	-50.4475	-565.4454	-127.1361	-90.6006	-312.9752
29	66.9308	10.2665	-565.9355	95.4716	-34.4232	-311.6265
30	128.1795	5.1647	-556.7833	117.1502	-3.5771	-313.4797
31	64.3827	46.9144	-567.4066	102.1670	46.7216	-313.6667
32	28.2069	42.5161	-573.6335	74.4089	8.8337	-310.4222
33	13.5157	-8.1312	-569.7059	53.4156	-31.5836	-315.0150
34	38.3705	-35.6255	-560.2751	71.1694	-65.0879	-314.3208
35	110.8944	-65.1957	-568.2821	83.0034	-90.7105	-307.6107
36	281.2500	8.4249	-548.2412	277.9888	20.4604	-299.2442
37	309.8546	3.7029	-554.3904	292.3153	58.1228	-290.9107
38	301.6371	47.6465	-541.9669	309.5932	95.1232	-300.8653
39	274.1711	37.5543	-554.4294	226.7347	33.0839	-300.4133

[6] Used with permission

Table 4-4. Reedlunn and Bean [8] compaction study of centroid locations for the upper and lower horizons (continued)

Centroid	Lower horizon			Upper horizon		
	x-coordinate	y-coordinate	z-coordinate	x-coordinate	y-coordinate	z-coordinate
40	242.5638	-9.9588	-554.2952	188.8528	-26.9823	-305.3414
41	241.4997	-48.9540	-547.1007	231.7606	-33.3423	-300.5899
42	295.4058	-59.4042	-552.7902	294.5557	-18.5864	-306.8297
43	-217.8443	6.5048	-544.1930	-265.4261	-12.0709	-268.1155
44	-153.4009	-53.6609	-548.4302	-235.0770	33.0402	-280.8256
45	-197.8117	80.2423	-550.1229	-248.4038	68.3274	-280.9737
46	-232.0676	61.1887	-517.6337	-264.8788	31.5113	-273.7527
47	-247.7792	16.2919	-511.9121	-287.8335	13.9891	-264.7854
48	-236.5811	-64.0944	-531.9523	-271.9484	-38.8405	-275.7612
49	-200.4602	-32.9123	-530.9564	-252.7562	-60.1307	-271.3269
50	64.5087	31.0070	-557.3813	121.3443	69.8568	-300.9824
51	143.1706	54.1248	-546.8746	254.0710	9.4251	-271.9287
52	117.8685	61.7223	-563.2603	235.1526	61.7990	-280.1688
53	87.5655	74.3758	-564.3316	34.4203	59.9985	-310.1965
54	6.3309	4.0348	-558.7176	-55.9454	19.2380	-306.0426
55	83.3233	-48.3772	-560.6623	11.9535	-72.6694	-308.7388
56	157.9896	-21.4957	-540.4430	191.609	-21.0098	-289.4311
57	288.3405	-26.3997	-500.3040	288.4938	-33.9050	-261.8424
58	305.0526	2.0657	-488.7934	304.4687	-40.9056	-253.1890
59	304.9013	60.9769	-488.0990	297.569	83.2448	-257.1121
60	297.5841	21.8671	-508.6516	302.8779	2.2301	-256.4747
61	263.3753	-3.1083	-512.8440	290.4659	-8.2906	-263.7739
62	302.8147	-88.9794	-499.9142	293.9906	-70.7845	-265.8125
63	305.0992	-54.2145	-495.0503	304.2196	-91.7415	-255.0902
64	-244.4525	-77.1758	-542.6508	-267.1711	-91.3518	-296.7223
65	-188.4417	-86.3376	-559.4857	-237.3205	-95.7182	-293.8821
66	-238.8877	-42.5505	-530.0501	-259.8012	-30.0669	-290.1501
67	-268.6379	-3.5462	-518.8964	-280.3122	-34.0868	-296.0446
68	-277.0882	-55.4640	-524.5588	-295.7452	-53.2454	-289.8989
69	-107.8975	-95.9258	-552.7917	-96.6793	-94.2065	-303.8164
70	-37.0657	-77.8336	-557.0315	6.4047	-95.7134	-315.0579
71	-63.3461	2.6602	-559.7408	-31.5007	-36.5975	-309.4587
72	-131.9347	-29.8631	-558.0907	-125.6904	-25.7994	-299.5687
73	-164.3553	-86.6192	-556.3458	-148.8238	-89.1546	-305.4559
74	210.3606	-96.2887	-543.9088	212.9723	-77.3391	-289.1568
75	251.8139	-86.6179	-518.6836	231.9386	-95.7353	-293.4954
76	236.0352	7.2155	-519.1767	227.2816	-38.7678	-293.8478
77	185.3908	-46.9649	-548.4143	195.7941	-16.1381	-294.3386
78	152.8983	-69.4795	-555.7515	172.8191	-64.4003	-294.0295
79	-243.7385	95.3014	-538.6218	-268.6026	94.9990	-298.3608
80	-212.0347	55.9720	-546.1598	-236.3573	94.7920	-287.0739
81	-271.4215	82.2483	-526.1757	-303.7671	92.0952	-295.0585
82	-265.7712	24.3046	-527.1078	-276.2057	5.1702	-294.8271
83	-239.3240	18.0546	-538.6019	-255.3651	23.1740	-299.7947
84	-112.4733	52.6610	-562.5813	-100.8276	95.6871	-303.3531

Table 4-4. Reedlunn and Bean [8] compaction study of centroid locations for the upper and lower horizons (continued)

Centroid	Lower horizon			Upper horizon		
	x-coordinate	y-coordinate	z-coordinate	x-coordinate	y-coordinate	z-coordinate
85	39.2405	87.0530	-562.6270	-40.6567	55.1499	-309.9441
86	-190.4090	98.7541	-550.0681	-145.5982	91.8613	-305.8976
87	-115.5552	24.8619	-559.7710	-138.6377	24.8523	-300.1584
88	-65.4479	23.4106	-554.6334	-79.5500	33.5978	-307.6583
89	232.1739	64.9417	-566.4858	222.0002	93.3458	-298.1699
90	272.3040	76.7184	-508.9081	263.9811	88.5637	-289.5813
91	126.5840	75.7607	-546.2491	186.6790	87.7788	-291.2231
92	167.1547	56.4320	-562.3259	206.7590	43.7193	-296.1452
93	213.2109	61.6758	-536.6561	235.5210	11.2188	-292.1886
94	-277.9814	-83.0493	-558.7073	-216.7393	-70.5421	-303.6883
95	-231.3040	-65.2024	-565.1735	-178.8628	-73.2675	-302.1743
96	-265.0780	-24.3620	-550.0945	-198.7380	-35.8451	-297.7332
97	-301.0789	-28.1433	-544.9897	-232.9369	-31.2563	-300.6552
98	-306.6950	-63.7129	-549.7599	-289.7868	-44.1079	-303.7186
99	-62.8465	-64.9939	-571.2789	-28.9445	-62.4375	-313.2632
100	-16.6897	-91.2152	-571.0237	37.9474	-73.1966	-312.4582
101	-11.3818	-26.1744	-567.7898	-4.0034	-28.3581	-315.3801
102	-69.6733	-31.5698	-569.2037	-50.3881	-9.1844	-317.6224
103	-118.9749	-76.3456	-555.6463	-81.3406	-74.7552	-313.1018
104	185.5332	-77.3915	-549.2069	154.2222	-96.4896	-309.3883
105	212.6486	-66.1513	-547.1550	188.9751	-73.9651	-303.9341
106	200.9535	-42.1123	-557.7798	160.2633	-46.2455	-302.7995
107	160.5359	-20.8914	-553.3461	127.2591	-31.9314	-310.4759
108	142.7483	-94.4954	-557.1335	124.9580	-87.5420	-311.3654
109	-274.7585	73.1582	-550.0604	-202.1909	91.6333	-308.3082
110	-254.6001	78.0200	-560.7598	-174.4730	92.2439	-307.3053
111	-313.6393	74.4106	-553.5117	-294.6694	27.0406	-299.4978
112	-308.0409	26.9075	-541.9002	-217.6602	10.3411	-304.9176
113	-268.5852	28.7860	-553.2664	-194.0969	29.7966	-303.6382
114	-15.4739	83.9212	-570.1639	-20.3665	80.1401	-312.0258
115	-5.6954	71.9634	-566.3322	71.7688	69.8459	-312.6709
116	-150.2334	77.8732	-558.4633	-75.0437	76.8131	-315.8768
117	-57.4474	45.4806	-562.1516	-64.8536	13.1179	-313.9009
118	-38.0596	19.6168	-570.9484	-9.0724	21.3081	-313.7538
119	170.7607	51.2304	-567.7764	154.6926	83.8294	-310.0220
120	240.4769	93.9066	-547.7869	204.8655	64.2860	-302.7075
121	135.4575	94.3221	-562.2151	121.9991	95.3049	-310.6237
122	179.6678	3.7066	-555.4600	147.7968	26.9379	-306.9927
123	212.8767	5.7786	-562.4326	175.2278	16.1506	-305.3567
124	-285.5110	-93.6461	-511.9963	-289.4428	-49.6838	-259.6640
125	-247.9282	-88.8492	-519.8870	-278.0818	-69.9646	-260.4170
126	-283.9506	-13.9425	-488.5638	-284.8696	-9.5179	-267.4761
127	-302.9387	-32.0402	-494.2332	-302.7002	-6.3955	-254.7843
128	-311.4812	-76.1218	-472.8971	-299.8982	-94.4408	-253.5523
129	-69.9875	-91.8442	-567.3457	-166.0907	-88.0975	-292.5673

Table 4-4. Reedlunn and Bean [8] compaction study of centroid locations for the upper and lower horizons (continued)

Centroid	Lower horizon			Upper horizon		
	x-coordinate	y-coordinate	z-coordinate	x-coordinate	y-coordinate	z-coordinate
130	37.6640	-92.6135	-563.6414	-91.2889	-61.8661	-303.2903
131	-48.5633	-57.9711	-565.9090	-124.5097	-0.6922	-299.9205
132	-89.8459	-42.1439	-554.3143	-205.2035	-47.2042	-287.0985
133	-180.4832	-96.3225	-535.7100	-245.0691	-96.7256	-276.4592
134	239.5603	-52.4520	-514.3432	267.7152	-87.6572	-273.3308
135	282.6324	-95.1450	-506.5219	277.9787	-96.8531	-271.5817
136	256.7301	-32.4694	-506.6623	278.1862	-57.5666	-267.7829
137	207.8105	12.4602	-527.3900	260.0825	-18.3410	-268.9344
138	167.7973	-95.8046	-552.2154	243.7051	-68.0402	-274.1189
139	-283.8441	75.4922	-492.0842	-287.7614	72.6029	-268.1458
140	-233.1853	72.6945	-530.3853	-279.8825	56.6815	-276.2016
141	-309.8401	81.3561	-480.5229	-293.8302	90.5573	-251.1806
142	-302.5714	28.8674	-484.8186	-303.7403	31.0081	-254.5943
143	-278.3352	50.5453	-504.1470	-288.1789	38.3306	-266.2597
144	-56.0811	92.8100	-559.7273	-182.8970	74.7467	-291.7416
145	-9.0936	66.5283	-559.0231	-111.8636	66.8251	-303.0716
146	-111.5024	79.3568	-553.5037	-219.6363	89.8358	-280.4688
147	-185.2346	-4.5709	-535.3569	-205.6745	45.3883	-286.7643
148	-81.4054	-16.8762	-552.1512	-146.6689	50.7662	-296.4557
149	211.6919	92.4383	-546.4770	276.1441	73.9273	-268.7344
150	279.3761	94.6427	-491.6647	290.6271	59.9997	-259.4299
151	175.3590	94.0269	-552.1094	258.1187	91.9249	-269.4827
152	185.9292	46.1741	-542.5692	263.9302	36.0571	-268.6708
153	248.2810	48.6150	-526.1100	288.0774	22.5152	-261.3250

4.2.2 Reflector Materials and Geometry

The reflector materials are those materials in the model located outside of the waste form—specifically, any material which is outside the outer diameter of the waste form. The reflector material has two possible configurations that may exist together in the same model: interstitial and discrete. The interstitial reflector materials are based on the work by Brickner [4] and are described in Section 4.2.1.1below. The discrete reflector described in Section 4.2.2.3 is directly adjacent to the waste form and has a thickness chosen to be very small (0.001 cm), or the thickness of a CCC (0.7112 cm), which was chosen to cover the existing arrangement, and for convenience. Additionally, the discrete thickness is used to evaluate the k_{eff} effect of polyethylene (an appropriate material because of its neutron-moderating/reflecting properties) from external sources that could be pressed around the waste stream under post-closure conditions.

For each waste form parametric sweep, the total mass and volume of the waste form define the waste form geometry dimensions (see Section 4.3 below). The discrete reflector has a fixed thickness which is applied to every parametric sweep over all the waste forms. Every calculation with the same waste form mass and volume has a consistent discrete-reflector-volume–to–waste-form-volume ratio. Parametric sweeps with a mix of waste form mass and volumes have varying discrete-reflector-volume–to–waste-form-volume ratios. Therefore, smaller waste form volumes with the 0.7112 cm thickness reflector have a much larger discrete-reflector-thickness-volume–to–waste-form-volume ratio than the largest waste form volume. In this manner, the source of external discrete reflector material is irrelevant, and each set of

parametric sweeps can establish the effect of the discrete reflector for its mass and volume combinations. Therefore, any combination that represents an actual waste form may be applicable. Since a very thin reflector and a thick discrete reflector are used, the effect of values in between can be estimated or bounded.

4.2.2.1 Salt and MgO for the interstitial reflector material

The interstitial reflector materials consist of material between CCCs. Because the material is between the waste forms, it reflects neutrons back into the waste forms. MgO and NaCl have very low moderating power. The treatment of the interstitial reflector here follows on the work by Brickner [4] and is described in detail below.

Salt is the most common and abundant material in the system and is considered in both the interstitial reflector and in the infinitely thick external reflector. The salt in the region of the waste forms is denoted as an *interstitial reflector* here because it lies between the waste forms, and it reflects some neutrons back into the waste forms. Salt can act either as a reflector or an absorber, depending on the neutron energy. In Brickner's work [4], the salt was evaluated as dry and modeled as NaCl. As saturated or brine it was modeled as NaCl and H_2O. The negative reactivity effect of the neutron absorptions in the brine precludes the necessity of repeating those studies here. The dry salt is assumed to always be present in the reflector.

MgO is present in Supersacks placed on top of about half of the stacks of three 7-packs. The MgO is used to absorb CO_2 produced by the decay of carbon-based materials such as wood, paper, plastic, or rubber. However, as noted in the High Bridge Associates report [23], the MgO has a large neutron scattering cross section and can therefore serve as a neutron reflector and/or moderator. Saylor and Scaglione [3] evaluated the impact of the MgO as a reflector in its as-emplaced configuration, which is essentially a layer of MgO on top of the stacks of three 7-packs (albeit an exaggeration of the total mass available). Brickner's 2019 [4] evaluations showed that increasing the amount of MgO that was uniformly mixed with salt increased the k_{eff}. Because of the far greater amount of salt compared to the MgO, Brickner [4] conservatively placed an upper limit of 50% on the amount of MgO compared to salt. The same approach is used here.

The mean free path of the salt/MgO mixture is shown below in Figure 4.10 as the solid orange line. The dotted line indicates the average distance that a neutron would travel between scattering events if no other interactions were to occur, and the dashed line shows the average distance that a neutron would travel before being captured—again assuming no other interactions. Above approximately 0.03 eV, scattering dominates the total interaction probability. However, because multiple scatters can occur, absorption can become important, even in the range of hundreds of eV, due to absorption resonances. These lengths were computed using the ENDF-7.1 252 group scale neutron cross sections. Total and capture microscopic cross sections were multiplied by the elemental abundances listed in the SCALE output for a Sampler case to obtain macroscopic cross sections. Mean free path is the multiplicative inverse of the total macroscopic cross section for a particular reaction.

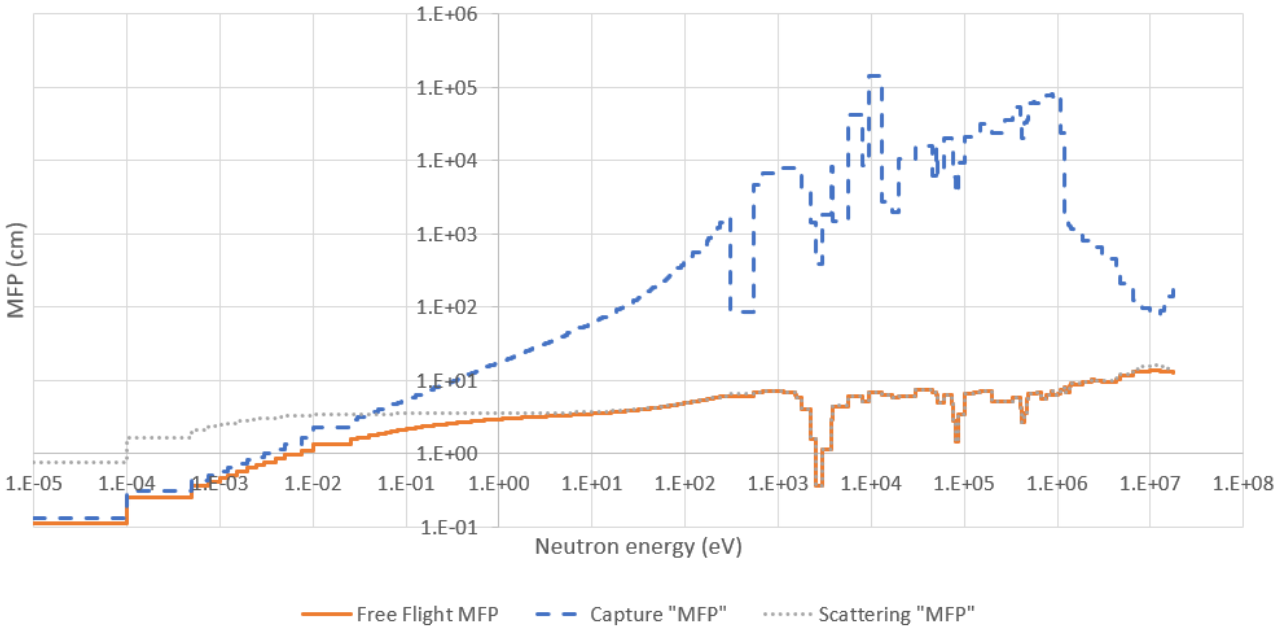

Figure 4.10. Mean free in the MgO/NaCl mixture.

Figure 4.11 below plots the macroscopic scattering cross sections of the major constituents of the salt/MgO mixture. As the figure shows, 100 eV ^{35}Cl contributes heavily to the total scattering cross section. In the keV range, there is a large scattering resonance for ^{23}Na. Mg and O play more prominent roles at higher energies, but they never truly dominate except at a few energy resonances. For convenience, scattering cross sections were taken as the difference between the total cross section and the capture cross section.

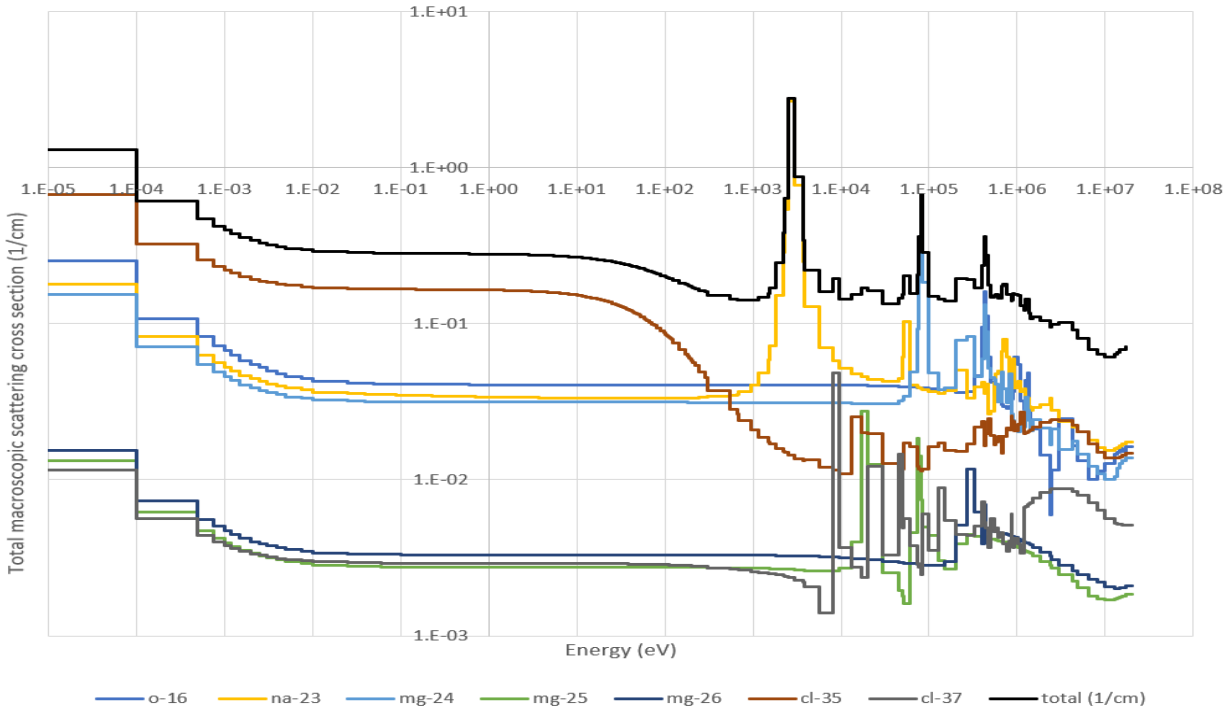

Figure 4.11. Macroscopic total interaction cross section for the the MgO/NaCl mixture components.

In Figure 4.12 below, capture cross sections of the salt/MgO mixture are dominated by ^{35}Cl at energies below 1 keV. Above 1 keV, ^{35}Cl remains a heavy contributor to the overall cross section with ^{23}Na.

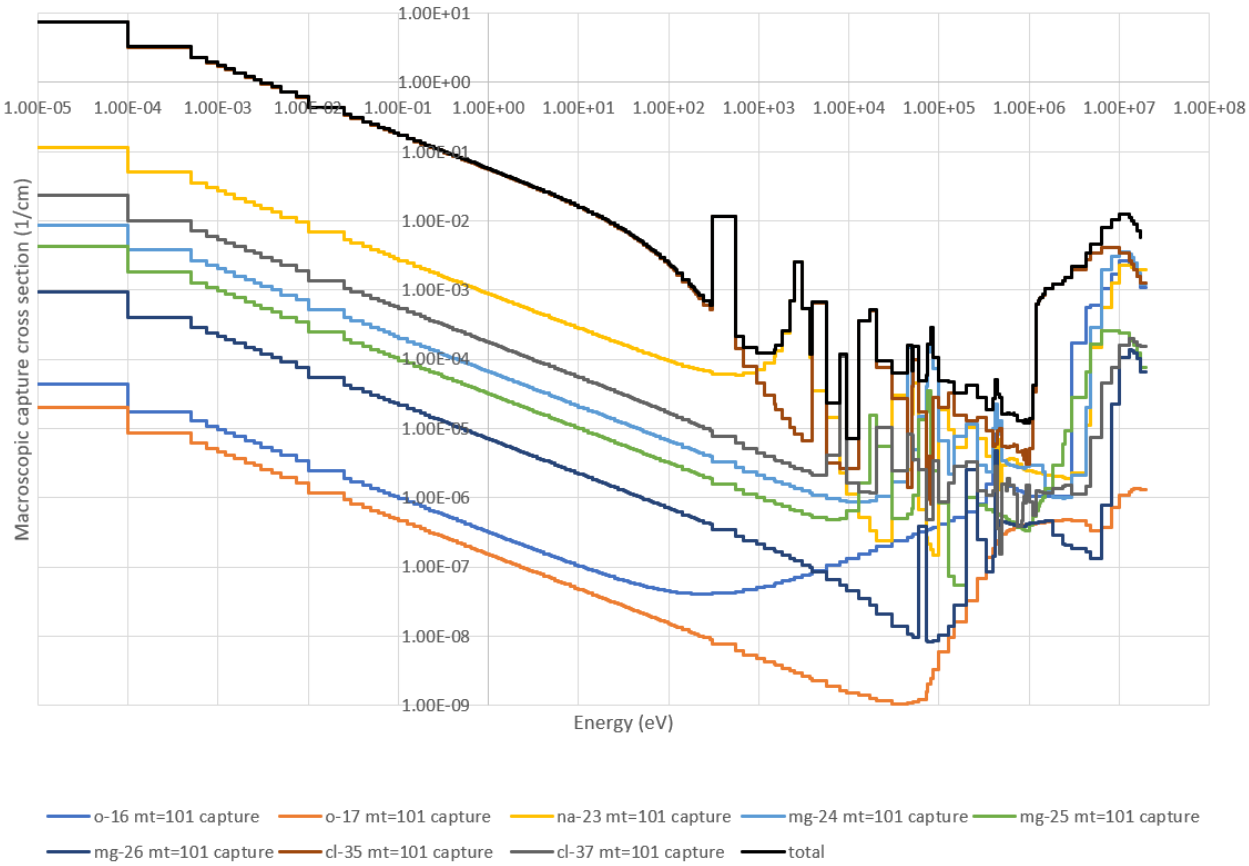

Figure 4.12. Macroscopic capture cross section for the the MgO/NaCl mixture components

4.2.2.2 Beryllium in the interstitial reflector

Because the special reflector as defined in the CCO *TRUPACT-II Safety Analysis Report* [9] can be transported using most container designs for shipment to WIPP, it is possible that Be may be present outside of the CCOs and could become intermixed with other materials. Calculations have been performed with Be uniformly mixed in the interstitial reflector material and are presented in publications by Saylor, Scaglione [3] and Brickner [4]. Those results show little or no difference in the presence of Be in the reflector vs. the waste form. For the present analysis, the Be is evaluated in the waste form only.

4.2.2.3 Steel and polyethylene for the discrete reflector material

The CCC is made of stainless steel and can function to reflect neutrons back into the CCC. The CCC is denoted as a *discrete reflector* in this document because it is not continuously distributed in the same manner as the salt/MgO mixture comprising the interstitial reflector. The stainless steel may be from the CCO, the CCC, or the packaging cans, and it can act as a reflector. Polyethylene is also used in packaging. Polyethylene is highly moderating, but it is also capable of scattering thermalized neutrons back into the CCO. Pu's fission cross section is orders of magnitude larger for thermal neutrons, which should produce a relatively large effect compared to the effect that would be achieved by simply reflecting faster neutrons back into the waste form. Polyethylene has a high moderating power, so it could bound other materials that may agglomerate into a discrete reflector around the waste form (i.e., cellulose from plywood) over long periods of time. For simplicity, the material card provided by the SCALE code package for 304 stainless steel and polyethylene is used.

4.2.3 WASTE FORM MATERIALS, COMPOSITION AND GEOMETRY

The CCO waste form materials are any materials that may be placed within the CCC of the CCO based on the defined limits contained in the CCO *TRUPACT-II Safety Analysis Report* [9] or otherwise limited by the WAC [5]. The CCO waste form materials include any possible materials which may be used as part of any waste stream processing. Generically, the waste form may potentially have up to 380 FGE ^{239}Pu, water and/or plastic materials, 585 g of special reflector material as defined in the CCO *TRUPACT-II Safety Analysis Report* [9] like Be, and no limits on any additional filler materials other than FGE and Be. These values bound the WAC limit. In this evaluation, H-bearing materials from any source are bounded by the H/^{239}Pu curves as water or polyethylene. In this report, all materials included in the waste form geometry are uniformly mixed. Any waste form which uses a configuration or process that creates a significant deviation in the waste form such that a uniform mixture may not be appropriate must be evaluated to determine the applicability of the results in this report. However, previous work has shown that the uniformly mixed case is an adequate approach to bound nonuniform mixing [24].

For this generic parametric evaluation of the CCO waste form, two filler materials[7] were evaluated separately: (1) a cementitious mixture herein termed a *generic material*, which was used by Saylor and Scaglione [3] to specifically evaluate the dilute surplus Pu waste stream, and (2) a *graphite material*, which was selected because it is expected to bound most if not all non-hydrogenous materials due to its neutron-moderating capabilities. The energy absorbed by nuclei in elastic collisions with neutrons decreases as atomic mass increases. A comparison of the moderating power of common moderator materials, as defined in Duderstadt and Hamilton [15], shows that lighter nuclei tend to have higher moderating powers (except for helium because it is a gas), so graphite is appropriate to consider, as shown in Table 4.5. Although other materials listed have higher moderator powers, they are either evaluated as moderators elsewhere in this study, or in the case of Be, they are restricted by the WAC.

Table 4.5. Comparison of the moderator power and moderating ratio of several materials

Material	Moderating power
water	1.28
heavy water	0.18
He	0.00001
Be	0.16
graphite	0.064
polyethylene	3.26

In addition to the generic and graphite filler materials, another material is included to provide a means to evaluate the impact of waste form processing cans (i.e., convenience cans) or other types of waste form container configurations. For this purpose, stainless steel is used for these cans because it is a likely candidate for such containers.

[7] A *filler material* is any material in the waste form that is ***not*** FGE, special reflector like beryllium as defined in the CCO *TRUPACT-II Safety Analysis Report [9]*, or H-bearing (i.e., water or polyethylene). For subsets of the parametric evaluations, stainless steel is included as a mass of material which represents a uniform mixing of the waste form and the stainless steel from either the convenience can type of configuration, as in the surplus plutonium from the CCC, or from some other external source. This context is considered part of the filler material. Specifically, when the stainless steel is mixed uniformly with the waste form, it is considered filler material that either replaces or is in addition to the other components of the filler material.

The reactivity effect of various filler materials (and the ingress of the can material) is expected to be dependent on the neutron spectrum and the size and shape of the waste form. The reactivity trend for filler materials is established in Section 6.1 below, but no effort is made to evaluate variations in the effect on reactivity for variations of the material components of the waste form, because the inclusion of filler materials shows a reduction in reactivity, and the materials considered are sufficiently conservative.

The waste form is modeled using two geometries: spherical and cylindrical. The use of spherical geometries to model long-term waste configurations is justified in Section 4 above. Additionally, Brickner [4] shows that using optimally moderated spheres (spheres that have moderator added to maximize reactivity) is extremely conservative compared to using other neutronically isolated shapes, and it provides ample technical justification for addressing the complexities of unknown configurations over the 10,000-year regulatory timeframe. However, to achieve optimal moderation for a sphere, the radius of the sphere must grow without bound until the optimum point is found. The radius of the optimally moderated sphere is seen to be well beyond the radius of the CCC for most cases; therefore, it is not realistic. However, the CCC is a cylindrical steel pipe which is expected to maintain its geometry for some significant period of time. Thus, results for calculations with sphere radii larger than the CCC should be viewed as information only and should not be considered likely. Furthermore, waste streams may be expected to use processes which result in rigid, fixed cylindrical shapes like the dilute surplus Pu can-bag-can configuration (see Figure 4.5, above). The dilute surplus Pu can-bag-can configuration is generically known to include an inner can wrapped in some form of plastic bagging which is then placed in another cylindrical can. This can-bag-can configuration is then placed in the cylindrical CCC pipe. If these cylindrical shapes are a part of any generic waste stream, then they should also be evaluated so that the FEP process may, at a minimum, consider the k_{eff} effect of the cylindrical geometry for the time periods in which they are expected to maintain their original geometry.

For both the spherical and cylindrical models, the waste forms are modeled for the parametric evaluations as follows:

1. The FGE volume is calculated from the FGE modeled based on one FGE equaling one gram ^{239}Pu in the form of PuO_2.

2. If Be is present, then the Be mass is used to calculate the volume of the Be.

3. The volume of moderator (water or polyethylene) is determined from the moderator mass at the point in the parametric sweep over moderator mass.

4. Each case, at a minimum, has FGE and moderator, while the Be is case dependent. Some additional cases include variations in filler mass and stainless steel for the can(s). For the spherical models, the total volume of these materials forms the basis for the radius of the sphere.

5. For the cylindrical models, the total volume of these materials is used to determine the cylinder height, based on the fixed radius for that case. Multiple cylindrical radii are considered because the radius and height have a direct impact on k_{eff}. Furthermore, the k_{eff} effects seen for the various parameter sweeps may be radii-dependent because of differing leakage for larger radii.

The *waste form parametric sweeps* consider FGE (380 or 190 for set-3), Be (0 and 585 g), and moderator (water and polyethylene) masses in the range of 100 to 3,000 g to establish a clear representation of the $H/^{239}Pu$ curve. The sweeps also consider filler material consisting of generic or graphite (0, 1,000, 2,000, 3,000 and 4,000 g), with and without the steel for the convenience can (0, 500 and 1,000 g). For all the variations of masses within the uniformly mixed waste form cylinders or spheres, the variation of the moderator generates k_{eff} curves as a function of the parametric sweeps.

4.3 OVERVIEW OF KENO MODEL GEOMETRY

The parametric evaluations described herein are based on the methodology in Saylor, Scaglione [3], and Brickner [4], as well as new methods that were developed to address emerging concerns. These evaluations consider two separate ways of modeling the system with CCOs: (1) uniform arrays of CCOs, and (2) nonuniform arrays of CCOs. The uniform arrays allow for the k_{eff} of the system to be evaluated in an idealized manner with 3 or 6 waste forms in close contact, whereas the nonuniform arrays are a best-estimate calculation using specific post-closure centroid locations based on the Reedlunn and Bean [8] data, with very few waste forms in close contact.

For both the spherical and cylindrical models, the discrete reflectors are modeled for the parametric evaluations as follows:

1. Both a thin 0.001 cm layer and a thick 0.7112 cm layer are modeled directly adjacent to the waste form shape.

2. The total mass and volume of the discrete reflector is allowed to vary based on the total volume of the shape for that sweep.

3. Sweeps are made over two materials: stainless steel and polyethylene.

Table 4-6 summarizes the parameters evaluated and the supporting rationales. The effects of these parameters on k_{eff} were evaluated using approximately 28,800 combinations per calculation set (155,520 total for six sets of calculations). Each set of calculations evaluated the array spacing variations listed in Table 6-1.

Table 4-6. Evaluated parameters and corresponding rationale for evaluating k_{eff} effect

PARAMETER	DESCRIPTION	VALUES USED	RATIONALE FOR EVALUATION
MODERATOR TYPE	Moderator uniformly mixed with waste form	Water, polyethylene	Both are powerful moderators (see Section 6.1). Furthermore, results show more moderation in the waste form increases k_{eff}
FILLER MASS	Filler uniformly mixed with waste form	0, 2, 4 kg	Range of interest
CYLINDER RADIUS	Radius of cylindrical waste form	4.8, 6.25, 7.7 cm	7.7 cm is the inner diameter of the CCC; smaller radii are listed to show a trend
CYLINDER HEIGHT	Height of cylindrical waste form	Set by waste form content	Dependent upon total volume
SPHERE RADIUS	Radius of spherical waste form	Set by waste form content	Dependent upon total volume: also provides some coverage of the space with radii > 7.7 cm
MODERATOR MASS	Mass of moderator mixed with waste form	0.1–3 kg	Range of interest to establish trend
STEEL PIPE OR POLYETHYLENE PIPE	Material of outer layer overlaying waste form	Stainless pipe or polyethylene	To show relative effect of bag, the CCC, and other materials that may accumulate like the polyethylene; polyethylene is expected to be an especially impactful material because of its high moderating power
PIPE THICKNESS	Outer layer overlaying waste form	0.001 cm, 0.7112 cm	Thickness of CCC is the default condition: thin layer is included to study the effect of removing the CCC, and the thick layer is included to study the effect of a layer of moderator immediately outside the waste form and the effect of any bagging material
CAN MASS MIXED WITH FILLER	Mass of steel convenience canister	0, 0.5, 1 kg	Values to establish trend
GRAPHITE OR DEFAULT		Graphite and cement	Cement is used; graphite is a good moderator but is not used elsewhere in the study; increased moderation tends to increase k_{eff}

Table 4-6. Evaluated parameters and corresponding rationale for evaluating k_{eff} effect (continued)

PARAMETER	DESCRIPTION	VALUES USED	RATIONALE FOR EVALUATION
GEOMETRY OF WASTE FORM	Shape of waste form	Sphere vs. cylinder	The cylinder is the initial condition of the system, and the sphere is a worst-case condition from the standpoint of single-waste form geometry
BE MASS	Mass of Be	0, 585 g	Transport limit
UNIFORM VS. NONUNIFORM	Uniform vs. nonuniform case	Triangular pitched 3- and six-high uniform arrays and centroid-specific nonuniform arrays	Uniform arrays are more conservative because they limit neutron leakage; nonuniform arrays are best-estimate arrays based on compaction data
PERTURBED CCO COORDINATES		Nominal, random sub-centroid, every sub centroid	In Appendix G, off-nominal CCO coordinates used to examine position sensitivity; the extent of CCO in the Reedlunn and Bean [8] model is taken as a reasonable range of uncertainty
PERTURBED ORIENTATION		Vertical orientation, random orientation, Reedlunn and Bean [8] best estimate	In Appendix G, off-nominal CCO orientation is used to examine sensitivity
B_4C CONTENT	B_4C uniformly mixed with waste form	0 g, 50 g (set-1, 1a, 2), 25 g (set-3)	0 g is the worst-case value; other values were included for comparison
MGO DENSITY	Density of MgO within envelope of CCOs	50%, Unperturbed	MgO is not placed on every stack and varies by what is in the stack of packages
MGO EXTENT	Size of MgO envelope	Around CCOs only	More than 1–2 mean free paths outside of envelope; neutrons leak or are absorbed by NaCl
PACKAGE LOCAL DENSITY		Unperturbed	Groups of 3 immediately adjacent waste forms evaluated in uniform array cases considered an unlikely condition
TIGHTER RUN PARAMETERS			Examined in Appendix E

Variations in array assumptions were achieved by grouping cases into different sets, as seen in Table 6-1. The full listing of results for these datasets is provided in Addendum 1.

The following diagrams (Figure 4.13 and Figure 4.14) provide additional information to illustrate the construction of the models and the use of the terminology.

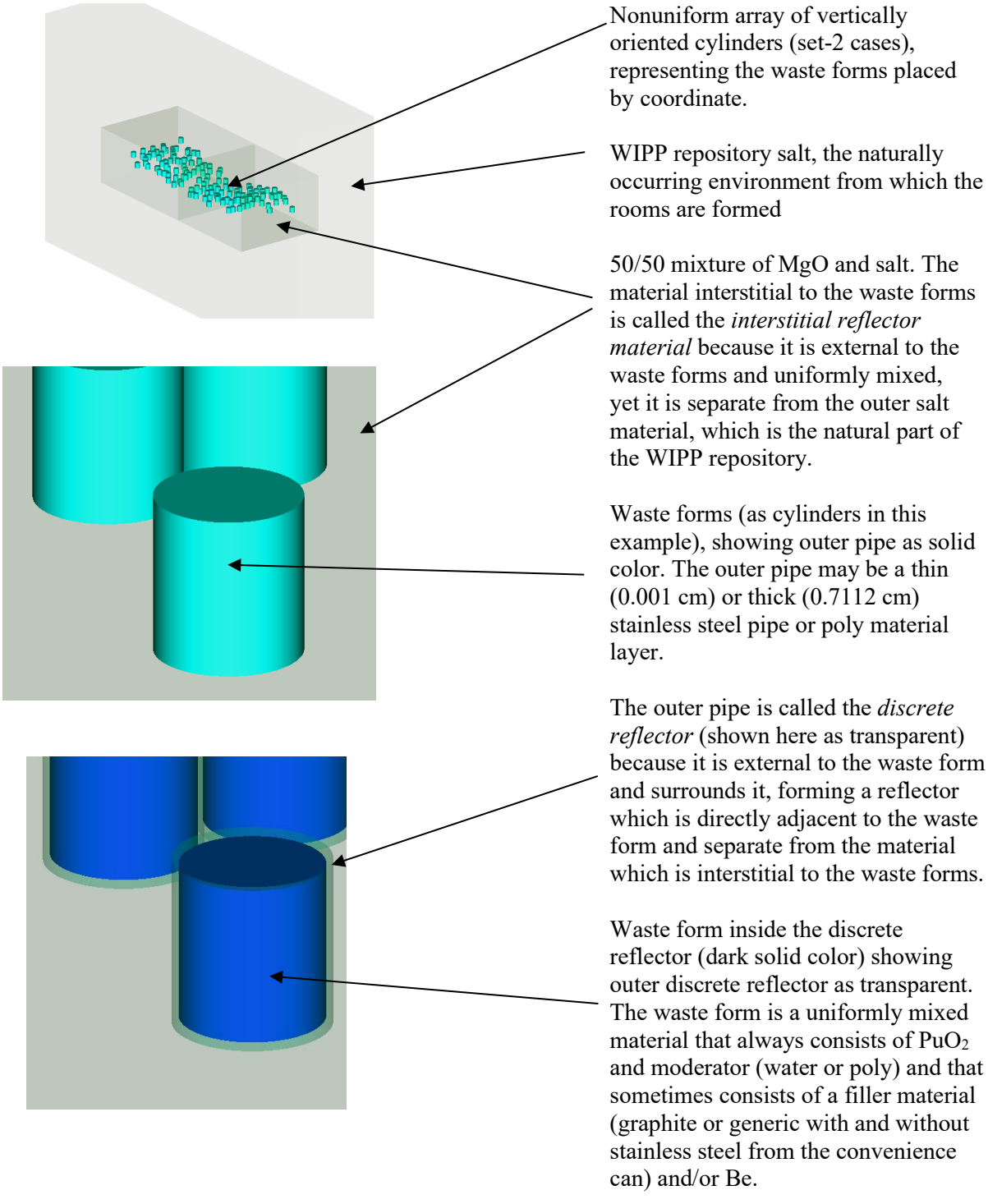

Figure 4.13. Diagram showing how the nonuniform array model is constructed with cylinders.

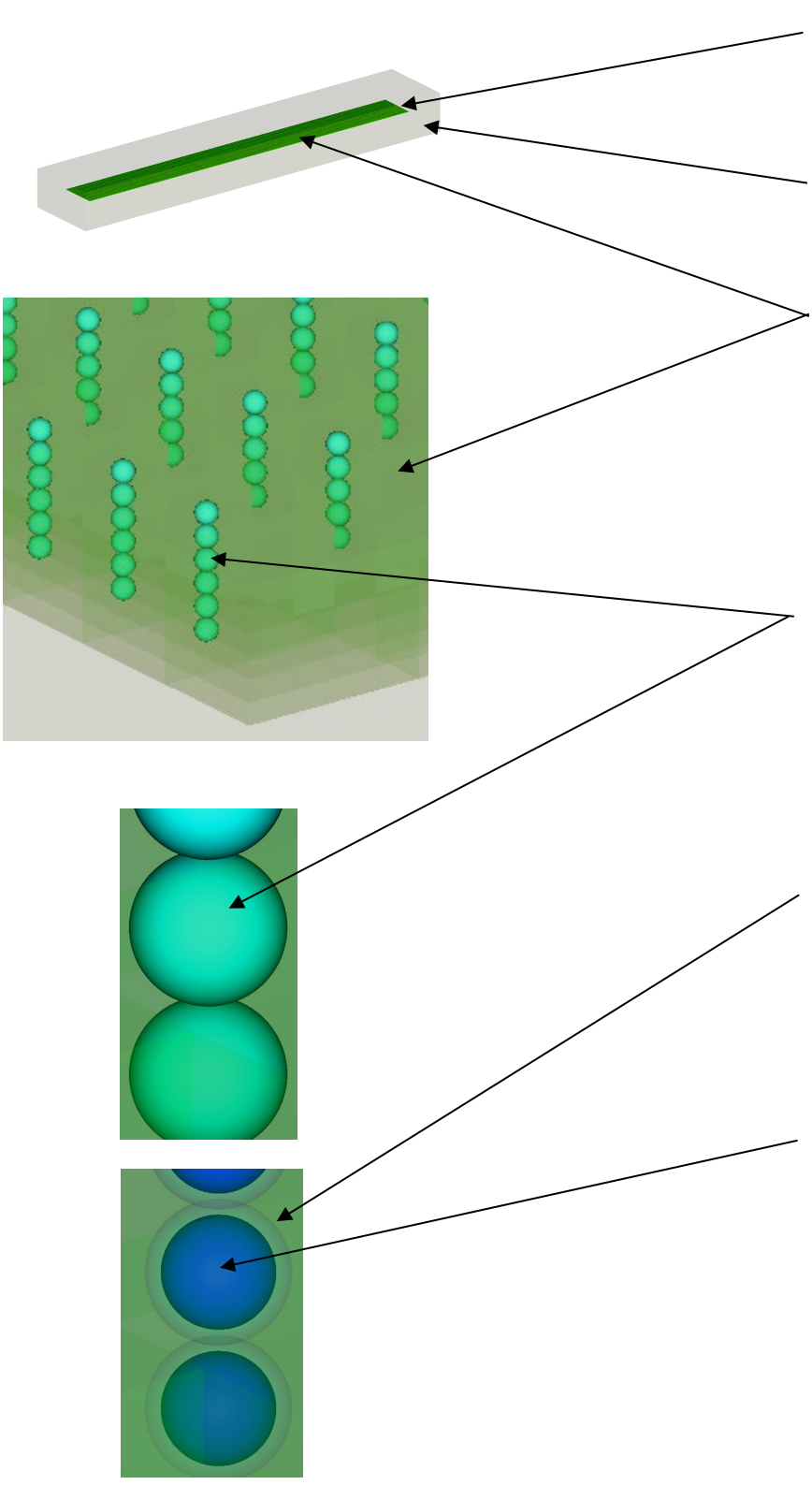

Uniform array representing the waste forms placed in a triangular pitch in six-high stacks of spheres (set-3 cases, detail shown in the following subfigures).

WIPP repository salt, the naturally occurring environment from which the rooms are formed.

50/50 mixture of MgO and salt. The material interstitial to the waste forms is called the *interstitial reflector material* because it is external to the waste forms and uniformly mixed, yet it is separate from the outer salt material, which is the natural part of the WIPP repository.

Waste forms (as spheres in this example) showing outer pipe as solid color. The outer pipe may be a thin (0.001 cm) or thick (0.7112 cm) stainless steel pipe or a poly material layer.

The outer pipe is called the *discrete reflector*, here shown as transparent, because it is external to the waste form and surrounds it, forming a reflector which is directly adjacent to the waste form and separate from the material which is interstitial to the waste forms.

Waste form inside the discrete reflector (dark solid color). The waste form is a uniformly mixed material that always consists of PuO_2 and moderator (water or poly) and that sometimes consists of a filler material (graphite or generic with and without stainless steel from the convenience can) and/or Be.

Figure 4.14. Diagram showing how a uniform array model is constructed with spheres.

4.4 GENERAL INPUT DATA TABLES AND MATERIAL COMPOSITIONS

Additional data used in the analysis are presented in Table 4.6 and Table 4.7.

Table 4.6. CCO and CCC data used with permission [3]

	Inches	Centimeters	Notes
CCO dimensions			
Outer diameter	22.618	57.45	Inner diameter plus wall thickness from CQ5508A5[a] (0.15cm/0.0590in [16 gauge])
Outer radius	11.309	28.725	
Inner diameter	22.50	57.15	From CCO-DWG-0001R3
Inner radius	11.25	28.575	
Wall/top/bottom thickness	.059	0.15	From CQ5508A5, 16 gauge (drawing gives range of 0.0543 - 0.0590 in)
Outside height (including bolt ring)	34.75[b]	88.265	Outside height of drum from CQ5508A5[a] (34.25 in) + 0.5 in (conservative underestimate of height added from bolt ring)
Outside height (drum only, not including additional height from bolt ring)	34.25	86.995	From CQ5508A5, includes additional height from curvature of top and bottom of drum (underestimate of 0.691 in for each) and top and bottom thickness
Inner height (at outermost edge)	32.75	83.185	From CCO-DWG-0001R3 (does not include drum top and bottom thickness)
Material			Carbon Steel
CCC dimensions			
Outer diameter	6.625	16.8275	From CCO-DWG-0001R3, nominal pipe size (NPS) 6, SCH 40
Outer radius	3.3125	8.4138	
Wall thickness	0.28	0.7112	
Inner diameter	6.065	15.4051	Outer dimension minus wall thickness
Inner radius	3.0325	7.7026	
Flange thickness	1.0	2.54	From CCO-DWG-0001R3, CLASS 150, NPS 6, top and bottom (diameter/radius may be modeled same as CCC pipe outer dimension)
Flange diameter	11.02	27.9908	
Flange radius	5.51	13.9954	
Ring gasket	1/16	0.1588	From CCO-DWG-0001R3, NPS 6, 1/16 THK
Cavity height	26.9425	68.4340	From CCO-DWG-0001R3 (26.50 + 0.38 + (1/16)), includes additional space from gasket
Material			From CCO-DWG-0001R3, stainless steel 304, use code standard composition
Dunnage			
Thickness	3/4	1.905	From CCO-DWG-0001R3, all plates (total of 10 plates – 2 end and 3 ring plates on bottom and 2 end and 3 ring plates on top
Outer diameter	22.0	55.88	
Outer radius	11.0	27.94	
Ring plate inner diameter	11.5	29.21	From CCO-DWG-0001R3
Ring plate inner radius	5.75	14.605	
Material			Plywood with density of 0.387 g/cm^3 (SCALE redwood standard composition)

[a] = CQ5508A5 is the drawing for the 55-gallon drum, as referenced in CCO-DWG-0001R3.
[b] = The total drum height given above (34.75 in) includes the spacing created by the curvature of the top and bottom of the drum and the spacing created by the bolt ring.

Table 4.7. Material densities (g/cm^3)

Parameter	Value (g/ cm^3)	Source
PuO_2	11.46[8]	Compendium of Material Composition Data for Radiation Transport Modeling [16]
Polyethylene (CH_2)	0.92	Saylor and Scaglione [3]
H_2O	0.9982	Compendium of Material Composition Data for Radiation Transport Modeling [16]
Be	1.848	Saylor and Scaglione [3]
MgO	1.45	Saylor and Scaglione [3]
Salt (NaCl)	2.165	Saylor and Scaglione [3]
graphite	2.3	Compendium of Material Composition Data for Radiation Transport Modeling [16]
generic	2.84375	Saylor and Scaglione [3]
50% mixture MgO/salt	1.737	calculated
brine	1.1602	calculated

[8] This value is slightly higher than the actual theoretical density.

This page is intentionally blank

5. ASSUMPTIONS

1. The WIPP repository accepts waste packages of varying designs and payloads [5], whereas this analysis is specific to CCOs. No analytical attempt is made to ascertain the reactivity impact of a room of CCOs mixed with other containers. Rather, the assumption being made is that the CCO with 380 FGE that was evaluated under very conservative assumptions is the bounding configuration of packages to date, so any other packages would have less reactivity from a FGE perspective. The geomechanical impacts are less well known. However, various justifications have been made when using the Reedlunn and Bean data [8].

2. The waste streams are assumed to be uniformly mixed. A significant precedence exists for assuming that uniform mixtures are appropriate to use when significant variations in particle sizes or lumping of constituents may be possible or expected. The ability of neutrons to travel and interact between heterogenous regions of fissile material is typically negated by the heterogeneity. Significant justification exists in the literature, and some analytical justification is also provided.

This page is intentionally blank

6. ANALYSIS DISCUSSION

The analysis presented herein is a parametric evaluation of the most important system parameters and provides results covering a large range of H/^{239}Pu variations. A large range of variations is included to inform an FEP evaluation regarding the conditions under which criticality may be possible, but it does not define the probability of such an occurrence. The very conservative nature of the analysis method does allow an FEP evaluation some latitude in that regard. Many of the analyzed configurations greatly exceed conditions and established controls defined for dilute and dispose waste stream in an attempt to establish a generic approach that may be used for packaging other waste streams using the CCO container.

The generic parametric evaluation that is presented in this report provides results for the broad range of system parameters. Not all of these parameters are expected to be part of any actual waste stream, nor are all configurations physically possible, but these results provide useful information to better understand repository behavior and to help define the unique neutron physics at work in the repository environment.

The generic parametric evaluation presented in this report is based on the previous post-closure criticality methods described by Saylor, Scaglione [3], and Brickner 2019 [4]. Saylor's work forms the basis for the generic waste form filler material (but without the 50 g B_4C included by Saylor), evaluated as an appropriate representation of the dilute surplus Pu waste from. The methodology in Brickner's document [4] forms the basis for modeling the waste from spacing and centroid locations according to geomechanical analysis from Reedlunn and Bean [7]. Brickner's work [4] also forms the basis for the interstitial reflector material considerations. Additional methods are introduced in this analysis, but they are extensions of the previous work.

Each model used in this analysis considers the waste forms based on a physically realistic representation of the masses of materials evaluated. Specifically, each variation of the waste form considers the theoretical density of the pure material and the mass for each case to determine the constituent's volume. An alternative approach would be to consider the initial volume of the waste form container and then to distribute the constituents over that volume. Because the main interest in this work is to evaluate the effect of compaction, it is desirable to eliminate spacing where possible. Therefore, removing the overall initial dimensions from consideration allows the analysis to proceed conservatively in that regard. Therefore, for each parametric sweep, the uniform waste form volume is calculated as the sum of individual components using the maximum or theoretical density for each constituent from Table 4.2. In this manner, the one constant in all cases is the FGE mass of ^{239}Pu per CCO so changes in the k_{eff} associated waste form composition can be evaluated for the many system parameters considered.

There are two waste form geometries evaluated: spherical and cylindrical. For the spherical geometry, as the parametric sweeps over waste form constituent masses are performed, the total volume defines the sphere radius. For the cylindrical cases, three radii are arbitrarily selected for evaluation—4.8, 6.25, and 7.7 cm—with 7.7 as the maximum because it defines the inner diameter of the CCC, and the total volume defines the cylinder height.

In general, the waste form's cylinder radius has a strong effect on k_{eff}, as shown in Section 6.1 (correlation study). The cylinder radius is related to how the other system parameters affect k_{eff}, especially at the extreme ends of the sweeps, and more particularly in moderation sweeps. Therefore, the parametric sweeps cover these various generic radii to (1) evaluate possible options for waste form processing, and (2) to determine the various system k_{eff} effects. For example, the dilute surplus Pu waste stream is known to use a can-bag-can configuration for which the inner diameter of the inner can or the outer diameter of either can could be used to define the radius of the waste form. The results for the desired radius case could be used to evaluate this waste stream geometry. Furthermore, the results from the equivalent volume sphere waste form models could also be used to evaluate this waste stream. Both geometries may

be used, for example, if the cylindrical geometry is used for early timeframes and the spherical geometry is used for later timeframes. Additional value is gained in allowing future modifications to be made to waste form geometries, as informed by the results of the additional radii sweeps. Generically, enough information is intended to be provided so that it is generically applicable to a wide range of waste streams.

For both waste form geometries, a discrete reflector is included so that the reactivity effect of material that is directly adjacent to the waste form can be evaluated. At emplacement, the CCC pipe wall is the discrete reflector and is modeled as stainless steel. Later, this may degrade or otherwise change, and other materials may collect around the waste forms. Therefore, polyethylene is also considered as a discrete reflector material. The stainless steel from the pipe or the cans represents a material known to be present at least initially and which should have some impact on the reflection of neutrons for low moderator cases. The polyethylene represents a thermalizing reflector which should have an impact along the entire neutron energy spectrum. These two materials are sufficient to cover the known and predominate quantities of materials in the system (see Section 4.2.2.3). No attempt is made to evaluate how much discrete reflector material from sources external to the CCO, from the CCO itself, or from CCO components may be present. This is intentional because such an evaluation could result in an unnecessary restriction or limit, and neither is necessary since this approach covers multiple scenarios over the long regulatory time frame. Therefore, the thickness of the CCC is used to evaluate the k_{eff} effect of a thick discrete reflector that may be directly adjacent to the waste form, and 0.001 cm is arbitrarily selected to evaluate the k_{eff} effect of a thin discrete reflector that may be directly adjacent to the waste form.

In this manner, the CCC thickness is essentially a surrogate for material forming a discrete reflector. Also, this allows waste stream analysis to consider all material present in the repository system during compaction as also being present in the actual waste form *and* its container(s) to be part of the uniformly mixed constituents for volumes up to the inner diameter of the CCC. For example, for the Savanah River Site (SRS) waste form, the can may or may not be included in the waste form. The thickness of the can is unknown, but it is expected to be adequately represented by either the thick or thin stainless steel discrete reflector. On the other hand, to cover the possibility of the can or stainless steel from another external source mixing with the waste form, sweeps with stainless steel as filler material are also considered (see Section 4.2.3). In that case, the waste form evaluation may use the full thickness of the CCC as a discrete reflector to evaluate the outside sources of discrete reflector materials, or the evaluation may use the known thickness of packaging inside the CCC such as the convenience can, or a combination of the two. Using the discrete reflector in this way allows for flexibility in how a waste form may be evaluated with respect to treating container material as either uniformly mixed with the waste form, or discreetly, or both, if the difference depends on how the configuration changes over time. It also allows for flexibility in future changes to waste form processing and packaging.

The analysis includes flexibility based on to the wide range of material sweeps for each configuration. For example, for the surplus Pu configuration, there are waste form sweeps with only filler material (generic or graphite) mixed uniformly with the waste form (no stainless steel from the convenience can), cases with only material from the convenience can mixed uniformly with the waste form (no filler), and cases with both mixed uniformly with the waste form. Therefore, if it is desirable to consider the waste form as a cylinder within a can, then those results are available with no can material uniformly mixed with the waste form. On the other hand, if it is desirable to consider the waste form with a radius equal to the outer diameter of either the inner can or the outer can, then there are cases with a range of steel masses mixed uniformly with the waste form and with discrete reflectors to account for the CCC or material from other outside sources.

The discrete reflector is evaluated at a very small thickness (0.001 cm) and at the CCC pipe thickness (0.7112 cm) for both steel and polyethylene. The use of a very small reflector allows the trend in k_{eff} due

to discrete reflector thickness to be analyzed, and it also provides results from the very thin discrete reflector in case these results are more conservative than those of the thick discrete reflector. The use of polyethylene allows for the consideration of external plastic sources which may be present and come to be compacted around the waste forms or for plastics known to reside adjacent to the waste form due to packaging. Because it is very unlikely that a large quantity of plastic from outside sources would collect around every waste form in the system, these results are extremely conservative and provide an upper bound of the possible scenarios.

For the waste form filler materials—i.e., nonfissile, non-hydrogenous, non-special reflector as defined in the CCO *TRUPACT-II Safety Analysis Report [9]*, and non-H bearing materials —two materials are selected to be bounding materials (see Section 4.2.3).

The SCALE models used in this generic evaluation are based on the WIPP repository room layout. Uniform and nonuniform arrays are the two model types used to evaluate a WIPP room full of CCOs. The uniform arrays mimic the as-loaded configuration at time zero with a triangular pitch, as seen in Figure 6.1. Although the WIPP panel rooms are actually currently loaded with 7-packs that have a hexagonal spacing in a three-high uniform array of waste forms, a three-high triangular pitch is used in the SCALE model as a conservatism from Saylor and Scaglione [3] and is consistent with Brickner [4]. The magnitude of the triangular pitch is based on the overall room closure from Reedlunn and Bean [8] (see Sections 4.2.1).

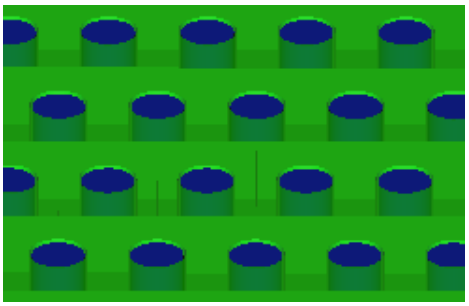

Figure 6.1. Diagram of the triangular pitch for the three-high uniform arrays.

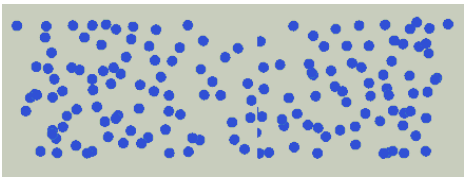

Figure 6.2. Diagram of the nonuniform arrays.

The nonuniform arrays are based on the actual centroid locations for both the lower and upper horizon calculations from Reedlunn and Bean [8], as shown in Figure 6.2.

One additional variation of the uniform array model is used to evaluate the k_{eff} effect of placing two waste forms per CCO [20]; this model is similar to the three-high uniform array, except it is a six-high configuration in which each waste form has half the allowable 380 FGE separated physically only by the discrete reflector thickness, as shown in Figure 6.3.

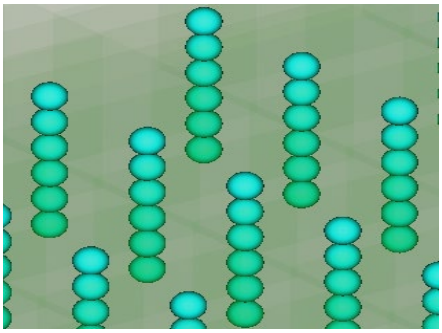

Figure 6.3. Diagram of the triangular pitch for the six-high uniform arrays two represent two waste forms per CCO.

For all uniform and nonuniform array models, both waste form geometries are evaluated for all parametric sweeps listed in Table 6.2. Where necessary, additional sweeps are added so that the neutron physics of the system can be evaluated.

As specified by Brickner [4], all evaluations use the bounding uniform mixture of 50% MgO and 50% salt for the interstitial reflector material. An interstitial reflector material of 50% salt and 50% MgO bounds pure salt, as previously shown by Brickner [4]. It is likely that as the Supersacks of MgO break during roof fall or otherwise decompose, the granules of MgO will fall down between the as-yet uncompacted CCOs and will form piles on the room floor. When the final compaction condition is

reached, it is most likely that the MgO granules will be underneath most waste forms. The final compaction configuration is a relatively high neutron leakage configuration, so the majority of the neutrons escaping the waste forms will not likely contact MgO. Therefore, considering the MgO uniformly mixed with salt in the interstitial reflector ensures that any neutron escaping the waste form will encounter MgO and will be less likely to be captured than if it had seen salt. This approach is conservative and bounding, indicating that it is appropriate to avoid unnecessary restrictions or constraints of limits due to use of MgO.

The principal criticality calculations of this study are categorized into the cases shown in Table 6.1 and the subcases shown in Table 6.2. Cases are defined based on array shape. Subcases are defined as parameter sweeps.

Table 6.1. Description of the cases to evaluate reactivity trends

Case	Description	Location of results
set-1	Uniform array with three-high spheres and cylinders, with the most conservative spacing based on the SNL compaction data. Waste forms are stacked directly on top of each other.	Appendix A Addendum 1
set-1a	Uniform array with three-high spheres and cylinders, with an alternative spacing based on the SNL compaction data. Waste forms are stacked directly on top of each other.	Appendix B Addendum 1
set-2	Nonuniform array with spacing based on SNL compaction data. Two sets are included: one set for the upper horizon (uh), and one set for the lower horizon (lh).	Appendix C Addendum 1 Appendix D Addendum 1
set-3	Uniform array with six-high spheres and cylinders, with the most conservative spacing based on the SNL compaction data. FGE limited to 180 per waste form. Waste forms are stacked directly on top of each other.	Appendix F Addendum 1
set-3a	Uniform array with six-high spheres and cylinders, with an alternative spacing based on the SNL compaction data. FGE limited to 180 per waste form. Waste forms are stacked directly on top of each other.	Appendix I Addendum 1

For each of the cases listed in Table 6.1 above, the full set of parametric sweeps is provided in Table 6.2 below.

Table 6.2. Summary of parametric sweeps for both cylindrical and spherical waste forms (values per CCO)

Subcase	Waste form geometry	FGE	Waste form moderator	Waste form filler material	Discrete reflector material	Waste form Be mass (g)	Interstitial reflector material	B_4C (g)
1	cylinder	380	water	graphite	SS (from the can)	0, 585	50/50 salt/MgO	0
2	cylinder	380	polyethylene	graphite	SS (from the can)	0, 585	50/50 salt/MgO	0
3	cylinder	380	water	graphite	polyethylene	0, 585	50/50 salt/MgO	0
4	cylinder	380	polyethylene	graphite	polyethylene	0, 585	50/50 salt/MgO	0
5	cylinder	380	water	generic	SS (from the can)	0, 585	50/50 salt/MgO	0
6	cylinder	380	polyethylene	generic	SS (from the can)	0, 585	50/50 salt/MgO	0
7	cylinder	380	water	generic	polyethylene	0, 585	50/50 salt/MgO	0
8	cylinder	380	polyethylene	generic	polyethylene	0, 585	50/50 salt/MgO	0
9	sphere	380	water	graphite	SS (from the can)	0, 585	50/50 salt/MgO	0
10	sphere	380	polyethylene	graphite	SS (from the can)	0, 585	50/50 salt/MgO	0
11	sphere	380	water	graphite	polyethylene	0, 585	50/50 salt/MgO	0
12	sphere	380	polyethylene	graphite	polyethylene	0, 585	50/50 salt/MgO	0
13	sphere	380	water	generic	SS (from the can)	0, 585	50/50 salt/MgO	0
14	sphere	380	polyethylene	generic	SS (from the can)	0, 585	50/50 salt/MgO	0
15	sphere	380	water	generic	polyethylene	0, 585	50/50 salt/MgO	0
16	sphere	380	polyethylene	generic	polyethylene	0, 585	50/50 salt/MgO	0
17	cylinder	380	polyethylene	graphite	polyethylene	0, 585	50/50 salt/MgO	50
18	sphere	380	polyethylene	graphite	polyethylene	0, 585	50/50 salt/MgO	50

6.1 DISCUSSION OF THE THREE-HIGH UNIFORM ARRAY PARAMETRIC SWEEPS

The three-high uniform array results for set-1 are provided in Appendix A, and the results for set-1a are provided in Appendix B. The results presented in Appendix A and Appendix B provide H/^{239}Pu curves which show the k_{eff} trend, with the following parameters associated with the waste form using 380 FGE as ^{239}Pu mass:

- waste form triangular pitch (the reactivity difference between set-1 and set-1a)
- waste form moderator material and mass
- waste form filler material and mass
- waste form Be mass
- discrete reflector material and thickness

The system's k_{eff} trends are divided into two categories: primary and secondary. Primary categories are k_{eff} trends which may have a direct, significant impact on a FEP. Secondary k_{eff} trends are important, but they may not have a significant impact on a FEP. Each trend is reviewed in third-tier headings of this subsection.

The full set of parametric sweeps provide information about the k_{eff} trends associated with the system, and the full set of results are found in Appendix A and Appendix B.

All of the results for set-1 and set-1a are plotted below in Figure 6.4 and Figure 6.5, respectively. For each set, representative curves for the cylinder and spheres are accentuated for both discrete reflector thicknesses. The representative curves are provided to show which curves could be selected for limits if appropriate. These curves typically bound their sub-set of results at the moderator mass, resulting in a k_{eff} of 1.

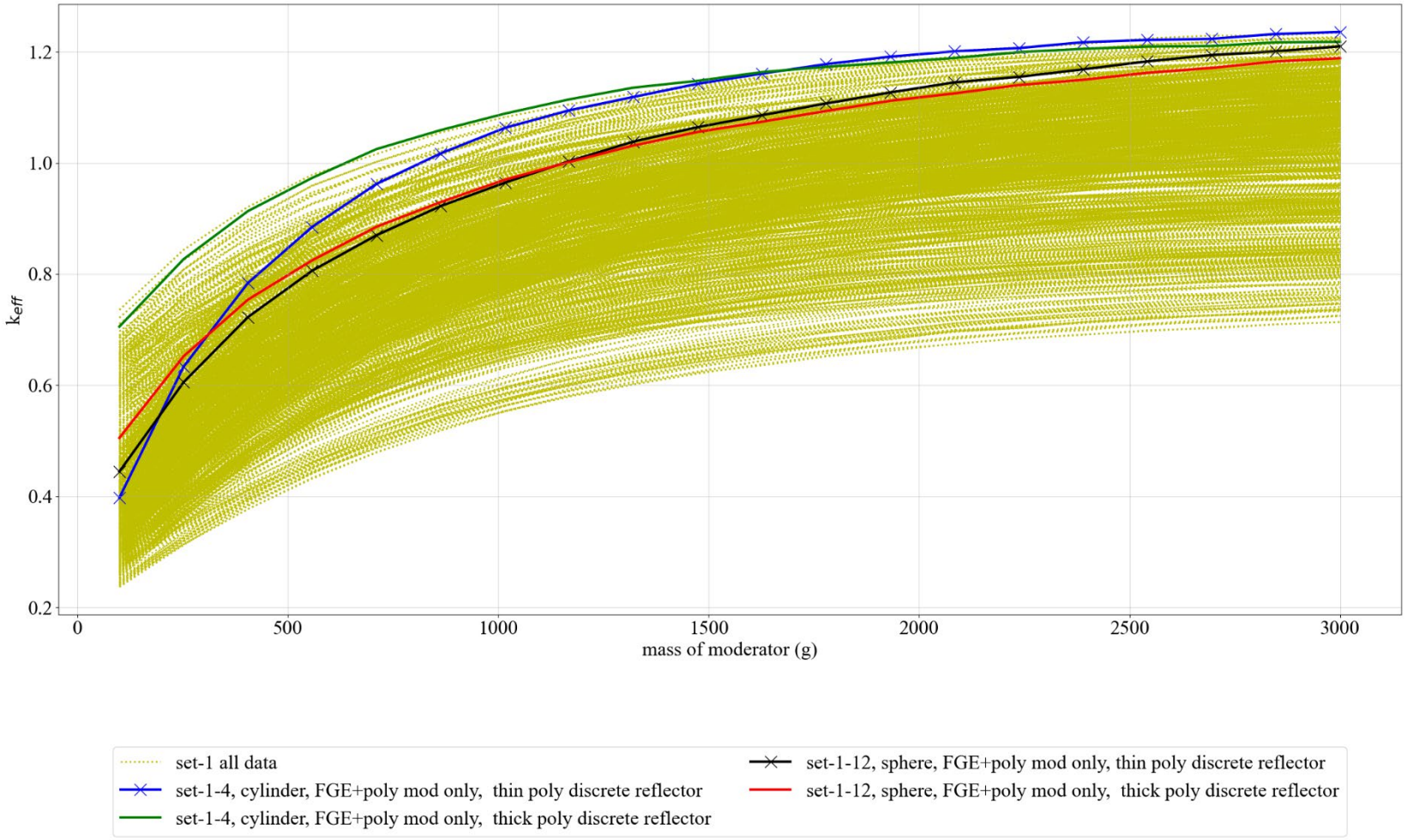

Figure 6.4. Full set of results for set-1 compared to various representative curves.

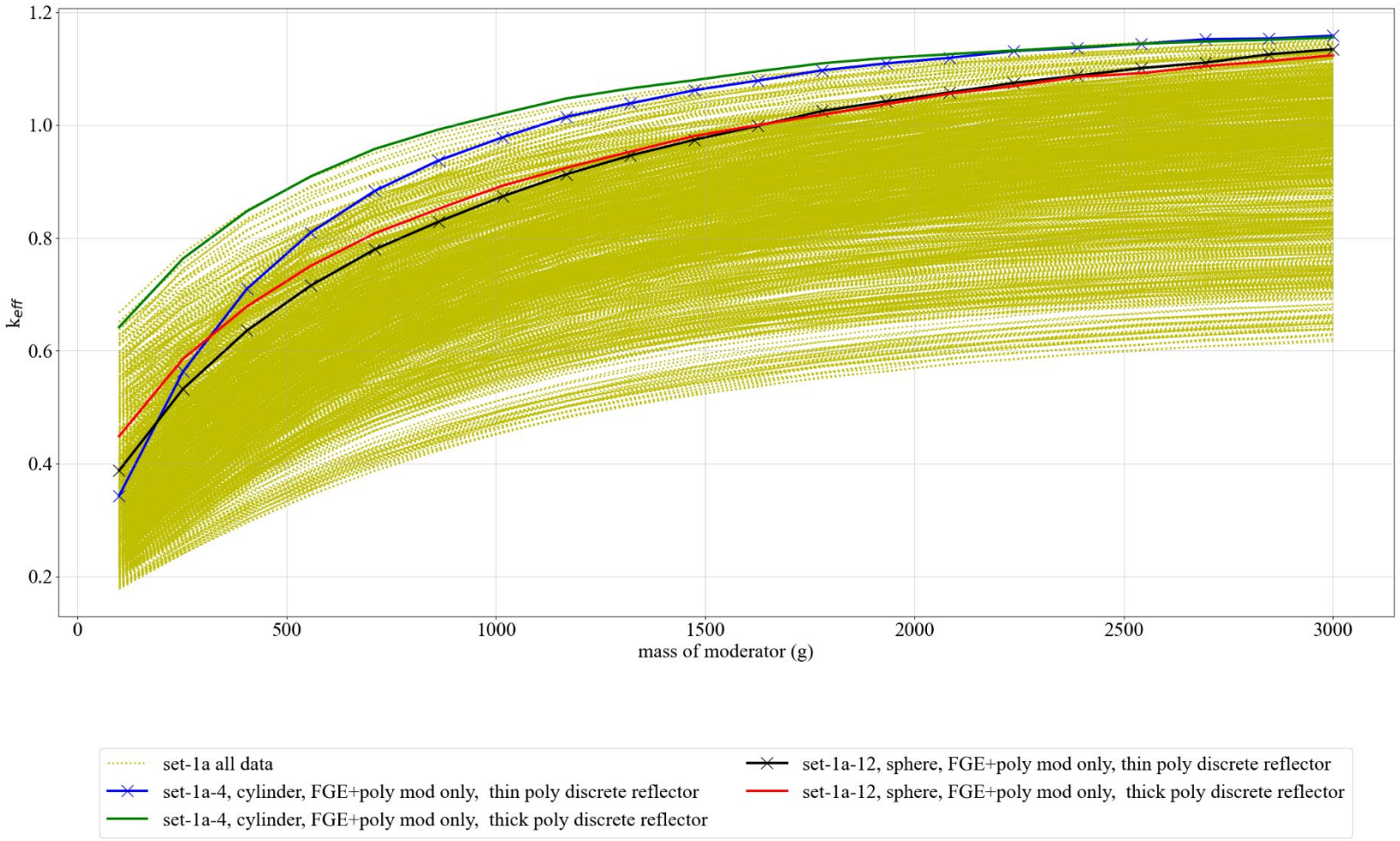

Figure 6.5. Full set of results for set-1a compared to various representative curves.

The primary k_{eff} trends of the system are highly dependent upon the spacing, moderator mass, geometry, and filler mass. These are discussed in more detail below.

6.1.1 Waste Form Spacing (Primary Trend)

The predominate reactivity effect of this system is driven by the spacing between the arrays of waste forms, and this effect is the primary motivation for the work described in this report. The previous analysis from Saylor and Scaglione [3] did not consider any spacing in triangular pitched uniform arrays, and the result was a requirement for 50 g B_4C per CCO. In this work, the spacing between the CCOs is evaluated based on the SNL compaction results from Reedlunn and Bean [8]. While the SNL compaction results yield a physically realistic nonuniform distribution of spacing between CCOs, the data can also be used to determine spacing for use in triangular pitched uniform arrays. The purpose for using uniform arrays is based on several objectives. First, is the objective to cover the entire regulatory timeframe, from emplacement to 10,000 years. At time zero, the CCOs are emplaced in a uniform array, and after 10,000 years, the final configuration of the CCOs is very nonuniform. Second, it is beneficial to use a uniform array to enable comparisons to previous work from Saylor, Scaglione [3], and Brickner [4] in which uniform arrays were also used. This will allow for comparison among all of the results. Third, the neutron physics of the system is highly dependent upon neutron leakage, and in the uniform array, the reactivity trends are therefore magnified by the uniform arrays (more sensitive). Furthermore, the lower leakage of the uniform arrays is expected to bound the nonuniform arrays in the moderator range of interest. Therefore, while the uniform arrays are not physically realistic at 10,000 years, they may be appropriate to use as bounding results over the nonuniform arrays so that unwarranted importance is not placed on the high uncertainty associated with the SNL compaction data.

Every case in set-1a has a corresponding case in set-1. The reactivity effect of the difference in spacing is shown by comparing the results of set-1 to set-1a as a delta-k in Figure 6.6 for every curve in the sets. The reactivity effect of the closer spacing for set-1 is in the range of 10–15% delta-k for the representative curves, and it is consistent across the range of moderator mass sweeps, showing that there is a large conservatism in using the set-1 dataset. Furthermore, the comparison which shows the delta-k between the representative curves illustrates how the spacing impacts the representative curves.

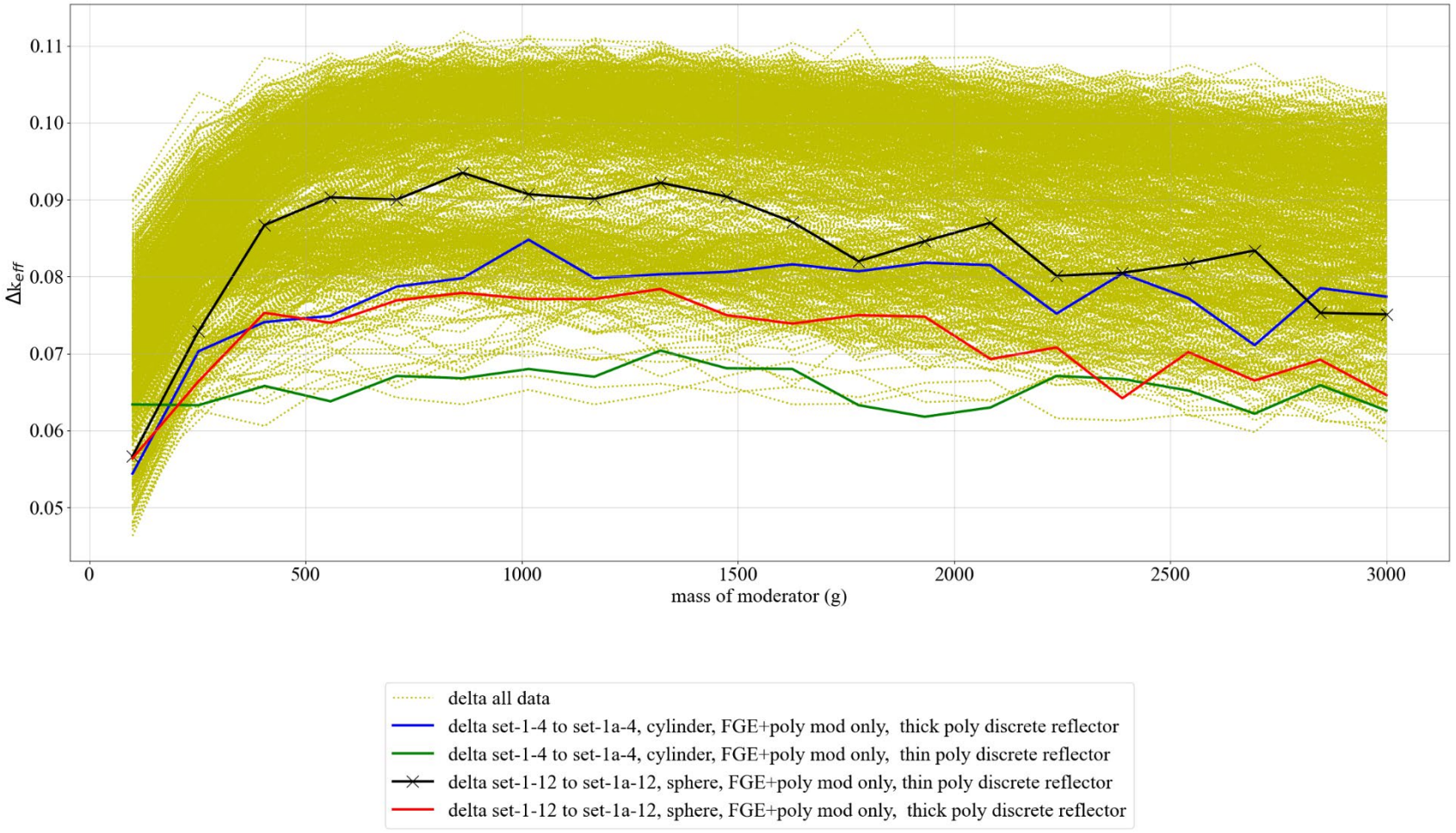

Figure 6.6. Comparison of the representative curves between set-1 and set-1a (set-1-set-1a).

6.1.2 Waste Form Moderator Mass (Primary Trend)

The sweeps over the mass of moderator in the waste form provide a variety of results depending on the other system parameters being swept over. In general, increasing moderator mass increases k_{eff}, but the magnitude and behavior of the trend is dependent on the subcase, the study of which is the purpose to this analysis. For the moderator material itself, the polyethylene bounds the water. These trends are expected because the system is very under-moderated initially, and polyethylene is more H-dense than water. While it is not likely to be physically realistic to have pure polyethylene as the moderator, the curves which use pure polyethylene are expected to conservatively bound other materials since polyethylene is a powerful moderator. Figure 6.7 below shows how the reactivity compares between water and polyethylene for various cases.

The results of the specific cases, presented in detail in APPENDIX A, show how reactivity changes as a function of moderation is reached varies according to the other system parameters for the various sweeps. Fissile mass mixtures are highly dependent on internal moderation, and this effect is clear in the results presented in this parametric evaluation. While most waste form processes are expected to be relatively dry, the CCO *TRUPACT-II Safety Analysis Report* [9] did not initially limit the mass of H-bearing materials such water or polyethylene. If actual waste forms are known (due to processing) to have masses of H-bearing materials within some range, then that range could be used to select results to limit moderator in the waste form.

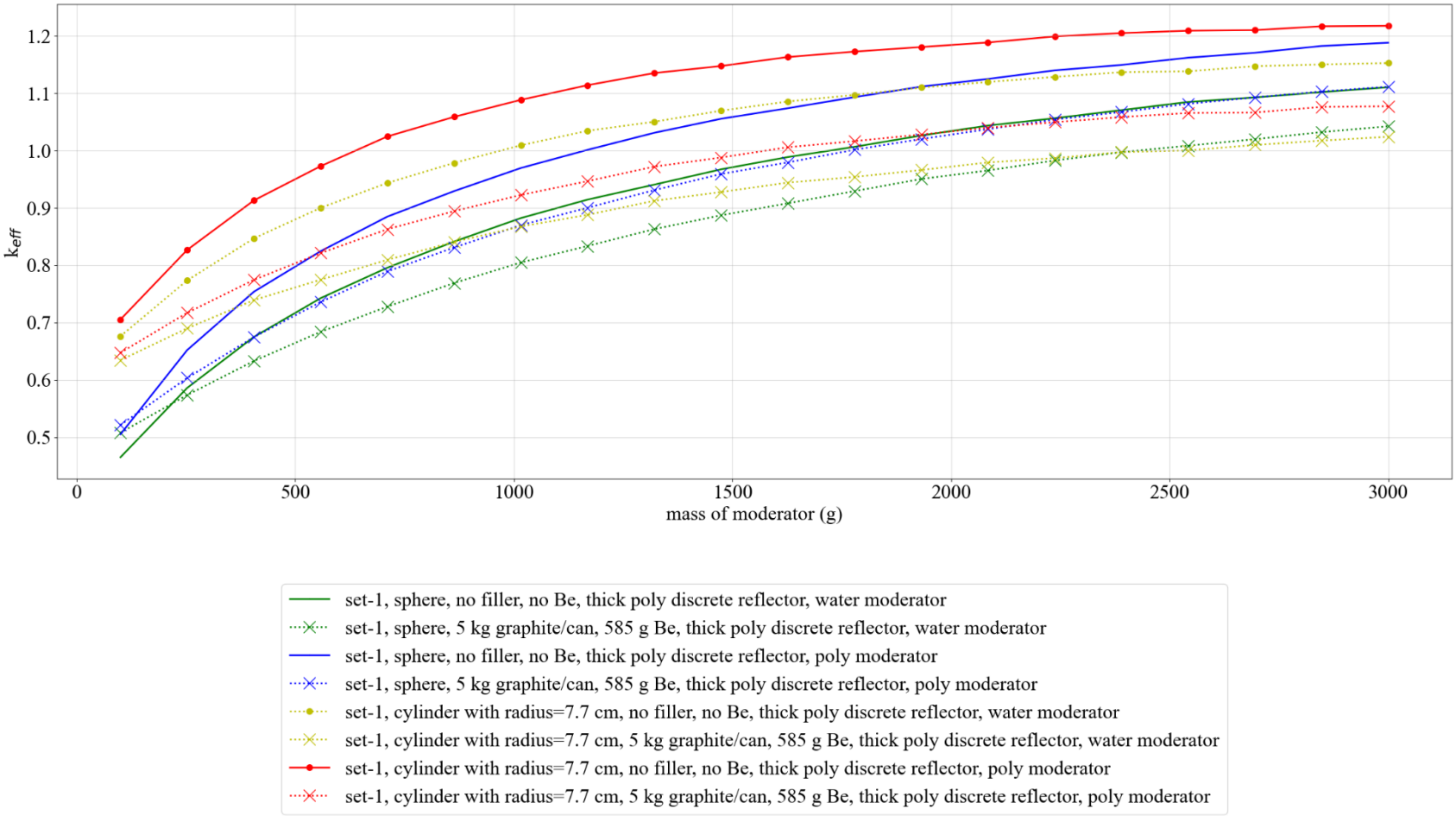

Figure 6.7. Comparison of various cases for both water and polyethylene waste form moderator mass.

6.1.3 Geometry and Filler Mass (Primary Trend)

The results summarized in Figure 6.7 demonstrate that it is necessary to restrict H-bearing materials (i.e., a moderator mass limit) because the waste form spacing and moderator mass have such a primary impact on system k_{eff}. While it is likely that such a moderator mass limit is realistic for many waste streams there may be some waste streams which will not meet that limit. Secondary to this type of requirement, it is also clear that most, if not all, actual waste forms also include filler material.

The sweeps over waste form geometry and filler mass trend typically indicate a trend of decreasing k_{eff} with expanding geometry for a fixed moderator content. This occurs as a consequence of the increasing filler mass. While the reactivity effect of geometry and filler mass is not as large as that caused by spacing or moderator mass, listing the impact as a primary effect is appropriate because it is a significant system component which is highly expected to be present in large mass quantities.

The reactivity effect of cylindrical shape is very dependent on size, whereas the spherical shape is less so. These trends are expected, especially for the cylindrical geometry (for cases with the same radius). For the cylinder shape, generally, decreasing radius and/or increasing height decreases k_{eff} for a fixed volume. For both shapes, increasing the mass of filler material decreases k_{eff} substantially, although it is much more pronounced for the cylindrical shape than the spherical shape.

The results shown in Figure 6.7 above provide some examples of the reactivity effect of geometry and filler material.

The secondary k_{eff} trends of the system are moderately dependent upon the discrete reflector material and thickness, the difference in generic filler material, and the graphite filler material and Be. These factors are discussed in more detail below.

6.1.4 Discrete Reflector Material and Thickness (Secondary Trend)

The trend associated with the discrete reflector material and thickness shows a strong dependence on the other waste form parameters. The dependence is very strong for the cylindrical waste form shape, whereas the dependence is greatly reduced for the spherical shape. The overall magnitude of the trends is small enough to be considered a secondary k_{eff} trend and to provide additional flexibility in determining how to consider packaging. Figure 6.8 below shows an example of the effect of discrete reflector material for thick discrete reflectors.

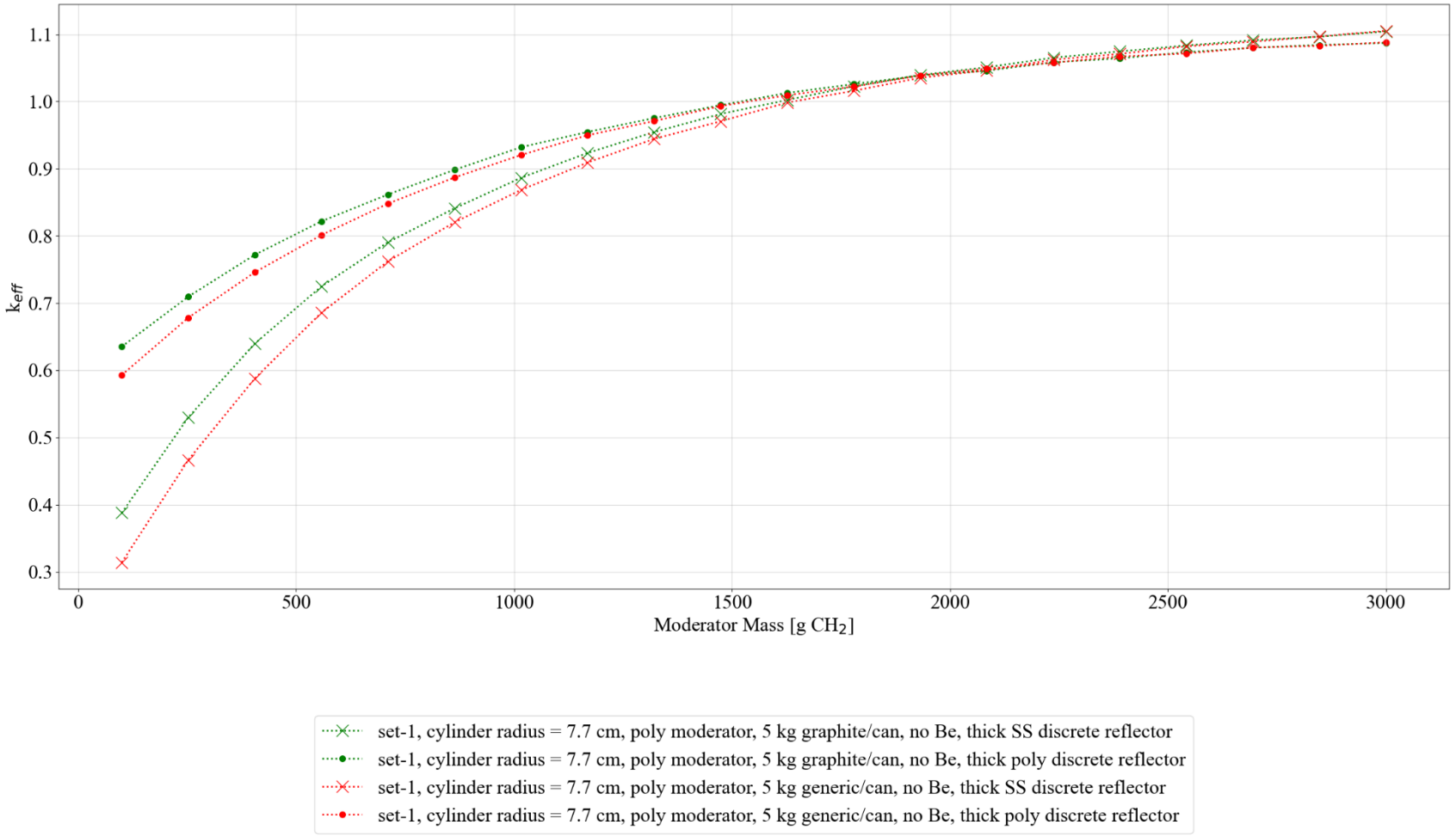

Figure 6.8. Comparison of the discrete reflector material and filler material on reactivity for cylindrical waste forms.

6.1.5 Difference in Generic Filler Material and the Graphite Filler Material (Secondary Trend)

The trend associated with the comparison between the generic filler material and the graphite filler material shows that the graphite filler material bounds the generic filler material for the most under-moderated cases. Both materials are essentially equivalent for well-moderated cases with generic filler perhaps bounding the graphite by a tiny amount. While the additional moderation effects from the carbon in the graphite material do increase k_{eff}, the overall effect of the change in volume of the waste form has a greater impact.

6.1.6 Beryllium in Waste Form (Secondary Trend)

The trend associated with the increasing the mass of Be is not significant and varies between the two waste form geometries. For the cylindrical waste form, the sensitivity of the reactivity of the system is high, depending on the overall mass of the system (nonfissile, non-H materials). The addition of Be to the system increases the reactivity of the system because it is a special moderator, but the magnitude of the increase is offset by the decrease in reactivity due to the additional mass (volume change). For the cylindrical waste forms, the decrease in reactivity is greater than the increase due to the special moderator. For the spherical geometry, the two competing factors are essentially offset.

6.2 DISCUSSION OF THE SIX-HIGH UNIFORM ARRAY PARAMETRIC SWEEPS

As discussed in Section 6.1, an alternative uniform array model is used to address the specific issues caused by having two waste forms per CCO. Additional sweeps are added to address the impact of separating the 50 g B_4C equally into those two waste forms per CCO. The set-3 cases evaluate this configuration by using a six-high uniform array with the same triangular pitch spacing as in the set-1 cases, as shown in Figure 6.9 below. The set-3 sweeps are the same as the set-1 sweeps. All set-3 cases have 380 total FGE per CCO and 190 FGE per waste form. For the B_4C cases, each waste form has 25 g B_4C and 50 g B_4C total for the CCO. The sweeps considered are summarized in APPENDIX F.

Figure 6.9 below shows the difference between the three-high and six-high models.

The full set of results for set-3 are found in APPENDIX F and are summarized in Figure 6.10 below. Additionally, a comparison of set-1 to set-3 by delta-k is presented in Figure 6.11 below.

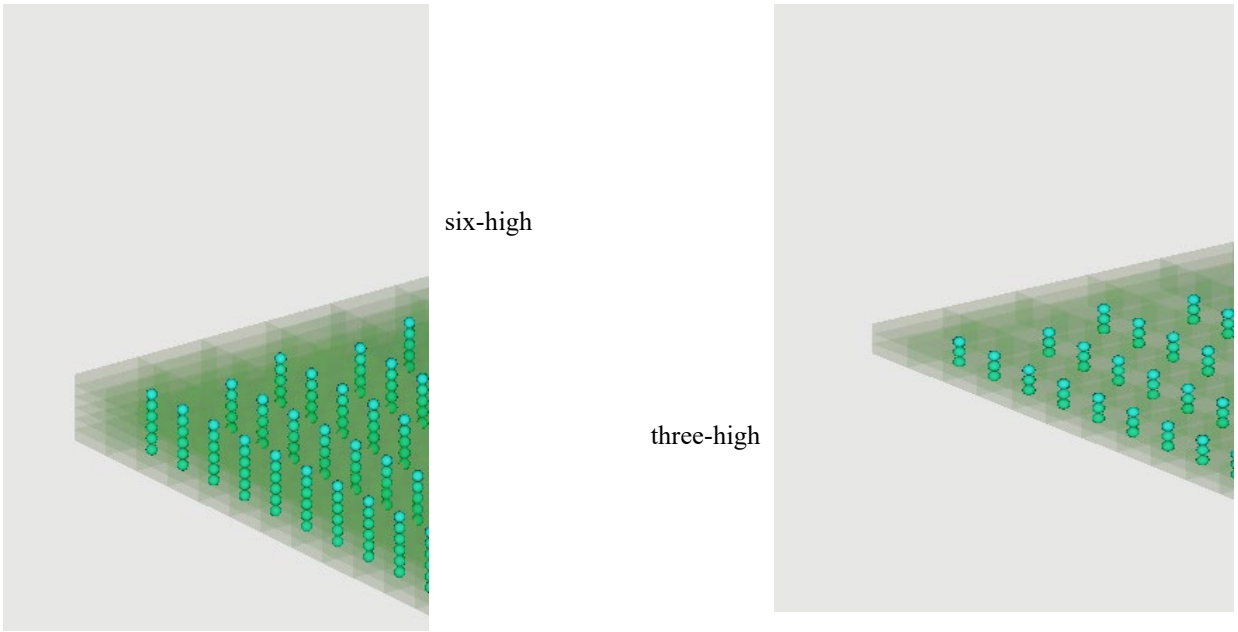

Figure 6.9. Comparison of the six-high and three-high arrays.

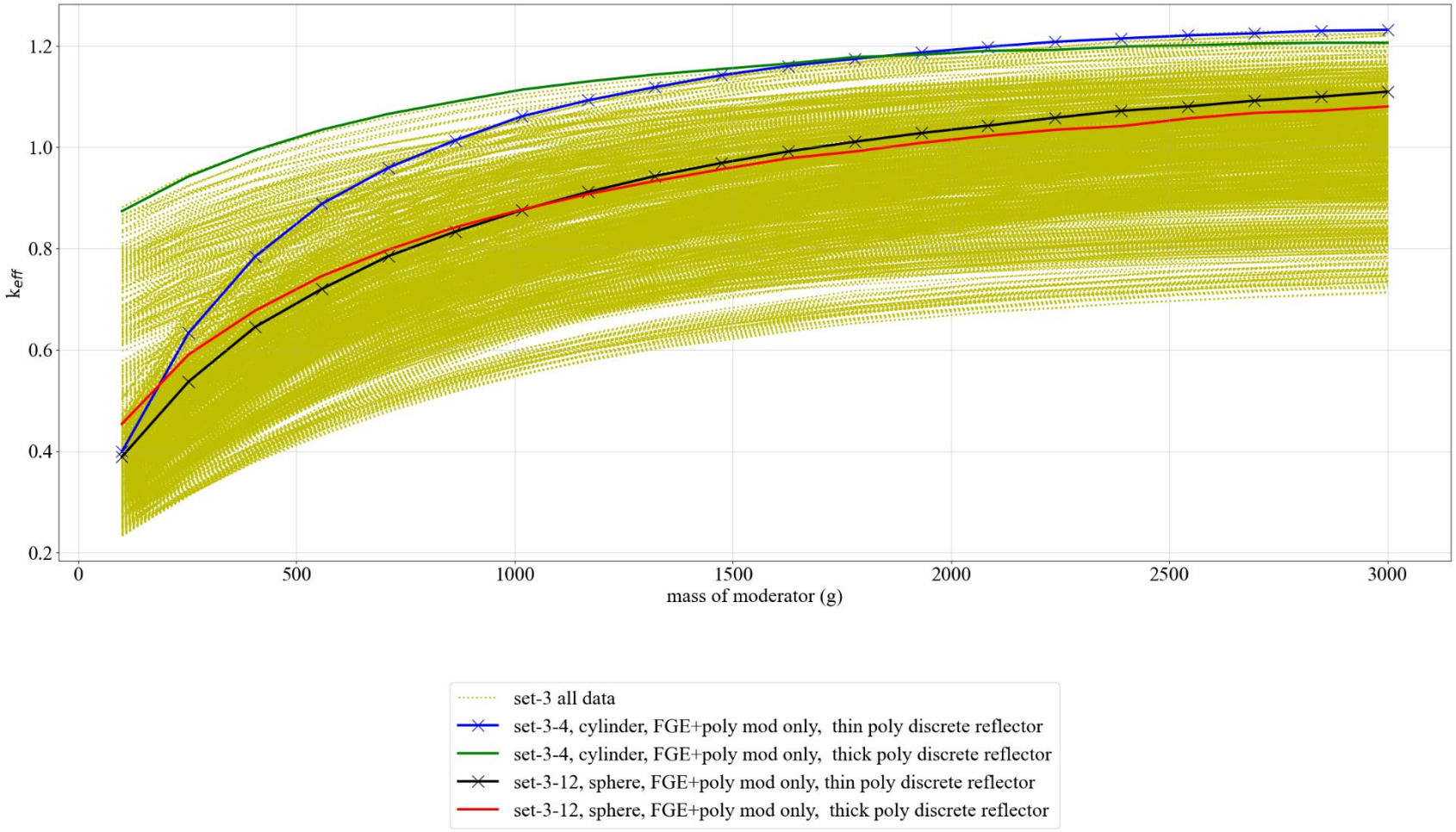

Figure 6.10. Full set of results for set-3 compared to various representative curves.

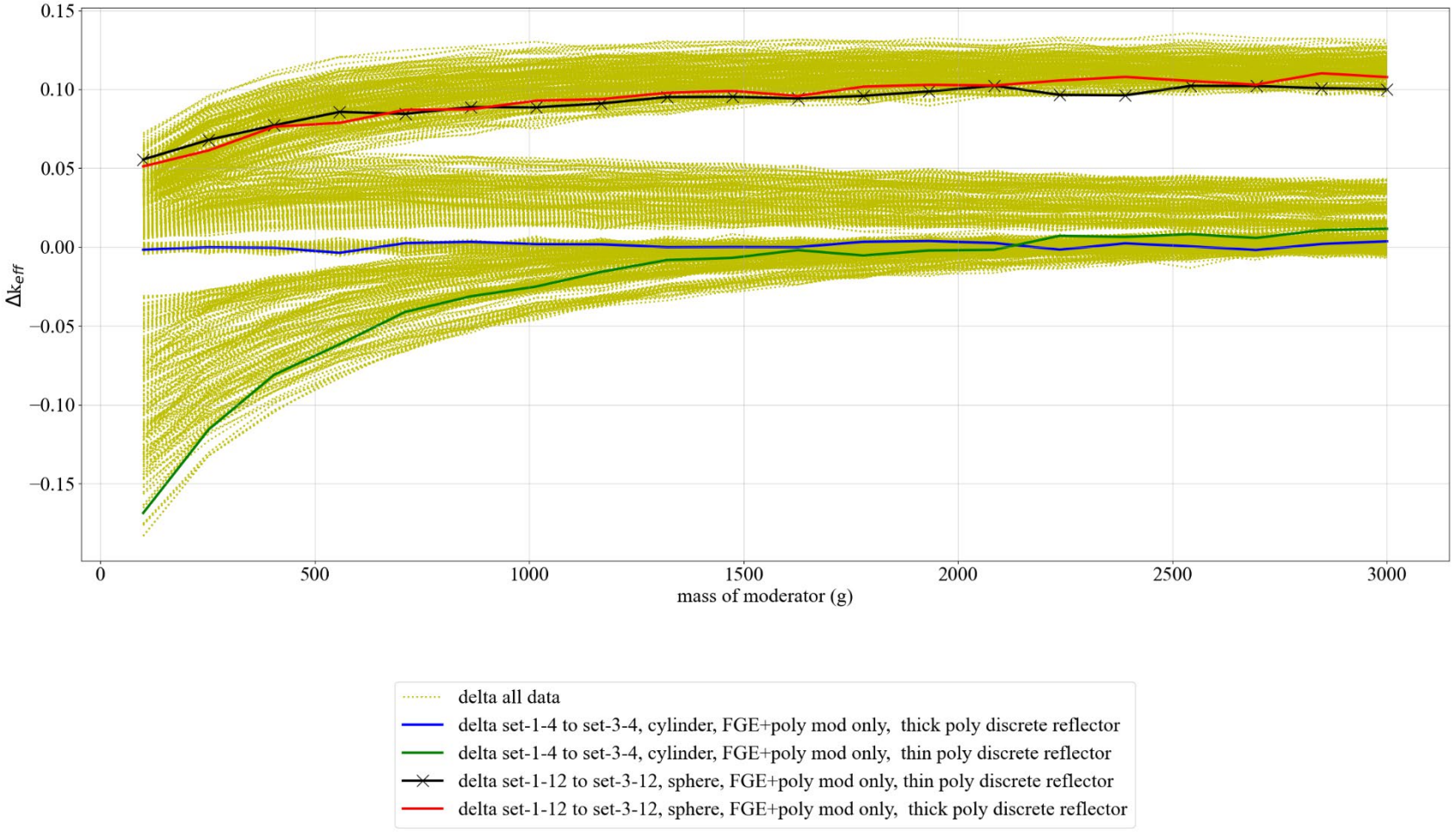

Figure 6.11. Full set of results for set-1 compared to set-3 with various representative curves (set-1 – set-3).

The results presented in Figure 6.10 and Figure 6.11 above and in APPENDIX F show that in general, all the reactivity trends evaluated in set-1 and set-1a remain consistent with those evaluated in set-3.

The set-3 results are also used to show that 25 g of B_4C per waste form (50 g B_4C per CCO) is adequate to reduce reactivity consistent with the Saylor and Scaglione [3] analysis. The issue addressed in the studies is that Saylor and Scaglione [3] used a single waste form per CCO. The use of two waste forms with a maximum 190 FGE per waste form had not been considered. This B_4C study was conducted using the same six-high uniform array model and SAMPLER sweeps as those used for set-3-4 and set-3-12 (see Table F.1 in APPENDIX F), albeit with 25 g of B_4C per waste form. These sweeps represent the most reactive sweeps in the range of interest for moderator mass. The results are summarized in Figure 6.12 below. The red bounding curve is for a radius of 7.7 cm, no filler, no Be, thick poly discrete reflector, and poly moderator has the largest value of k_{eff}. The purple curve is exactly the same, except with 25 g of B_4C added, and it can be seen that k_{eff} is reduced substantially. The results provide sufficient data to show that 25 g B_4C per waste form (50 g B_4C per CCO) is acceptable and meets the requirement of 50 g per CCO as stipulated by Saylor and Scaglione [3].

Additionally, as was done for set-1 and set-1a, set-3a results are for cases with the alternative spacing (see Table 6.1). The results for set-3a are provided in APPENDIX I.

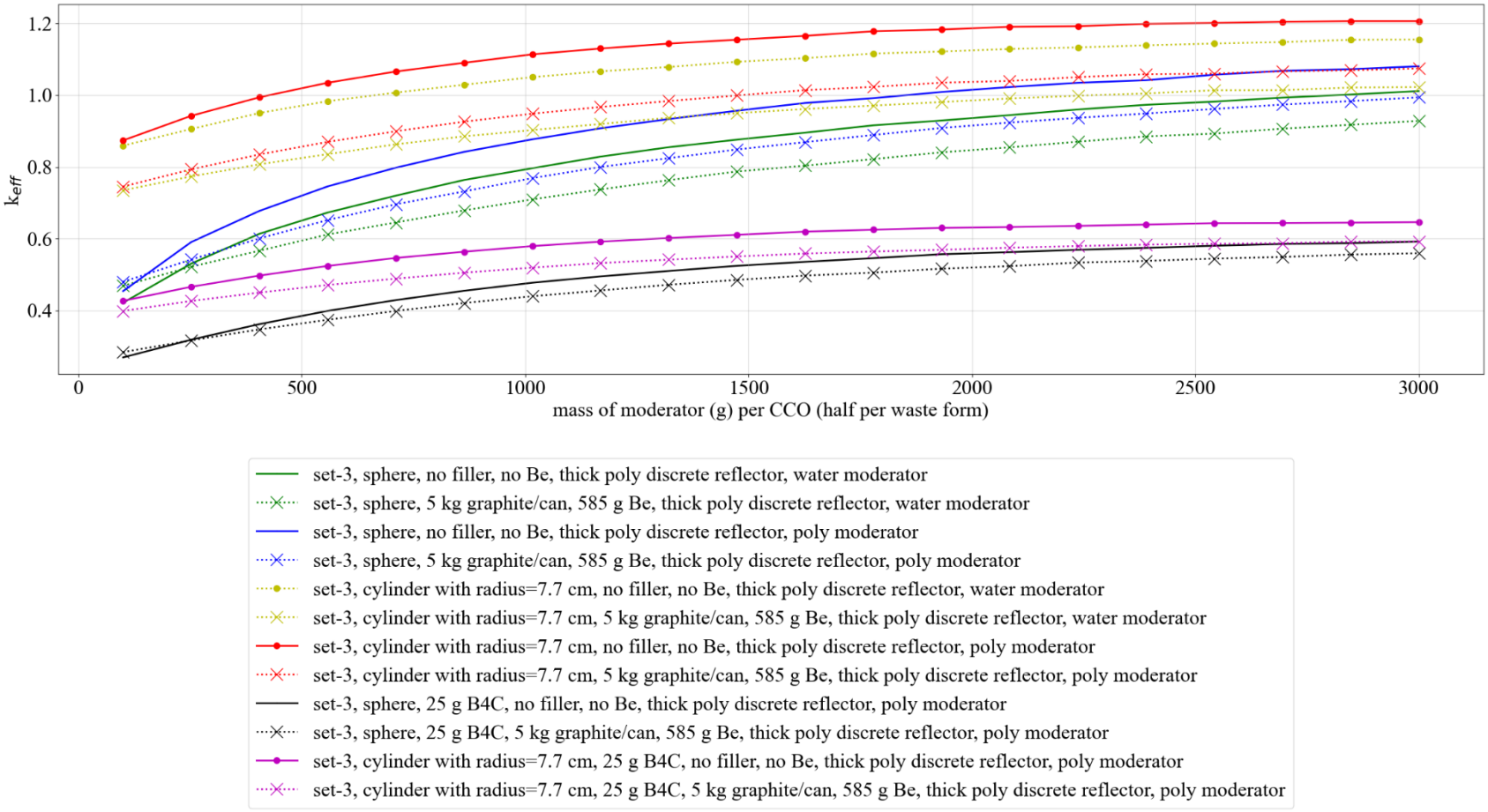

Figure 6.12. Reactivity effect of 25 g B_4C compared to representative curves.

6.3 DISCUSSION OF THE NONUNIFORM ARRAY PARAMETRIC SWEEPS

As discussed in Section 6.1 and Section 6.2, the Reedlunn and Bean [8] data may be used in various ways for uniform array models. The data which provide the room closure information used in those uniform array models are based on the calculated compaction results which yield orthogonal locations for the CCC (pipes). The data generated by the compaction calculations are a set of data in which each pipe in the compaction model yields nonuniform location datasets, as shown in Figure 6.13 below.

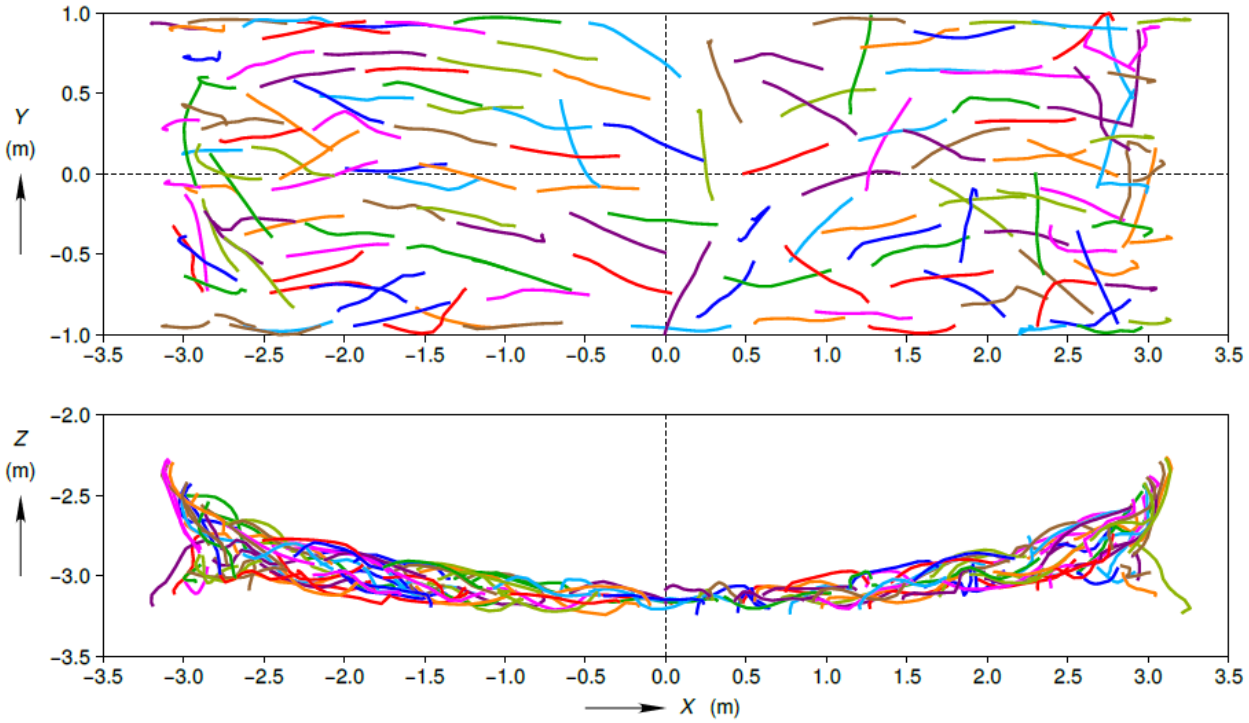

Figure 6.13. An example representation of the Reedlunn and Bean [8] data in the form of "spaghetti" plots, used with permission.

The utilization of the Reedlunn and Bean [8] data for the nonuniform cases (i.e., set-2-uh and set-2-lh) is consistent with the use of similar data in Brickner [4]: that is, that the location of the center of the compacted pipe is used to define a centroid location. The Reedlunn and Bean [8] data provide these results for both the upper and lower horizon, as discussed in Section 4.2.1. To show how the reactivity trends in the system behave for nonuniform arrays, the same sweeps that were used for the uniform arrays (see Section 6.1 and Section 6.2) are also evaluated. A complete description of the sweeps is provided in APPENDIX C (set-2-uh for upper horizon cases) and APPENDIX D (set-2-lh for lower horizon cases).

The nonuniform array model construction is the same as that used previously in Brickner [4]. The 153 data points provided by Reedlunn and Bean [8], shown in Table 4.4, are used to define the center of the vertically oriented cylinder base or the center of a sphere. The nonuniform array model is constructed in a manner similar to that used for the uniform array model in that the waste form geometry is defined by the amount of mass associated with each constituent. Consistent with the method used by Brickner [4], the centroid locations are set in the interstitial reflector material volume of the model (i.e., the "reflector box"). The reflector box is a rectangular volume for which the sides and top are fitted directly adjacent to the outer edge of the outer waste form, and the y-direction reflective boundary conditions are set just outside the outermost waste form in both y-directions. The reflective boundary conditions result in a room

that is effectively infinite in the y-direction. A diagram of the model construct is shown in Figure 6.14 below. Additional discussions about this model and the assumptions used to construct it are provided in APPENDIX E.

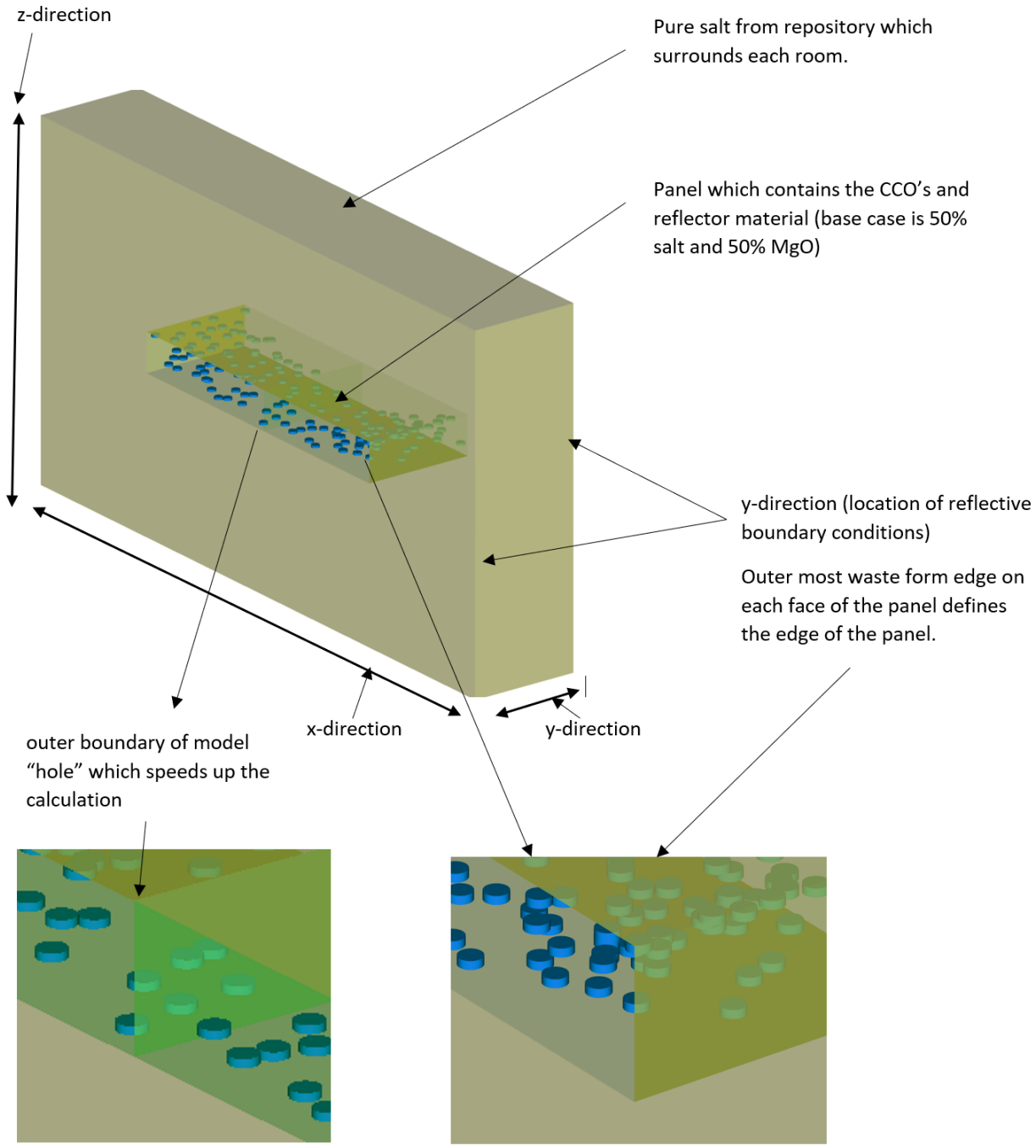

Figure 6.14. Diagram of the nonuniform array model.

The full set of results for the nonuniform array cases is presented in APPENDIX C (set-2-uh for upper horizon cases) and APPENDIX D (set-2-lh for lower horizon cases). The same set of plots shown in

APPENDIX A and APPENDIX B are shown in APPENDIX C and Appendix D so that comparisons can be made for the FEP analysis. The full set of results with the representative curves are provided in Figure 6.15 and Figure 6.16 below for the upper and lower horizons, respectively, whereas Figure 6.17 provides the delta-k comparison between the upper and lower horizons. The results show that the upper horizon is always more reactive than the lower horizon.

The most meaningful comparisons for these results are shown as delta-k comparisons between set-1 and set-2-uh and set-1a and set-2-uh in Figure 6.18 and Figure 6.19, respectively. These delta-k comparisons show that set-1 is significantly more reactive than the other sets, and they also show that the important reactivity trends discussed in Section 6.1 remain consistent between set-1 and set-2 cases, with some important exceptions as discussed further below. Figure 6.20 compares set-1 to set-2-lh.

The reactivity of the nonuniform spacing is dramatically lower in k_{eff} than in set-1. CCO centroid locations in their compacted configurations have significantly lower neutronic coupling than the uniform array. This is likely because in the compacted configuration, neutrons escaping a CCO can only cause fission in other CCOs if they travel in a relatively horizontal direction. However, in the uniform direction, neutrons can travel in more non-horizontal directions and still cause fission. Furthermore, the tangential impact is that the spherical shape is more reactive than the cylinder shape because now that the waste forms are more neutronically isolated from each other, the geometric impact of the surface-to-volume ratio dominates. It should be noted also that many of these differences in trend effectively cancel out at very high moderator mass.

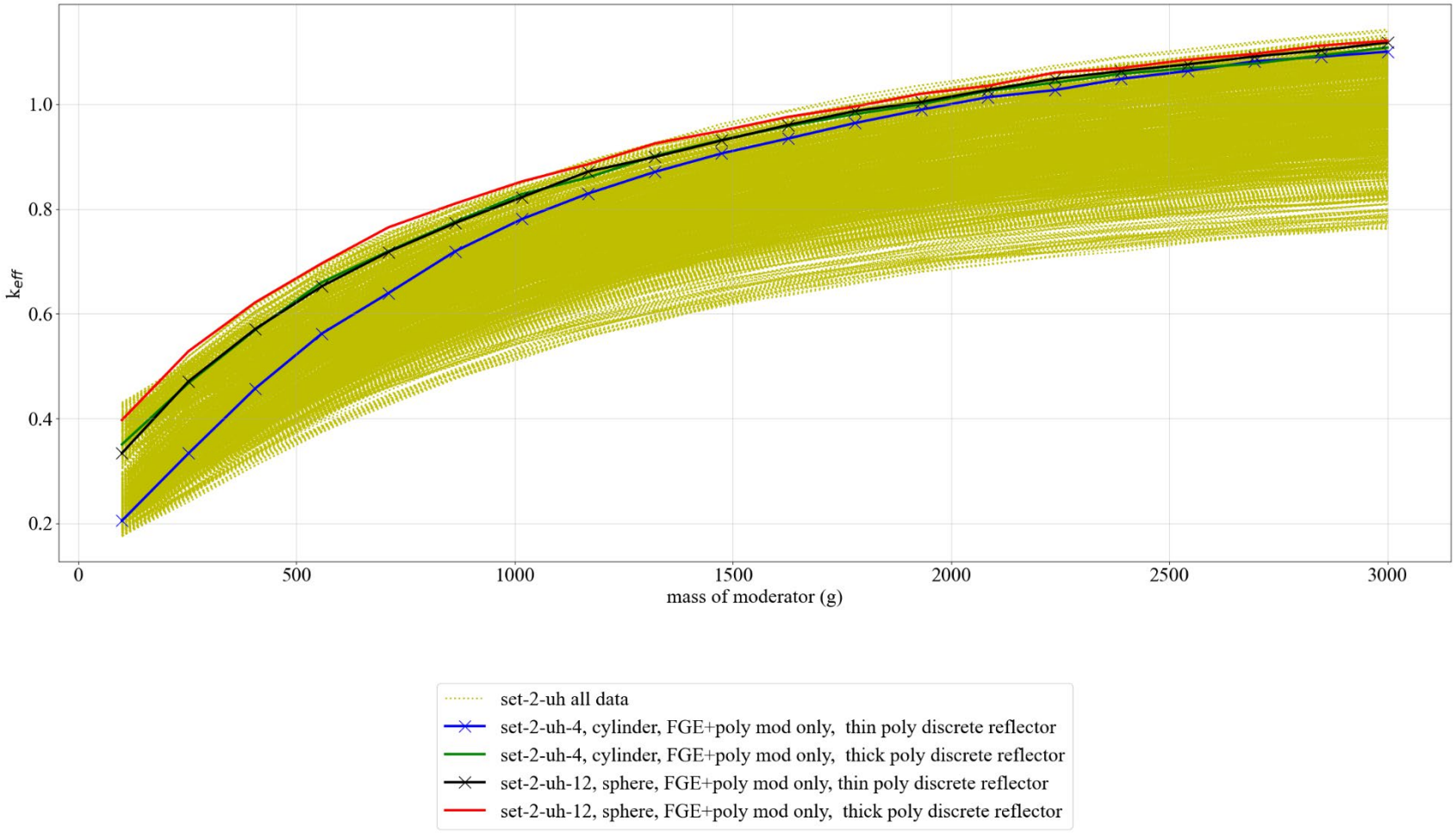

Figure 6.15. Full set of results for set-2-uh compared to various representative curves.

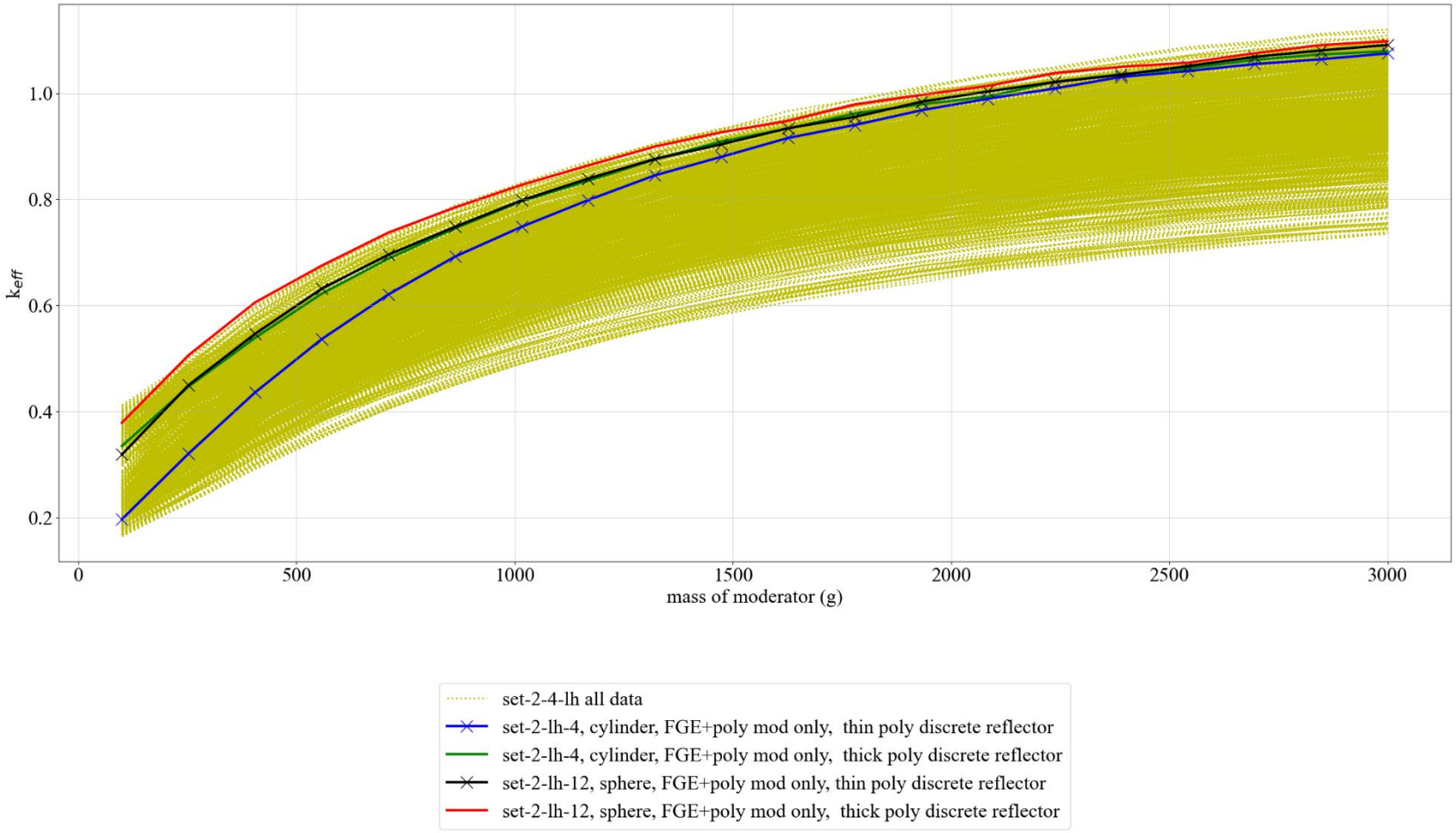

Figure 6.16. Full set of results for set-2-lh compared to various representative curves.

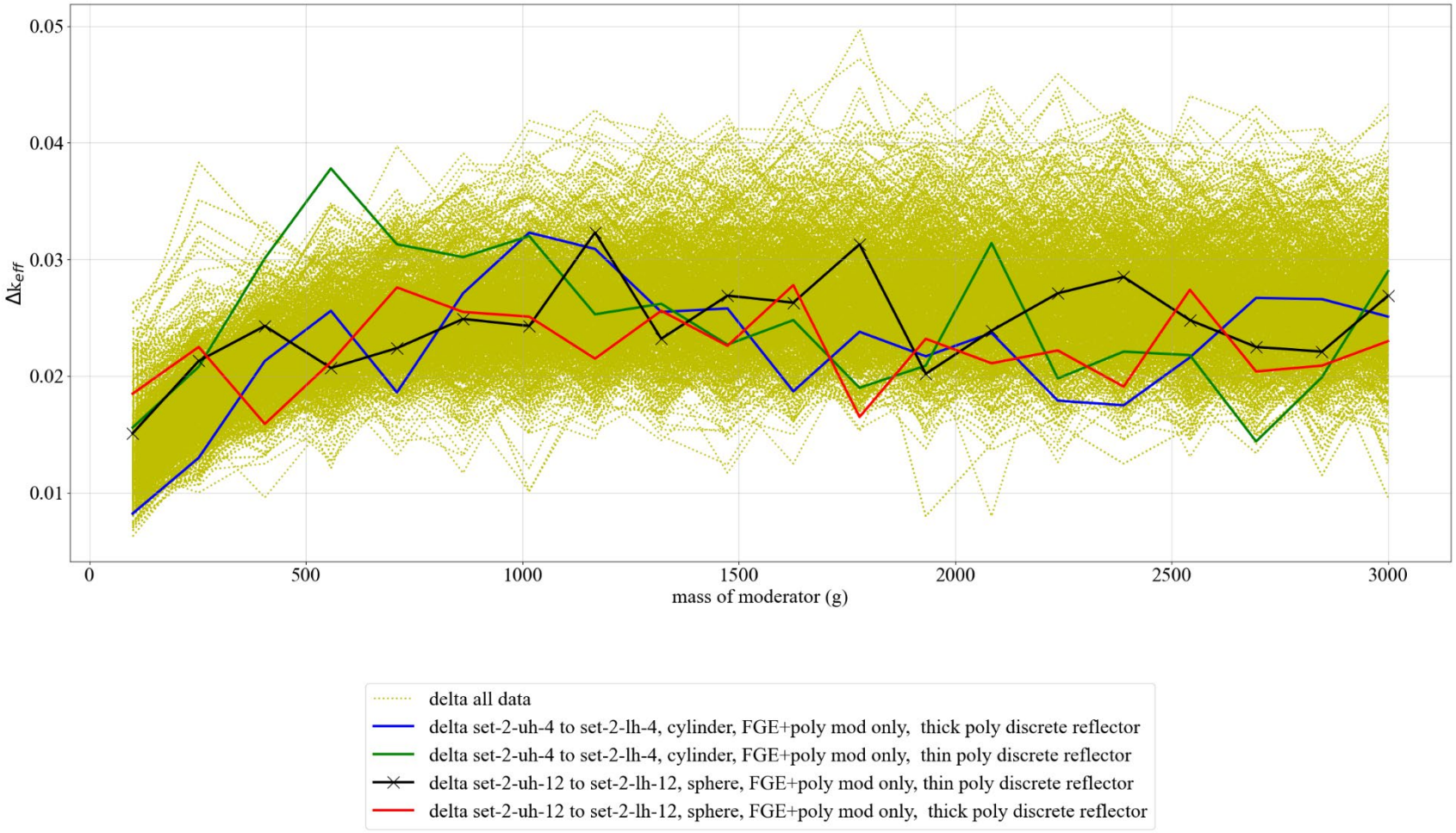

Figure 6.17. Delta k of set-2-uh compared to set-2-lh with various representative curves (set-2-uh – set-2-lh).

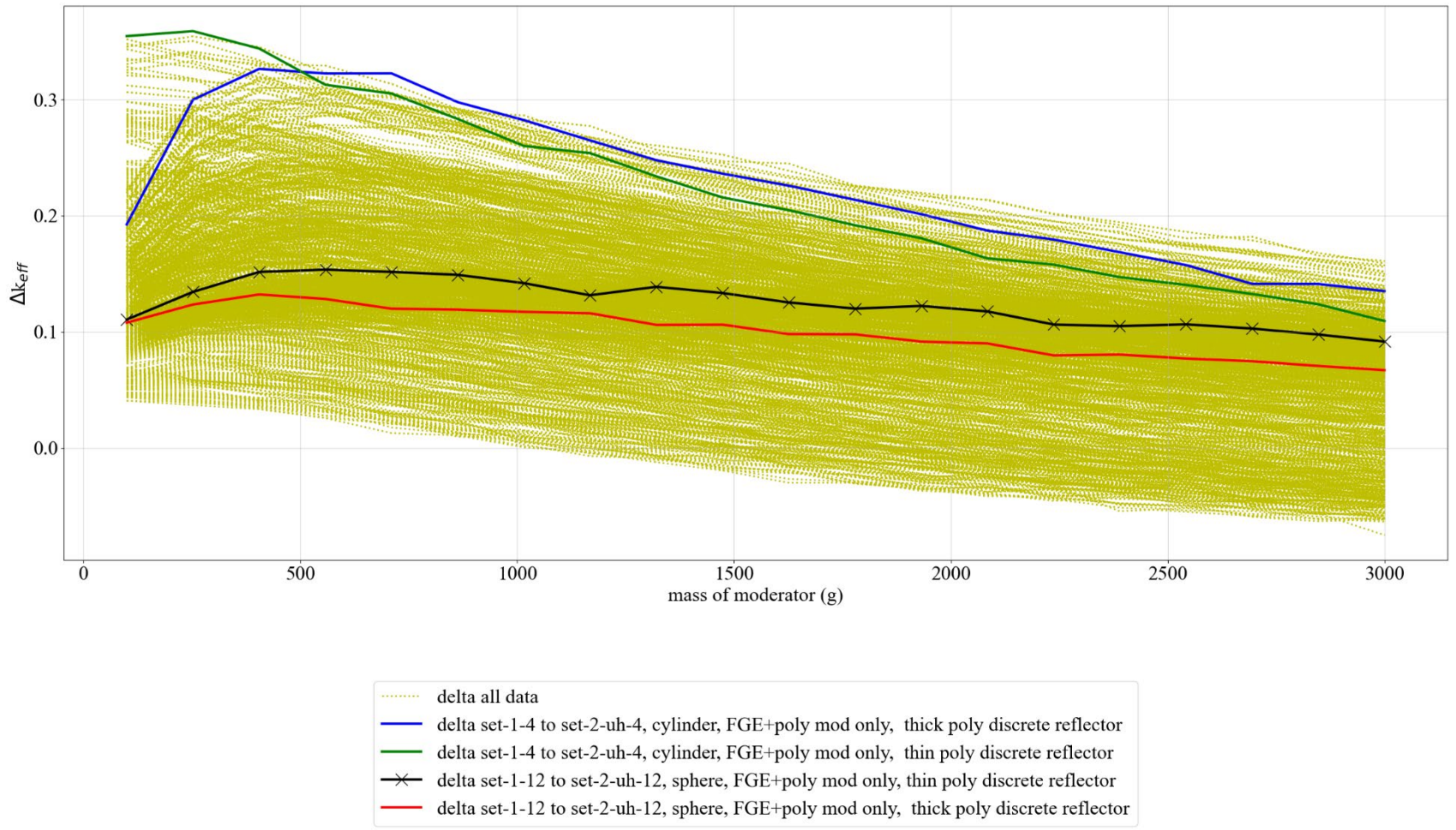

Figure 6.18. Full set of results for set-1 compared to set-2-uh with various representative curves (set-1 – set-2-uh).

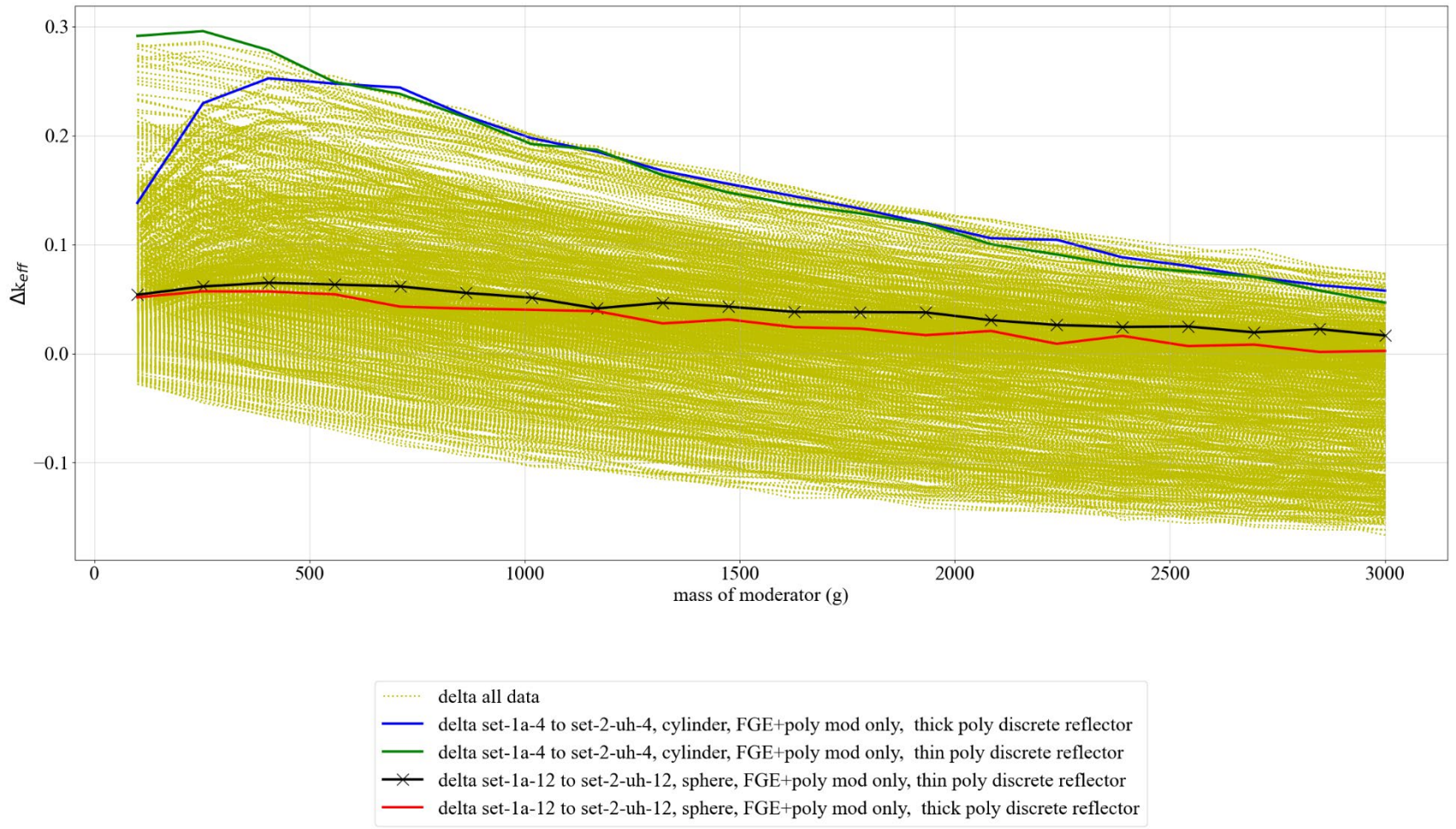

Figure 6.19. Full set of results for set-1a compared to set-2-uh with various representative curves (set-1a – set-2-uh).

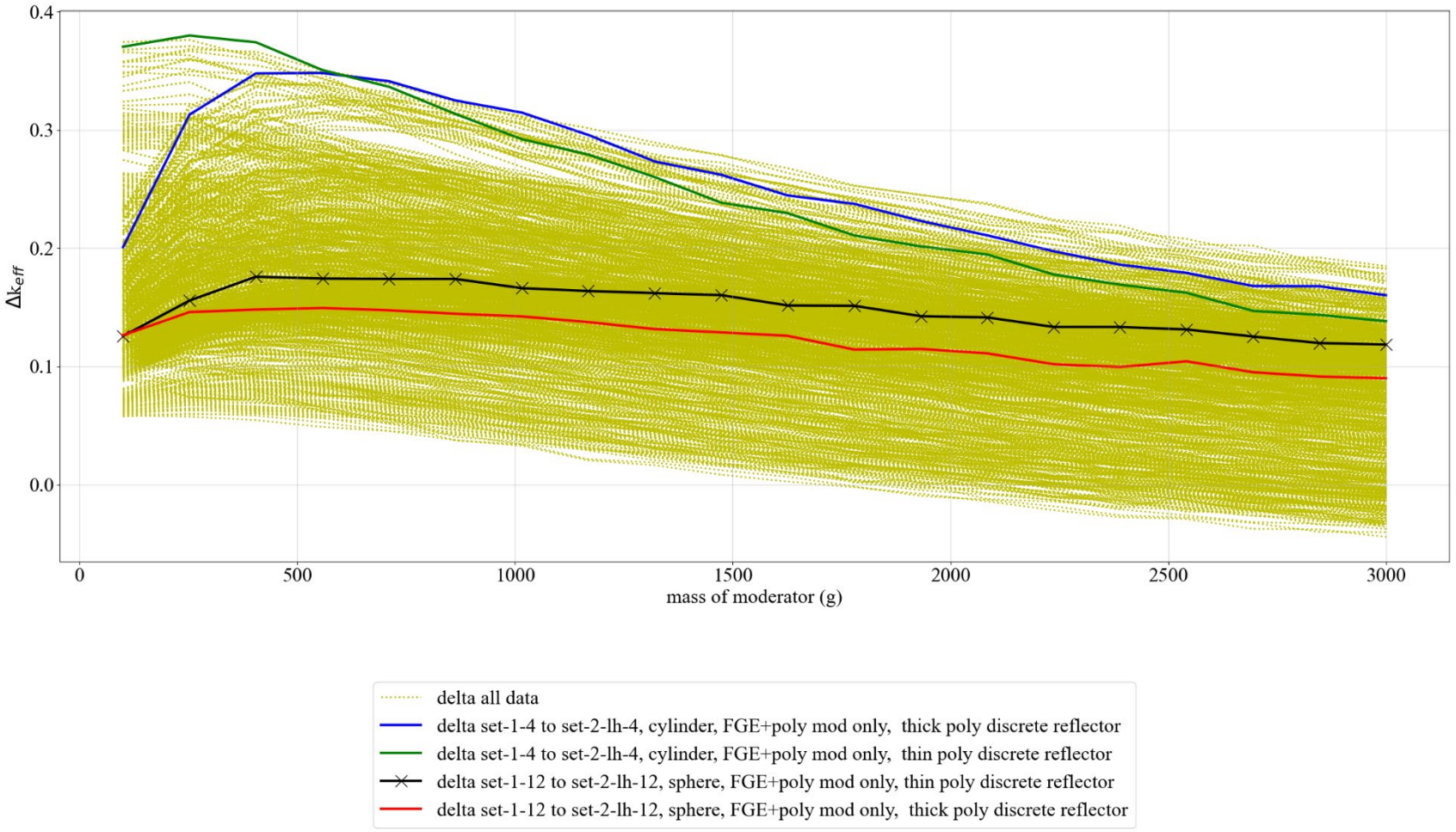

Figure 6.20. Full set of results for set-1 compared to set-2-lh with various representative curves (set-1 – set-2-lh).

6.4 ADDITIONAL NONUNIFORM ARRAY ANALYSIS

As is discussed in Section 6.3, the nonuniform array models for set-2-uh and set-2-lh are used to provide a comparison of reactivity between using the Reedlunn and Bean [8] data with uniform arrays (set-1 and set-1a) vs. nonuniform arrays. The set-2 -uh and set-2-lh results are considered appropriate for that purpose and could also be used as best-estimate guidance if needed.

To provide additional technical justification for the appropriateness of specific aspects of the nonuniform array model for set-2 -uh and set-2-lh calculations, additional analysis is provided. Specifically, the following items are addressed:

1. Compaction is a time-dependent process in which the location of the compacted CCOs changes over time. The results in Section 6.3 are for the "final" location at 10,000 years, with 1,000 years being used because there is little change after the first few hundred years. Additional analysis evaluated if there is an intermediate time step that could be more reactive between 0 years and 1,000 years. It also evaluates whether 1,000 years is the most reactive time and if it would be appropriate to use to represent 10,000 years.

2. Satisfactory computational performance is essential to any modeling effort. Additional cases were run to verify that the reactivity difference between a 1-unit KENO model vs. the 2-unit KENO model (used for nonuniform arrays throughout this report) is small. Furthermore, cases with more stringent control parameters examined whether cases are properly converged. The convergence of Monte Carlo criticality calculations is an important feature for providing meaningful results. The nature of the calculational model for the nonuniform array is a computationally intensive calculation for Monte Carlo codes like KENO in the SCALE system because of the nonuniform nature of the location of the fissile regions with multiple surfaces. While the long historic precedence in running criticality calculations provides sufficient support for the Monte Carlo calculations' control parameters used in these KENO inputs, the use of a model enhancement described in Marshall and Brickner [26] motivated this inquiry.

3. The sensitivity of nonuniform models upon boundary conditions was evaluated. Specifically, the reactivity effect of using the reflective boundary conditions vs. a thick layer of reflector box material (salt+MgO) or periodic boundary conditions was examined. The Reedlunn and Bean [8] data are based on geomechanical models that utilize boundary conditions to limit the overall calculational effort and runtime. The underlying effect of such little movement in the y-direction (down the length of the room) supports the use of boundary conditions in that direction for the compaction studies. However, the use of boundary conditions is not as clear in criticality models of such nonuniform distributions of fissile regions. Three options are available: (1) no boundary conditions but instead a thick layer of reflecting media, (2) reflective boundary conditions, and (3) periodic boundary conditions. Brickner's original approach [4] was to assume that due to the crushing of the salt during creep, all other materials

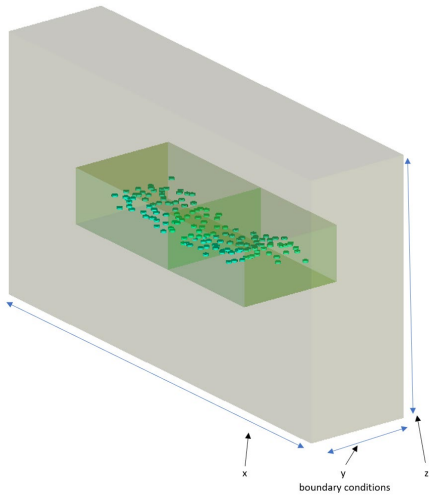

Figure 6.21. Illustration of boundary conditions.

would be very closely packed against the waste forms. Therefore, it would be appropriate for the reflector box to be defined as directly adjacent to the waste forms. In the z-direction and x-direction, a thick salt layer was then modeled, whereas in the y-direction, reflective boundary conditions were applied.

4. The original approach for modeling cylinders from Brickner [4] was to use the Reedlunn and Bean [7] data centroid (as determined to be a weighted average center pipe locations) to locate the center of the base of upright cylinders. An in-depth evaluation was performed to examine this assumption. Some cases evaluated if the centroid was located in the physical center of the cylinder instead of the base. In another group of cases, the centroid was oriented according to the pipe orientation at 1,000 years as calculated by Reedlunn and Bean [8]. In more cases, centroid location was varied along the length of the pipe was a more reactive configuration than the center. Also, a random distribution of centroid locations along the lengths of the cylinders was evaluated in search of a more reactive configuration. In addition, random distribution of cylinder orientations was evaluated. Finally, a combination of random distributions of both centroid location and orientations was evaluated.

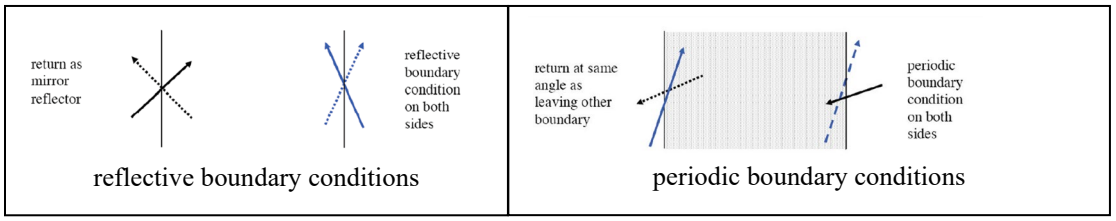

The calculations presented in APPENDIX E address items 1–3, and the calculations presented in APPENDIX G address item 4. Additional discussions are provided below.

In APPENDIX E, time-dependent models are created which use a 1-unit model rather than the 2-unit model, the Monte Carlo calculations control parameters are modified, and variations in boundary condition use are included (see Figure 6.26). The time dependence is for the locations of CCO centroid coordinates only; it does not include decay of ^{239}Pu to ^{235}U, corrosion, mass transport, or any other geometric or compositional change. Calculations are performed for the upper horizon dataset from Reedlunn and Bean [8] in 10-year increments up to 300 years and in 100-year increments up to 1,000 years. The full set of time-dependent results is summarized in Figure 6.24 below (see APPENDIX E for more information). The time-dependent results show that there is an expected time-dependent trend in reactivity (reactivity goes up over time due to compaction) and that there are no intermediate time steps which show any significant increase in reactivity. The results also show that after 300 years, there is little change in reactivity because there is little-to-no further movement of the fissile regions due to compaction.

For all the set-2 calculations in APPENDIX E which use the 2-unit model and are compared to 1-unit model, the comparison includes the reactivity effect of the change in Monte Carlo calculations control parameters to verify convergence in the set-2 1-unit model (e.g., larger number of cycles, neutron histories), as seen in Table E.1 in APPENDIX E). The difference in reactivity shown in Figure 6.255 below for the comparison between the 1-unit and 2-unit models shows that the Monte Carlo calculations control parameters used in set-1 and set-2 calculations are appropriate because the cases with much larger parameters do not change the result. The cases to verify convergence and to demonstrate adequate sampling use time step data from Reedlunn and Bean [8] (i.e., centroid datasets in 10-year increments). For the Monte Carlo cases with the alternative control parameters to verify convergence, flux distribution data were visualized using FULCRUM in the SCALE system, as shown in Figure 6.22 (presented in detail in APPENDIX E). The meaning and significance of these plots is discussed below.

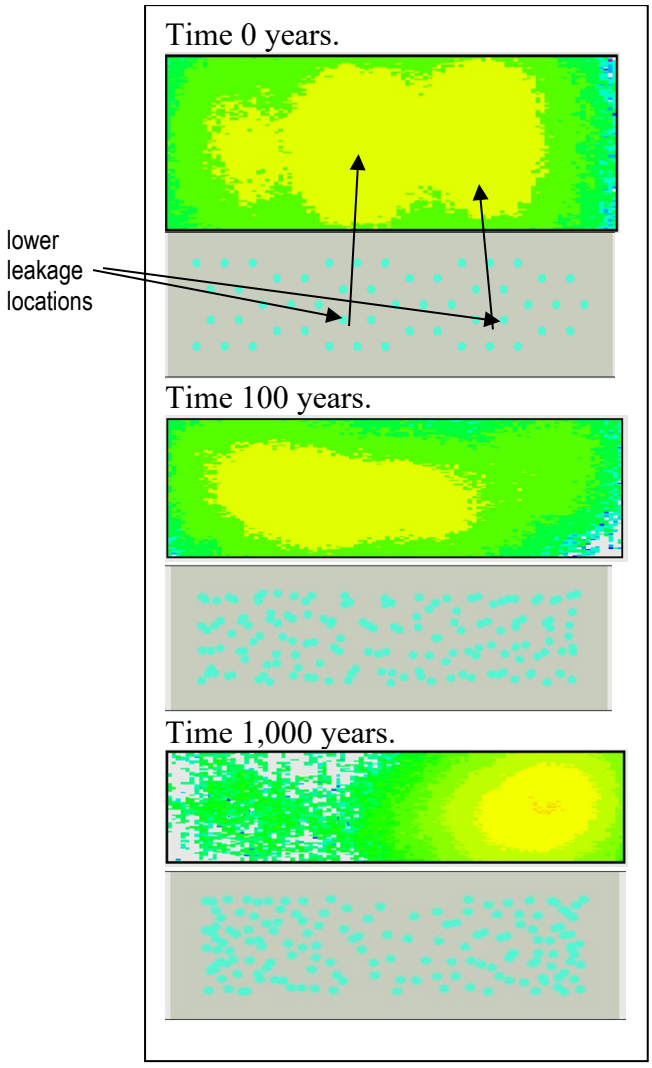

Figure 6.22. Diagram of flux for time-dependent cases.

The quantity of interest in this entire study is k_{eff}. By definition, k_{eff} is the number of child neutrons produced per parent neutron in a system. Any number of systems or configurations which are very different from each other and which have very different flux distributions may have the same k_{eff} value. Ultimately, k_{eff} is a system characteristic independent of flux distribution. However, flux information in (n/cm^2) is provided for these KENO calculations to (1) show that the geometry is adequately sampled, and (2) show the location of maximum reactivity which is of interest since several geometry configurations from Reedlunn and Bean [8] are evaluated (see examples from APPENDIX E in the diagram to the right). The flux computed in KENO is non-physical and is only used as a means to analyze the system. Due to the way Monte Carlo computations proceed, where neutrons in higher multiplication areas reproduce more, the areas with larger fluxes contribute more multiplication to the system and have a higher reactivity—defined as (k-1)/k)—than areas with smaller fluxes. However, because k_{eff} is a system characteristic independent of flux distribution, there is no unique function that maps a value of flux to a value of reactivity in a region, so *flux magnitudes only indicate whether an area has a higher or lower reactivity than another region*.

The KENO calculation is time-independent, and it proceeds by providing an assumed fission source defined by the control parameters (here the increased values, see Table E.1 in APPENDIX E), neglecting the intrinsic source of neutrons (radioactive decay-based reactions) in the system from the waste forms.

The initial generation source distribution is a guess that is uniform across the fissionable material in the model, and it is updated in each generation based on the location's fissions that occurred in the previous generation. The number of neutrons in each generation is forced to remain constant, despite the actual system k_{eff}. This process leads to the term "iterated source" for a k_{eff} calculation in a Monte Carlo code such as KENO. As the calculation proceeds, the source distribution should stabilize into a converged distribution representative of the fission source, and thus relative reactivities, *in all regions of the problem*. The number of skipped generations in the calculation should be selected to be greater than the number of generations necessary to achieve this convergence, and several outputs from the simulation are provided to help the user assess that this source convergence has been achieved (all of which has been done and verified by these comparisons). In each active generation, the tallied flux is a result of the fission sites from the previous generation and the multiplication of each portion of the system. As the calculation proceeds, the iterative nature of the simulation causes the flux to become higher and higher in the most reactive portion of the system. This means that less and less attention is paid to the lower value regions. Therefore, for the 1,000-year case (see bottom image in Figure 6.22), the lack of shading on the left side of the room indicates a very high degree of convergence, whereas for the 0-year case (top image in Figure 6.22), both sides remain equally important because of the symmetry of the fissile region distribution.

It is worth noting that in the subcritical configurations considered, the real flux in the room would be quite low. The intrinsic source from the waste forms would provide a constant small source of neutrons (from radioactive decay) that would be multiplied in the surrounding fissionable material. The real, time-dependent flux distribution would look sparser and more sporadic with occasional peaks that quickly faded away. This sort of calculation is extremely expensive and is not necessary for the analysis presented in this report.

Results are plotted for a number of time steps in APPENDIX E (summarized in Figure 6.22 above) and can be used to observe the following trends:

- At time 0 years, the hexagonally arranged fissile regions show how the calculation converges on the locations where the most fissions occur.
- At time 100 years, the location where the flux is greatest has shifted to the left side of the room, indicating that the compacted arrangement yields a configuration where the calculation focuses to converge its solution.

At time 1,000 years, the location in the model which yields the maximum k_{eff} has shifted to the far-right side, and the flux indicates that the calculation has determined that this location is of much more importance than the left side. To support this statement, another set of calculations was performed in which one half of the room has no FGE. As can be seen in Figure 6.233, the "half-room" calculations support these conclusions.

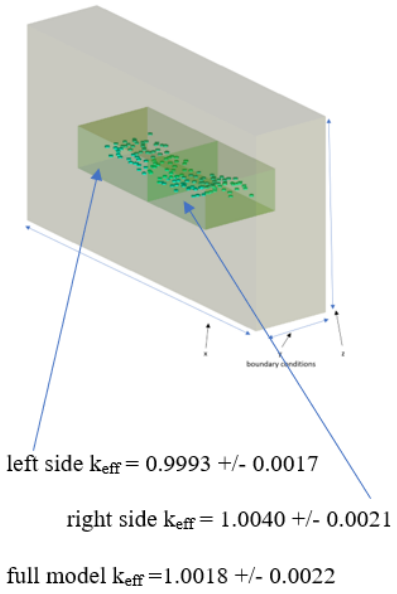

Figure 6.23. Results of the "half-room" calculations.

The results of the calculations to address item 4 (above) are found in APPENDIX G and are summarized in Figure 6.27 through Figure 6.29 below. Three sets of evaluations were performed: *centroid studies, rcoord studies*, and *rA studies.* Each set includes multiple subsets, as explained in detail in APPENDIX G and summarized below.

The centroid studies evaluate the effect of using each of the 13 SNL centroids independently, along with a midpoint. For these cases, each pipe in the model uses the same centroid for that case. For example, if the case is centroid1, then each pipe in the model uses the centroid1 coordinates. The results are summarized in Figure 6.27.

The rcoord studies evaluate the effect of randomly selecting the 13 centroid coordinates to be used. Each pipe in the model has its own unique, random selection. For these studies, 100 rcoord cases were generated. The results are summarized in Figure 6.28.

The rA studies evaluate the effect of randomly selecting the cylinder orientation. These studies are performed independently and in conjunction with rcoord sets. The results are summarized in Figure 6.29.

The results show that the set-2 approach for using upright cylinders with the Reedlunn and Bean [8] centroid data for the average central centroid defining the center of the bottom of the cylinder is an acceptable approach.

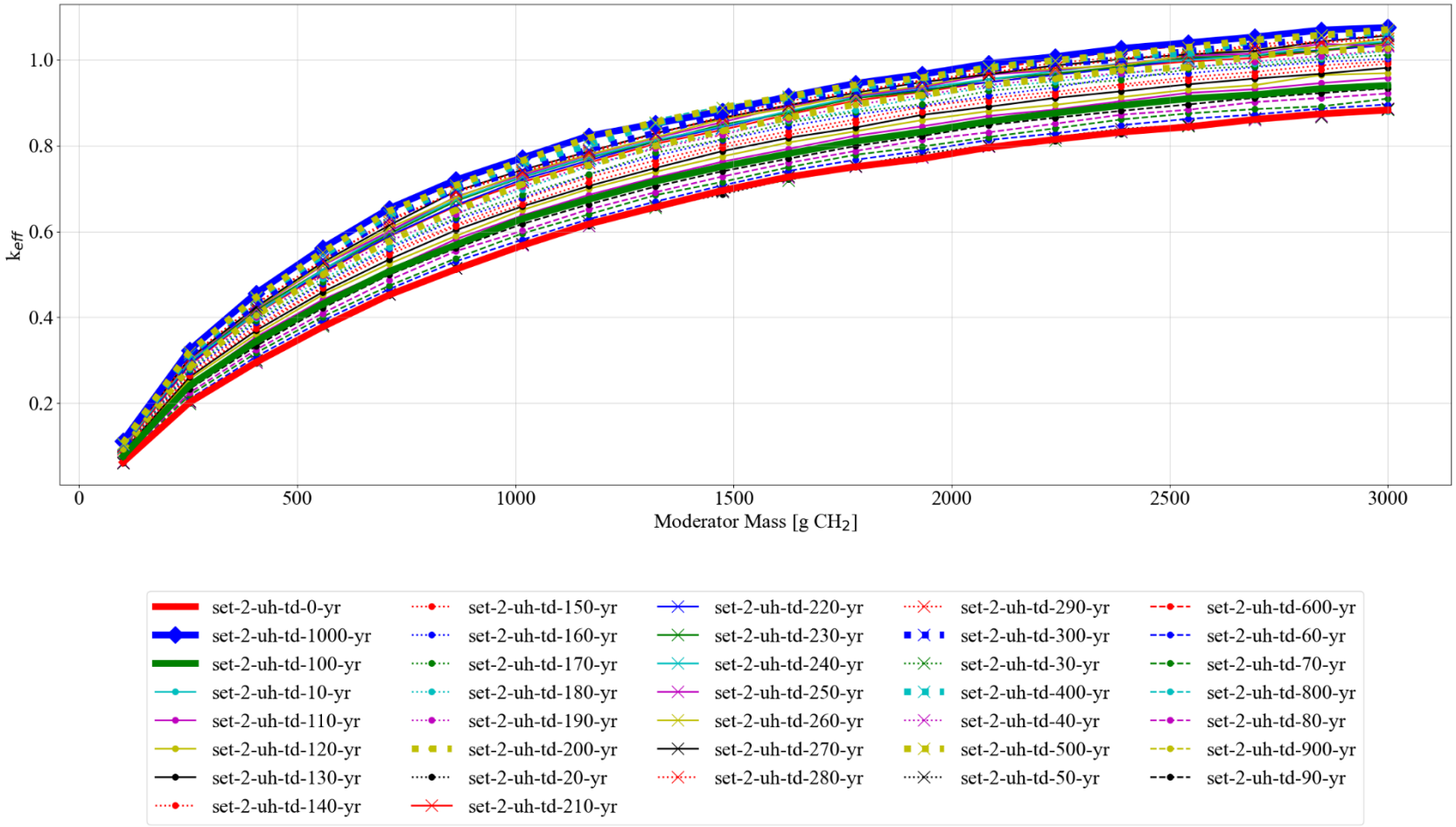

Figure 6.24. Results of the time-dependent calculations (set-2-4 with no filler).

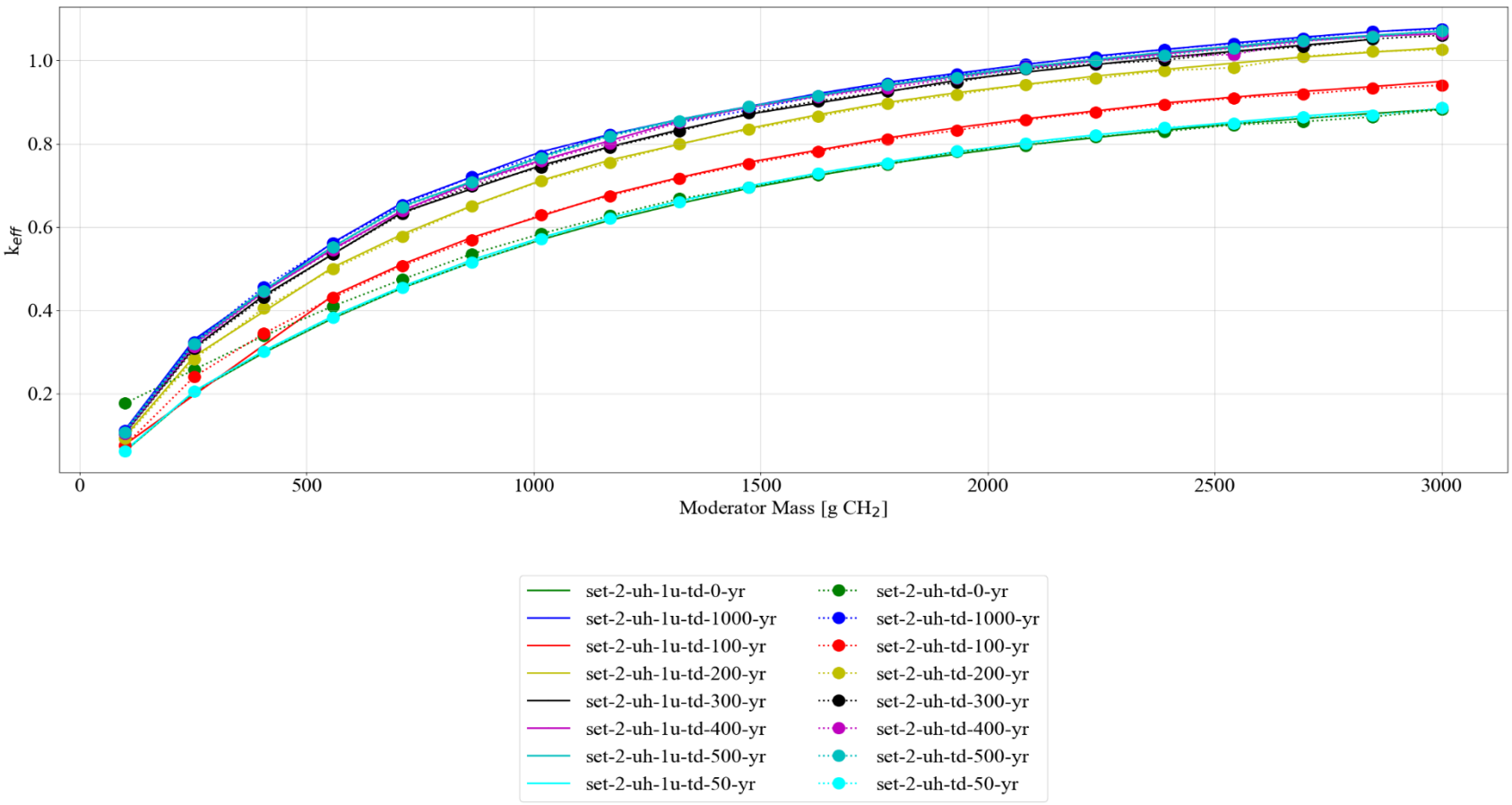

Figure 6.25. Comparison between the 1-unit model and the 2-unit model (set-2-4 with no filler).

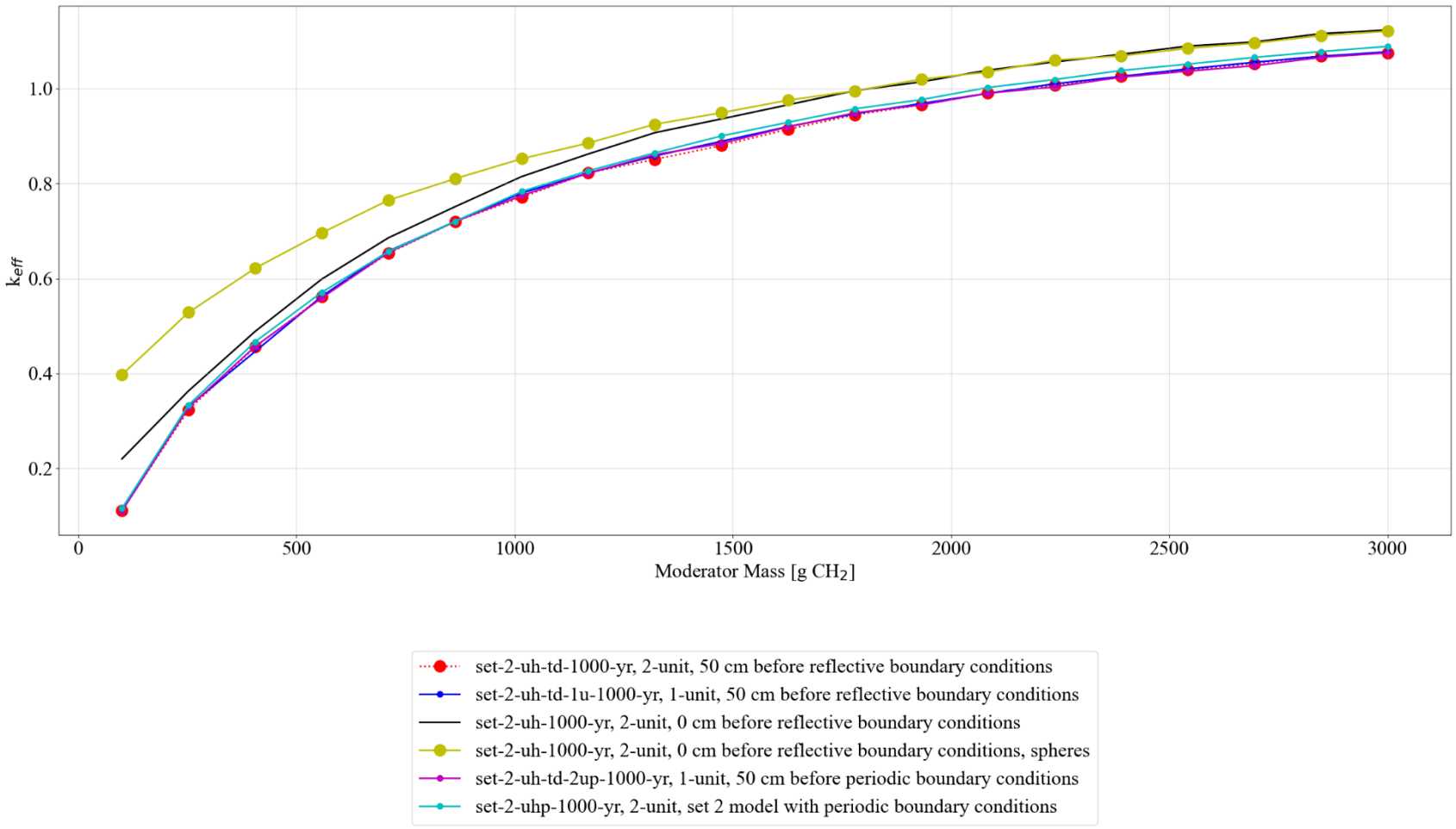

Figure 6.26. Comparison of various boundary conditions (set-2-4 with no filler).

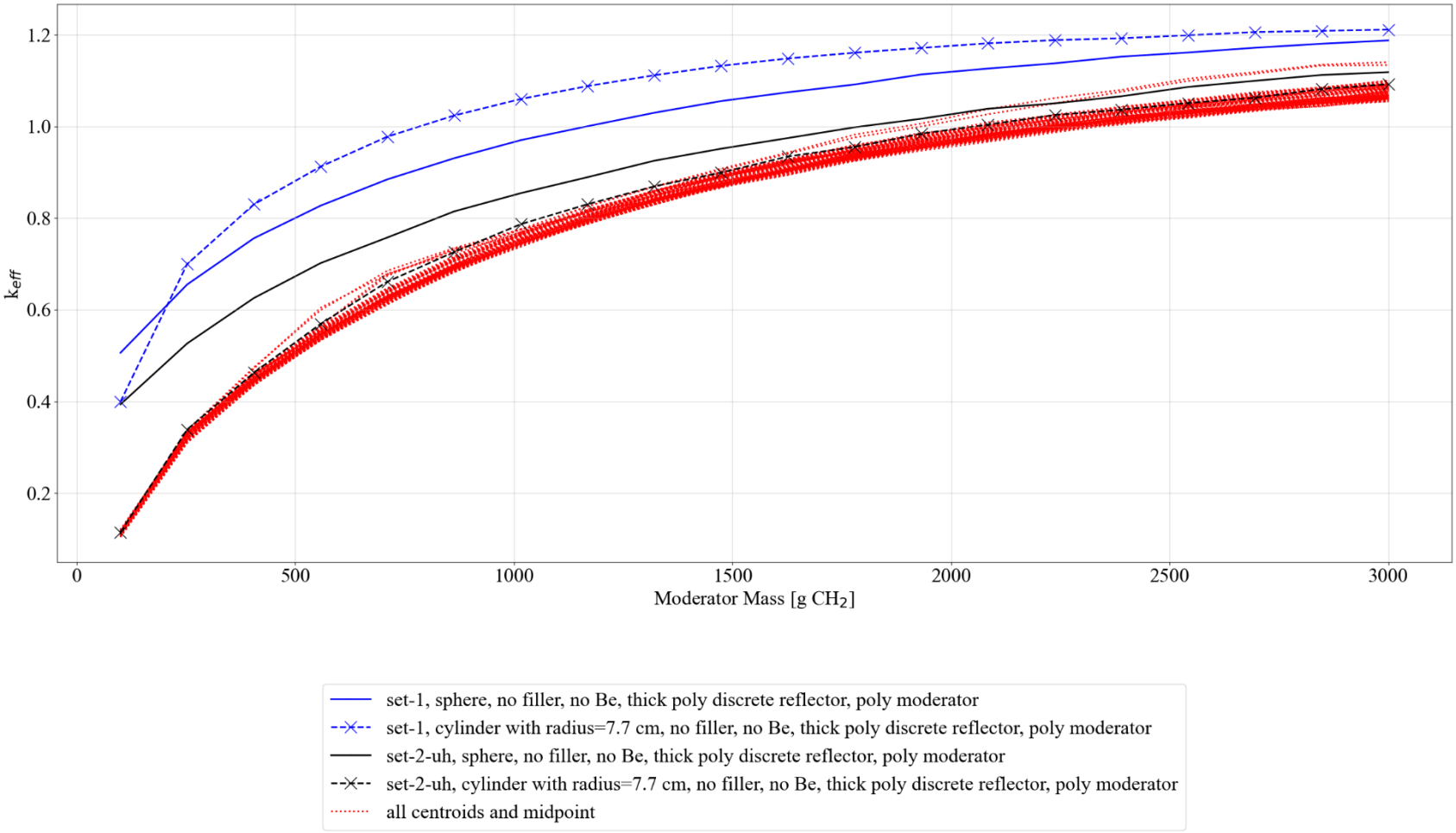

Figure 6.27. Summary of centroid study results.

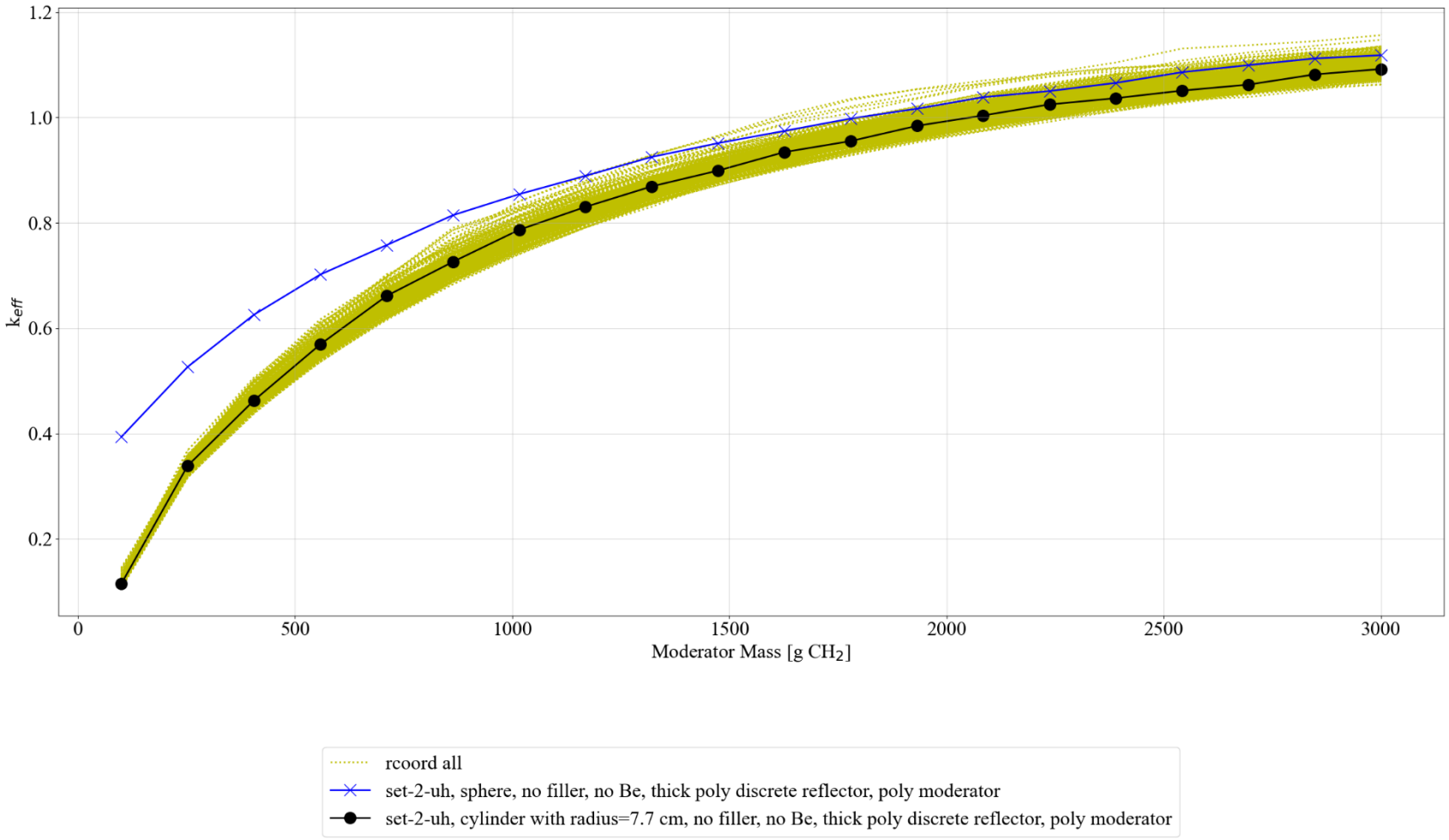

Figure 6.28. Summary of rcoord study results.

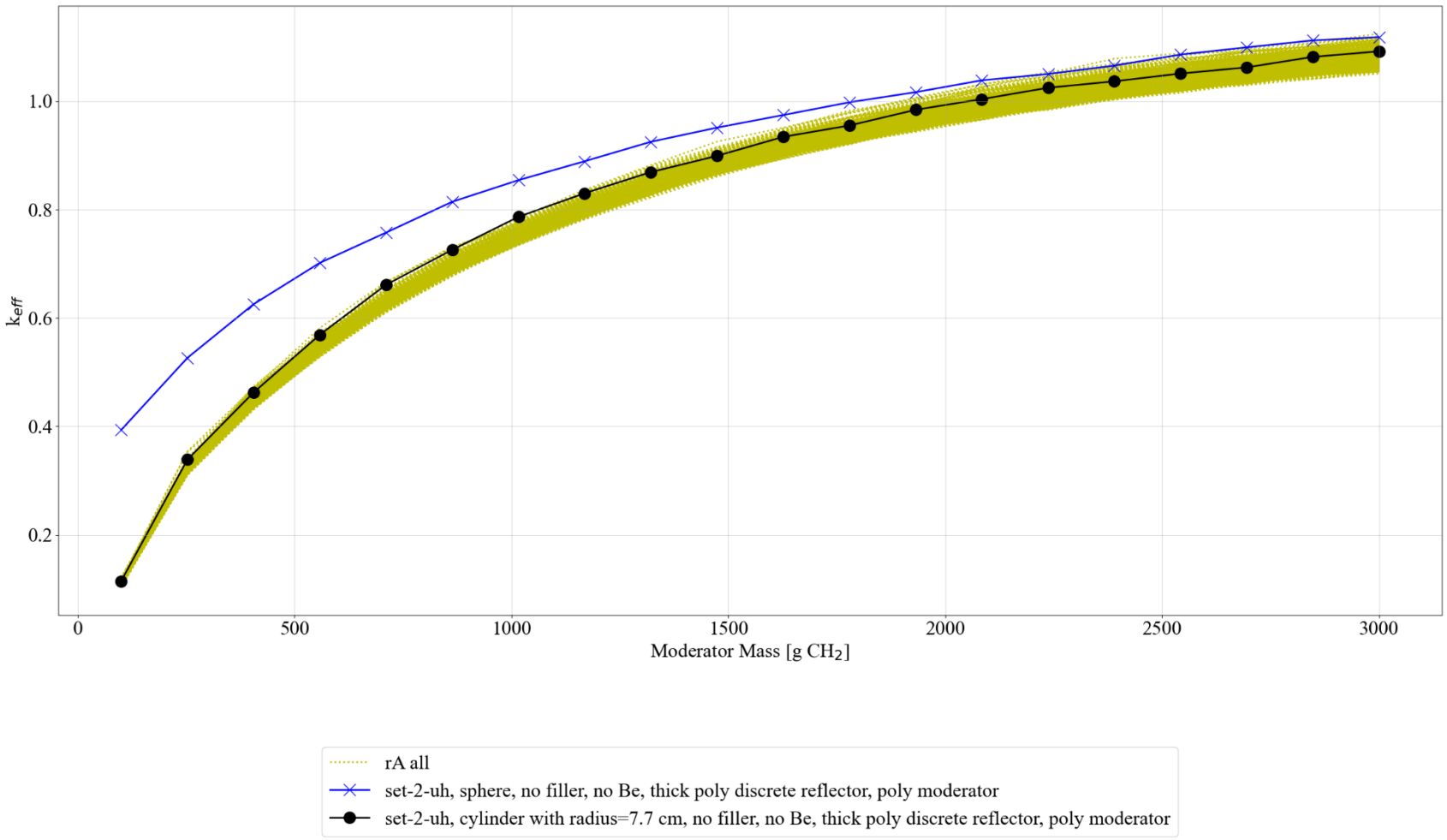

Figure 6.29. Summary of rA study results.

6.5 SENSITIVITY OF RESULTS TO PARAMETERS VARIED

While manual examination played a large part in the interpretation of the resulting k_{eff} trends, a multivariate linear regression was used to determine the importance of each parameter for a subset of k_{eff} models. In the production of the linear model, each parameter (p) was rescaled to a range of -1 to 1 to represent "low" and "high," as shown in Eq. (6-1) below

$$x_{i,j} = \frac{2 \cdot p_{i,j}}{\max_j(p_{i,j}) - \min_j(p_{i,j})} - 1, \quad (6\text{-}1)$$

where x is the rescaled parameter, i is the parameter type, and j indexes the value for the j-th output. Parameters having a high covariance with parameters included in the correlation must be excluded. For example, sphere radius and cylinder height cannot be included because they are correlated to moderator mass. If they were included, then the impact of both sphere radius and moderator mass would become arbitrary. Some of the studied parameters such as moderator content, array spacing, and waste form shape were not linearizable, so a correlation was produced for each combination of those parameters instead.

After rescaling, correlation coefficients (m) and a correlation constant (c) were found by fitting the functional form in Eq. (6-2) below.

$$k_{eff,j} = \sum_i m_i x_{i,j} + c, \quad 6\text{-}2$$

The resulting regression coefficients indicate the parameters driving system behavior. The correlations suggest the typical behavior of the system, but it is not a substitute for physics simulations.

Figure 6.310 shows the absolute value of the linear correlation coefficient (the relative importance) of each parameter for various moderator masses evaluated for a set of cylinder cases in a uniform array (set-1). It is clear that variations in B_4C content have the largest effect on k_{eff}; filler mass, radius, pipe material, and pipe thickness are less impactful on k_{eff} over the ranges in which the parameters were varied. Although the correlations are not definitive, they can quickly summarize trends in the data. Since the correlation parameters were normalized to a range of -1 to 1, multiplying the correlation coefficient by 2 gives the typical delta k introduced by a given parameter within the evaluation ranges. Thus, 50 g per CCO of B_4C leads to a 0.4 change in k_{eff} at higher moderator masses.

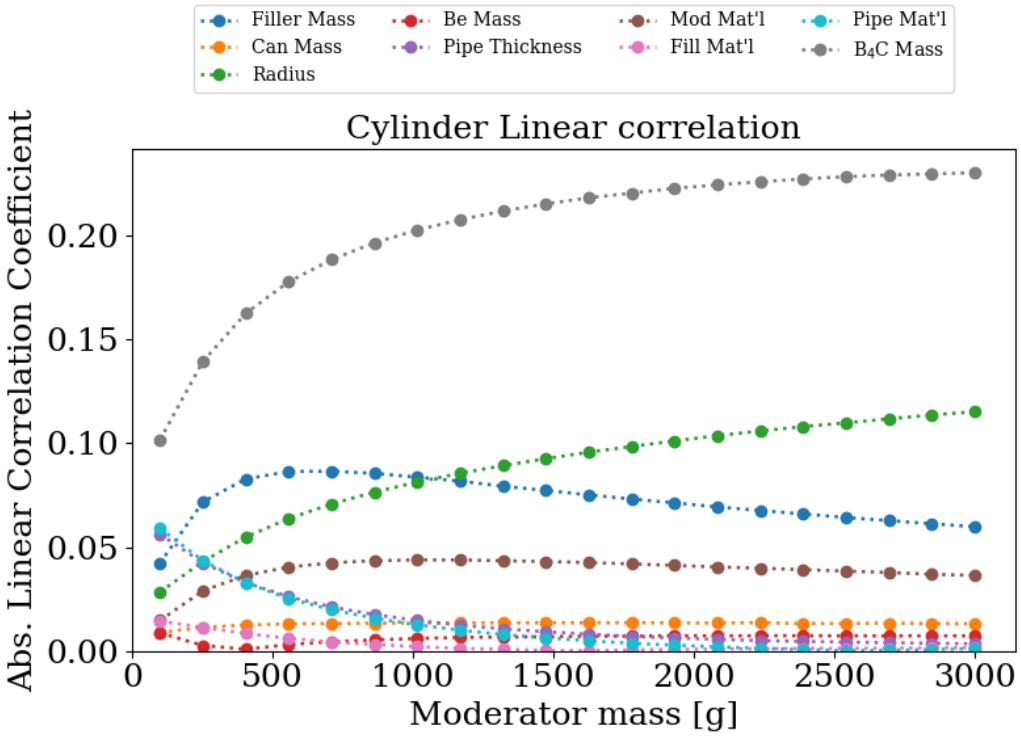

Figure 6.30. Absolute values of linear correlation coefficients for set-1 cylinders showing the relative impact of each parameter upon k_{eff}.

Because each parameter was normalized to center the range about zero, the correlation constants reflect the average behavior of the system (i.e., when all parameters are set to their midpoints). Since the real system is nonlinear, the linear approximation is only useful to gather general trends. By exploring the differences between correlation constants for different sets of parameter sweeps, the approximate average impact on k_{eff} that results from changing between sets (array spacings in this case) can be observed. Figure 6.321 shows the differences in correlation constants (approximately the change in k_{eff}) between set-1 and set-3 cylinder cases (both uniform arrays) and the other datasets. In the figure, sphere cases were compared to sphere cases, and cylinder cases to cylinder cases. As all of the values in Figure 6.321 are negative, it is clear that set1 and set-3 cylinders are the most reactive array configurations. Set-3 and 3a subdivide the waste forms in sets 1 and 1a, respectively, into two per CCO, so set-3 waste forms have half the volume of set-1 waste forms. The cylinder radii are set parameters, and because the cylinders are stacked in set-1, and because total mass is the same between both sets, set-3 cylinders have roughly the same stack height as set-1 cylinders. However, they are not identical because of discrete reflector usage. The spheres do not make an equivalent configuration in set-3 and set-1 because the differing volume produces differing radii.

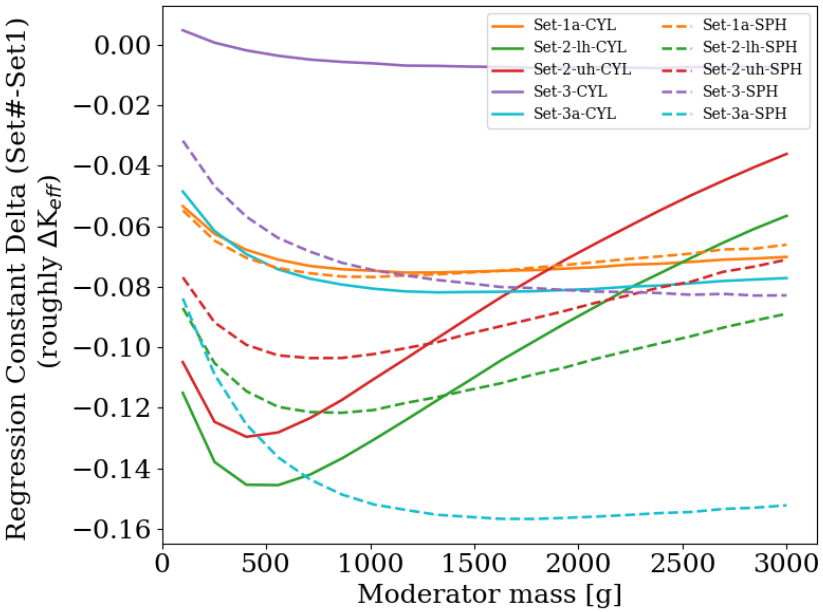

Figure 6.31. Differences in linear correlation constant terms relative to set-1 values.

To show that the correlations are applicable, and there are few nonlinearities or interaction terms, r^2 values are plotted in Figure 6-32 below. These scores indicate that the correlations are sufficiently good to identify the primary system drivers.

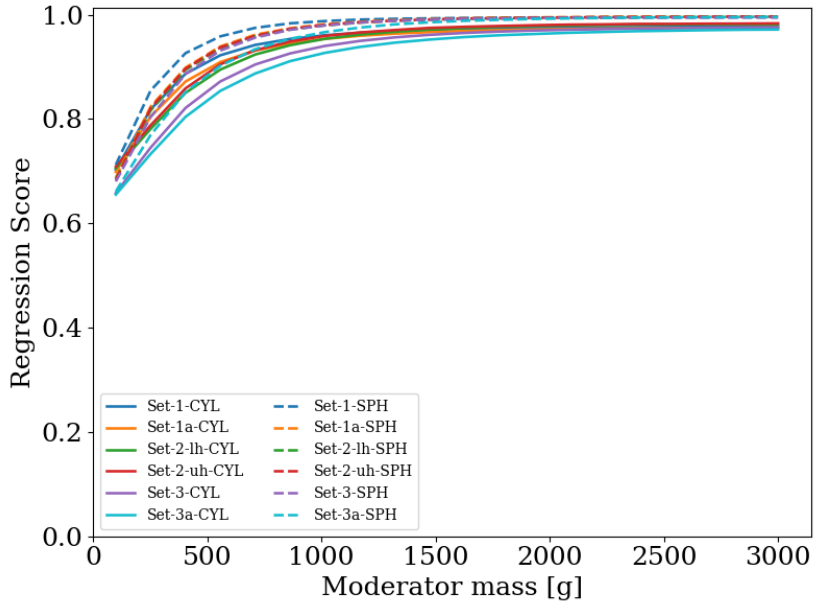

Figure 6.32. r^2 values for various moderator masses.

6.5.1 Correlation Coefficients for Additional Sets

Correlation coefficients for set-1 spheres are shown in Figure 6-33 below. The coefficients are roughly similar in trend in magnitude to set-1 cylinders.

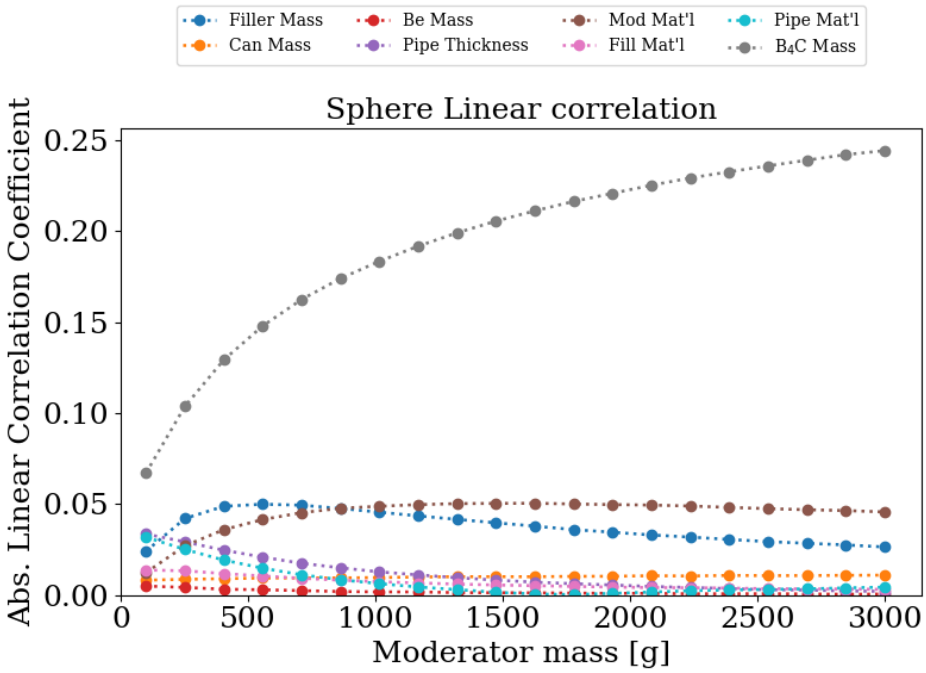

Figure 6.33. Absolute values of linear correlation coefficients for set-1 spheres showing the relative impact of each parameter upon k_{eff}.

Correlation coefficients for set-2 lower horizon data are shown in Figure 6-34 below. The radius coefficient is particularly affected as compared to that of set-1. This may be caused by the set-2 cylinders being separated, as opposed to cylinders in set-1 being stacked three high in direct contact. This results in different stack height and leakage for a given radius vs. that in a group of three-stacked cylinders.

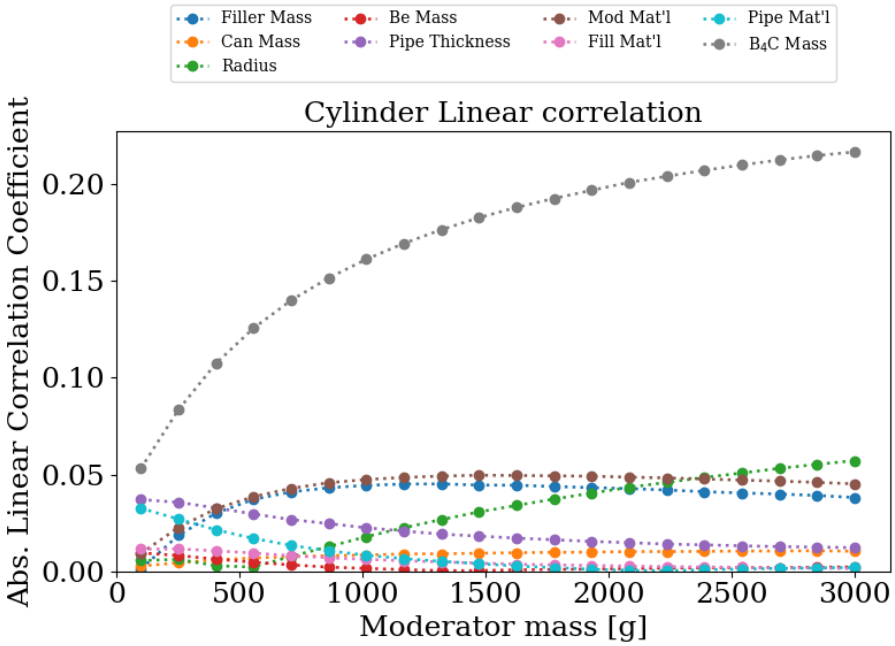

Figure 6.34. Absolute values of linear correlation coefficients for set 2-lh cylinders showing the relative impact of each parameter upon k_{eff}.

Correlation coefficients for set-2-lh spheres are shown in Figure 6-35 below. The trends are roughly similar to those in the cylinder case.

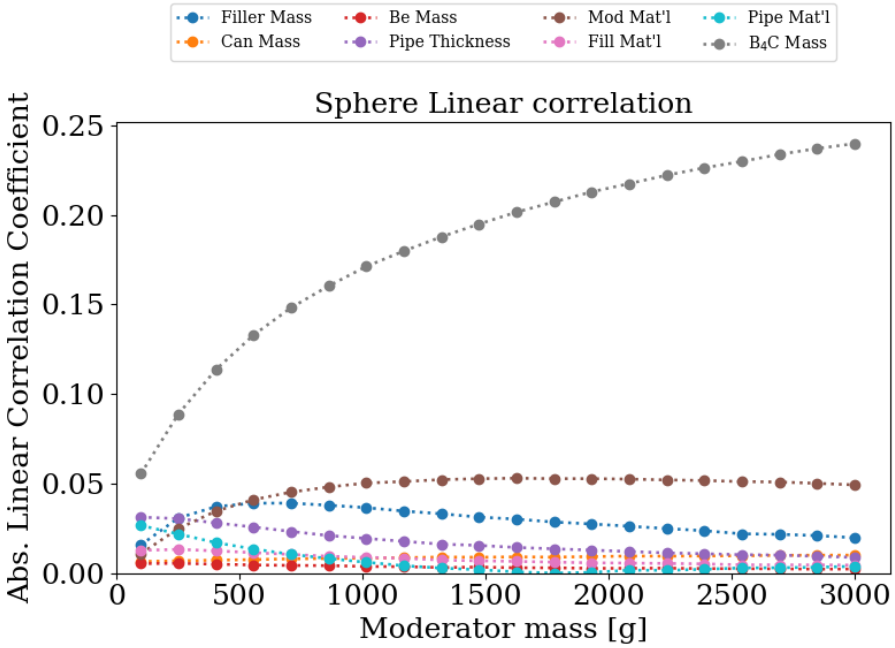

Figure 6.35. Absolute values of linear correlation coefficients for set-2lh spheres showing the relative impact of each parameter upon k_{eff}.

6.6 UPPER SUBCRITICAL MODERATOR MASSES

Upper subcritical masses were evaluated for various configurations of each set of cases evaluated in this work. They are presented here. Note that in these analyses the upper interpolation point was 3000 g of moderator. For points at 3000 g of moderator in plots in this subsection, this indicates that no upper value for subcritical moderator mass was found. The lines indicating sphere do not correspond to the radius listed in the plot. The lines for spheres instead simply indicate the upper subcritical mass for all spheres.

6.6.1 Set-1 Uniform Array of Waste Forms Stacked Three High with Closer Spacing

Table 6-3, Figure 6-36 and Figure 6-37 below shows the masses that were always associated with subcriticality in this study and did not produce k>1 for various types of scenarios evaluated in set-1. These masses were determined by interpolating between datapoints. Addition of filler and reduction of cylinder radius substantially increases the calculated maximum subcritical mass. To a lesser degree, the thick polyethylene pipe (i.e., discrete reflector) reduced the maximum subcritical mass. No such polyethylene geometry exists in the initial waste form configuration, and this case was examined to identify the effect of moderator directly outside of the waste form.

Because the polyethylene is modeled as sandwiched between three cylindrical waste forms, the stack obtains higher reactivity. A similar configuration may be conceivable assuming no decay of the plywood dunnage in the CCOs and perfect stacking in compaction.

Table 6.3. Moderator masses that did not produce $k > 1$ for evaluations in set-1

Set-1 interpolated mass of waste form moderator (g)						
No filler mass						
Pipe material	**Pipe thickness (cm)**	**Be (g)**	**cyl R = 4.8**	**cyl R = 6.25**	**cyl R = 7.7**	**sph**
Polyethylene	0.001	0	1,626	900	816	1,156
Polyethylene	0.7112	0	1,497	776	637	1,161
Polyethylene	0.001	585	No upper bound	1,013	821	1,171
Polyethylene	0.7112	585	No upper bound	860	646	1,169
Steel	0.001	0	1,631	907	823	1,152
Steel	0.7112	0	1,441	932	876	1,093
Steel	0.001	585	3,000	997	820	1,164
Steel	0.7112	585	2,068	1,000	880	1,107
4 kg filler mass						
Pipe material	**Pipe thickness (cm)**	**Be (g)**	**cyl R = 4.8**	**cyl R = 6.25**	**cyl R = 7.7**	**sph**
Polyethylene	0.001	0	No upper bound	2,432	1,441	1,561
Polyethylene	0.7112	0	No upper bound	2,288	1,301	1,617
Polyethylene	0.001	585	No upper bound	2,758	1,497	1,549
Polyethylene	0.7112	585	No upper bound	2,628	1,344	1,593
Steel	0.001	0	No upper bound	2,403	1,450	1,566
Steel	0.7112	0	No upper bound	2,181	1,445	1,471
Steel	0.001	585	No upper bound	2,688	1,508	1,538
Steel	0.7112	585	No upper bound	2,379	1,485	1,448

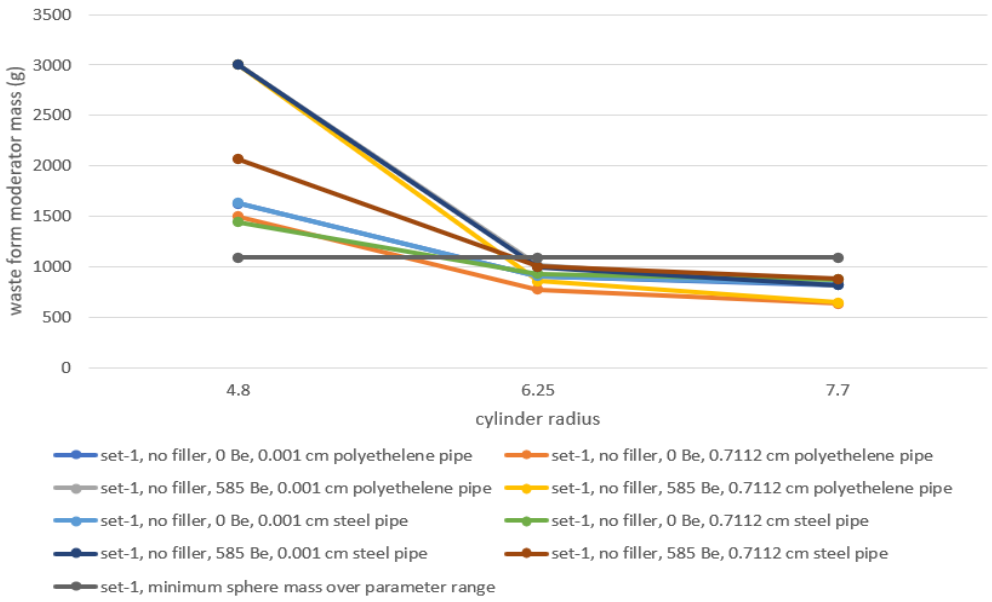

Figure 6.36. Subcritical moderator masses for evaluations in set-1 without filler vs. cylinder radius.

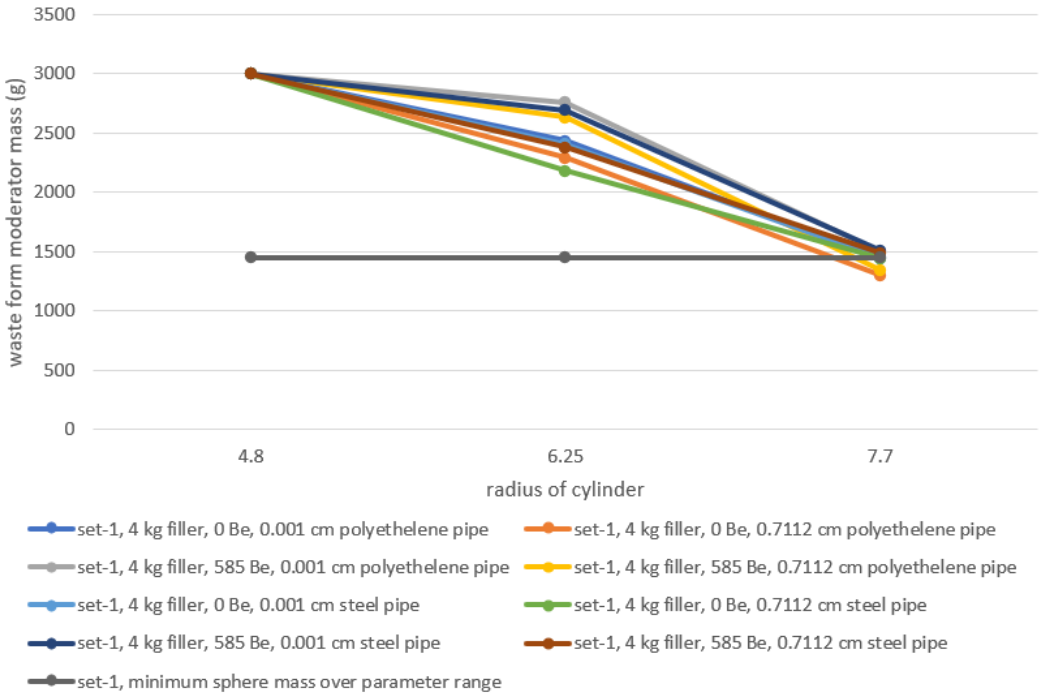

Figure 6.37. Subcritical moderator masses for evaluations in set-1 with filler vs. cylinder radius.

6.6.2 Set-1a Uniform Array of Waste Forms Stacked Three High with Wider Spacing

Table 6-4, Figure 6-38 and Figure 6-39 below shows the masses that were always associated with subcriticality in this study and did not produce k>1 for various types of scenarios evaluated in set-1a. These were determined in the same manner as the plot in Section 6.6.1, and they have similar trends and caveats overall. Due to the increased spacing in set-1a, upper subcritical masses are larger than those in set-1. This is due to the less restrictive assumption regarding horizontal compaction in the x-direction of the room.

Table 6.4. Moderator masses that did not produce $k > 1$ for evaluations in set-1a

Set-1a interpolated mass of waste form moderator (g)						
No filler mass						
Pipe material	**Pipe thickness (cm)**	**Be (g)**	**cyl R = 4.8**	**cyl R = 6.25**	**cyl R = 7.7**	**sph**
Polyethylene	0.001	0	No upper bound	1,448	1,107	1,634
Polyethylene	0.7112	0	No upper bound	1,216	905	1,625
Polyethylene	0.001	585	No upper bound	1,683	1,160	1,639
Polyethylene	0.7112	585	No upper bound	1,468	948	1,649
Steel	0.001	0	No upper bound	1,438	1,110	1,650
Steel	0.7112	0	No upper bound	1,458	1,189	1,560
Steel	0.001	585	No upper bound	1,719	1,165	1,658
Steel	0.7112	585	No upper bound	1,672	1,251	1,576
4 kg filler mass						
Pipe material	**Pipe thickness (cm)**	**Be (g)**	**cyl R = 4.8**	**cyl R = 6.25**	**cyl R = 7.7**	**sph**
Polyethylene	0.001	0	No upper bound	No upper bound	2,233	2,182
Polyethylene	0.7112	0	No upper bound	No upper bound	2,023	2,196
Polyethylene	0.001	585	No upper bound	No upper bound	2,372	2,169
Polyethylene	0.7112	585	No upper bound	No upper bound	2,152	2,184
Steel	0.001	0	No upper bound	No upper bound	2,264	2,186
Steel	0.7112	0	No upper bound	No upper bound	2,254	2,057
Steel	0.001	585	No upper bound	No upper bound	2,389	2,174
Steel	0.7112	585	No upper bound	No upper bound	2,377	2,058

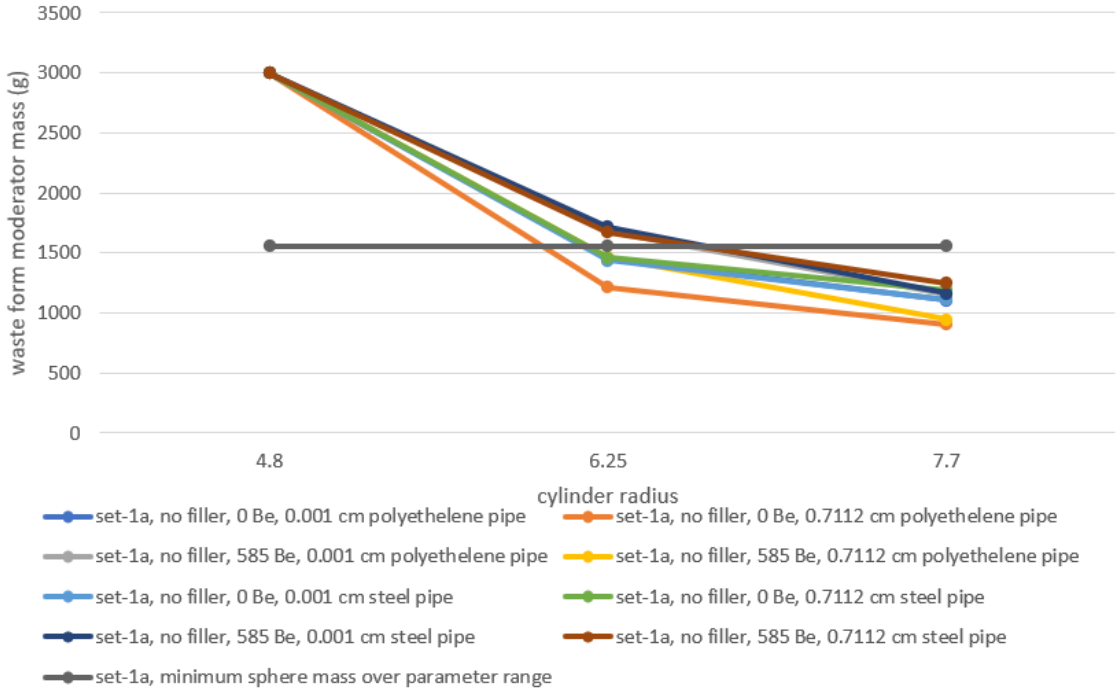

Figure 6.38. Subcritical moderator masses for evaluations in set-1a without filler vs. cylinder radius.

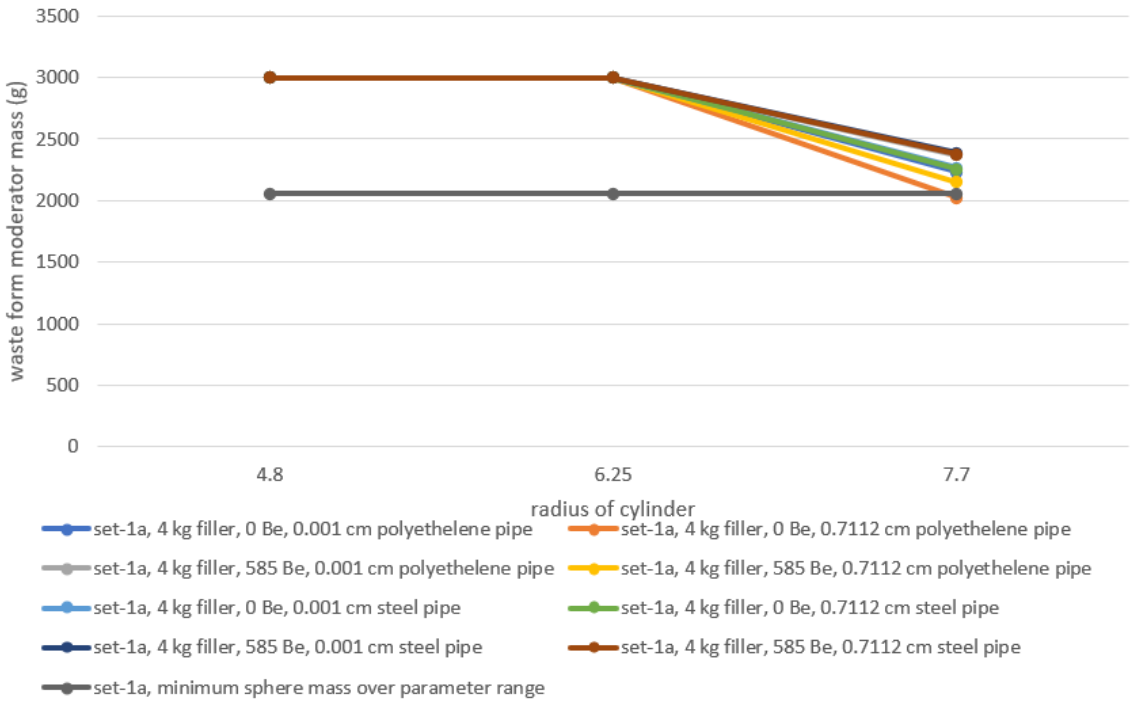

Figure 6.39. Subcritical moderator masses for evaluations in set-1a with filler vs. cylinder radius.

6.6.3 Set-2 Nonuniform Array of Waste Forms.

Table 6-5, Figure 6-40, and Figure 6-41 show upper subcritical moderator masses for set-2. Because individual waste forms are spaced farther apart compared to sets 1, 1a, 3, and 3a, the mass limits are higher. Other trends are roughly similar to set-1. This set has limited close contact between waste forms and is based on a sampling of 153 CCOs. It constitutes a best estimate array spacing assumption for the worst-case time step for the simulation at 1,000 years after emplacement.

Given that the neutron flux from a package tapers off quickly over half a meter (see Appendix K), the closest grouping of CCOs in a nonuniform array would be the most reactive. Assuming fair odds and representative sampling, roughly one stack of three waste forms would occur in a collection of 153^2 (over 20,000) waste forms. Thus, for such a case, set-1 or set1a may provide k_{eff} values and mass limits that better approximate a realistic configuration that includes a triple-stack of compacted CCOs.

Table 6.5. Masses that did not produce $k > 1$ for evaluations in set-2

Set-2 interpolated mass of waste form moderator (g)						
No filler mass						
Pipe material	**Pipe thickness (cm)**	**Be (g)**	**cyl R = 4.8**	**cyl R = 6.25**	**cyl R = 7.7**	**sph**
Polyethylene	0.001	0	2849	2,015	1,997	1,893
Polyethylene	0.7112	0	2702	1,947	1,930	1,806
Polyethylene	0.001	585	No upper bound	2,072	1,936	1,876
Polyethylene	0.7112	585	2994	1,954	1,871	1,792
Steel	0.001	0	2805	2,059	2,018	1,897
Steel	0.7112	0	2262	1,791	1,811	1,722
Steel	0.001	585	No upper bound	2,073	1,980	1,867
Steel	0.7112	585	2457	1,849	1,774	1,693
4 kg filler mass						
Pipe material	**Pipe thickness (cm)**	**Be (g)**	**cyl R = 4.8**	**cyl R = 6.25**	**cyl R = 7.7**	**sph**
Polyethylene	0.001	0	No upper bound	No upper bound	2,481	2,259
Polyethylene	0.7112	0	No upper bound	No upper bound	2,384	2,198
Polyethylene	0.001	585	No upper bound	No upper bound	2,546	2,230
Polyethylene	0.7112	585	No upper bound	No upper bound	2,394	2,132
Steel	0.001	0	No upper bound	No upper bound	2,520	2,271
Steel	0.7112	0	No upper bound	2,704	2,207	2,059
Steel	0.001	585	No upper bound	No upper bound	2,496	2,229
Steel	0.7112	585	No upper bound	2,727	2,235	2,022

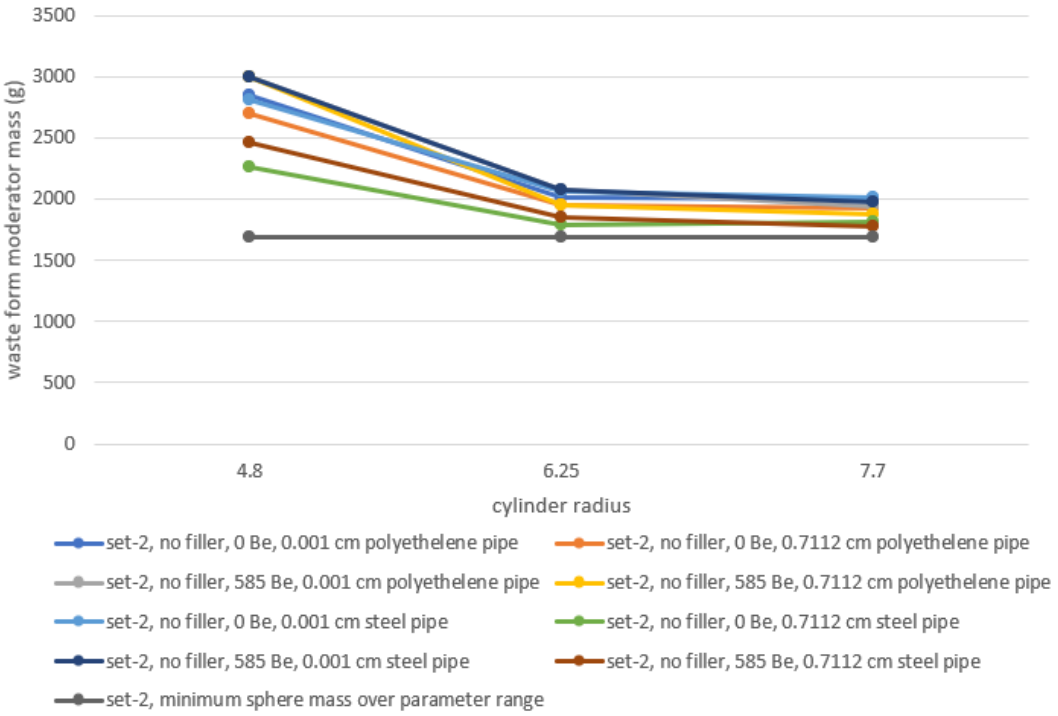

Figure 6.40. Subcritical masses for evaluations in set-2 without filler vs. cylinder radius.

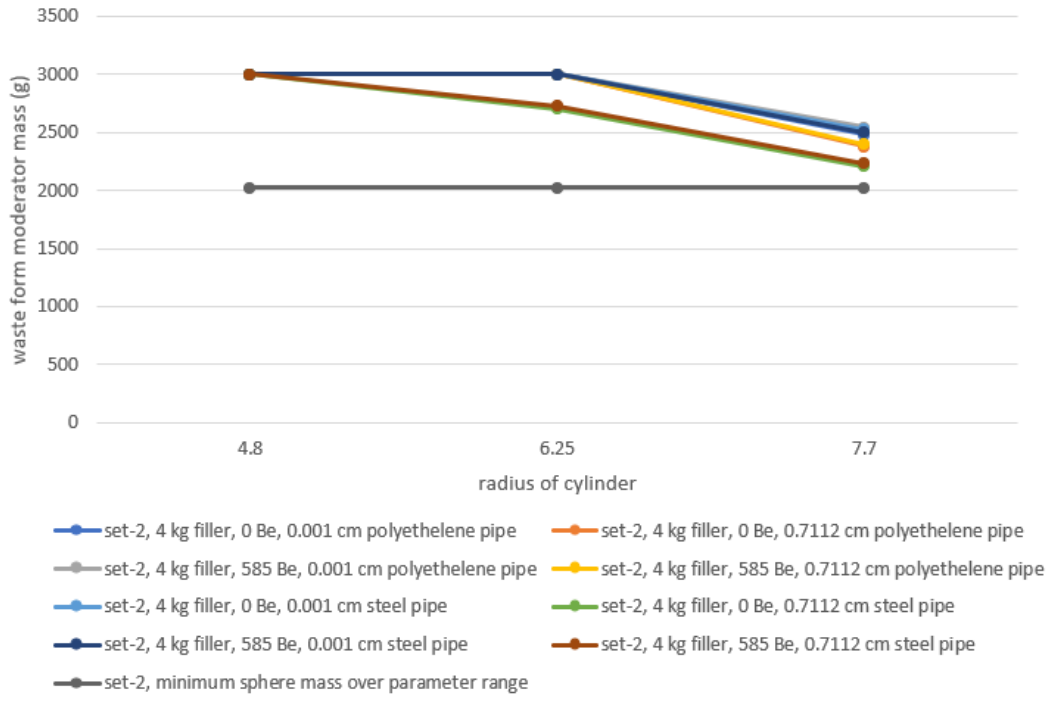

Figure 6.41. Subcritical masses for evaluations in set-2 with filler vs. cylinder radius.

6.6.4 Set-3 Uniform Array of Waste Forms Stacked Six High with Closer Spacing

Table 6-6, Figure 6-42, and Figure 6-431 show upper subcritical moderator masses for set-3. Set-3 is similar to Set-1 with the exception that it subdivides the contents of each CCO into two waste forms. Masses are listed per CCO. Dividing by 2 gives masses per waste form. The trends are roughly similar to those for set-1, especially for cylinders, which stack to form a similar geometry to set-1, with the exception that there are six cylinders rather than three, and therefore more discrete reflector material.

Table 6.6. Masses that did not produce $k > 1$ for evaluations in set-3

Set-3 interpolated mass of waste form moderator (g) per CCO (2 waste forms per CCO)						
No filler mass						
Pipe material	**Pipe thickness (cm)**	**Be (g)**	**cyl R = 4.8**	**cyl R = 6.25**	**cyl R = 7.7**	**sph**
Polyethylene	0.001	0	1,599	906	825	1,692
Polyethylene	0.7112	0	1,569	675	427	1,853
Polyethylene	0.001	585	No upper bound	1,006	826	1,736
Polyethylene	0.7112	585	No upper bound	765	436	1,907
Steel	0.001	0	1,633	906	823	1,700
Steel	0.7112	0	1,813	1,140	1,076	1,655
Steel	0.001	585	No upper bound	992	825	1,765
Steel	0.7112	585	No upper bound	1,226	1,095	1,717
4 kg filler mass						
Pipe material	**Pipe thickness (cm)**	**Be (g)**	**cyl R = 4.8**	**cyl R = 6.25**	**cyl R = 7.7**	**sph**
Polyethylene	0.001	0	No upper bound	2,398	1,447	2,445
Polyethylene	0.7112	0	No upper bound	2,316	1,131	2,697
Polyethylene	0.001	585	No upper bound	2,691	1,474	2,488
Polyethylene	0.7112	585	No upper bound	2,689	1,205	2,775
Steel	0.001	0	No upper bound	2,385	1,449	2,443
Steel	0.7112	0	No upper bound	2,613	1,710	2,332
Steel	0.001	585	No upper bound	2,728	1,493	2,484
Steel	0.7112	585	No upper bound	2,928	1,762	2,368

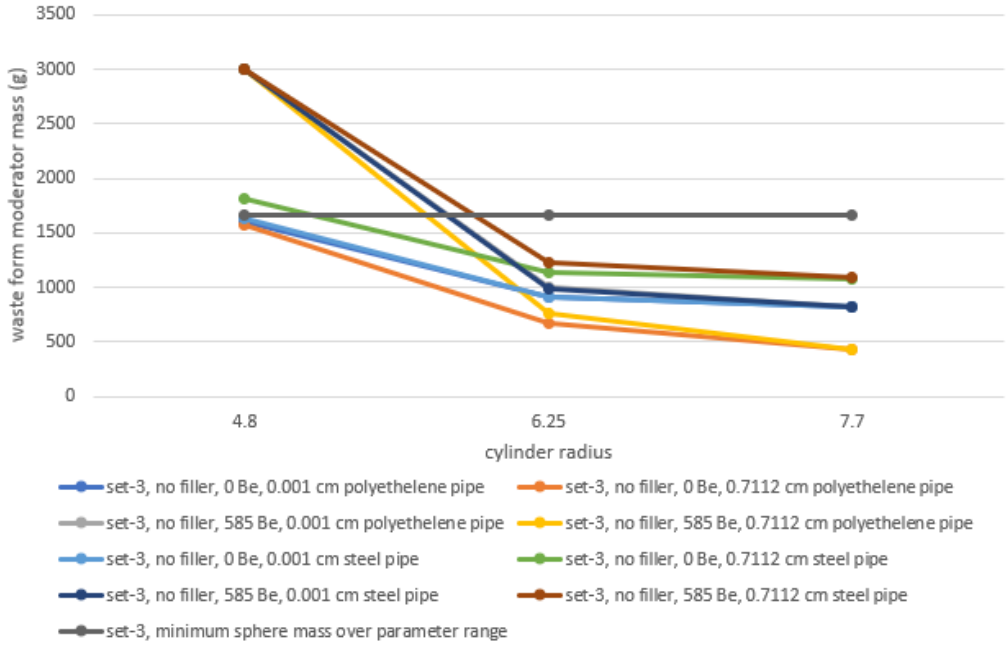

Figure 6.42. Subcritical masses for evaluations in set-3 without filler vs. cylinder radius.

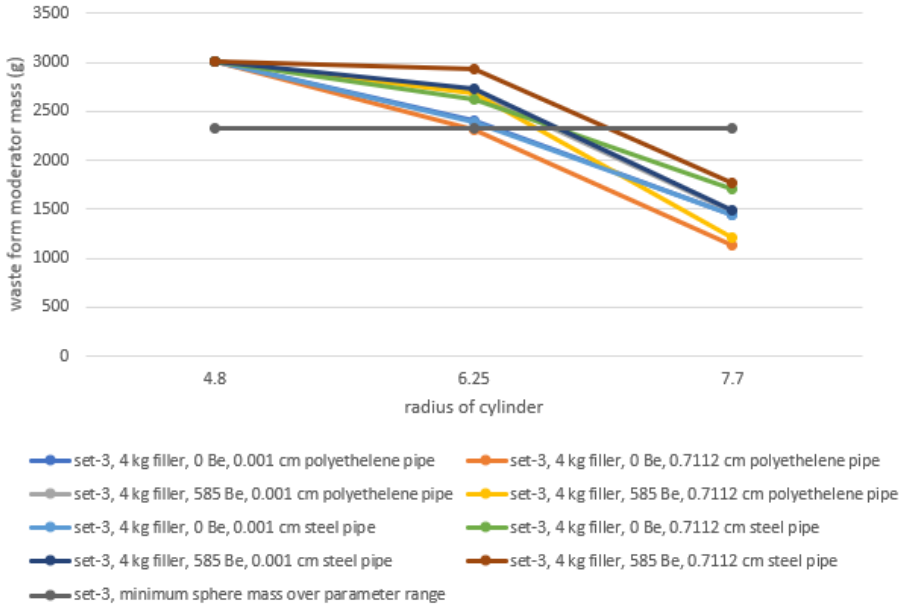

Figure 6.43. Subcritical masses for evaluations in set-3 with filler vs. cylinder radius.

6.6.5 Set-3a Uniform Array of Waste Forms Stacked Six High with Wider Spacing

Table 6-7, Figure 6-44, and Figure 6-45 show upper subcritical moderator masses for set-3a. Set-3a is similar to Set-1a with the exception that it subdivides the contents of each CCO into two waste forms. Masses are listed per CCO. Dividing by 2 gives masses per waste form. The trends are roughly similar to set-1a, especially for cylinders, which stack to form a similar geometry to set-1a, with the exception that

there are six cylinders rather than three, and therefore more discrete reflector material. Set-3a has a larger spacing than set-3, so it has higher upper moderator masses.

Table 6.7. Masses that did not produce $k > 1$ for evaluations in set-3a

Set-3a interpolated mass of waste form moderator (g) per CCO (2 waste forms per CCO)						
No filler mass						
Pipe material	**Pipe thickness (cm)**	**Be (g)**	**cyl R = 4.8**	**cyl R = 6.25**	**cyl R = 7.7**	**sph**
Polyethylene	0.001	0	No upper bound	1,447	1,106	2,596
Polyethylene	0.7112	0	No upper bound	1,187	704	2,785
Polyethylene	0.001	585	No upper bound	1,694	1,158	2,691
Polyethylene	0.7112	585	No upper bound	1,430	767	2,903
Steel	0.001	0	No upper bound	1,450	1,103	2,628
Steel	0.7112	0	No upper bound	1,890	1,523	2,560
Steel	0.001	585	No upper bound	1,701	1,149	2,720
Steel	0.7112	585	No upper bound	2,131	1,597	2,662
4 kg filler mass						
Pipe material	**Pipe thickness (cm)**	**Be (g)**	**cyl R = 4.8**	**cyl R = 6.25**	**cyl R = 7.7**	**sph**
Polyethylene	0.001	0	No upper bound	No upper bound	2,256	No upper bound
Polyethylene	0.7112	0	No upper bound	No upper bound	1,940	No upper bound
Polyethylene	0.001	585	No upper bound	No upper bound	2,389	No upper bound
Polyethylene	0.7112	585	No upper bound	No upper bound	2,091	No upper bound
Steel	0.001	0	No upper bound	No upper bound	2,278	No upper bound
Steel	0.7112	0	No upper bound	No upper bound	2,767	No upper bound
Steel	0.001	585	No upper bound	No upper bound	2,374	No upper bound
Steel	0.7112	585	No upper bound	No upper bound	2,949	No upper bound

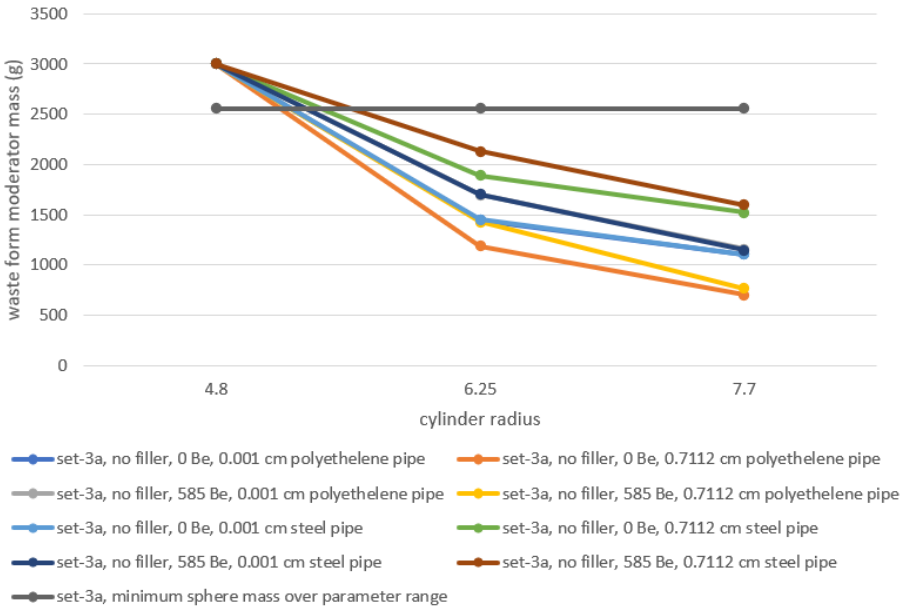

Figure 6.44. Subcritical masses for evaluations in set-3a without filler vs. cylinder radius.

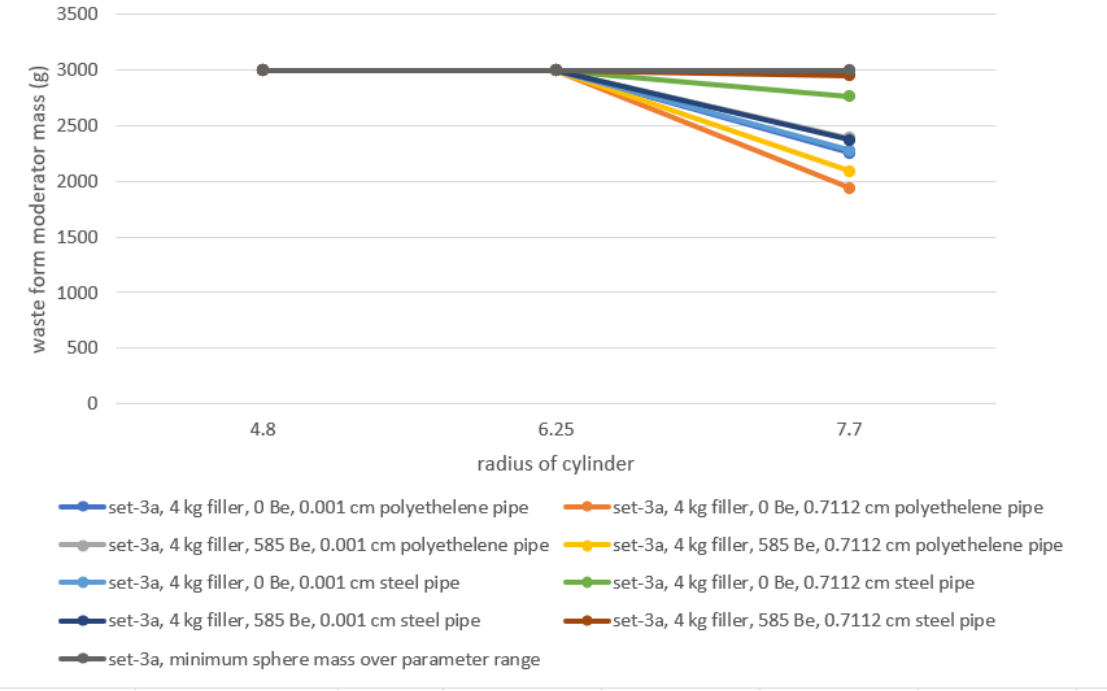

Figure 6.45. Subcritical masses for evaluations in set-3a with filler vs. cylinder radius.

6.7 EFFECT OF WASTE FORM HETEROGENEITY

The criticality safety analysis presented in this report uses the same assumption regarding waste form mixtures being uniformly mixed that was used by Saylor [3] and Brickner [4]. To provide additional technical justification for that uniform mixing assumption, studies are presented in Appendix J which constitute set-4. Specifically, the purpose of Appendix J is to evaluate the validity of the assumption that the PuO_2 is uniformly mixed within the waste form. This evaluation examines the effect of locally increased fissile concentration in the waste from in terms of k_{eff}. This appendix is not intended to address all possible heterogeneous configurations, but only a selection of cases that correspond to the analyses performed and which cover a range of sizes which would allow larger particle sizes within a mixture to be acceptable.

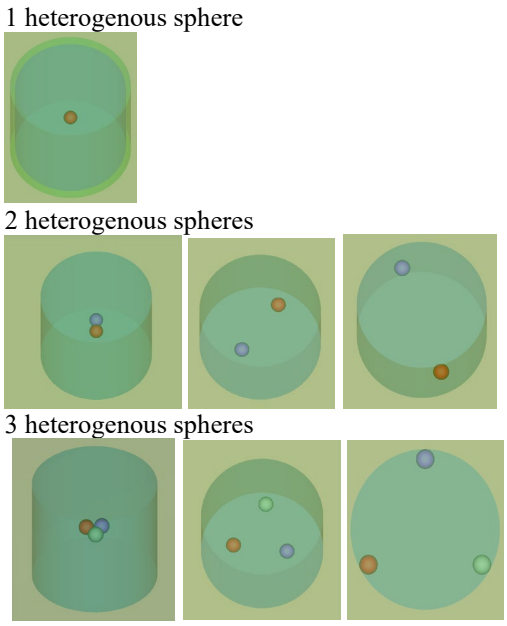

Figure 6.46. Diagram of the various heterogenous sphere cases and spacings.

Appendix J evaluates the assumption that a uniform mixture for the waste form is acceptable by evaluating a unit cylindrical waste form (with set-2-uh subset 2-4 parameters, i.e., polyethylene waste form moderator, polyethylene discrete reflector, and graphite filler material) with variations in the number, size, and location of pure PuO_2 spheres (heterogenous spheres) embedded in a mixture of filler and PuO_2. Spheres are used because the neutron leakage is bounding compared to similar sized chunks of FGE. Geometries evaluated are shown in Figure 6.46.

The results presented in Appendix J and summarized in Figure 6.47 below for the worst-case configuration show that the heterogeneity may have some positive reactivity impact for waste form cases which are under-moderated and in which the impact to k_{eff} is not significant because these cases are very subcritical.

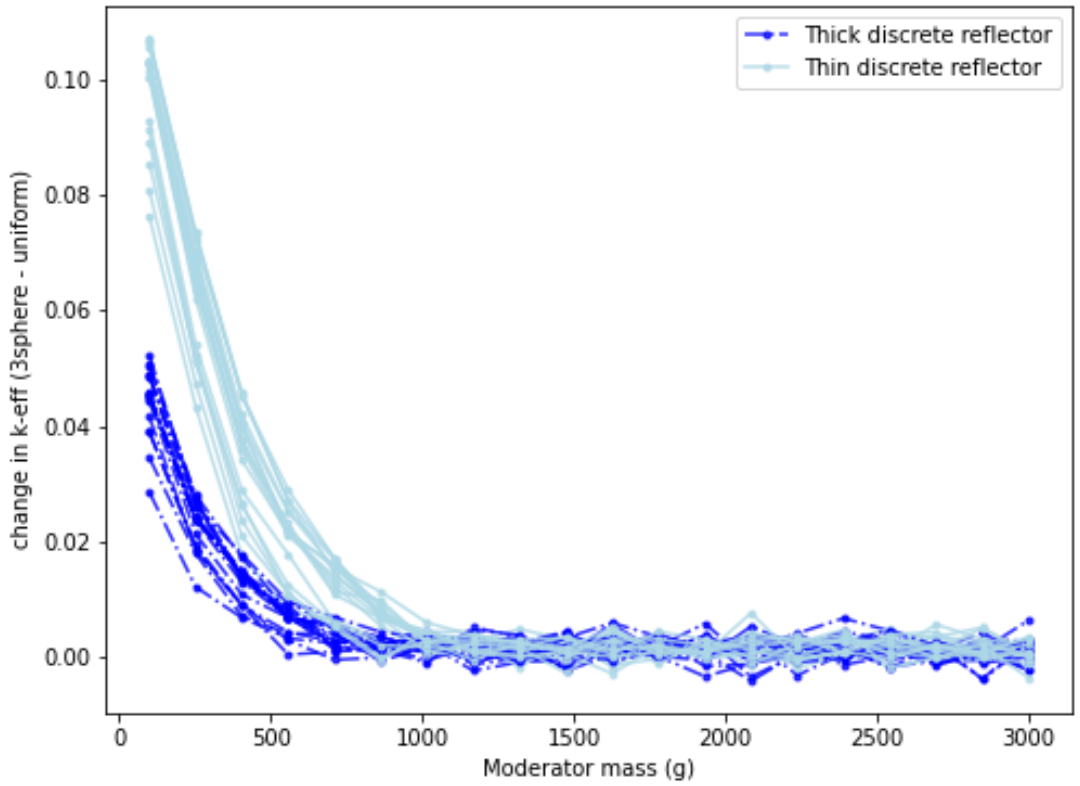

Figure 6.47. Delta-k_{eff} when comparing highest reactivity three-sphere case to a uniform case (positive values correspond to cases in which the highest reactivity three-sphere configuration has higher k_{eff} than uniform configuration.

6.8 STUDY OF NEUTRON TRANSMISSION FROM CCO SOURCE THROUGH INTERSTITIAL MEDIA

The interstitial material between the waste forms plays a significant part in overall system reactivity. Given the predominance of salt and MgO in that interstitial mixture, study results are presented in Appendix K which evaluate the transmission of neutrons from the waste form through this media. Specifically, the results in Appendix K evaluate the sphere of influence of a waste form assuming a waste form in a cuboid of material. The waste form itself is not of particular importance here because the primary concern is the rate at which neutron flux tapers (magnitude goes down) in the salt/MgO mixture.

The results in Appendix K provide neutron intensities at various distances for various types of interstitial reflector media and are shown in Figure 6.48 below. When neutrons escape from a waste form, the neutron intensity decreases roughly exponentially, which is consistent with the solution to the diffusion equation for a point source in non-multiplying media [15]. Note that the waste form used in this study is assumed to be a sphere with a 10 cm diameter.

As seen in Figure 6.48 below, the flux at the waste form's surface decreases by a factor of 10 in the first 20 cm outside the waste form. An important conclusion to be drawn from this result is that t a few closely spaced packages may locally produce higher values of reactivity.

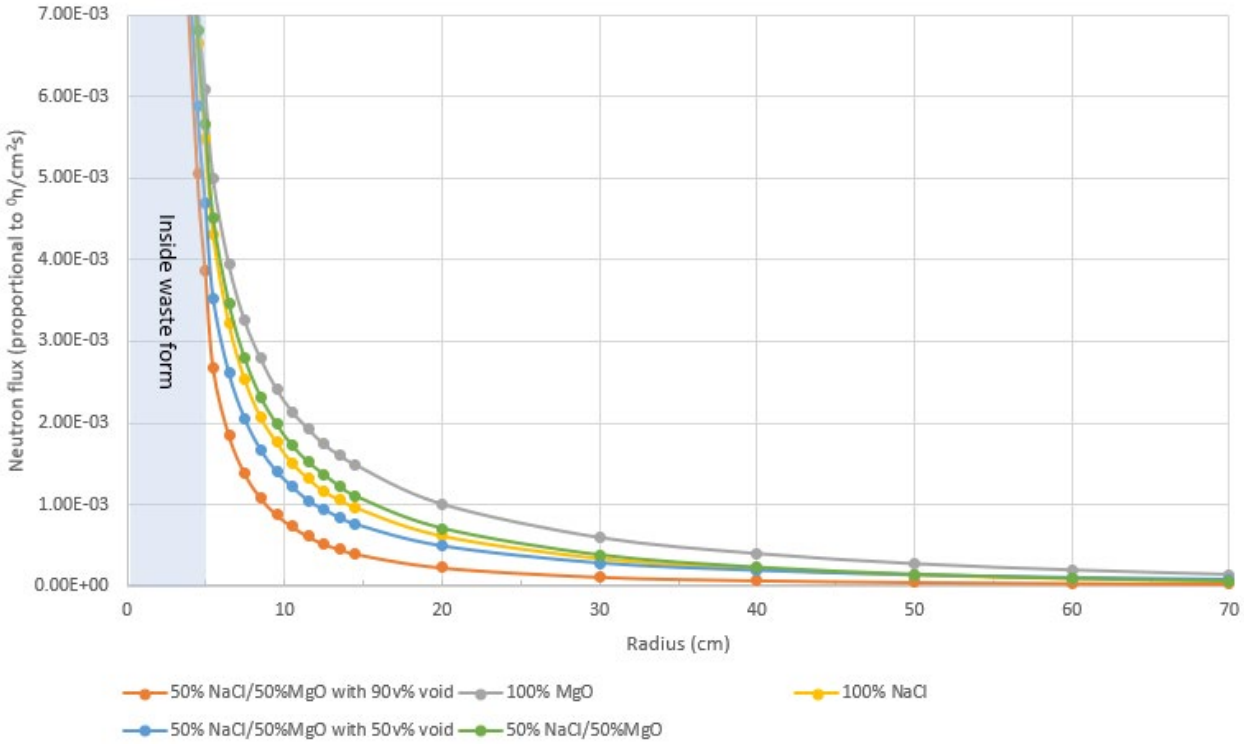

Figure 6.48. Flux per source particle at various distances in the salt form the source (linear scale).

6.9 STUDIES ON THE REACTIVITY EFFECT OF BRINE AND THE ASSUMPTIONS RELATED TO INTERSTITIAL REFLECTOR MATERIAL DENSITY AND COMPOSITION

The criticality safety analysis in this report uses a specific mixture of salt and MgO for the interstitial material between waste forms. To provide additional technical justification for that assumption and to include studies with brine as an interstitial material, the reactivity effects of various interstitial material assumptions were examined using set-5 nomenclature, as shown in Appendix L.

For the results presented in Appendix L, the compositions interstitial material were perturbed. This included altering the material densities, modifying the mixing ratio of salt and MgO, and evaluating the reactivity effect of a brine intrusion. Full sets of parametric sweeps were evaluated for nine different interstitial reflector types. For the case with the brine intrusion into the waste form mixture itself (case 5h), the brine mixture replaces the filler mass (graphite is replaced by brine). Set-2-uh, the nonuniform array for the upper horizon calculations, provided the baseline configuration.

The results in Appendix L show that the assumptions for the salt and MgO mixture density used in the criticality safety analysis in this report are conservative for moderator loadings in excess of 200 g. The results in Appendix L also show that the effect of brine replacing the interstitial material was seen to largely decrease k_{eff}, summarized below in Figure 6.49. However, this trend does not hold for under-moderated waste forms. For cases in which the brine cases exceeded k_{eff} values of set-2, the moderator

contents were at moderator masses below approximately 200 g, and they did not increase k_{eff} above that of set-2 at 200 g of moderator.

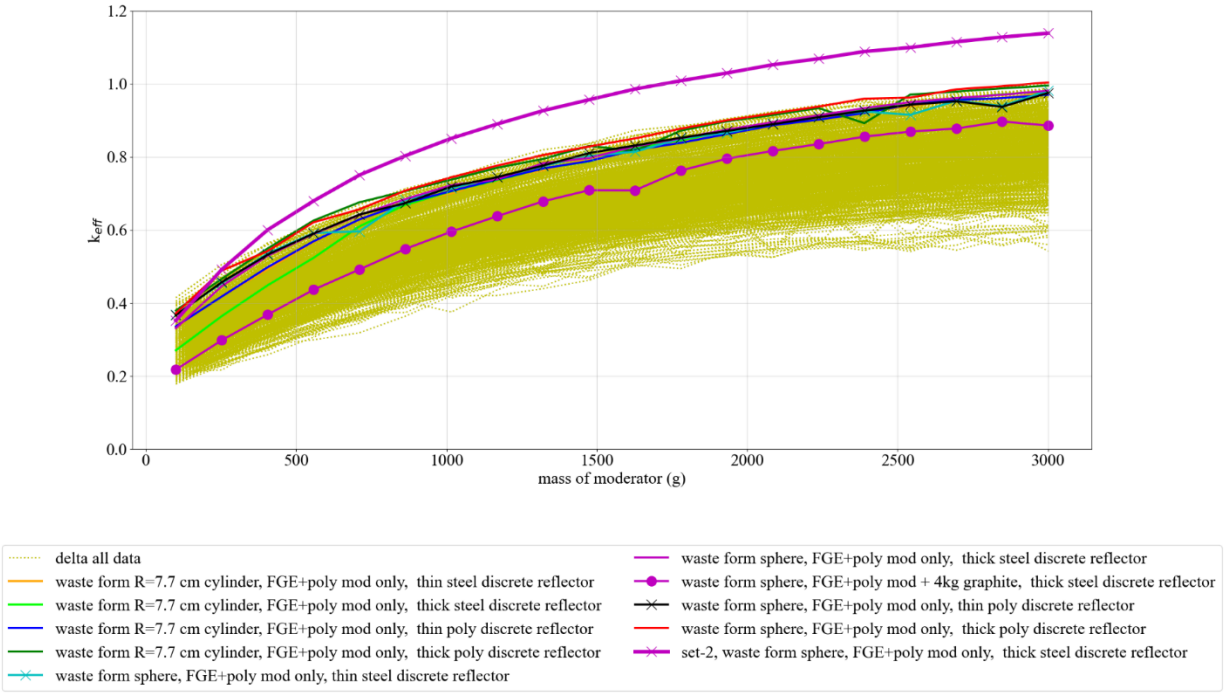

Figure 6.49. Reactivity of set-5e compared to a single set-2 representative curve to evaluate the effect of brine (no MgO) as interstitial reflective material.

Of the set-5 cases, the effect of brine intrusion into waste forms had the largest positive effect on k_{eff}. It increased k_{eff} at moderator compositions below 600 g, but at no time did the k_{eff} values exceed the set-2 k_{eff} at 600 g of moderator. In other words, k_{eff} was shown to increase only when the system was already deeply subcritical.

The effect of replacing MgO with NaCl slightly decreased k_{eff} in all cases evaluated, supporting the assumption that the interstitial material is at 100% density.

Decreasing the density of interstitial material decreased k_{eff} in all cases evaluated, supporting the assumption that the interstitial material is at 100% density.

6.10 STUDIES WITH ADDITIONAL CENTROID LOCATIONS FOR VARIOUS CONTAINER DESIGNS AND INITIAL SPATIAL ARRANGEMENTS (APPENDIX M)

As previously discussed, the CCO arrive for emplacement in seven-packs, which resemble a hexagonal array (shown in Figure 4-3). For conservatism, the uniform arrays arrange the packages in a triangular pitch, as discussed in Section 4.2.1.1, which conservatively adds more waste forms to the system. The compaction studies from Reedlunn and Bean [8] that provide the centroid locations of the compacted containers considered hexagonal pitched arrays at time = 0 as a starting point for the simulations. Of some interest is the potential impact of beginning those same compaction studies with the containers in a triangular pitch at time = 0 because then the comparison between the uniform arrays and nonuniform arrays have more technical commonality, and the additional number of containers in the compacted

models (167 vs. 152) provides results that have more mass (i.e., more centroids) for the set-2 studies in nonuniform arrays.

Of additional interest is the evaluation of centroid data for other container designs, specifically the POCs evaluated in Brickner [4], using the same methodology outlined in this report—that is, not modifying the parametric sweeps to be specific to the POC designs but applying the CCO sweeps to the centroids provided by the other container while using the lower FGE for the POC (200 g). The main interest is to provide more technical justification that the reactivity of the system using the compaction data centroids in Table 4-4 is not highly susceptible to variations in initial starting conditions for the compaction analysis.

Furthermore, the evaluation provided in Appendix K was used in Reedlunn and Bean [46] to define a method that predicts maximum reactivity locations using the centroid datasets directly. Therefore, a small subset of the calculations presented in Appendix M is used to generate flux maps and maximum reactivity orthogonal locations in the model for comparison purposes to that method in Reedlunn and Bean [46]. Finally, the additional datasets provide additional means to further evaluate (Appendix E) the studies that were performed to show the effect of the two boundary conditions for these models.

To address these interests, additional centroid datasets were provided in Reedlunn and Bean [46]. These data include CCO centroid locations for simulations that begin in a triangular pitch (yields 167 centroids) and POCs for both hexagonal and triangular pitch simulations scenarios. The differences between the CCO and POC are presented generically in Figure 6.50.

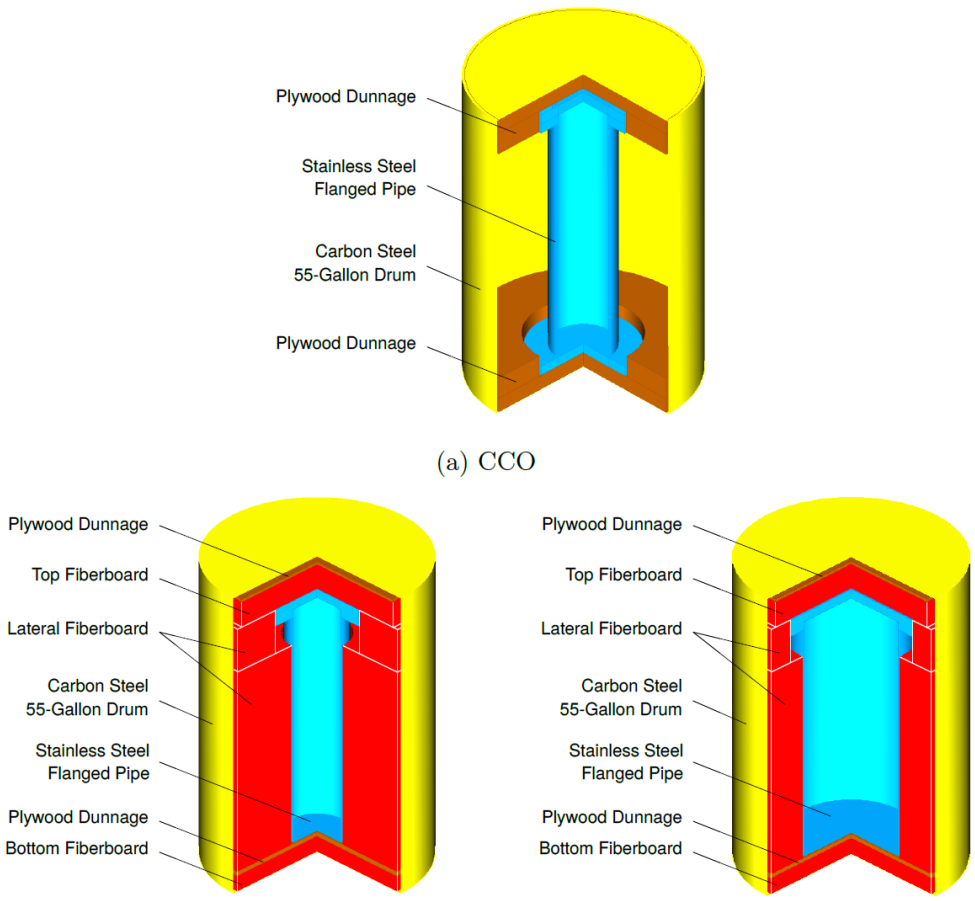

Figure 6.50. Diagrams of the CCO compared with the POCs evaluated in Appendix M (used with permission from Reedlunn and Bean [46]).

Although the CCO and POC are similar, design differences exist. Additional POC design information is available in Brickner [4]. Although the various POC package dimensions and materials are different, the actual values fall within the range of the parametric sweeps used.

The data provided and additional information, including results, are presented in Appendix M and summarized in Figure 6.51 and Figure 6.52.

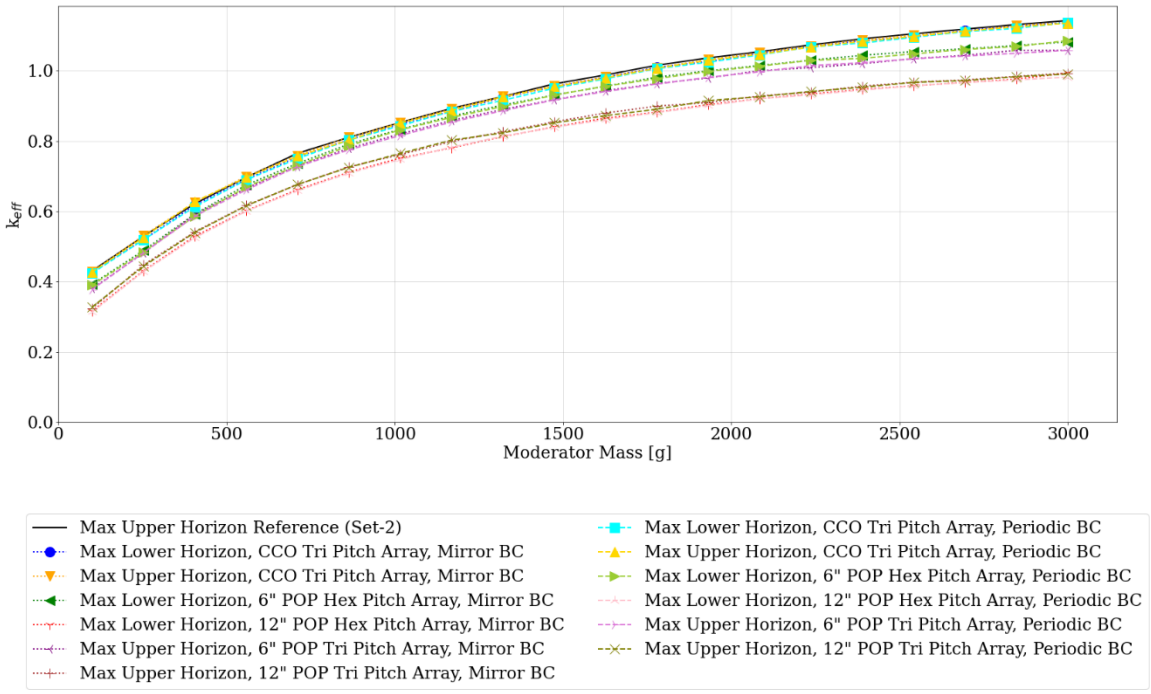

Figure 6.51. Max k_{eff} of all subsets of all CCO and POC centroid configurations at time = 1,000 years compared with max k_{eff} of all subsets of set-2-uh hexagonal pitch (mirror boundary conditions) as k_{eff} vs. moderator mass, time = 1,000 years.

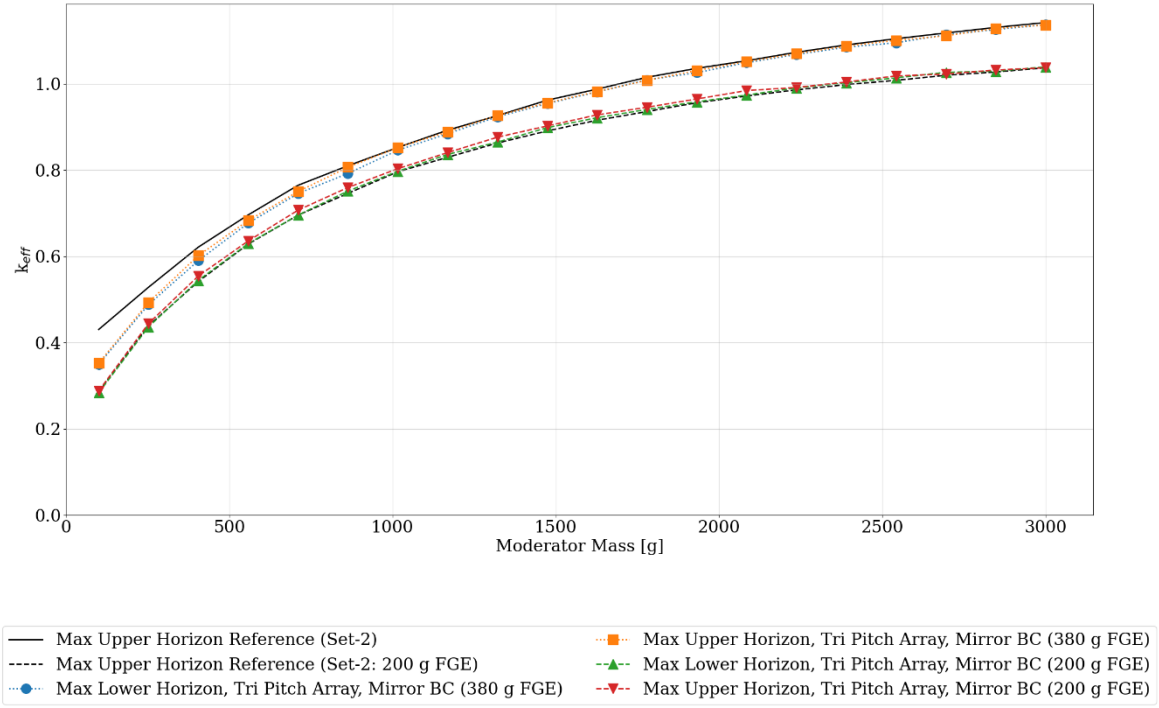

Figure 6.52. Comparison of the effect of FGE on the maximum k_{eff} of all subsets of all CCO and POC centroid configurations at time = 1,000 years (mirror boundary conditions).

6.11 STUDIES TO EVALUATE THE IMPACT OF LARGER DISCRETE REFLECTOR THICKNESSES (APPENDIX O)

As previously discussed in Section 4.2.2, two discrete reflector thicknesses were used in the analysis in this report to evaluate the reactivity impact of various materials. Of interest is the evaluation of thicker discrete reflectors because the discrete reflector model allows materials that may be compacted directly adjacent to the waste form to be evaluated. These studies are presented in Appendix O and summarized in Figure 6.53 and Figure 6.54.

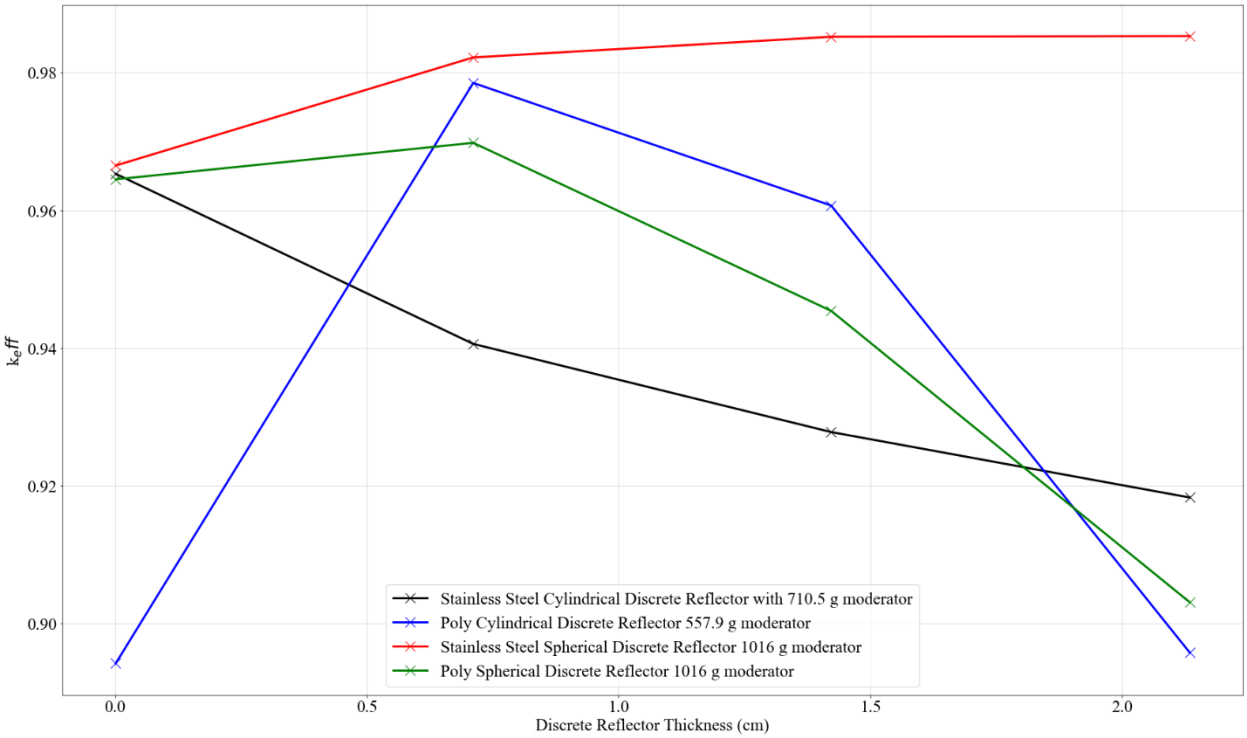

Figure 6.53. Set-8a and set-1 maximum k_{eff} results (three-high uniform array model) overall sublistings as a function of discrete reflector thickness.

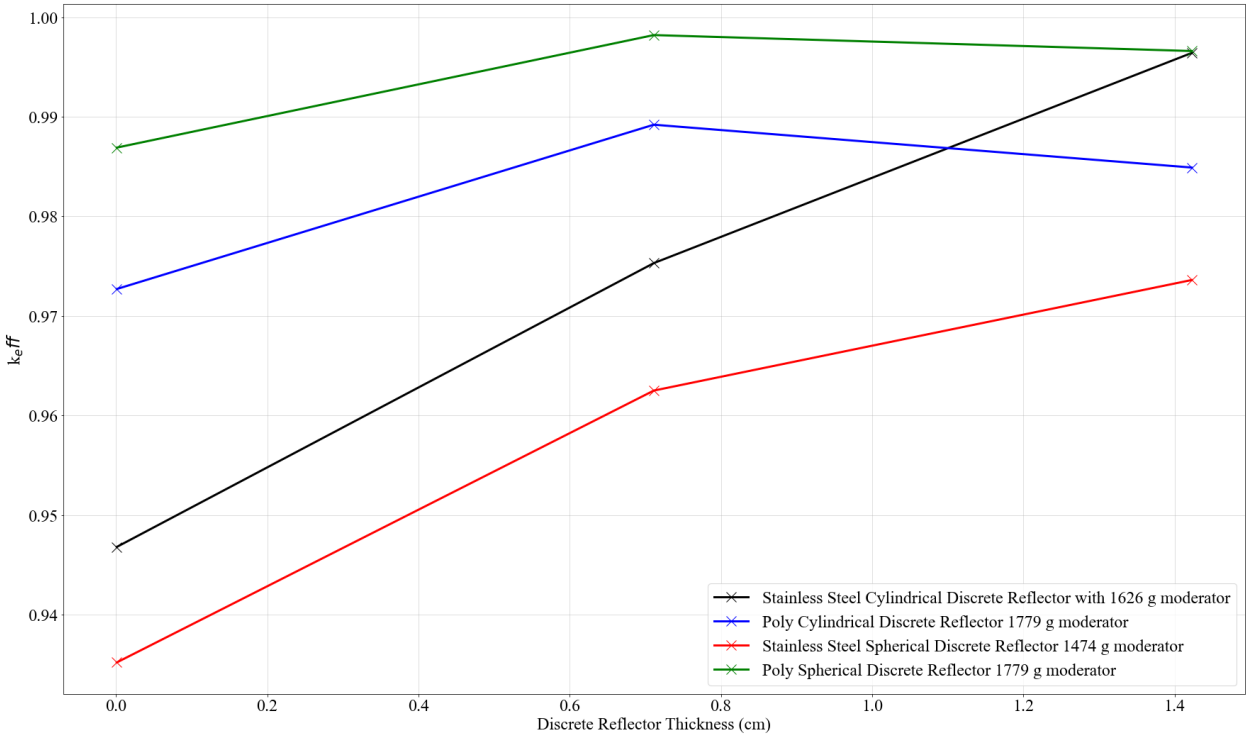

Figure 6.54. Set-8b and set-2-uh maximum k_{eff} results (nonuniform array model) overall sublistings as a function of discrete reflector thickness.

6.12 STUDIES TO EVALUATE VARIOUS AMOUNTS OF B_4C MIXED UNIFORMLY IN THE WASTE FORM (APPENDIX N).

As previously discussed in Section 6 and shown in Table 6-2, a subset of calculations in this report considered 50 g of B_4C mixed uniformly with the waste form. Additional calculations are provided in Appendix O to show the complete set of parametric sweeps with various amounts of B_4C to provide more technical justification for using B_4C as control. These studies are presented in Appendix N and summarized in Figure 6.55 through Figure 6.58.

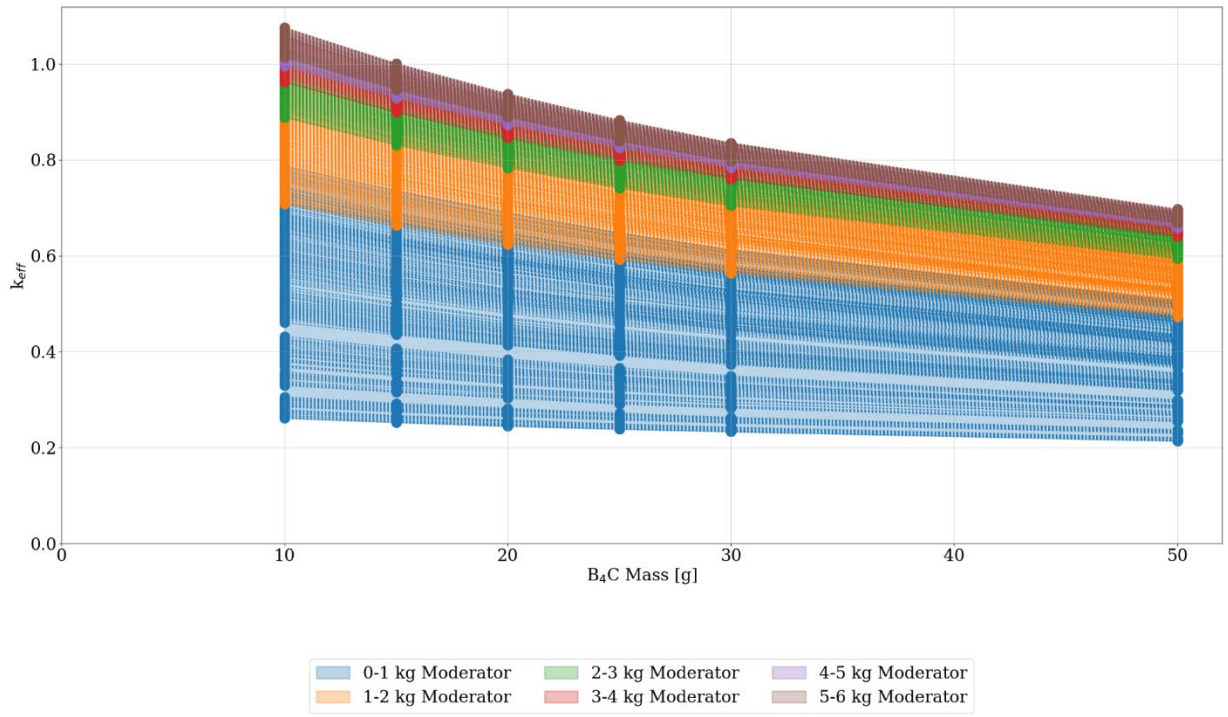

Figure 6.55. Set-7a results (three-high uniform array model) for 10, 15, 20, 25, 30, and 50 g of B_4C for all subcases. Reactivity trends of all subcase-10 as k_{eff} as a function of B_4C mass.

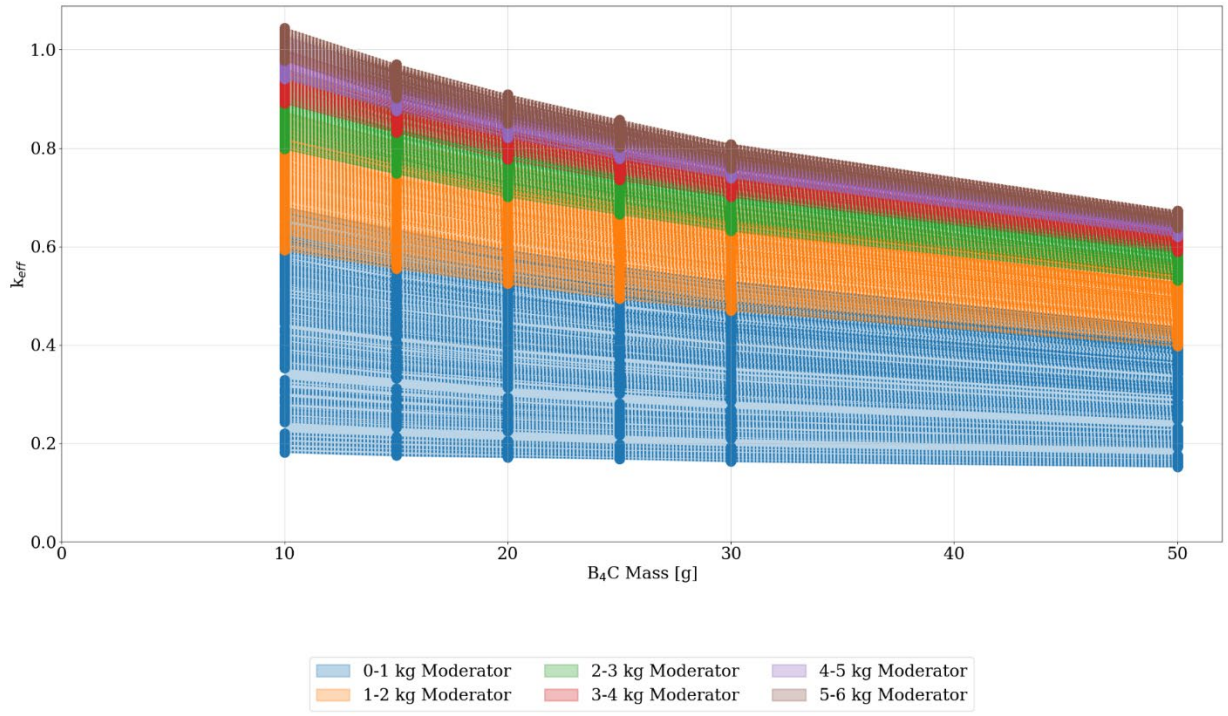

Figure 6.56. Set-7c results (nonuniform array model) for 10, 15, 20, 25, 30, and 50 g of B_4C for up to a 6 kg moderator. Reactivity trends of subcase-10 as k_{eff} as a function of B_4C mass.

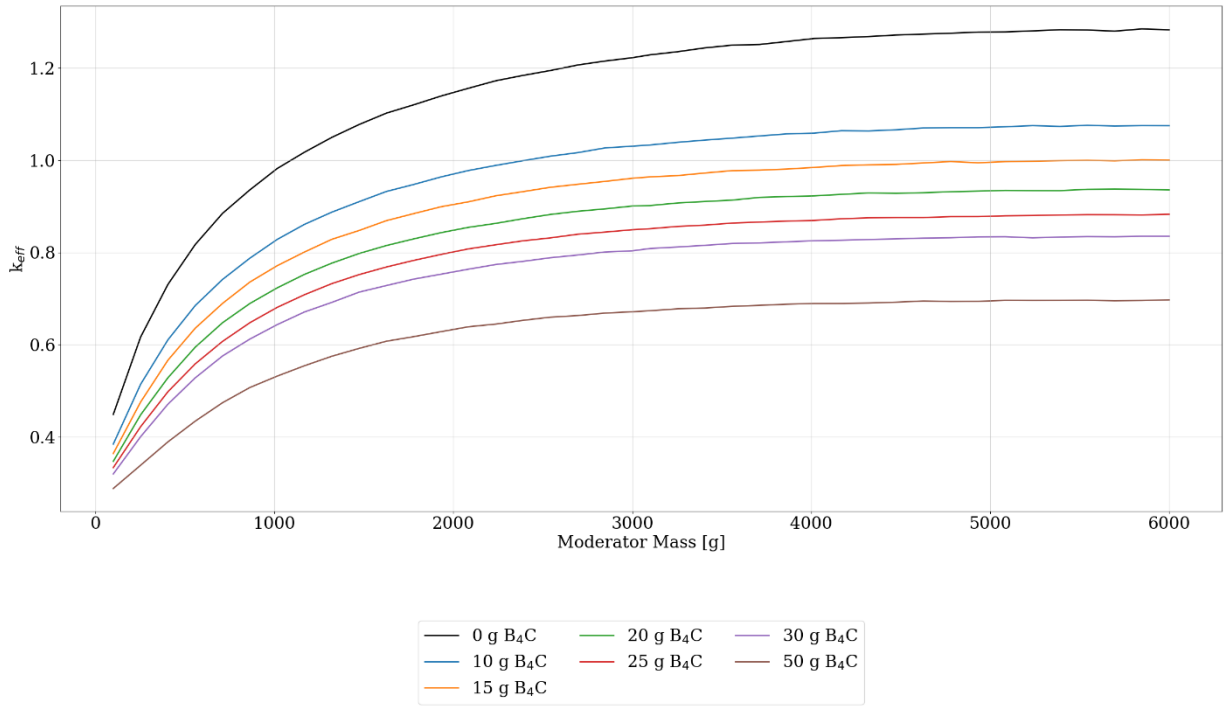

Figure 6.57. Set-7a results (three-high array model) for 10, 15, 20, 25, 30, and 50 g of B_4C for up to a 6 kg moderator. Reactivity trends of subcase-14 as k_{eff} as a function of B_4C mass.

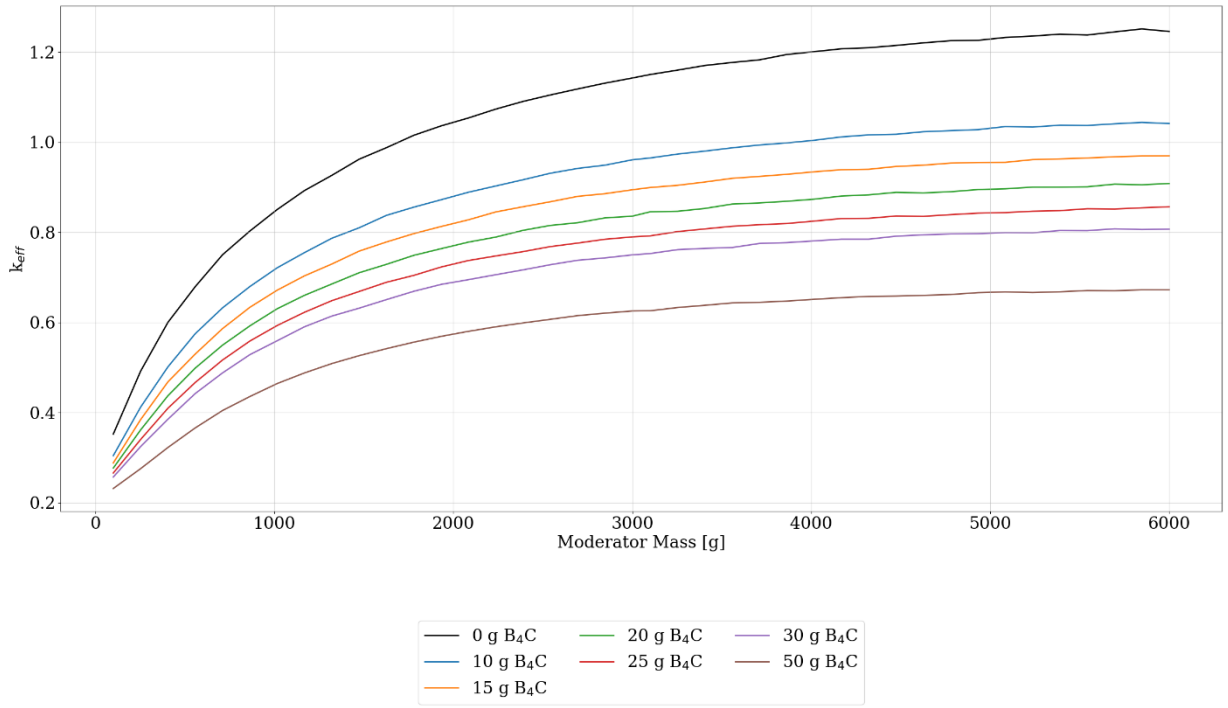

Figure 6.58. Set-7c results (nonuniform array model) for 10, 15, 20, 25, 30, and 50 g of B_4C for up to a 6 kg moderator. Reactivity trends of subcase-14 as k_{eff} as a function of B_4C mass.

6.13 DISCUSSION REGARDING THE EXTENSION OF THE TSUNAMI VALIDATION TO ANALYSIS DATASETS

The criticality calculations in this report were validated using the TSUNAMI sequence in the SCALE code package. Because of the many calculations performed and the resource-consuming nature of the TSUNAMI method, the validation documented in Appendix H considers a small subset of cases entirely from set-1 (subcase 1-8). This section discusses how the Appendix H validation may be extended to all the results in this analysis. As an example, set-2-uh subcase 10 (set-2-10-uh) is used in the following discussion.

When performing a validation, one important step is determining the "area of applicability" of the validation and limitations. NUREG/CR-6698, *Guide for Validation of Nuclear Criticality Safety Calculational Methodology* [47], provides insight into parameters to consider for determining the area of applicability. This is typically used to select nuclear criticality experiments in which bias and bias uncertainty are determined for nuclear criticality applications.

The key physical parameters when defining the area of applicability include the materials, geometry, and neutron energy. Table 2.3 of NUREG/CR-6698 [47] describes these three parameters. If set-2-10-uh is within the area of applicability of set-1-2 per NUREG/CR-6698, then this would imply that the bias and bias uncertainty determined for set-1-2 would be applicable for set-2-10-uh. First, the parameters evaluated for set-2-uh-10 compared with the closest set-1 case (Appendix H) that parameterizes the same materials were consider.

Table 6.8. Comparison of set-2-10-uh parameters with set-1-2 parameters.

Case	Model type	Waste form shape	Waste form moderator	Filler material	Metal in filler discrete reflector	Discrete reflector
Set-2-10-uh	Nonuniform array with centroids based on upper horizon data. Centroid from pipe center is used as the point in center of base of cylinders or the center of spheres.	Sphere (radius defined by volume of mass)	Poly	Graphite	Stainless steel	Steel
Set-1-2	Uniform array stacked three high with CCO pitch reduction. x = 50%, y = 10%, and z = no space.	Cylinder (radius range 4.8, 6, and 7.7 and height defined by total volume of mass)	Poly	Graphite	Stainless steel	Steel

Because the physical parameters within Table 2.3 of NUREG/CR-6698 [47] show sufficient agreement between set-1-2 and set-2-10-uh for the fissionable materials, moderation material within fuel, interstitial moderation, reflector material, and absorber material (i.e., all the parameters and materials are evaluated the same), the only sections that need additional discussion are the geometry and neutron energy.

For geometry, NUREG/CR-6698 [47] notes that the geometry should be as similar as possible. The figures provided in Appendix A and Appendix C shows the uniform array arrangement of set-1 and the placement of waste forms in set-2-uh, respectively. The geometry is sufficiently different to warrant an examination of the waste form shape.

The area of applicability guide refers to shape comparison by the mean cord length. There is an allowable +/-50% variation on mean cord length for non-reentrant bodies and a +/- 25% variation for reentrant bodies. Reentrant bodies have a condition in which a particle leaving the body could possibly reenter without any additional events occurring. An example of a reentrant body would be an annulus geometry. The cylinder and spherical waste forms modeled are considered non-reentrant bodies.

Volumes are determined by the amount of material within the waste form and are the same regardless of the geometric shape of the waste form. The range of volume is 146 to 5,480 cm^3 with the primary driver of change being the moderation mixed with the waste. Set-1-2 models the waste form as cylinders that are fixed with a radius of 4.8, 6, and 7.7 cm, whereas set-2-10-uh models the waste form as a sphere. Figure 6.59 compares the mean chords lengths of these waste forms.

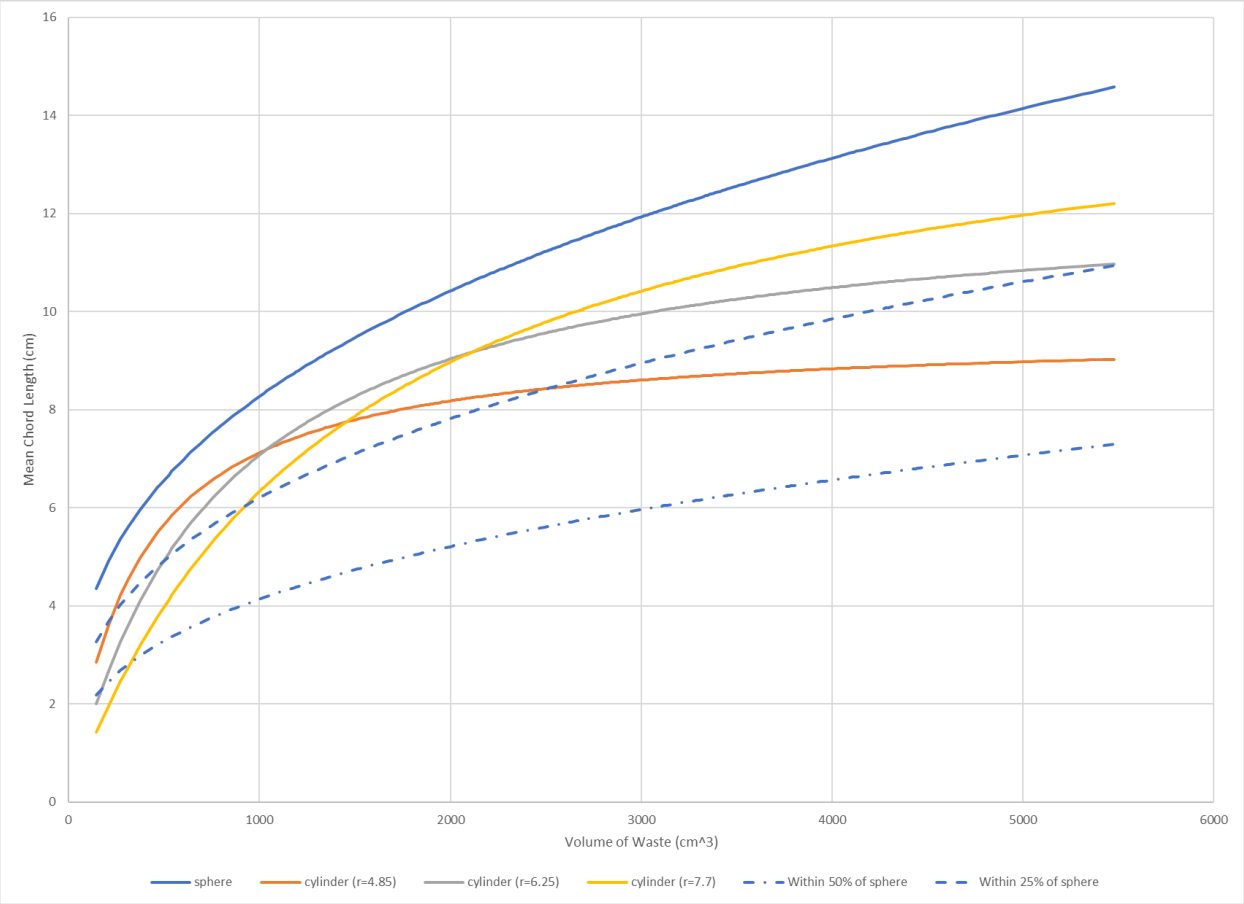

Figure 6.59. Comparison of mean chord length for the different geometric configurations.

The comparison presented in Figure 6.59 shows that, as expected, the mean chord length for the sphere is the largest. Set-1-2 cylinders with radii of 6.25 and 7.7 cm are essentially within 25% of the spherical mean cord length for set-2-10-uh when volumes of the waste are around 525 cm^3 and 1,000 cm^3, respectively. The set-1-2 cylinders with a radius of 4.85 cm remains within 50% of the sphere mean chord length. This indicates that the waste form shapes are similar enough that set-2-10-uh is within set-1-2. The set-1-2 models used for validation all use a cylinder radius with 7.7 cm.

For neutron energy, NUREG/CR-6698 [47] notes that the neutron energy spectra should cover the same energy range. A wide tolerance is given based on thermal (0–0.1 eV), intermediate (1–100 KeV), or fast (100 KeV–20 MeV). The energy of average lethargy causing fission (EALF) is a provided value that

gives a good indication of the neutron energy spectrum. Neutrons produced from fission are typically in the megaelectron volt range and lose fractions of its energy through scattering before it causes another fission. Figure 6.60 shows how the EALF changes as a function of moderator mass within the waste.

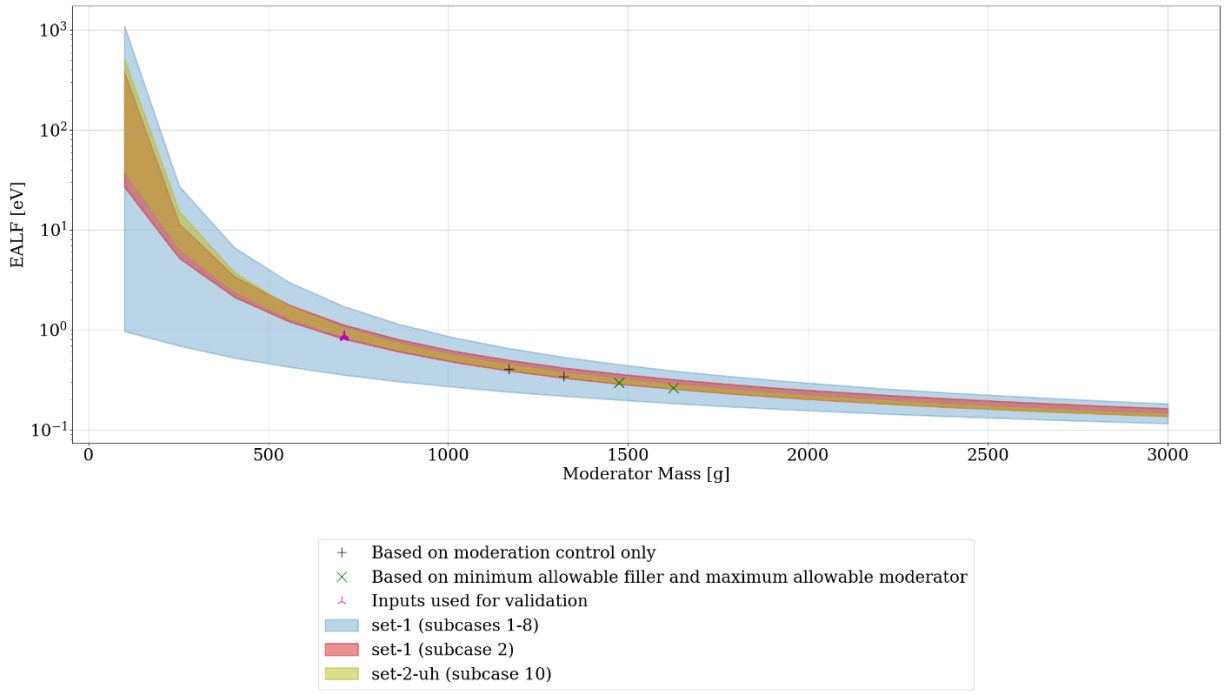

Figure 6.60. EALF of set-1 (all cases), set-2-uh (subcase 10 only), and set-1 subcase 2 (cylinder radius fixed at 7.7 cm)

The comparison presented in Figure 6.60 shows that, as expected, the EALF dramatically reduces as moderator is added to the waste forms. These also indicate that the EALF for set-2-10-uh is within the boundaries of the EALF for set-1-2. The individual points indicate the location of (1) where the set-1-2 models are used for validation, (2) the bounding set-2-uh subcase 10 models for moderation control (1.3 kg moderator in this example), and (3) the bounding set-2-uh subcase 10 models for controls with a minimum filler content (6 × FGE mass) and maximum allowable moderator (1.5 kg moderator in this example).

The above discussion provides sufficient justification to conclude that the validation in the Appendix H area of applicability covers the other results in this analysis with set-2-10-uh as an example.

An additional discussion is required to address the use of the results in Appendix H because of the lack of applicable benchmark experiments and the way that TSUNAMI was used for them.

For this discussion, the same example controls on moderator mass for set-2-10-uh are used: 1.3 kg with no filler mass requirement, and with 6 × FGE mass as a filler mass requirement, the moderator control is 1.5 kg.

The analysis models with the maximum k_{eff} that occur with a moderator mass of 1.168 kg and 1.321 kg of moderator in the waste were selected for this example for the control of limiting the moderator within the waste to 1.300 kg (i.e., an interpolation was performed). These models are presented in Table 6.9.

Table 6.9. Set-2-uh subcase 10 sweeps that bound the current controls

Control	Bounding inputs
Moderator in waste limited to 1.300 kg	set-2-10-nuac_uh_m2_graphite_sph_ps_1000_yr_para_00256
	set-2-10-nuac_uh_m2_graphite_sph_ps_1000_yr_para_00292
Filler in waste is a minimum of 2280 kg Moderator in waste limited to 1.500 kg	set-2-10-nuac_uh_m2_graphite_sph_ps_1000_yr_para_00340
	set-2-10-nuac_uh_m2_graphite_sph_ps_1000_yr_para_00376
	set-2-10-nuac_uh_m2_graphite_sph_ps_1000_yr_para_00352
	set-2-10-nuac_uh_m2_graphite_sph_ps_1000_yr_para_00388

Selecting the most appropriate validation models was done by matching the parameters as closely as possible. All the set-2-uh inputs selected in Appendix H have no filler mass or can mass, use a thick discrete reflector (i.e., 0.7112 cm thick), and contain 585 g Be. The sweeps used for validation that match these criteria are selected from Table H-2. These are:

- set-1-2-uac1_uh_m2_graphite_cyl_ps_1000_yr_para_00444 and
- set-1-2-uac1_uh_m2_graphite_cyl_ps_1000_yr_para_00480.

TSUNAMI-IP determines the similarity value, c_k, of benchmarks to the selected validation inputs. The correlation coefficient, c_k, is used to determine the similarity between an application (e.g., a model within set-1-2) and a nuclear criticality benchmark experiment. A $c_k \geq 0.8$ is considered to have a high degree of similarity between application and experiment. No experiments with a $c_k \geq 0.7$ were evaluated in this analysis (Appendix H). However, a trend can be determined and a bias and bias uncertainty can be applied regardless. It is not unusual to have difficulty in finding experiments with a high c_k, and usually some compensatory action may be applicable, if desired. The number of benchmarks that met the c_k criteria in are listed in Table 6.10.

Table 6.10. Number of benchmark experiments in Appendix H with various c_k criteria

Input	Number of benchmark models	
	$C_k > 0.6$	$C_k > 0.5$
set-1-2-uac1_uh_m2_graphite_cyl_ps_1000_yr_para_00444	68	131
set-1-2-uac1_uh_m2_graphite_cyl_ps_1000_yr_para_00480	16	92

The various bias and bias uncertainty values for the sets of c_k criteria can be used via the approach provided by USLstats, which takes the c_k values and trends the bias and bias uncertainty as c_k approaches 1. There are two methods for USL: a confidence band with an administrative margin method and uniform width closed interval technique (single-sided tolerance). The latter cannot be used to extrapolate, only the first method can be used for c_k trending. This is because the USL is determined when the similarity matches the application (i.e., $c_k = 1$). The first method is discussed as follows [31].

Confidence band with administrative margin:

$$USL_1(x) = 1 + \beta(x) - W - \Delta k_m$$
(for $\beta(x) < 0$)

$$USL_1(x) = 1 - W - \Delta k_m$$
(for $\beta(x) > 0$)

Where

β(x) is the bias;
W is the confidence band interval [New reference];
And Δk_m is additional administrative margin applied to cover validation gaps.

Figure 6.61 through Figure 6.63 are plots of the USL trends where set-1-2-00480 with a $c_k \geq 0.6$ was not included because there are not enough benchmarks for an appropriate statistical analysis. The trends in each plot show a positive bias. When there is a positive, the bias is assumed to be zero. Therefore, the bias and bias uncertainty in Table H-34 is only the bias uncertainty for set-1-2-para_00444 and set-1-2-para_00480. When extrapolating the confidence band interval, W is a curvilinear function that considers the number of experiments, the confidence level desired (e.g., 95% confidence level), and extrapolation beyond the range of experimental data points. The values in Table H-34 are the applicable bias and bias uncertainty to use when extending the validation to set-2-10-uh. Additional margin to cover validation gaps. The absolute data-induced uncertainty in Table H-34 could be the applicable margin applied.

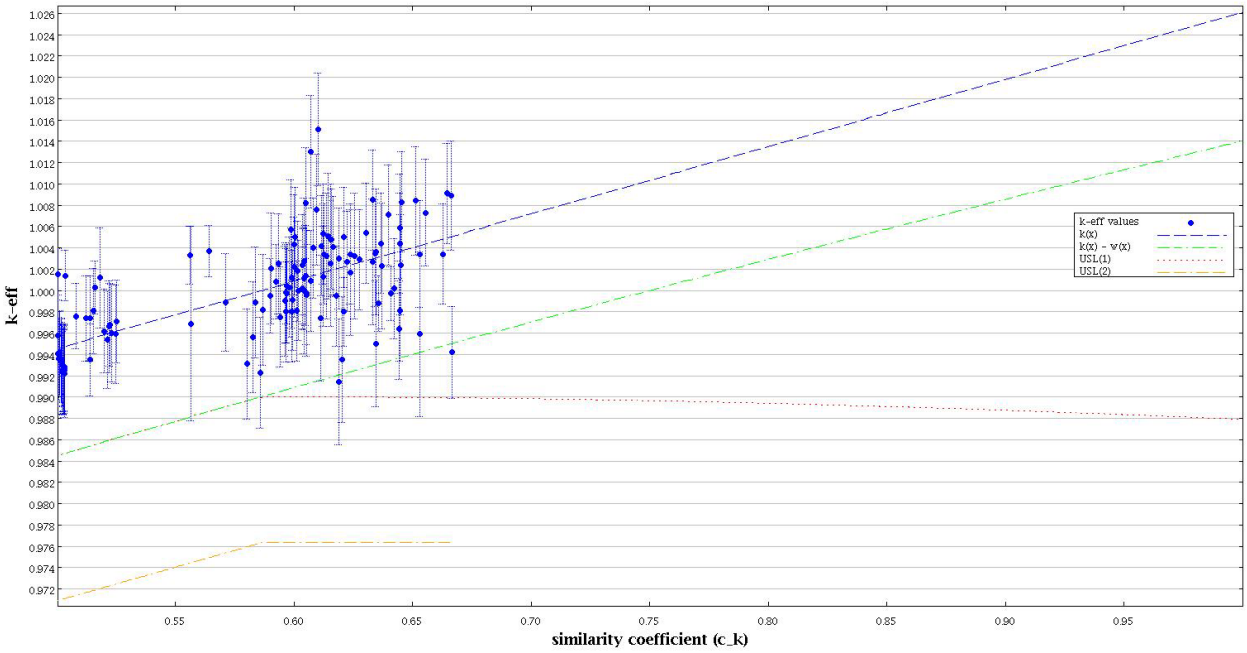

Figure 6.61. Trend of bias and bias uncertainty as c_k approaches 1 for set-1-2-uac1_uh_m2_graphite_cyl_ps_1000_yr_para_00444 for $c_k \geq 0.5$.

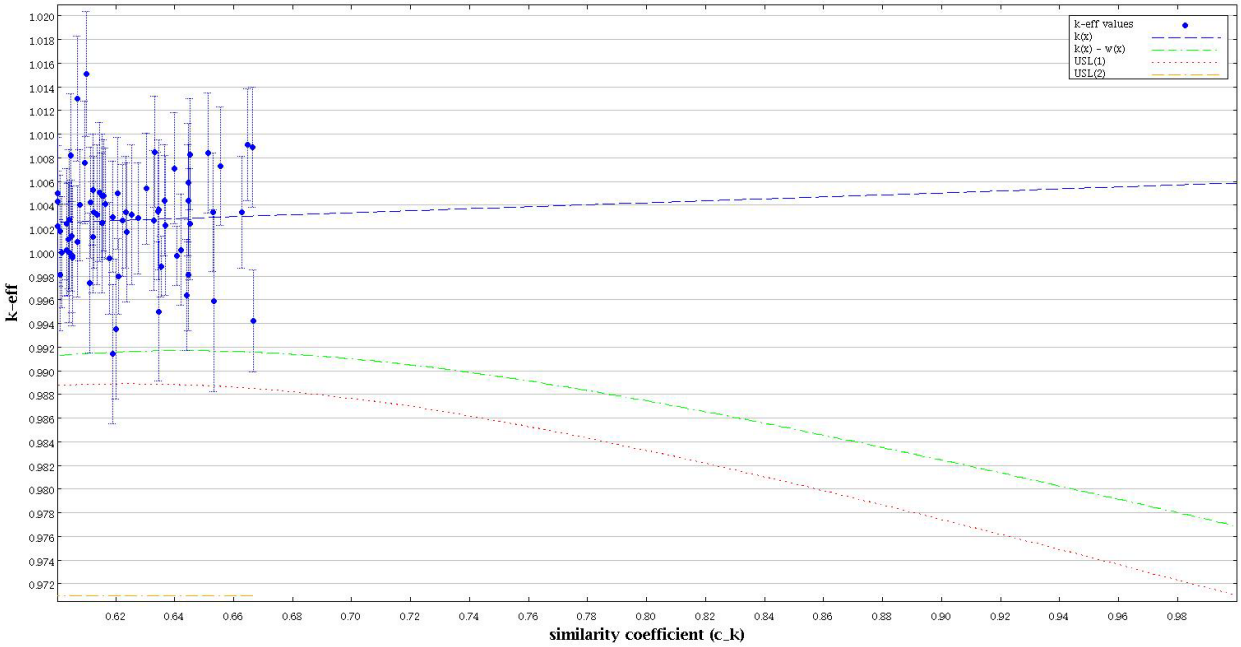

Figure 6.62. Trend of bias and bias uncertainty as c_k approaches 1 for set-1-2-uac1_uh_m2_graphite_cyl_ps_1000_yr_para_00444 for $c_k \geq 0.6$.

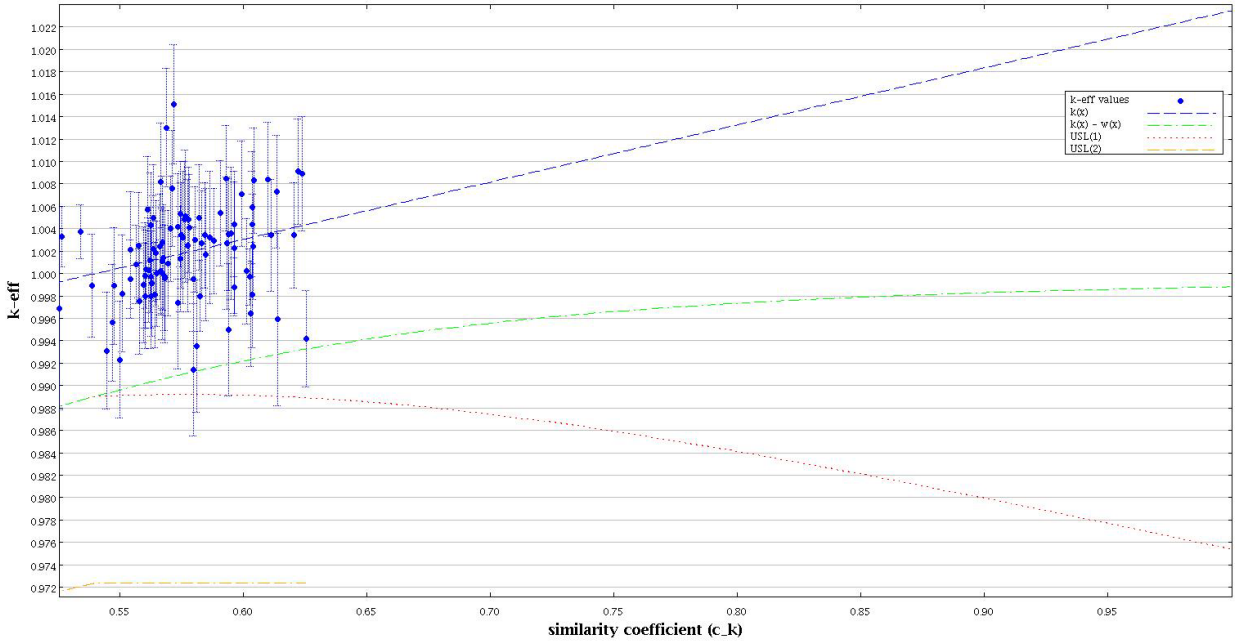

Figure 6.63. Trend of bias and bias uncertainty as c_k approaches 1 for set-1-2-uac1_uh_m2_graphite_cyl_ps_1000_yr_para_00480 for $c_k \geq 0.6$.

7. CONCLUSIONS

By evaluating k_{eff} for multiple arrays and CCO configurations and establishing the H/^{239}Pu curves related to them, this work establishes a relationship between the controlling parameters and the associated criticality-based system reactivity (k_{eff}) during the post-closure repository performance period spanning 10,000 years, given the results of Sandia geomechanical analysis provided by Reedlunn and Bean [8]. Building upon the methodology developed by Brickner [4], parametric sweeps were performed to gauge possible k_{eff} values over the performance period. The parametric sweeps demonstrated the primary reactivity impact of waste form moderator material and mass, array spacing, fissile region geometry, filler material and mass, and external reflector effects; other parameters studied introduced variation into the k_{eff} results but did not dominate the system.

Moderator content, spacing, waste form volume and B_4C content are the principal drivers of system behavior. Therefore, subcriticality can be maintained by managing these parameters. Waste form moderator mass is the primary means to limit system reactivity. As a secondary means, non-hydrogenous waste form filler mass can be used to increase the volume of the waste form to limit the reactivity of the system. Additionally, as previously established, B_4C can be added to maintain subcriticality. Finally, applicable combinations of these three parameters can be used together to maintain subcriticality with the post-closure repository environment.

The results provided also allow other combinations of parameters to be used as control limits. Although the report documents a small subset of the results, the full set of results applicable to potential control limits are provided in Addendum 1.

Although this report provides results that are potential B_4C mass limits (i.e., 30 g is sufficient up to at least 6 kg moderator) lower than previously provided in Saylor and Scaglione [3], the difference is primarily due to the differences in how the two analyses model the compaction of the CCOs. Therefore, both remain valid and either analysis may be used to provide technical justification for B_4C mass limits.

Of additional interest is the implication of the results provided for the potential heterogeneity of the FGE. The analysis provides studies that show the behavior of the system—excluding the very low waste form moderator cases, which are also very low reactivity systems—is consistent with historical evaluations of FGE heterogeneity. As such, the well-mixed or heterogenous assumption for distribution of FGE within the waste form is a conservative assumption. Consequently, the inclusion of fissile materials that are not well mixed does not increase k_{eff}. Because the analysis is generic, it is intended to cover a wide range of potential scenarios. For example, a waste form may be identified from unused commercial nuclear fuel assembly fuel rods or other noncommercial fuel-related activities that manufactured cylindrical fuel components. As long as the component limits are met (e.g., FGE mass, moderator mass), the shape, size, and number of the FGE pieces is of no concern.

Finally, this report provides a very large set of results (see Addendum 1) that may be utilized to define limits in various ways for various parameters. The mixing of CCOs at emplacement which are qualified under different limits is acceptable as long as the subcritical limit used to define the various limits is similar because using the same subcritical limit to determine a set of limits for different parameters means that the CCOs would all have essentially the same maximum reactivity.

This page is intentionally blank

8. REFERENCES

[1] Sandia National Laboratories, *Consideration of Nuclear Criticality When Disposing of Transuranic Waste at the Waste Isolation Pilot Plant*, SAND99-2898, 2,000.

[2] Nuclear Waste Partnership, LLC, *Nuclear Criticality Safety Evaluation for Contact-Handled Transuranic Waste Containers at the Waste Isolation Pilot Plant*, WIPP-016, Revision 6, 2021.

[3] Saylor, Ellen M. and John M. Scaglione, *Nuclear Criticality Safety Assessment of Potential Disposition at the Waste Isolation Plant*, ORNL/TM-2017/751/R1, 2017.

[4] Brickner, Bret D., *Post Placement Nuclear Criticality Evaluations Involving 6- and 12-Inch Pipe Overpack TRU Waste Containers at the Waste Isolation Pilot Plant*, Oak Ridge National Laboratory, ORNL/TM-2019/1222/R0, 2019.

[5] DOE/WIPP-02-3122, *Transuranic Waste Acceptance Criteria for the Waste Isolation Pilot Plant*, Revision 8, July 5, 2016.

[6] PO 1990300

[7] Reedlunn, B., and J. Bean. *Simulations of Pipe Overpack Container Compaction at the Waste Isolation Pilot Plant; Memorandum to Distribution*, July 18, 2019. Sandia National Laboratories, 2019.

[8] Reedlunn, B. and J. Bean. *Further Simulations of Criticality Overpack Container Compaction at the Waste Isolation Pilot Plant; Memorandum to Distribution,* May 14, 2020. Sandia National Laboratories, 2020.

[9] US Department of Energy Carlsbad Field Office, *TRUPACT-II Safety Analysis Report*, Revision 23, Carlsbad, New Mexico, 2013a.

[10] US Department of Energy, "Surplus Plutonium Disposition, Record of Decision," *Federal Register*, **81**(*65*), 19588–19594 (2016).

[11] R. P. Rechard, *Improbability of Nuclear Criticality in TRU Waste in Criticality Control Overpacks at WIPP after Salt Creep Compaction*.

[12] US Environmental Protection Agency, "40 CFR Part 191: Environmental Radiation Protection Standards for the Management and Disposal of Spent Nuclear Fuel, High-Level and Transuranic Radioactive Wastes, Final Rule," *Federal Register*, **58**(*242*), 66398–66416, 1993.

[13] US Environmental Protection Agency, "40 CFR Part 191: Environmental Standards for the Management and Disposal of Spent Nuclear Fuel, High-Level and Transuranic Radioactive Wastes: Final Rule," *Federal Register*, **50**(*182*), 38066–38089, 1985.

[14] US Environmental Protection Agency, "40 CFR Part 194: Criteria for the Certification and Re-Certification of the Waste Isolation Pilot Plant's Compliance with the 40 CFR Part 191 Disposal Regulations; Final Rule," *Federal Register*, **61**(*28*), 5224–5245, 1996.

[15] Duderstadt, J. J. and L. J. Hamilton, *Nuclear Reactor Analysis*, John Wiley & Sons (1976).

[16] Marshall, W. J., et al., "Validation of SCALE 6.2 Criticality Calculations Using KENO V.a and KENO-VI," In: *Proceedings, International Conference on Nuclear Criticality Safety* (ICNC 2015), Charlotte, North Carolina, Sept. 13–17, 2015.

[17] American National Standards Institute, *An American National Standard for Nuclear Criticality Safety in Operations with Fissionable Materials Outside Reactors*, ANSI/ANS-8.1-2014, 2014.

[18] Geotechnical Analysis Report for July 2015 – June 2016

[19] Reedlunn, B., et al., *Initial Simulations of Empty room Collapse and Reconsolidation at the Waste Isolation Pilot Plant*, Sandia National Laboratories, SAND2019-15351, date TBD

[20] Williamson, B. M., ANSI/ANS-8.7 Applications for the Storage of Criticality Control Overpacks, Savannah River Nuclear Solutions, Aiken, South Carolina.

[21] National Academies of Sciences, Engineering, and Medicine. *Disposal of Surplus Plutonium at the Waste Isolation Pilot Plant: Interim Report.* Washington, DC: The National Academies Press, 2018. https://doi.org/10.17226/25272.

[22] PUB. L. 102-579, "Waste Isolation Pilot Plant Land Withdrawal Act" (106 Stat. 4777), 1992.

[23] High Bridge Associates, Inc., *Comparison of Plutonium Disposition Alternatives: WIPP Diluted Plutonium Storage and MOX Fuel Irradiation*, 2016.

[24] Clark, H. K., et al. 1965, "Effect of Distribution of Fissile Material on Critical Mass," *Nuclear Science and Engineering*, **24**, 133–141, 1966.

[25] Reedlunn, B. and Bean, J. (May 2020). Further Simulations of Criticality Control Overpack Container Compaction at the Waste Isolation Pilot Plant. Tech. rep. SAND2020-5105 CTF. Sandia National Laboratories.

[26] W.J. Marshall and B.D. Brickner, "Improved Runtime Performance in KENO-VI Models Using Arrays and Holes," *Trans. Am. Nucl. Soc.* **123**, 937-940 (2020).

[27] W.J. Marshall, T.M. Greene, B.D. Brickner, and R.A. Hall, "Description and Use of SCALE Sampler Parametric Capability for Engineering Analysis and Optimization," *Trans. Am. Nucl. Soc.* **122**, 471-474 (2020).

[28] Email from Ben Reedlunn to Bret Brickner et al, 2/3/21, "Re: [EXTERNAL] RE: CCO Post-closure Criticality Safety," and attachments.

[29] Saylor, Ellen M., *Nuclear Criticality Safety Assessment of Criticality Control Containers without Moderation Control at the Waste Isolation Pilot Plant*, ORNL/TM-2020/1713, 2020.

[30] DOE/WIPP-19-3609, *Title 40 CFR Part 191 Subparts B and C Compliance Recertification Application 2019 for the Waste Isolation Pilot Plant, Appendix PA-2019 Performance Assessment*, US Department of Energy, Carlsbad Field Office, Carlsbad, New Mexico, 2020

[31] Christopher M. Perfetti & Bradley T. Rearden (2019) *Estimating Code Biases for Criticality Safety Applications with Few Relevant Benchmarks*, Nuclear Science and Engineering, 193:10, 1090-1128 https://doi.org/10.1080/00295639.2019.1604048.

[32] D. E. Peplow, "Monte Carlo Shielding Analysis Capabilities with MAVRIC," *Nucl. Technol.* 174(2), 289–313 (2011).

[33] B. T. Rearden, M. T. Sieger, S. M. Bowman, and J. P. Lefebvre, *Quality Assurance Plan for the SCALE Code System*, SCALE-QAP-005, Rev. 4, May 2013.

[34] American Nuclear Society, *Nuclear Criticality Safety in Operations with Fissionable Materials Outside Reactors*, ANSI/ANS-8.1-2014, R2018, La Grange Park, IL (2018).

[35] American Nuclear Society, *Validation of Neutron Transport Methods for Nuclear Criticality Safety Calculations*, ANSI/ANS-8.24-2017, American Nuclear Society, La Grange Park, IL (2017).

[36] *International Handbook of Evaluated Criticality Safety Benchmark Experiments*, NEA/NSC/DOC(95)03, NEA Nuclear Science Committee (2020).

[37] W. A. Wieselquist, R. A. Lefebvre, and M. A. Jessee, Eds., *SCALE Code System*, ORNL/TM-2005/39, Version 6.2.4, Oak Ridge National Laboratory, Oak Ridge, TN (2020).

[38] B. T. Rearden, M. L. Williams, M. A. Jessee, D. E. Mueller, and D. A. Wiarda, "Sensitivity and Uncertainty Analysis Capabilities and Data in SCALE," *Nucl. Technol.* **174** (2), pp. 236–288 (2011).

[39] ORNL. 2013. *The SCALE Verified, Archived Library of Inputs and Data – VALID*, Oak Ridge National Laboratory, transactions of ANS NCSD 2013, Wilmington, NC, September 29 – October 31, 2013.

[40] Division of Spent Fuel Storage and Transportation, *Interim Staff Guidance—8, Revision 3, Burnup Credit in the Criticality Safety Analyses of PWR Spent Fuel in Transportation and Storage Casks*, US Nuclear Regulatory Commission (2012).

[41] W. J. Marshall, B. J. Ade, S. M. Bowman, I. C. Gauld, G. Ilas, U. Mertyurek, and G. Radulescu, *Technical Basis for Peak Reactivity Burnup Credit for BWR Spent Nuclear Fuel in Storage and Transportation Systems*, NUREG/CR-7194 (ORNL/TM-2014/240), prepared for the US Nuclear Regulatory Commission by Oak Ridge National Laboratory, Oak Ridge, TN (2015).

[42] W. J. Marshall, J. B. Clarity, and S. M. Bowman, *Validation of k_{eff} Calculations for Extended BWR Burnup Credit*, NUREG/CR-7252 (ORNL/TM-2018/797), prepared for the US Nuclear Regulatory Commission by Oak Ridge National Laboratory, Oak Ridge, TN (2018).

[43] J. M. Scaglione, D. E. Mueller, J. C. Wagner, and W. J. Marshall, *An Approach for Validating Actinide and Fission Product Burnup Credit Criticality Safety Analyses-Criticality (k_{eff}) Predictions*, NUREG/CR-7109 (ORNL/TM-2011/514), prepared for the US Nuclear Regulatory Commission by Oak Ridge National Laboratory, Oak Ridge, TN (2012).

[44] K. S. Krane, *Introductory Nuclear Physics*, John Wiley & Sons (1988).

[45] International Atomic Energy Agency Nuclear Data Section, *Livechart – Table of Nuclides*, Online, Accessed July 2021, https://www-nds.iaea.org/relnsd/vcharthtml/VChartHTML.html.

[46] B. Reedlunn and J. Bean, *Additional Studies of Criticality Control Overpack and Pipe Overpack Container Compaction at the Waste Isolation Pilot Plant. Sandia Memorandum*. SAND2021-11268 CTF (2021).

[47] NUREG/CR-6698, *Guide for Validation of Nuclear Criticality Safety Calculational Methodology*

This page is intentionally blank

APPENDIX A. SET-1: RESULTS OF THE THREE-HIGH UNIFORM ARRAY WITH BOUNDING SPACING CALCULATIONS

This page is intentionally blank

APPENDIX A. SET-1: RESULTS OF THE THREE-HIGH UNIFORM ARRAY WITH BOUNDING SPACING CALCULATIONS

The analysis methodology for the uniform arrays is discussed in detail in Section 6.1 of the main report.

This appendix serves as a repository of those results for the set-1 calculations.

The complete results for all SAMPLER sweeps are provided in ADDENDUM 1.

The analysis model use for the calculations in this appendix is shown in Figure A-1 below.

The SAMPLER case sweeps presented in this appendix are summarized in Table A-1 below.

LIST OF FIGURES

LIST OF TABLES

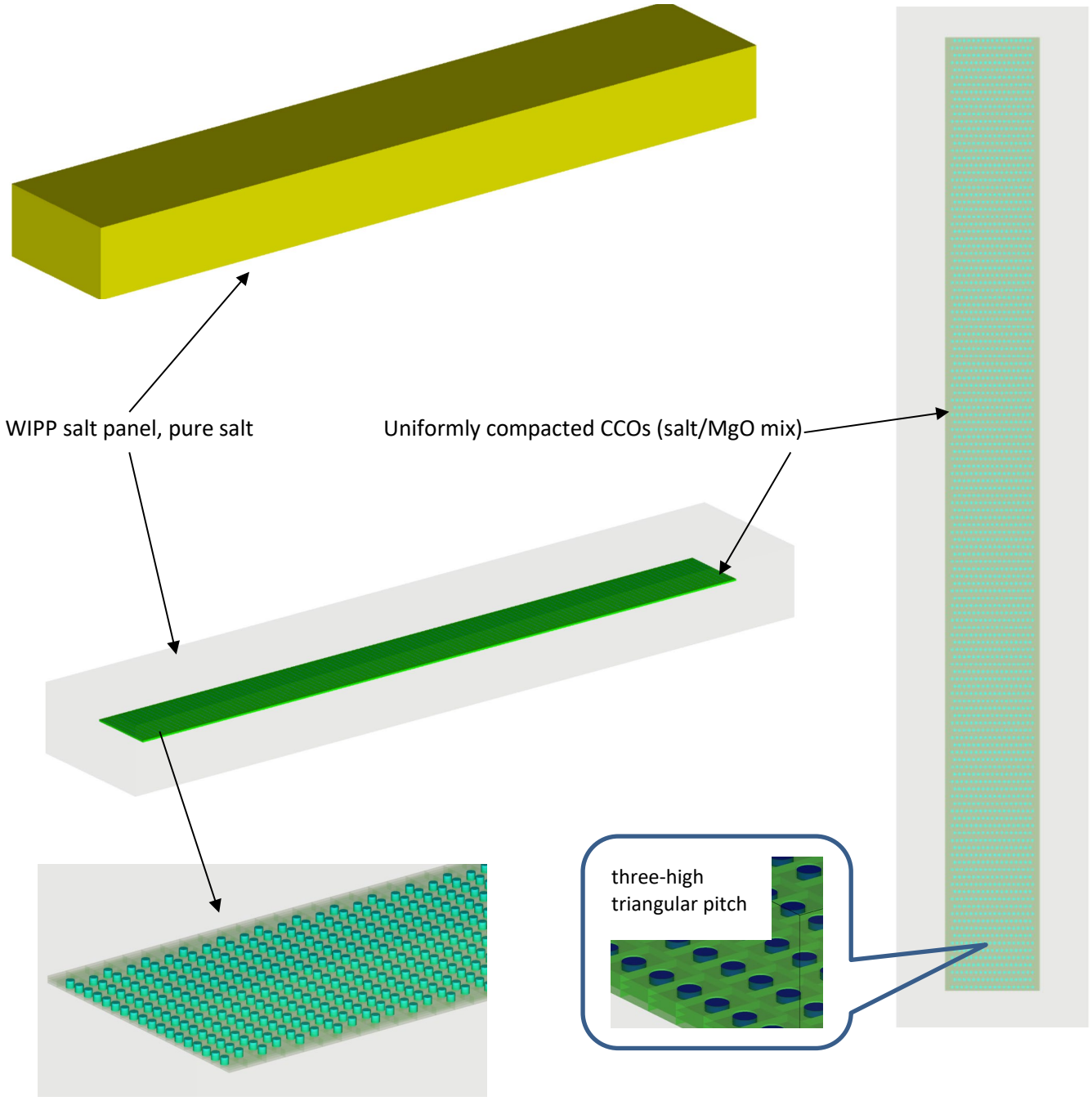

Figure A-1. Diagram of the uniform array three-high model.

Table A-1. Summary of cases for det-1

Case	Model type	Waste form shape	Waste form moderator	Filler material (0, 2,000, 4,000 g)	Metal in filler	Discrete reflector (thin 0.001 and thick 0.7112 cm)	Be (g)	Subcase
Set-1	Uniform array stacked three high with CCO pitch reduction x = 50%, y = 10%, z = no space	Cylinder (radius range 4.8, 6, 7.7 and height defined by total volume of mass)	water	c12	SS from can (0, 500, 1,000 g)	steel	0 to 585	set-1-1
			poly	c12		steel		set-1-2
			water	c12		poly		set-1-3
			poly	c12		poly		set-1-4
			water	generic		steel		set-1-5
			poly	generic		steel		set-1-6
			water	generic		poly		set-1-7
			poly	generic		poly		set-1-8
		Sphere (radius defined by total volume of mass)	water	c12		steel		set-1-9
			poly	c12		steel		set-1-10
			water	c12		poly		set-1-11
			poly	c12		poly		set-1-12
			water	generic		steel		set-1-13
			poly	generic		steel		set-1-14
			water	generic		poly		set-1-15
			poly	generic		poly		set-1-16
			poly + 50 g B_4C (cyl)	c12		poly (0.7112)		set-1-17
			poly + 50 g B_4C (sph)	c12		poly (0.7112)		set-1-18

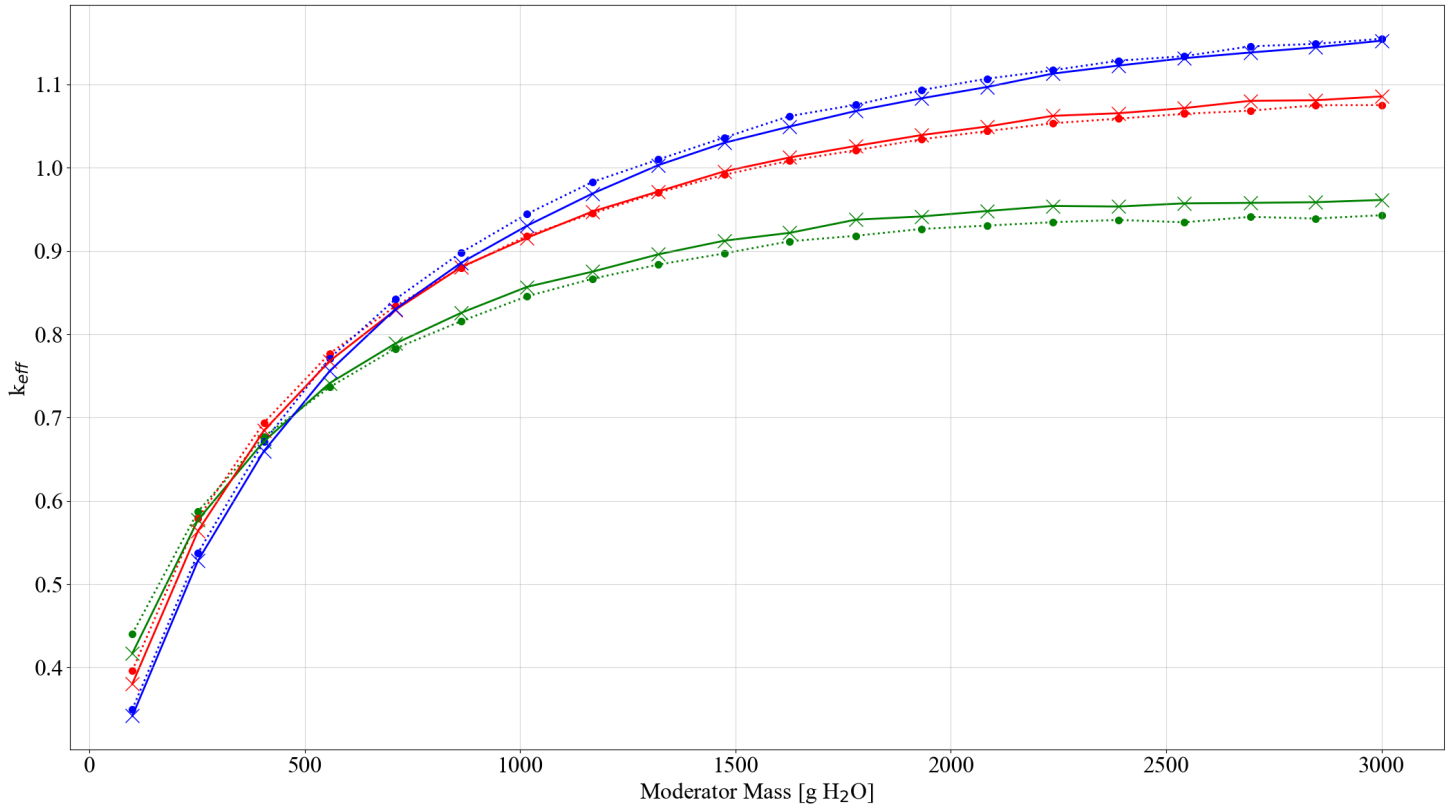

Figure A-2. Set-1 results, plot 1: reactivity effect of cylinder radius, pipe steel, no filler, no Be, water moderated.

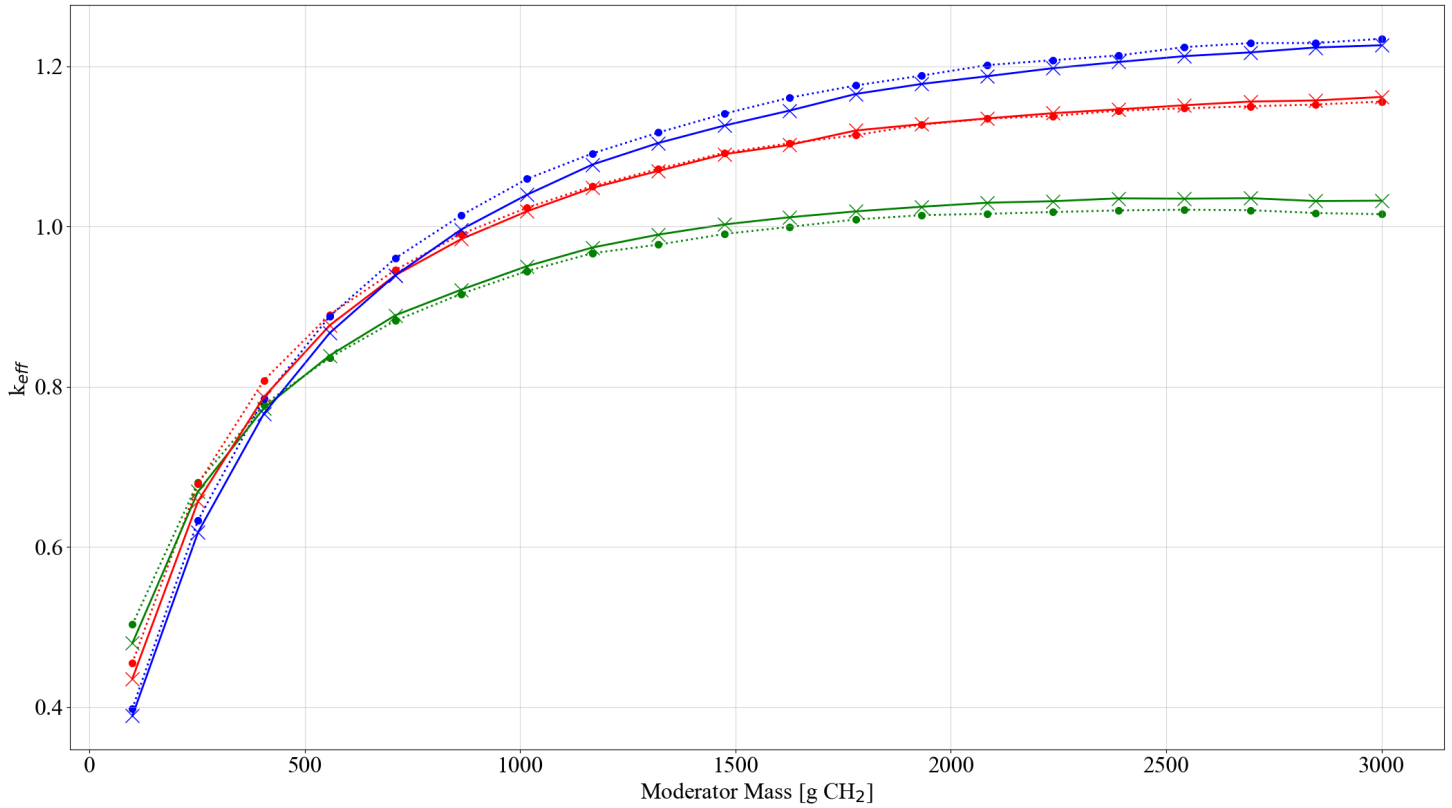

Figure A-3. Set-1 results, plot 2: reactivity effect of cylinder radius, pipe steel, no filler, no Be, poly moderated.

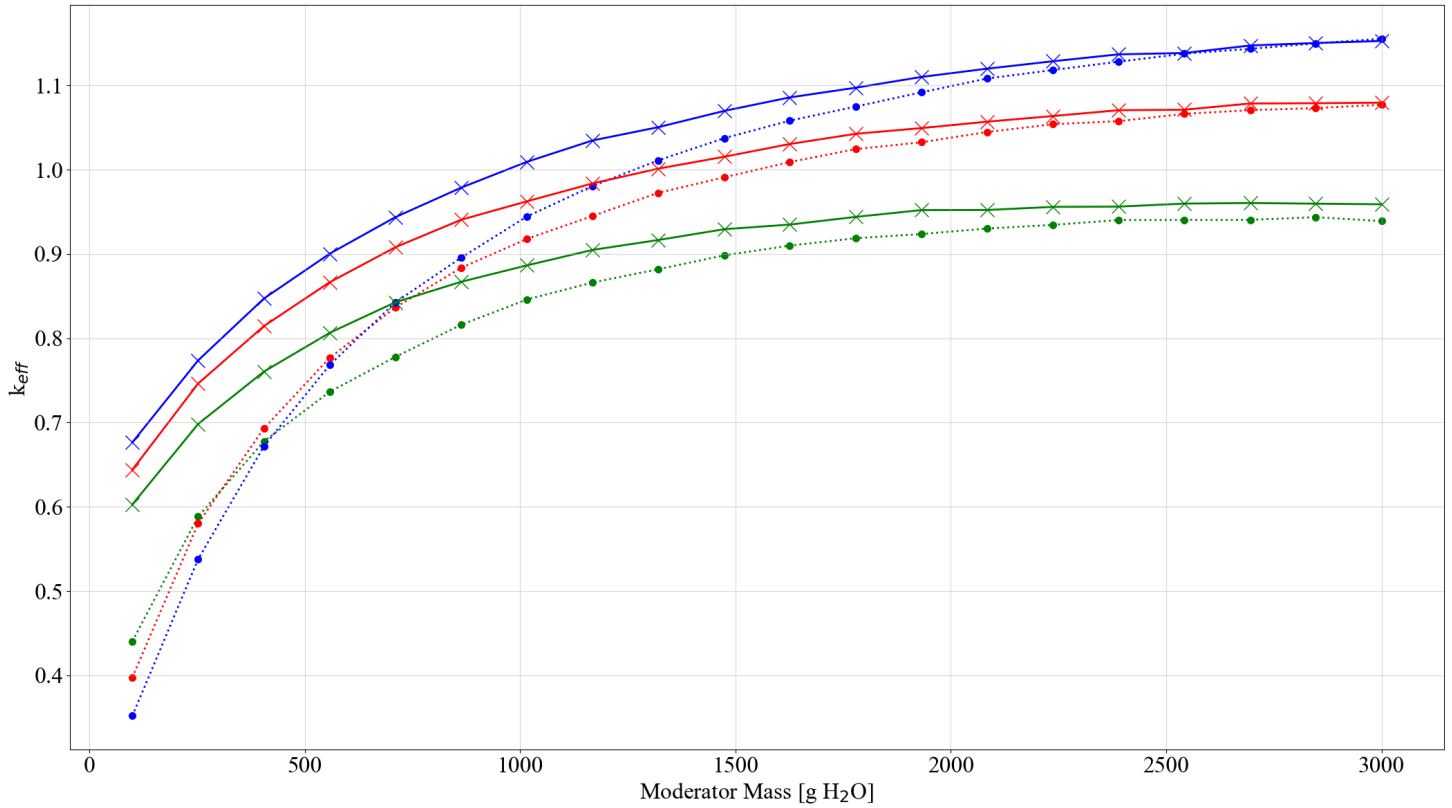

Figure A-4. Set-1 results, plot 3: reactivity effect of cylinder radius, pipe poly, no filler, no Be, water moderated.

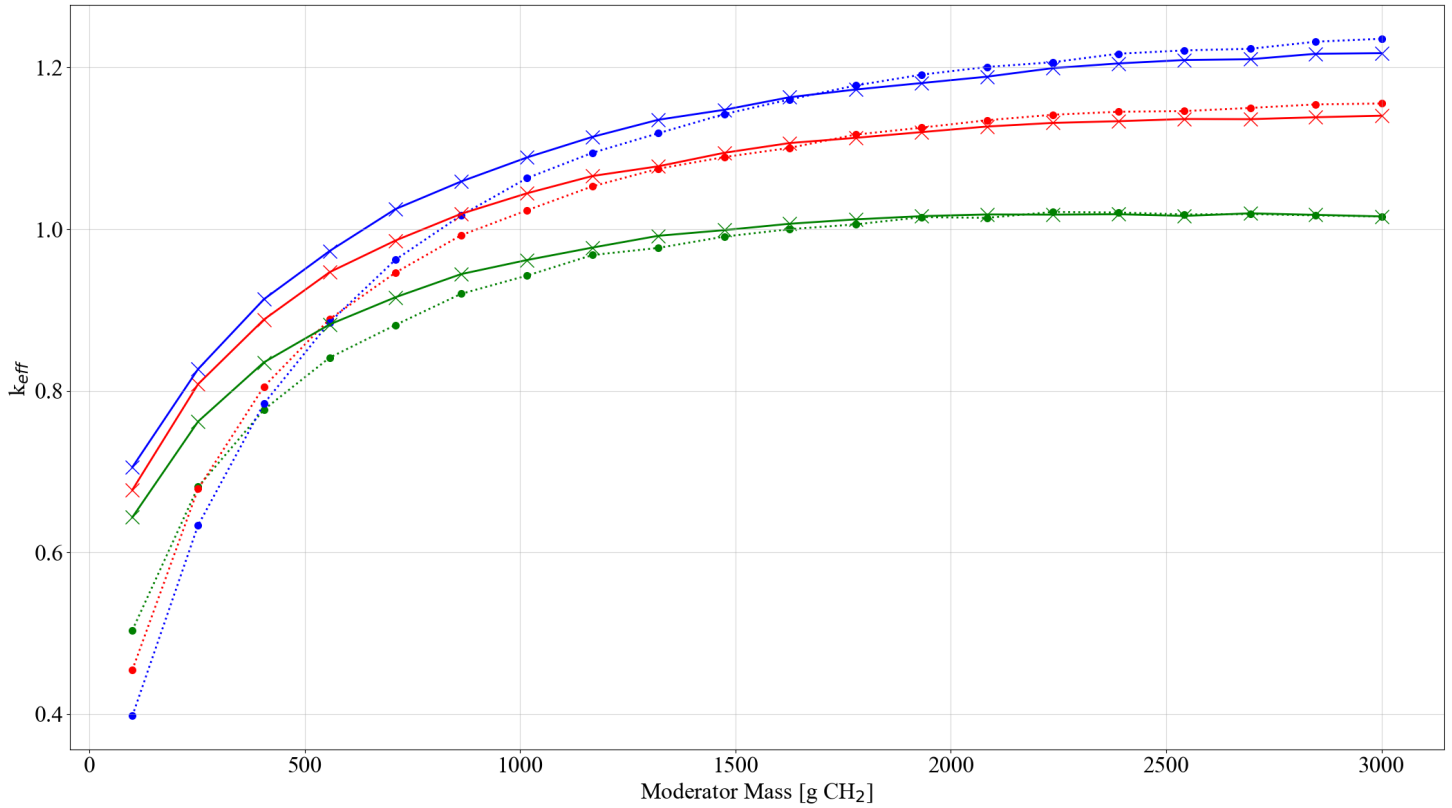

Figure A-5. Set-1 results, plot 4: reactivity effect of cylinder radius, pipe poly, no filler, no Be, poly moderated.

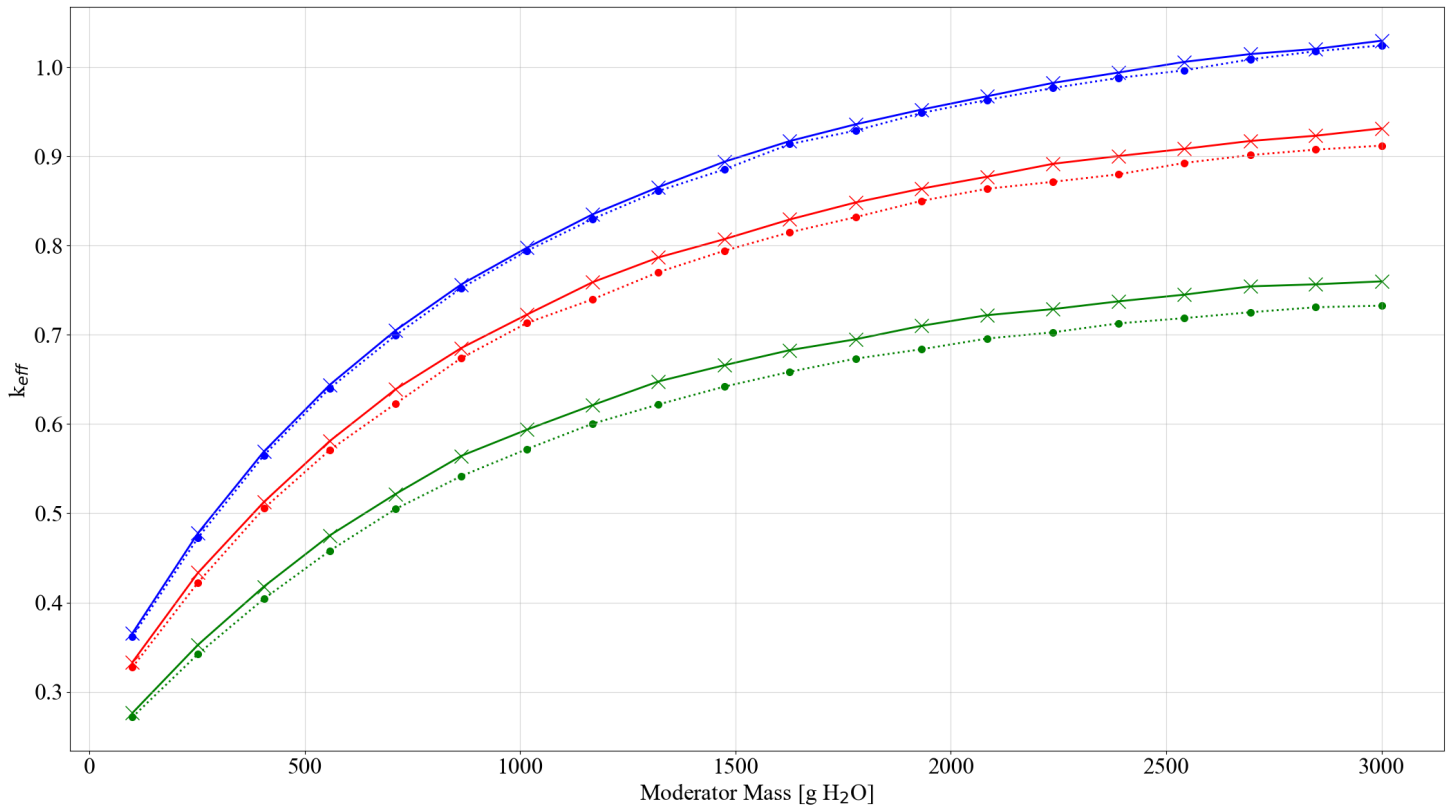

Figure A-6. Set-1 results, plot 5: reactivity effect of cylinder radius, pipe steel, 5 kg graphite/can, no Be, water moderated.

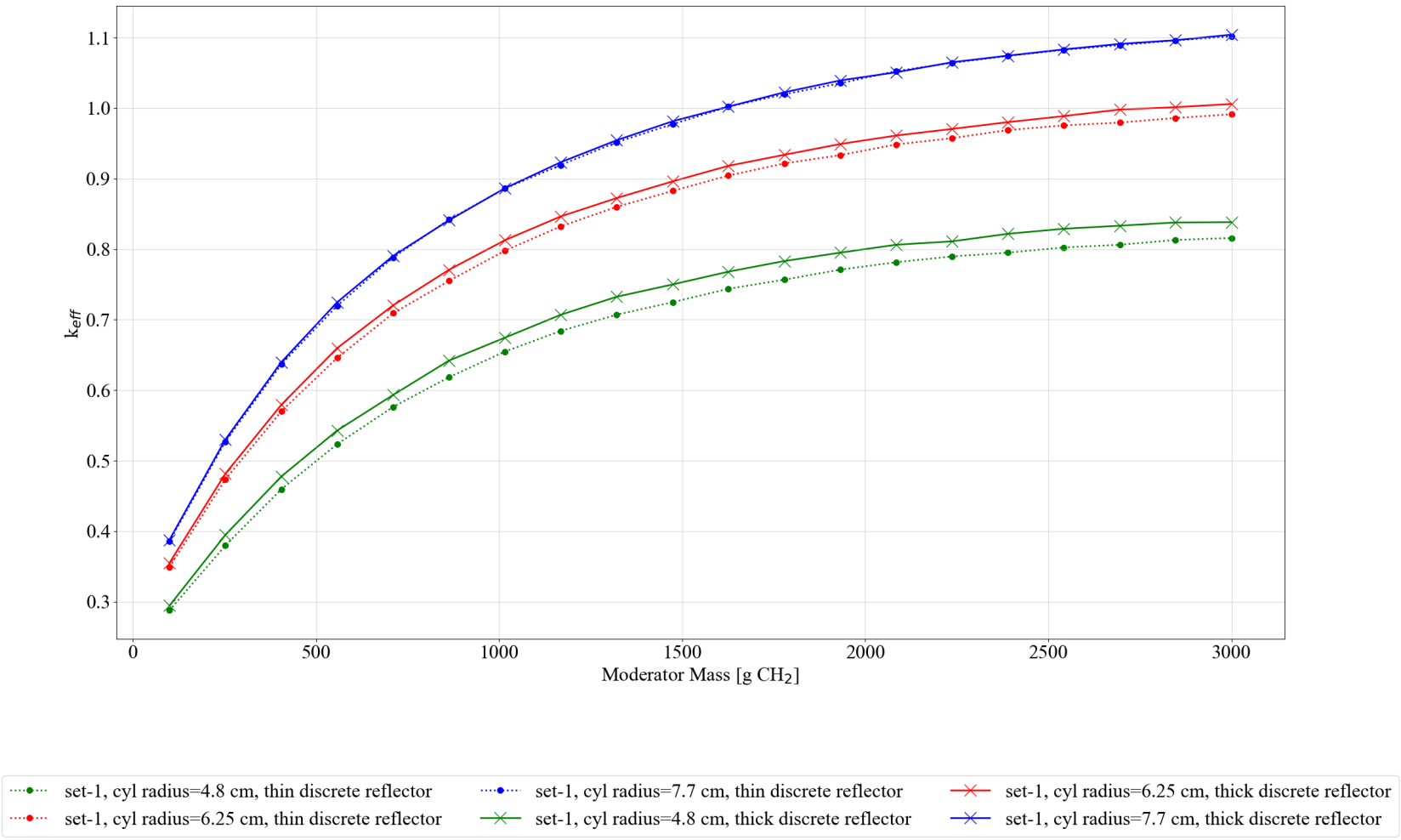

Figure A-7. Set-1 results, plot 6: reactivity effect of cylinder radius, pipe steel, 5 kg graphite/can, no Be, poly moderated.

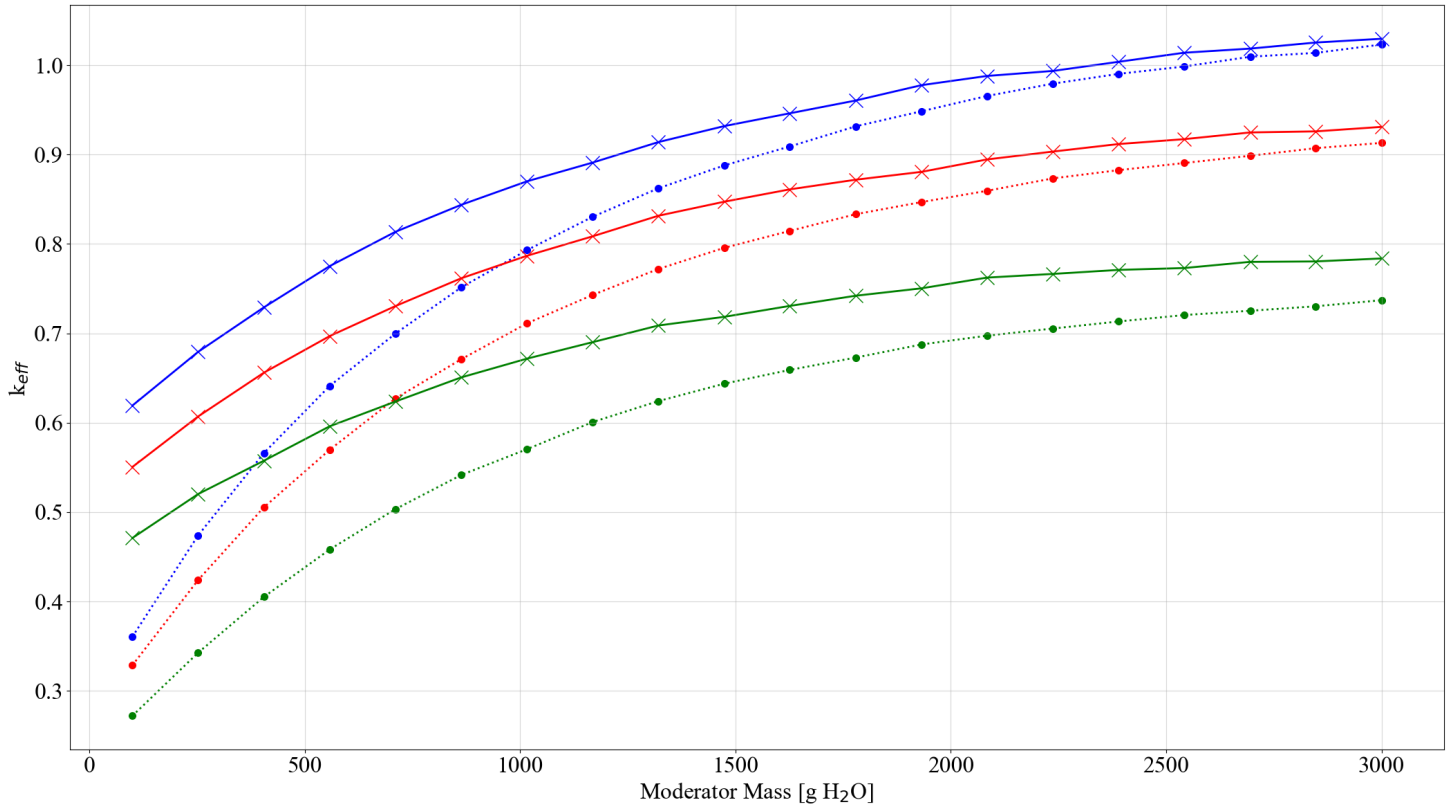

Figure A-8. Set-1 results, plot 7: reactivity effect of cylinder radius, pipe poly, 5 kg graphite/can, no Be, water moderated.

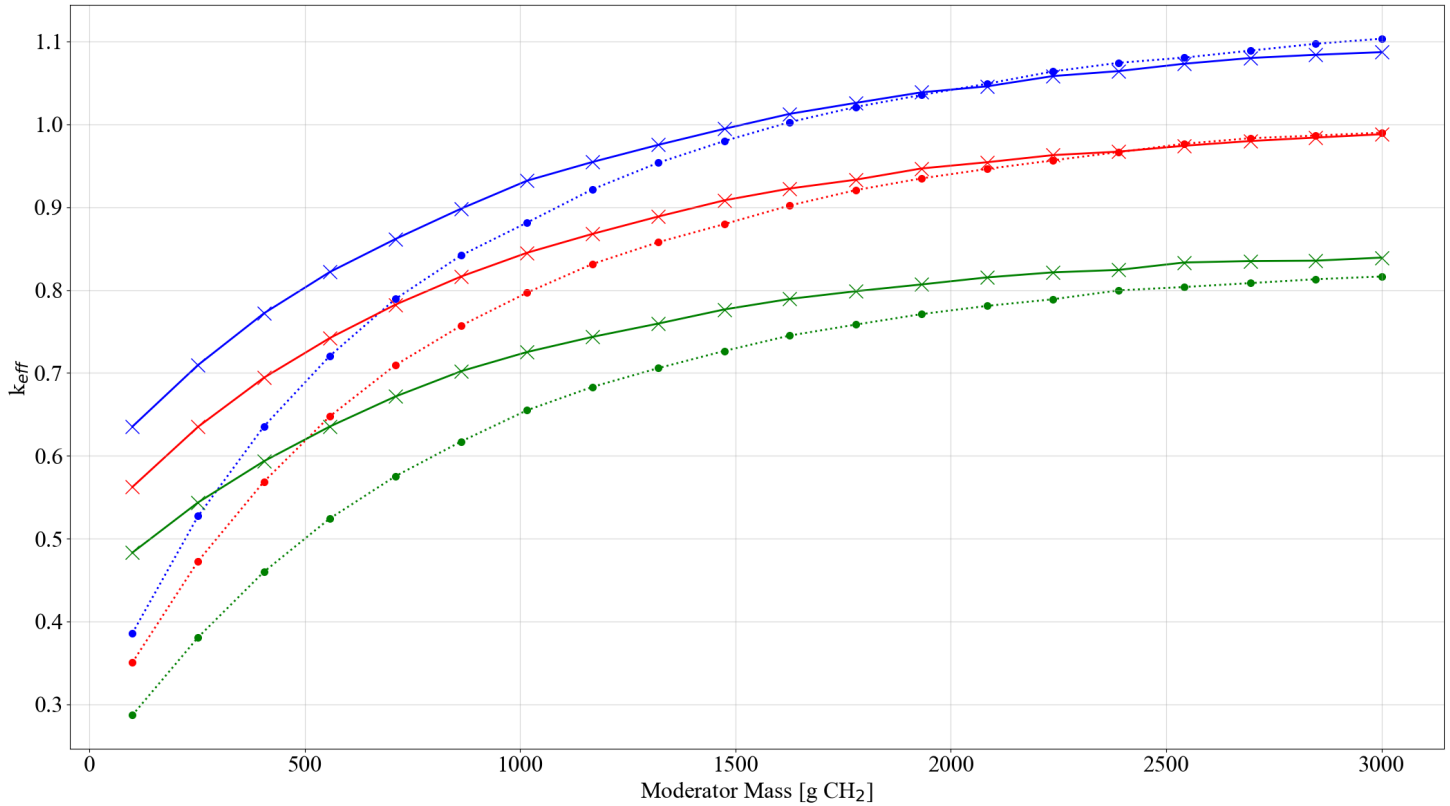

Figure A-9. Set-1 results, plot 8: reactivity effect of cylinder radius, pipe poly, 5 kg graphite/can, no Be, poly moderated.

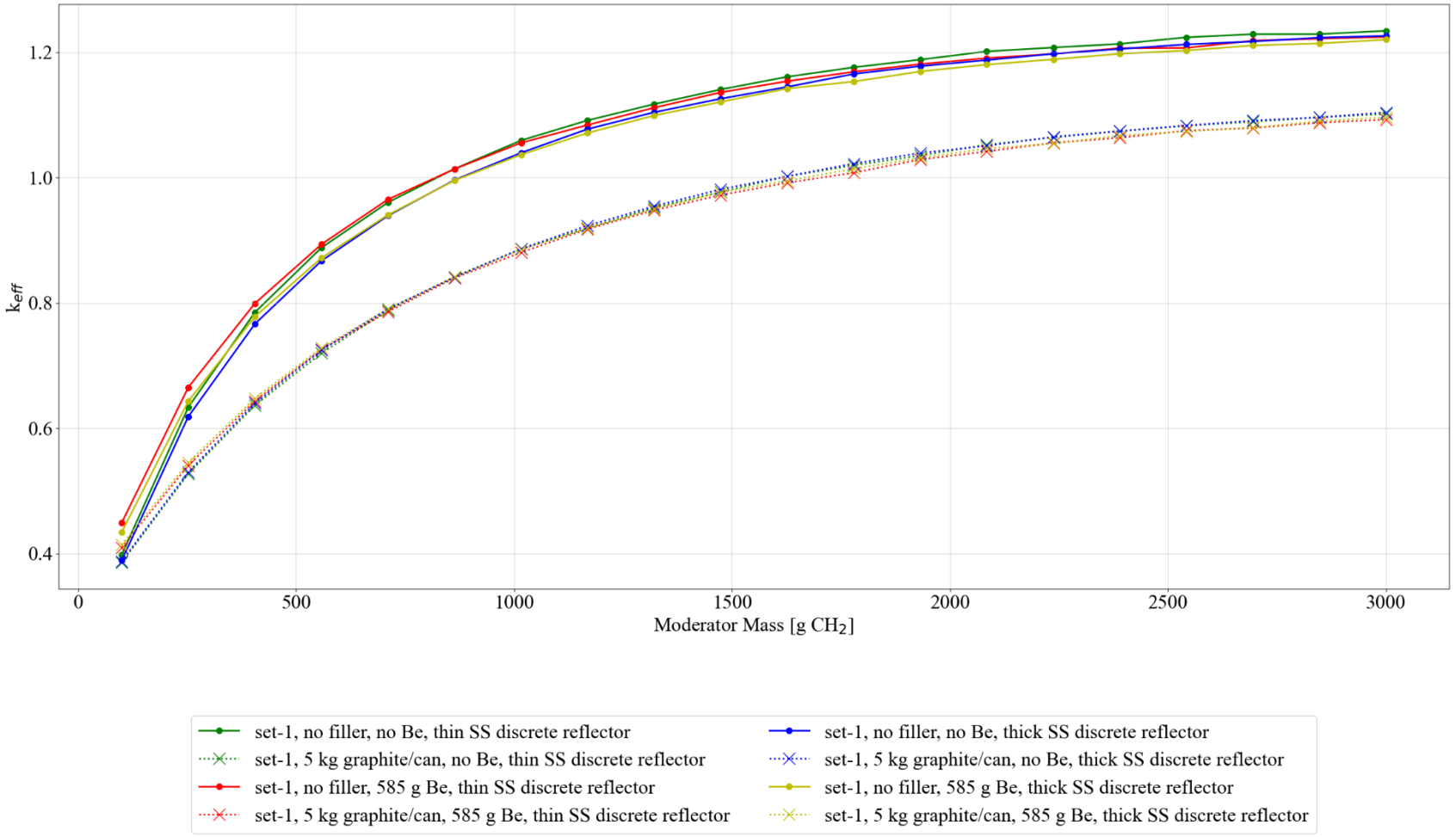

Figure A-10. Set-1 results, plot 9: reactivity effect of various parameters with 7.7 cm cylinder radius, graphite filler, poly moderated.

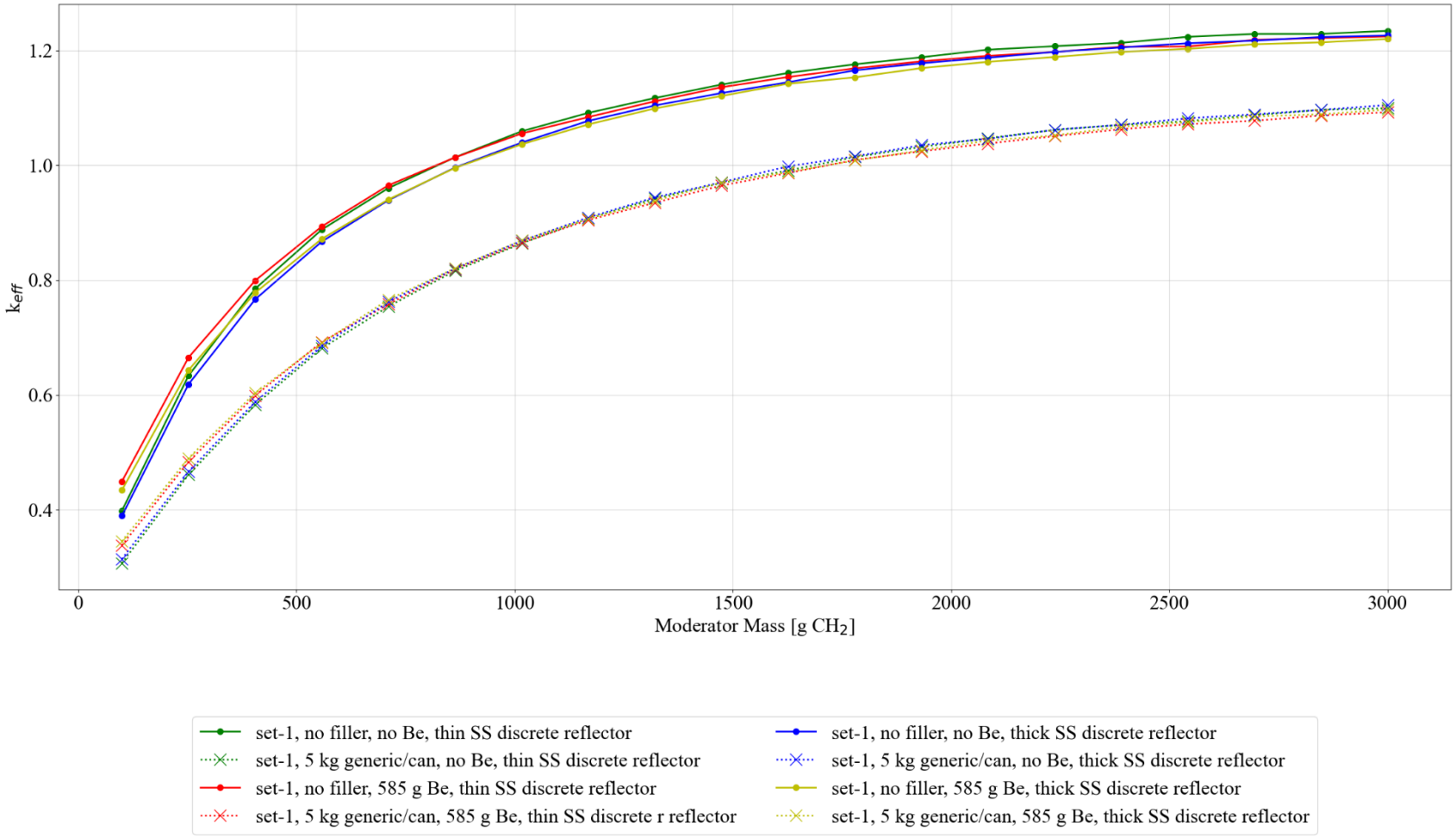

Figure A-11. Set-1 results, plot 10: reactivity effect of various parameters with 7.7 cm cylinder radius, generic filler, poly moderated.

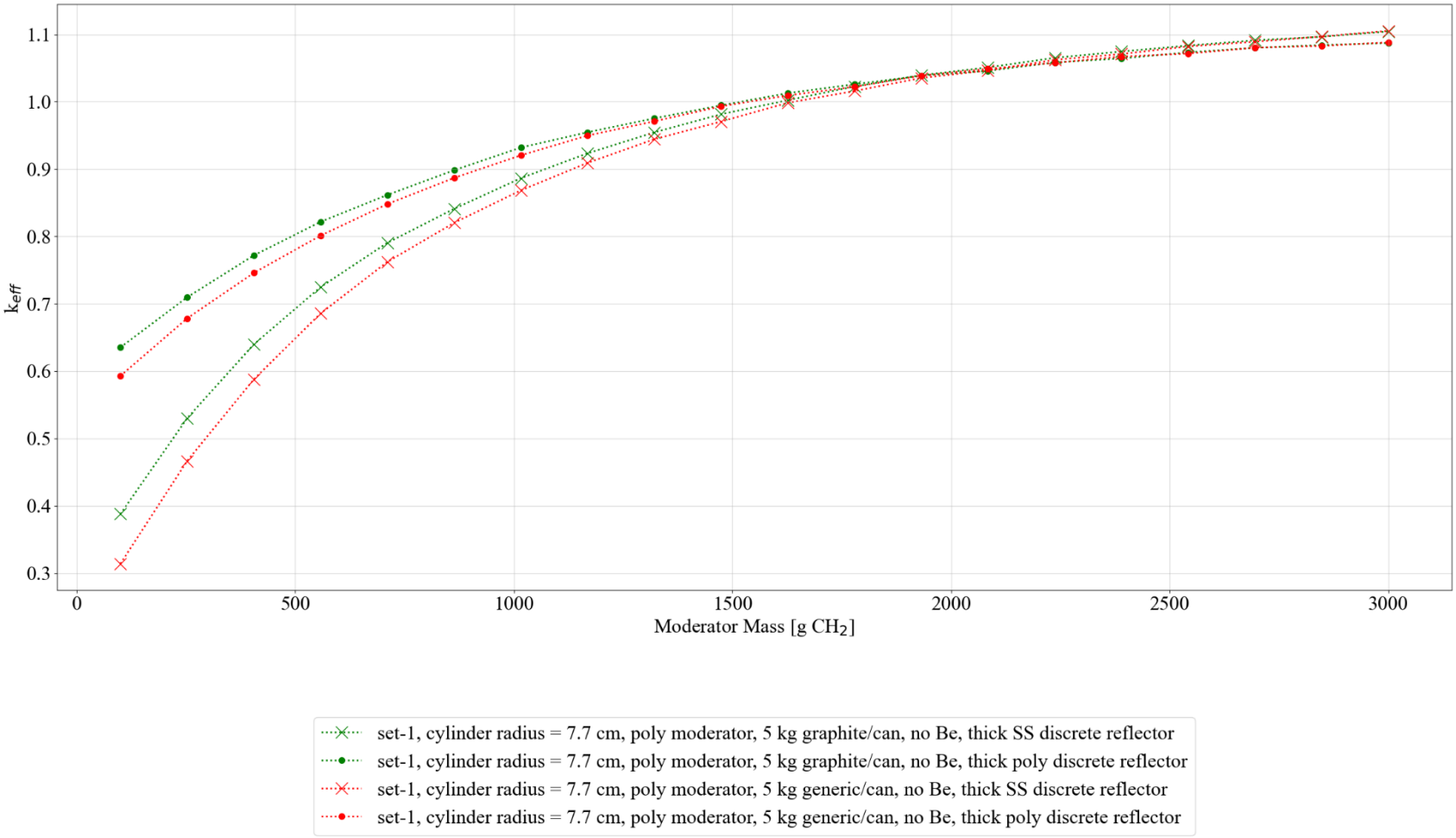

Figure A-12. Set-1 results, plot 11: comparison of graphite and generic filler with 7.7 cm cylinder radius, no Be, poly moderated, thick discrete reflector.

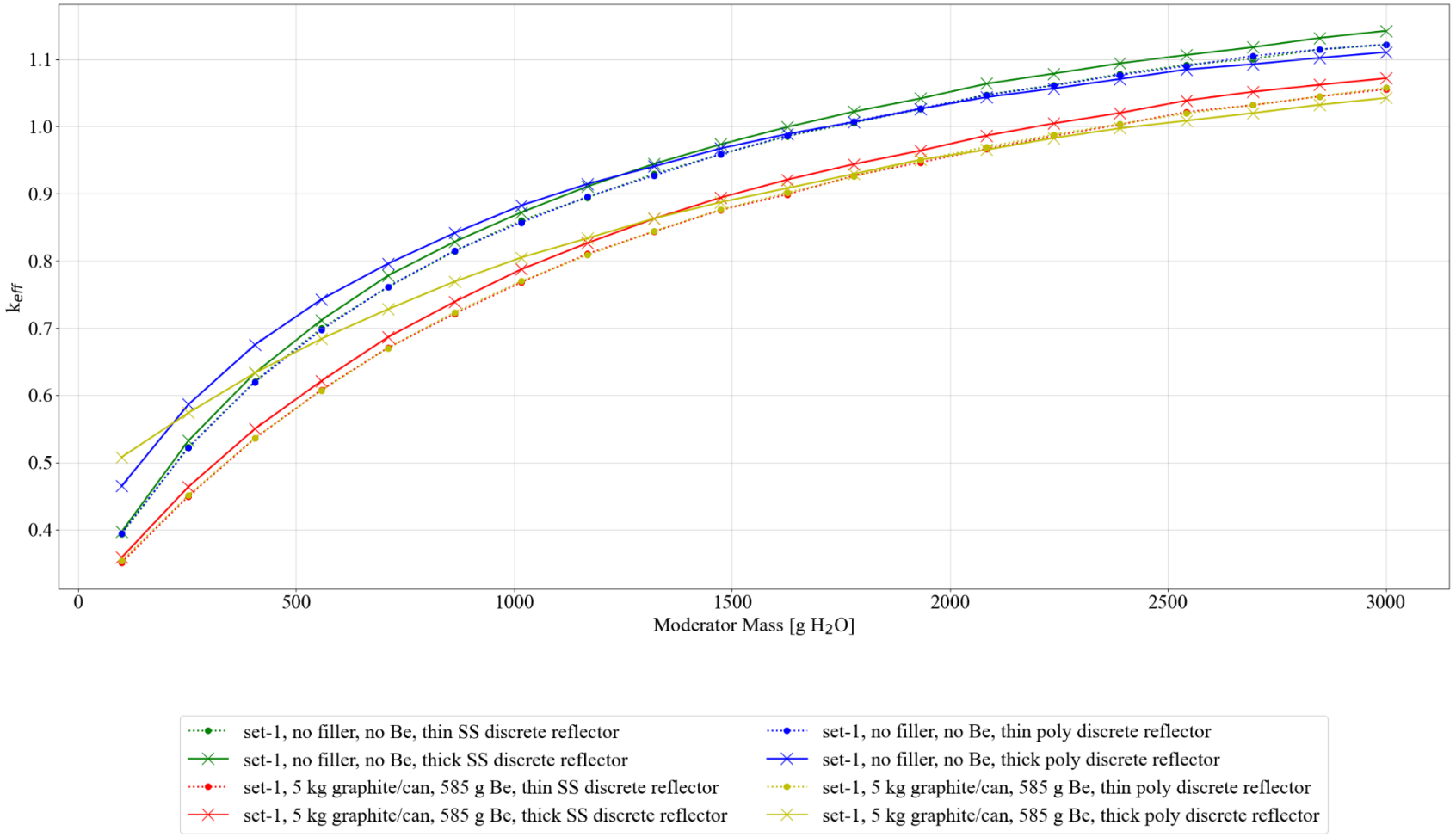

Figure A-13. Set-1 results, plot 12: reactivity effect of various parameters with spherical waste form geometry, graphite filler, water moderated.

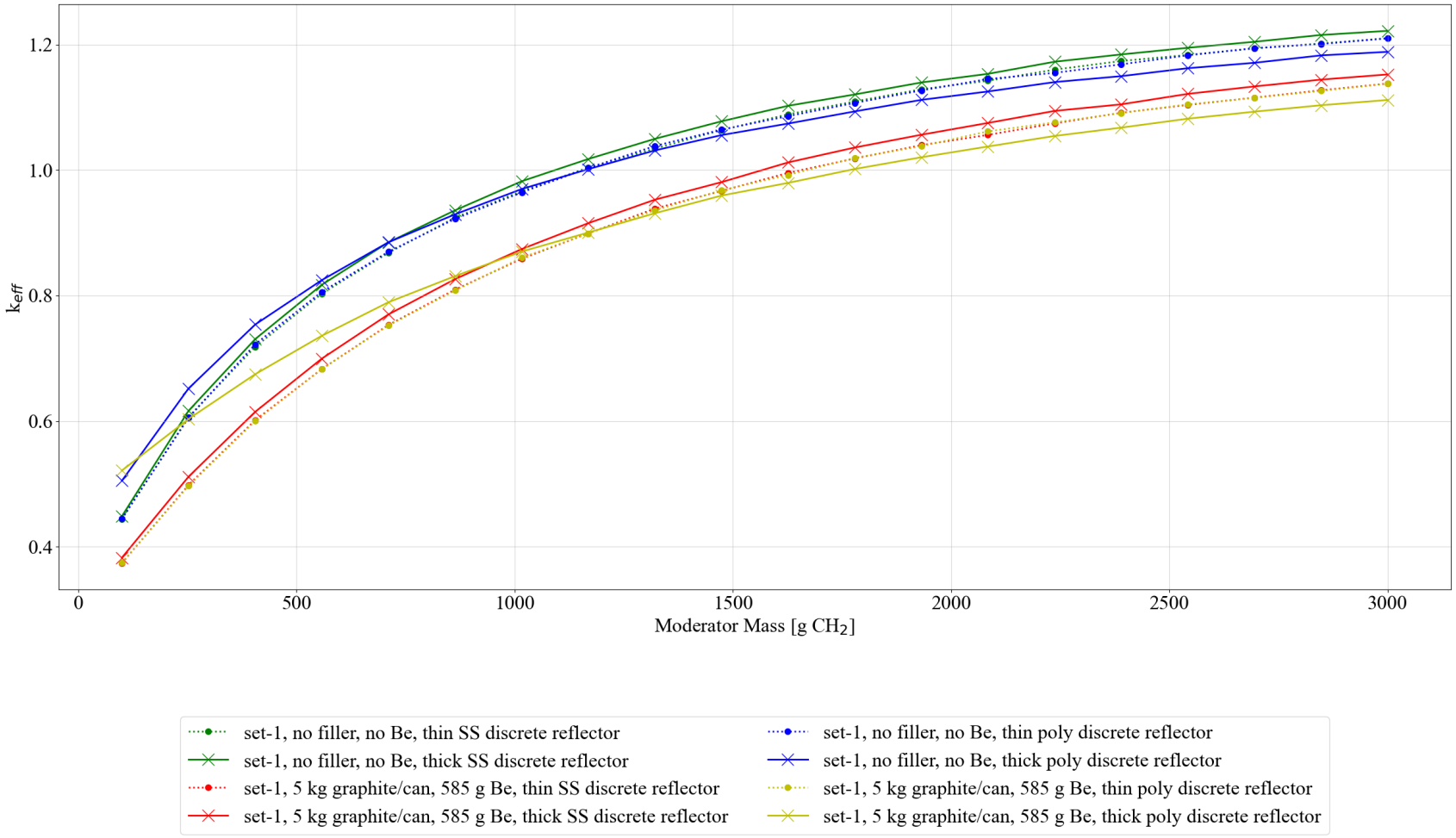

Figure A-14. Set-1 results, plot 13: reactivity effect of various parameters with spherical waste form geometry, graphite filler, poly moderated.

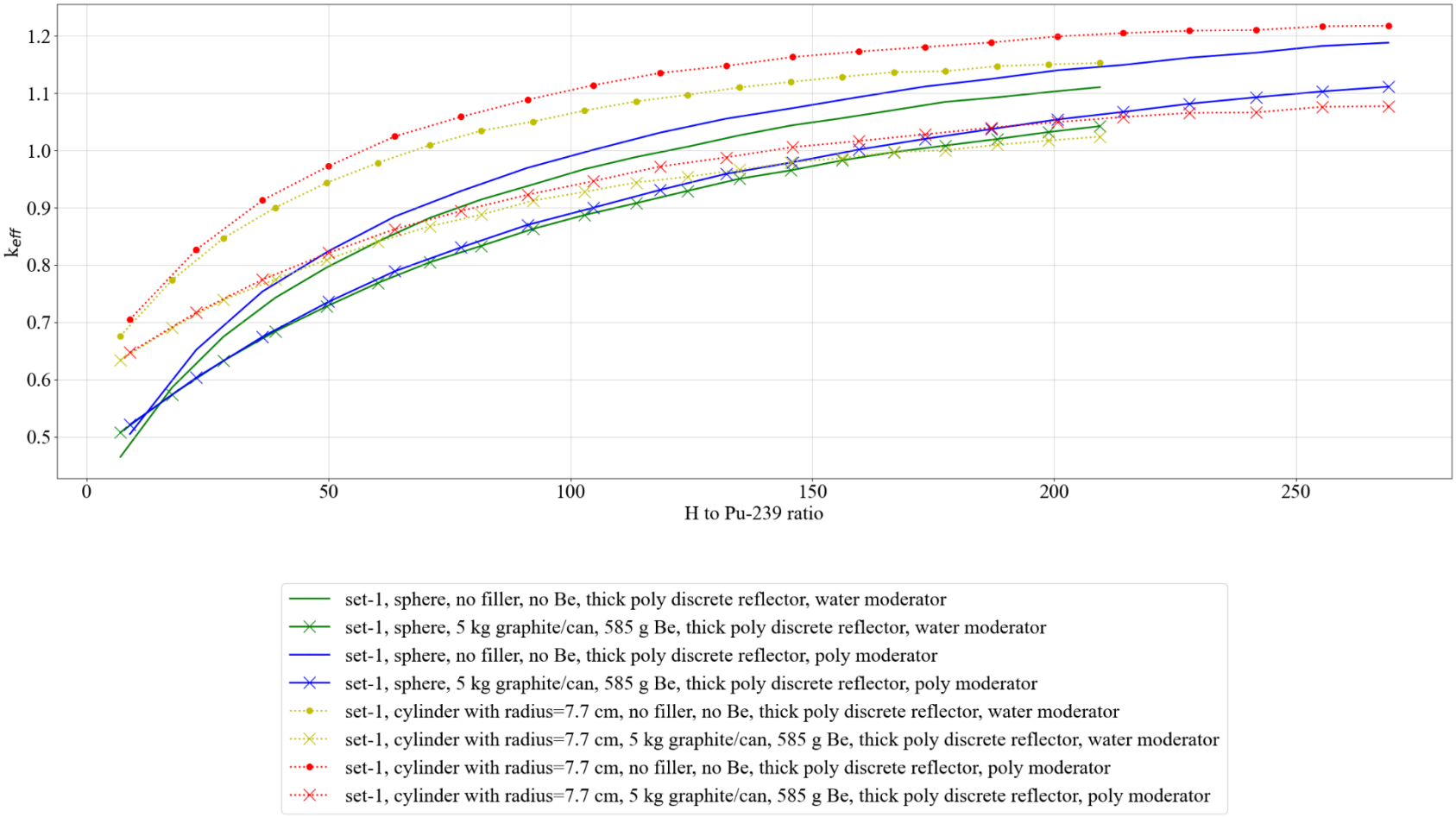

Figure A-15. Set-1 results, plot 14: comparison of spherical and cylindrical geometries (h/x).

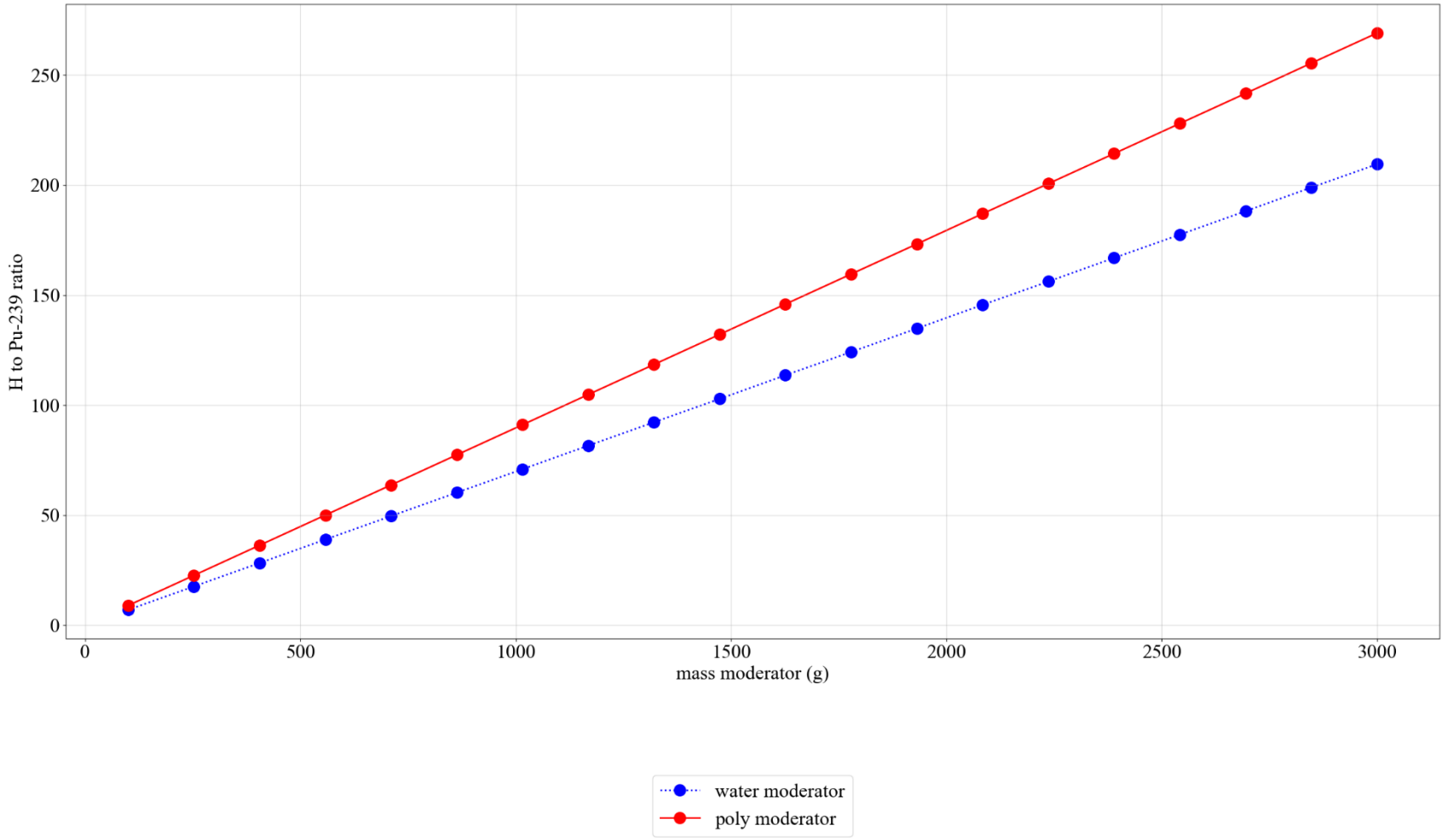

Figure A-16. Set-1 results, plot 15: comparison of water and poly h/x.

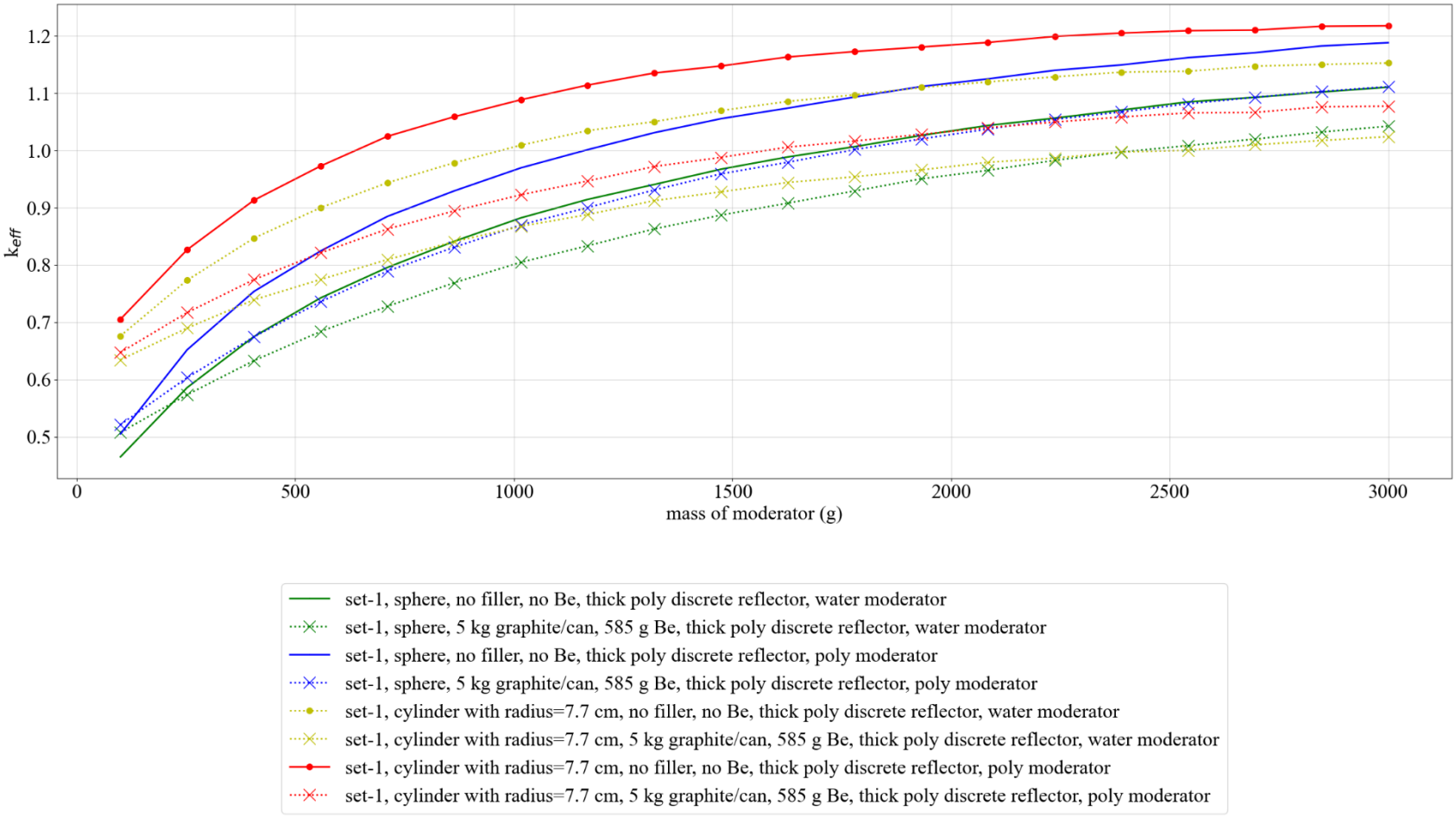

Figure A-17. Set-1 results, plot 16: comparison of spherical and cylindrical geometries (mod mass).

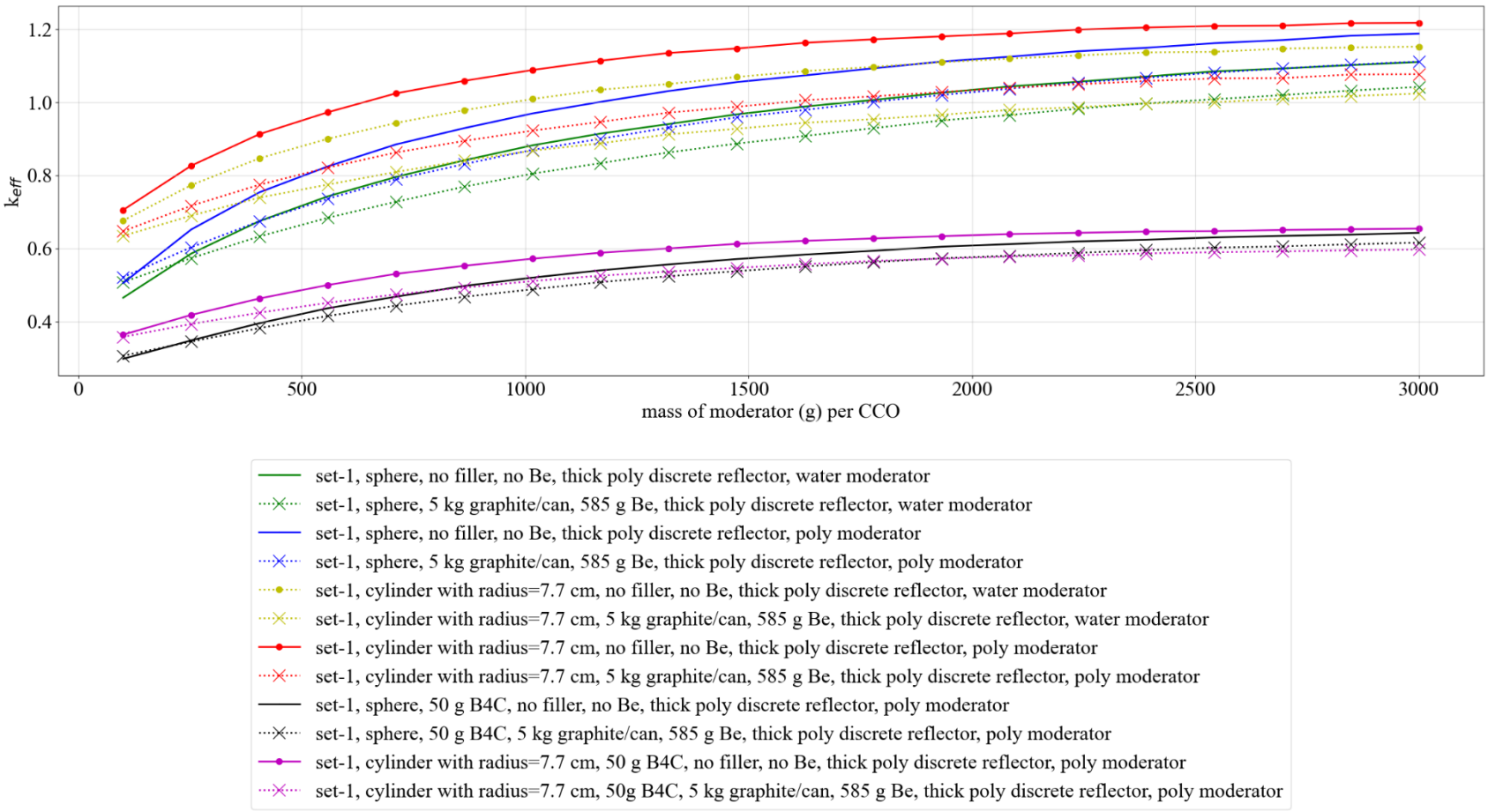

Figure A-18. Set-1 results, plot 17: comparison of 50 g B_4C vs. no B_4C for spherical and cylindrical geometries (mod mass).

This page is intentionally blank

APPENDIX B. SET-1A: RESULTS OF THE THREE-HIGH UNIFORM ARRAY WITH ALTERNATIVE SPACING CALCULATIONS

This page is intentionally blank

APPENDIX B. SET-1A: RESULTS OF THE THREE-HIGH UNIFORM ARRAY WITH ALTERNATIVE SPACING CALCULATIONS

The analysis methodology for the uniform arrays is discussed in detail in Section 6.2 of the main report.

This appendix serves as a repository of those results for the set-1a calculations.

The complete results for all SAMPLER sweeps are provided in ADDENDUM 1.

The analysis model use for the calculations in this appendix is shown in Figure B-1 below.

The SAMPLER case sweeps presented in this appendix are summarized in Table B-1 below.

LIST OF FIGURES

LIST OF TABLES

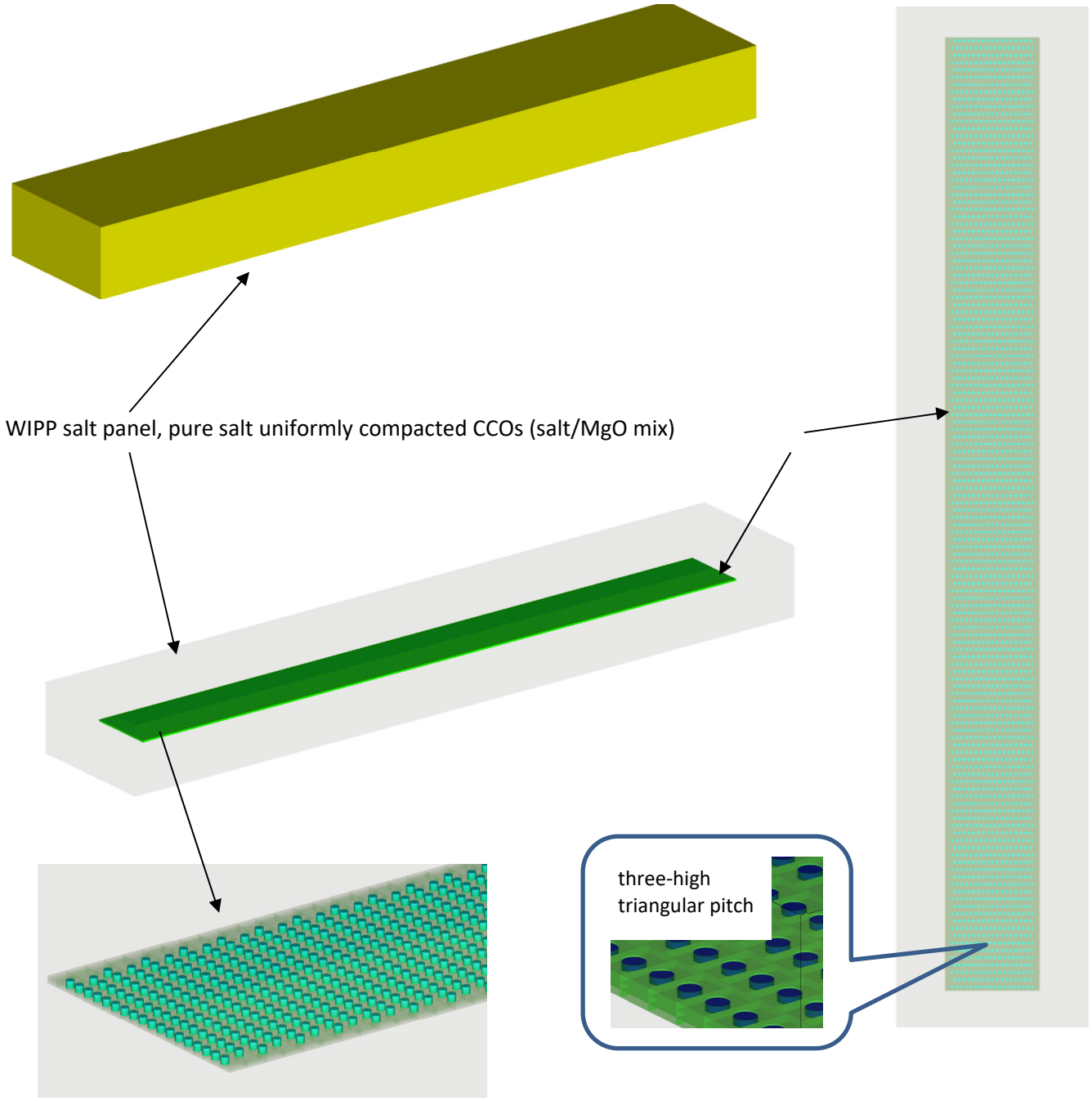

Figure B-1. Diagram of the uniform array three-high model. This is not an actual analysis model: it is a diagram of a model used by SAMPLER to generate the analysis models.

Table B-1. Summary of cases for Set-1a

Case	Model type	Waste form shape	Waste form moderator	Filler material (0, 2,000, 4,000 g)	Metal in filler	Discrete reflector (thin 0.001 and thick 0.7112 cm)	Be (g)	Subcase
Set-1a	Uniform array stacked three high with CCO pitch reduction x = 25%, y = 10%, z = no space	Cylinder (radius range 4.8, 6, 7.7 and height defined by total volume of mass)	water	c12	SS from can (0, 500, 1,000 g)	steel	0 to 585	set-1a-1
			poly	c12		steel		set-1a-2
			water	c12		poly		set-1a-3
			poly	c12		poly		set-1a-4
			water	generic		steel		set-1a-5
			poly	generic		steel		set-1a-6
			water	generic		poly		set-1a-7
			poly	generic		poly		set-1a-8
		Sphere (radius defined by total volume of mass)	water	c12		steel		set-1a-9
			poly	c12		steel		set-1a-10
			water	c12		poly		set-1a-11
			poly	c12		poly		set-1a-12
			water	generic		steel		set-1a-13
			poly	generic		steel		set-1a-14
			water	generic		poly		set-1a-15
			poly	generic		poly		set-1a-16
			poly + 50 g B_4C (cyl)	c12		poly (0.7112)		set-1a-17
			poly + 50 g B_4C (sph)	c12		poly (0.7112)		set-1a-18

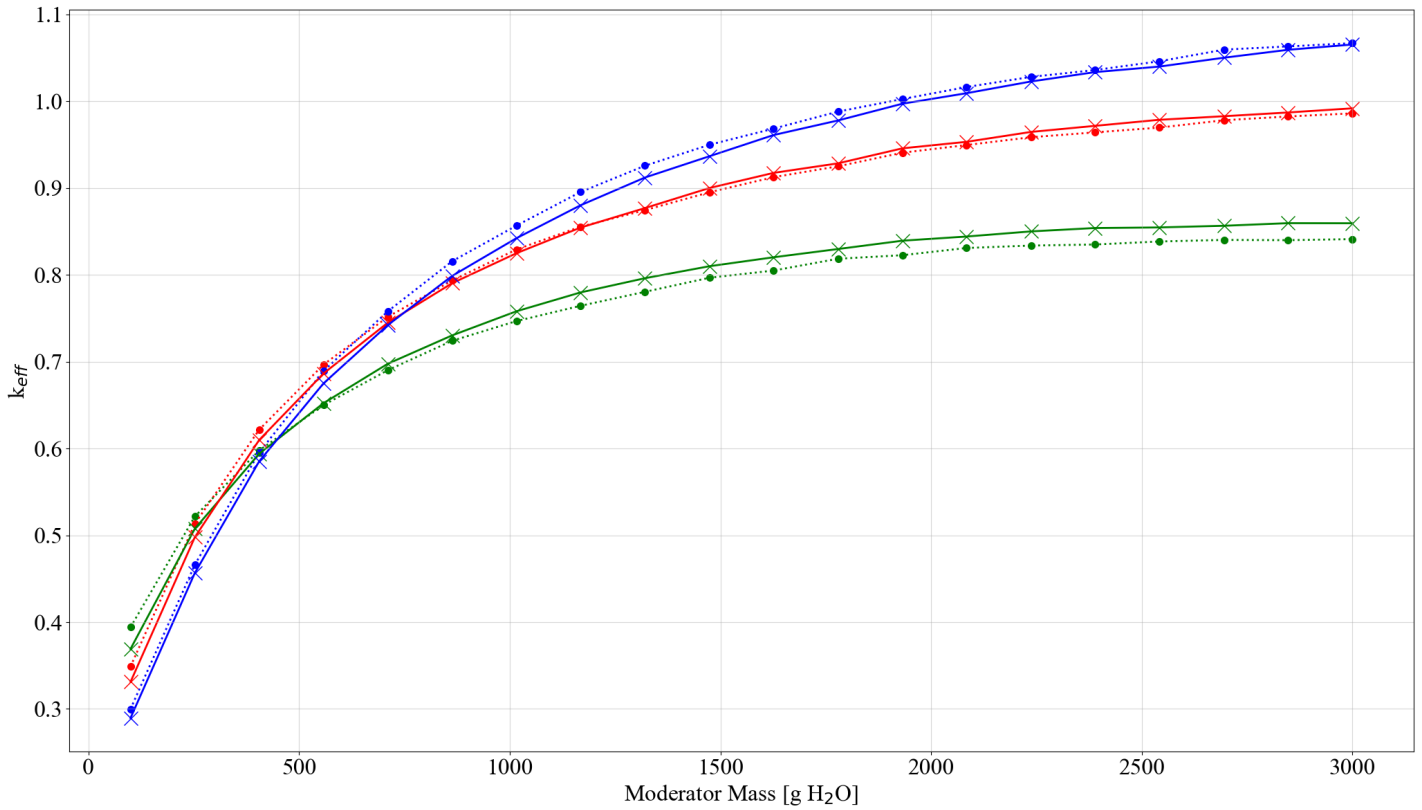

Figure B-2. Set-1a results, plot 1: reactivity effect of cylinder radius, pipe steel, no filler, no Be, water moderated.

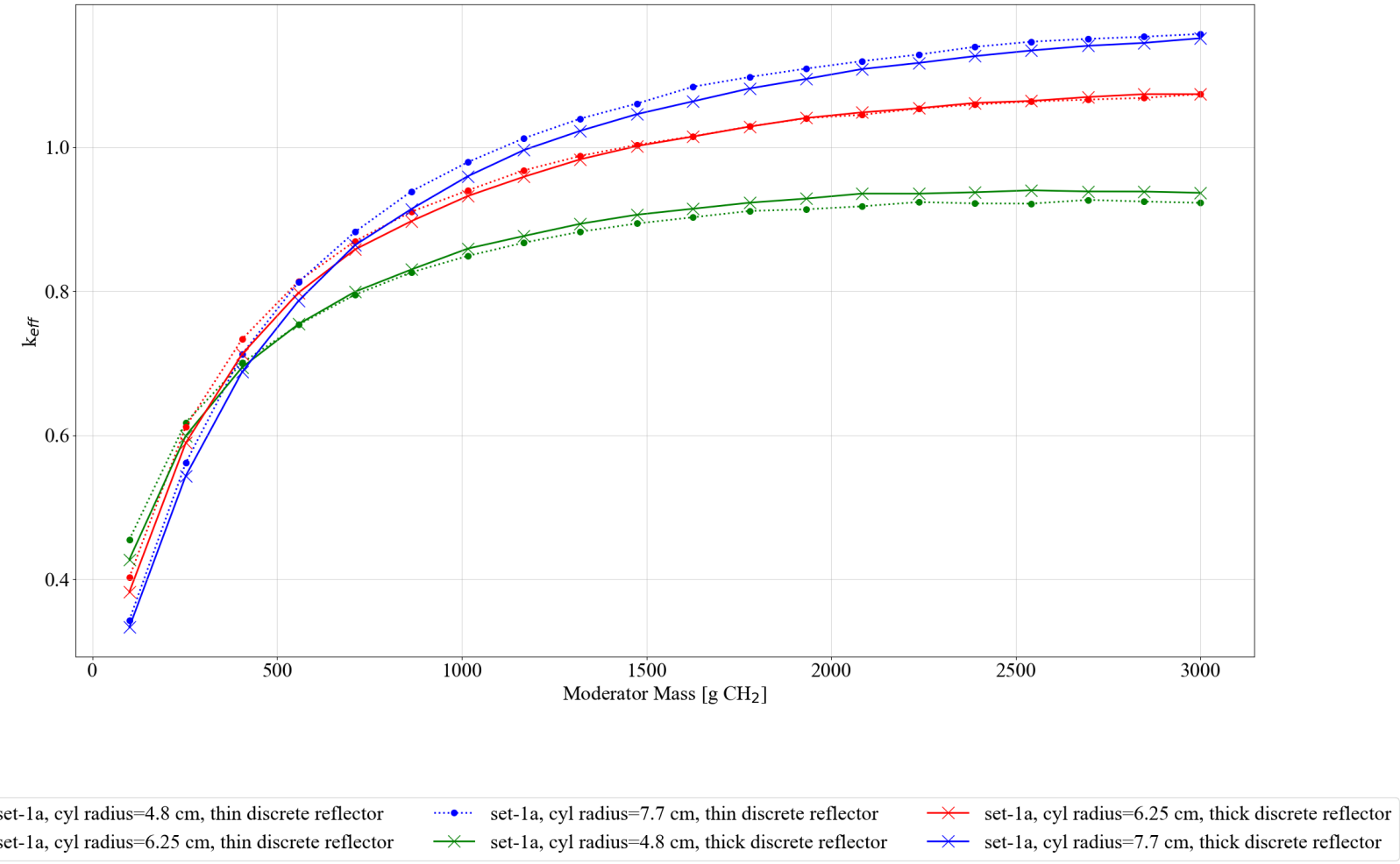

Figure B-3. Set-1a results, plot 2: reactivity effect of cylinder radius, pipe steel, no filler, no Be, poly moderated.

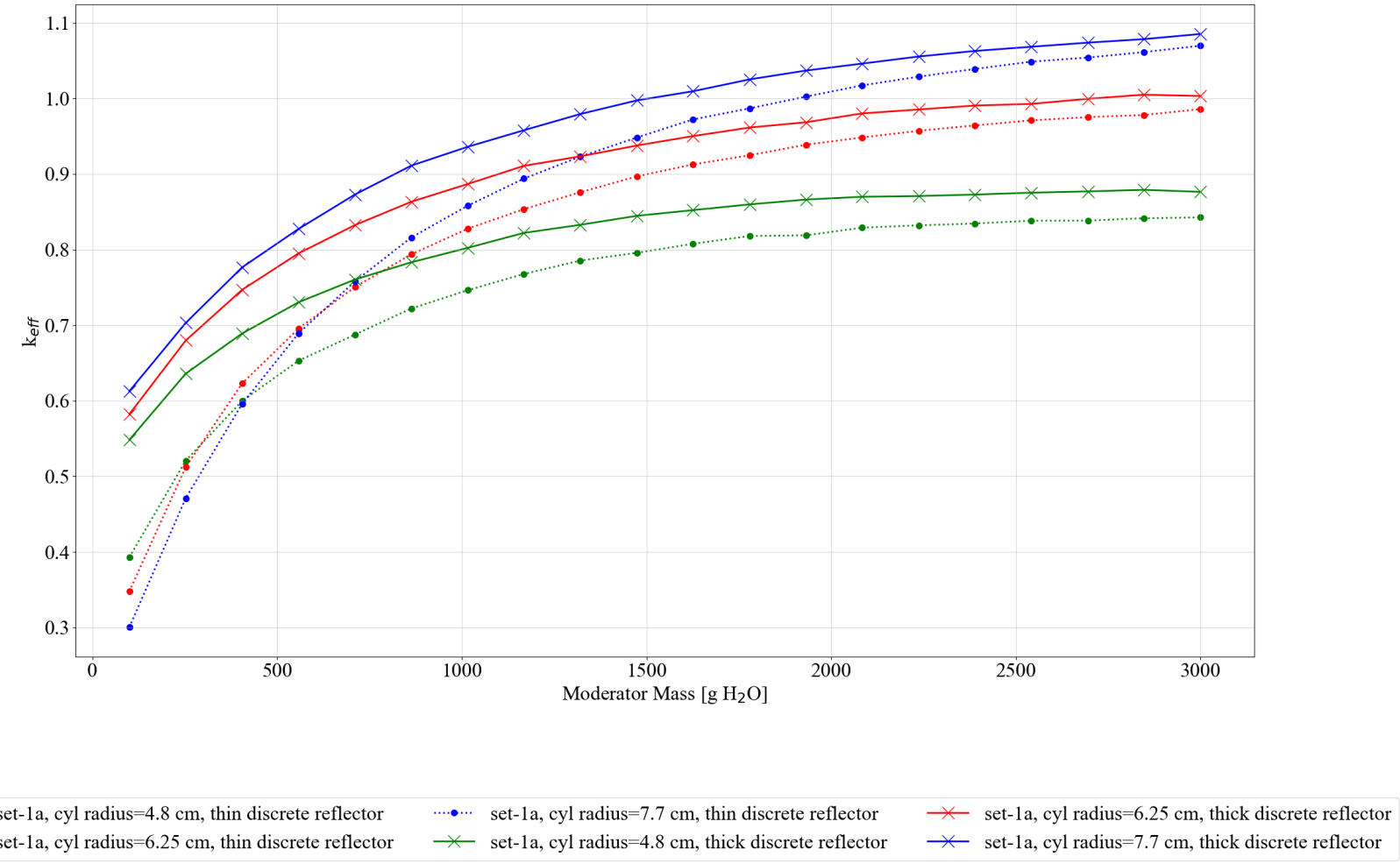

Figure B-4. Set-1a results. plot 3: reactivity effect of cylinder radius, pipe poly, no filler, no Be, water moderated.

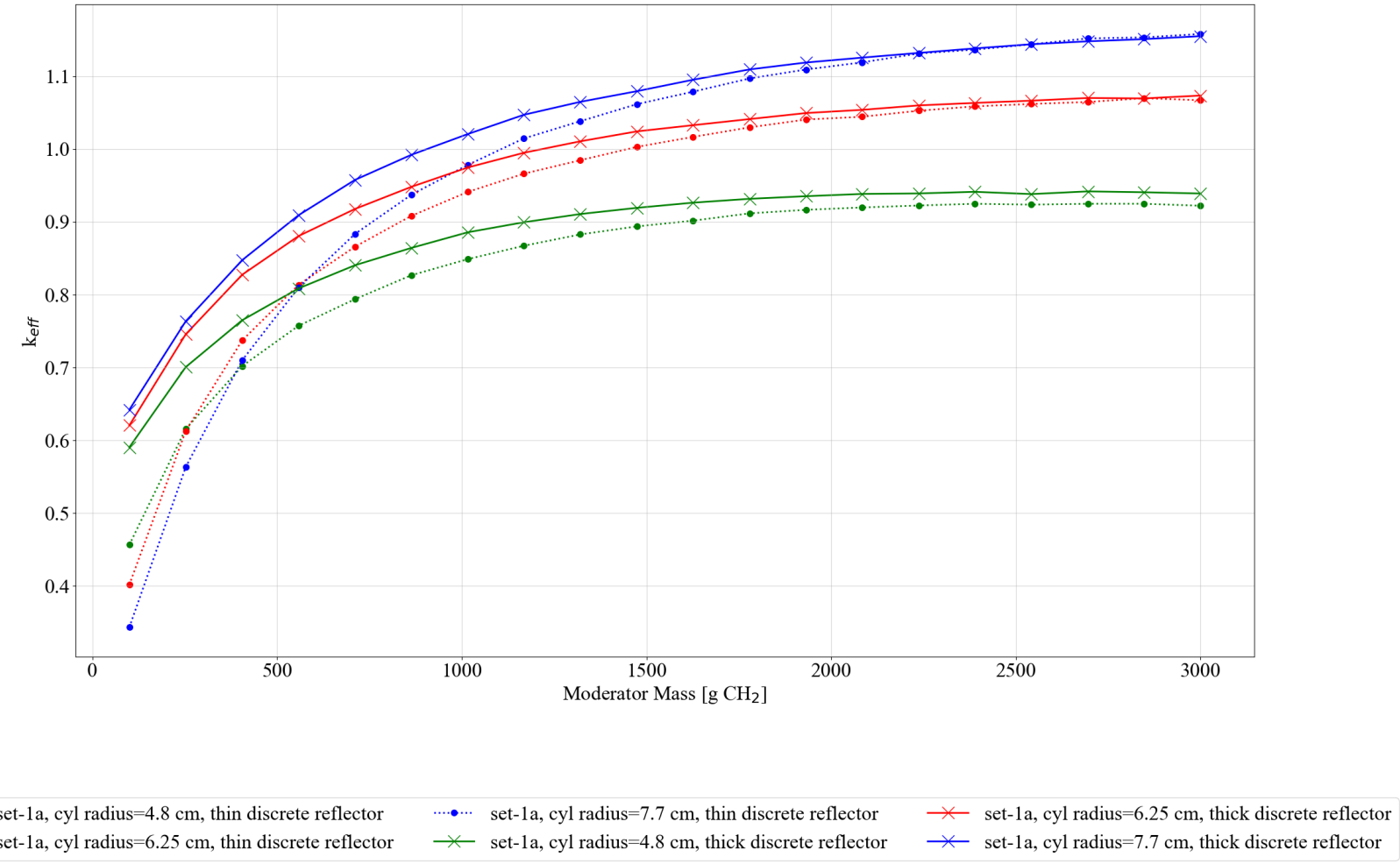

Figure B-5. Set-1a results, plot 4: reactivity effect of cylinder radius, pipe poly, no filler, no Be, poly moderated.

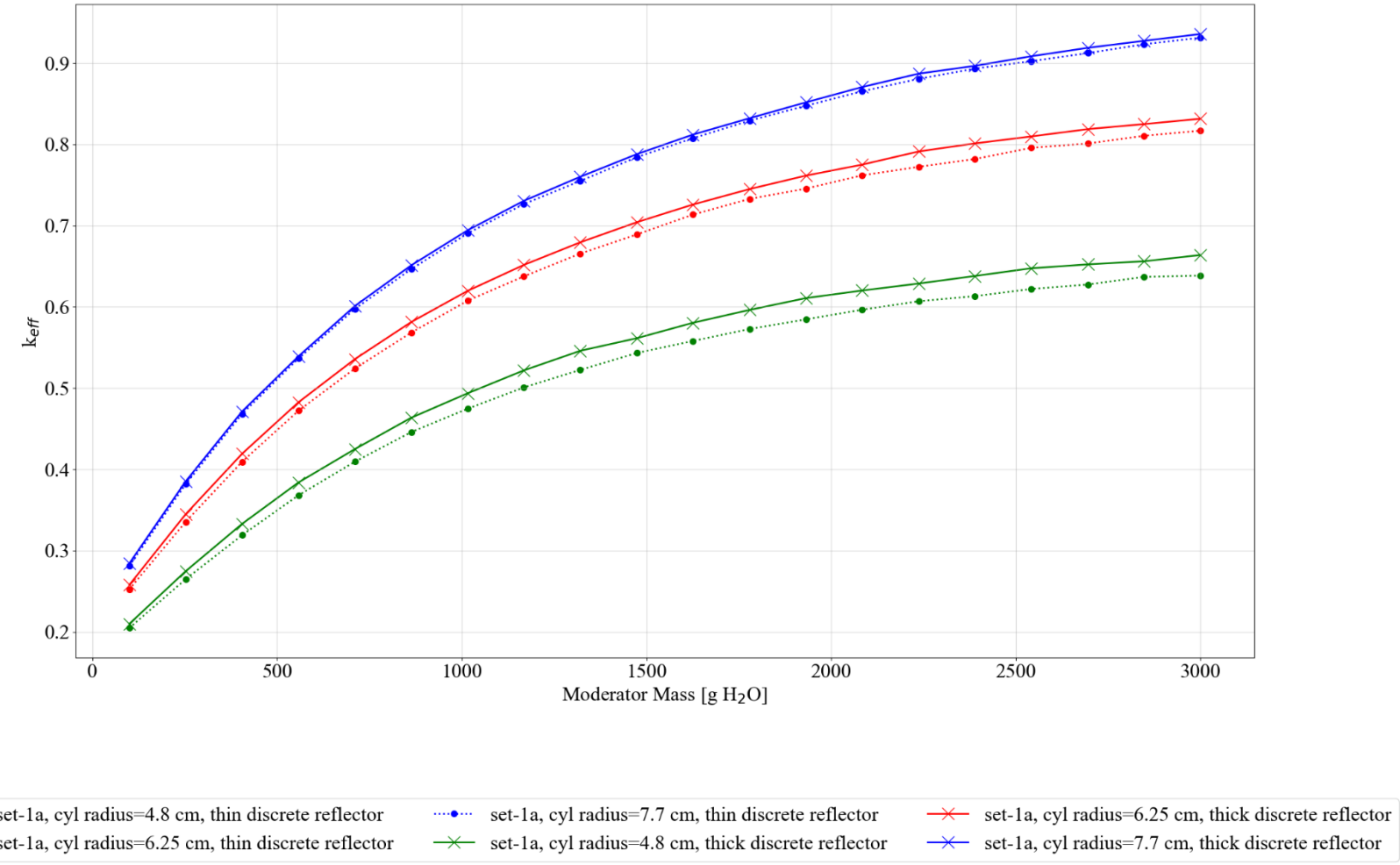

Figure B-6. Set-1a results, plot 5: reactivity effect of cylinder radius, pipe steel, 5 kg graphite/can, no Be, water moderated.

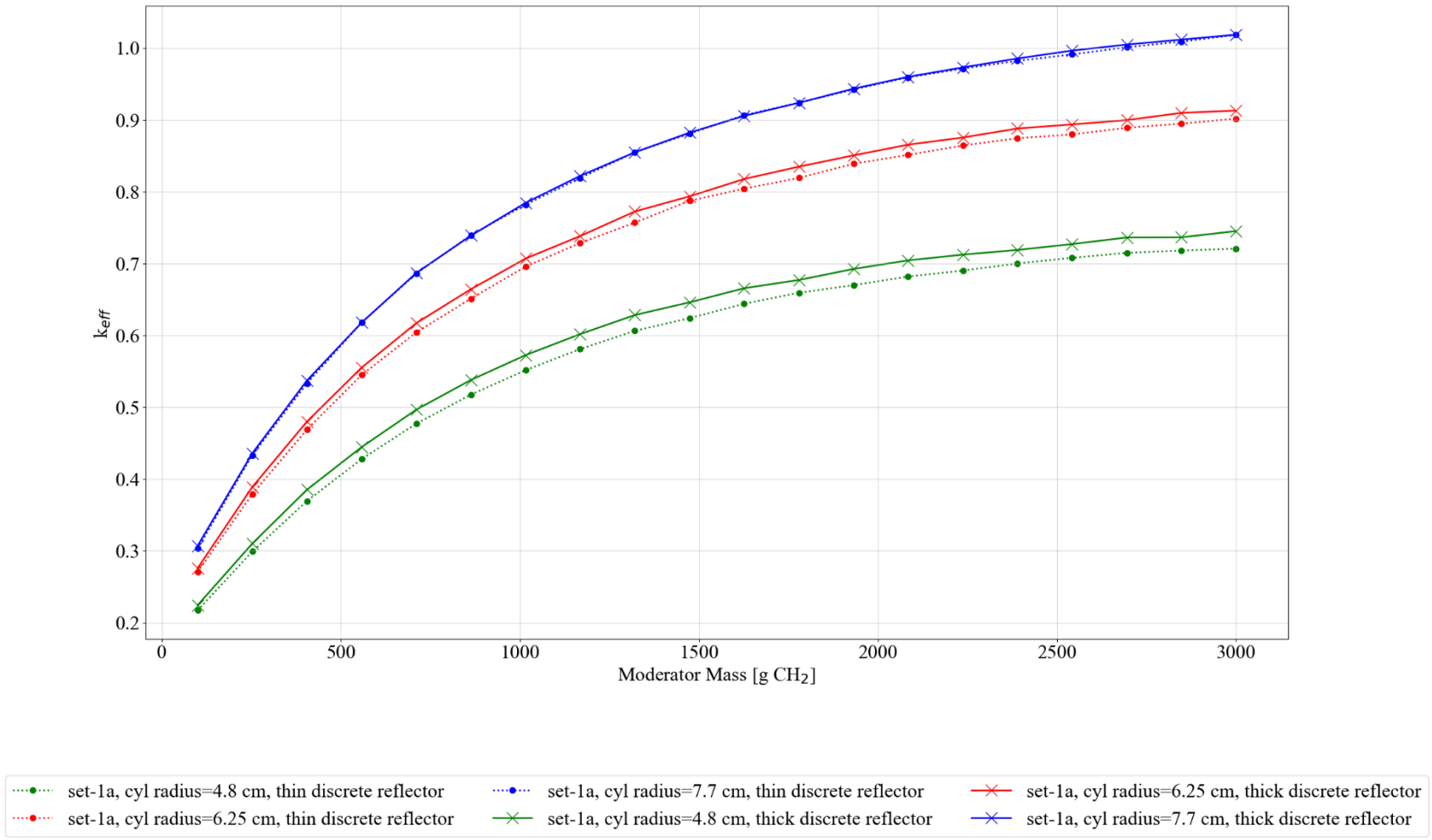

Figure B-7. Set-1a results, plot 6: reactivity effect of cylinder radius, pipe steel, 5 kg graphite/can, no Be, poly moderated.

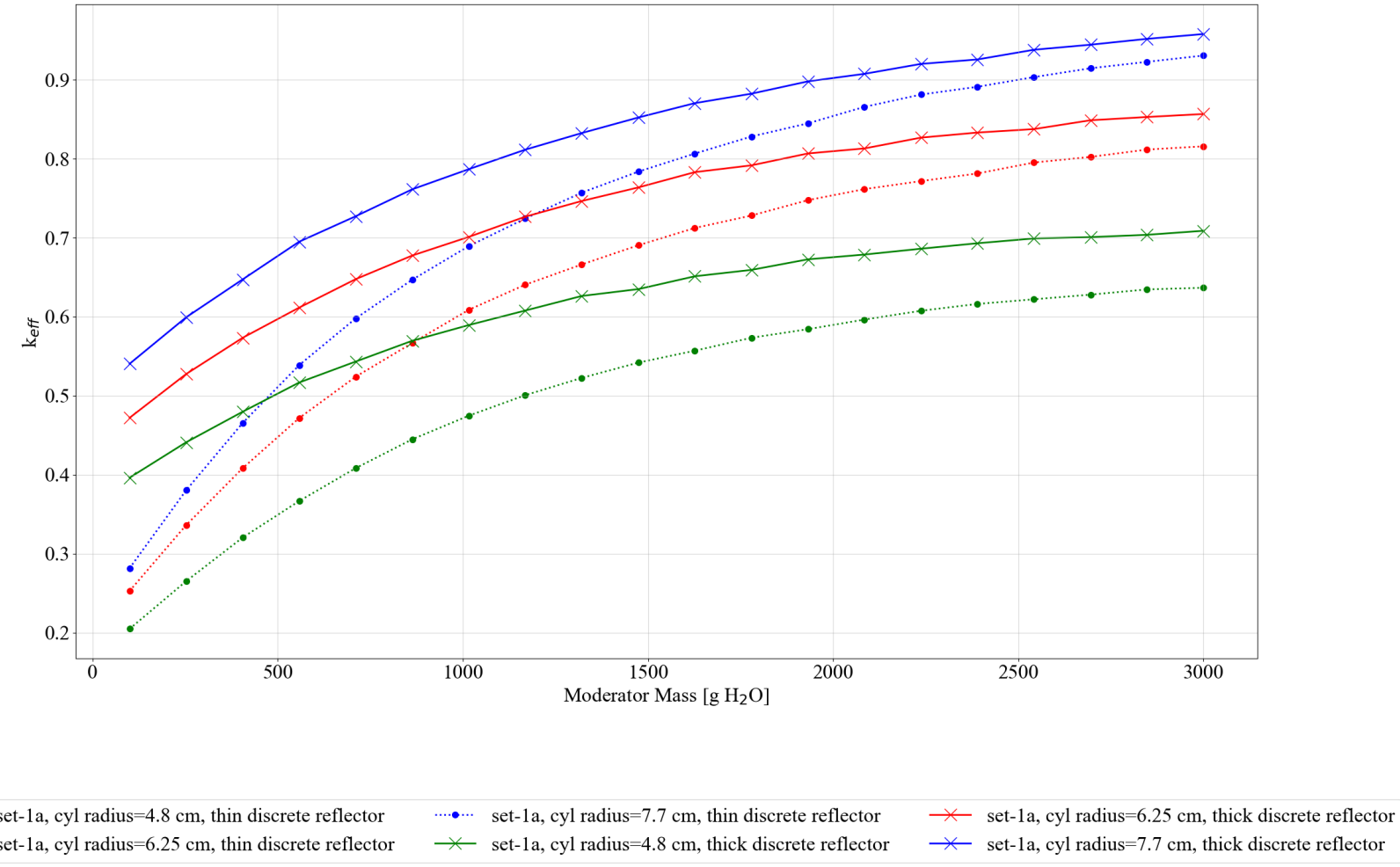

Figure B-8. Set-1a results, plot 7: reactivity effect of cylinder radius, pipe poly, 5 kg graphite/can, no Be, water moderated.

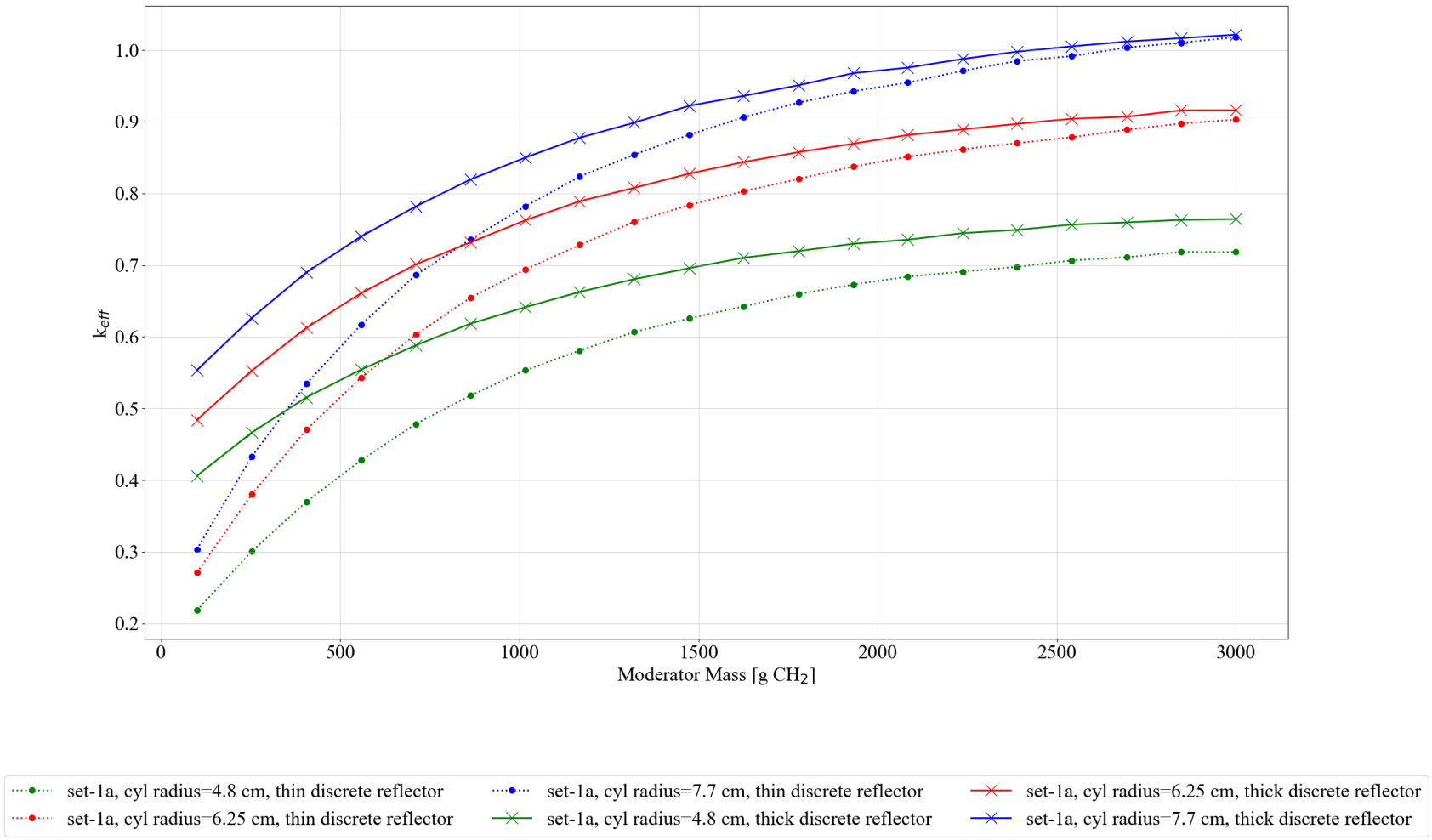

Figure B-9. Set-1a results, plot 8: reactivity effect of cylinder radius, pipe poly, 5 kg graphite/can, no Be, poly moderated.

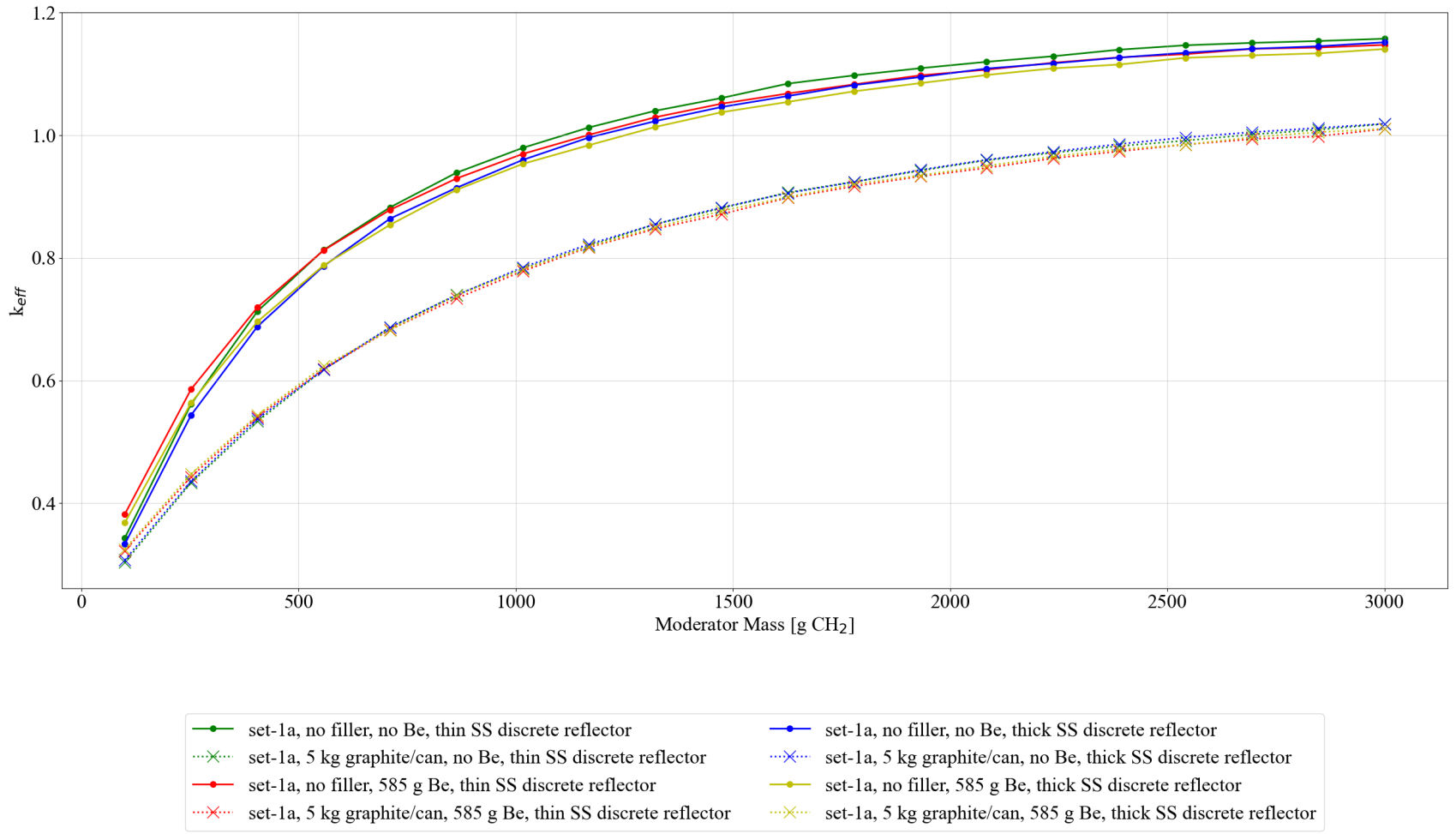

Figure B-10. Set-1a results, plot 9: reactivity effect of various parameters with 7.7 cm cylinder radius, graphite filler, poly moderated.

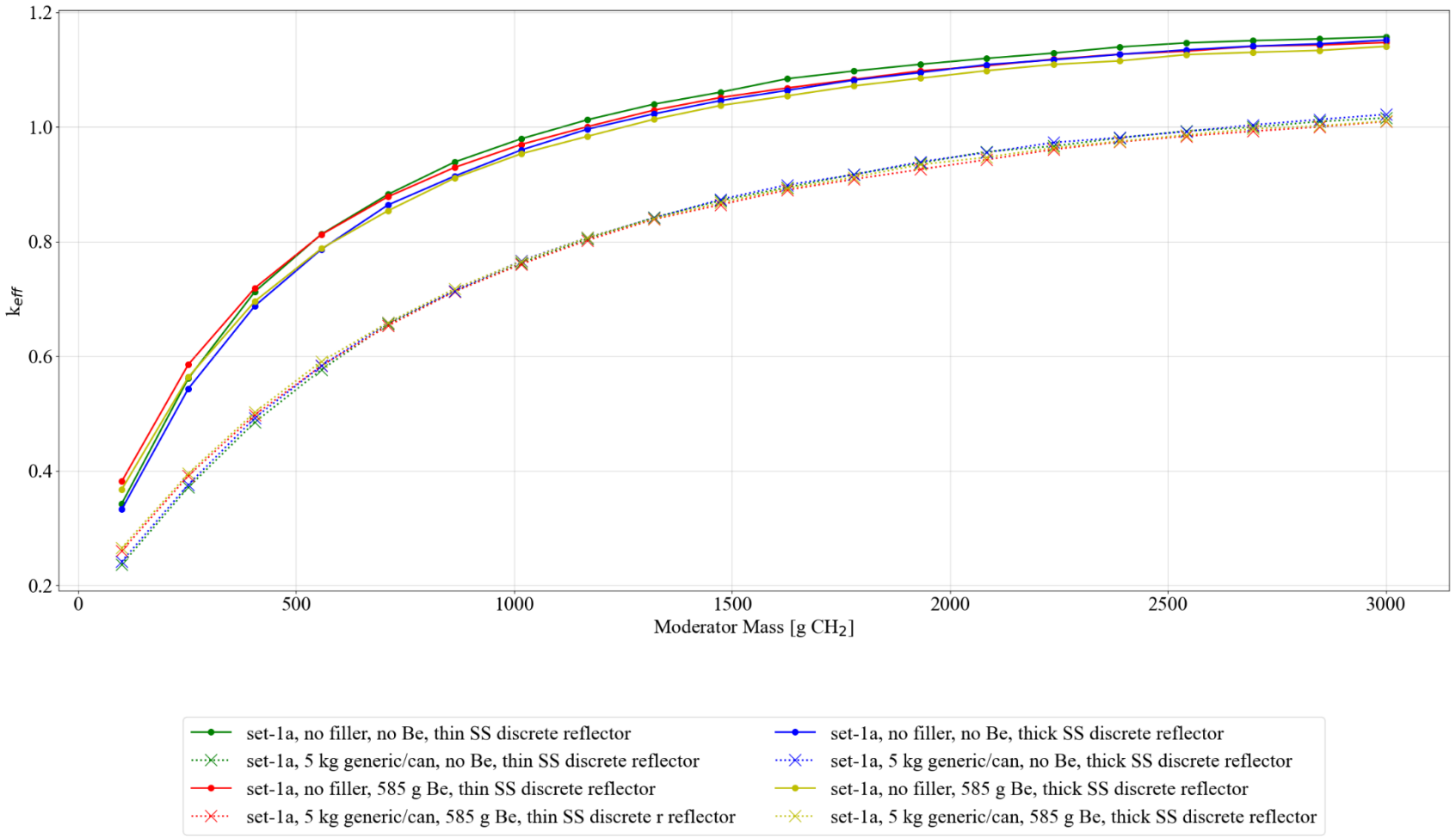

Figure B-11. Set-1a results, plot 10: reactivity effect of various parameters with 7.7 cm cylinder radius, generic filler, poly moderated.

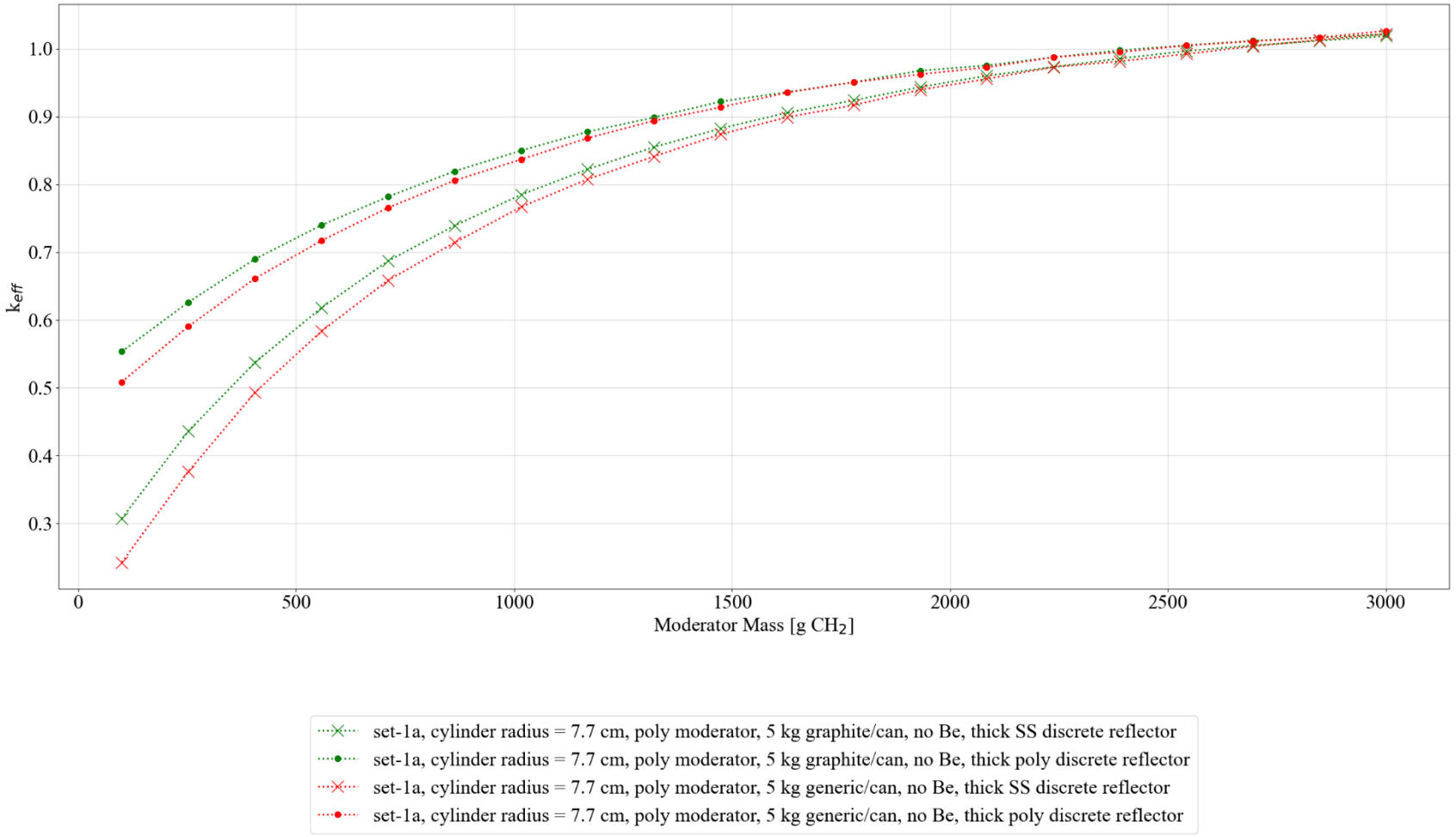

Figure B-12. Set-1a results, plot 11: comparison of graphite and generic filler with 7.7 cm cylinder radius, no Be, poly moderated, thick discrete reflector.

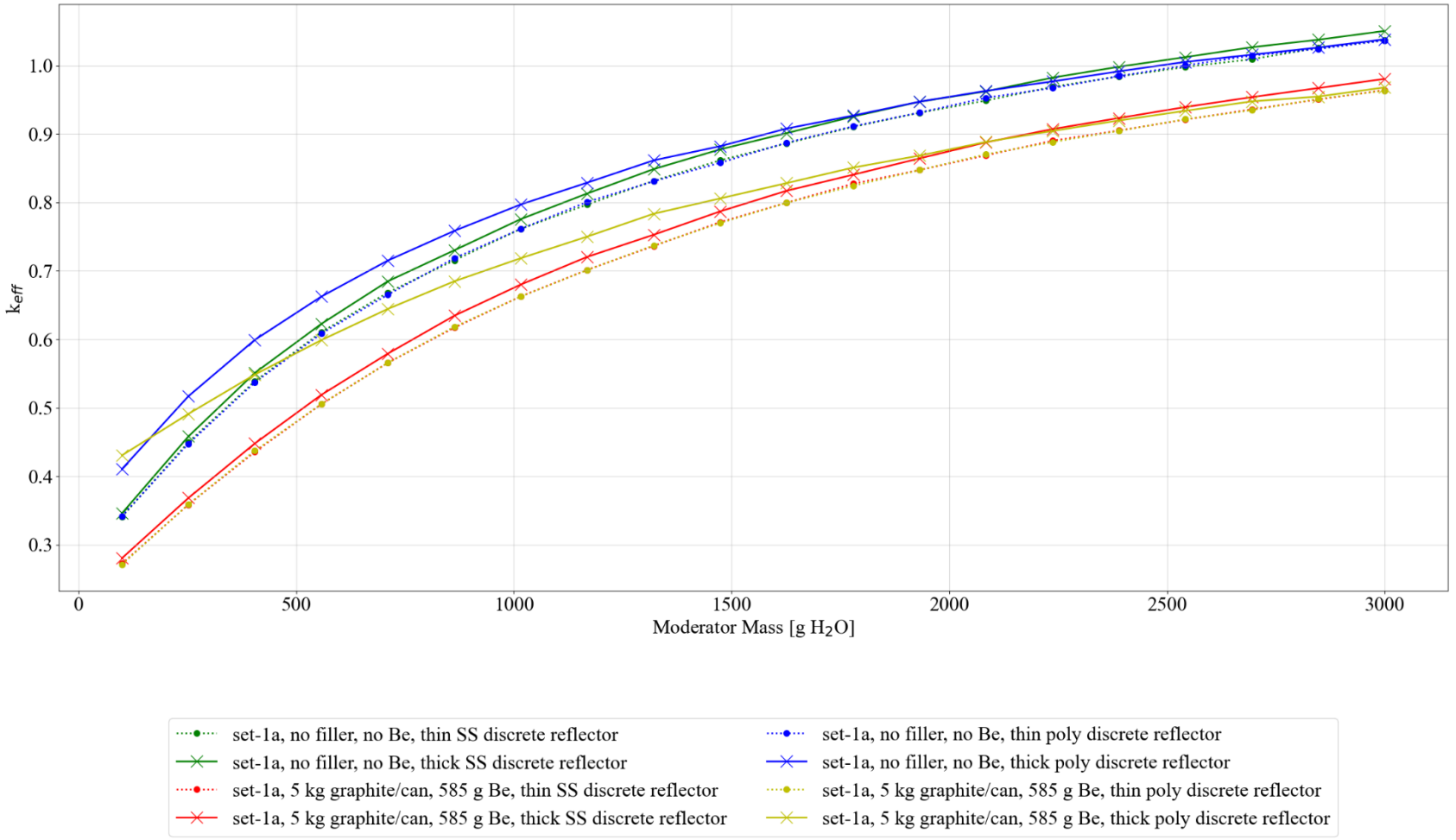

Figure B-13. Set-1a results, plot 12: reactivity effect of various parameters with spherical waste form geometry, graphite filler, water moderated.

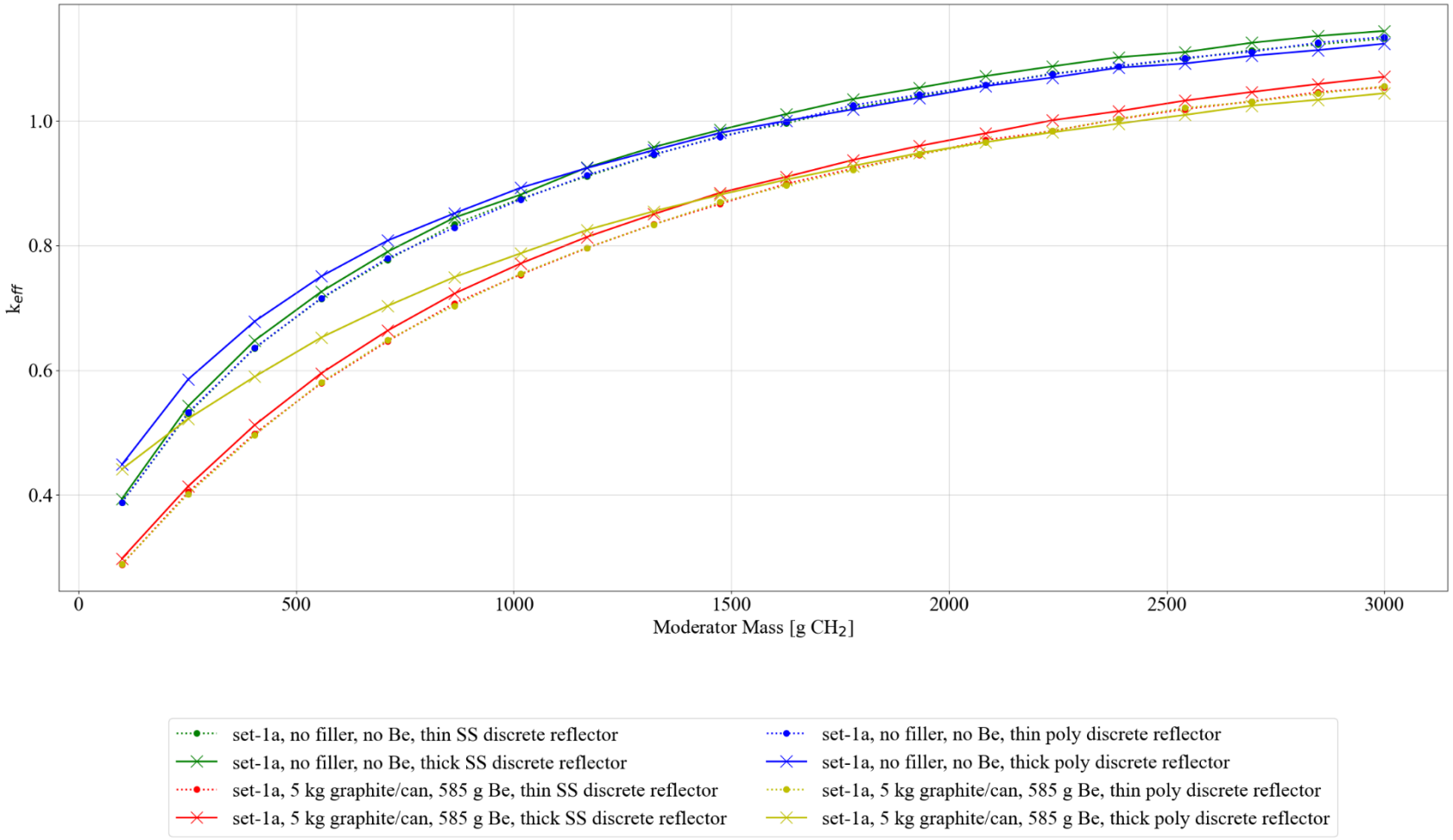

Figure B-14. Set-1a results, plot 13: reactivity effect of various parameters with spherical waste form geometry, graphite filler, poly moderated.

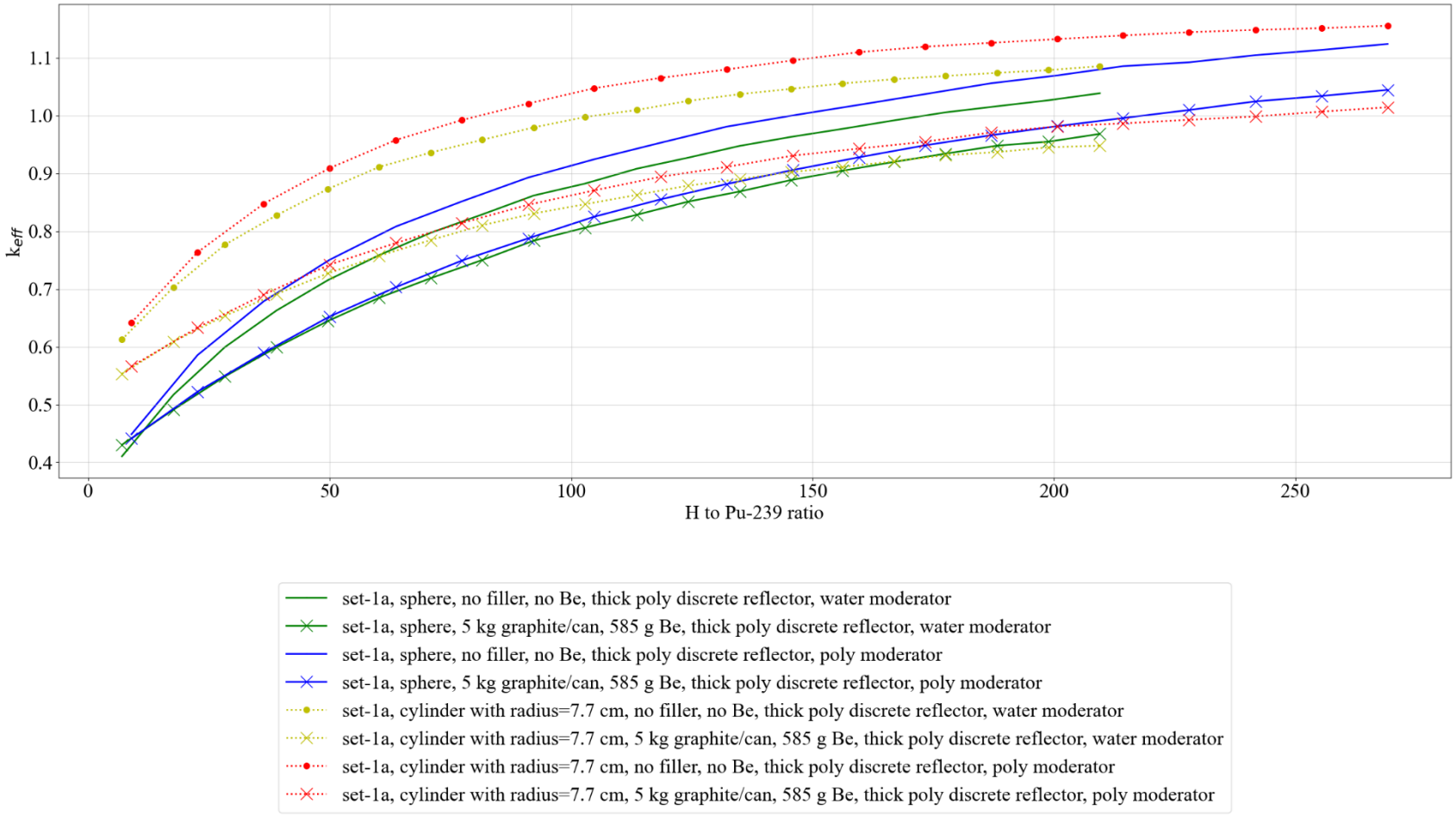

Figure B-15. Set-1a results, plot 14: comparison of spherical and cylindrical geometries (h/x).

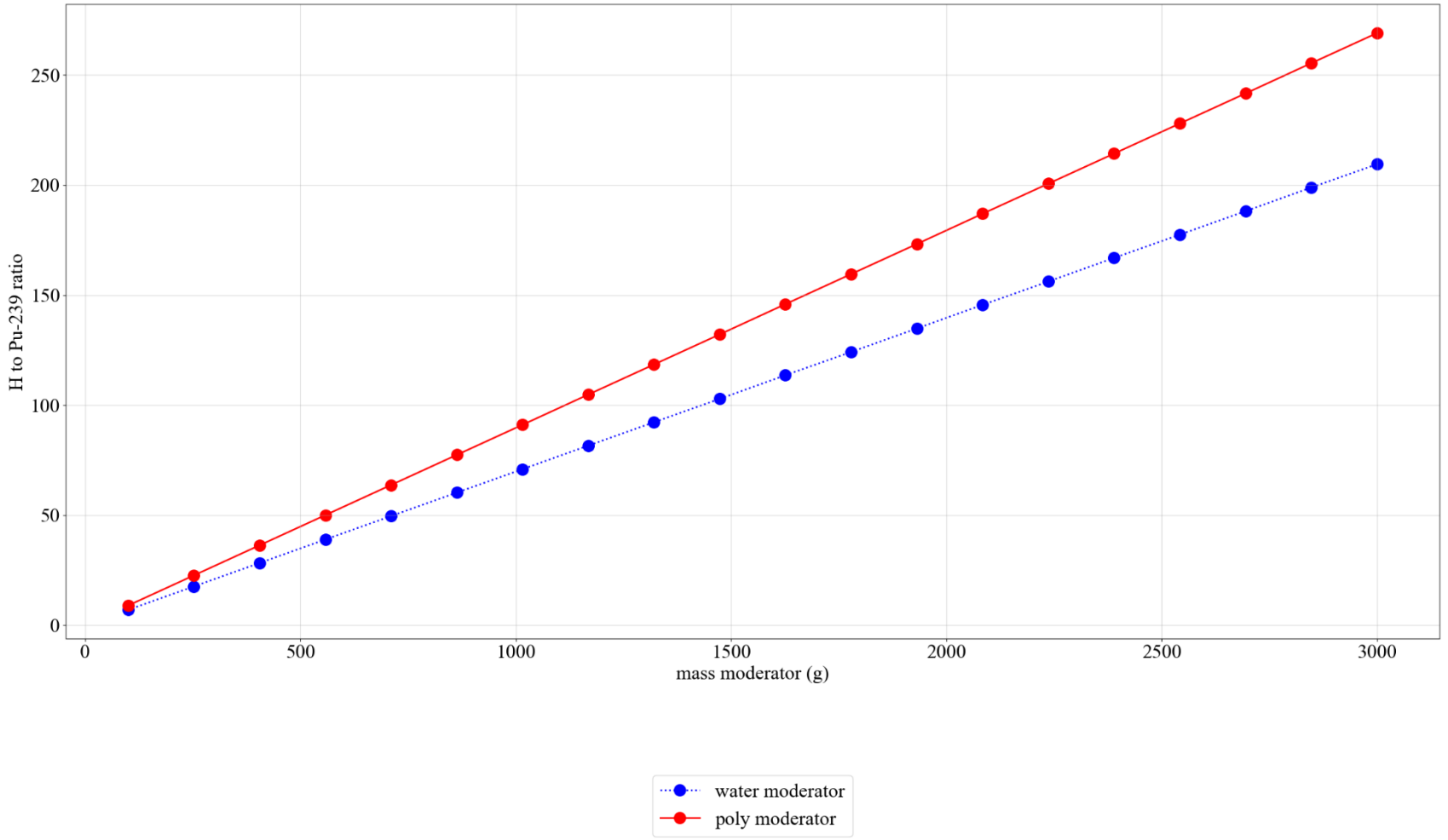

Figure B-16. Set-1a results, plot 15: comparison of water and poly h/x.

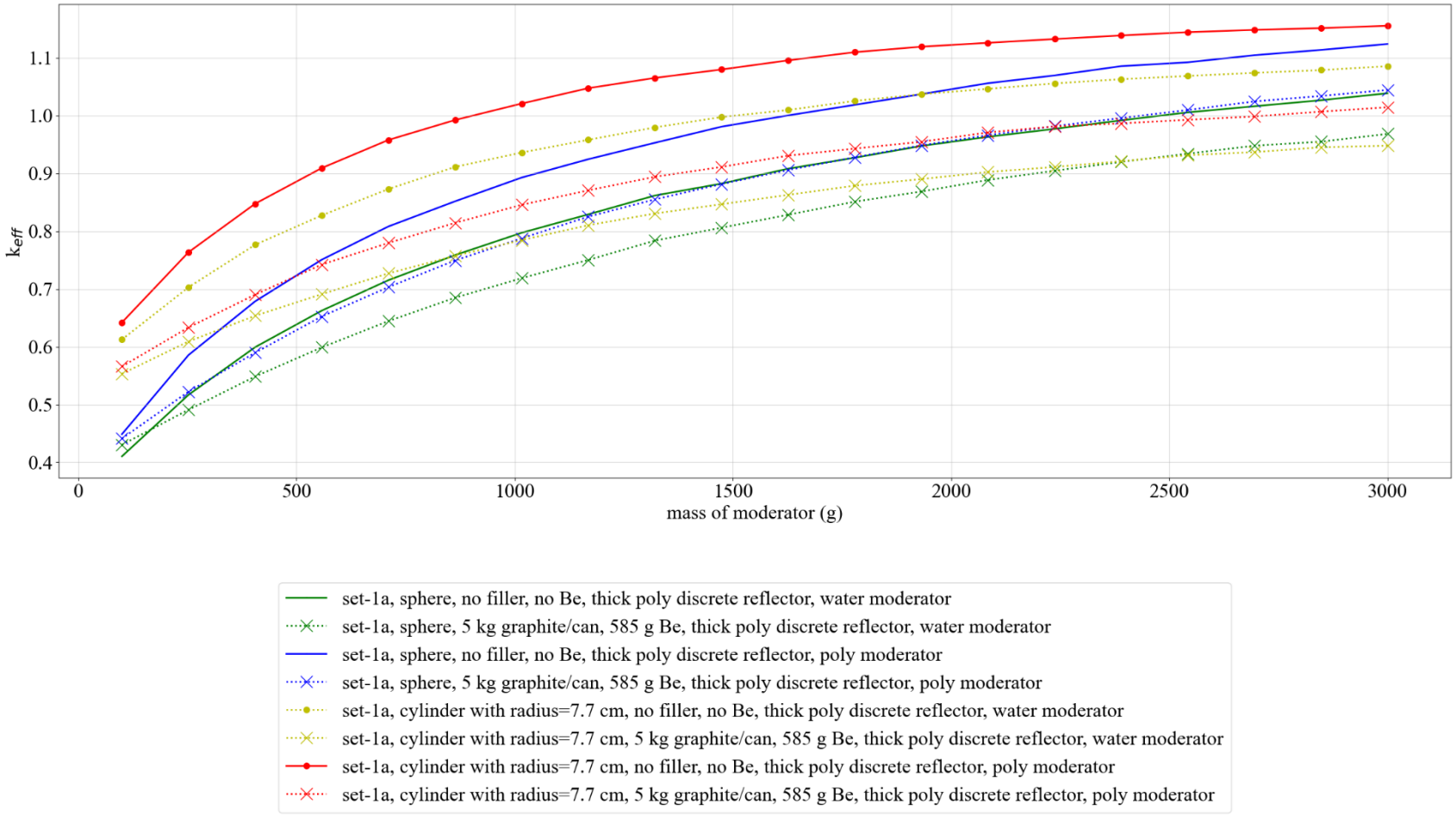

Figure B-17. Set-1a results, plot 16: comparison of spherical and cylindrical geometries (mod mass).

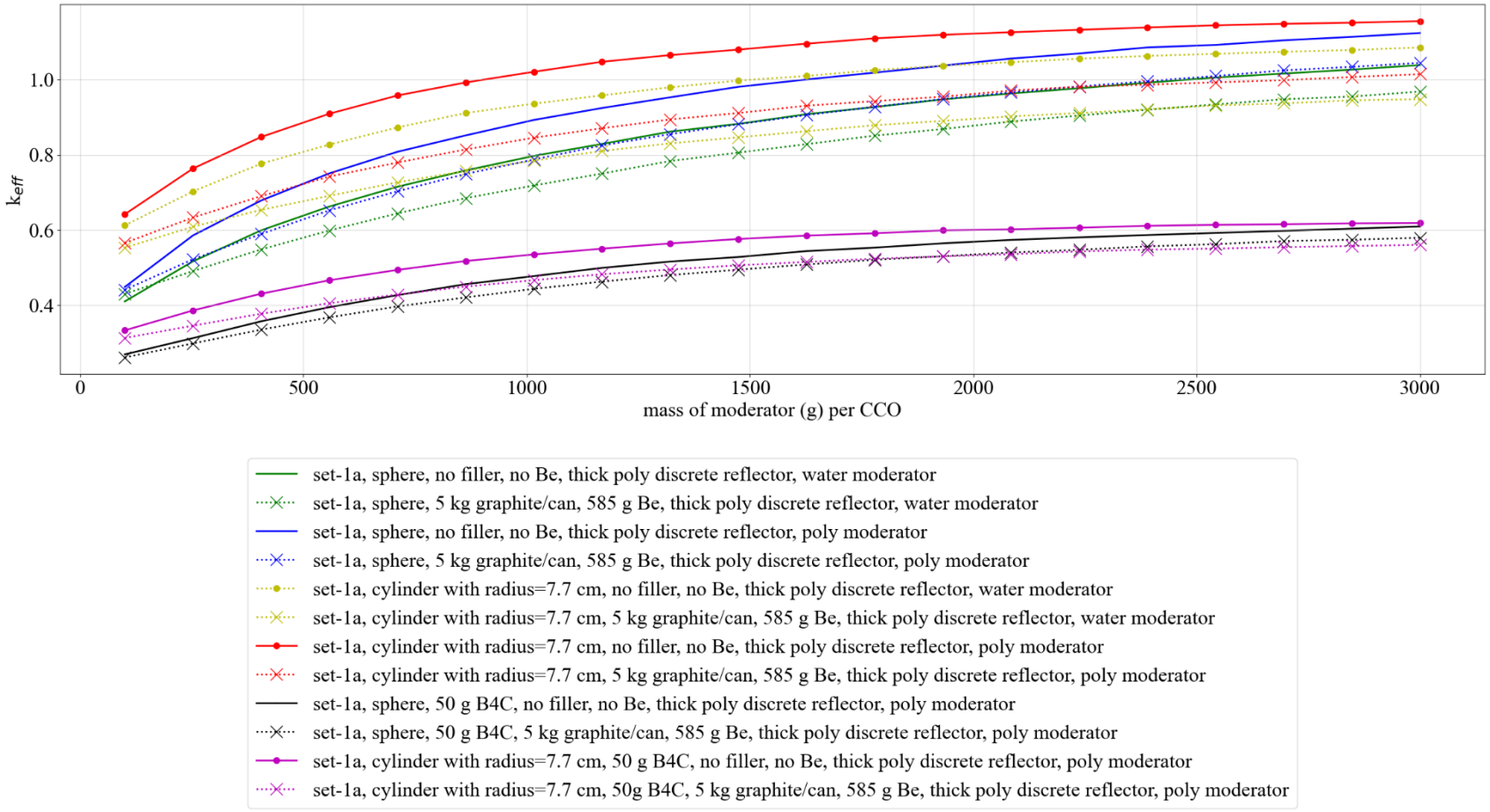

Figure B-18. Set-1a results, plot 17: comparison of 50 g B_4C vs. no B_4C for spherical and cylindrical geometries (mod mass).

This page is intentionally blank

APPENDIX C. SET-2: RESULTS OF THE NONUNIFORM ARRAY FOR THE UPPER HORIZON CALCULATIONS

This page is intentionally blank

APPENDIX C. SET-2: RESULTS OF THE NONUNIFORM ARRAY FOR THE UPPER HORIZON CALCULATIONS

The analysis methodology for the uniform arrays is discussed in detail in Section 6.3 of the main report.

This appendix serves as a repository of those results for the set-2-uh calculations.

The complete results for all SAMPLER sweeps are provided in ADDENDUM 1.

The analysis model use for the calculations in this appendix is shown in Figure C-1 below.

The SAMPLER case sweeps presented in this appendix are summarized in Table C-1 below.

LIST OF FIGURES

LIST OF TABLES

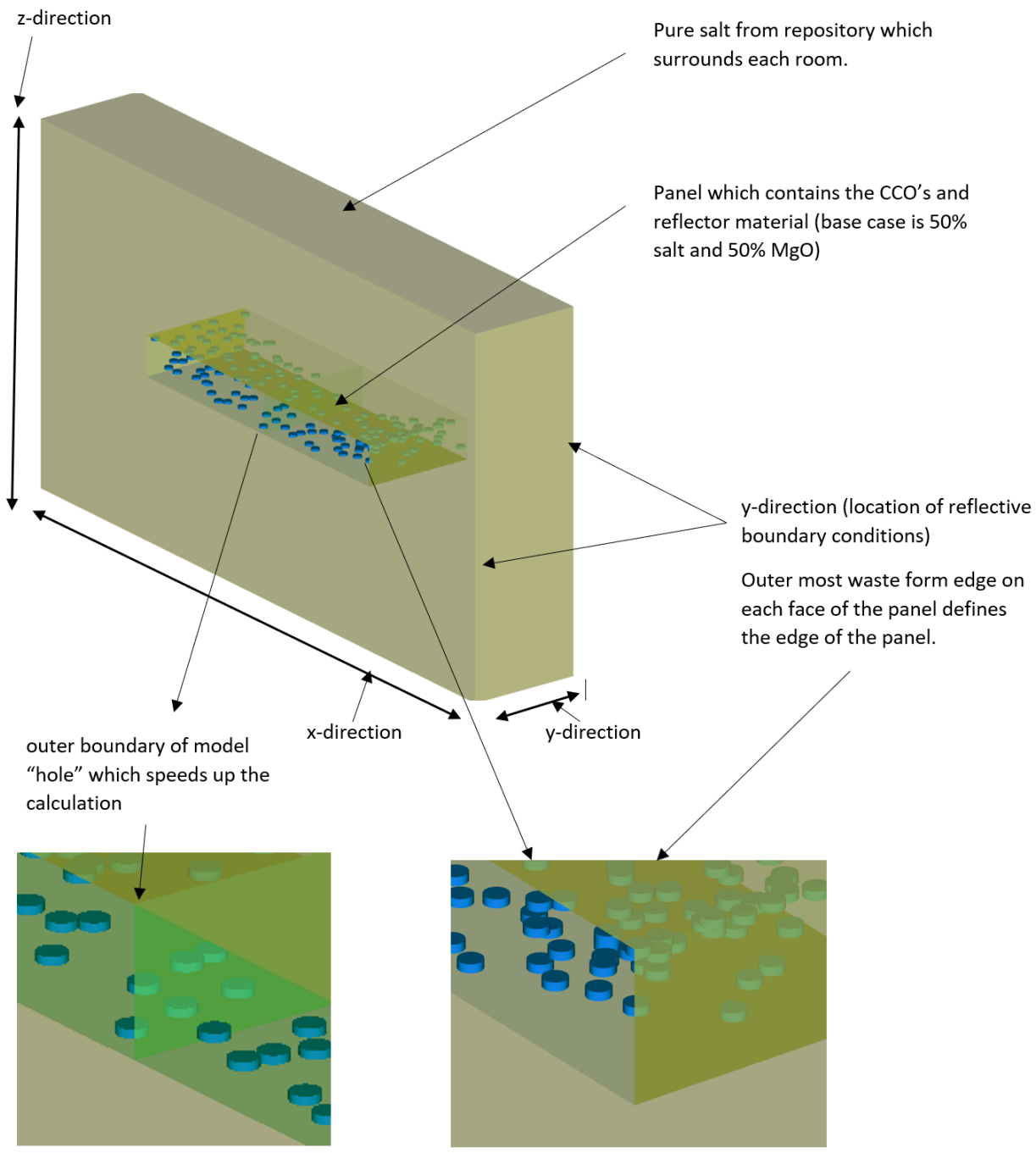

Figure C-1. Diagram of the nonuniform array model.

Table C-1. Summary of cases for set-2-uh for the upper horizon compaction data

Case	Model type	Waste form shape	Waste form moderator	Filler material (0, 2,000, 4,000 g)	Metal in filler	Discrete reflector (thin 0.001 and thick 0.7112 cm)	be (g)	Subcase
Set-2-uh	Nonuniform array with centroids based on upper horizon data. Centroid from pipe center is used as the point in center of base of cylinders or the center of spheres.	Cylinder (radius range 4.8, 6, 7.7 and height defined by total volume of mass)	water	c12	SS from can (0, 500, 1,000 g)	steel	0 to 585	set-2-uh-1
			poly	c12		steel		set-2-uh-2
			water	c12		poly		set-2-uh-3
			poly	c12		poly		set-2-uh-4
			water	generic		steel		set-2-uh-5
			poly	generic		steel		set-2-uh-6
			water	generic		poly		set-2-uh-7
			poly	generic		poly		set-2-uh-8
		Sphere (radius defined by total volume of mass)	water	c12		steel		set-2-uh-9
			poly	c12		steel		set-2-uh-10
			water	c12		poly		set-2-uh-11
			poly	c12		poly		set-2-uh-12
			water	generic		steel		set-2-uh-13
			poly	generic		steel		set-2-uh-14
			water	generic		poly		set-2-uh-15
			poly	generic		poly		set-2-uh-16
			poly + 50 g B_4C (cyl)	c12		poly (0.7112)		set-2-uh-17
			poly + 50 g B_4C (sph)	c12		poly (0.7112)		set-2-uh-18

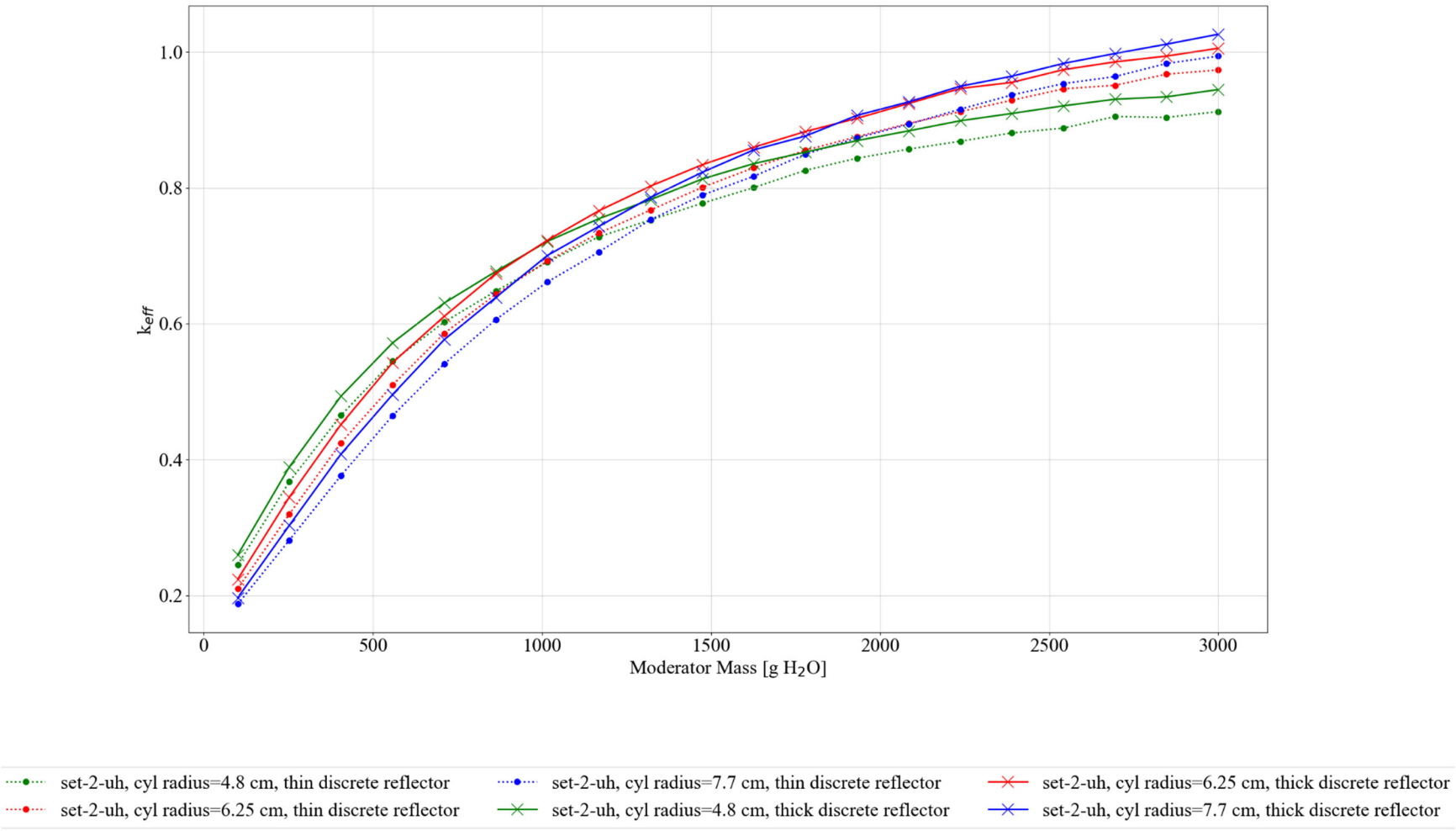

Figure C-2. Set-2-uh results, plot 1: reactivity effect of cylinder radius, pipe steel, no filler, no Be, water moderated.

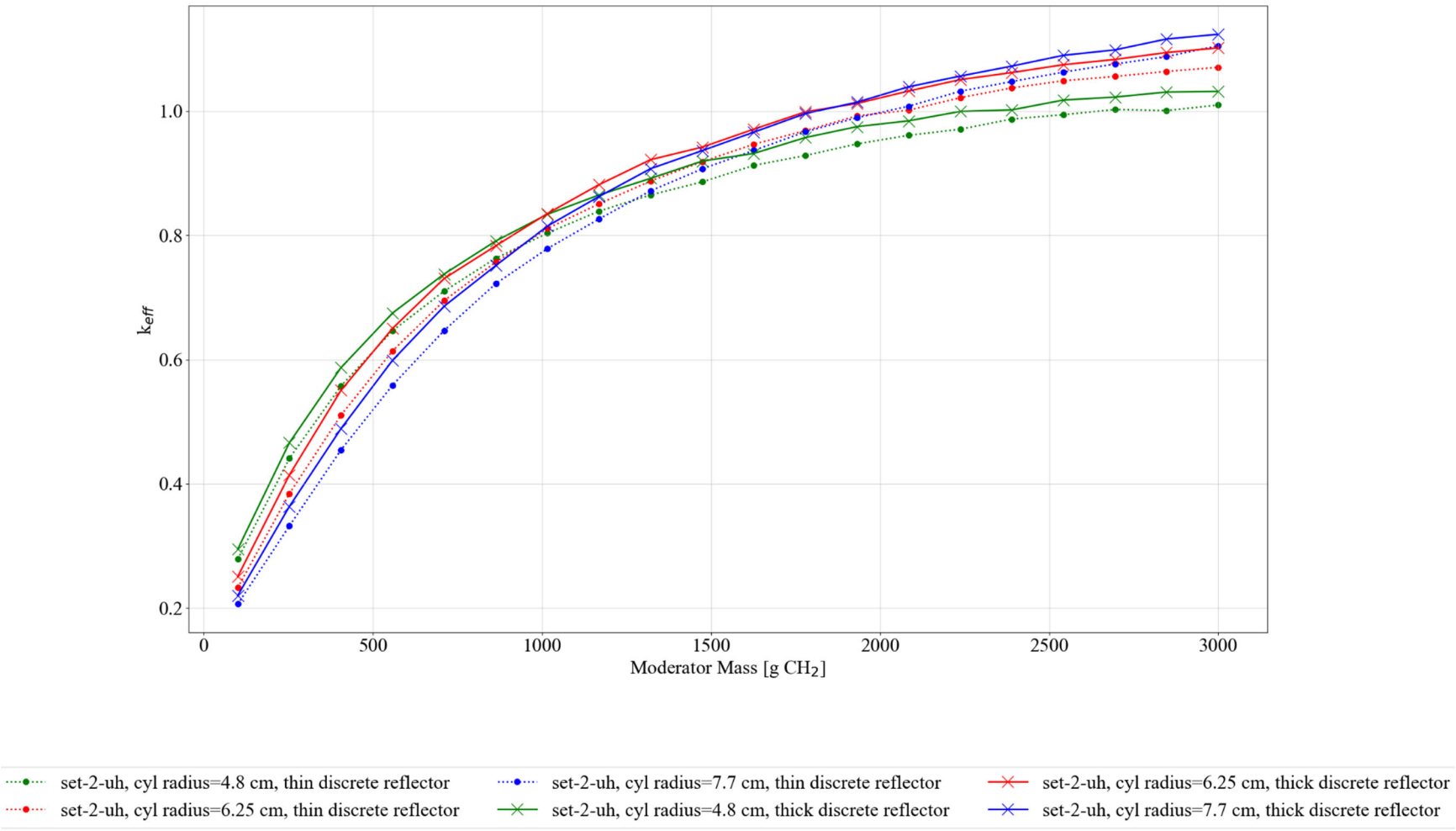

Figure C-3. Set-2-uh results, plot 2: reactivity effect of cylinder radius, pipe steel, no filler, no Be, poly moderated.

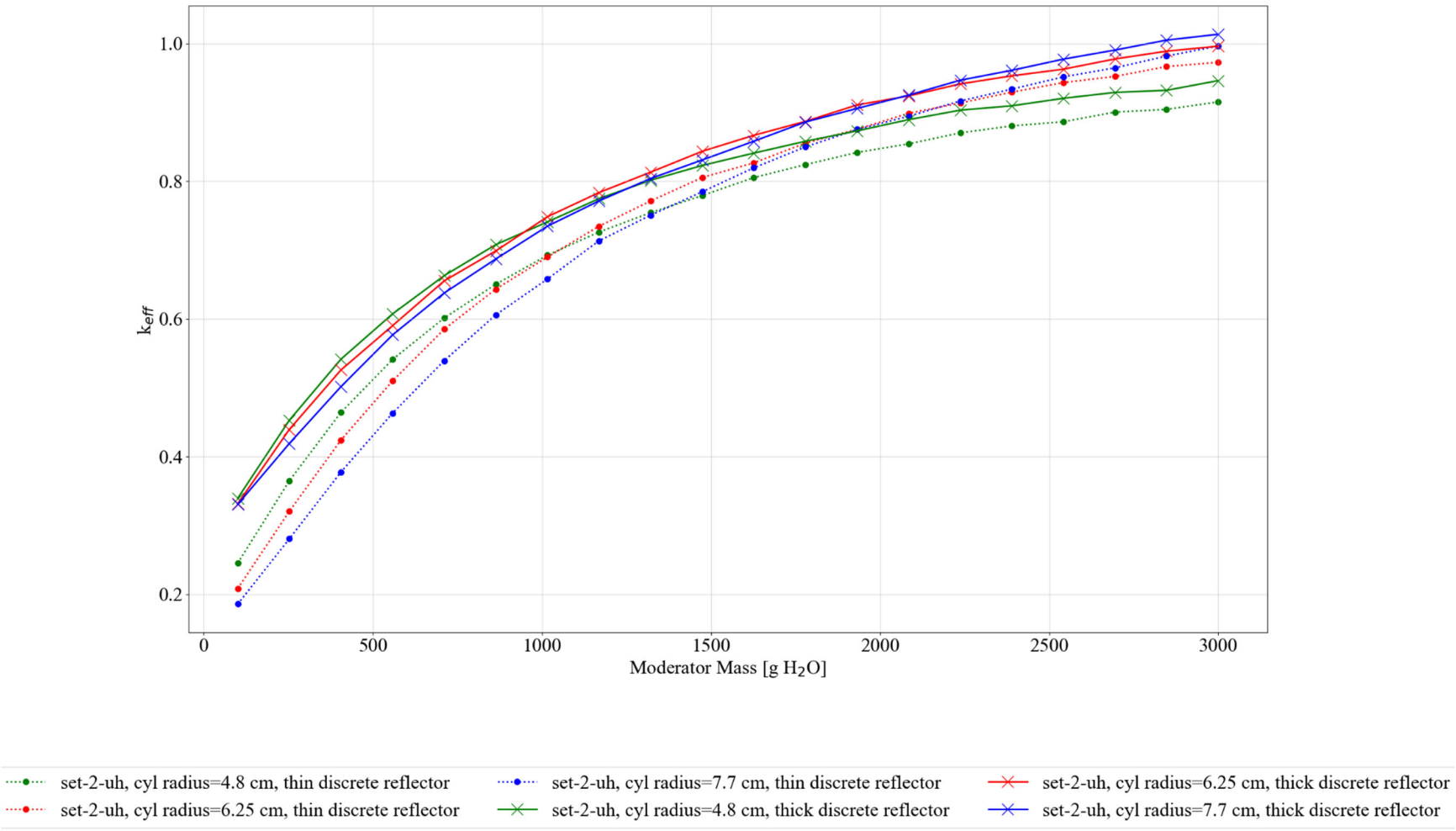

Figure C-4. Set-2-uh results, plot 3: reactivity effect of cylinder radius, pipe poly, no filler, no Be, water moderated.

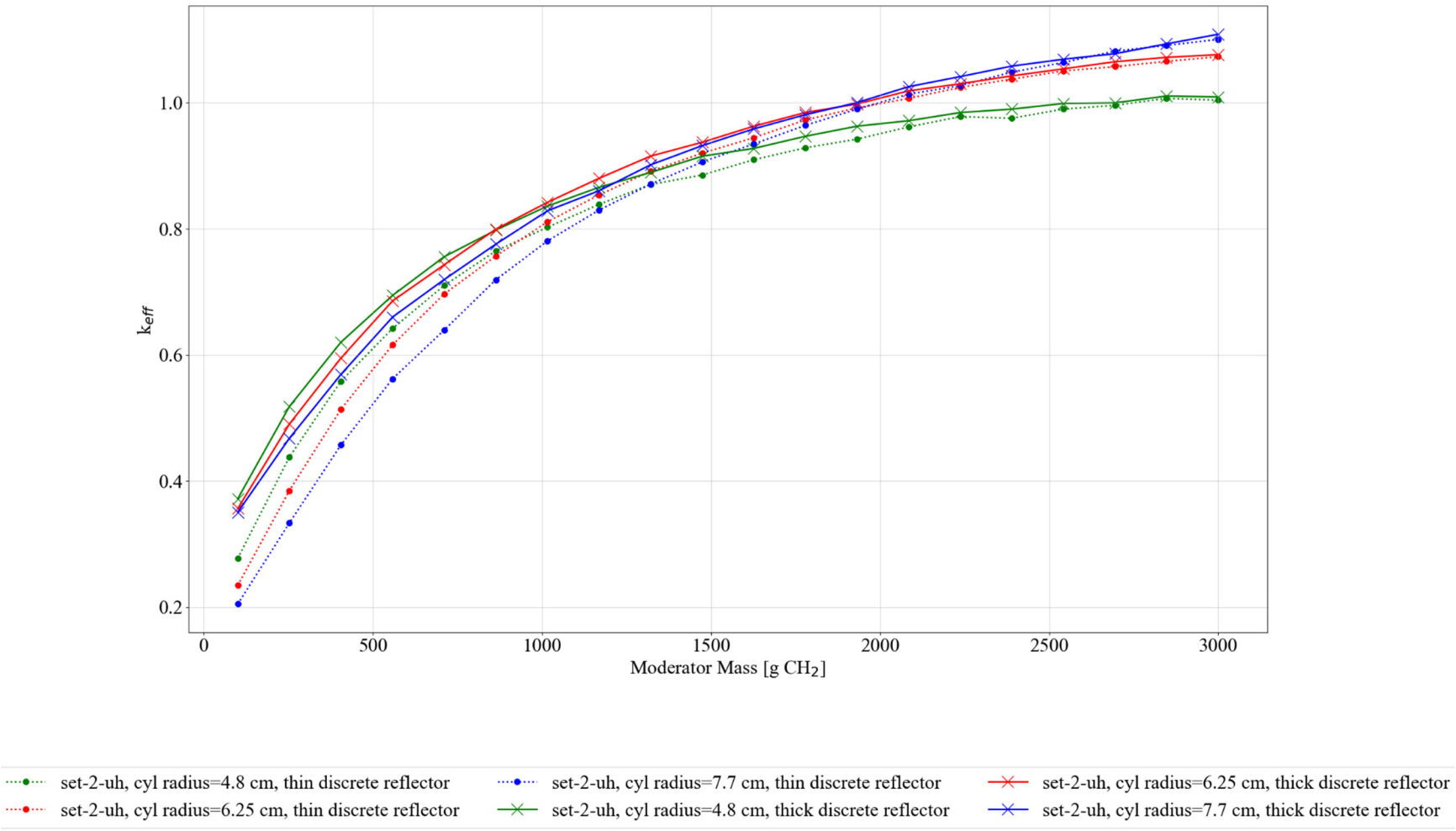

Figure C-5. Set-2-uh results, plot 4: reactivity effect of cylinder radius, pipe poly, no filler, no Be, poly moderated .

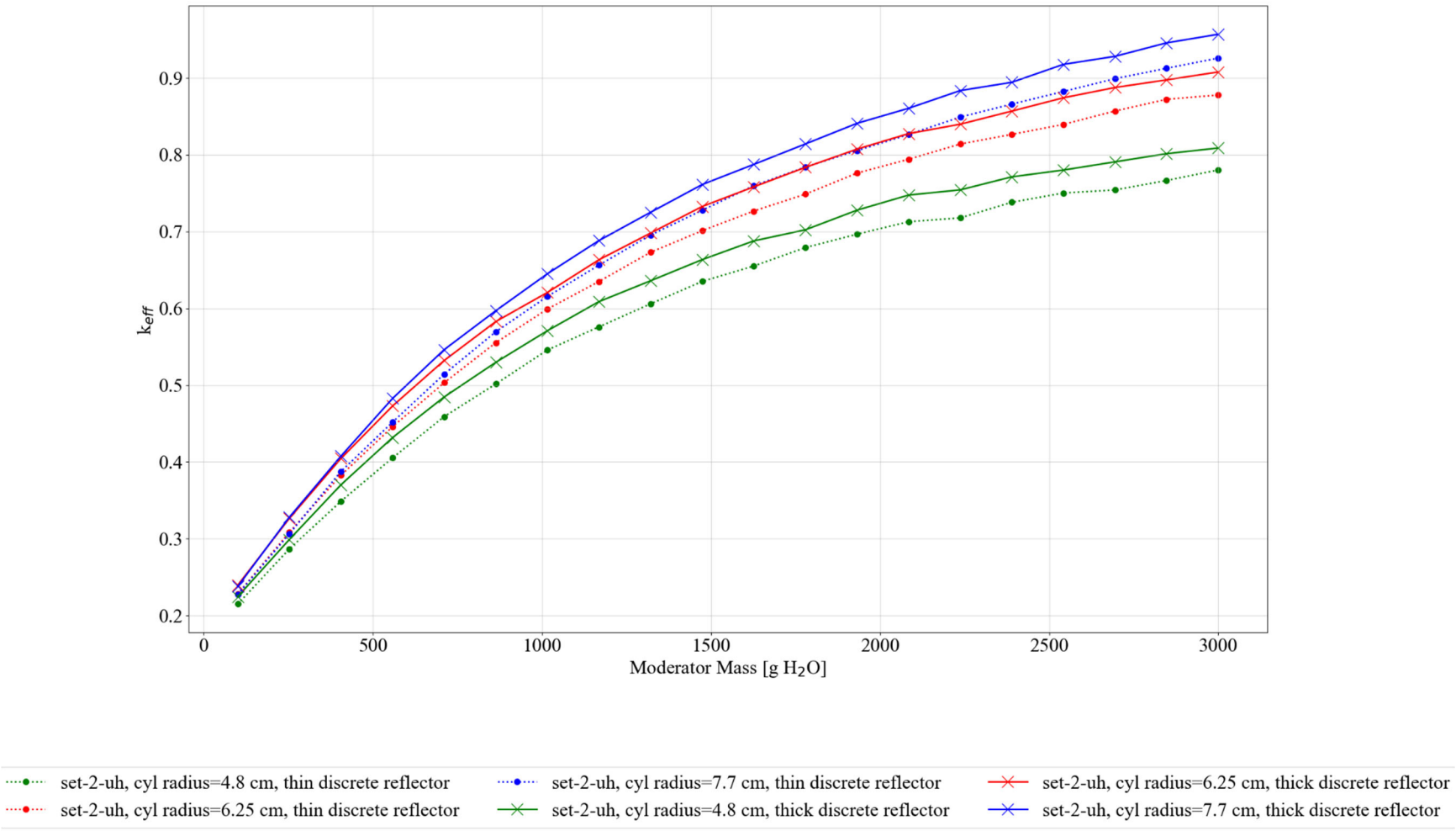

Figure C-6. Set-2-uh results, plot 5: reactivity effect of cylinder radius, pipe steel, 5 kg graphite/can, no Be, water moderated.

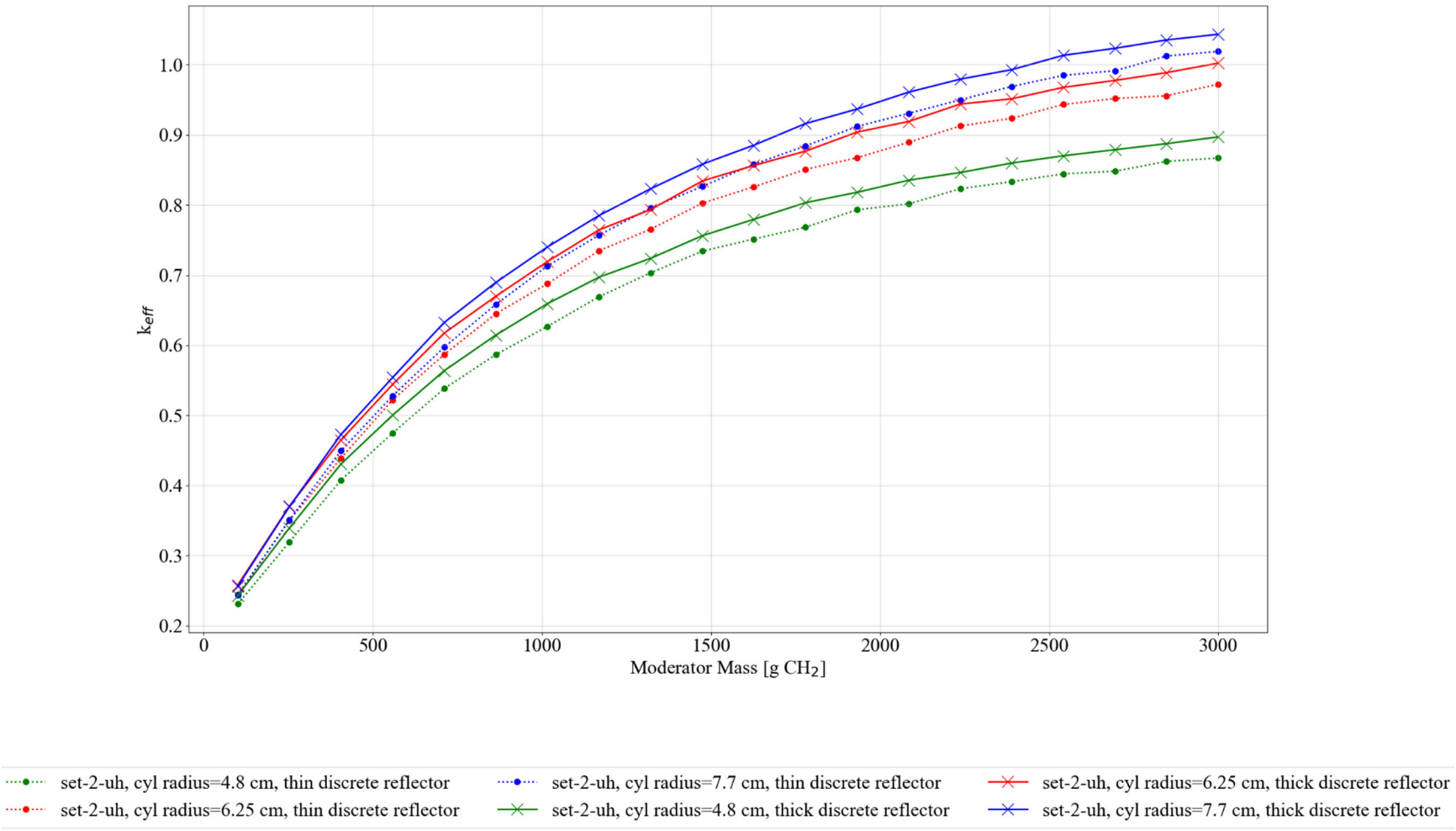

Figure C-7. Set-2-uh results, plot 6: reactivity effect of cylinder radius, pipe steel, 5 kg graphite/can, no Be, poly moderated.

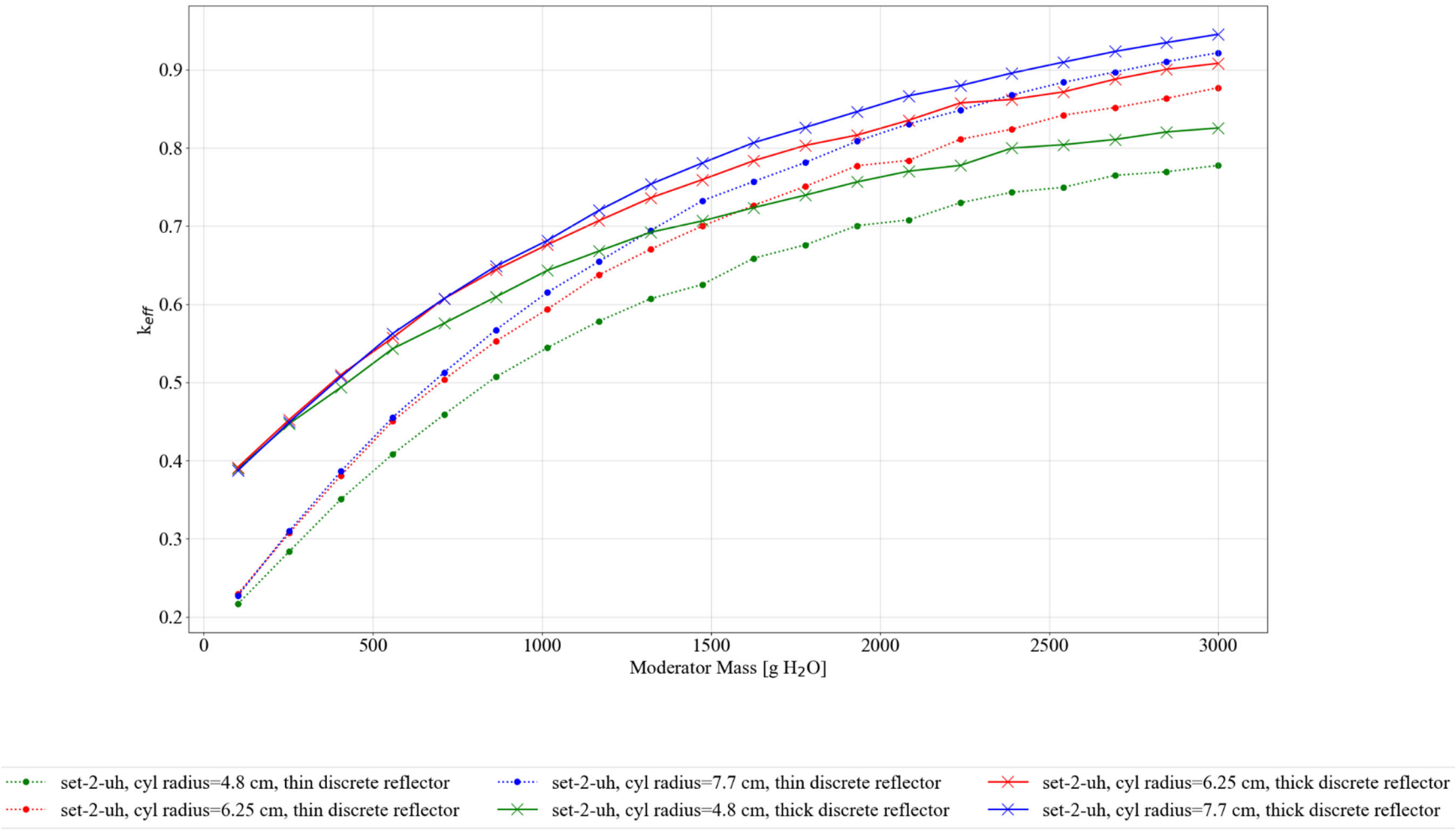

Figure C-8. Set-2-uh results, plot 7: reactivity effect of cylinder radius, pipe poly, 5 kg graphite/can, no Be, water moderated.

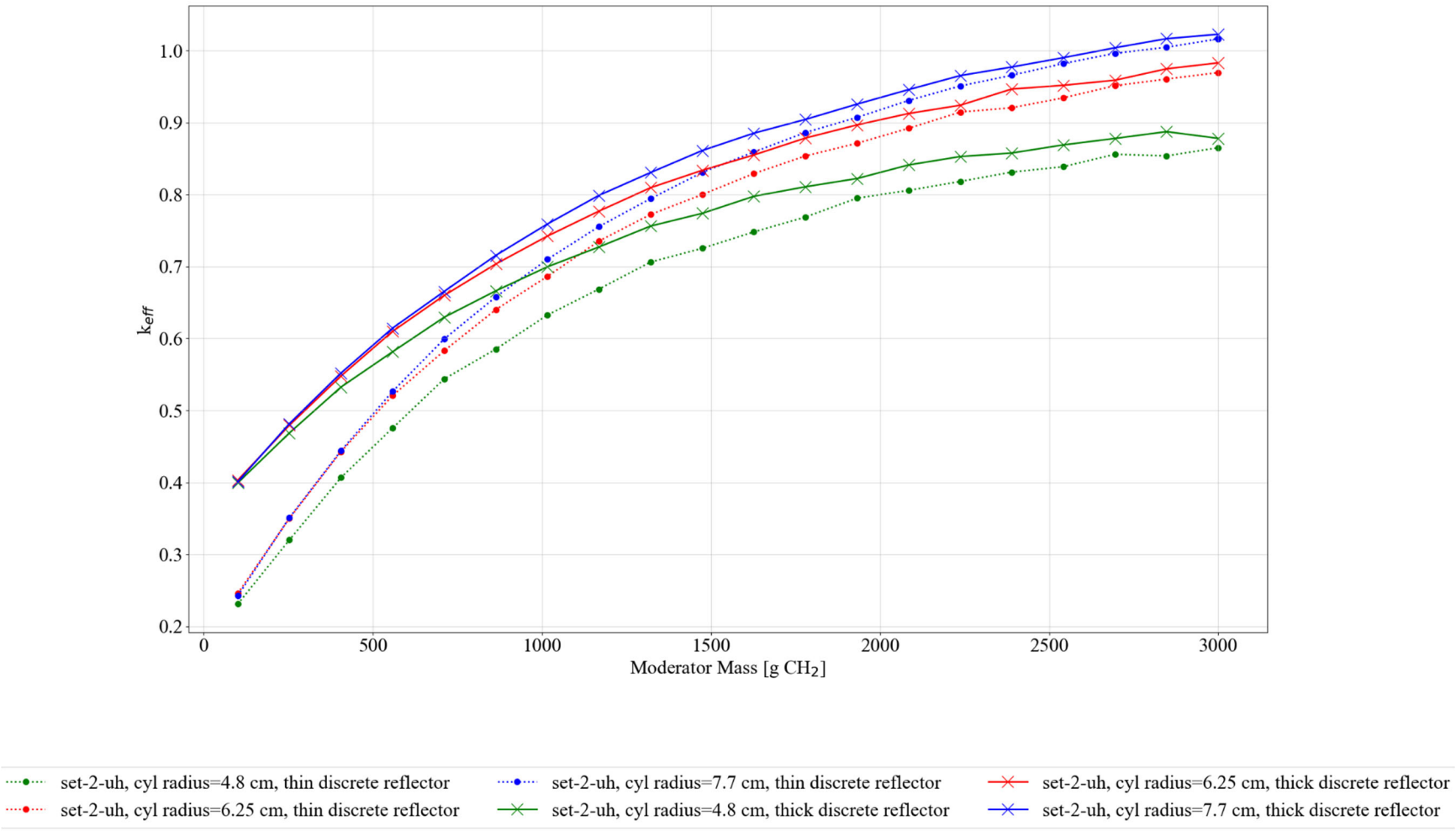

Figure C-9. Set-2-uh results, plot 8: reactivity effect of cylinder radius, pipe poly, 5 kg graphite/can, no Be, poly moderated.

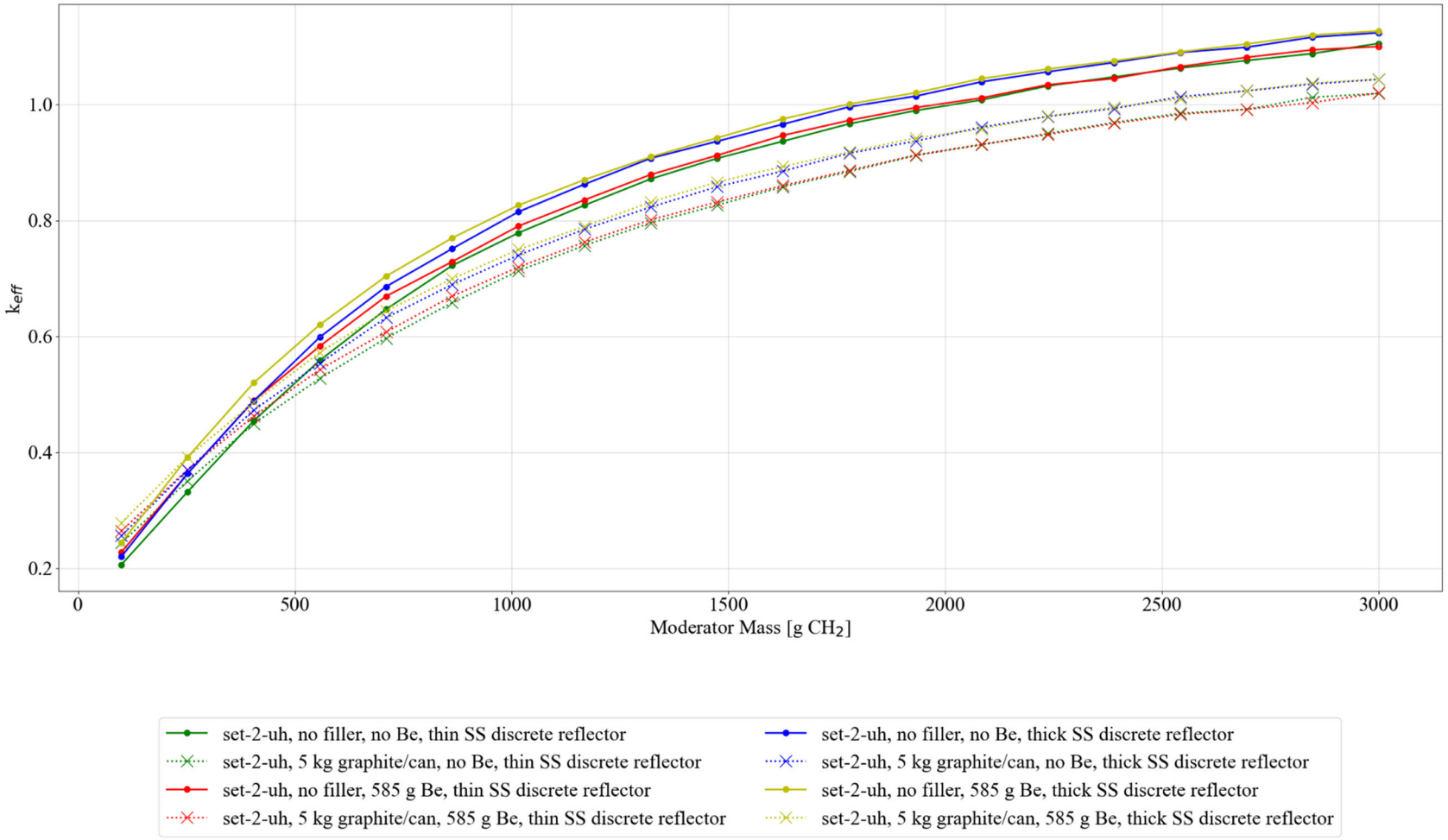

Figure C-10. Set-2-uh results, plot 9: reactivity effect of various parameters with 7.7 cm cylinder radius, graphite filler, poly moderated.

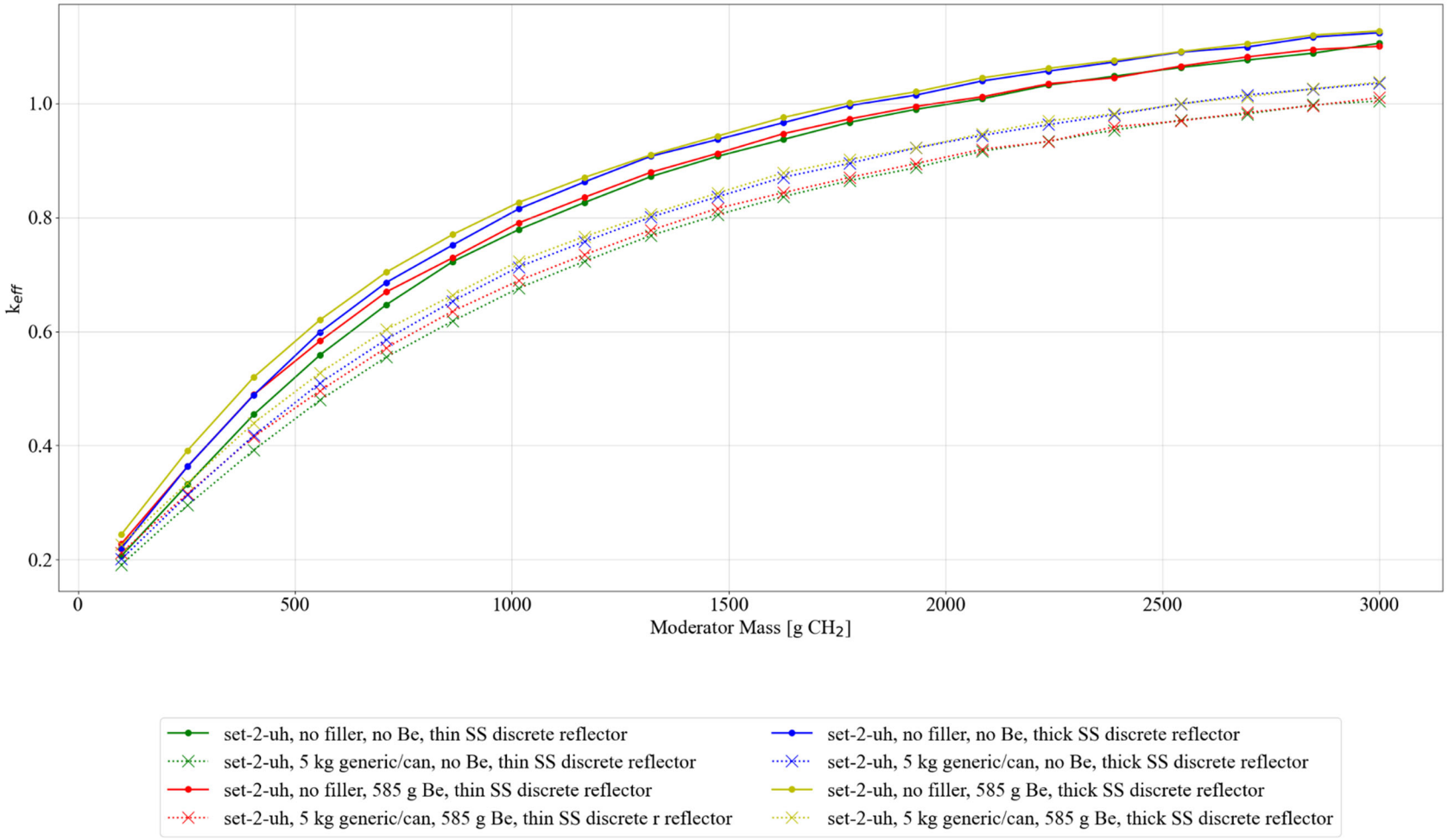

Figure C-11. Set-2-uh results, plot 10: reactivity effect of various parameters with 7.7 cm cylinder radius, generic filler, poly moderated.

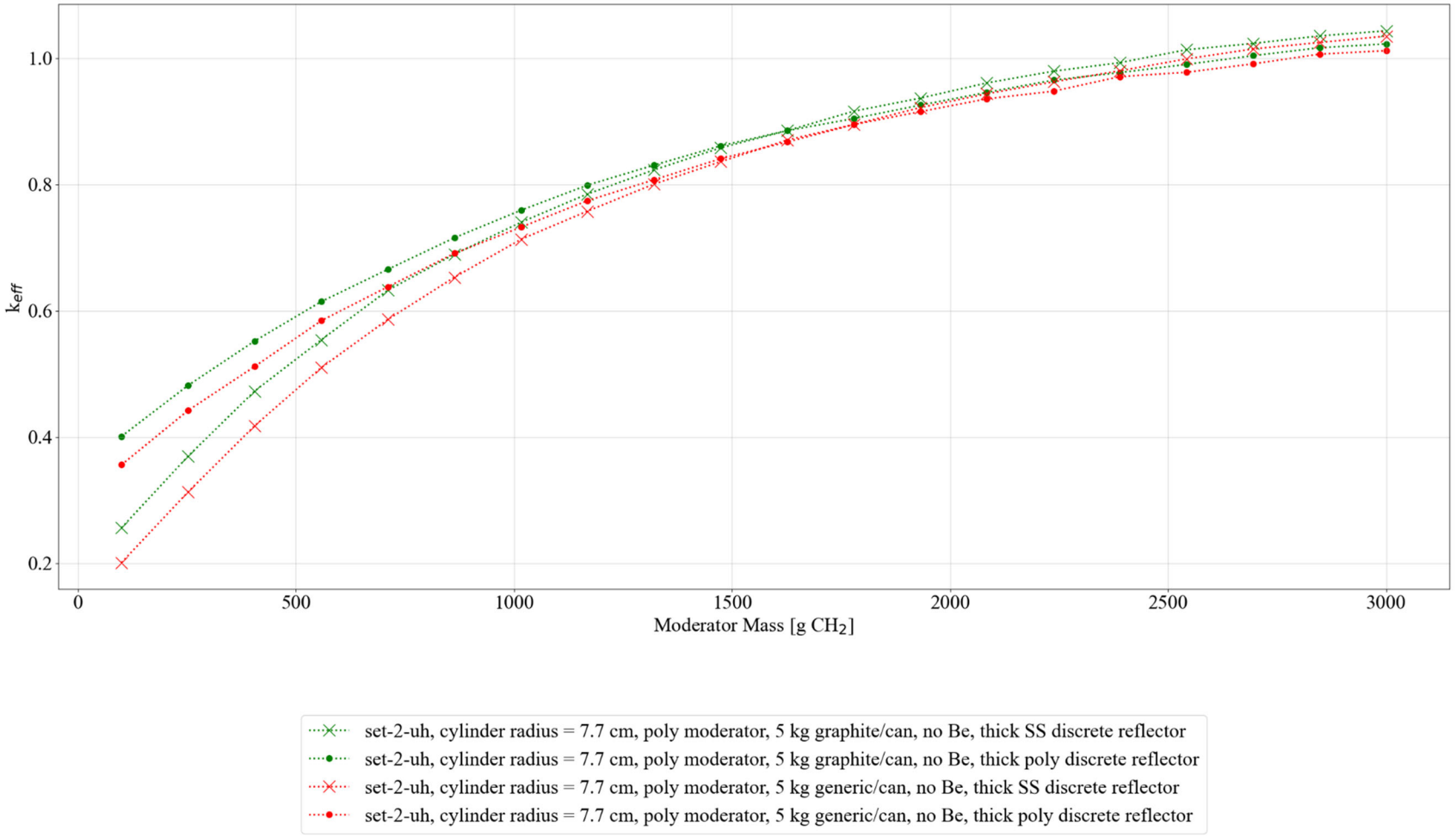

Figure C-12. Set-2-uh results, plot 11: comparison of graphite and generic filler with 7.7 cm cylinder radius, no Be, poly moderated, thick discrete reflector.

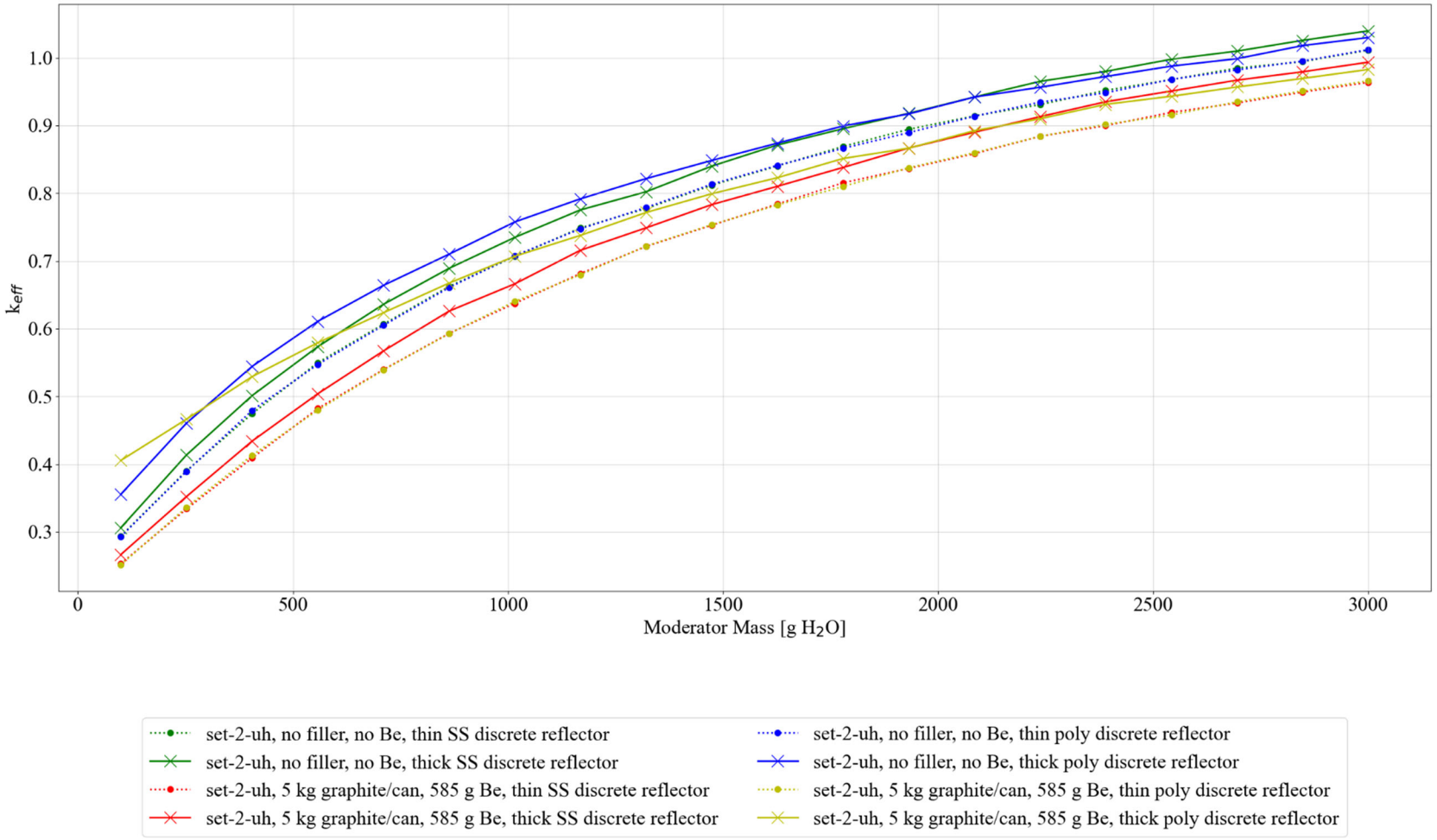

Figure C-13. Set-2-uh results, plot 12: reactivity effect of various parameters with spherical waste form geometry, graphite filler, water moderated.

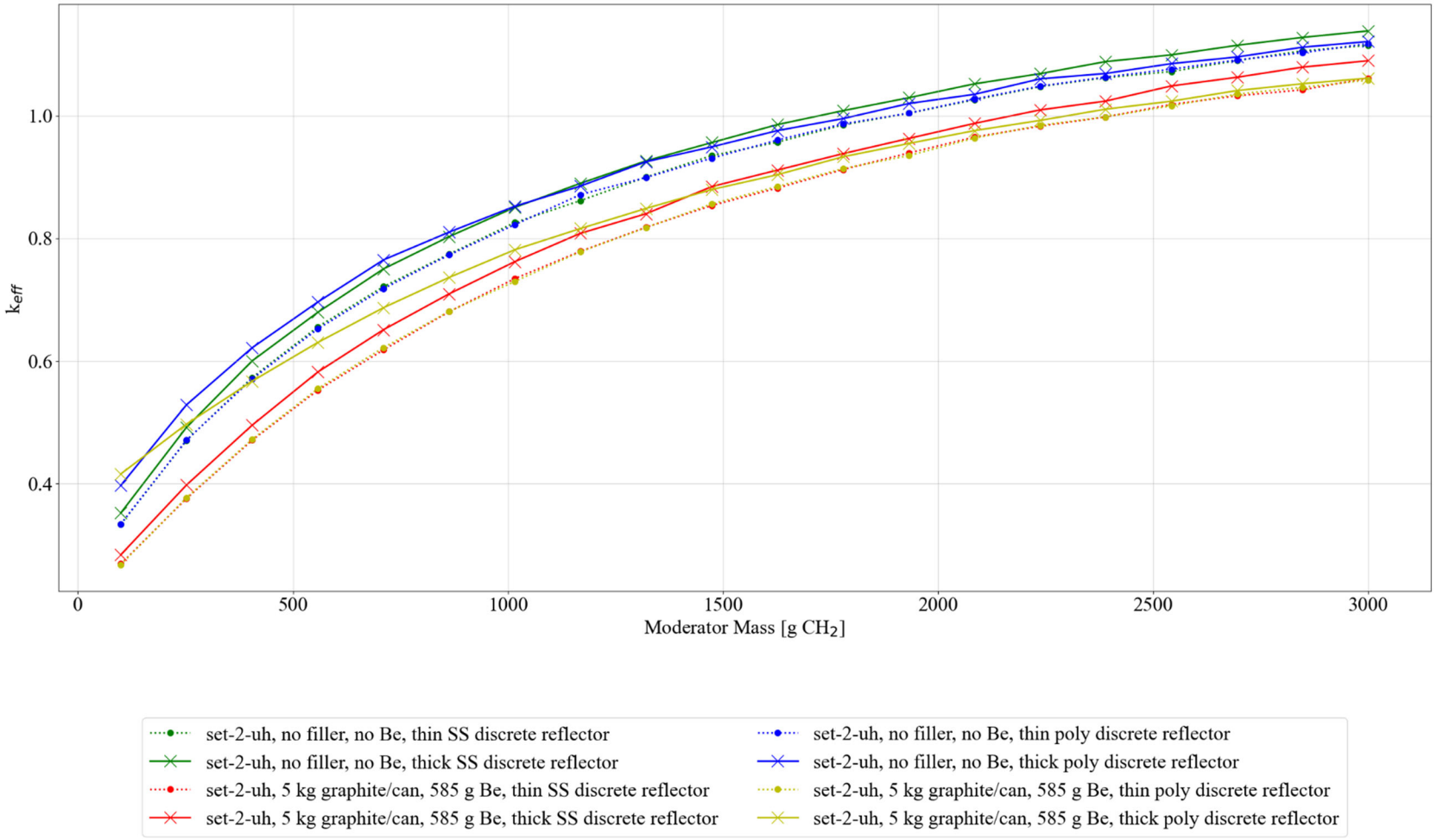

Figure C-14. Set-2-uh results, plot 13: reactivity effect of various parameters with spherical waste form geometry, graphite filler, poly moderated.

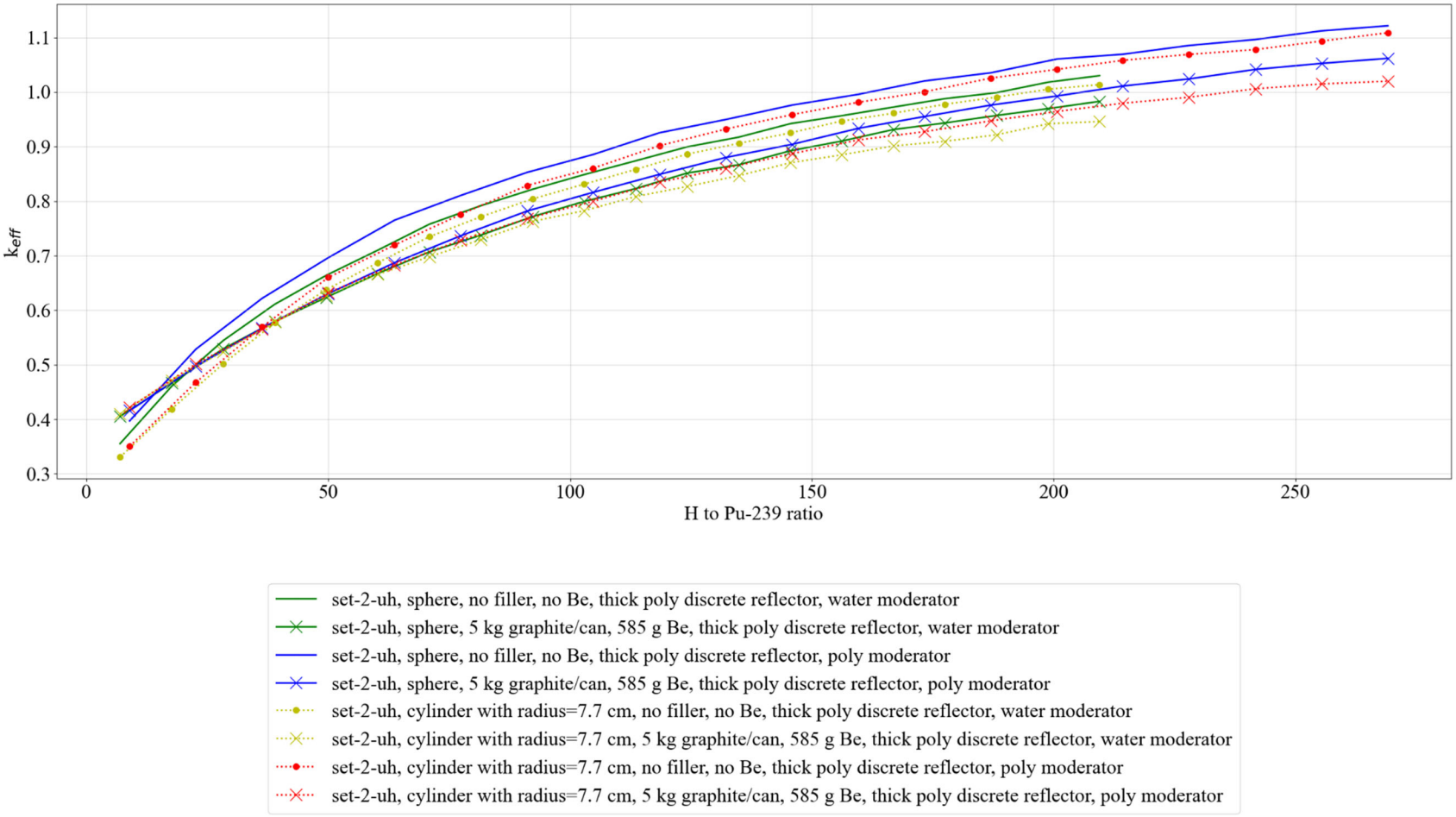

Figure C-15. Set-2-uh results, plot 14: comparison of spherical and cylindrical geometries (h/x).

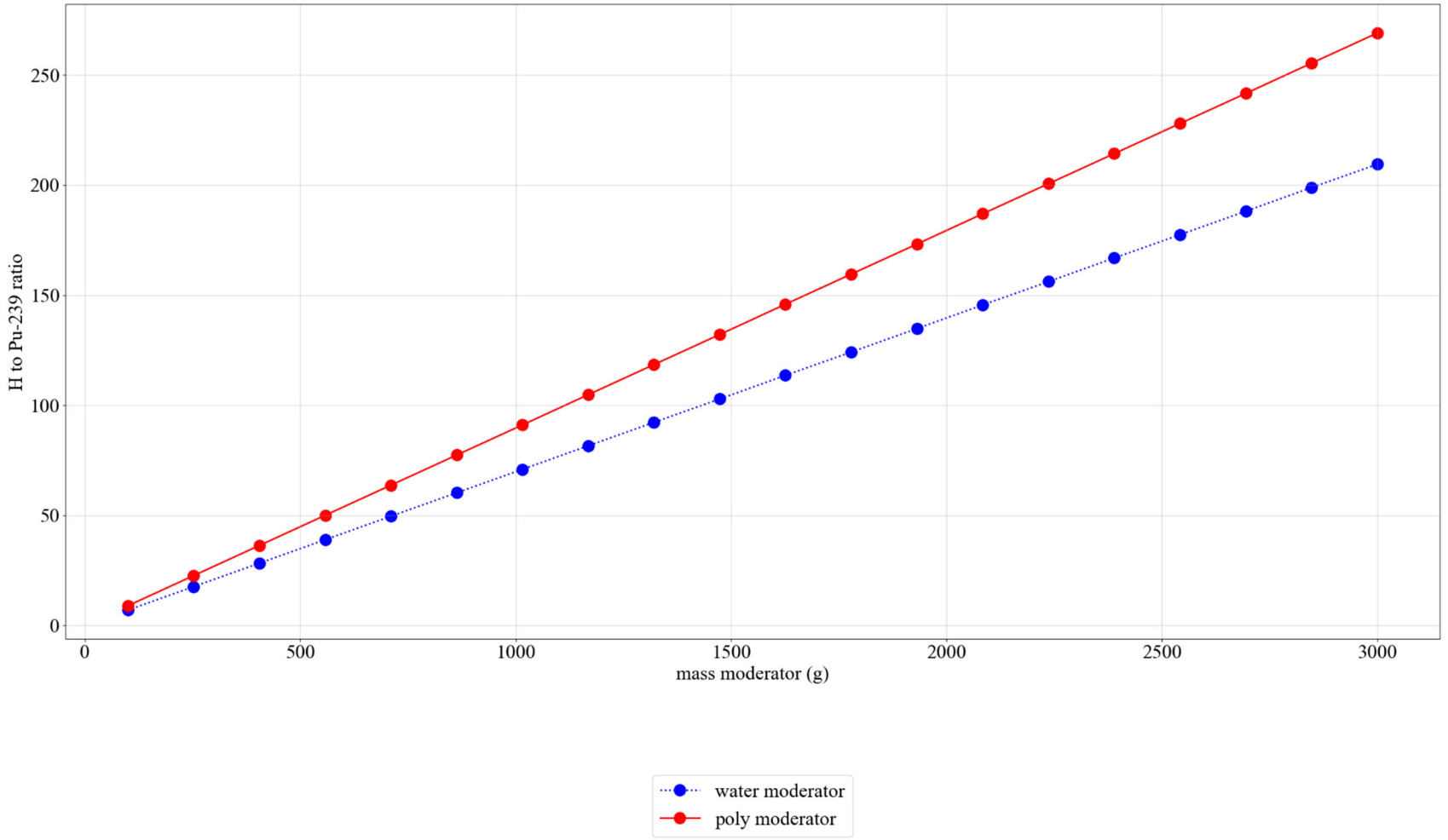

Figure C-16. Set-2-uh results, plot 15: comparison of water and poly h/x.

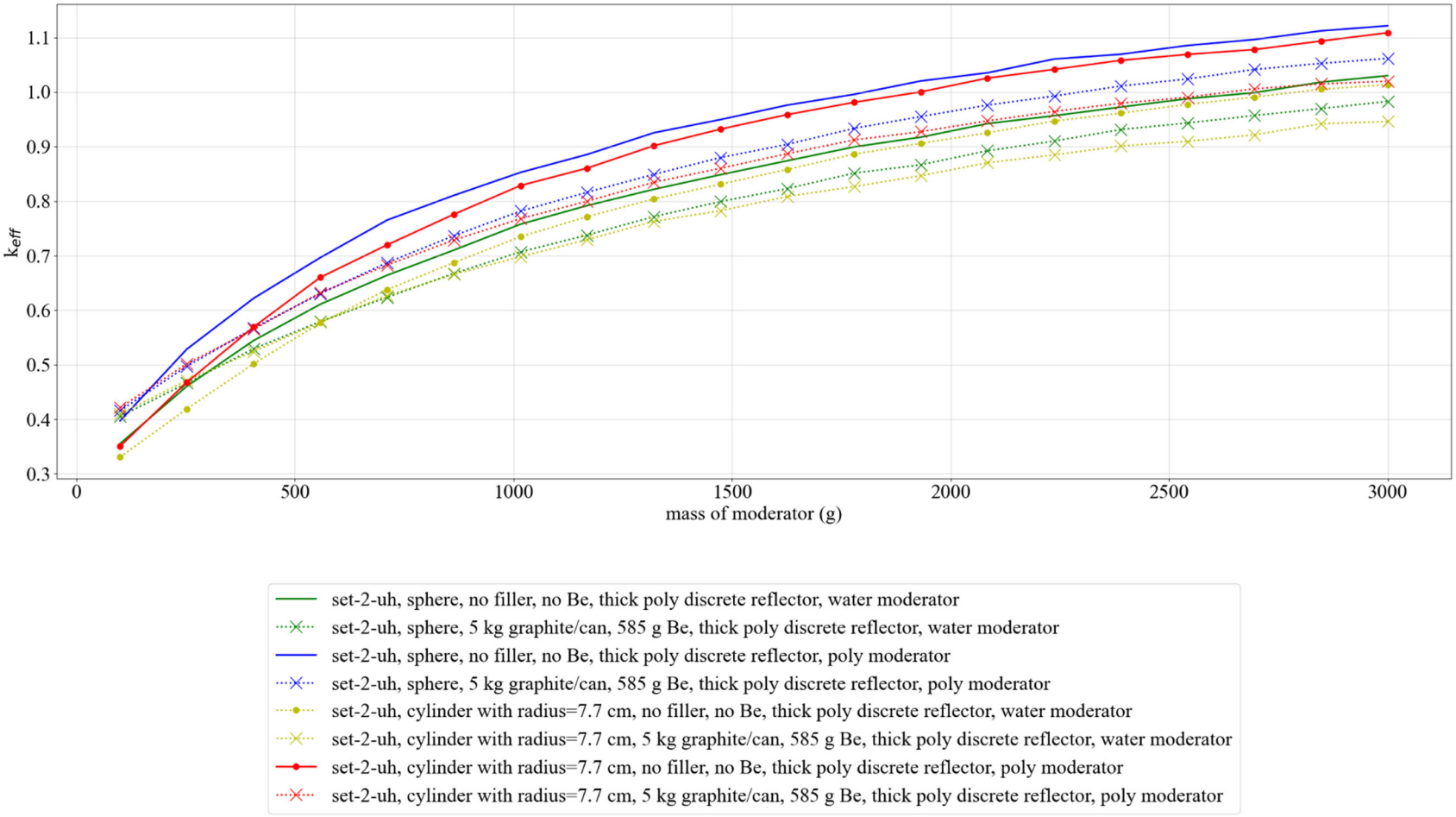

Figure C-17. Set-2-uh results, plot 16: comparison of spherical and cylindrical geometries (mod mass).

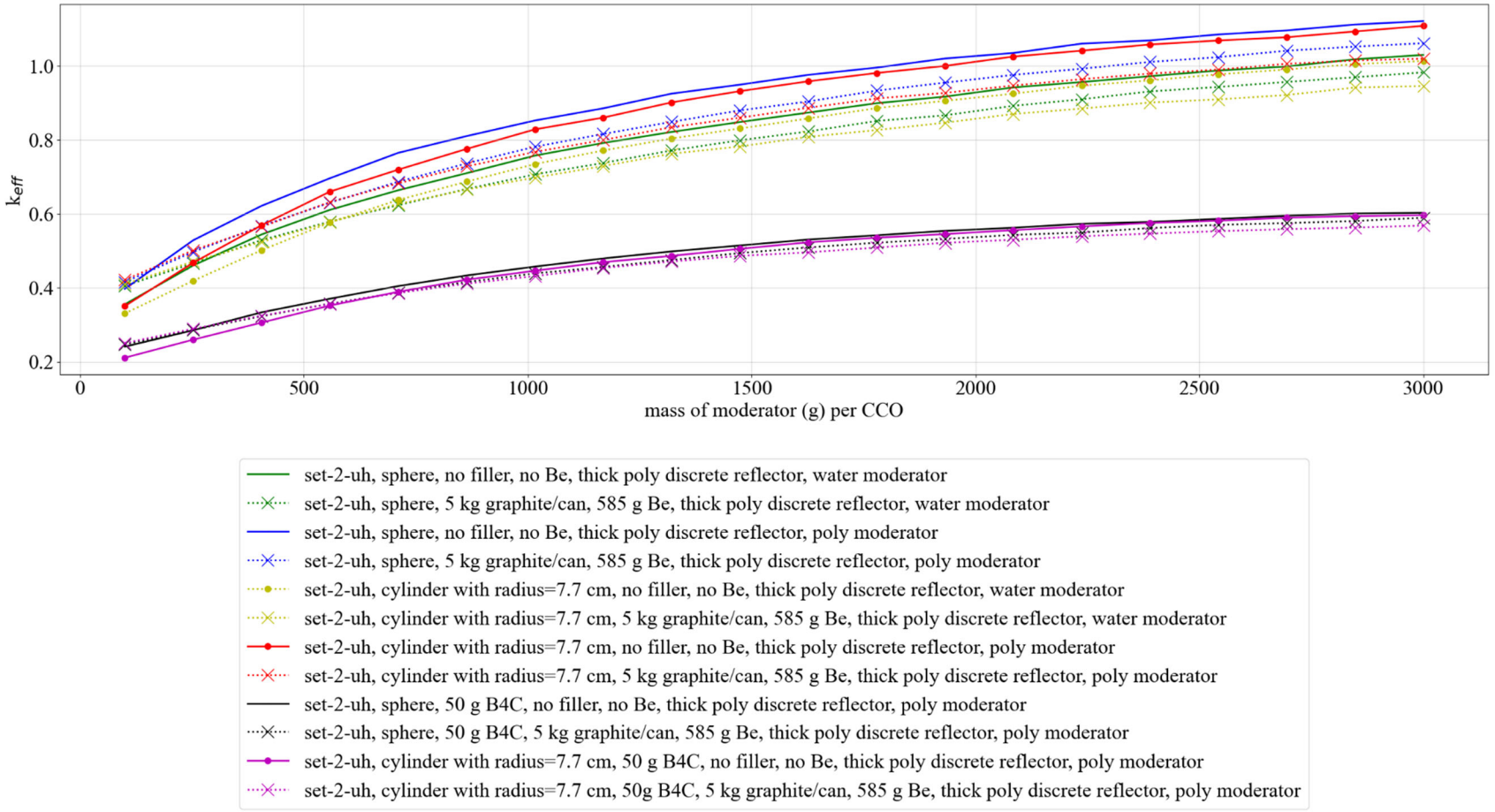

Figure C-18. Set-2-uh results, plot 17: comparison of 50g B_4C vs. no B_4C for spherical and cylindrical geometries (mod mass).

APPENDIX D. SET-2-LH: RESULTS OF THE NONUNIFORM ARRAY FOR THE LOWER HORIZON CALCULATIONS

This page is intentionally blank

APPENDIX D. SET-2-LH: RESULTS OF THE NONUNIFORM ARRAY FOR THE LOWER HORIZON CALCULATIONS

The analysis methodology for the uniform arrays is discussed in detail in Section 6.3 of the main report.

This appendix serves as a repository of those results for the set-2-lh calculations.

The complete results for all SAMPLER sweeps are provided in ADDENDUM 1.

The analysis model use for the calculations in this appendix is shown in Figure D-1 below.

The SAMPLER case sweeps presented in this appendix are summarized in Table D-1 below.

LIST OF FIGURES

LIST OF TABLES

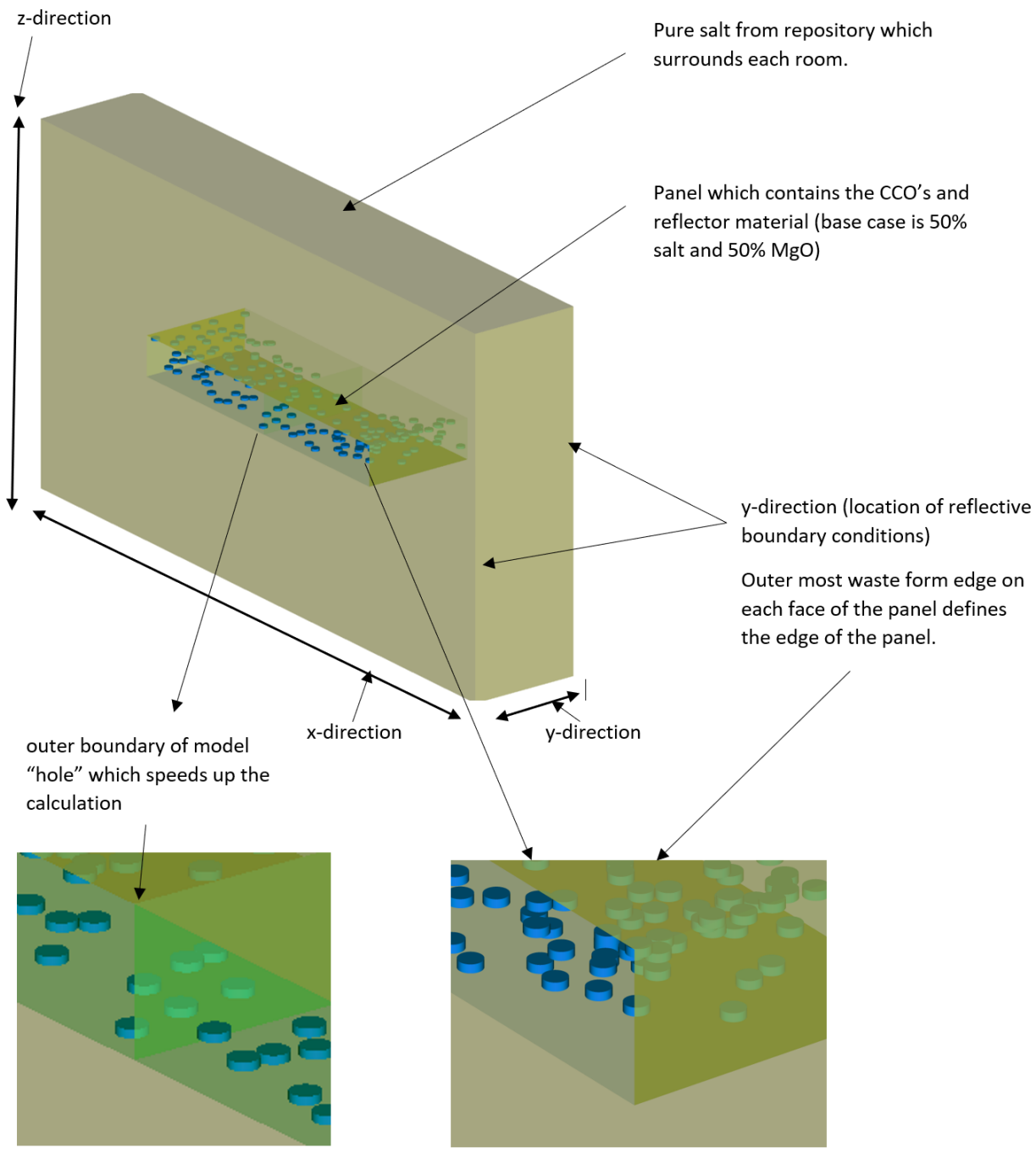

Figure D-1. Diagram of the nonuniform array three-high model.

Table D-1. Summary of cases for Set-2-uh for the lower horizon compaction data

Case	Model type	Waste form shape	Waste form moderator	Filler material (0, 2,000, 4,000 g)	Metal in filler	Discrete reflector (thin 0.001 and thick 0.7112 cm)	Be (g)	Subcase
Set-2-lh	Nonuniform array with centroids based on upper horizon data. Centroid from pipe center is used as the point in the center of the base of cylinders or the center of the spheres.	Cylinder (radius range 4.8, 6, 7.7 and height defined by total volume of mass)	water	c12	SS from can (0, 500, 1,000 g)	steel	0 to 585	set-2-lh-1
			poly	c12		steel		set-2-lh-2
			water	c12		poly		set-2-lh-3
			poly	c12		poly		set-2-lh-4
			water	generic		steel		set-2-lh-5
			poly	generic		steel		set-2-lh-6
			water	generic		poly		set-2-lh-7
			poly	generic		poly		set-2-lh-8
		Sphere (radius defined by total volume of mass)	water	c12		steel		set-2-lh-9
			poly	c12		steel		set-2-lh-10
			water	c12		poly		set-2-lh-11
			poly	c12		poly		set-2-lh-12
			water	generic		steel		set-2-lh-13
			poly	generic		steel		set-2-lh-14
			water	generic		poly		set-2-lh-15
			poly	generic		poly		set-2-lh-16
			poly + 50 g B_4C (cyl)	c12		poly (0.7112)		set-2-lh-17
			poly + 50 g B_4C (sph)	c12		poly (0.7112)		set-2-lh-18

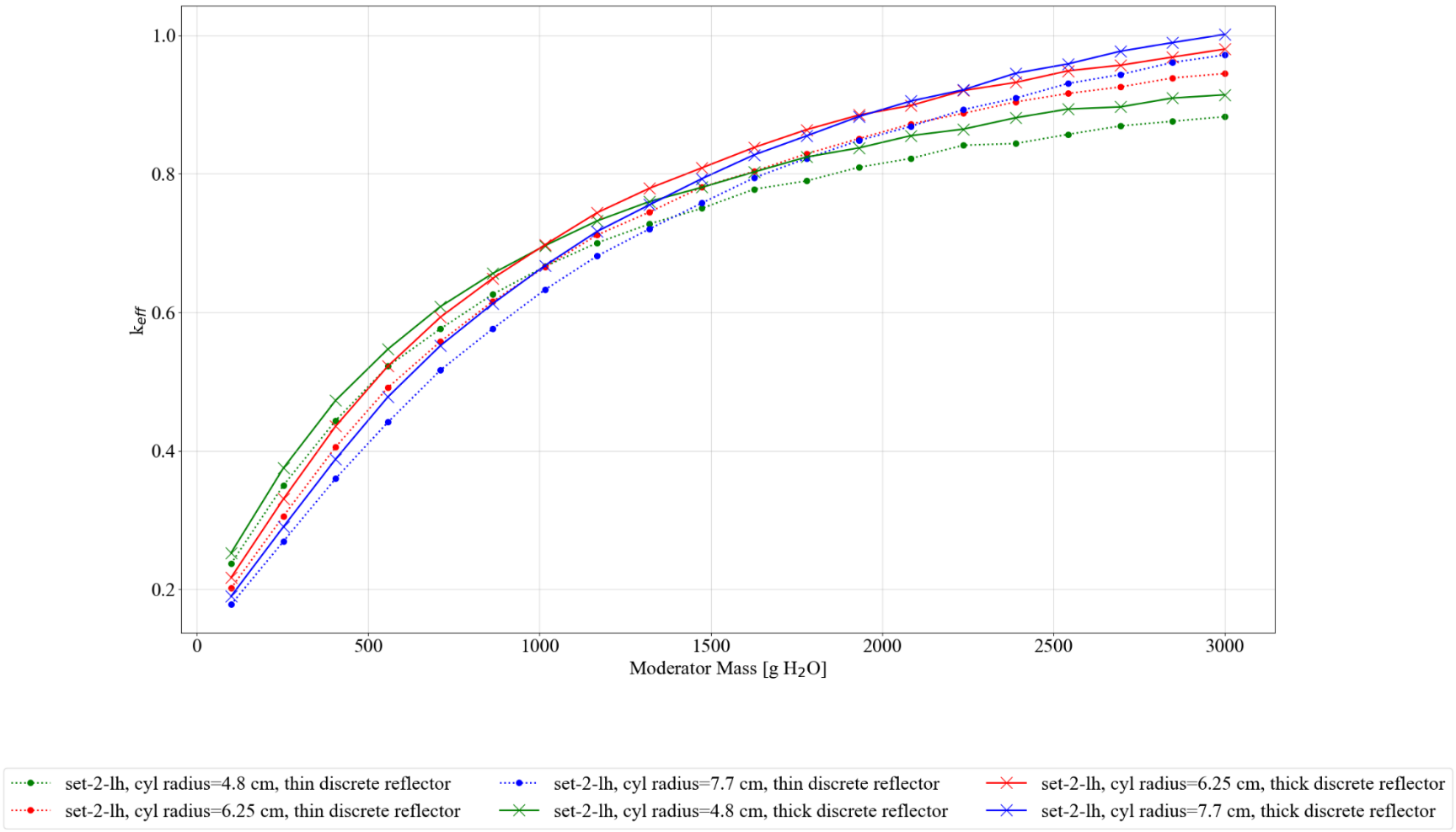

Figure D-2. Set-2-lh results, plot 1: reactivity effect of cylinder radius, pipe steel, no filler, no Be, water moderated.

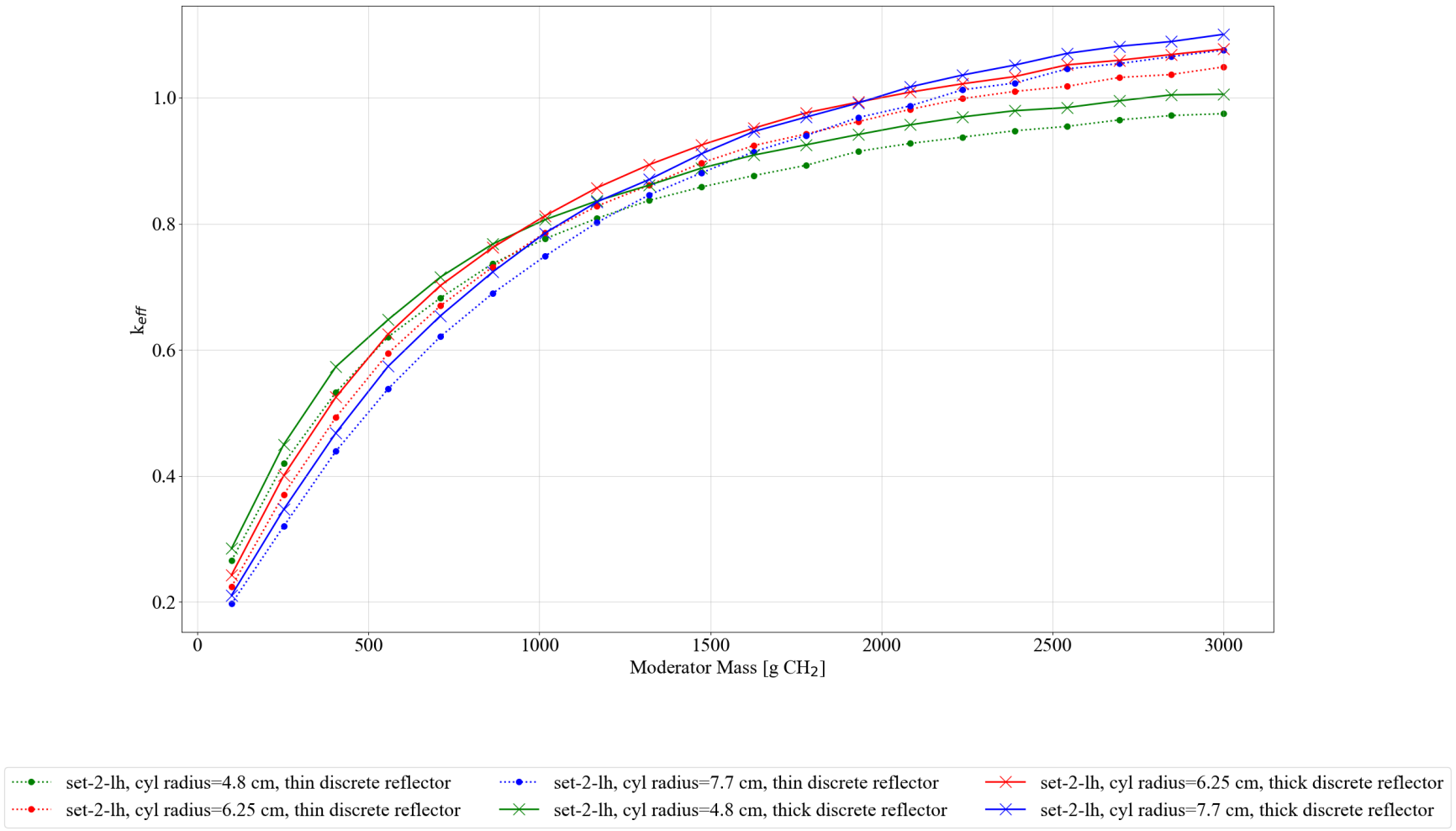

Figure D-3. Set-2-lh results, plot 2: reactivity effect of cylinder radius, pipe steel, no filler, no Be, poly moderated.

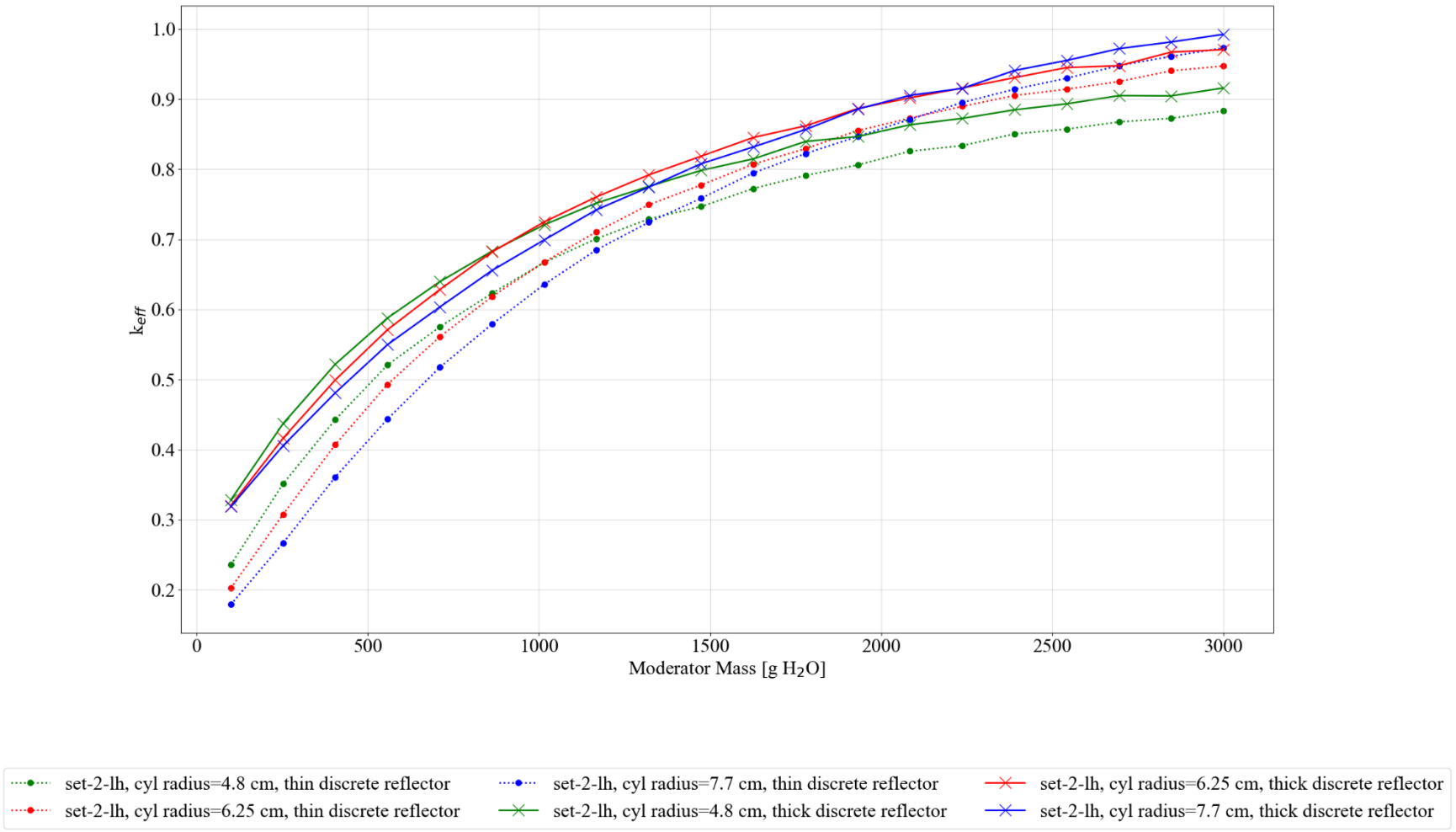

Figure D-4. Set-2-lh results, plot 3: reactivity effect of cylinder radius, pipe poly, no filler, no Be, water moderated.

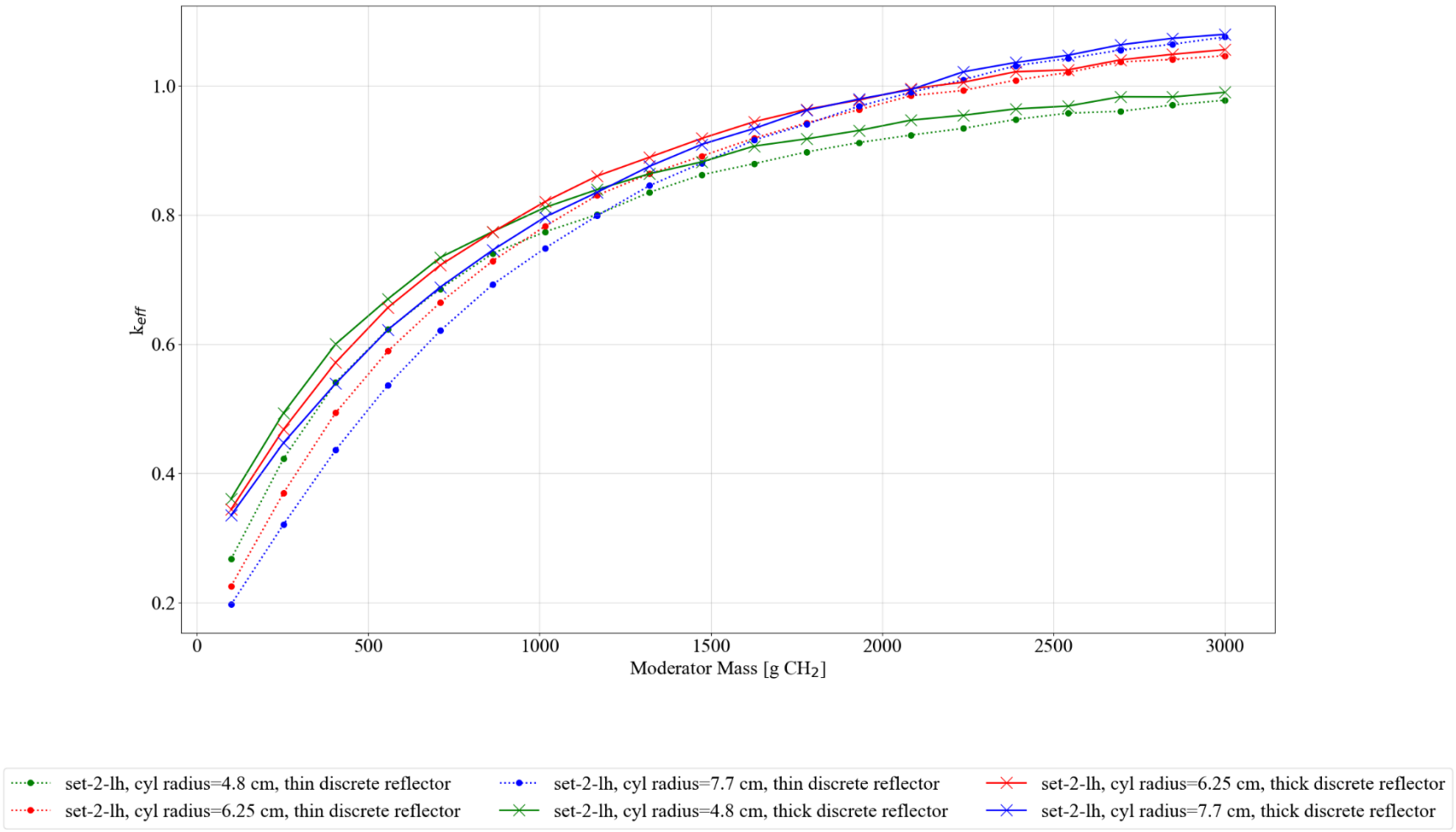

Figure D-5. Set-2-lh results, plot 4: reactivity effect of cylinder radius, pipe poly, no filler, no Be, poly moderated.

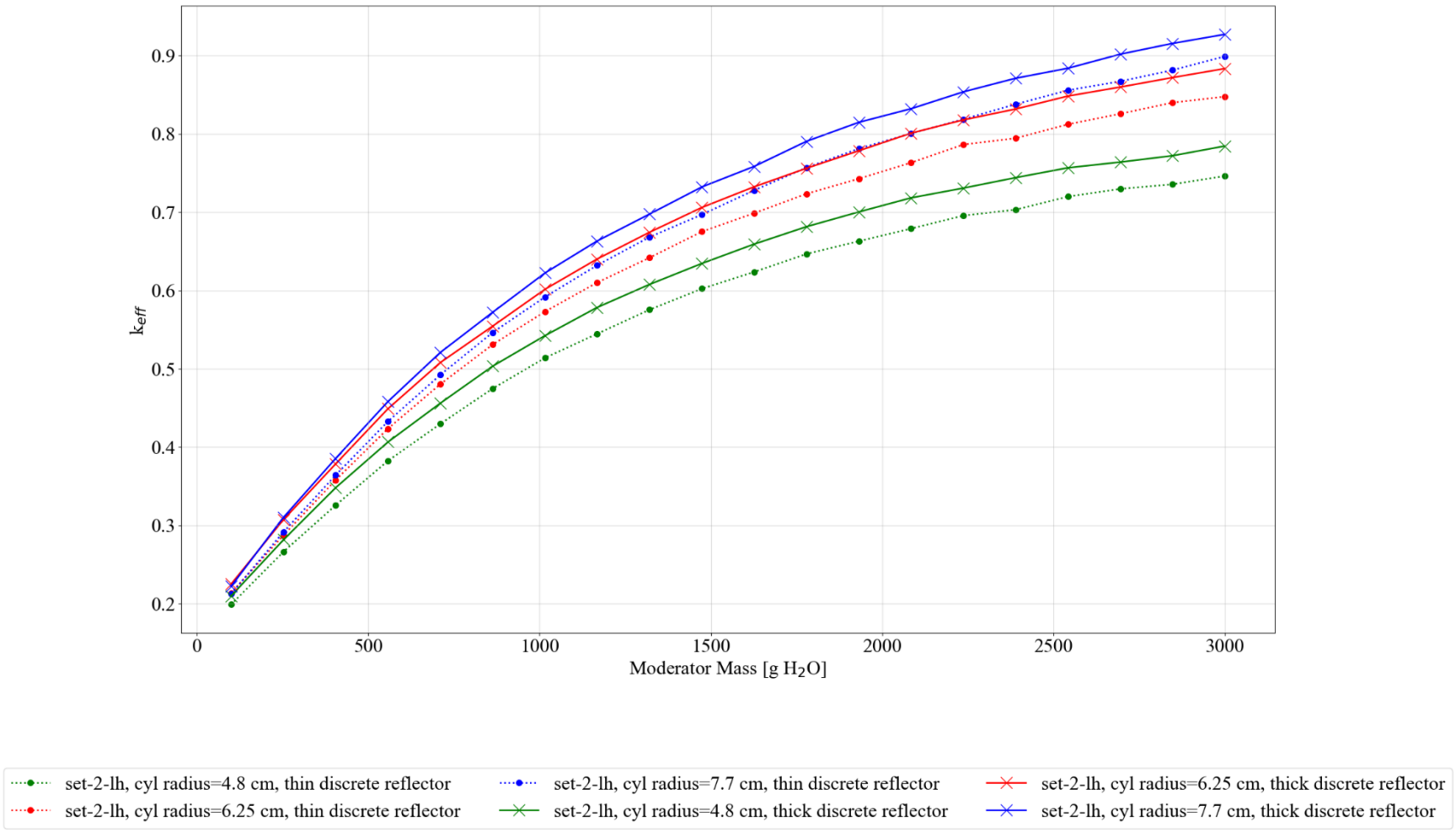

Figure D-6. Set-2-lh results, plot 5: reactivity effect of cylinder radius, pipe steel, 5 kg graphite/can, no Be, water moderated.

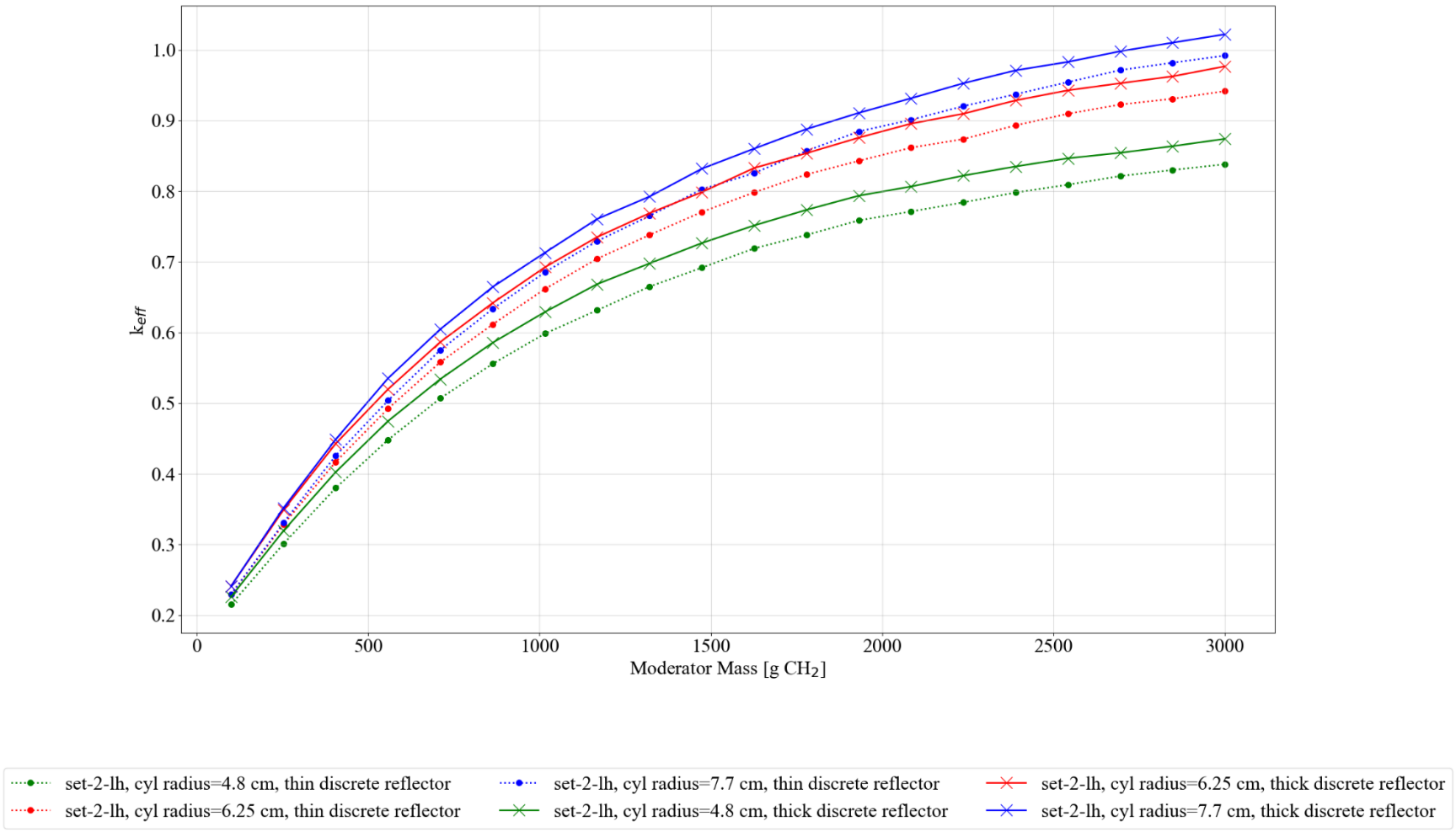

Figure D-7. Set-2-lh results, plot 6: reactivity effect of cylinder radius, pipe steel, 5 kg graphite/can, no Be, poly moderated.

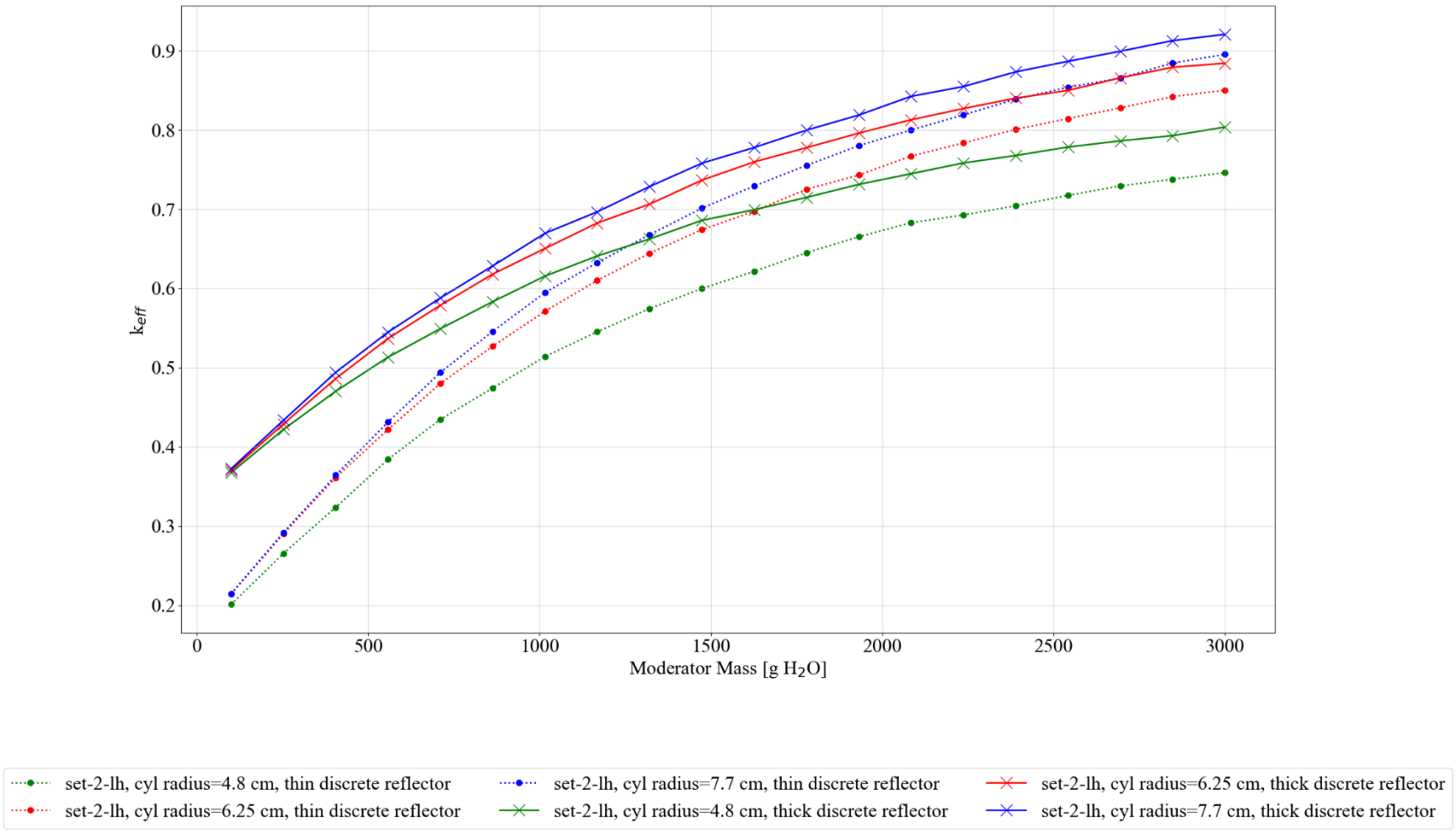

Figure D-8. Set-2-lh results, plot 7: reactivity effect of cylinder radius, pipe poly, 5 kg graphite/can, no Be, water moderated.

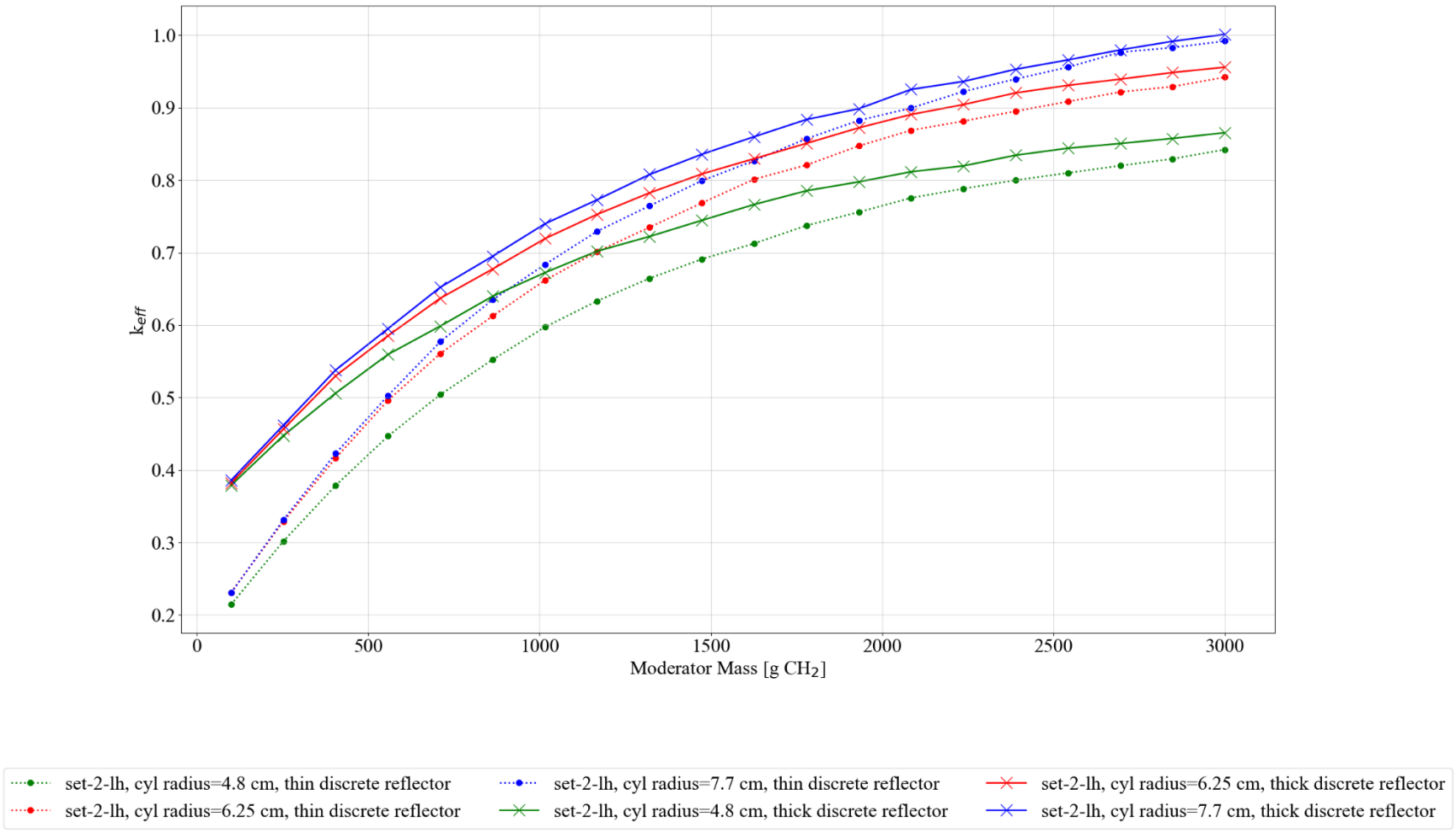

Figure D-9. Set-2-lh results, plot 8: reactivity effect of cylinder radius, pipe poly, 5 kg graphite/can, no Be, poly moderated.

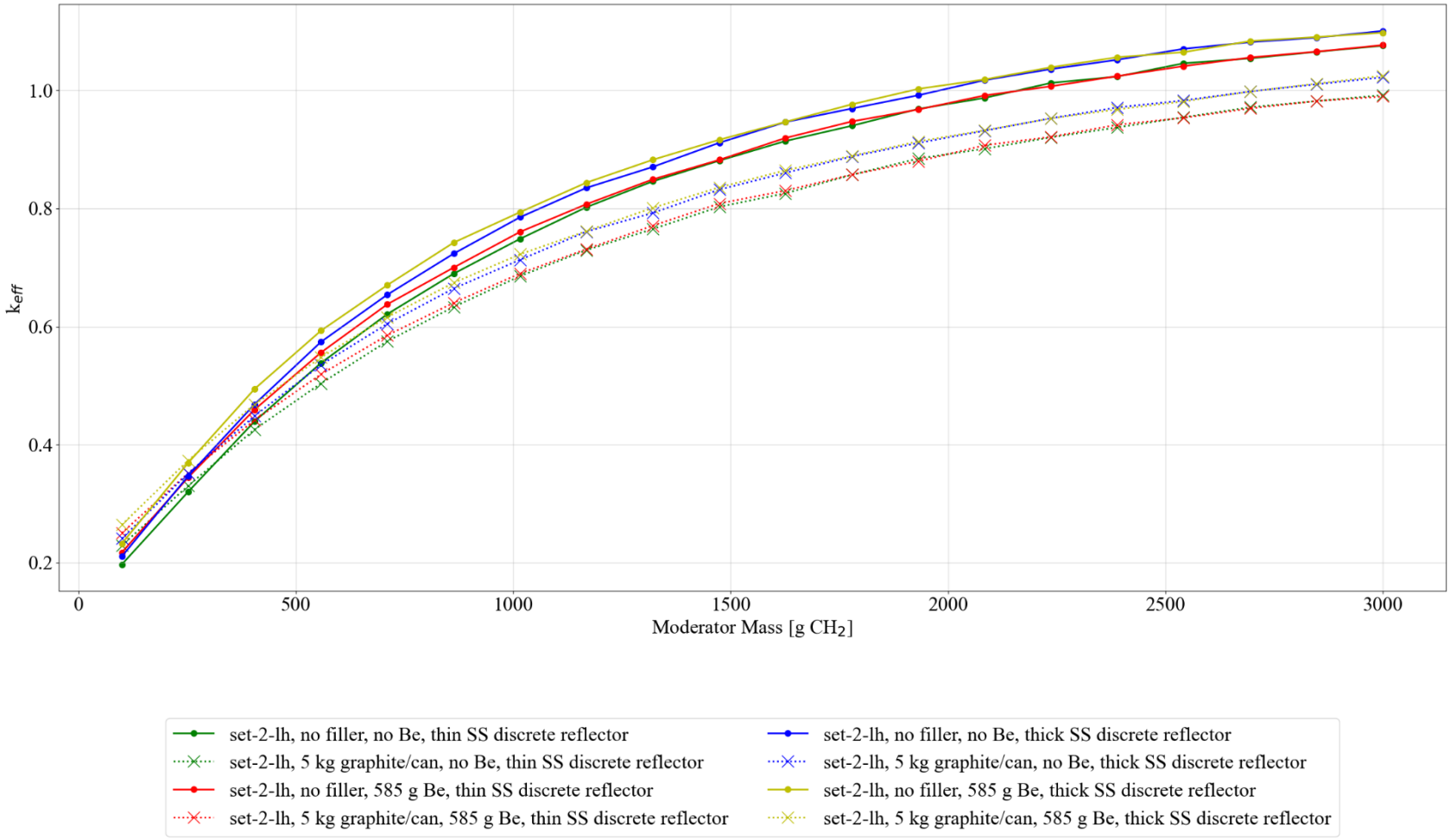

Figure D-10. Set-2-lh results, plot 9: reactivity effect of various parameters with 7.7 cm cylinder radius, graphite filler, poly moderated.

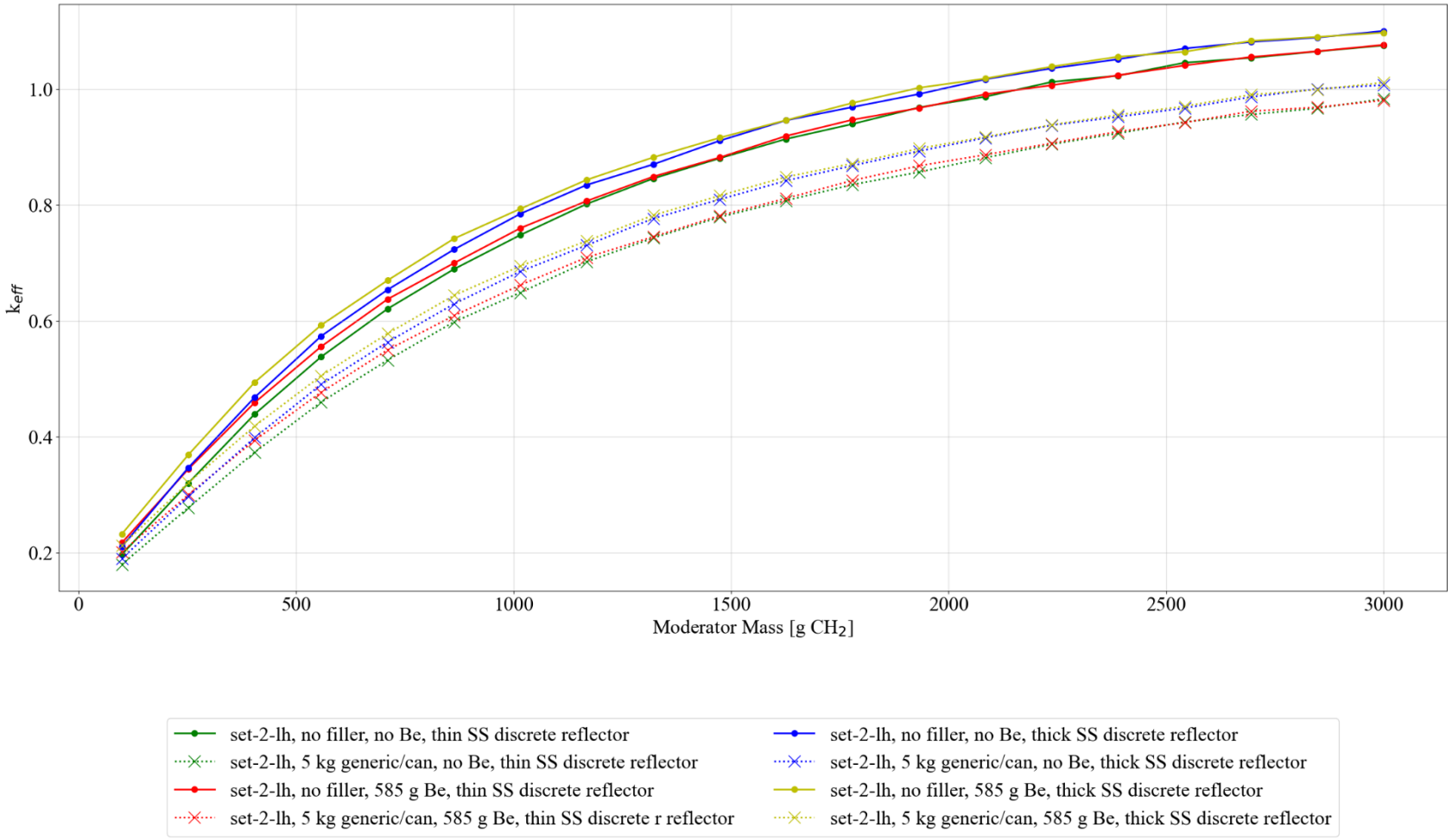

Figure D-11. Set-2-lh results, plot 10: reactivity effect of various parameters with 7.7 cm cylinder radius, generic filler, poly moderated.

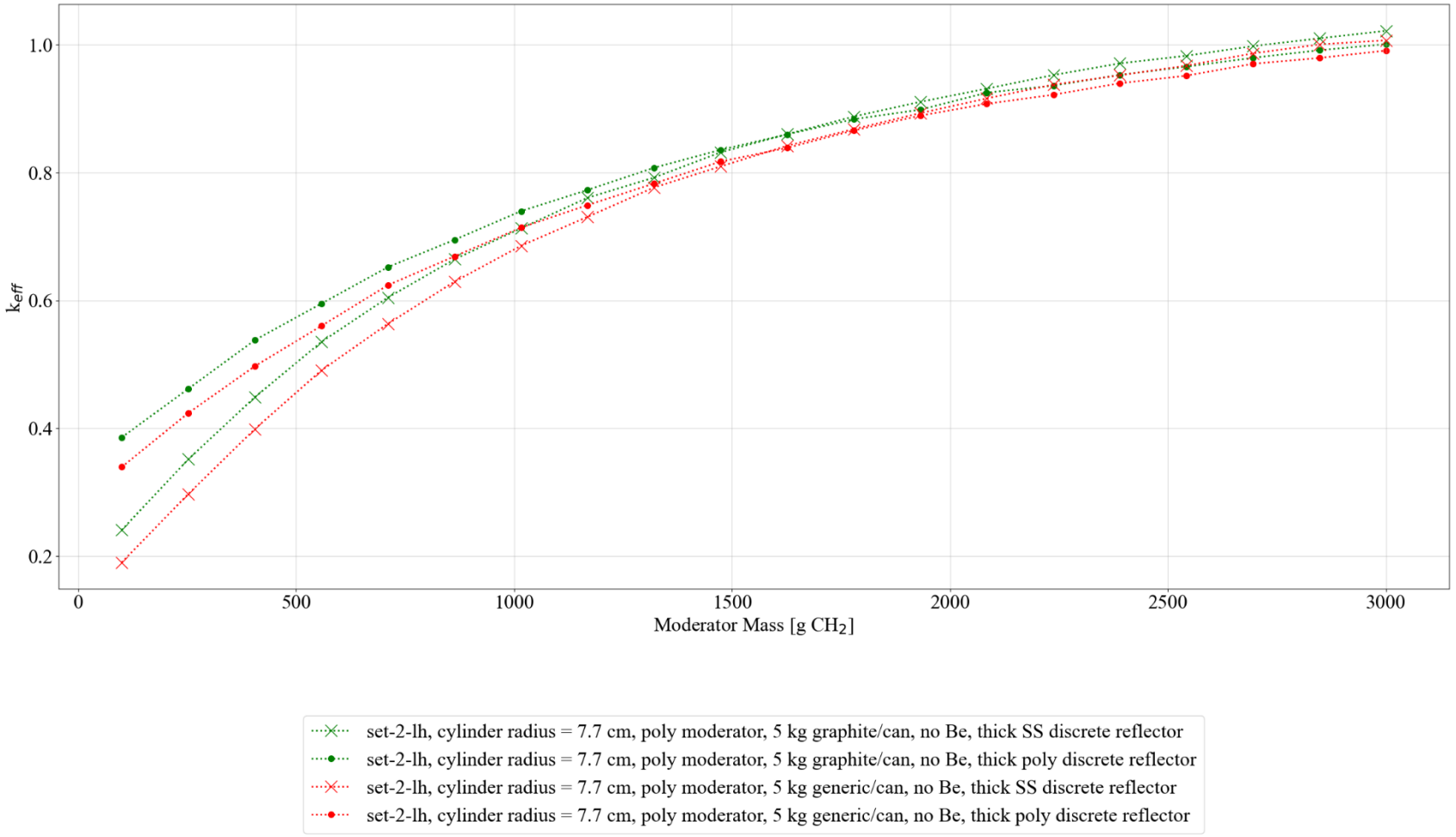

Figure D-12. Set-2-lh results, plot 11: comparison of graphite and generic filler with 7.7 cm cylinder radius, no Be, poly moderated, thick discrete reflector.

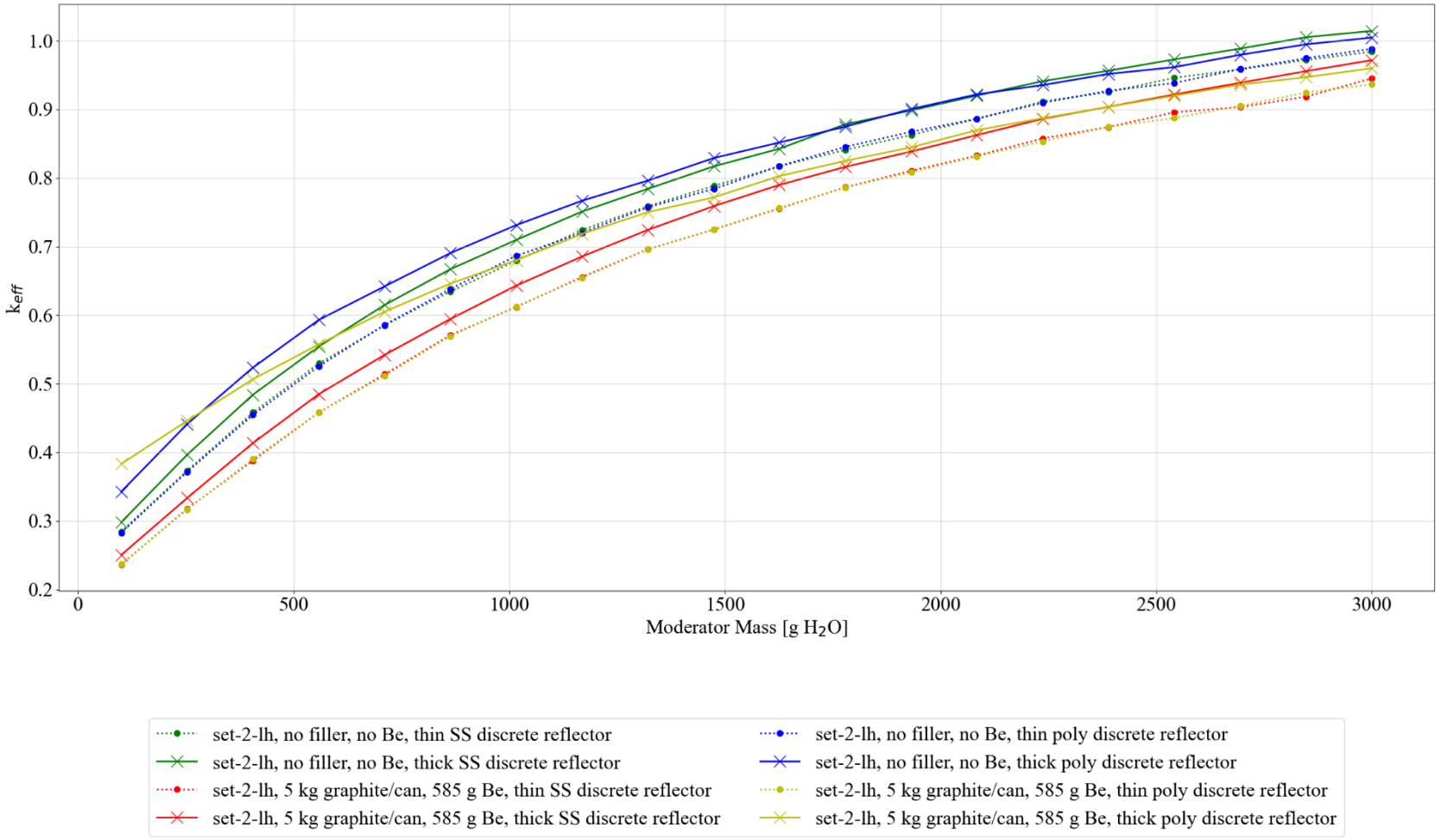

Figure D-13. Set-2-lh results, plot 12: reactivity effect of various parameters with spherical waste form geometry, graphite filler, water moderated.

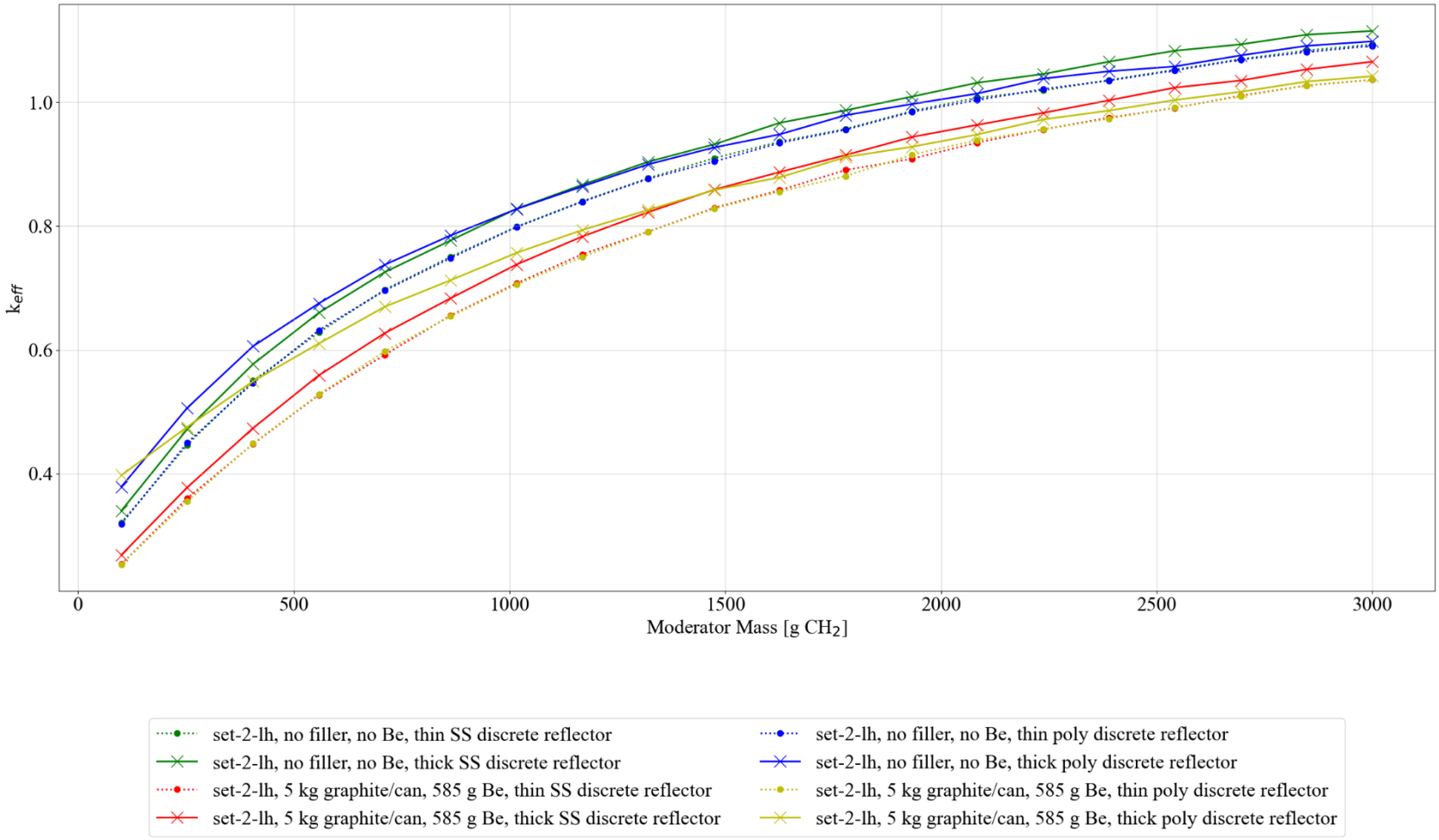

Figure D-14. Set-2-lh results, plot 13: reactivity effect of various parameters with spherical waste form geometry, graphite filler, poly moderated.

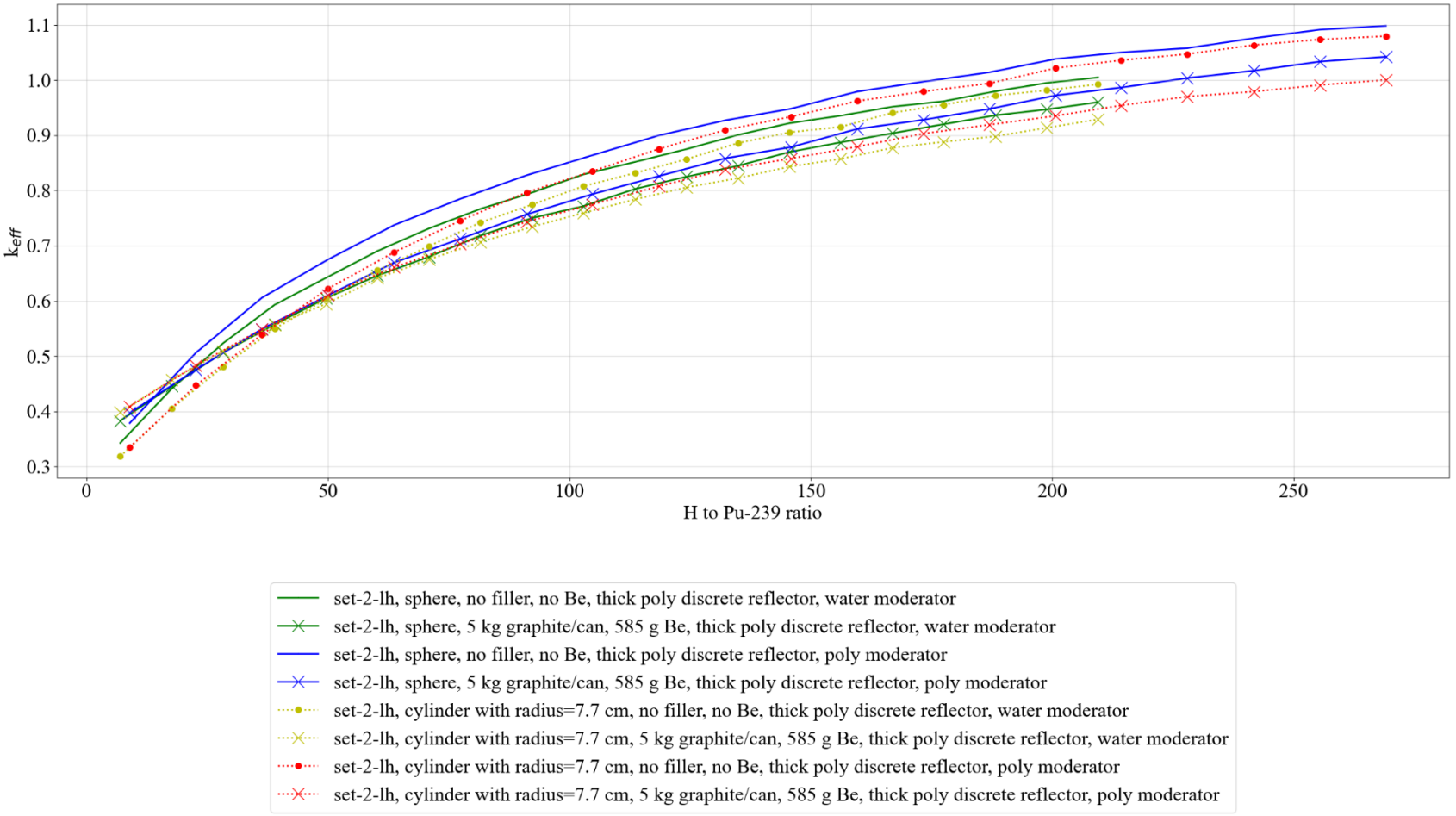

Figure D-15. Set-2-lh results, plot 14: comparison of spherical and cylindrical geometries (h/x).

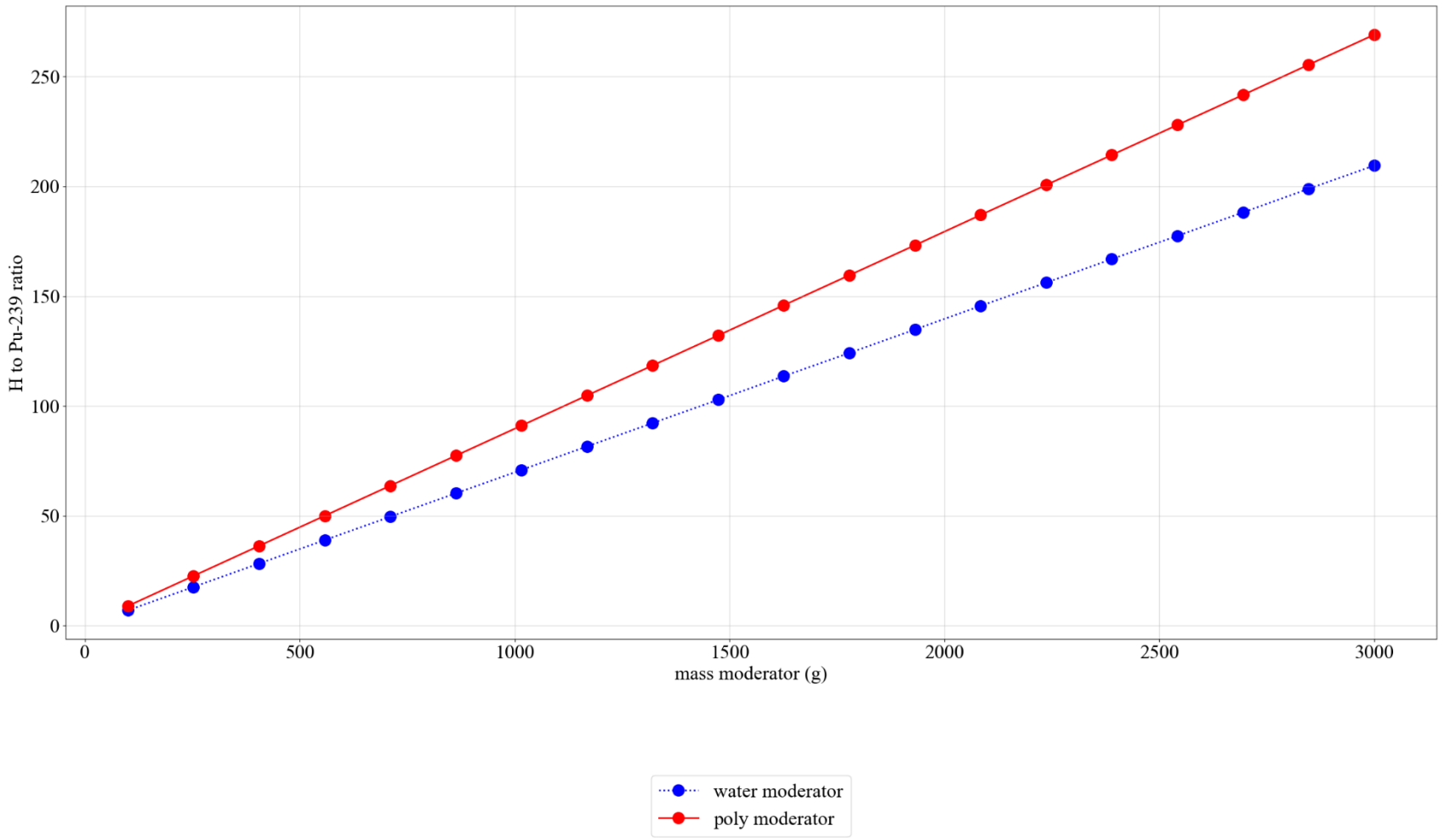

Figure D-16. Set-2-lh results, plot 15: comparison of water and poly h/x.

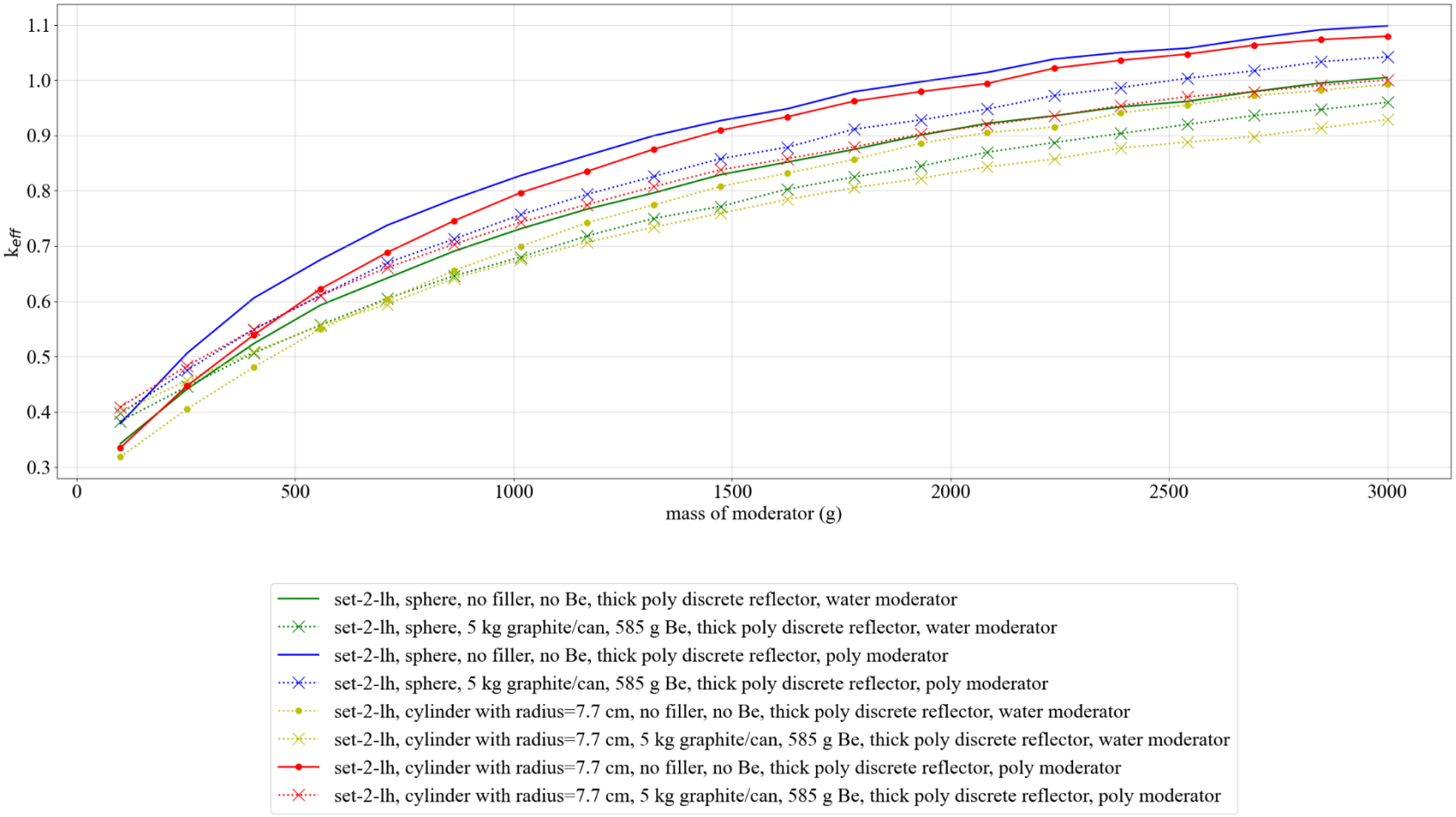

Figure D-17. Set-2-lh results, plot 16: comparison of spherical and cylindrical geometries (mod mass).

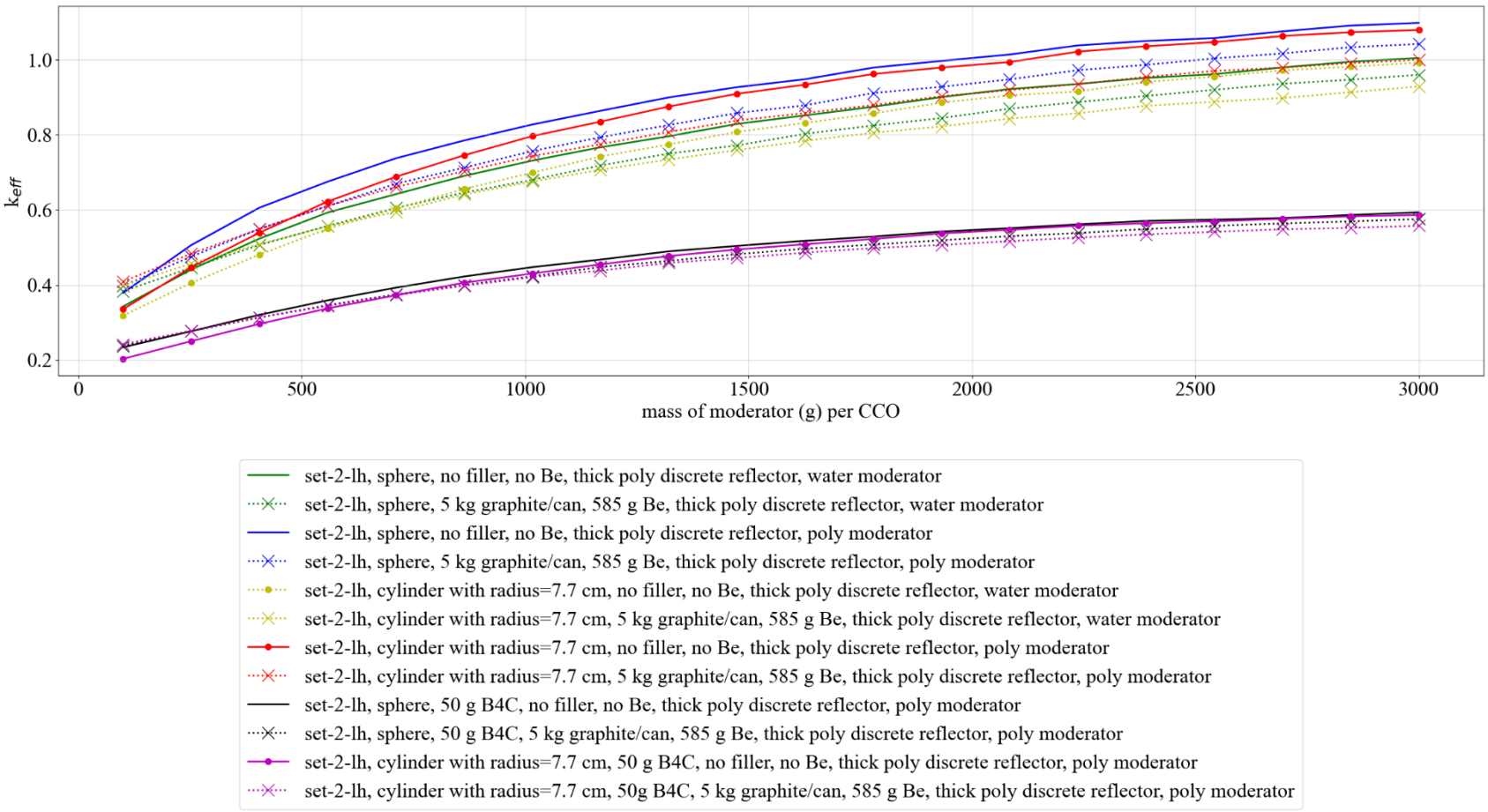

Figure D-18. Set-2-lh results, plot 17: comparison of 50g B_4C vs. no B_4C for spherical and cylindrical geometries (mod mass).

This page is intentionally blank

APPENDIX E. SET-2-TD: RESULTS OF THE TIME DEPENDENT NONUNIFORM ARRAY CALCULATIONS

This page is intentionally blank

APPENDIX E. SET-2-TD: RESULTS OF THE TIME DEPENDENT NONUNIFORM ARRAY CALCULATIONS

The analysis methodology for the time dependent nonuniform array studies is discussed in detail in Section 6.4 of the main report.

This appendix serves as a repository of the results for the time-dependent calculations.

The analysis model used for the calculations in this appendix is shown in Figure E-1 below. Additional discussions are provided in Section 6.3 of the main report.

The SAMPLER case sweeps presented in this appendix are summarized in Table E-1 below.

Results are presented in the following figures:

LIST OF FIGURES

LIST OF TABLES

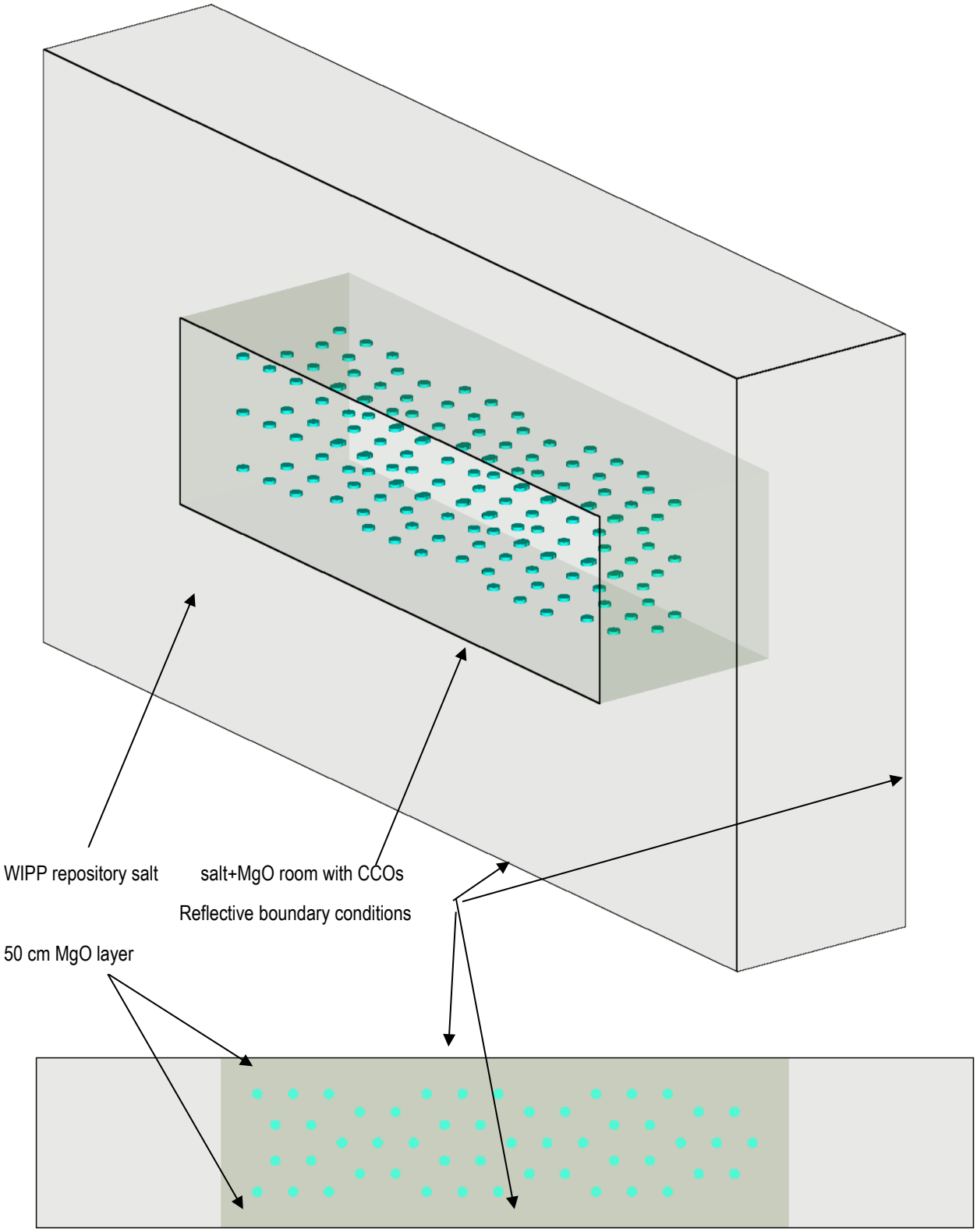

Figure E-1. 3D Isometric view (top) and 2D top view (bottom) representations of the 1-unit SCALE model.

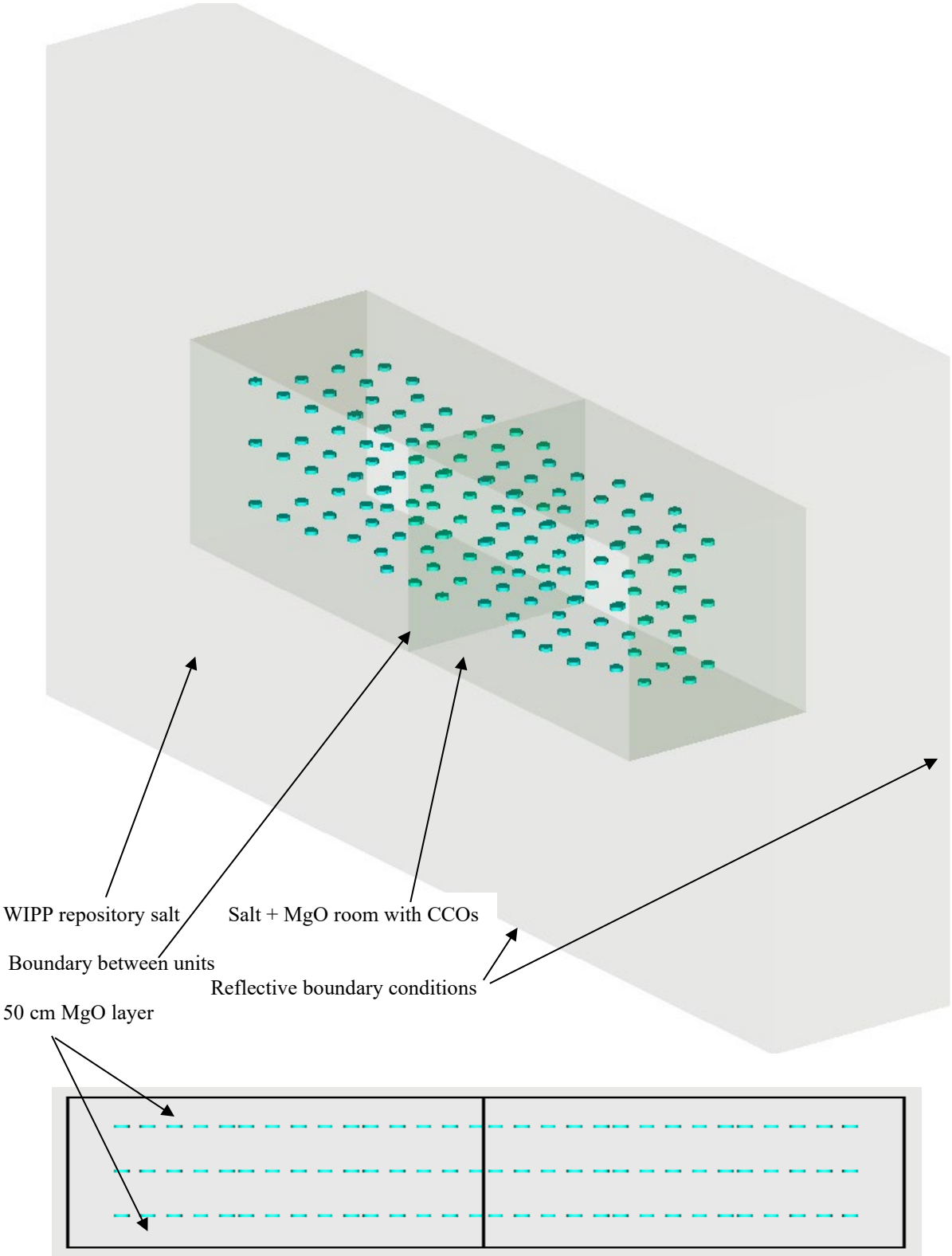

Figure E-2. 3D isometric (top) and 2D front (bottom) representations of the 2-unit SCALE model.

Table E-1. SAMPLER sweeps for the time-dependent studies

Case	Model type	Waste form shape	Waste form moderator	Filler material (0, 2,000, 4,000 g)	Metal in filler	Discrete reflector (thin 0.001, thick 0.7112 cm)	Be (g)	Subcase (time-step years)
Set-2-4-td	2-unit nonuniform array with centroids based on upper horizon data. Centroid from pipe center is used as the point in the center of the cylinder bases. Reflective boundary conditions are moved 50 cm off the outermost centroid positions in the y-direction. 50 cm is also used to offset the remainder of the reflective material box in the x and z directions. ***1,000 generations, 100 skipped cycles, 10,000 neutrons per generation.***	Cylinder (radius range 4.8, 6.25, 7.7 cm and height defined by total volume of mass)	water	c12	SS from can (0, 500, 1,000 g)	steel	0 to 585	0
			poly	c12		steel		
			water	c12		poly		
			poly	c12		poly		
			water	generic		steel		
			poly	generic		steel		
			water	generic		poly		
			poly	generic		poly		
		Cylinder with radius of 7.7 cm and height defined by total volume of mass.	poly	none	0	poly (thick 0.7112 cm)	0	10–300 in 10-year increments; 400–1,000 in 100-year increments
	1-unit nonuniform array with centroids based on upper horizon data. Centroid from pipe center is used as the point in the center of the cylinder bases. Reflective boundary conditions are directly adjacent to the outermost waste form in the y-direction, and the reflector box is also directly adjacent to the waste forms in the x and z directions***. 300 generations, 50 skipped cycles, 1,000 neutrons per generation.***	Cylinder with radius of 7.7 cm and height defined by total volume of mass.	poly	none	0	poly (thick 0.7112 cm)	0	0, 50, 100, 200, 300, 400, 500, 1,000 years

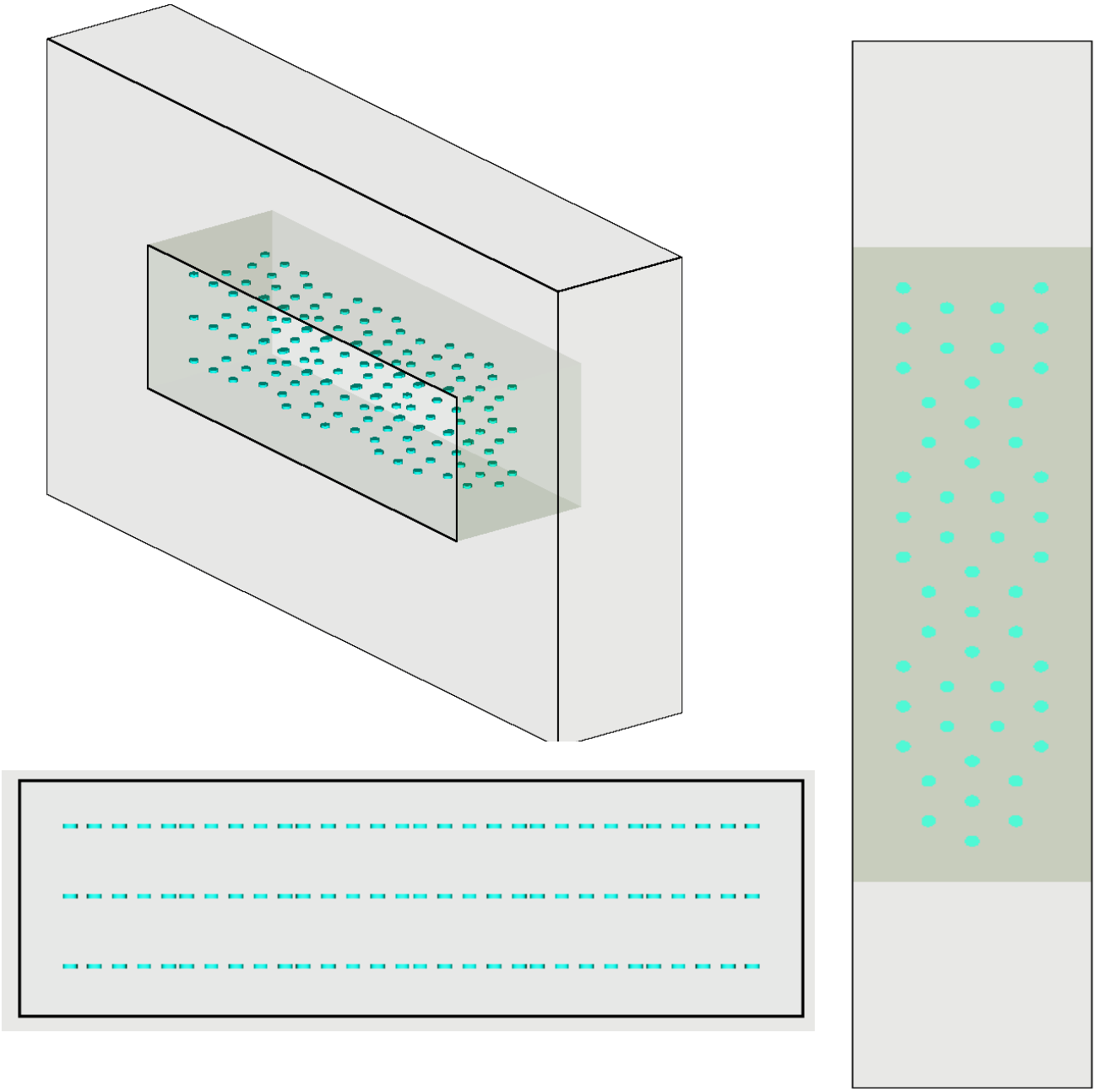

Figure E-3. Layout of the 1-unit, 0-year CCO locations in 3D isometric (top left), top view (right) and front (bottom left).

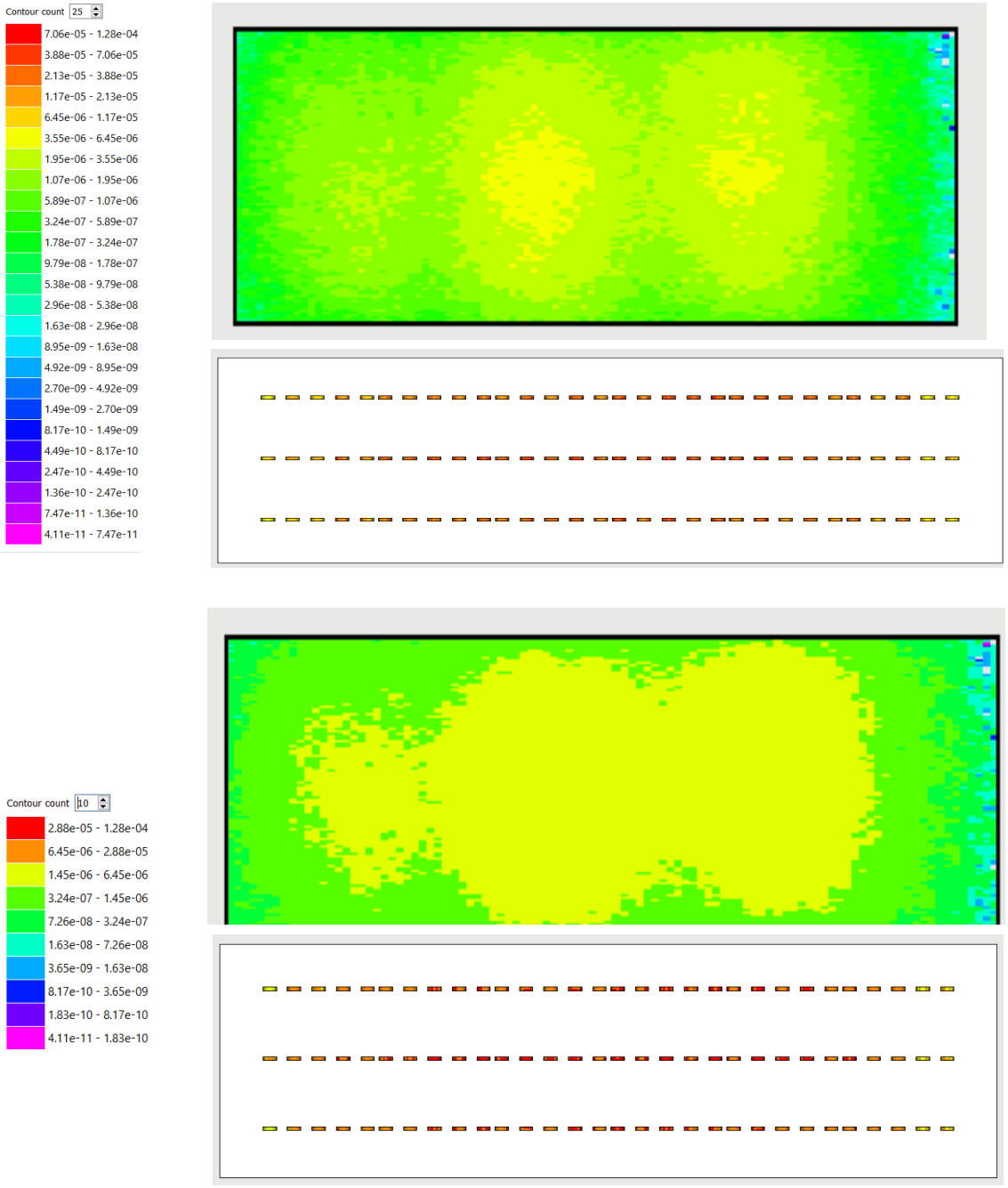

Figure E-4. Distribution of the flux for the x-z direction (top and bottom) with contour count of 10 for 0 years for the SNL upper horizon compaction results. All cases use set-2-4 bounding conditions (cylindrical waste forms with no filler, no can, no Be, thick poly discrete reflector, and approximately 700 g poly moderator in the 1-unit model).

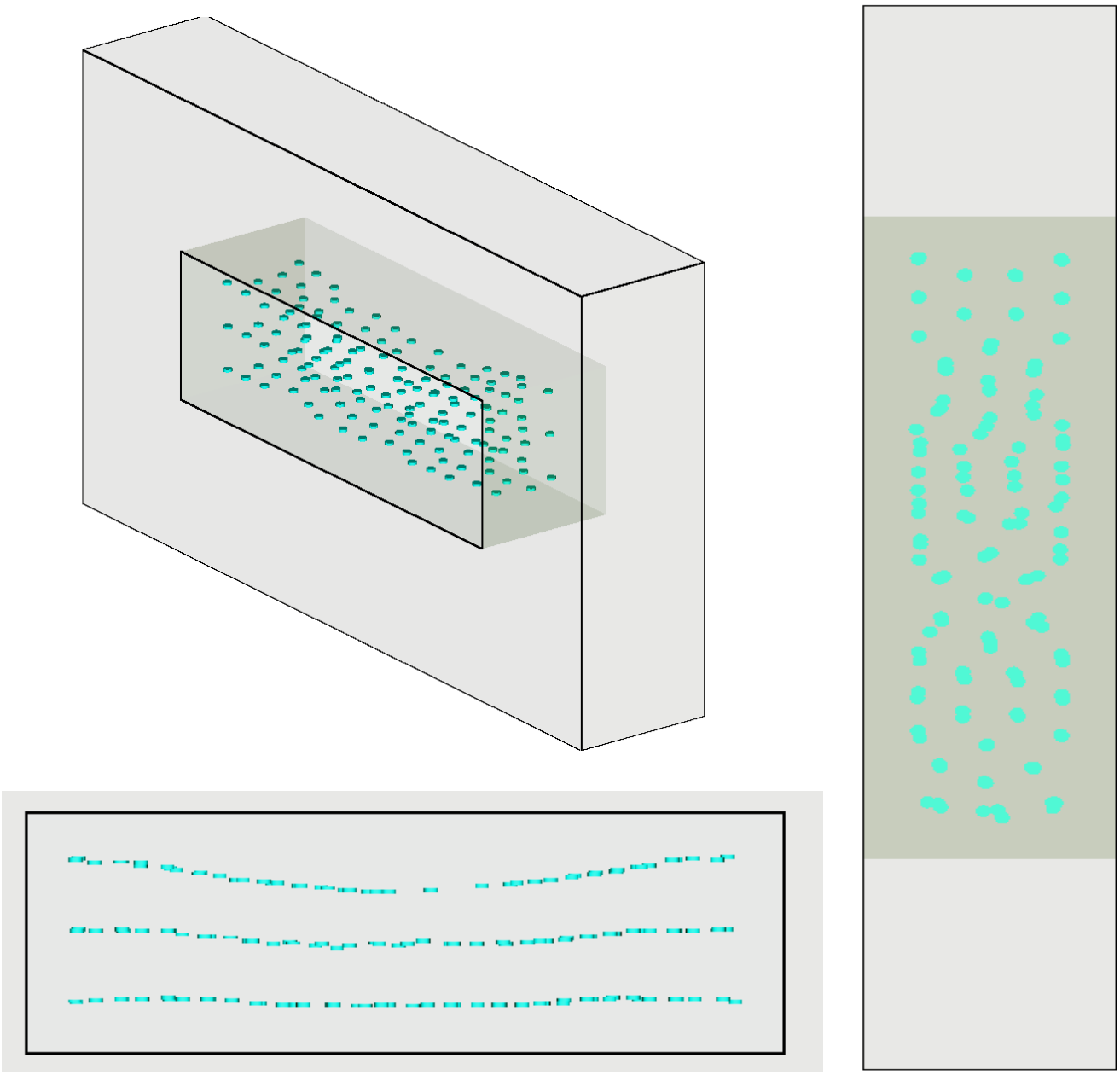

Figure E-5. Layout of the 1-unit, 50-year CCO locations in 3D isometric (top left), top view (right) and front (bottom left).

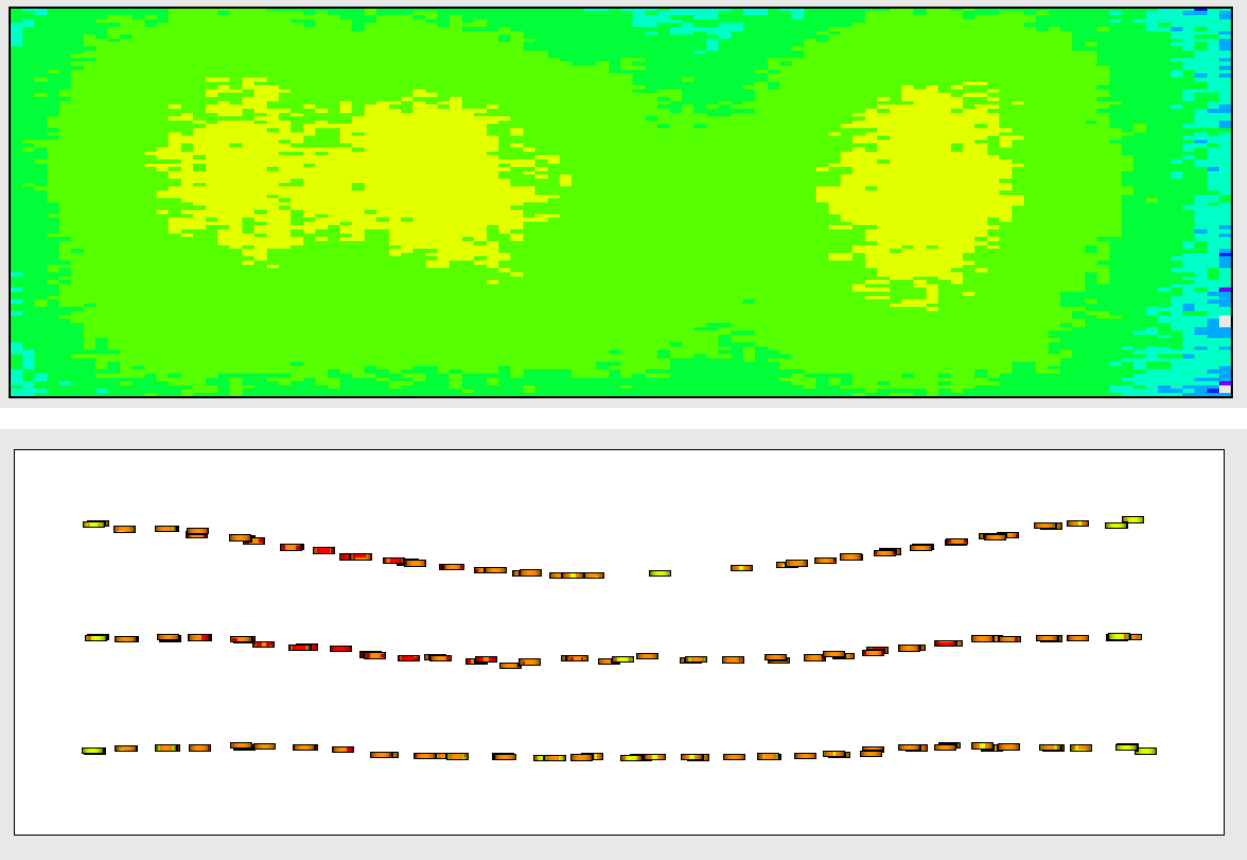

Figure E-6. Distribution of the flux for the x-z direction (top and bottom) with contour count of 10 for 50 years for the SNL upper horizon compaction results. All cases use the set-2-4 bounding conditions (cylindrical waste forms with no filler, no can, no Be, thick poly discrete reflector, and approximately 700 g poly moderator in the 1-unit model).

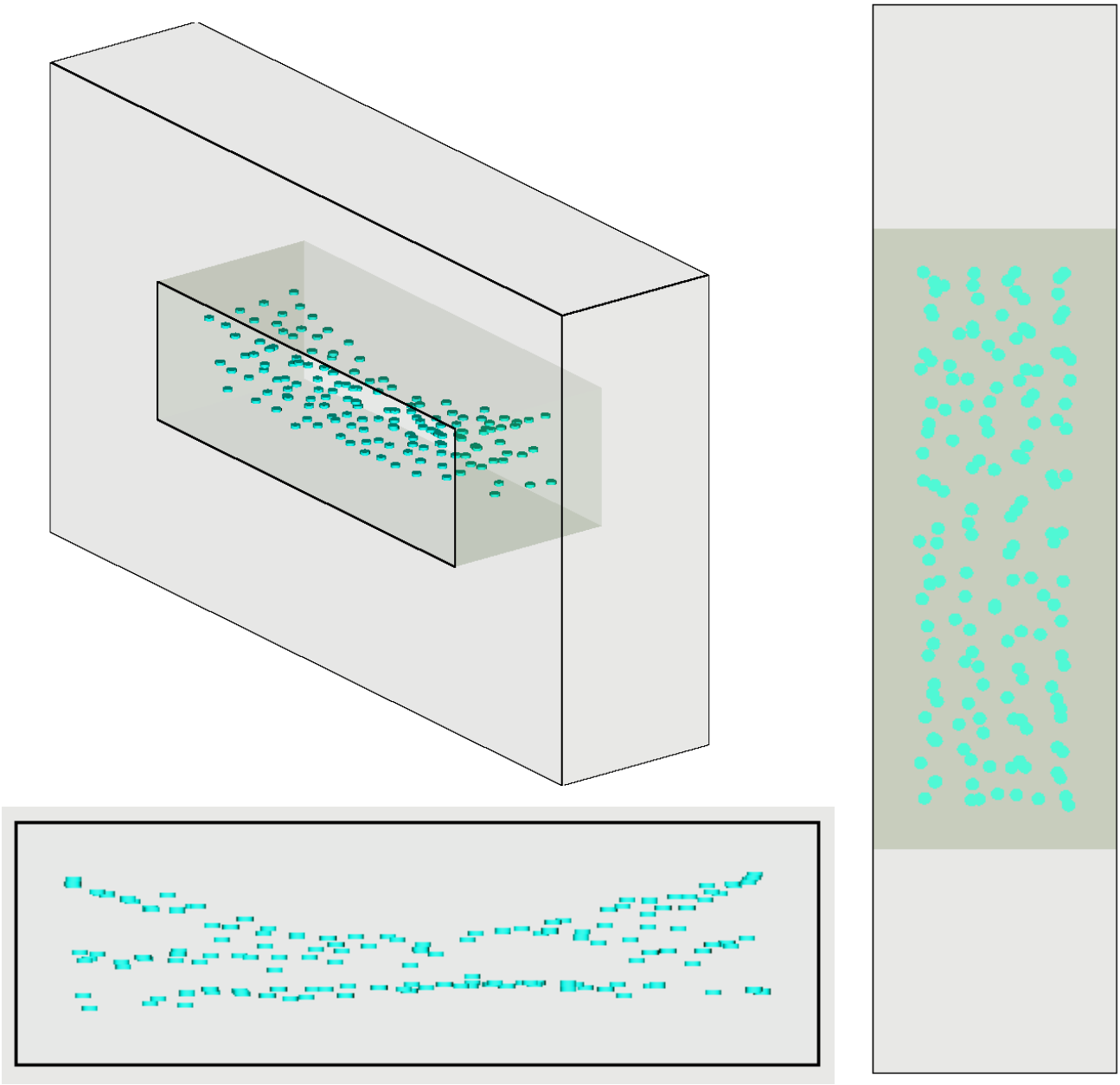

Figure E-7. Layout of the 1-unit, 100-year CCO locations in 3D isometric (top left), top view (right) and front (bottom left).

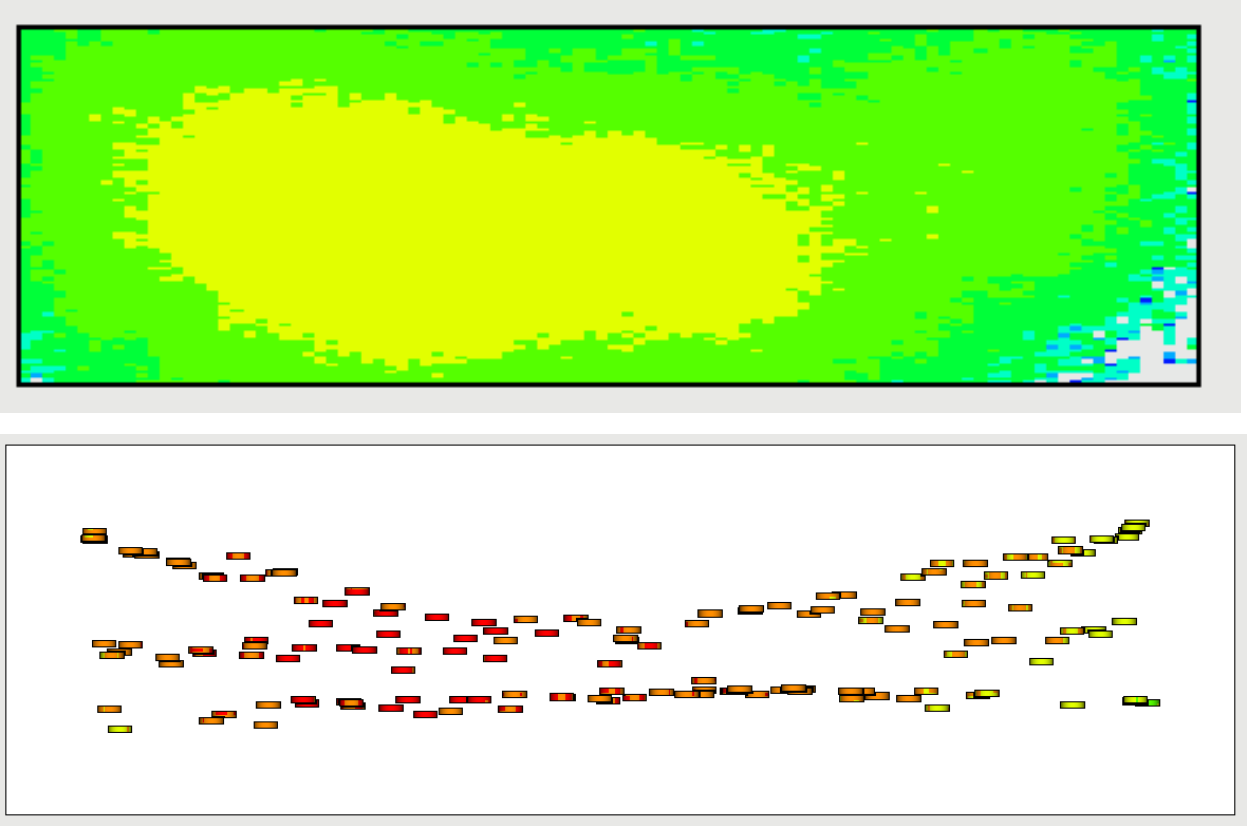

Figure E-8. Distribution of the flux for the x-z direction (top and bottom) with contour count of 10 for 100 years for the SNL upper horizon compaction results. All cases use the set-2-4 bounding conditions (cylindrical waste forms with no filler, no can, no Be, thick poly discrete reflector, and approximately 700 g poly moderator in the 1-unit model).

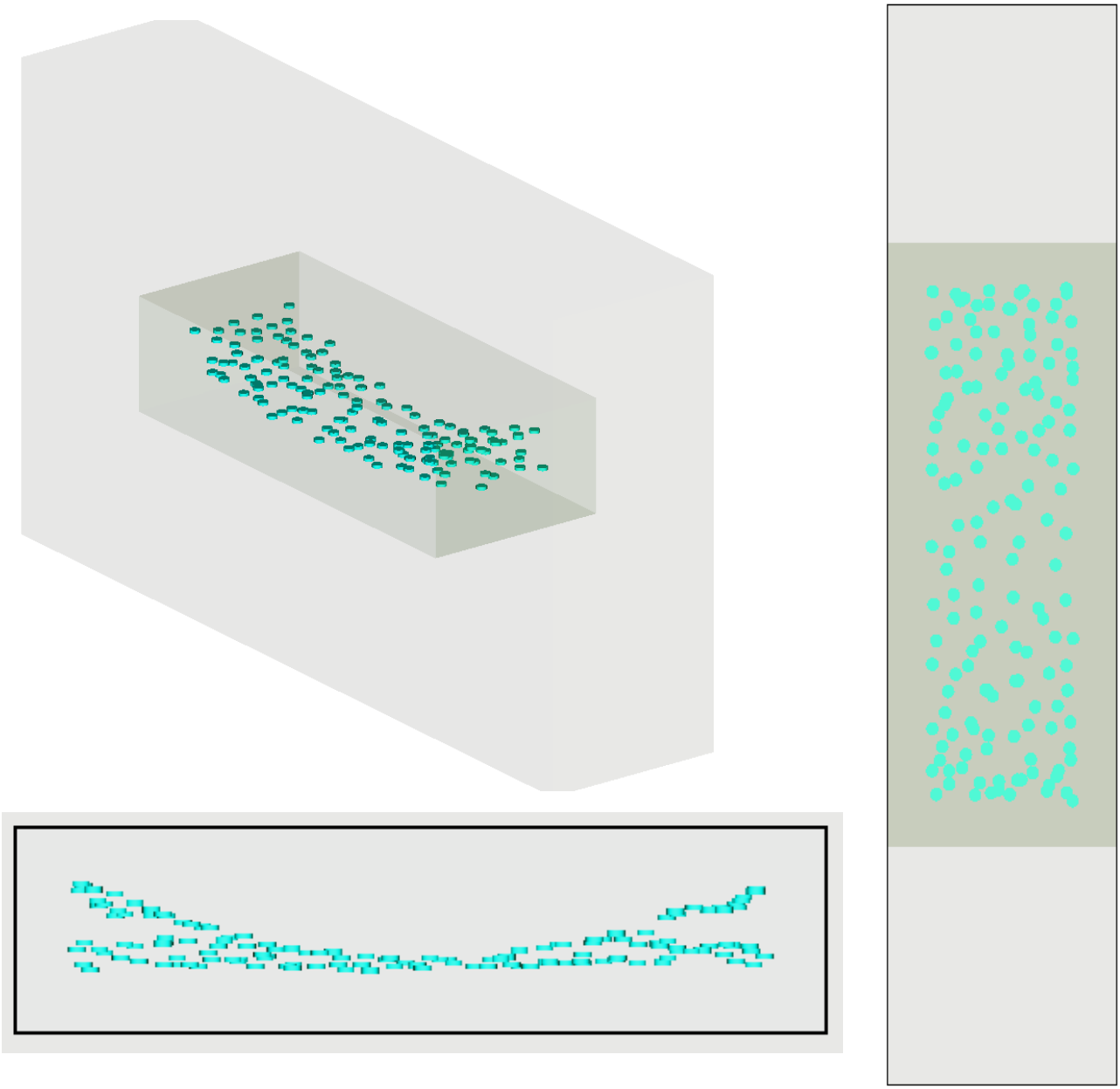

Figure E-9. Layout of the 1-unit, 200-year CCO locations in 3D isometric (top left), top view (right) and front (bottom left).

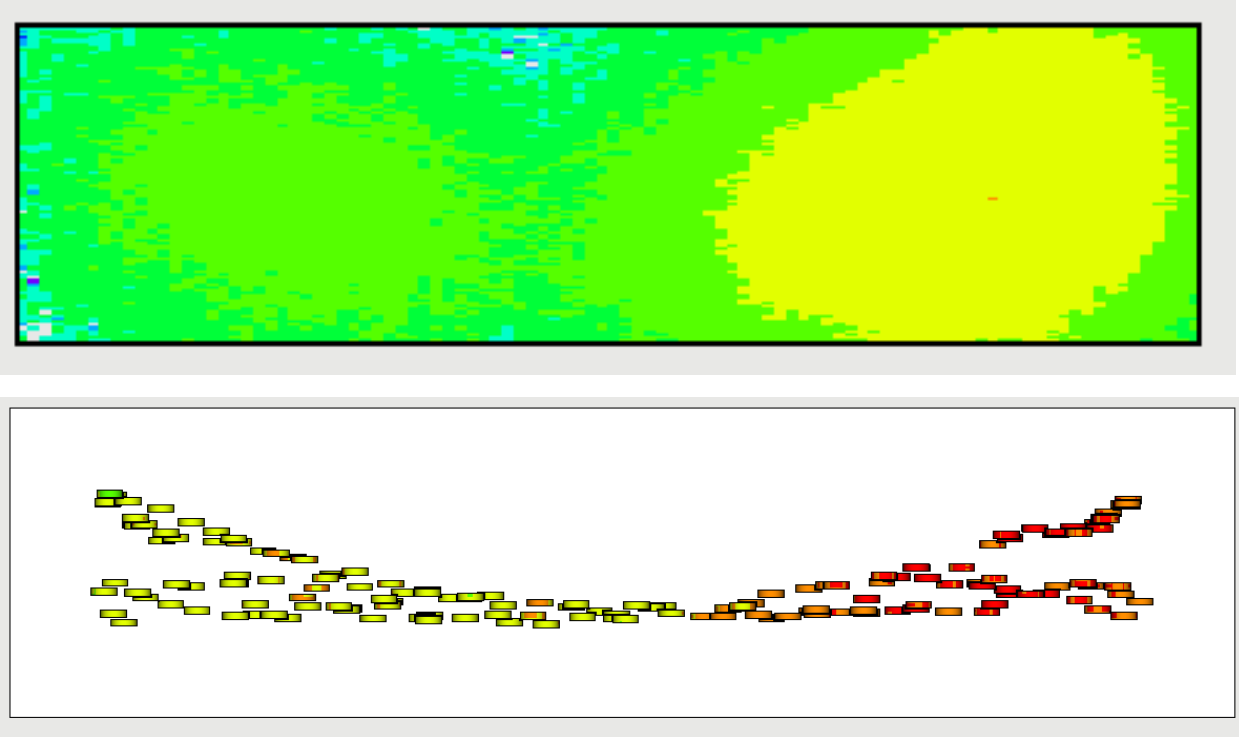

Figure E-10. Distribution of the flux for the x-z direction (top and bottom) with contour count of 10 for 200 years for the SNL upper horizon compaction results. All cases use the set-2-4 bounding conditions (cylindrical waste forms with no filler, no can, no Be, thick poly discrete reflector, and approximately 700 g poly moderator in the 1-unit model)

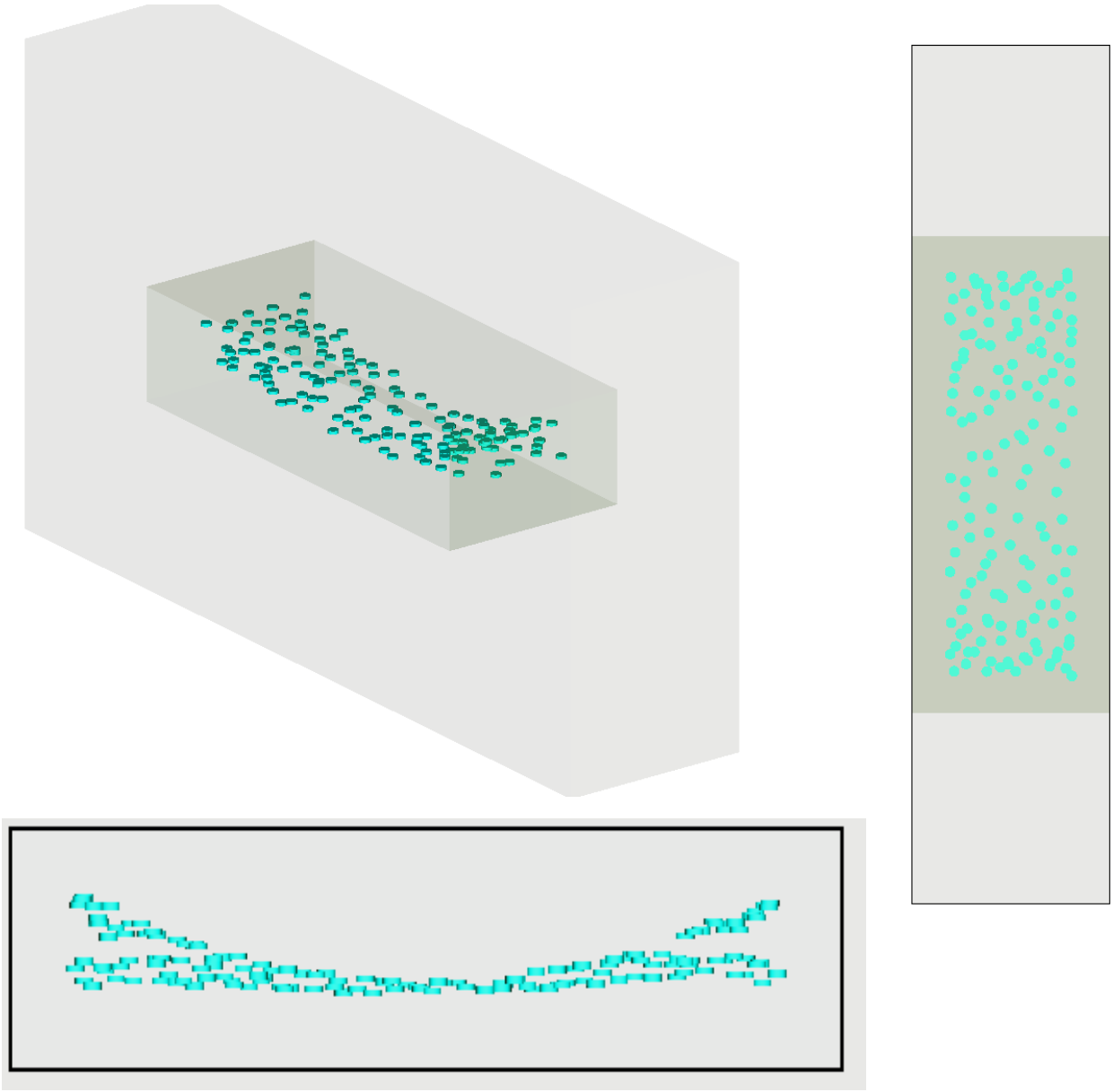

Figure E-11. Layout of the 1-unit, 300-year CCO locations in 3D isometric (top left), top view (right) and front (bottom left).

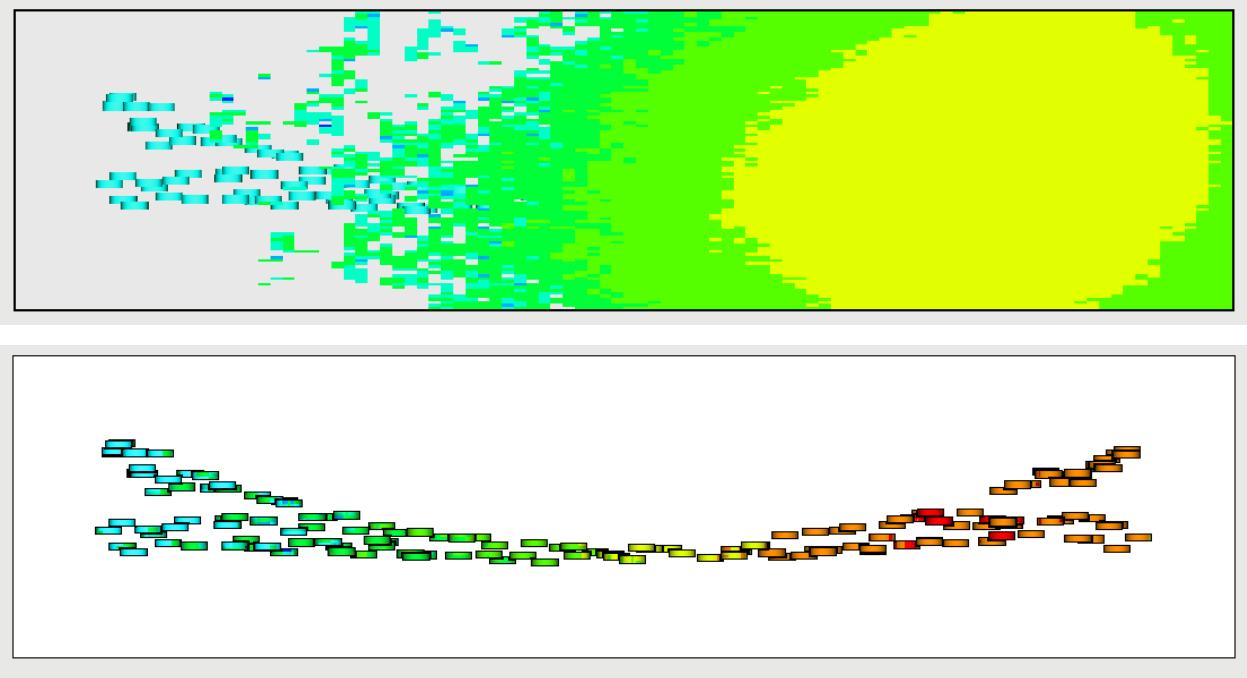

Figure E-12. Distribution of the flux for the x-z direction (top and bottom) with contour count of 10 for 300 years for the SNL upper horizon compaction results. All cases use the set-2-4 bounding conditions (cylindrical waste forms with no filler, no can, no Be, thick poly discrete reflector, and approximately 700 g poly moderator in the 1-unit model)

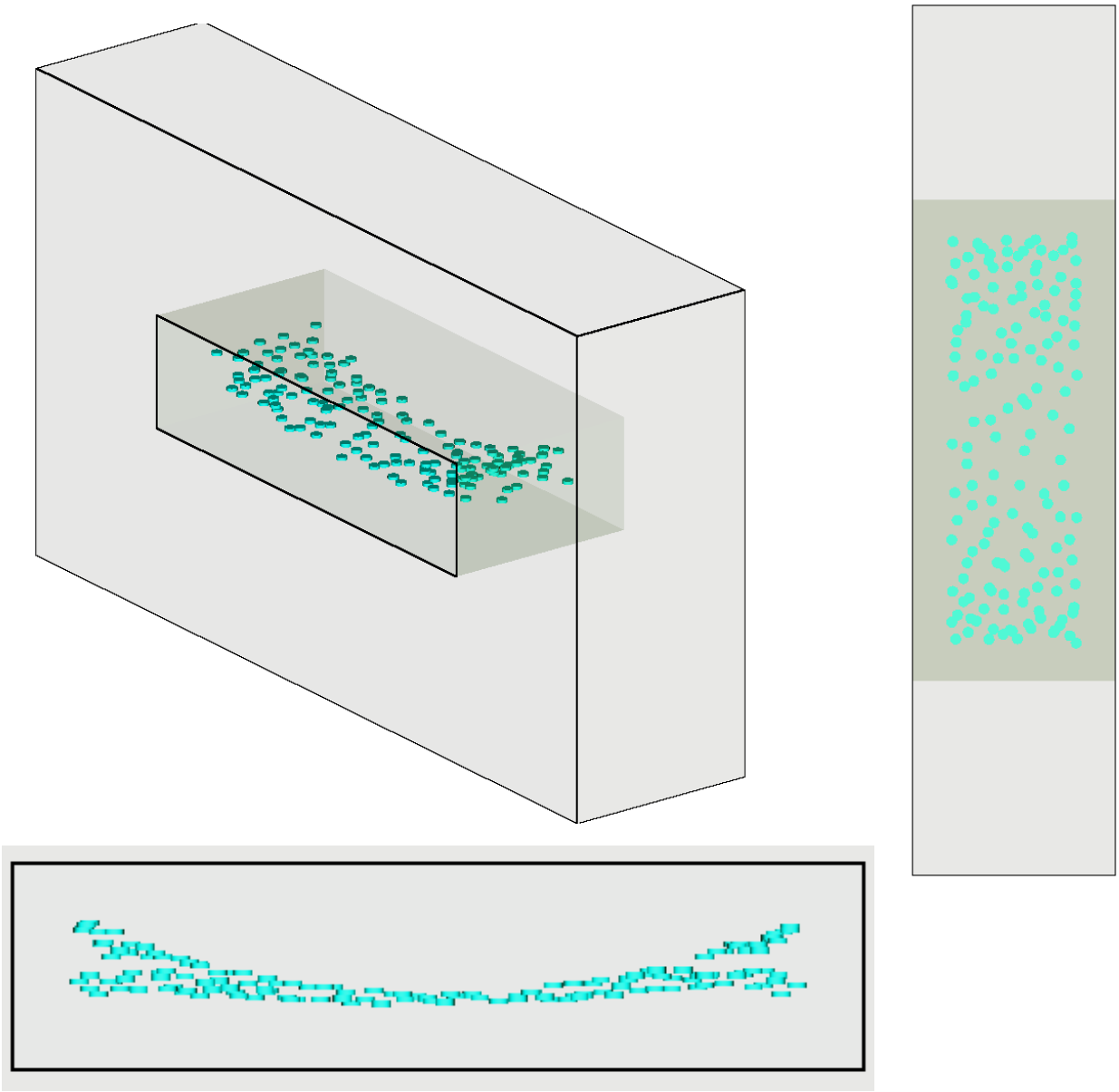

Figure E-13. Layout of the 1-unit, 400-year CCO locations in 3D isometric (top left), top view (right) and front (bottom left).

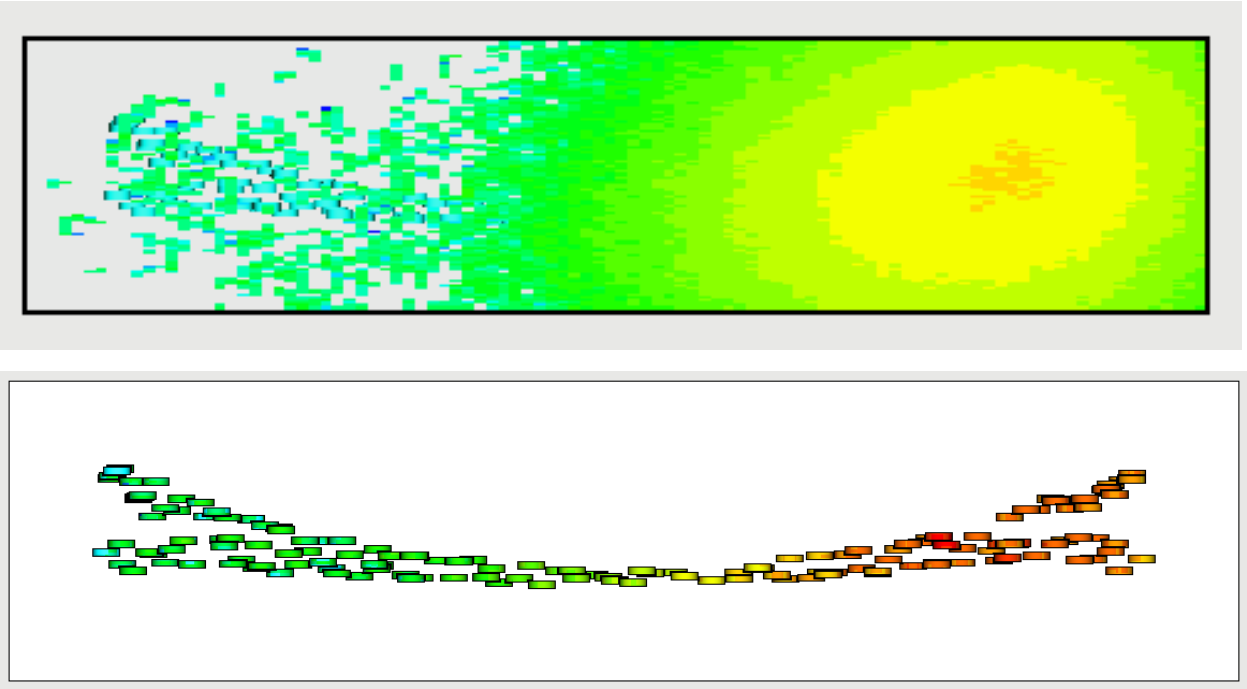

Figure E-14. Distribution of the flux for the x-z direction (top and bottom) with contour count of 10 for 400 years for the SNL upper horizon compaction results. All cases use the set-2-4 bounding conditions (cylindrical waste forms with no filler, no can, no Be, thick poly discrete reflector, and approximately 700 g poly moderator in the 1-unit model)

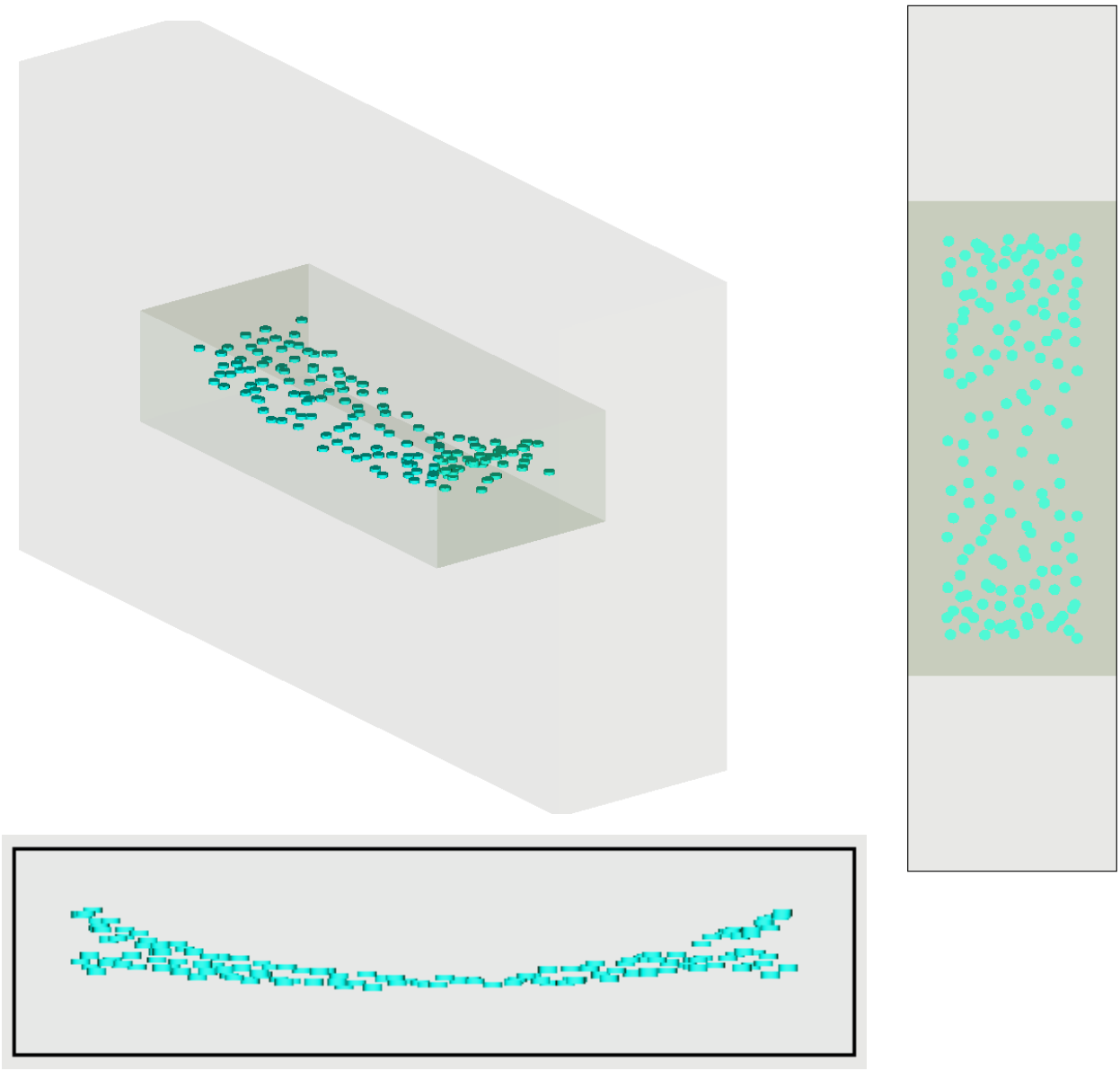

Figure E-15. Layout of the 1-unit, 1,000-year CCO locations in 3D isometric (top left), top view (right) and front (bottom left).

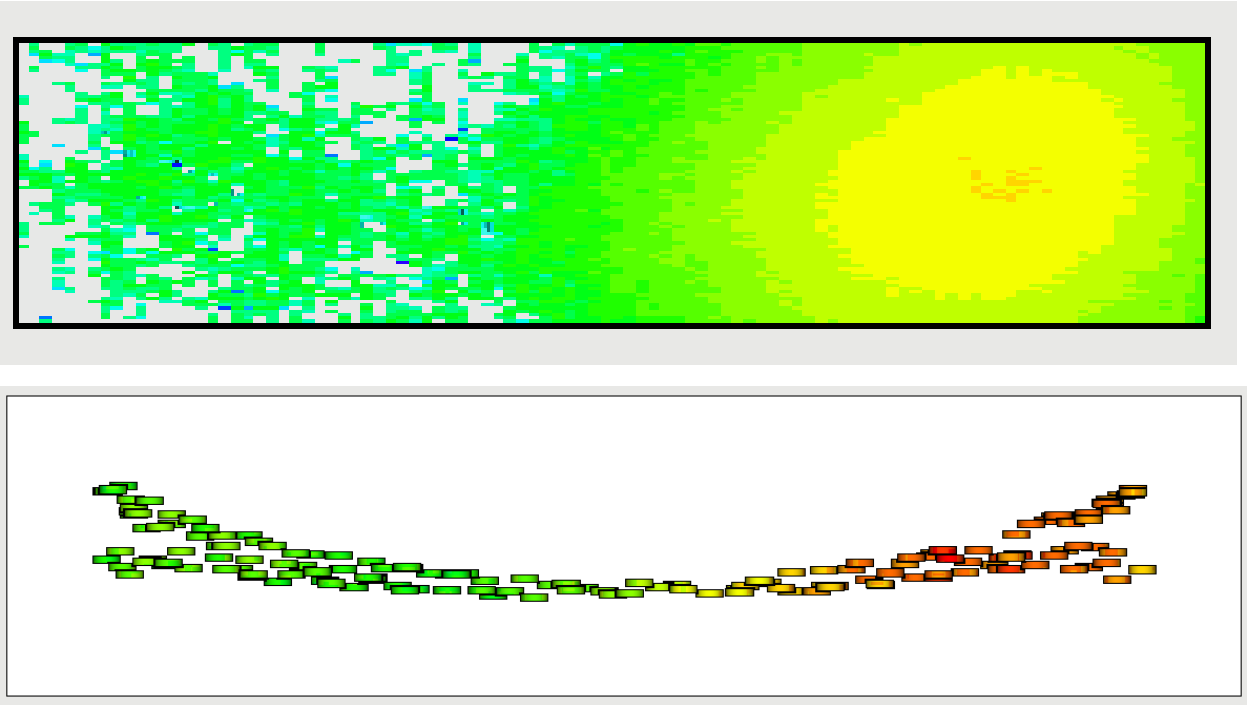

Figure E-16. Distribution of the flux for the x-z direction (top and bottom) with contour count of 10 for 1,000 years for the SNL upper horizon compaction results. All cases use the set-2-4 bounding conditions (cylindrical waste forms with no filler, no can, no Be, thick poly discrete reflector, and approximately 700 g poly moderator in the 1-unit model)

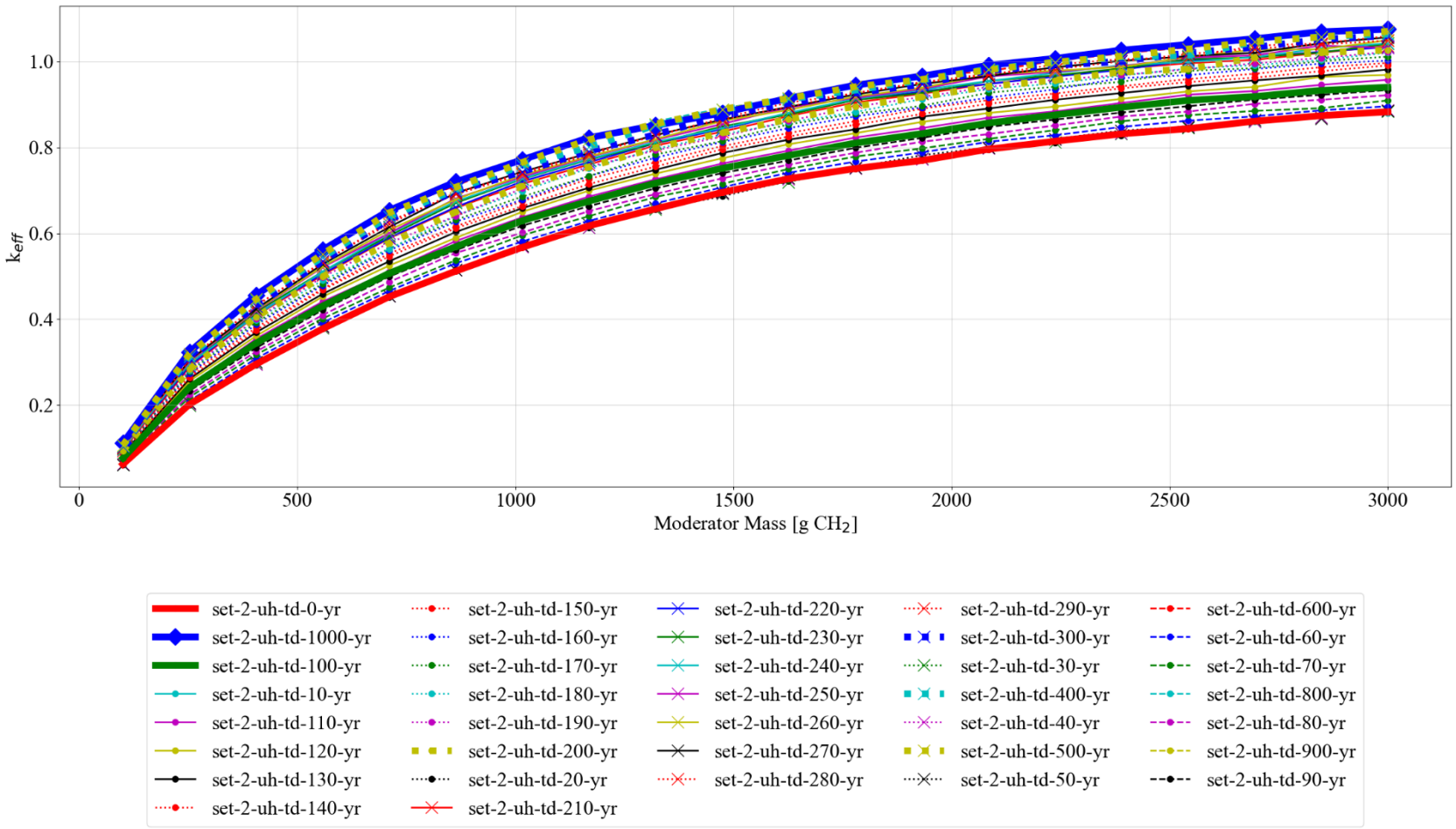

Figure E-17. Comparison of various small-step time-dependent compaction steps for the SNL upper horizon compaction results. All cases use the set-2-4 bounding conditions (cylindrical waste forms with no filler, no can, no Be, thick poly discrete reflector, and poly moderator).

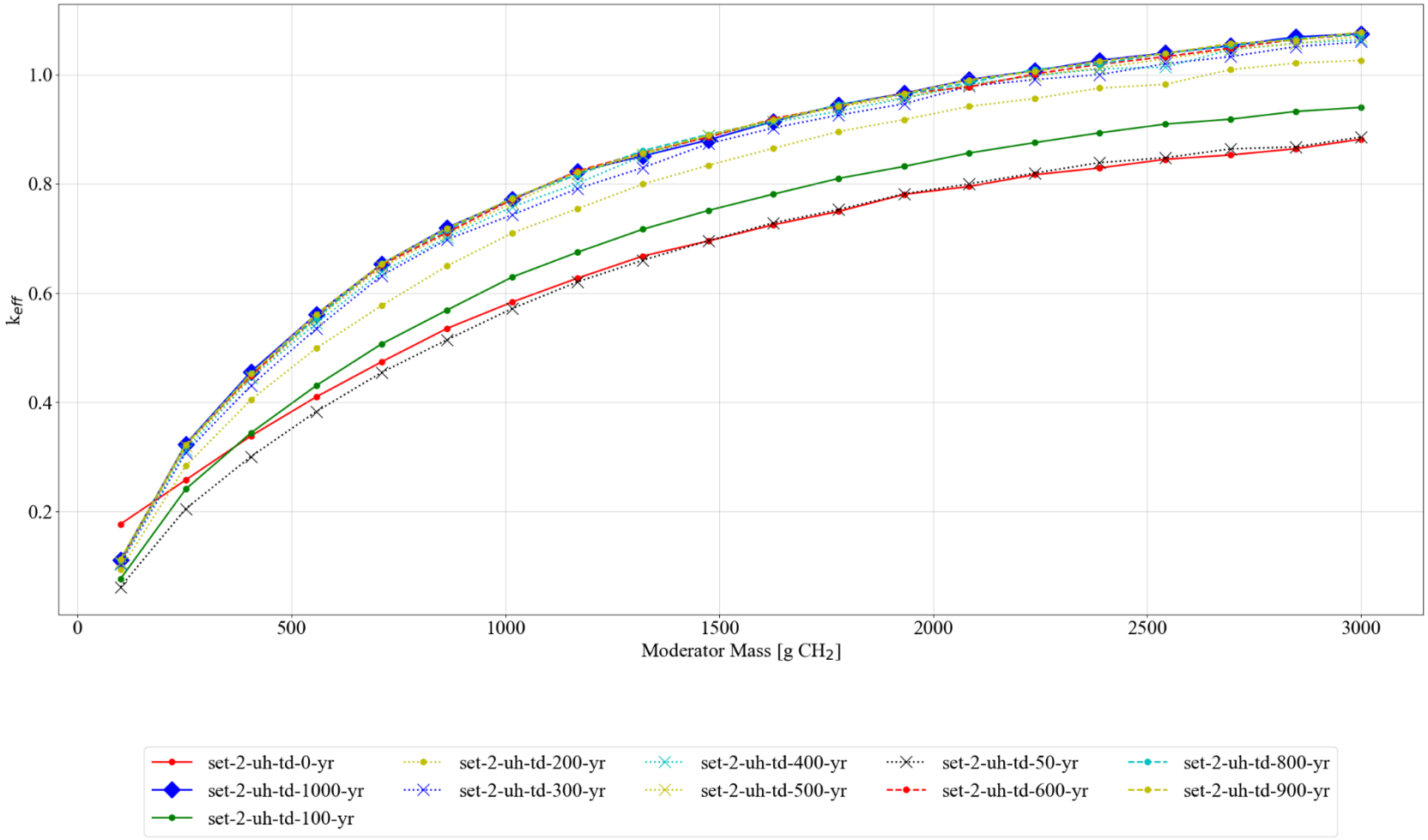

Figure E-18. Comparison of various large-step time-dependent compaction steps for the SNL upper horizon compaction results. All cases use the set-2-4 bounding conditions (cylindrical waste forms with no filler, no can, no Be, thick poly discrete reflector, and poly moderator).

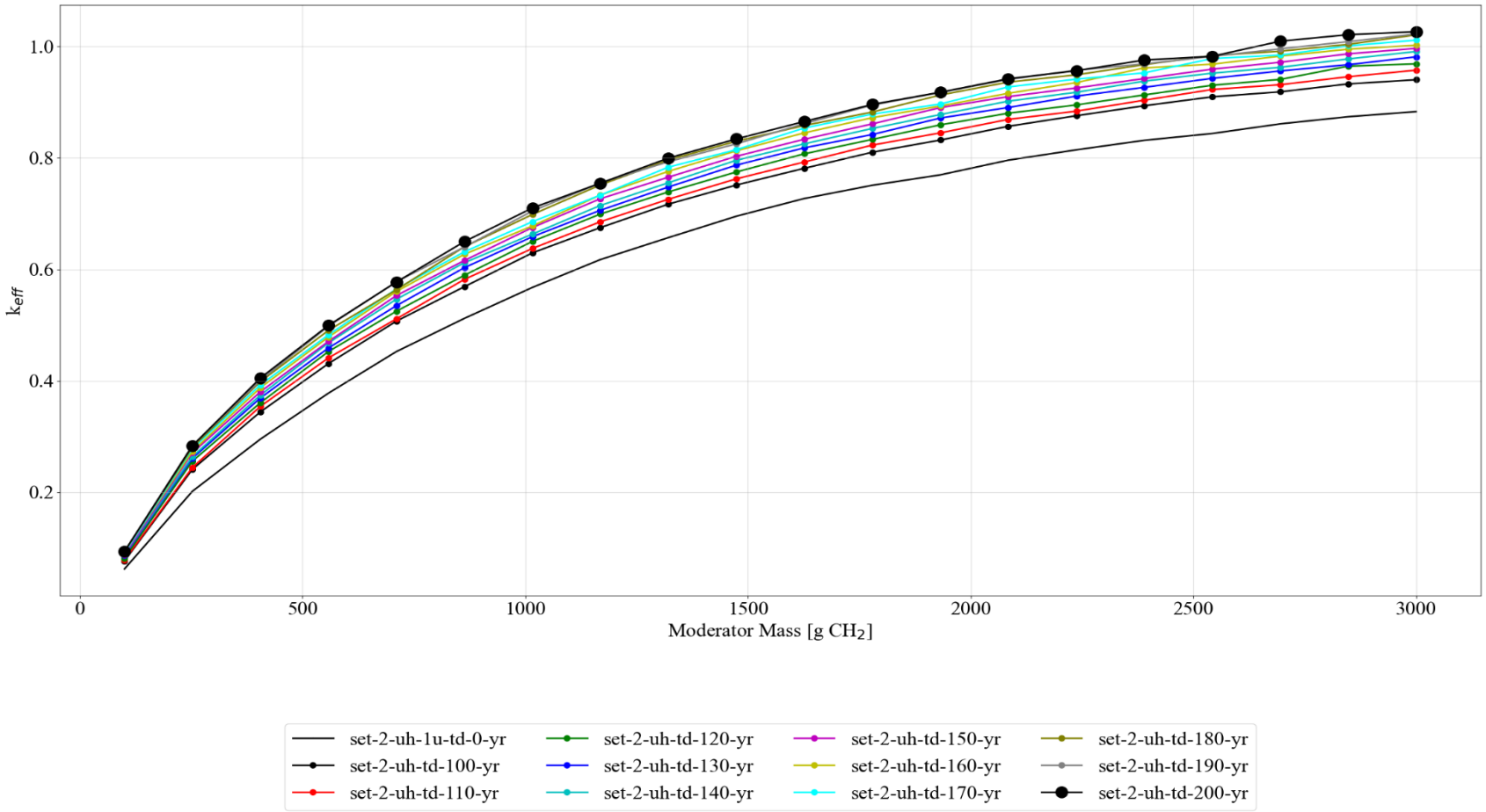

Figure E-19. Comparison of various small-step time-dependent compaction steps between 100 and 200 years for the SNL upper horizon compaction results. All cases use the set-2-4 bounding conditions (cylindrical waste forms with no filler, no can, no Be, thick poly discrete reflector, and poly moderator).

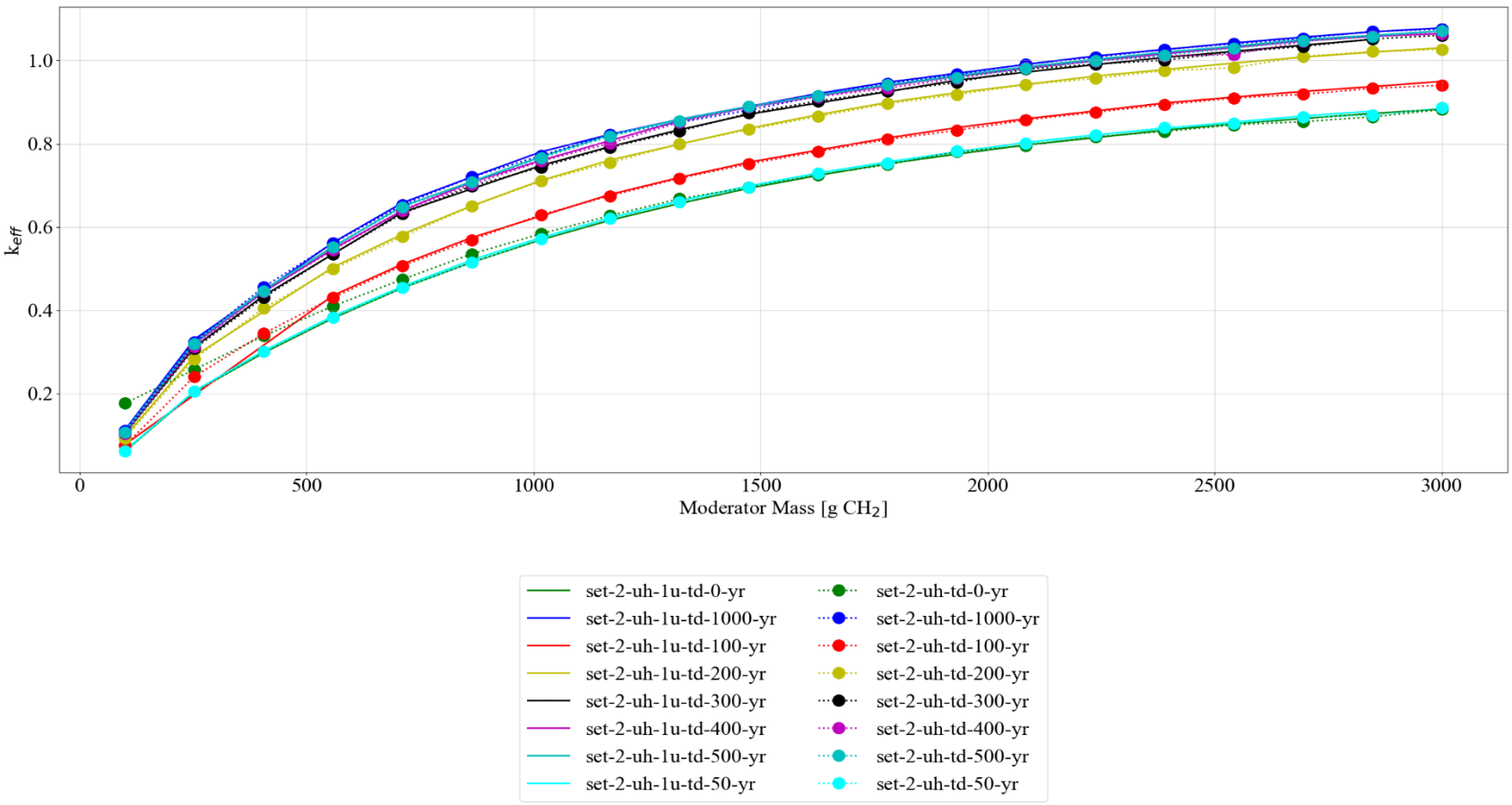

Figure E-20. Comparison of the 1- (-1u-) to 2-unit SCALE models for various time dependent cases for the SNL upper horizon compaction results. All cases use the set-2-4 bounding conditions (cylindrical waste forms with no filler, no can, no Be, thick poly discrete reflector, and poly moderator).

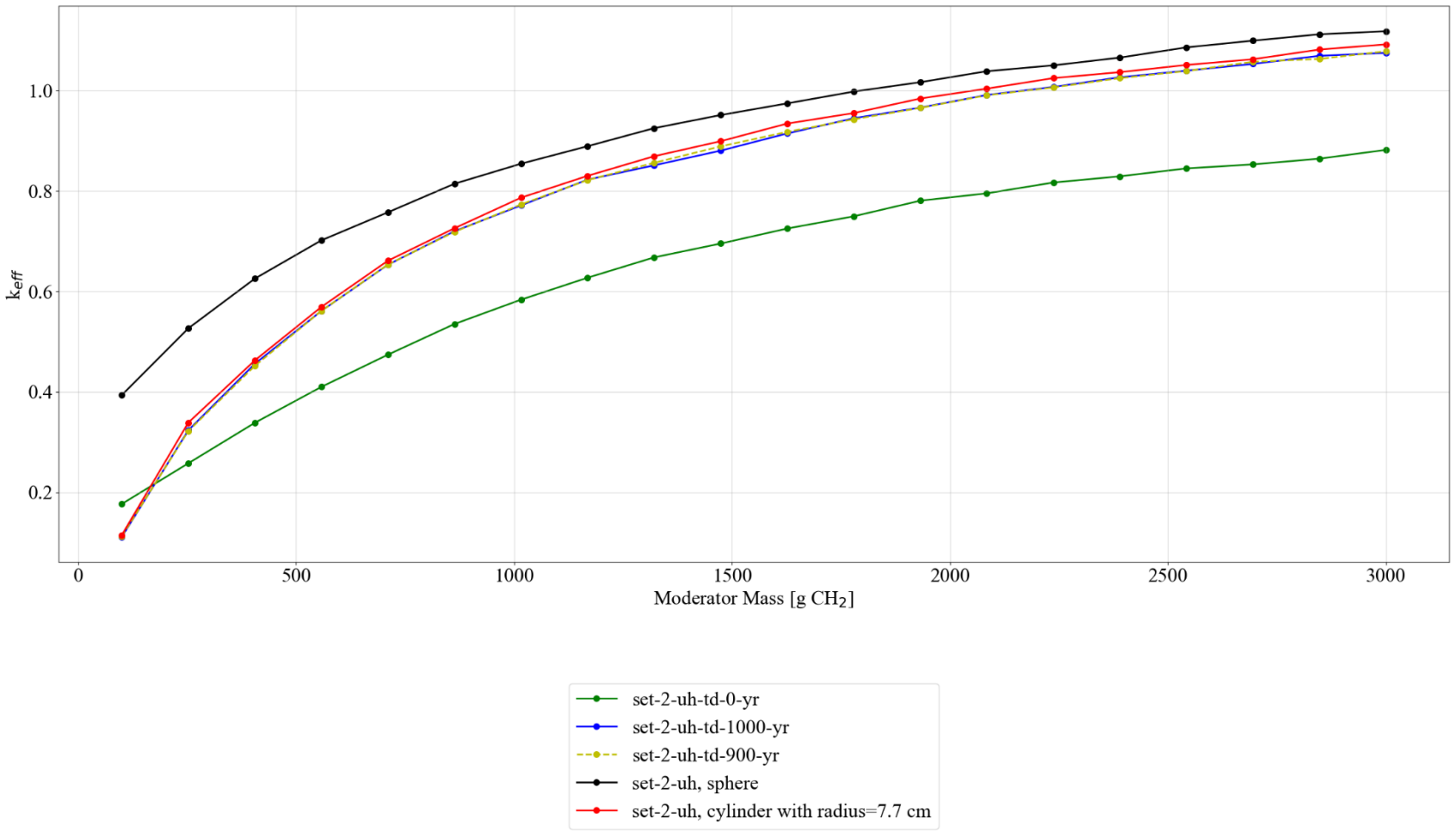

Figure E-21. Comparison of the sphere and cylinder models for various time-dependent cases for the SNL upper horizon compaction results. All cases use the set-2-4 bounding conditions (cylindrical or spherical waste forms with no filler, no can, no Be, thick poly discrete reflector, and poly moderator).

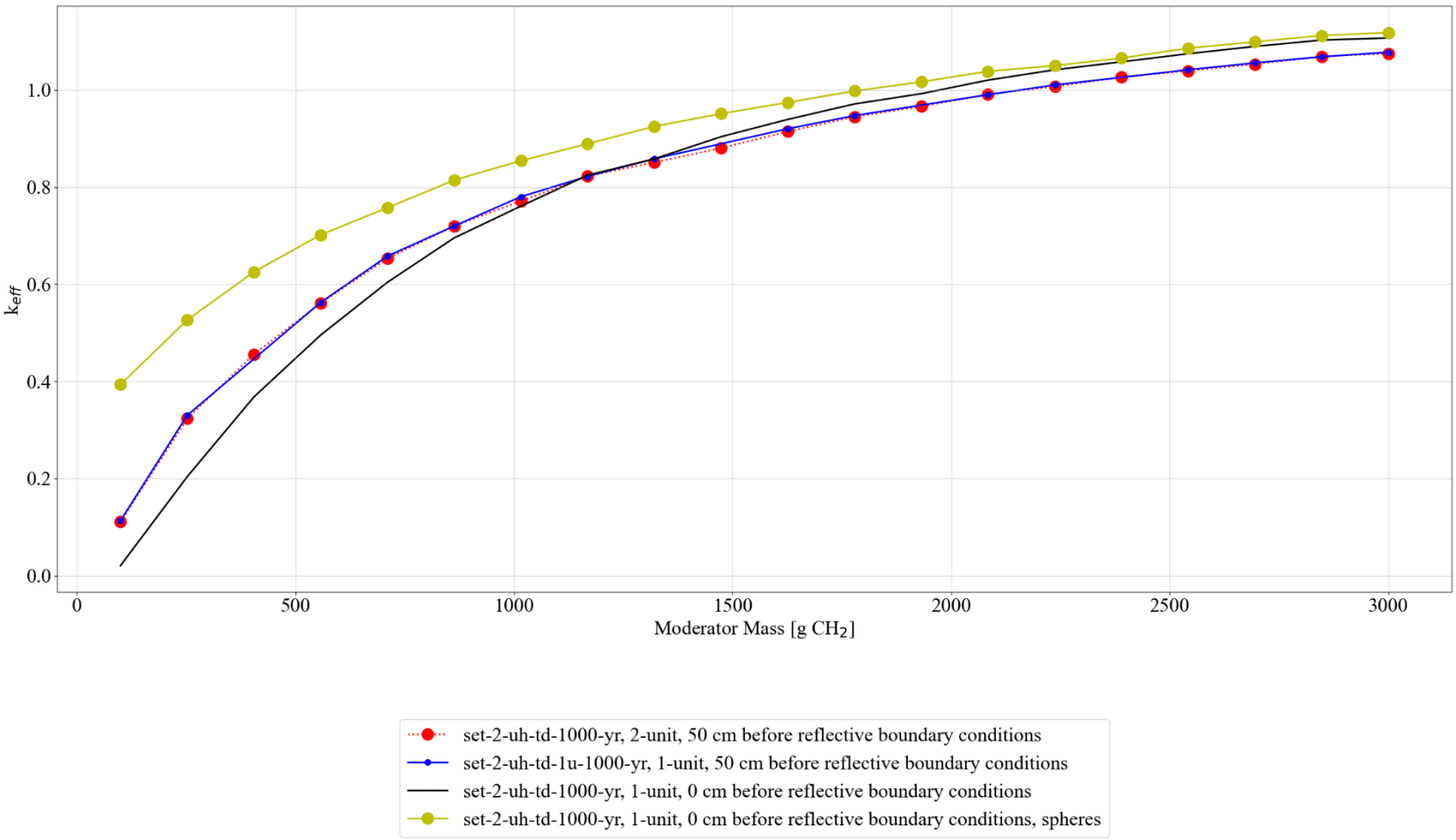

Figure E-22. Comparison of the reactivity effect of location of the reflective boundary conditions, KENO parametric block parameters for the 1- and 2-unit SCALE sphere, and cylinder models for the 1,000-year time-dependent case for the SNL upper horizon compaction results. All cases use the set-2-4 bounding conditions (cylindrical or spherical waste forms with no filler, no can, no Be, thick poly discrete reflector, and poly moderator).

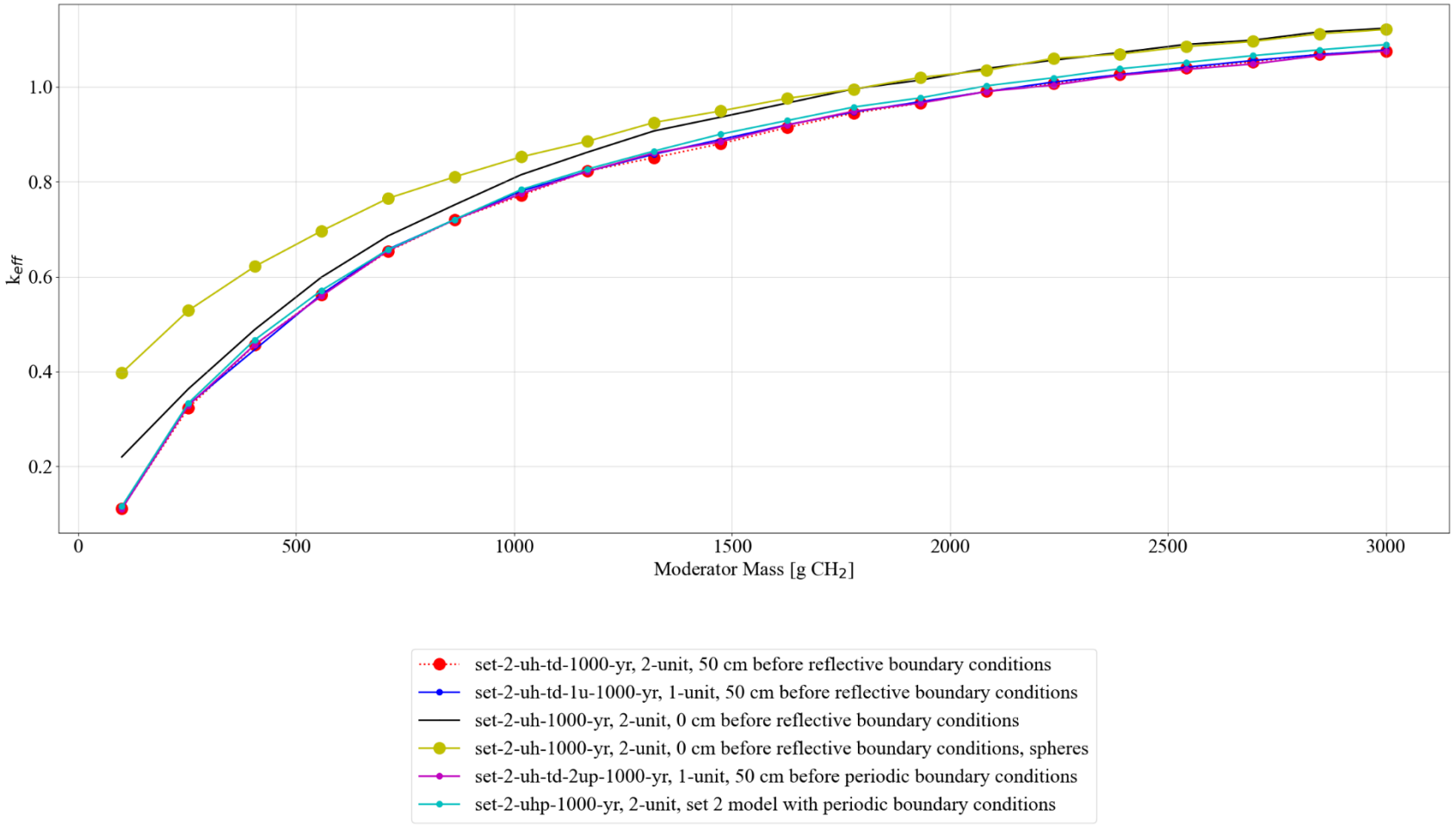

Figure E-23. Comparison of the reactivity effect of various boundary conditions for the 1- and 2-unit SCALE sphere and cylinder models for the 1,000-year time-dependent case for the SNL upper horizon compaction results. All cases use the set-2-4 bounding conditions (cylindrical or spherical waste forms with no filler, no can, no Be, thick poly discrete reflector, and poly moderator).

APPENDIX F. SET-3: RESULTS OF THE SIX-HIGH UNIFORM ARRAY WITH BOUNDING SPACING CALCULATIONS

This page is intentionally blank

APPENDIX F. SET-3: RESULTS OF THE SIX-HIGH UNIFORM ARRAY WITH BOUNDING SPACING CALCULATIONS

The analysis methodology for the uniform arrays is discussed in detail in Section 6.2 of the main report.

This appendix serves as a repository of those results for the set-1 calculations.

The complete results for all SAMPLER sweeps are provided in ADDENDUM 1.

The analysis model use for the calculations in this appendix is shown in Figure F-1 below.

The SAMPLER case sweeps presented in this appendix are summarized in Table F-1 below.

LIST OF FIGURES

LIST OF TABLES

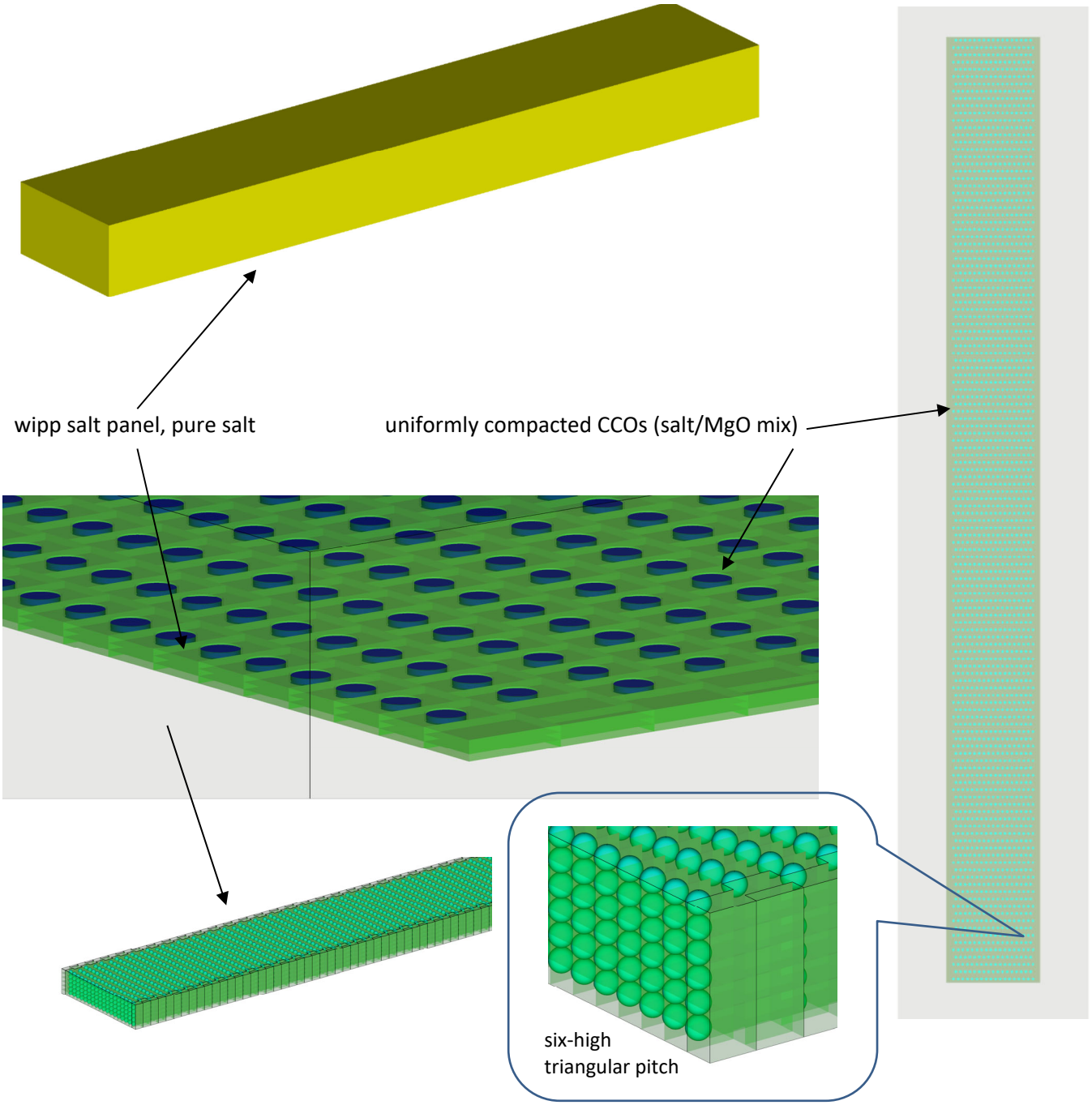

Figure F-1. Diagram of the uniform array six-high model.

Table F-1. Summary of cases for set-3

Case	Model type	Waste form shape	Waste form moderator	Filler material (0, 2,000, 4,000 g)	Metal in filler	Discrete reflector (thin 0.001 and thick 0.7112 cm)	be (g)	Subcase
Set-3	Uniform array stacked six-high with CCO pitch reduction x = 25%, y = 10%, z = no space	Cylinder (radius range 4.8, 6, 7.7 and height defined by total volume of mass)	water	c12	SS from can (0, 500, 1,000 g)	steel	0 to 585	set-3-1
			poly	c12		steel		set-3-2
			water	c12		poly		set-3-3
			poly	c12		poly		set-3-4
			water	generic		steel		set-3-5
			poly	generic		steel		set-3-6
			water	generic		poly		set-3-7
			poly	generic		poly		set-3-8
		Sphere (radius defined by total volume of mass)	water	c12		steel		set-3-9
			poly	c12		steel		set-3-10
			water	c12		poly		set-3-11
			poly	c12		poly		set-3-12
			water	generic		steel		set-3-13
			poly	generic		steel		set-3-14
			water	generic		poly		set-3-15
			poly	generic		poly		set-3-16
		Cylinder (radius range 4.8, 6, 7.7 and height defined by total volume of mass) with 25 g B_4C	poly	c12		poly		set-3-17
		Sphere (radius defined by total volume of mass) with 25 g B_4C	poly	c12		poly		set-3-18

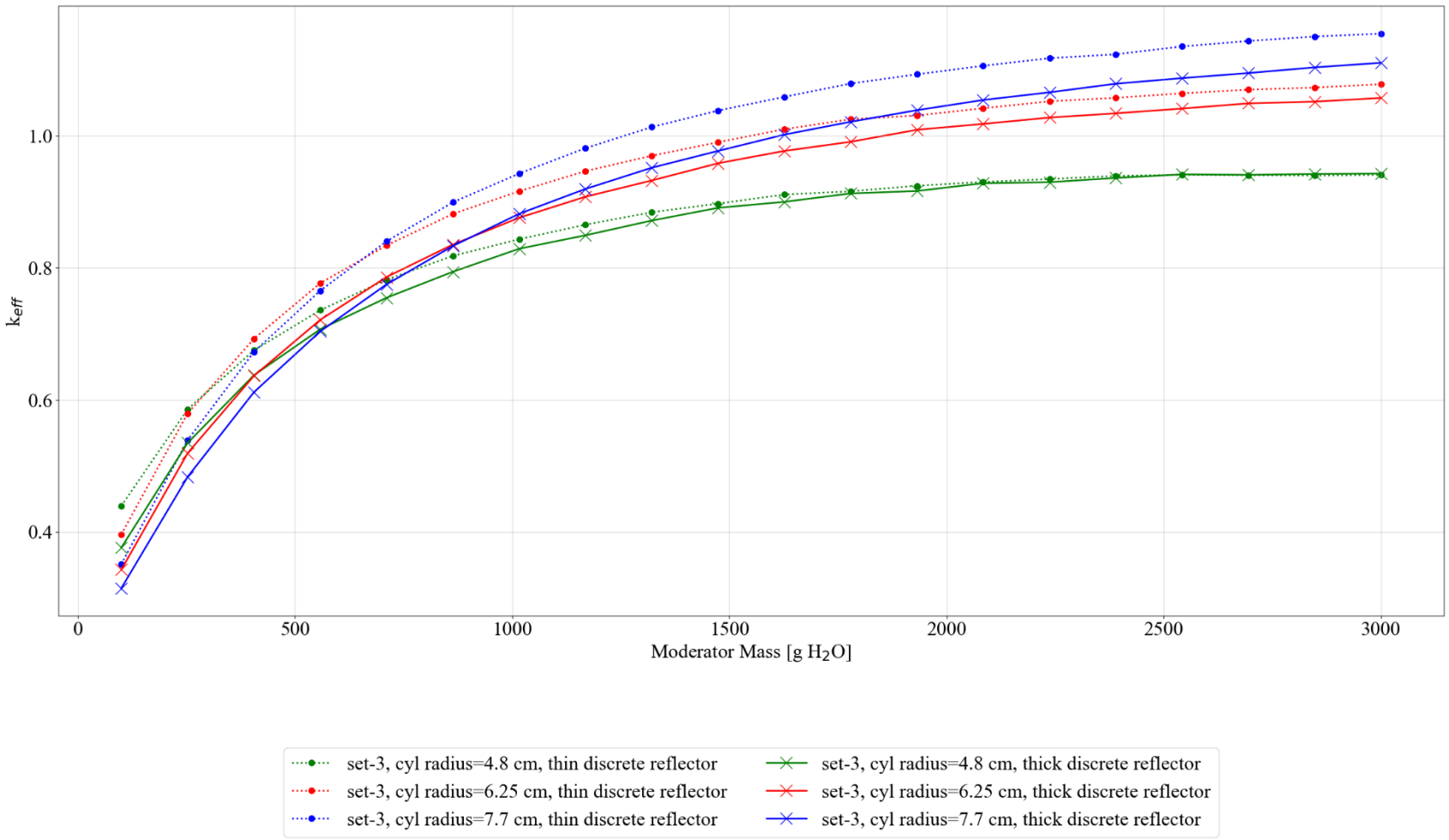

Figure F-2. Set-3 results, plot 1: reactivity effect of cylinder radius, pipe steel, no filler, no Be, water moderated.

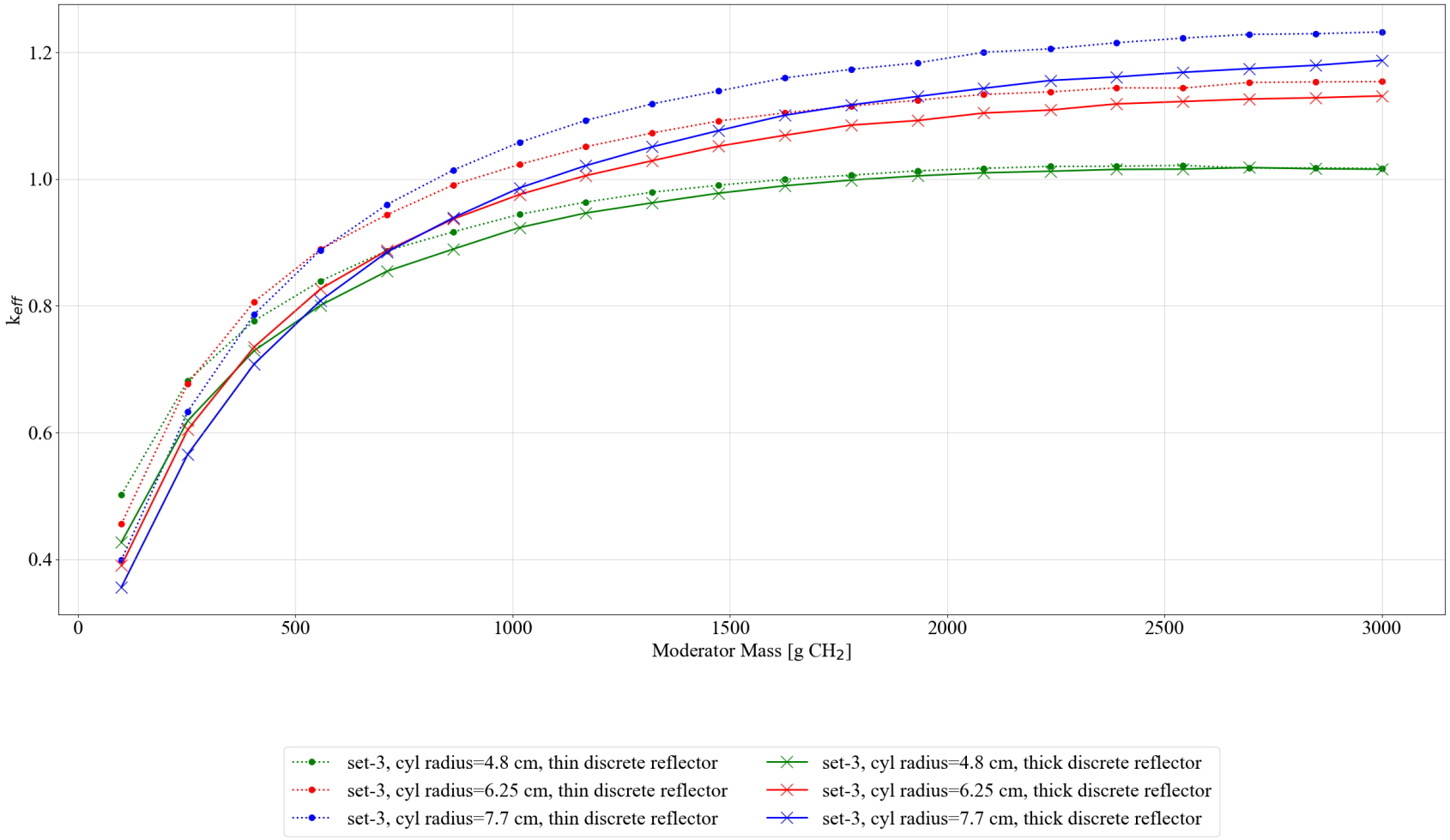

Figure F-3. Set-3 results, plot 2: reactivity effect of cylinder radius, pipe steel, no filler, no Be, poly moderated.

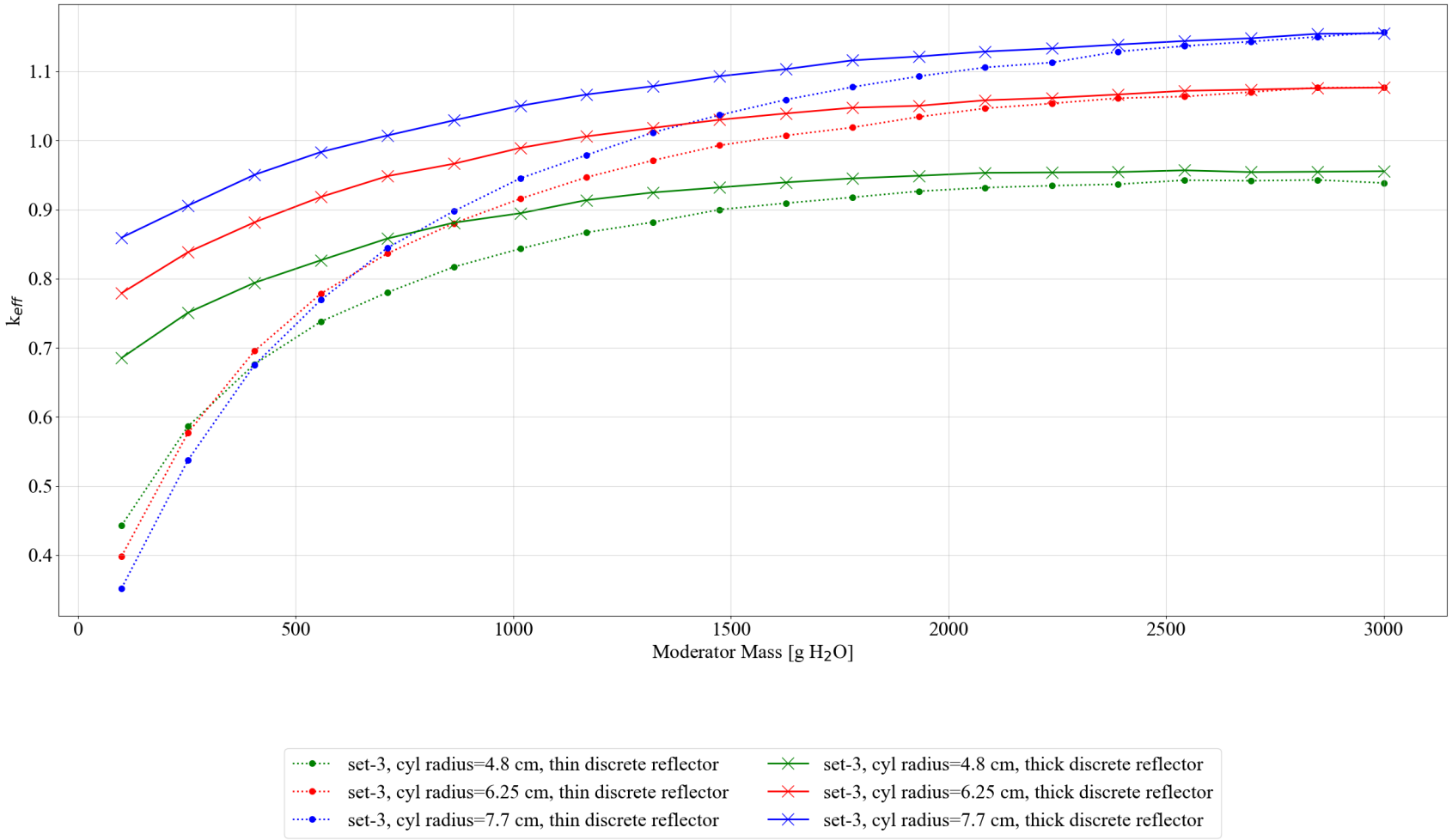

Figure F-4. Set-3 results, plot 3: reactivity effect of cylinder radius, pipe poly, no filler, no Be, water moderated.

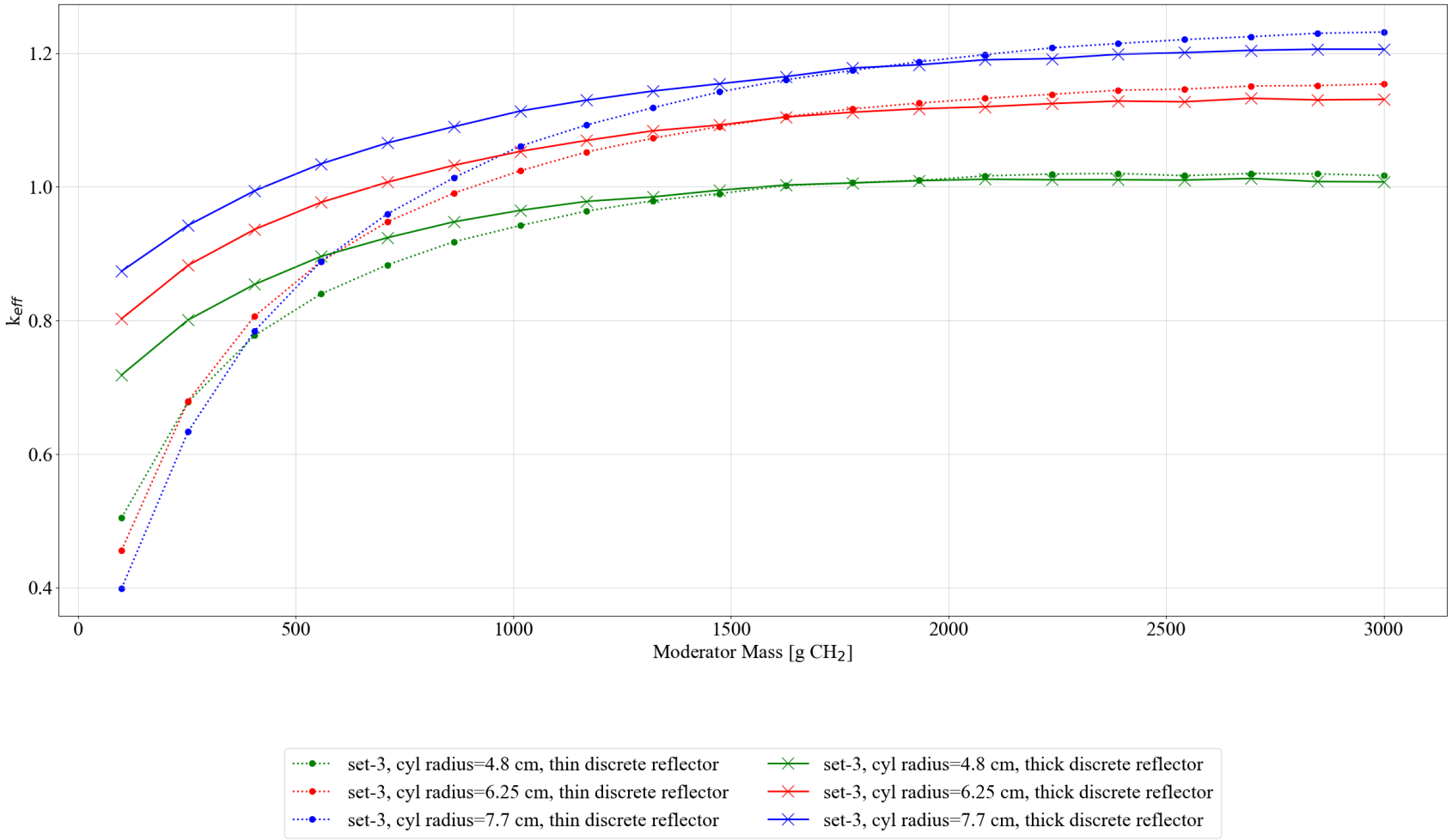

Figure F-5. Set-3 results, plot 4: reactivity effect of cylinder radius, pipe poly, no filler, no Be, poly moderated.

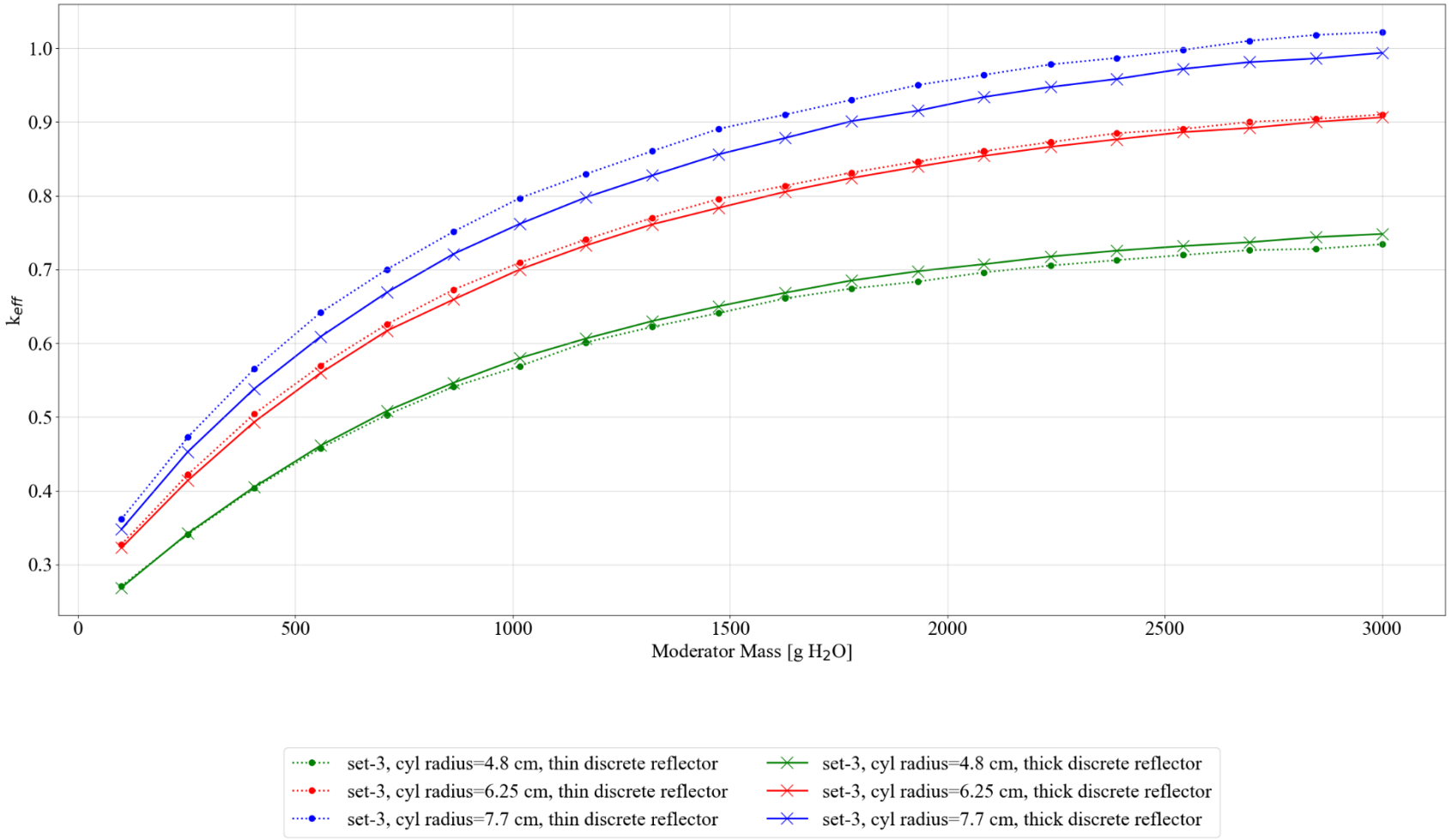

Figure F-6. Set-3 results, plot 5: reactivity effect of cylinder radius, pipe steel, 5 kg graphite/can, no Be, water moderated.

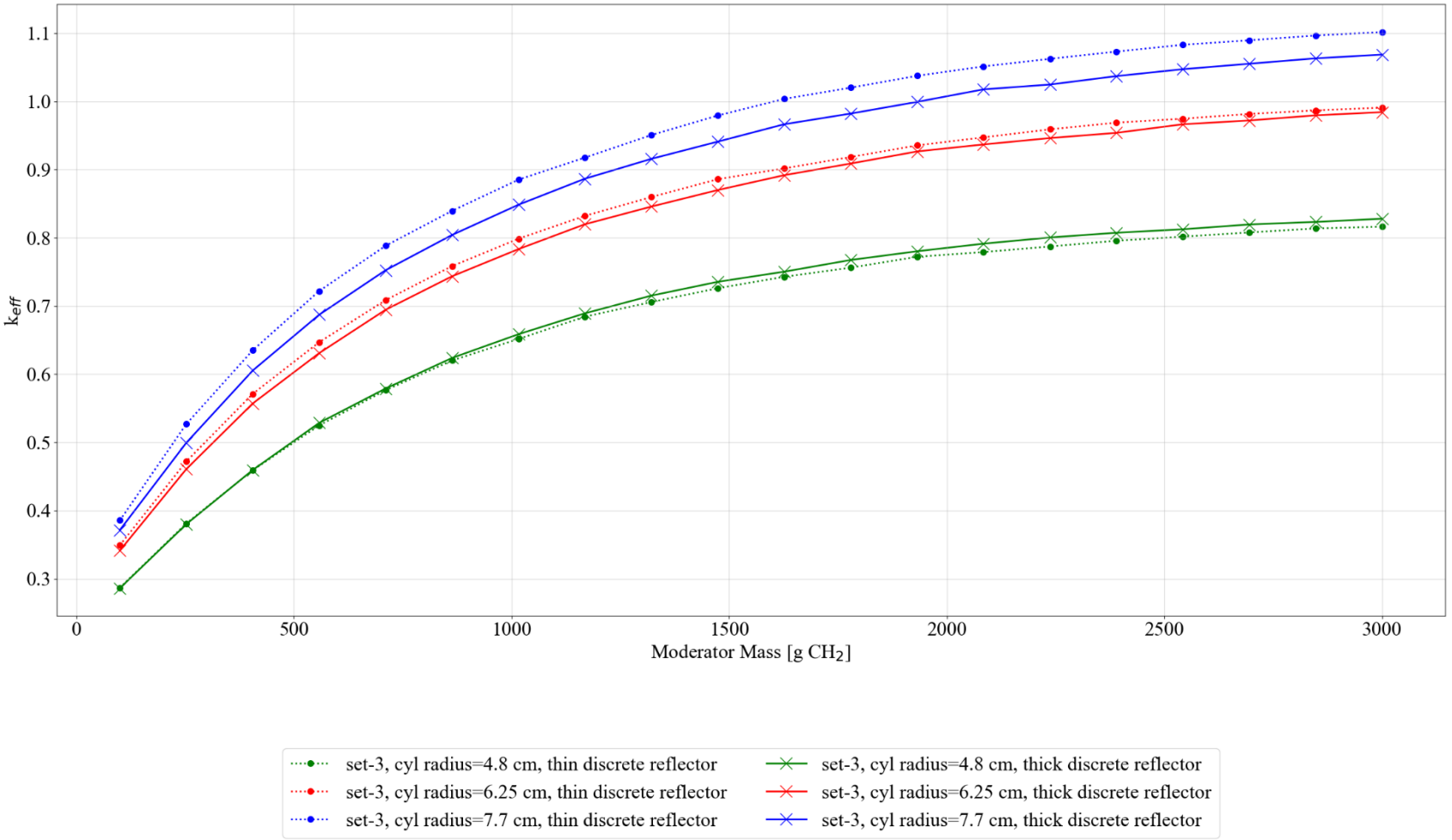

Figure F-7. Set-3 results, plot 6: reactivity effect of cylinder radius, pipe steel, 5 kg graphite/can, no Be, poly moderated.

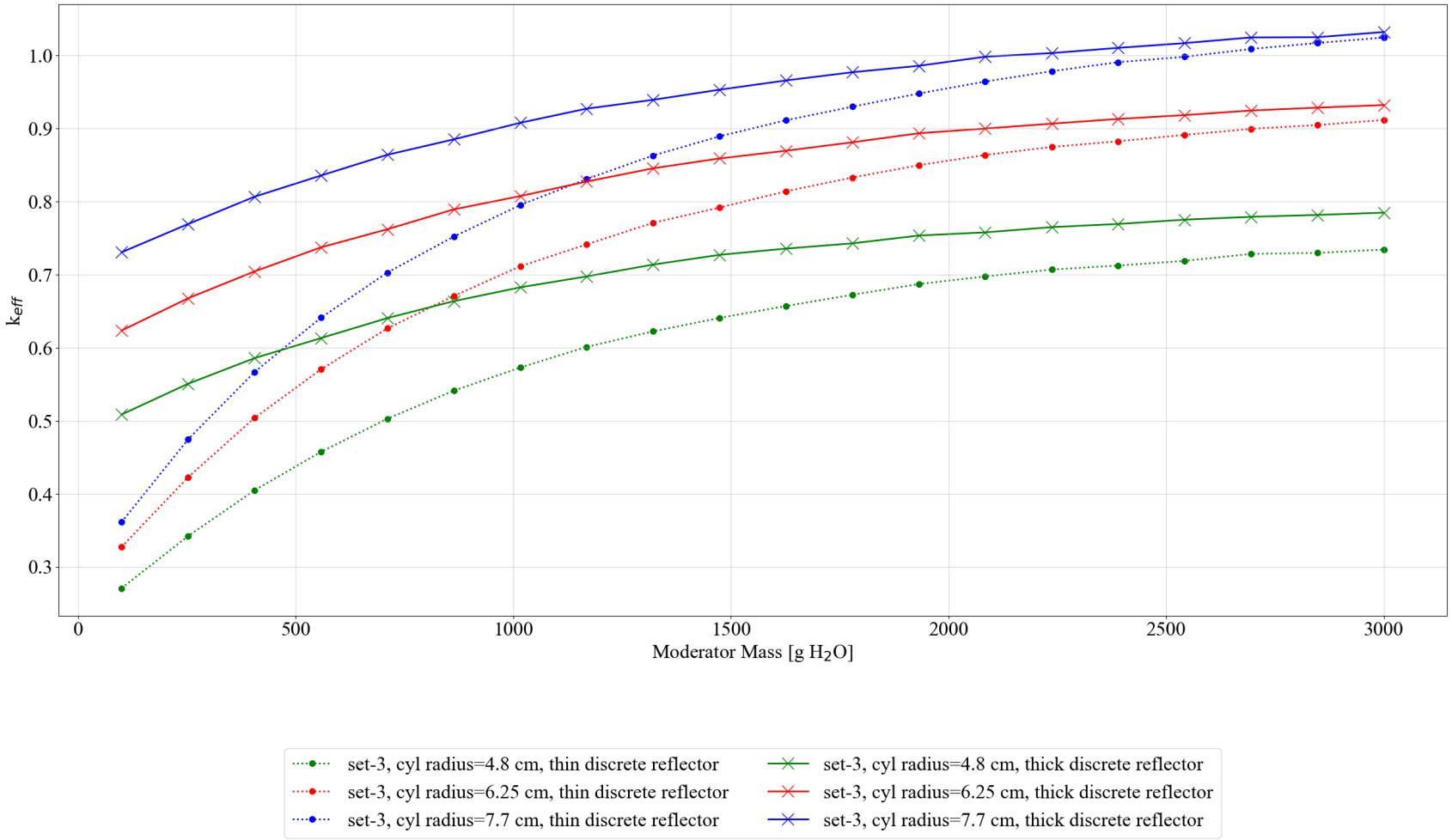

Figure F-8. Set-3 results, plot 7: reactivity effect of cylinder radius, pipe poly, 5 kg graphite/can, no Be, water moderated.

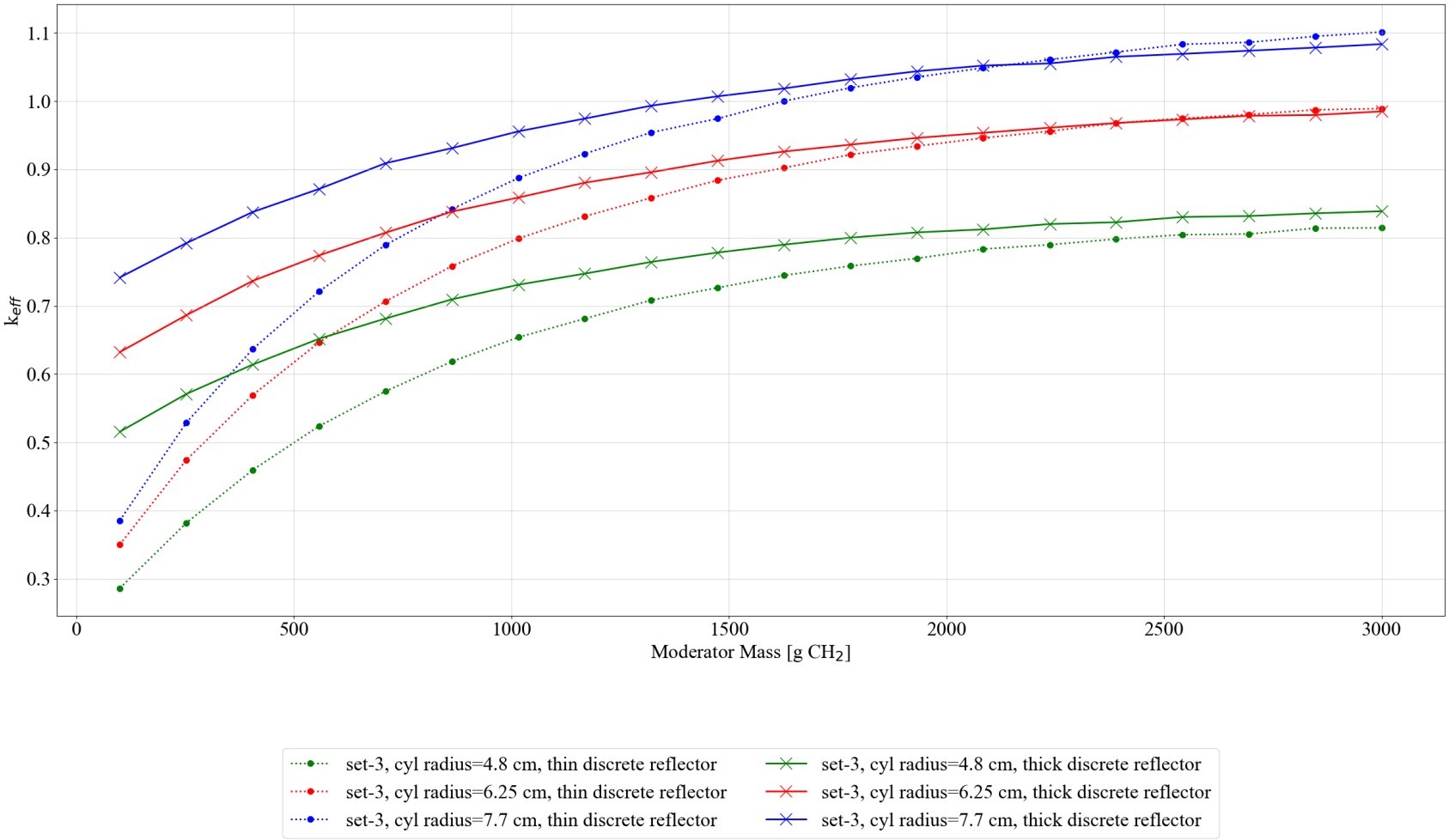

Figure F-9. Set-3 results, plot 8: reactivity effect of cylinder radius, pipe poly, 5 kg graphite/can, no Be, poly moderated.

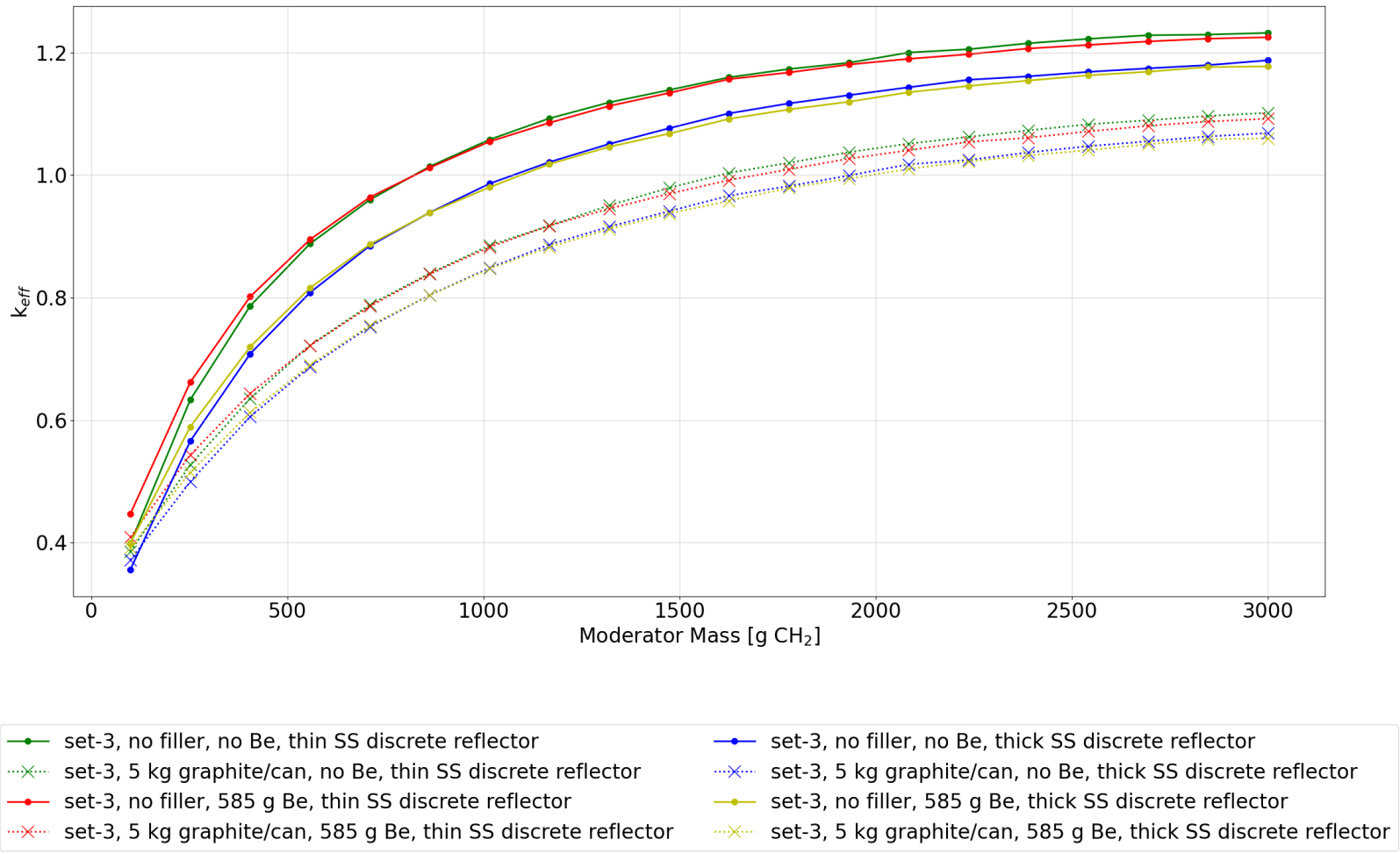

Figure F-10. Set-3 results, plot 9: reactivity effect of various parameters with 7.7 cm cylinder radius, graphite filler, poly moderated.

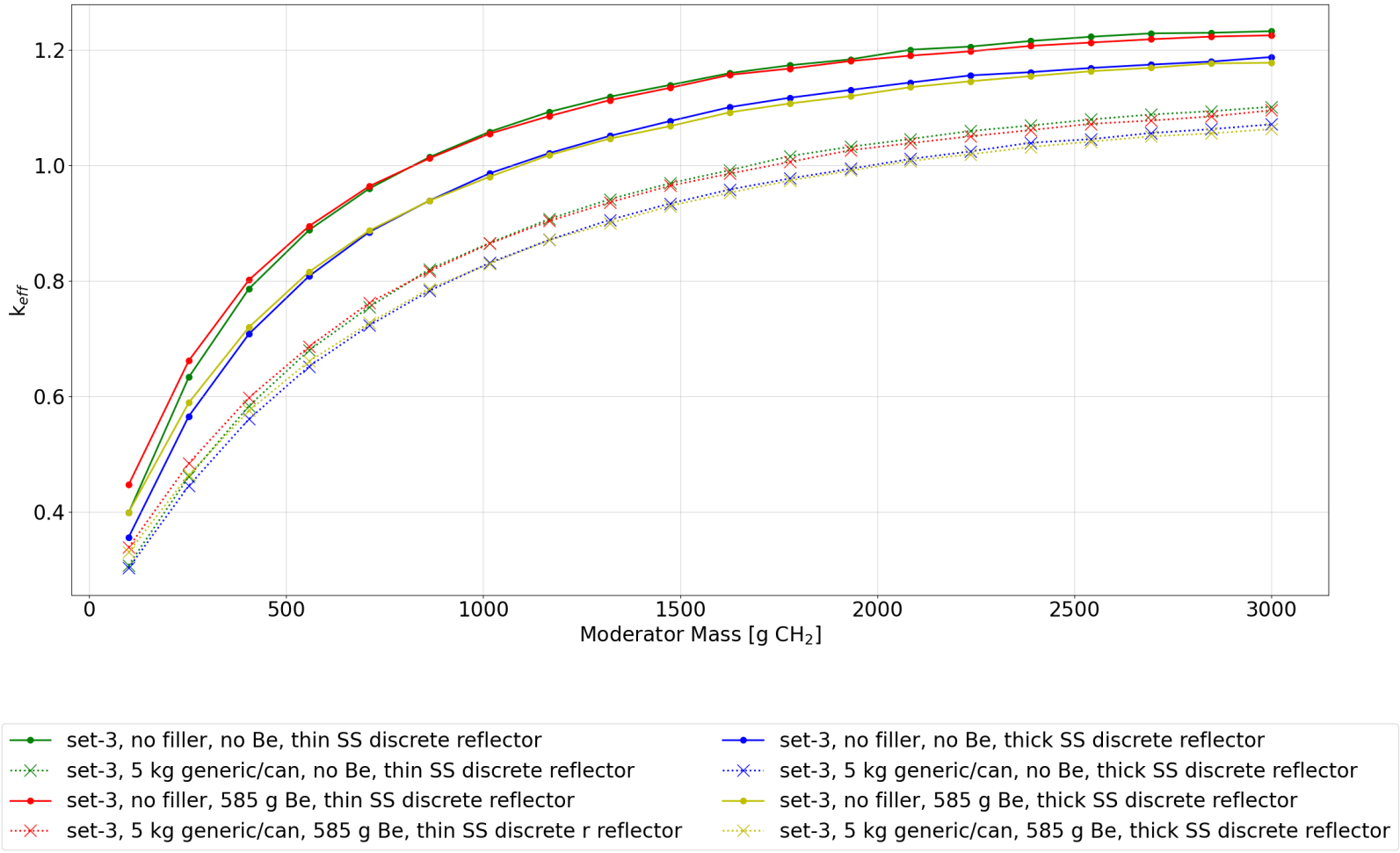

Figure F-11. Set-3 results, plot 10: reactivity effect of various parameters with 7.7 cm cylinder radius, generic filler, poly moderated.

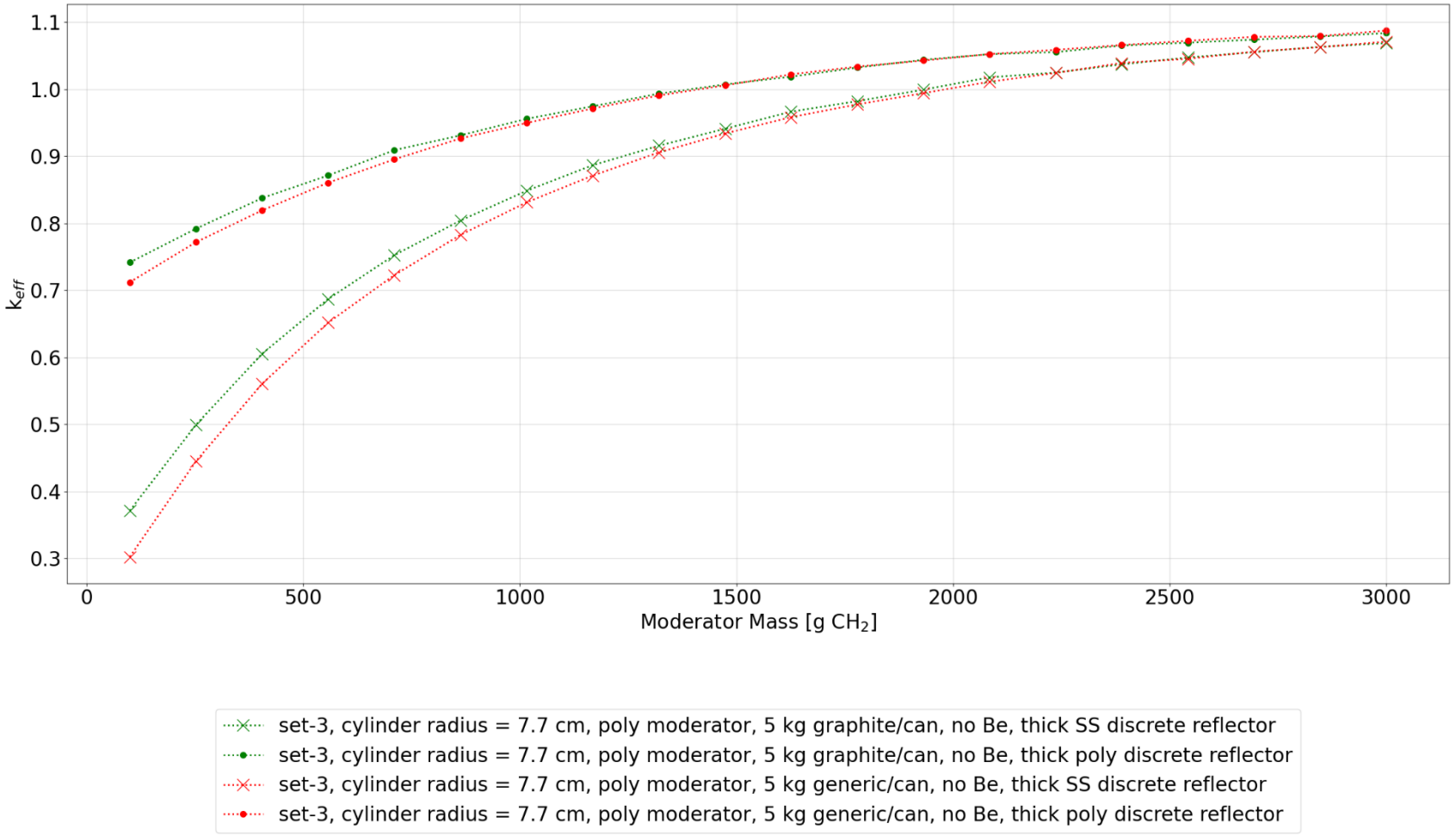

Figure F-12. Set-3 results, plot 11: comparison of graphite and generic filler with 7.7 cm cylinder radius, no Be, poly moderated, thick discrete reflector.

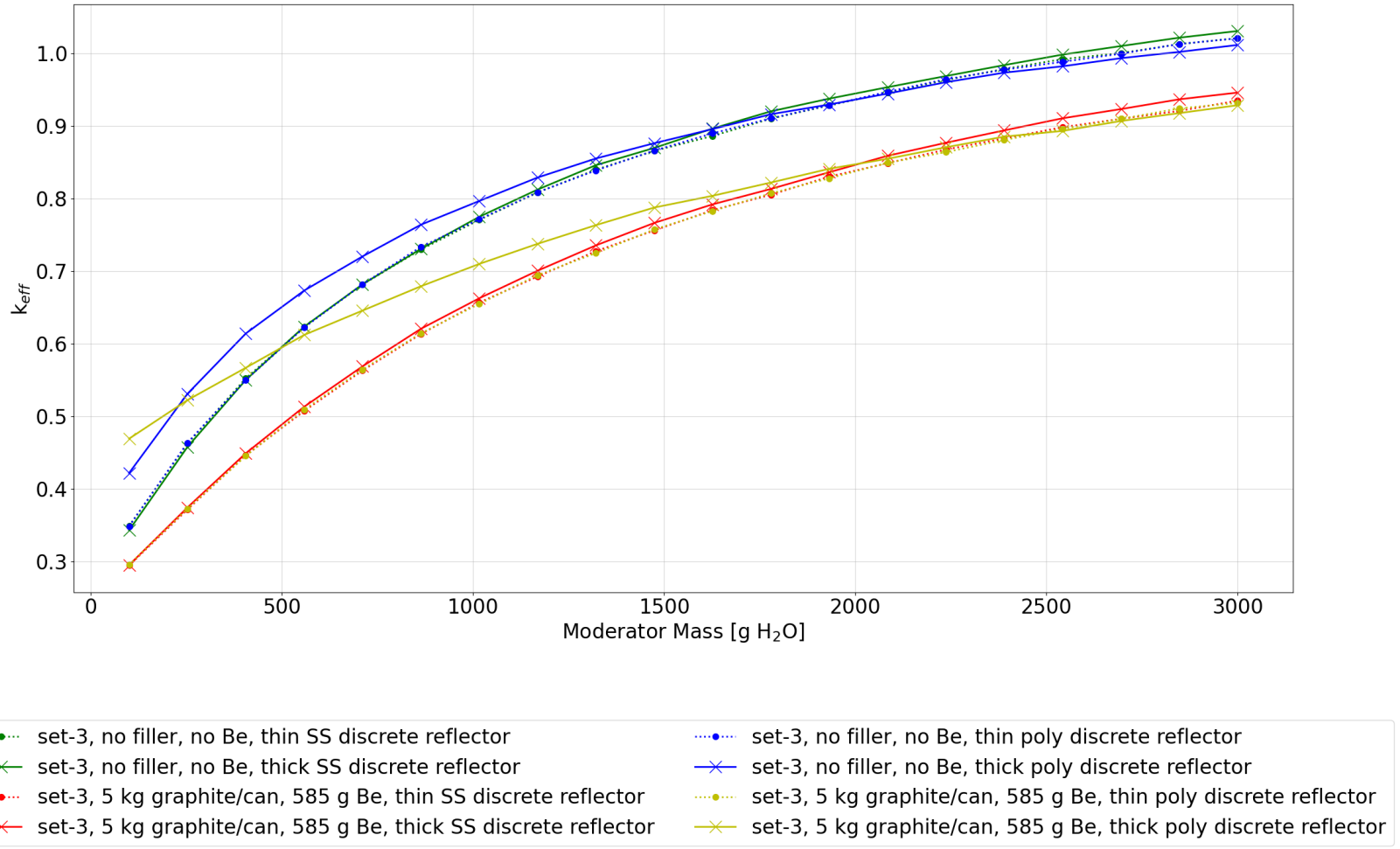

Figure F-13. Set-3 results, plot 12: reactivity effect of various parameters with spherical waste form geometry, graphite filler, water moderated.

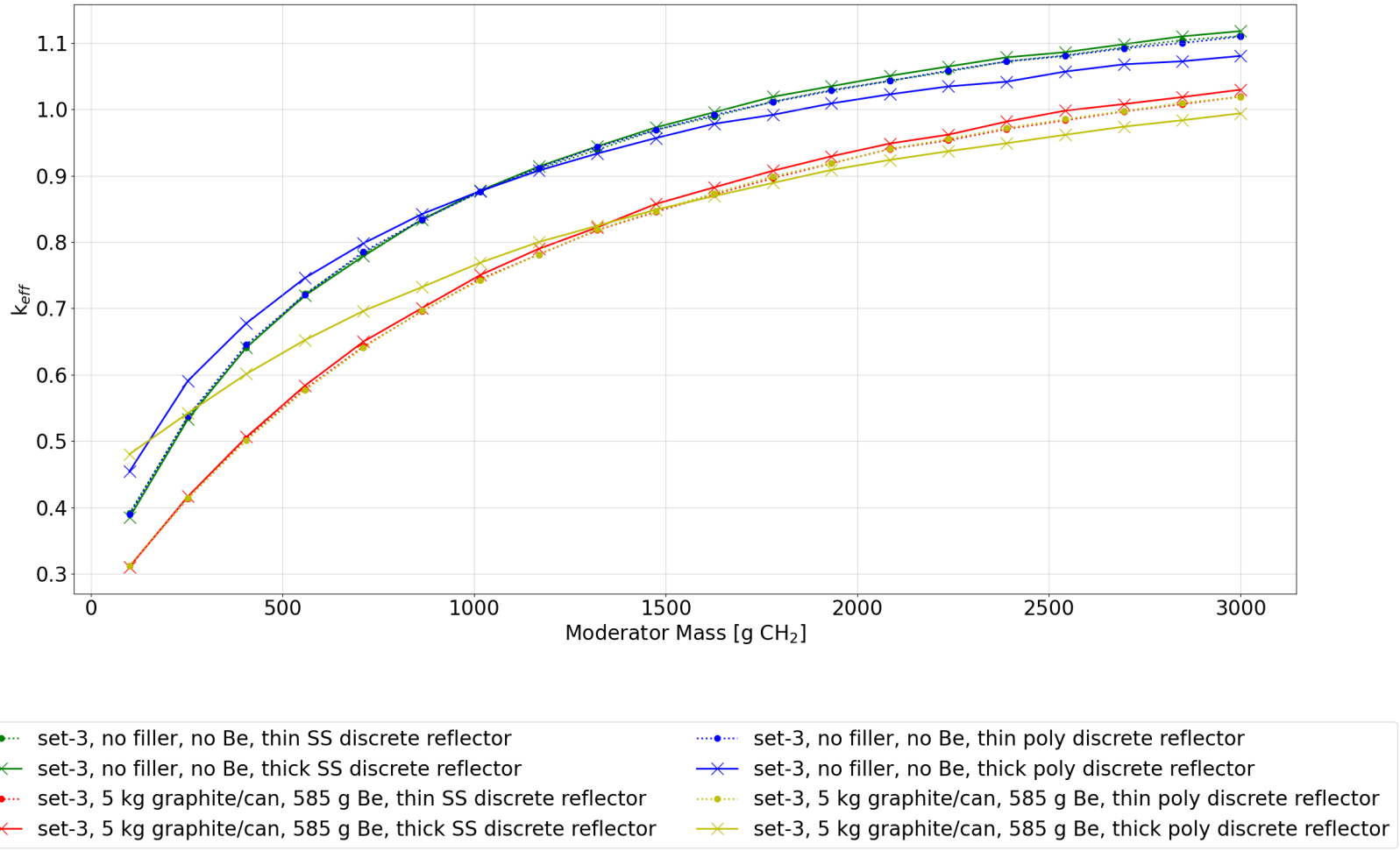

Figure F-14. Set-3 results, plot 13: reactivity effect of various parameters with spherical waste form geometry, graphite filler, poly moderated.

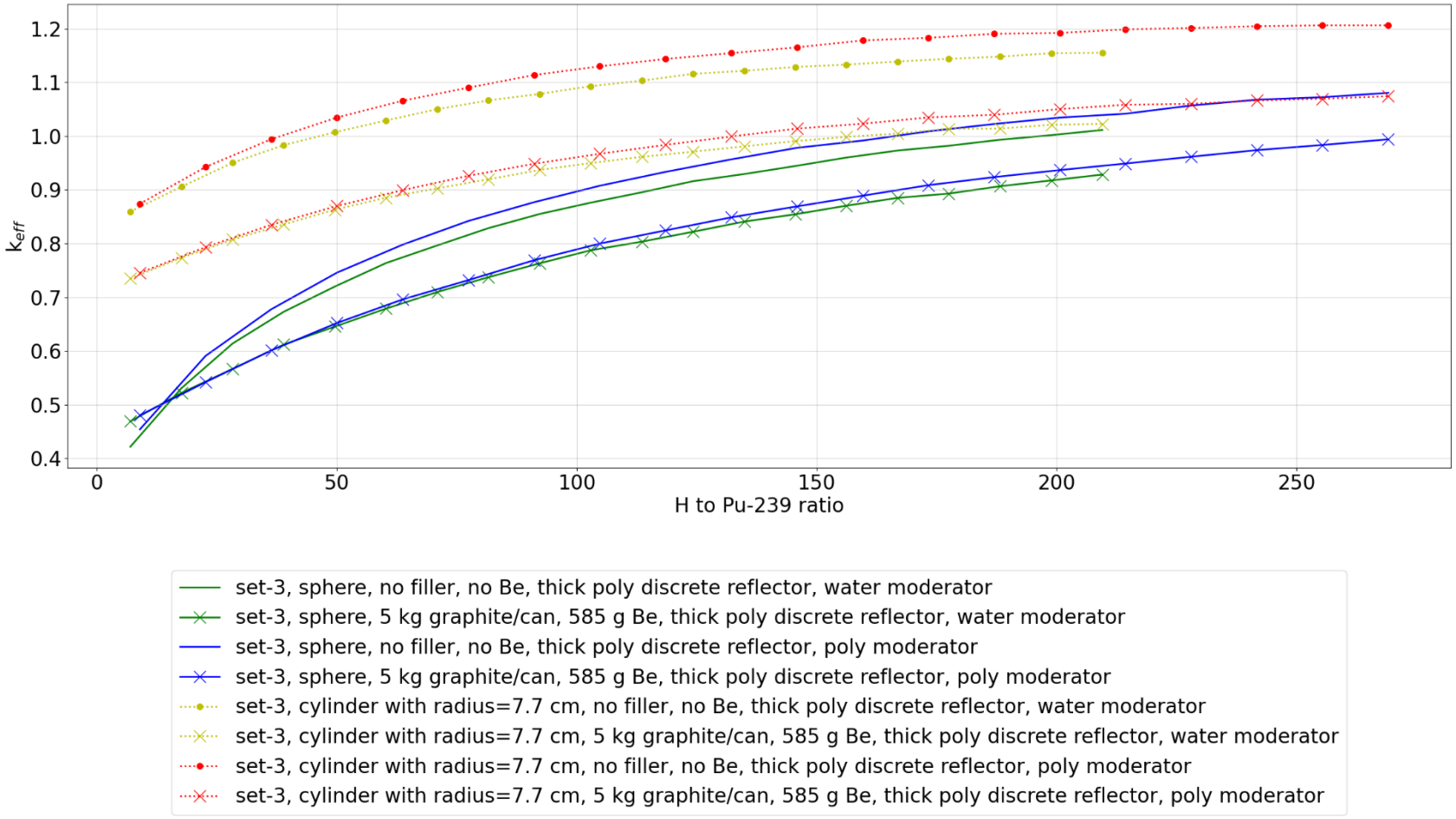

Figure F-15. Set-3 results, plot 14: comparison of spherical and cylindrical geometries (h/x).

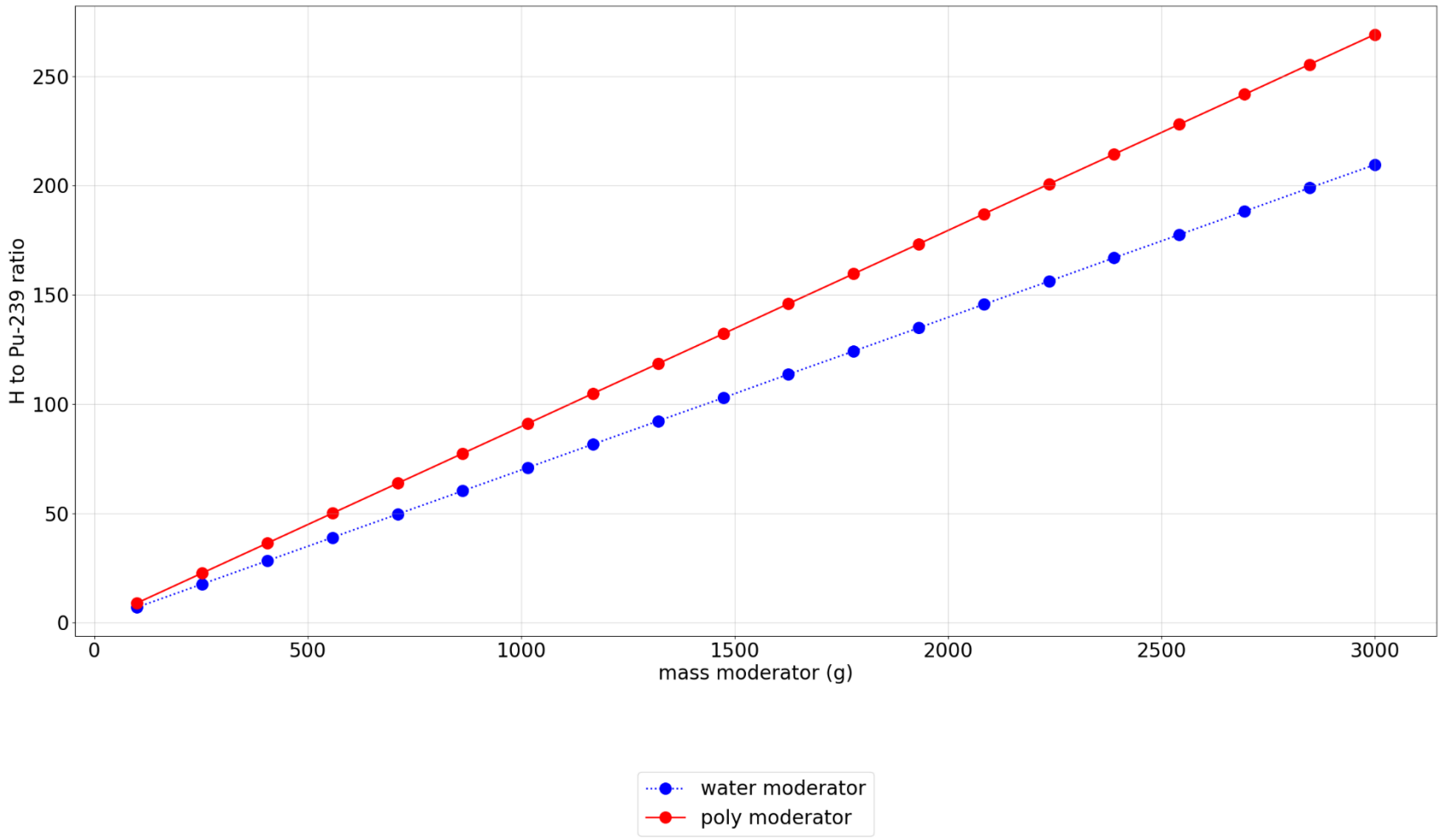

Figure F-16. Set-3 results, plot 15: comparison of water and poly h/x.

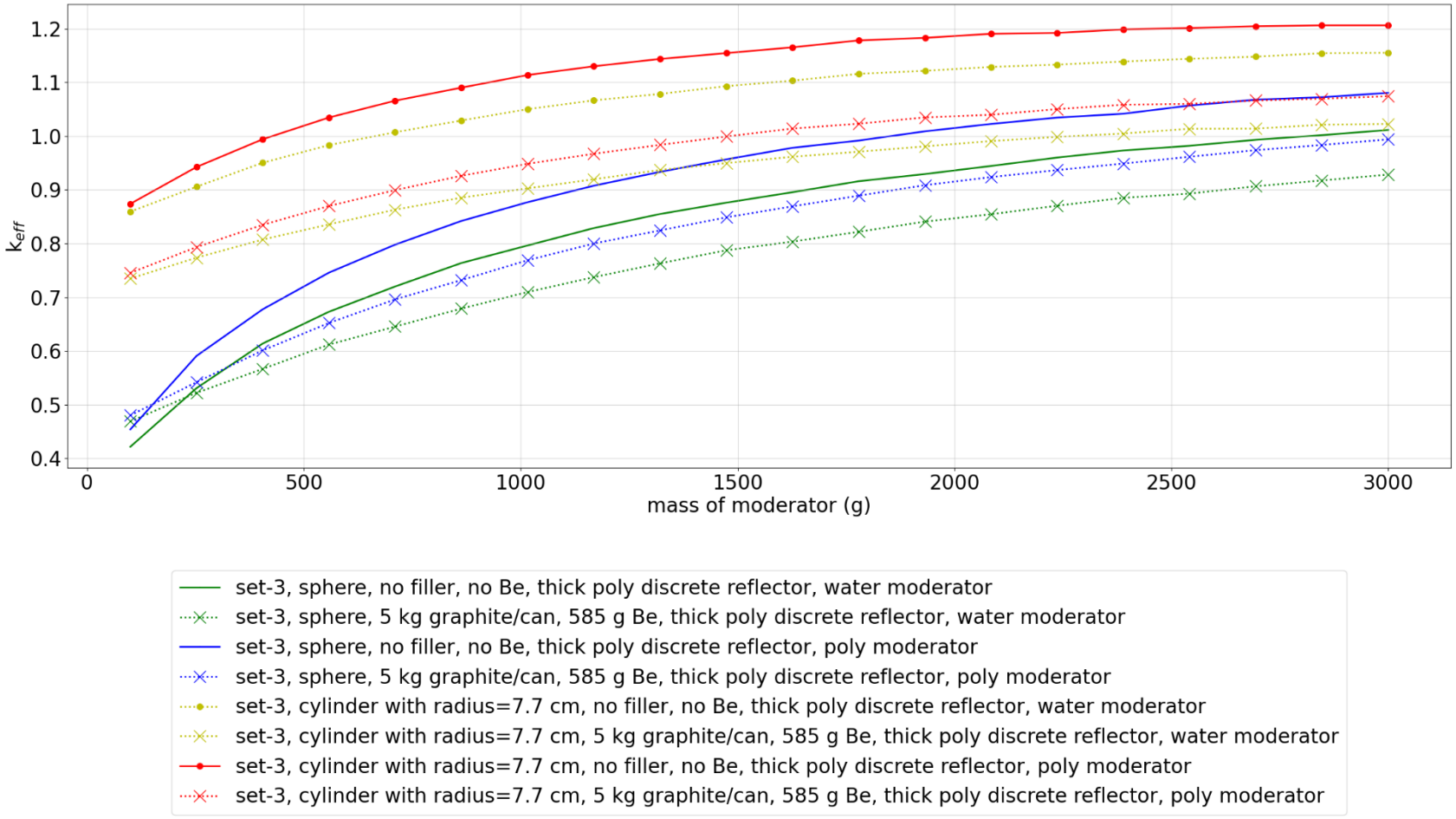

Figure F-17. Set-3 results, plot 16: comparison of spherical and cylindrical geometries (mod mass).

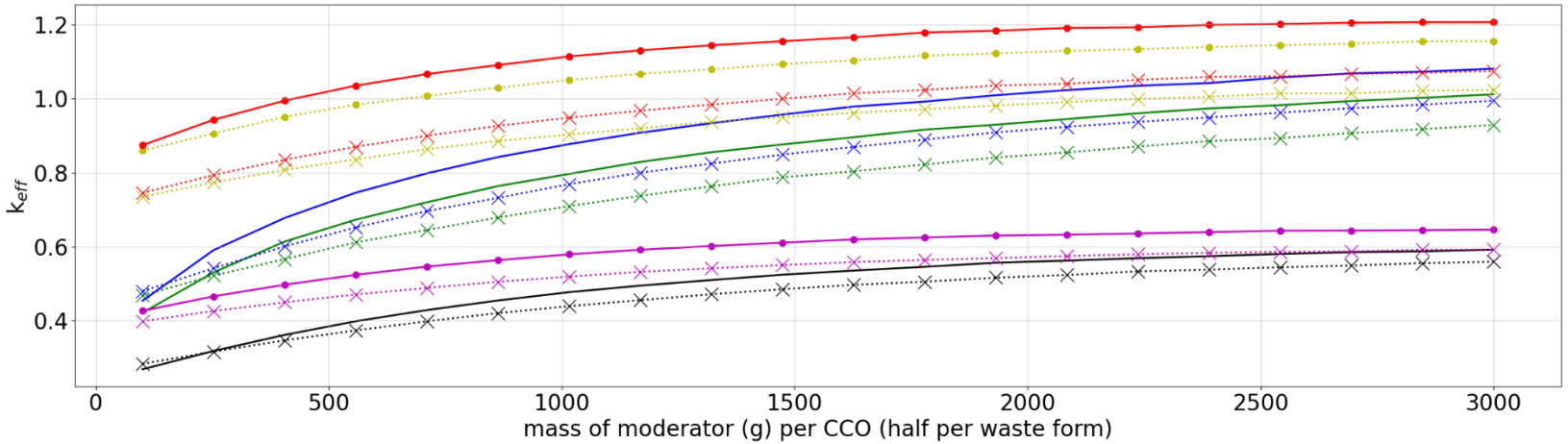

Figure F-18. Set-3 results, plot 17: Reactivity effect of 25 g B_4C per waste form (2 per CCO)

This page is intentionally blank

APPENDIX G. SET-2 UPPER HORIZON CENTROID LOCATION AND ORIENTATION STUDIES

This page is intentionally blank

APPENDIX G. SET-2 UPPER HORIZON CENTROID LOCATION AND ORIENTATION STUDIES

The analysis methodology for the nonuniform array studies is discussed in detail in Section 6.2 and Section 6.4 of the main report.

This appendix serves as a repository of the results for the centroid location and orientation study calculations.

The analysis model used for the calculations in this appendix is shown in Figure G-1 below. Additional discussions are provided in Section 6.4 of the main report.

The SAMPLER case sweeps presented in this appendix limited to those which have the same parameters as set-2-4 and with no filler material.

Results are presented in the following figures:

LIST OF FIGURES

The analysis methodology for the nonuniform arrays, which are models that utilize the Reedlunn and Bean [7] data exclusively, was previously based on the work performed for the POCs by Brickner [4]. That previous work used the centroid positions provided by the SNL compaction studies by Reedlunn and Bean [7] to locate the waste forms in the model. Spheres and cylinders were used to geometrically represent the waste forms with ideal shapes. Both shapes were placed into the model based on the 153 individual pipe coordinate data. For the spheres, the coordinates defined the center point of the sphere. For the cylinders, the coordinates defined the center of a vertically oriented cylinder's base. These coordinate points for each pipe are termed *centroids*.

The results of the SNL compaction studies provide 153 pipe centerlines. A visualization of these pipe centerlines is shown in the figure below.

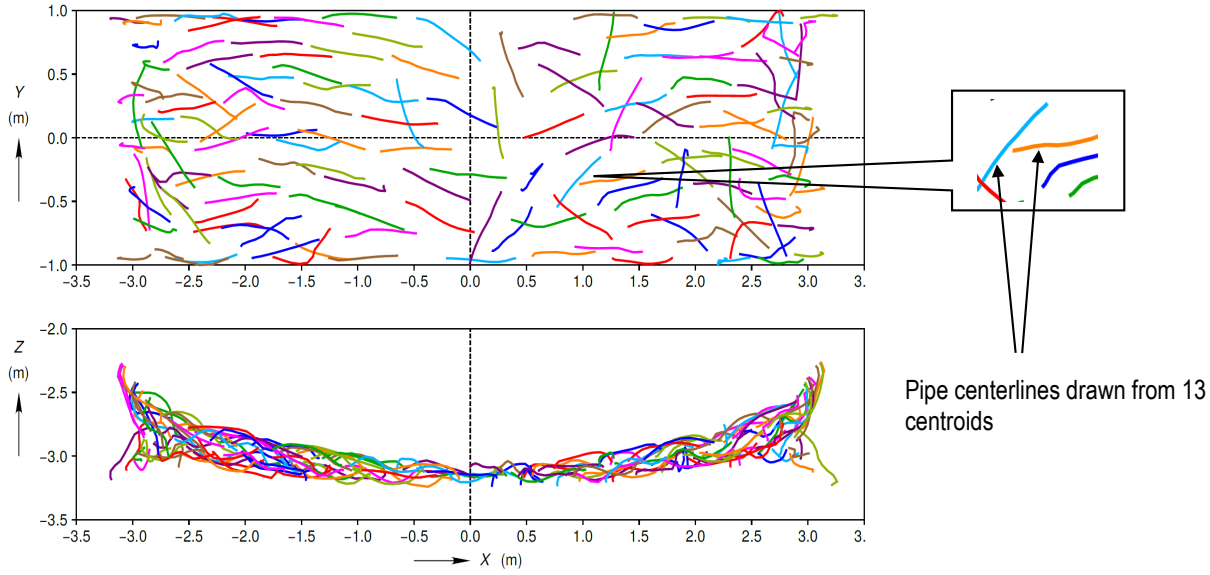

Figure G-1. Representation of the compacted CCO pipe centerline "spaghetti model" drawn from 13 centroids per pipe centerline from [28] with permission. Note that this is not an actual analysis model; it was generated from the centroid dataset.

Each of the 153 pipe centerlines is constructed from 13 points, or centroids, spaced evenly along the compacted pipe centerline. Visualizations of these centroids are shown in the figure below.

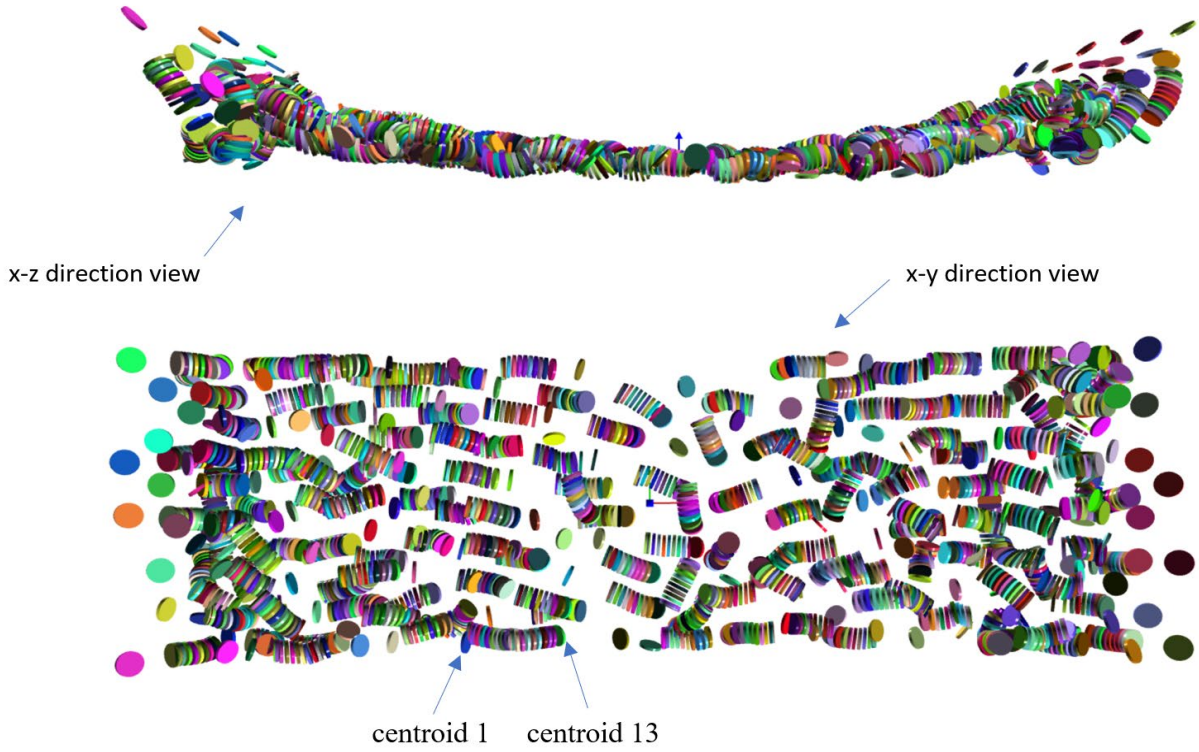

Figure G-2. Example of centroid locations within compacted pipes. This 3D representation of the compacted pipe centerline and centroid locations uses disks to show the locations of individual centroids. Note that this is not an actual analysis model but rather it is a python-generated representation of the centroid dataset.

One important assumption inherent to the previous analysis—as well as the calculations presented in this analysis for the set-2 upper horizon and lower horizon compaction results in APPENDIX C and APPENDIX D—is related to which of the 13 centroids along the compacted pipe centerlines is used to place the waste forms in the model relative to each other. For the calculations in APPENDIX C and APPENDIX D, a point close to the center centroid was used. Furthermore, the centroid was used to center the base of the upright cylinders, as shown in the figure below.

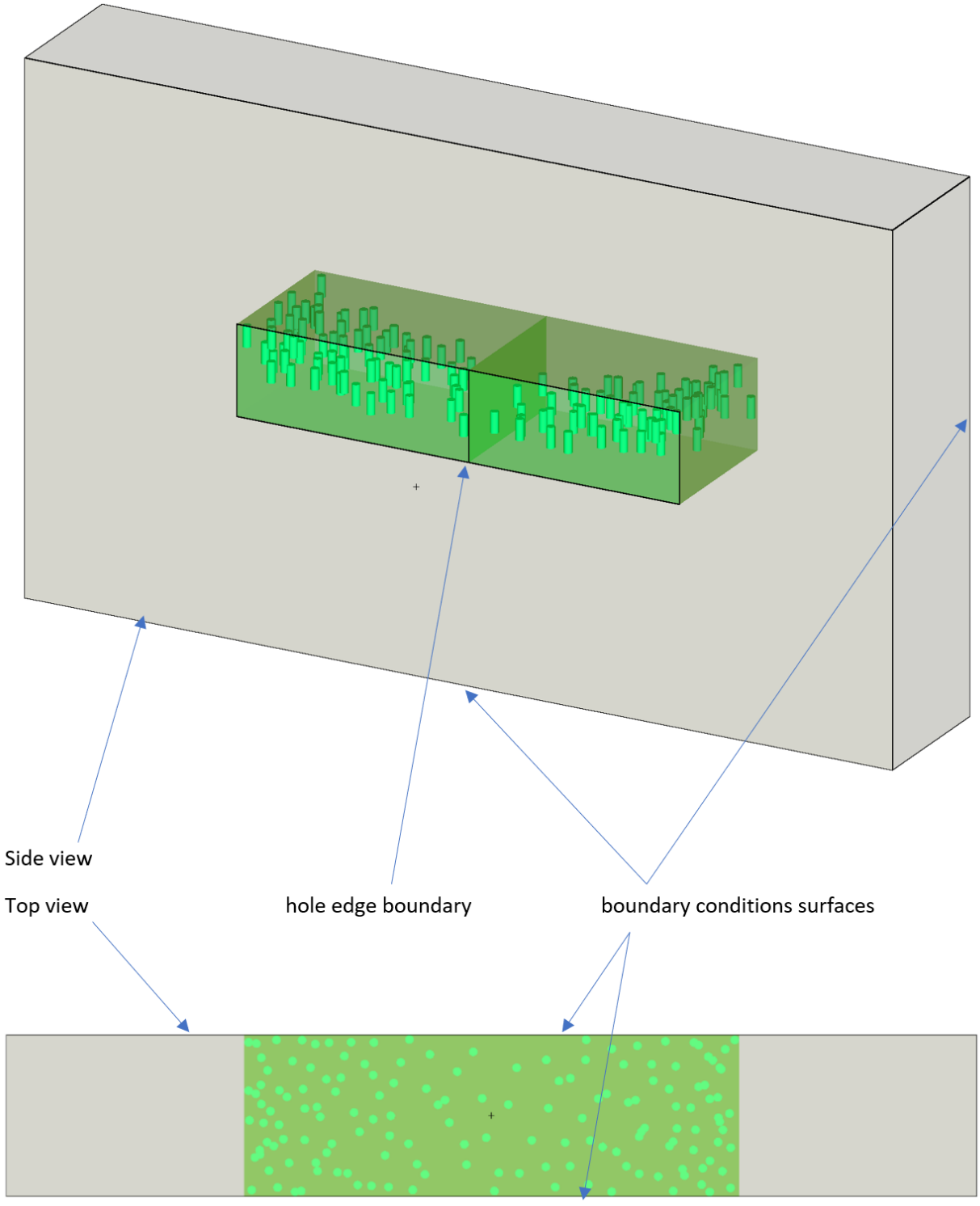

Figure G-3. 3D representation of the Appendix C and Appendix D 2-unit analysis model illustrating how pipe center centroid data were used to orient vertical cylinders.

In the figure above, the model's reflective boundary conditions are conservatively placed just adjacent to the outmost edge of the waste forms along both boundaries. This assumption regarding the placement of the reflective boundary conditions is discussed further in APPENDIX E.

For the purpose of the studies presented in this appendix, many of which will change the orientation of the cylinders in the model, there will be instances in which this change in orientation will result in the cylinder extending far past the reflective boundary plane, thus causing the reflective boundary conditions to be farther away from the waste form than shown in this example. Rather than change the location of the reflective boundary condition for each sweep, it is more appropriate to move the reflective boundary condition to a fixed point for all cases so that the reactivity effect of the changes in orientation can be evaluated with like-for-like comparisons. Therefore, for all cases, the outermost centroid's coordinates are used to define the boundaries of the interstitial filler material (MgO+salt), and an additional 50 cm is applied so that all cases have a more uniform application of reflection. For these models, the 50 cm of reflector material was applied in all directions. The impact of this is expressly evaluated in APPENDIX E.

All cases in this appendix use similar models, and they also use the same set of conditions associated with set-2-4 for the upper horizon calculations presented in APPENDIX C. Specifically, these cases are for sweeps with poly moderator, graphite filler, and poly pipe material with cylinders.

It is possible that an alternate orientation configuration may yield a significant reactivity increase that could invalidate the conclusion that set-1 results are bounding of all nonuniform array results. Furthermore, these calculations provide a methodology to conclude that under the CCO emplacement strategy used at WIPP, an insufficient amount of fissile material can be expected to collect in a given area of the room, thus significantly increasing the risk of criticality.

The specific nomenclature used for the studies in this appendix is provided below:

- **centroid**: location of a point defined by (x,y,z) coordinates from SNL compaction studies.

Each pipe in the dataset of 153 compacted pipes contains 13 centroids defined by their (x,y,z) position along the pipe centerline.

- **base case**: the centroid defines the center of the cylinder base. The term *base* is not included in the case nomenclature, but in the absence of other case designations, it is considered consistent with the Appendix C and Appendix D calculations.
- **shifted**: the centroid defines the geometric center of the cylinder rather than the center of the bottom face.
- **midpoint**: the (x,y,z) position calculated at the center of the vector between the endpoints (not a specific SNL-defined centroid, but calculated from the SNL data).
- **orientation**: direction of the cylinder relative to the x-y plane. Following are specific orientation terms:

base case orientation is with the orientation in the vertical direction, and is a term which is not specifically used but is considered consistent with the Appendix C and Appendix D calculations.
local orientation is determined by calculating the angles from a vector between two adjacent points (adjacent to the centroid). For endpoints (centroids at either end of the pipe), it is calculated from the endpoint to the adjacent centroid. For non-endpoints, it is calculated from the centroids adjacent to either side. For example, the local orientation for centroid 5 is calculated using a vector between centroids 4 and 6.
global orientation is taken from the vector between the two endpoints.
rA is the random orientation taken by a python generated random angle pair (-180 < = phi < = 180 , 0< = theta< = 180) for the two SCALE variables which control orientation.
relLocal is the local orientation provided for rcoord cases.

Three sets of evaluations are performed, each having multiple subsets. These are *centroid studies*, *rcoord studies* and *rA* studies. These are explained below.

The centroid studies evaluate the effect of using each of the 13 SNL centroids independently, along with a midpoint. For these cases, each pipe in the model uses the same centroid for that case. For example, if the case is centroid1, then each pipe in the model uses the centroid 1 coordinates.

The rcoord studies sets evaluate the effect of randomly selecting which of the 13 centroid coordinates is used. Each pipe in the model has its own unique random selection. For these studies, 100 rcoord cases are generated.

The following six subsets of calculations are evaluated for each of the centroid and rcoord sets:

- **base case with no orientation of the cylinder**: the centroid is at the center of the cylinder base.
- **base-with-local-orientation case**: a local orientation is applied as determined specifically for each pipe based on the relative local centroid vectors, with the centroid at the center of the cylinder base.
- **base-with-global-orientation case**: a global orientation is applied as determined specifically for each pipe based on the pipe endpoint centroid vectors, with the centroid at the center of the cylinder base.
- **shifted case**: no orientation of the cylinder, with the centroid at the geometric center of the cylinder.
- **shifted-with-local-orientation case**: a local orientation is applied as determined specifically for each pipe based on the relative local centroid vectors, with the centroid at the geometric center of the cylinder.
- **shifted-with-global-orientation case**: a global orientation is applied as determined specifically for each pipe based on the pipe endpoint centroid vectors, with the centroid at geometric center of the cylinder.

The rA studies sets evaluate the effect of randomly selecting both phi and theta for the orientation of the cylinders. Each of the pipes in the model has its own unique random phi and theta selection. For these studies, 20 random phi and theta cases were generated for each of 13 centroids plus the midpoint. rA studies were performed in conjunction with rcoord cases, considering a set of 10 rcoord cases with 10 rA sets each.

The following illustration provides additional clarity for how the cylinder orientations were evaluated. For each pipe in the model, a pipe centerline was defined by the 13 centroids. For example, a local orientation or a global orientation was determined by a vector between either two centroids adjacent to the pipe or at the ends of the pipe, respectively. This is illustrated by the straight lines in the figure below. The cylinder's orientation is shown by how it follows the orientation of that line.

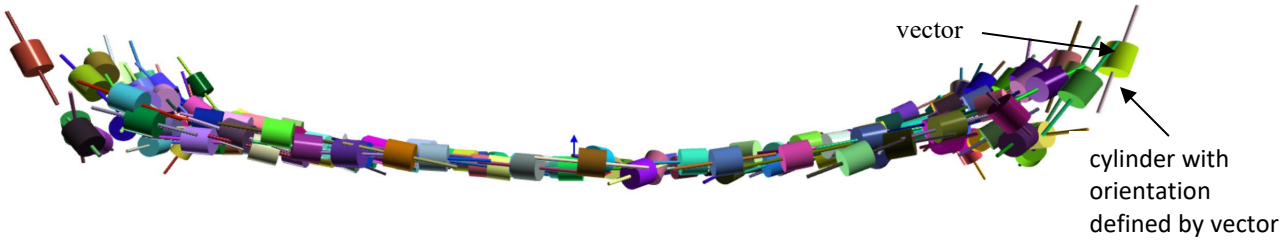

Figure G-4. A 3D python-generated illustration of how cylinder orientations follow pipe centerline orientations. Note that this illustration is not an actual analysis model.

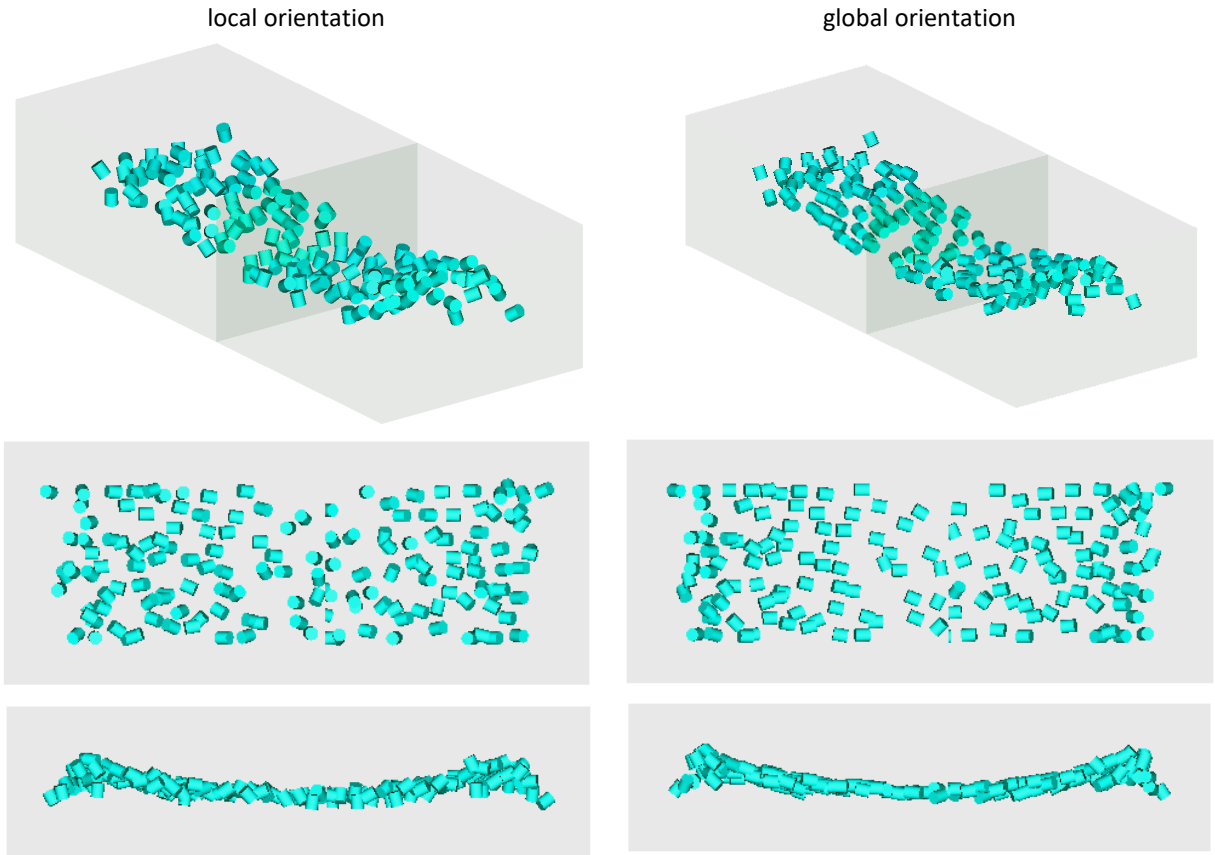

Figure G-5. Comparison of local and global orientations for centroid 1 using the isometric, top, and front view angles.

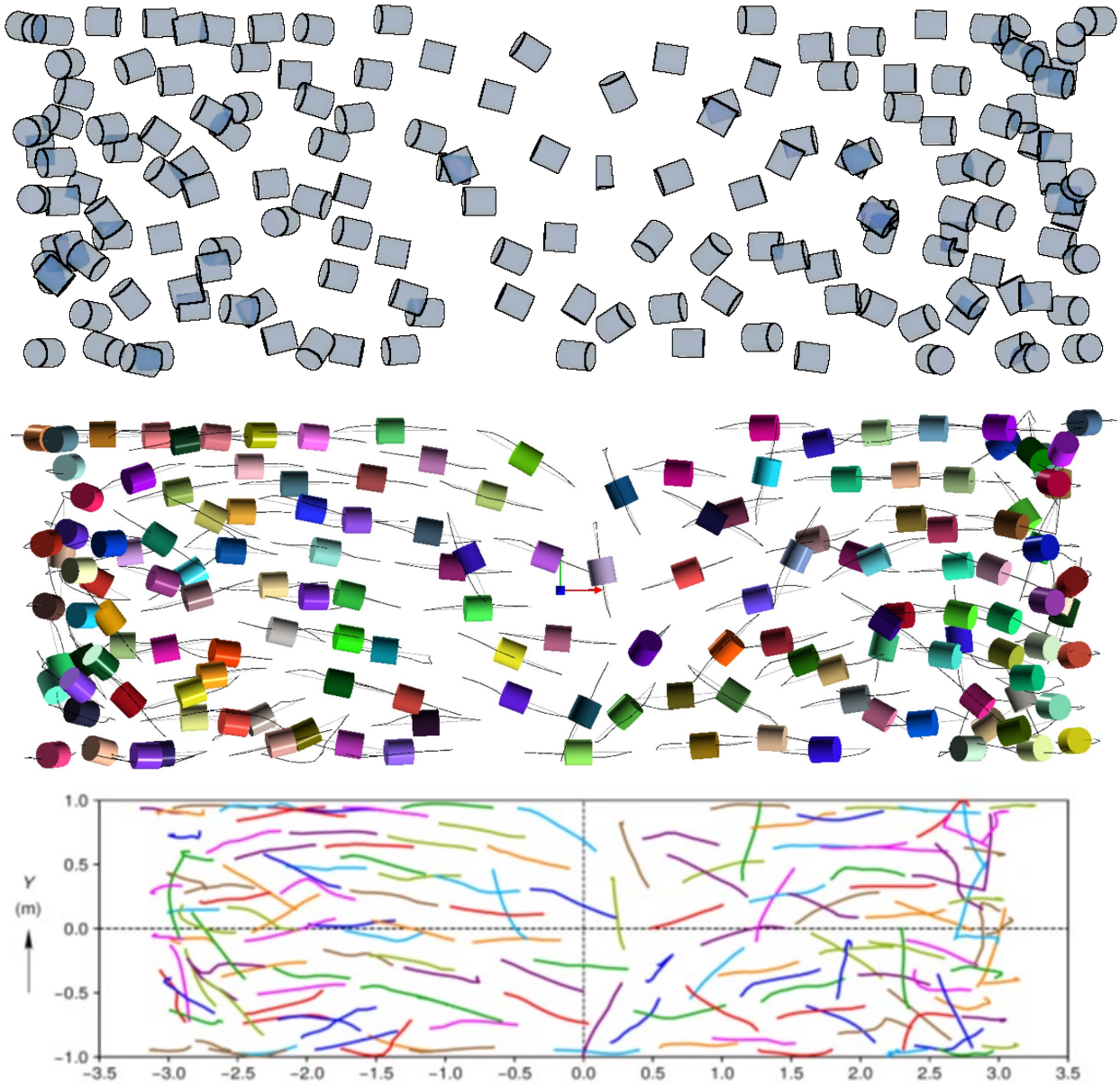

Figure G-6. Comparison of different visualizations of Centroid 6 shifted with global orientation case, x-y plane (top view).

Front view

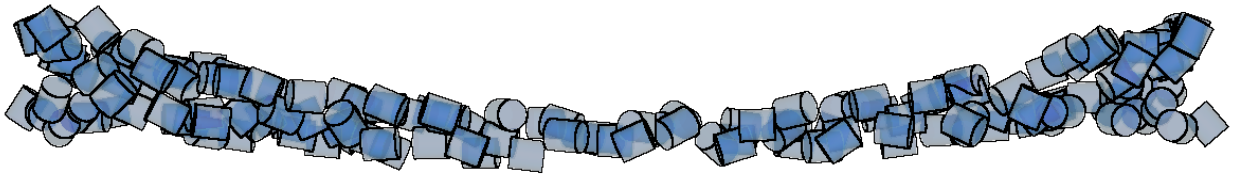

Front view rotated 180 degrees

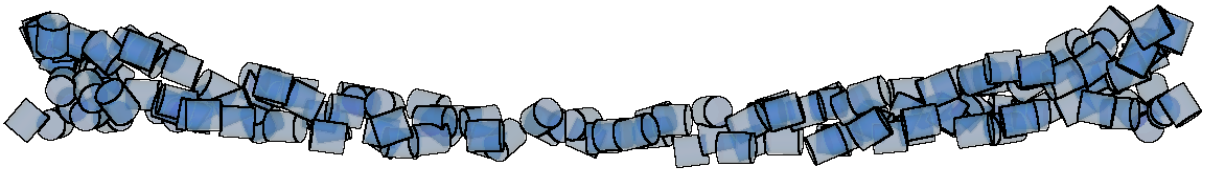

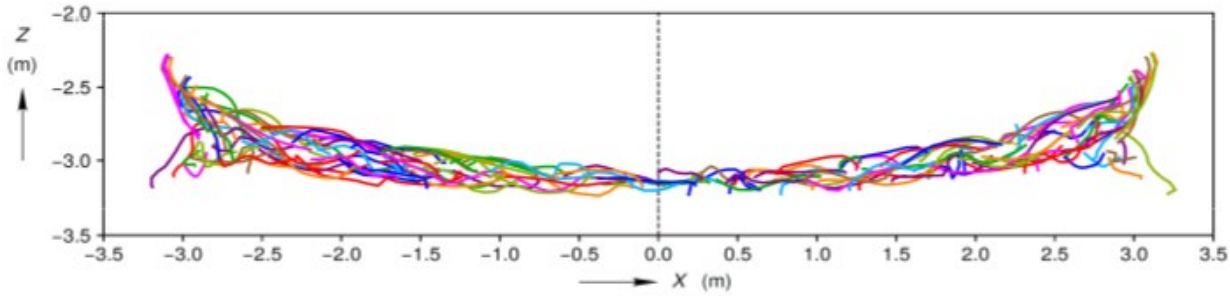

Figure G-7. Comparison of different visualizations of the Centroid 6 shifted with global orientation case, x-z plane (front/back view).

The results of these studies are provided in the figures and lists below. The following nomenclature is used for the cases provided in the listings:

- **centroid*n* (where *n* is a number between 1 and 13)**: indicates which centroid location is used for each pipe in the model.
- **_c1-1_**: indicates that there is no orientation of the cylinder in the model, or the base case.
- **_c*n*_*m***: indicates that a local orientation is determined from a vector taken from centroid *n* to *m*.
- **_c1-13_**: indicates a global orientation of the cylinders
- **shifted**: indicates that the geometric center of the cylinder is used for the centroid (x,y,z) rather than the SCALE default center of the cylinder base.
- **relLocal*n* (where *n* is a number between 1 and 100)**: indicates which random number in the series of random coordinate sweeps is being used, and that the local orientation relative to that selection is being applied.

Centroid study results

The following diagrams (Figures G-8 through G-21) show the results for centroid location and orientation for the base, local, and global orientations. Shifted cases are also included. The results show that there is little variation due to orientation for each centroid location, whereas some variation in reactivity due to centroid number exists. Centroids 8, 10 and 11 are slightly more reactive than the other centroids. Figure G-22 shows all the data combined, along with the bounding set-2-4 curves (under same the conditions).

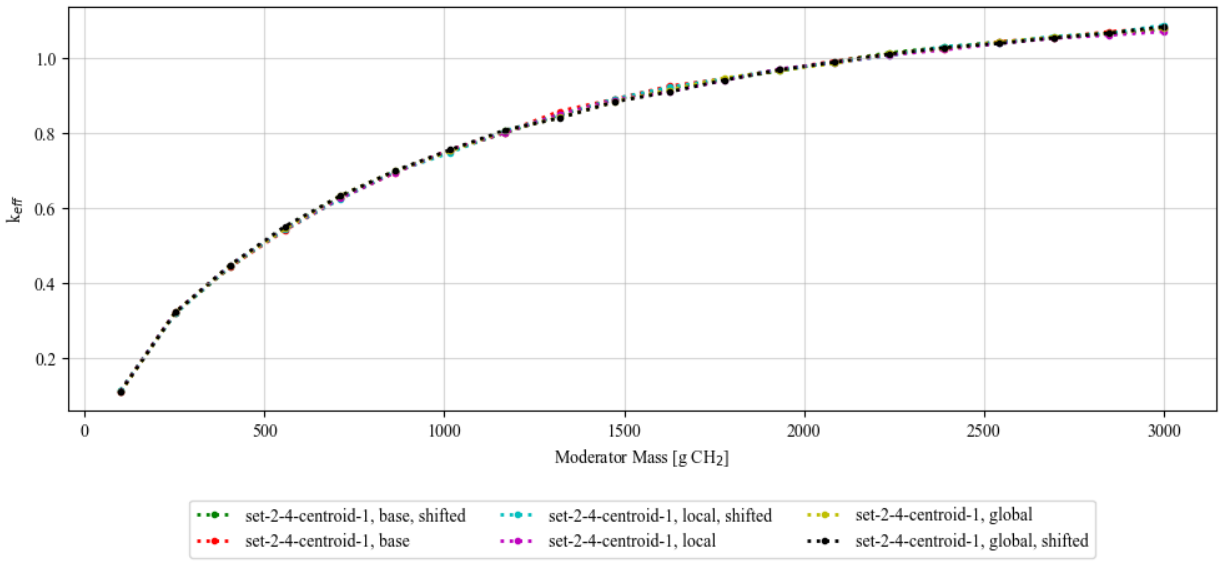

Figure G-8. Results of the centroid studies for centroid 1.

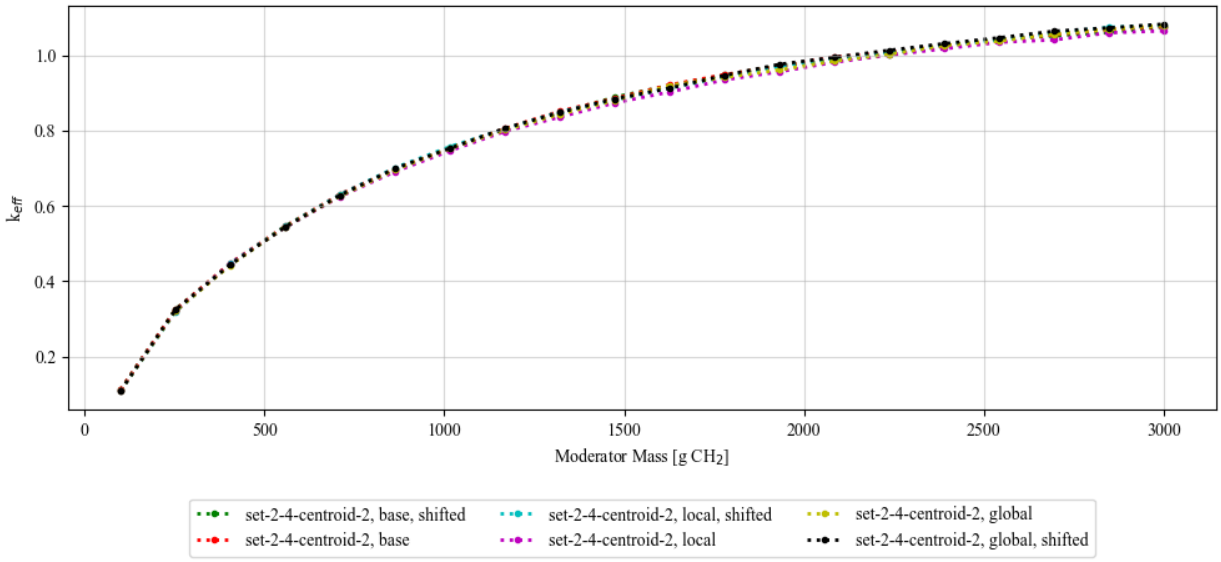

Figure G-9. Results of the centroid studies for centroid 2.

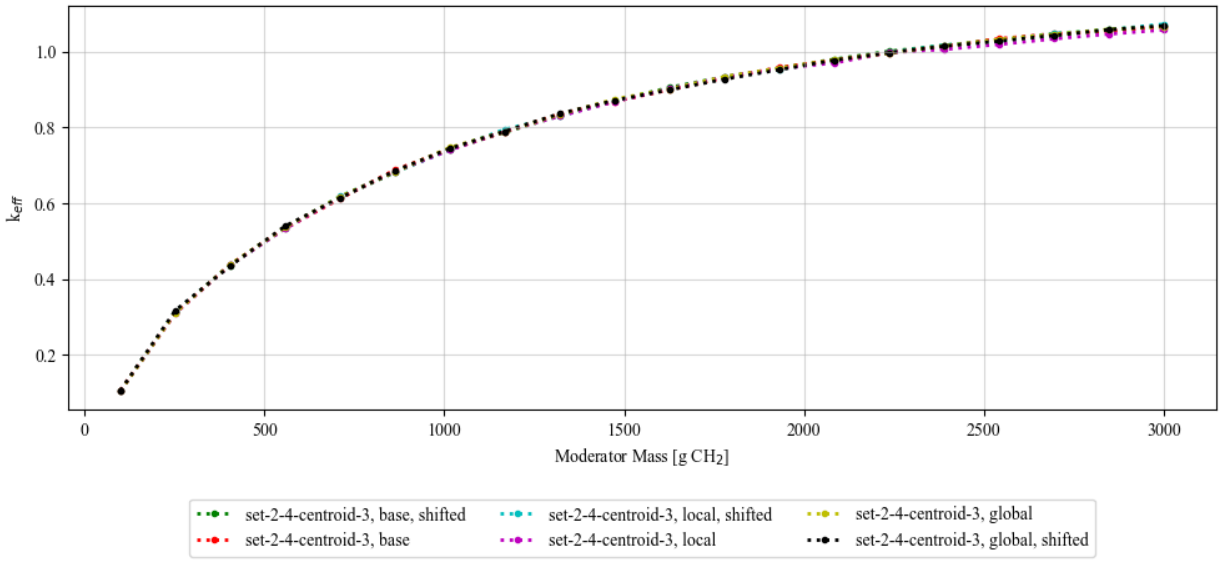

Figure G-10. Results of the centroid studies for centroid 3.

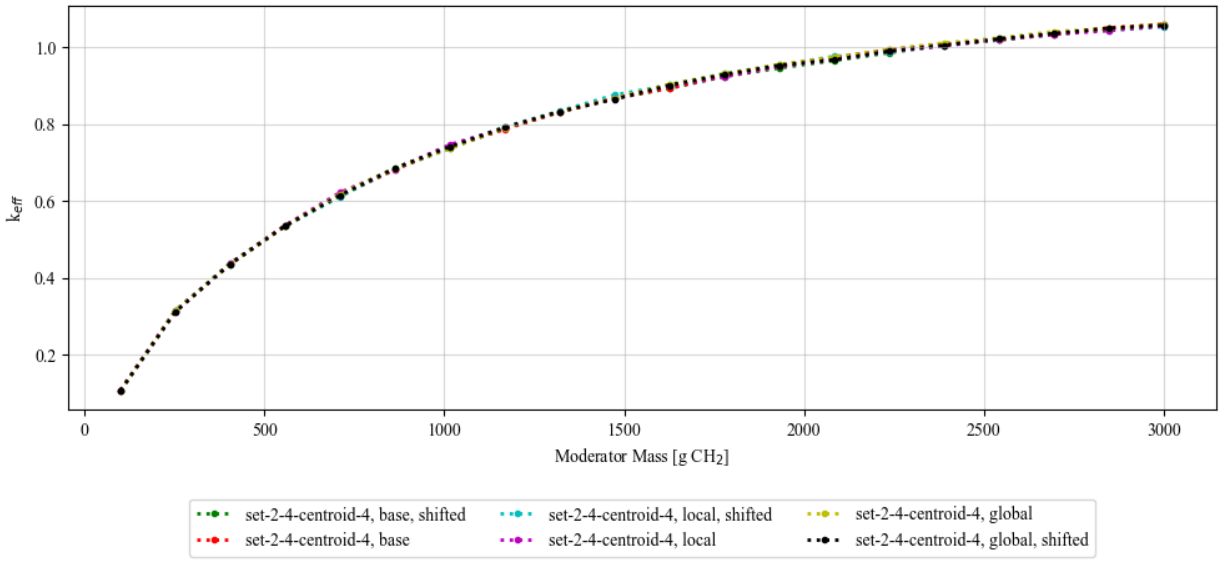

Figure G-11. Results of the centroid studies for centroid 4.

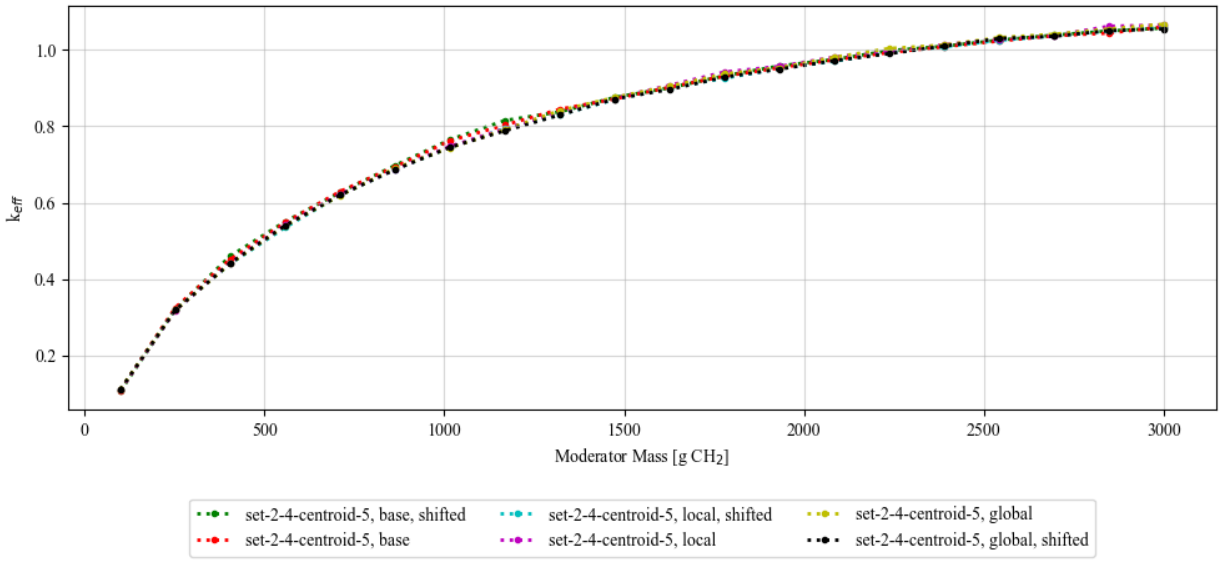

Figure G-12. Results of the centroid studies for centroid 5.

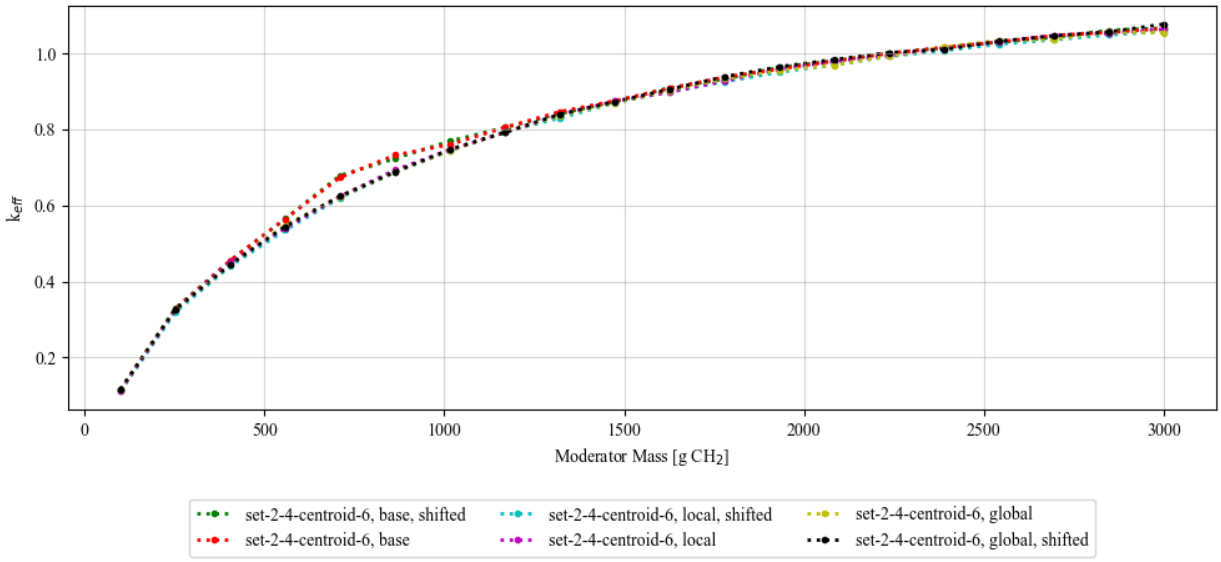

Figure G-13. Results of the centroid studies for centroid 6.

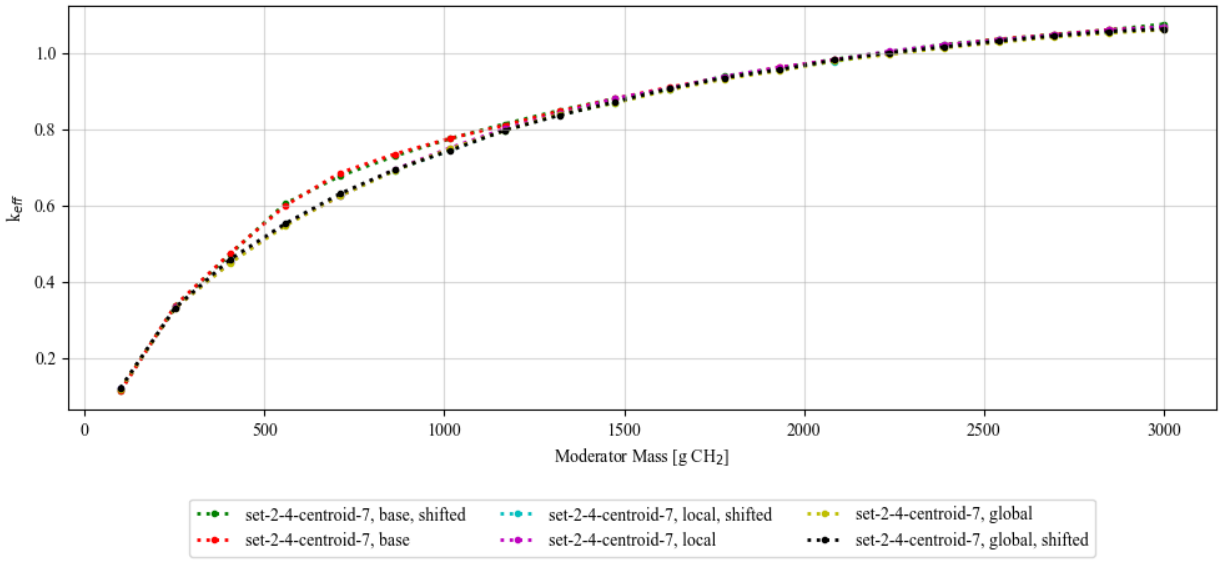

Figure G-14. Results of the centroid studies for centroid 7.

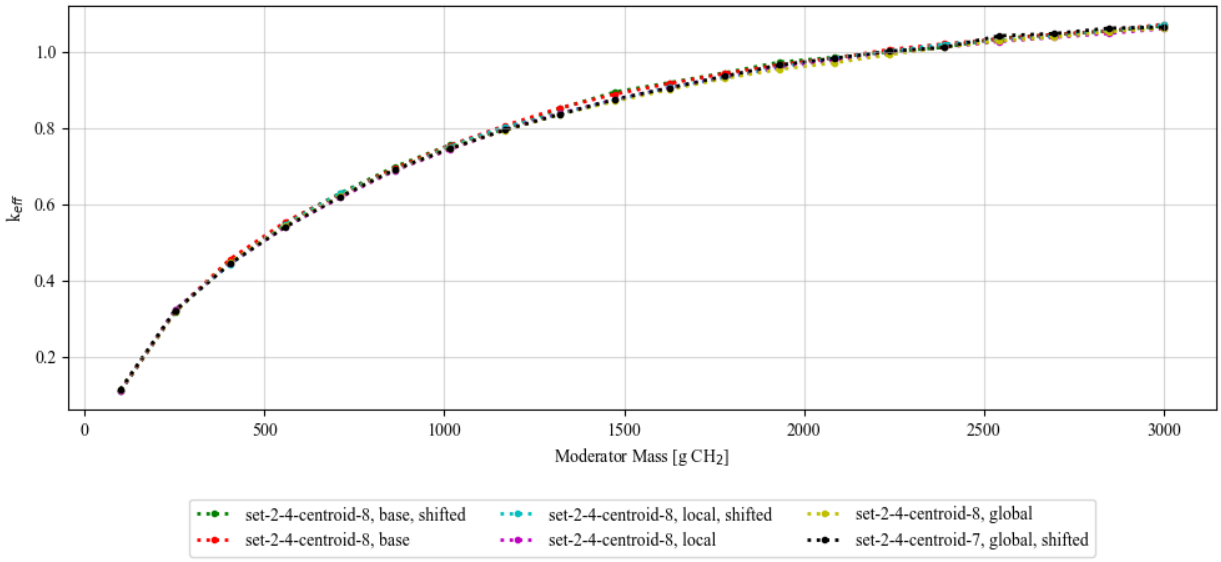

Figure G-15. Results of the centroid studies for centroid 8.

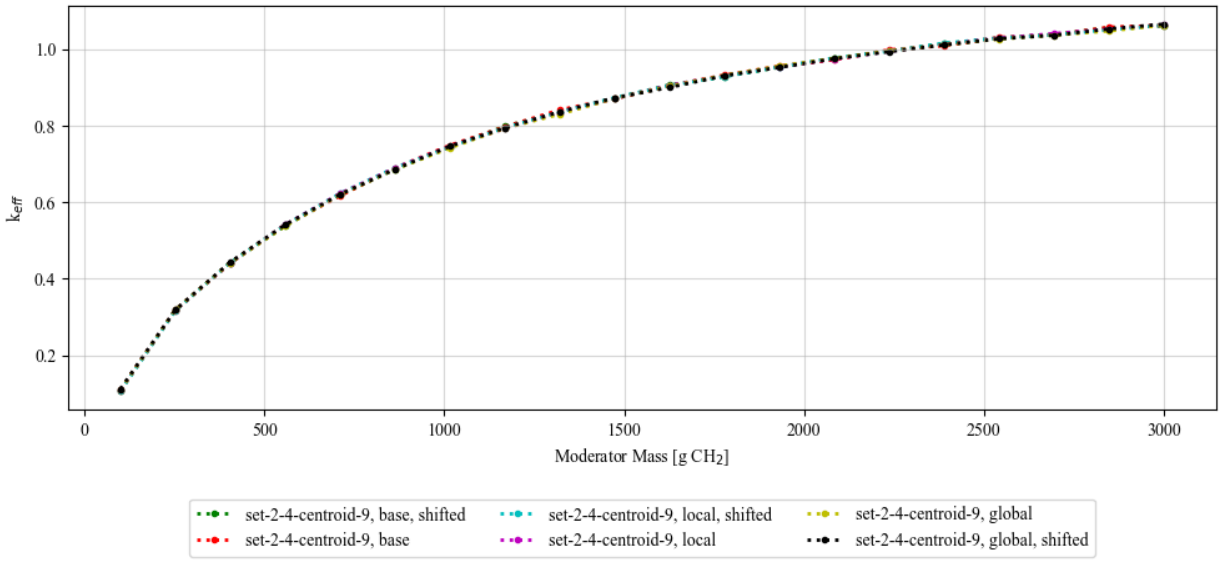

Figure G-16. Results of the centroid studies for centroid 9.

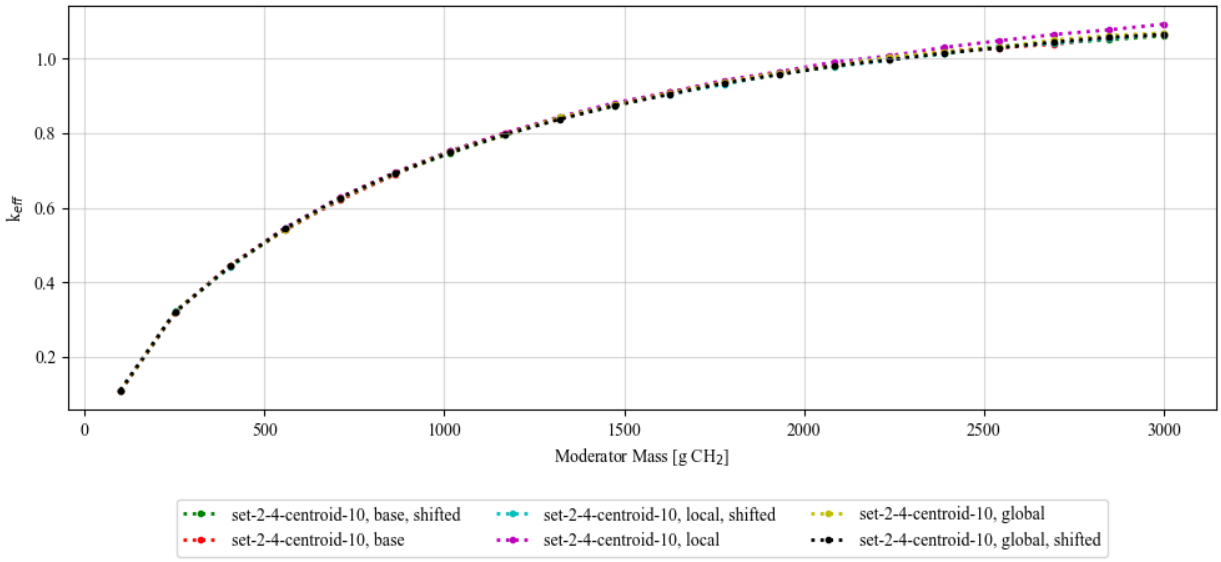

Figure G-17. Results of the centroid studies for centroid 10.

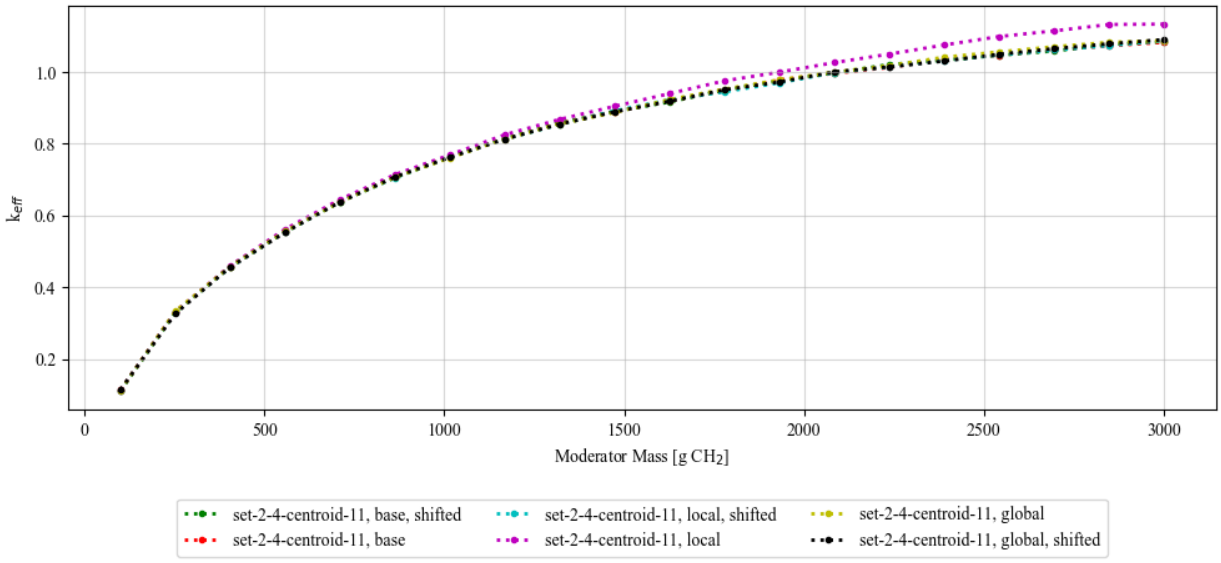

Figure G-18. Results of the centroid studies for centroid 11.

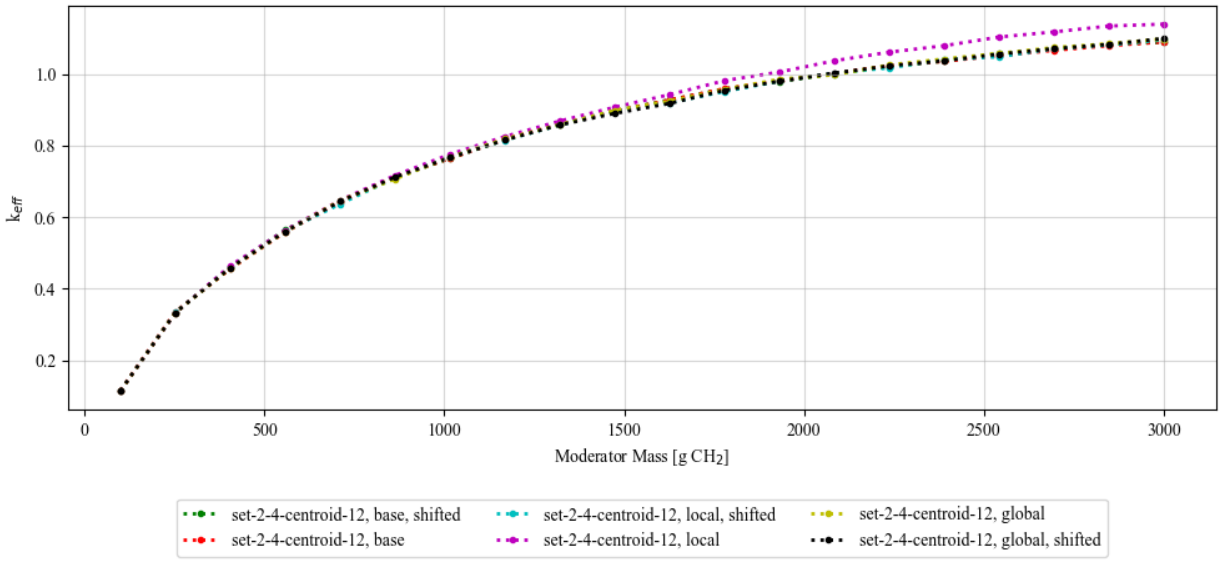

Figure G-19. Results of the centroid studies for centroid 12.

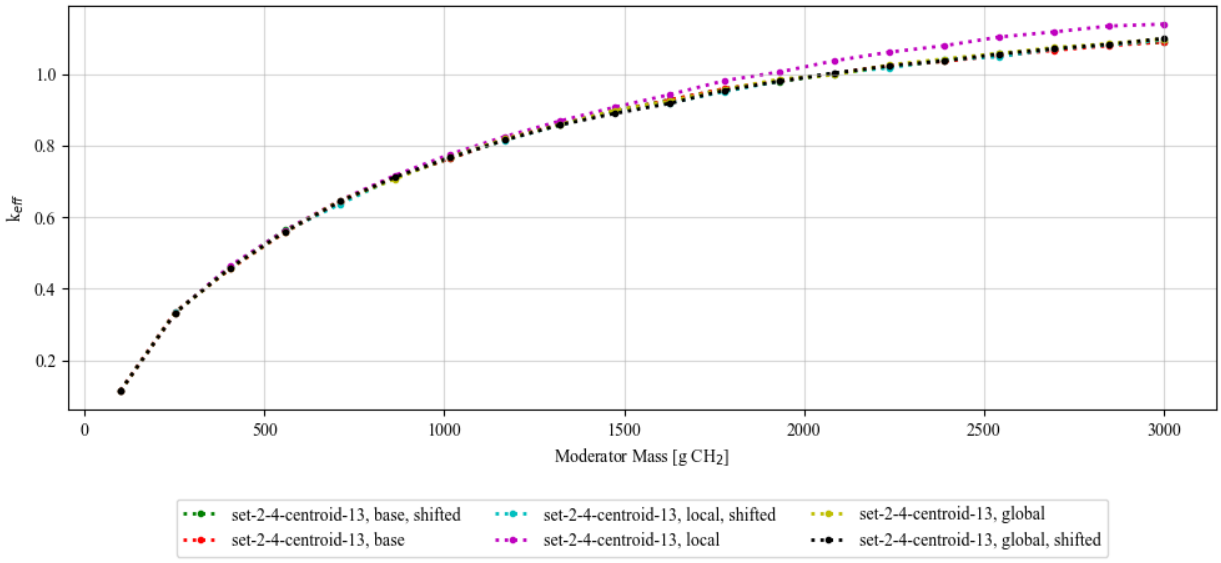

Figure G-20. Results of the centroid studies for centroid 13.

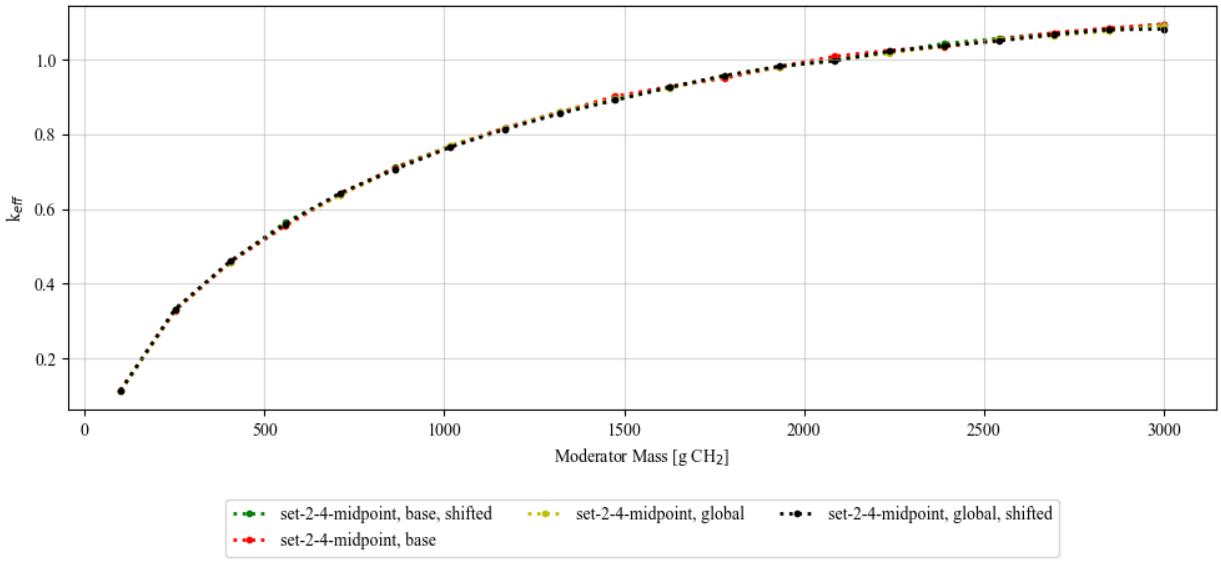

Figure G-21. Results of the centroid studies for the "midpoint" centroid.

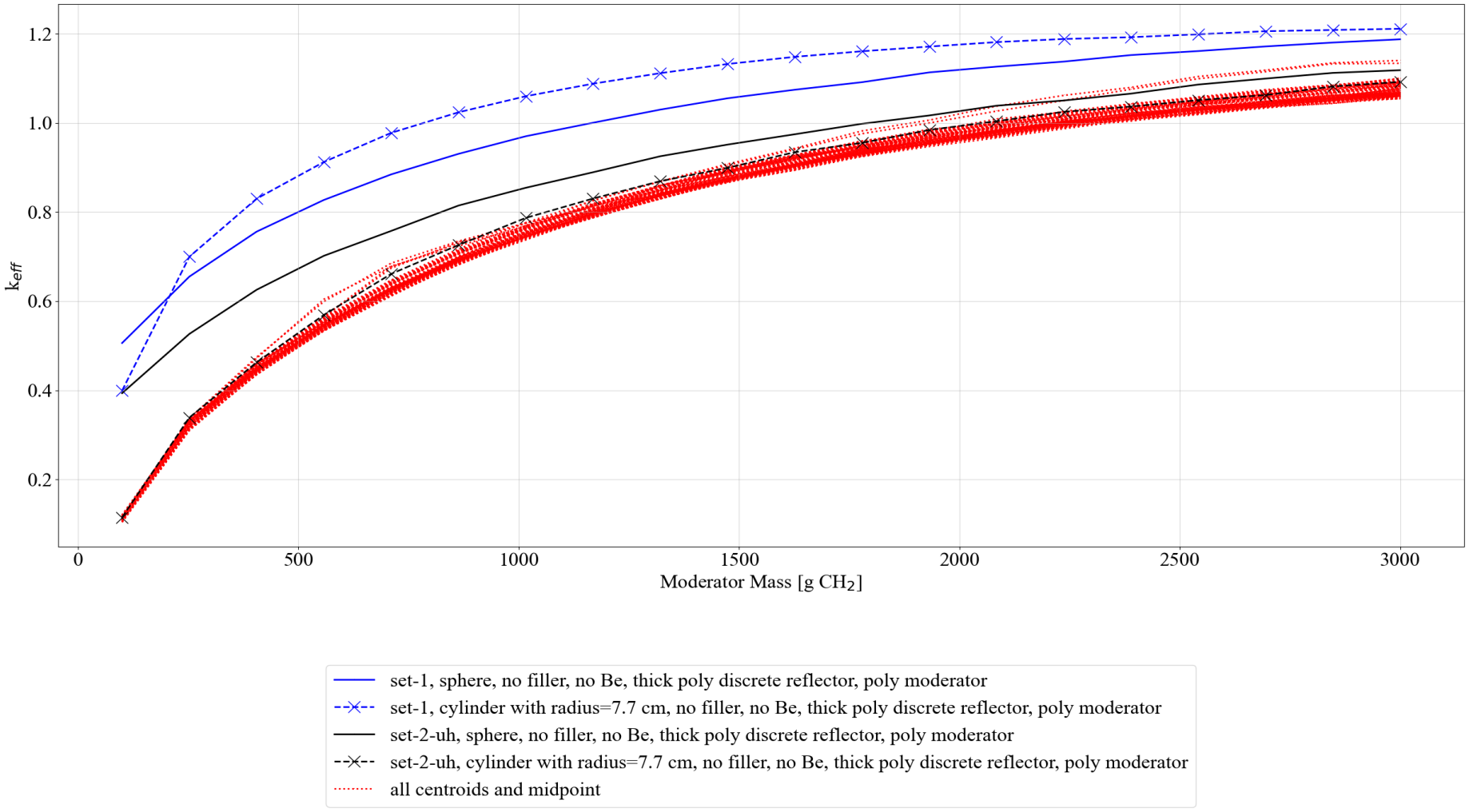

Figure G-22 Comparison of all centroids and midpoint to various representative curves.

rcoord study results

Additional studies were performed to evaluate the impact of randomly selecting which centroid location each pipe in the model used. The results are summarized in the Figure G-23 below.

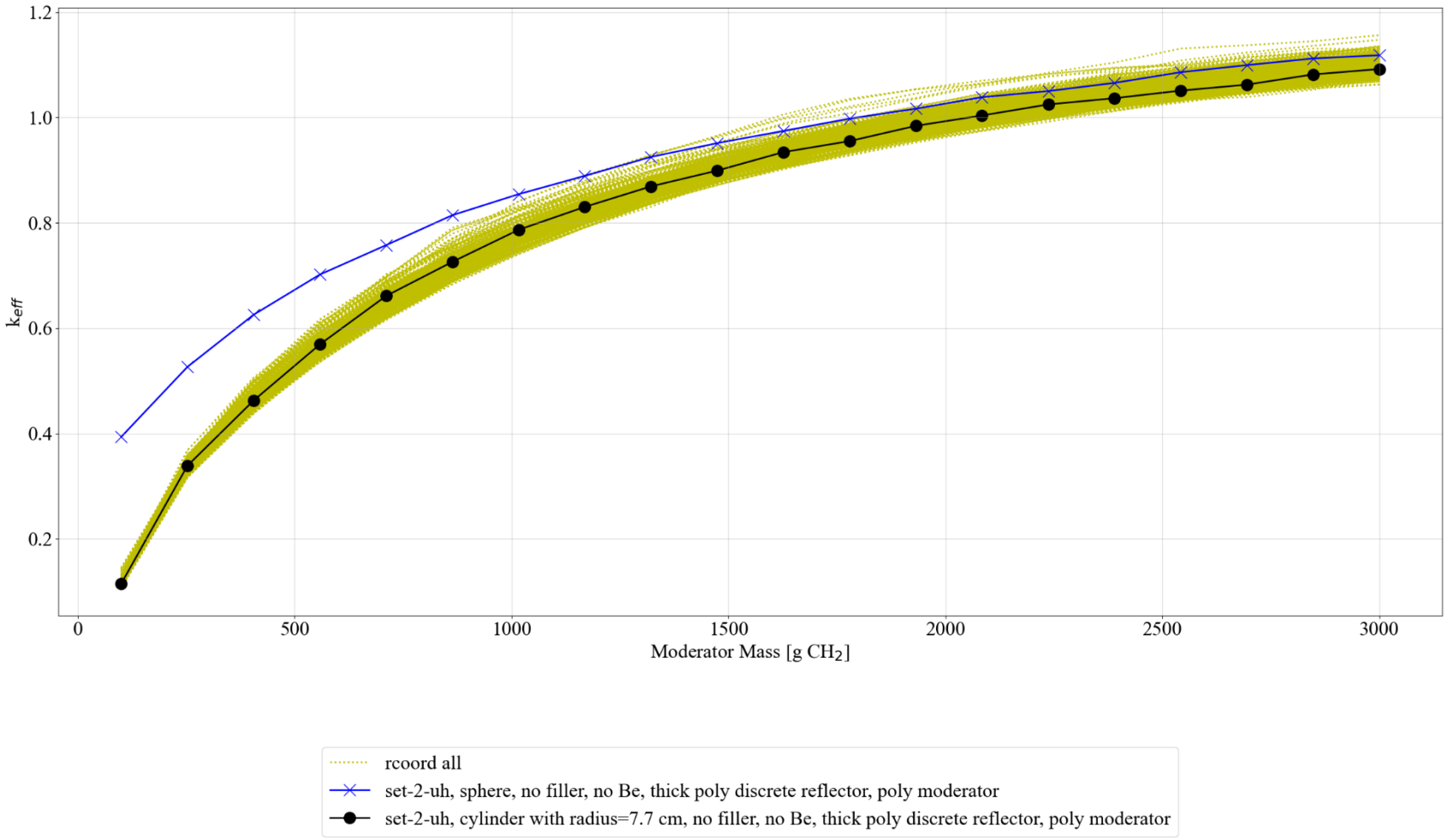

Figure G.23. Set-2-4 orientation study, random coordinate studies, results for 100 randomly selected centroid locations for each subset.

rA study results

The final set of studies presented in this appendix were performed to randomly select the rotation angles for the orientation of the cylinders. The results are summarized in the Figure G-24 and G-25 below.

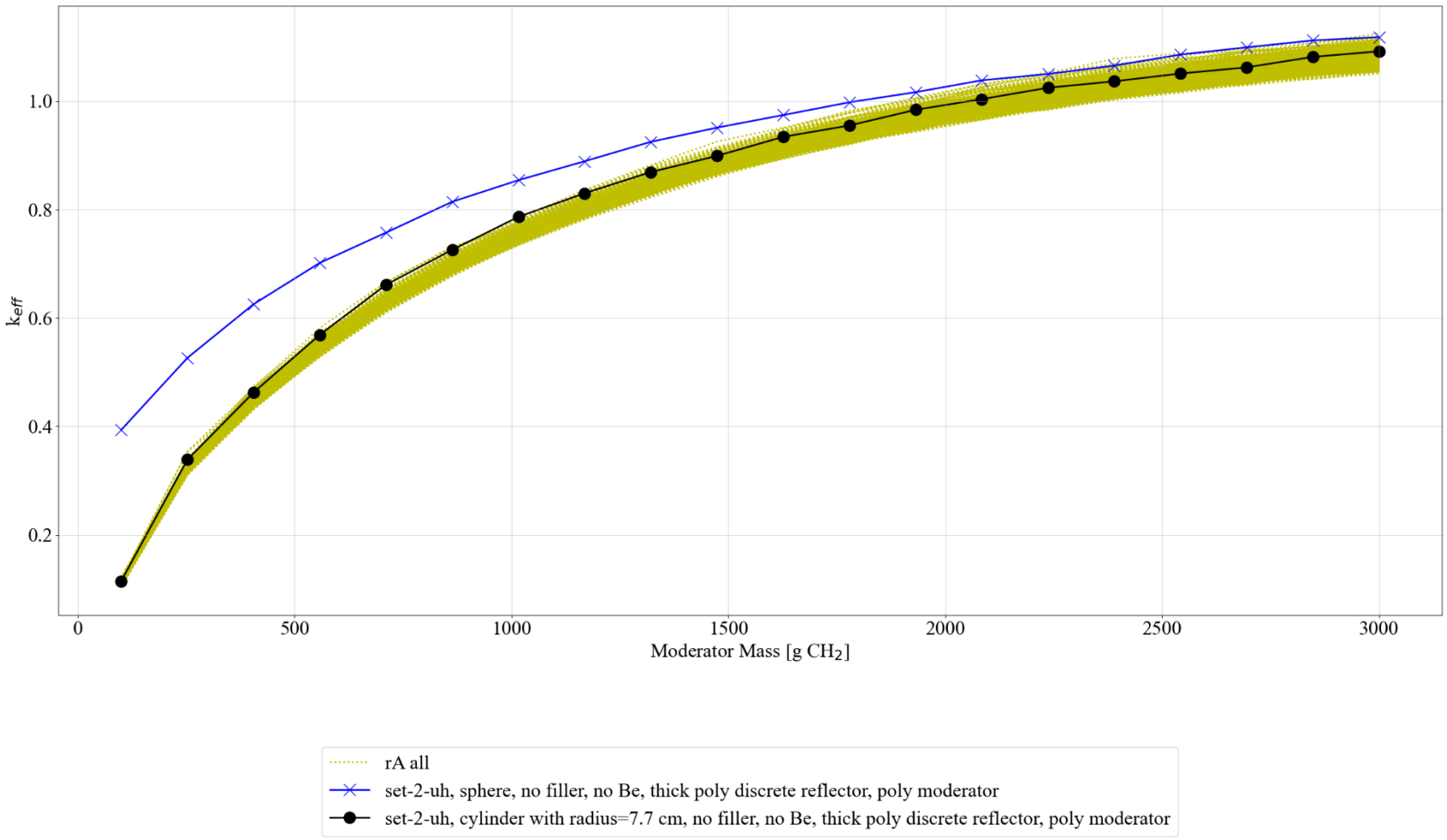

Figure G.24. Set-2-4 orientation study, random angle studies, results for 20 randomly selected angles for the 13 centroids plus the midpoint for each subset.

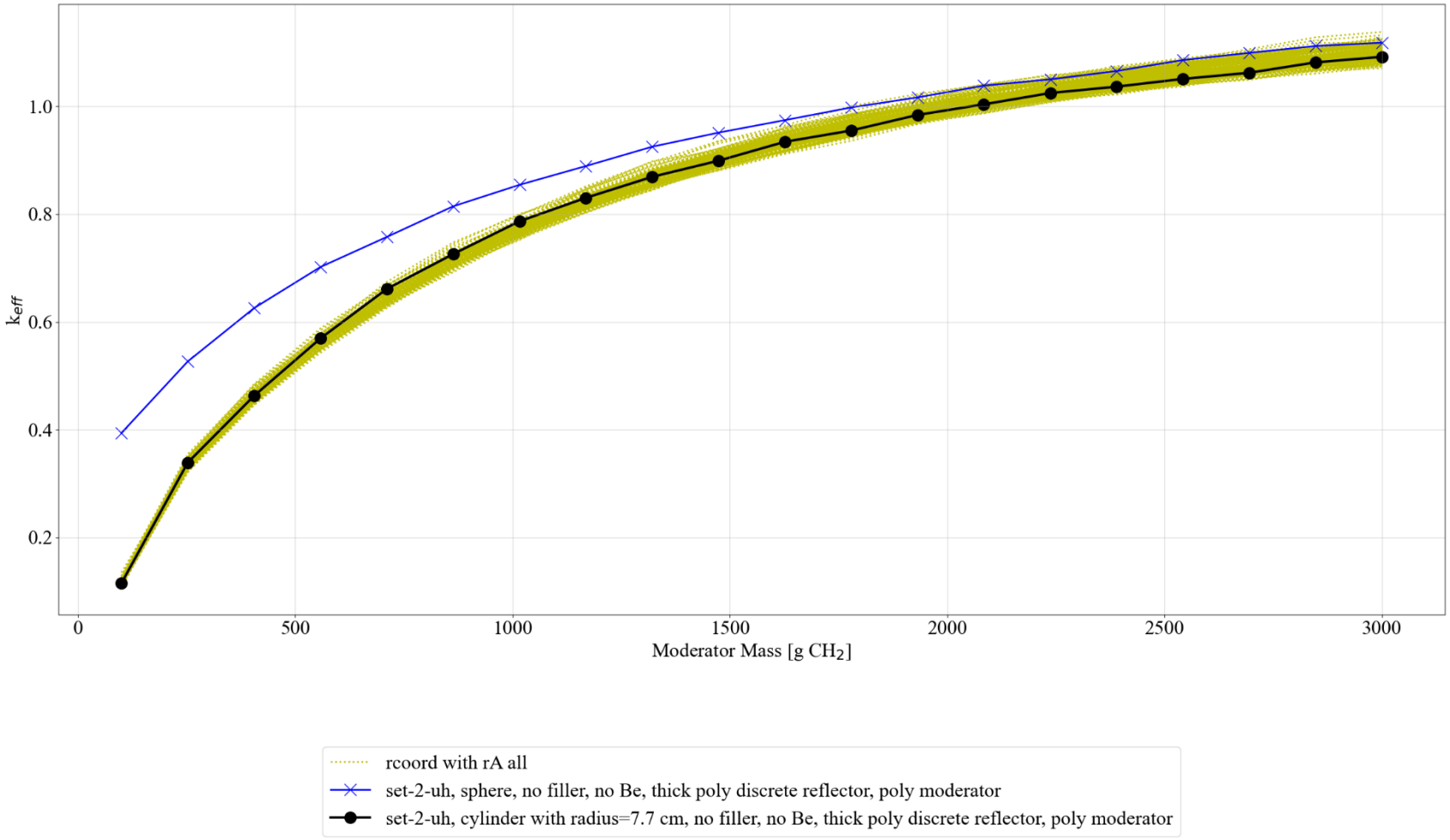

Figure G.25. Set-2-4 orientation study, random angle studies, results for 10 randomly selected angles for the 10 randomly selected centroids plus midpoint for each subset.

This page is intentionally blank

APPENDIX H. CALCULATIONAL VALIDATION

This page is intentionally blank

CONTENTS

LIST OF FIGURES

LIST OF TABLES

APPENDIX H. CALCULATIONAL VALIDATION

The calculations for this report were performed using the SCALE code system, version 6.2.4. The Criticality Safety Analysis Sequence (CSAS) with KENO-VI (CSAS6) was used to calculate effective neutron multiplication factors, or k-effective (k_{eff}) values, for the various configurations analyzed. As with any computer code or calculation used in relation to safety analyses and assessments, the ability of the calculational methodology to prove a configuration subcritical is obtained through a validation process.

The validation process assesses how well a computational method predicts reality (e.g., whether a system that was calculated to be subcritical is in reality subcritical). Validation of computational methods used in criticality safety analyses is required by consensus standards [34, 35]. These requirements are derived from the need for operational (notably worker) safety. Post-closure analyses of waste disposal sites do not fall directly under these requirements partly because there are no operations (other than static storage) or personnel presence. Post-closure analyses are also different because of the uncertainty in the waste composition/configuration due to the degradation of the waste and container materials over time. Even if it is not specifically required for post-closure analyses of waste disposal sites, the need for computational validation still exists.

The referenced consensus standards require validation to be conducted through comparisons of computed results with experimental data. Typically, well-documented critical experiments (critical benchmarks) are used for these comparisons. Documented critical experiments can be found in a variety of resources, including the *International Handbook of Evaluated Criticality Safety Benchmark Experiments* [36]. Ideally, calculational models of critical experiments would calculate results that are exactly equal to experimental results. In reality, calculational results do not exactly match experimental results because of simplifications and approximations made in the computational models to facilitate solutions on computer systems. Furthermore, the nuclear data used may include errors associated with the measurement, evaluation, and/or representation of the data. The validation process provides an understanding of the difference between calculated and experimental results, or *bias*, and the uncertainty in this difference, or *bias uncertainty*.

For a validation to yield an appropriate bias and bias uncertainty, the critical experiments used for comparison must be as similar as possible to the application being validated. Critical experiments are arrangements of fissile material and structural materials usually performed to support operational needs and processes. Validation of waste disposal operations can be challenging because of the difficulty in finding experiments similar in nature to waste disposal materials and operations.

The validation results (bias and bias uncertainty) are used to determine an upper subcritical limit (USL). Calculated results (including calculational uncertainty, $k_{eff\text{-}calc} + 2\sigma_{calc}$) below the USL are considered subcritical; results above the USL (even those below 1.0) are not considered to be subcritical. This number could also be considered as the maximum subcritical k_{eff}, referred to here as the *MSk*. Determination of the MSk can also include an additional margin of subcriticality to account for dissimilarities between the experiments used and the application and identified gaps in the nuclear data. The MSk can be considered as the magnitude of the sum of the biases, uncertainties, and administrative and/or statistical margins applied to a set of critical benchmarks. Because a positive bias may be nonconservative, all positive biases are set to zero. An allowance to use a positive bias, if the cause of the positive bias is well understood and justified, has been established in ANSI/ANS-8.24-2017 [35], but this is not typical. The MSk can be represented by the following:

$$\text{MSk} = 1.0 + \text{bias} - \text{bias uncertainty} - \text{administrative margin}$$

$$k_{eff\text{-}calc} + 2\sigma_{calc} < \text{MSk}. \quad (1)$$

Historically, the expected computational bias is established with the use of trending analyses of the bias for the critical experiments as a function of their physical characteristics such as H/X or energy of average neutron lethargy causing fission (EALF). The bias uncertainty is then determined through a statistical analysis of the trend, accounting for the uncertainty in each k_{eff} data point and the distribution of the data. The trending analysis can also be performed with sensitivity/uncertainty (S/U) tools. The S/U tools are used to determine correlation coefficients—c_k value or c(k)—for trending analysis. This report uses both c(k) and EALF values for trending analyses.

For the S/U method, the SCALE S/U analysis sequences, or TSUNAMI, is used. The TSUNAMI methods are based on the premise that the primary source of computational biases are the errors in the cross section data as bounded by their uncertainties, which can be tabulated in cross section covariance data. TSUNAMI quantifies the predicted change in k_{eff}, reaction rates, or the reactivity differences that result from changes in the energy-dependent, nuclide-reaction–specific cross section data, whether CE or MG. The sensitivity data are useful because they indicate the differences in system k_{eff} that would result from small changes in the underlying nuclear data. The sensitivity data can be used to quantify nuclear data uncertainties and to assess similarity between pairs of systems based on the shared nuclear data–induced uncertainty. This shared data uncertainty is expected to be a strong indicator of applicable benchmark experiments for use in validation of neutron transport methods. The two modules used in this report are TSUNAMI-3D and TSUNAMI-IP, both of which are described in more detail below.

The TSUNAMI-3D sequence is used for 3D cross section sensitivity generation in S/U analysis. The sequence provides automated processing of material input and cross section data, neutron transport, calculation of sensitivity coefficients (i.e., sensitivity of k_{eff} to nuclear data variation), and determination of uncertainty in k_{eff} caused by cross section covariances. Sensitivities based on the fluxes calculated by KENO are written to a sensitivity data file (SDF) containing the nuclide-, energy-, and reaction-dependent k_{eff} sensitivity coefficients. These energy-dependent sensitivities are determined for each nuclide in the model using first-order perturbation theory. SCALE 6.2.4 can generate sensitivity data using either CE or MG methods, but only MG calculations are used or reported in this work. Further details of the MG sensitivity calculation methodologies are available in Section 6 of the SCALE 6.2.4 manual [37].

TSUNAMI-IP is used to evaluate the similarity of critical experiments and application models and to determine uncertainties in system reactivity due to cross section covariance data. The similarity metric calculated here is c_k, which is the correlation coefficient of the effect of nuclear data uncertainty on k_{eff} of the application and experiment. c_k can be determined by dividing the covariance between the experiment and application by the product of the uncertainties in the experiment and the application [5], as shown in Eq. (2),

$$c_k = \frac{\sigma^2_{AppExp}}{\sigma_{App}\sigma_{Exp}}, \tag{2}$$

where: c_k is the similarity between an application and an experiment,
σ^2_{AppExp} is the covariance between the application and the experiment,
σ_{App} is the uncertainty in the application k_{eff} resulting from cross section covariances (uncertainties), and
σ_{Exp} is the uncertainty in the experiment k_{eff} caused by cross section covariances (uncertainties).

In essence, c_k is the fraction of the cross section–induced uncertainty in k_{eff} that is shared by two systems. A c_k value of 1 indicates that the k_{eff} values for two compared systems would be affected identically by

nuclear data errors, which are the primary contributors to the computational method's bias. Based on the assumption that computational biases are due primarily to nuclear data errors and that the nuclear data uncertainty values should indicate the potential for such nuclear data errors, two highly correlated systems should exhibit the same computational bias. A c_k value ≥ 0.8 is considered to have a high enough degree of similarity to be acceptable for use in validation studies [38]; this value is used as the cutoff for the acceptably similar experiments identified below.

TSUNAMI-IP can also generate additional inputs to be used with the Upper Subcritical Limit Statistics (USLSTATS) program, a statistical analysis program distributed with SCALE. USLSTATS can then be used to perform a trending analysis on the c_k value (or any other parameter suitable for trending analysis, e.g., EALF) to calculate a bias and bias uncertainty.

H.1 SENSITIVITY COEFFICIENT GENERATION

The TSUNAMI-3D sequence discussed above was used to generate sensitivity data for several cases ("application" cases). Cases from the uniform array parameter studies were chosen to represent the different material/container configurations modeled in this report. All cases had k_{eff} values close to 1.0, or slightly lower in similar material configuations. Limiting analysis conditions were used because the generation of SDFs requires significantly greater computational resources than the calculations of k_{eff}. The MG TSUNAMI method is used, which is consistent with the use of MG data in the analyses.

The uniform array models were large arrays, and the calculations were run with multigroup cross sections. Running multigroup TSUNAMI-3D to generate sensitivity data files with these cases as-is required the definition of a grid mesh, and it also required an extremely large amount of computer memory, taking up an extremely large computer footprint. The finer the grid mesh, the larger the computer footprint. Direct perturbation calculations were used to verify the TSUNAMI-3D–generated sensitivities, which indicated the mesh size necessary to generate valid sensitivity data, required a memory footprint not available on the current computer system in the necessary time frame. Therefore, the cases were modified by decreasing the length of the room modeled and using mirror boundaries on the positive and negative *y* faces. Figure H-1 shows an example top view for these configurations.

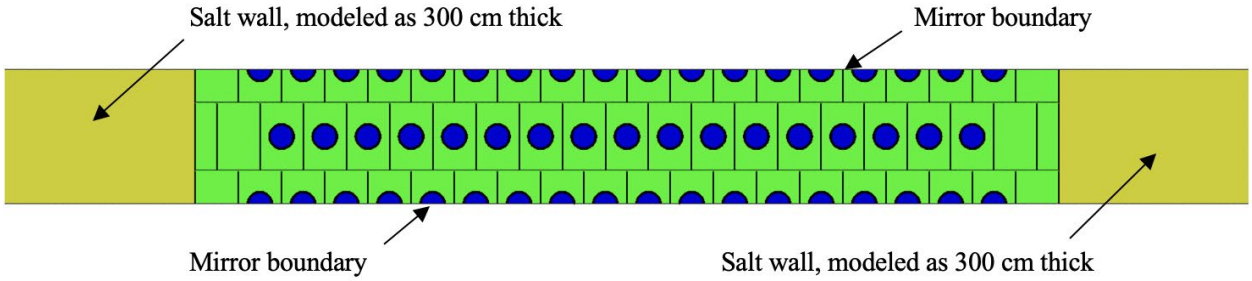

Figure H-1. Top view of modified configuration.

H.2 SELECTION OF APPLICATION CASES

The validation here considered only set-1 cases: specifically set-1-1, set-1-2, set-1-3, set-1-4, set-1-5, set-1-6, set-1-7, and set 1-8. The results were plotted by subset, as shown in Figures H-2 through H-9, to determine bounding cases to use as the application cases. The cases including Be were not included in the plots. For each set, the cases adding filler material and/or can material decrease the system k_{eff}. The more material added, the larger the decrease. Cases chosen as application cases included those with no filler or can material, as well as cases with 2,000 g filler material and/or 500 g can material. The same cases including Be were also chosen. Tables H-1 through H-8 list the application cases.

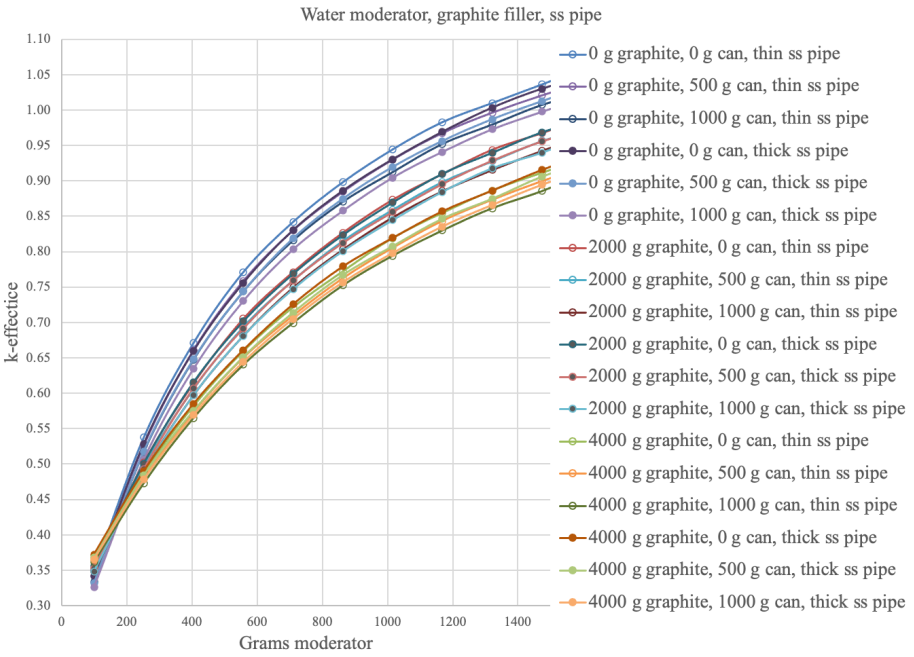

Figure H-2. Set-1-1 cases, water moderator, graphite filler, stainless steel pipe.

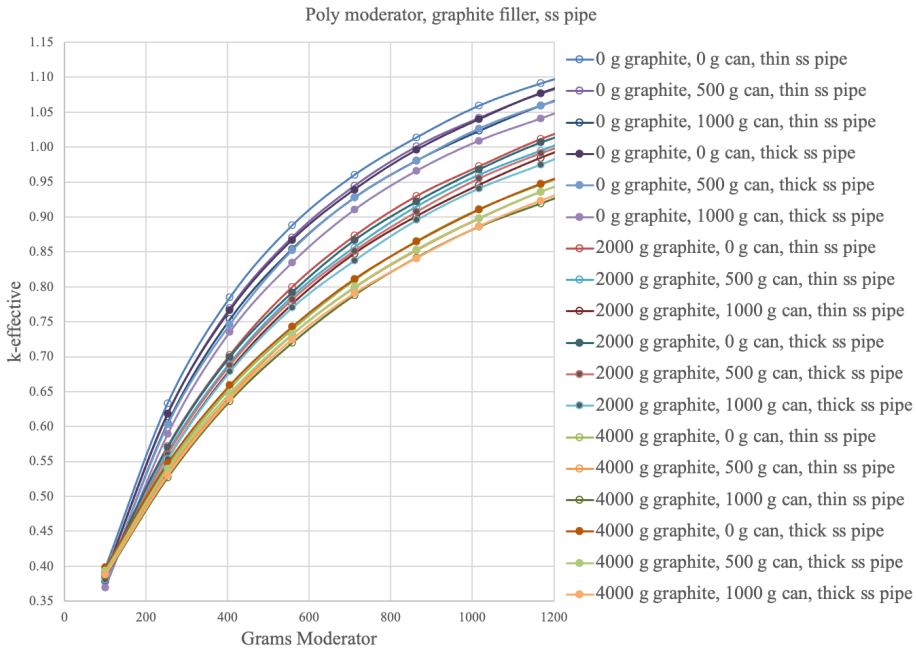

Figure H-3. Set-1-2 cases, poly moderator, graphite filler, stainless steel pipe.

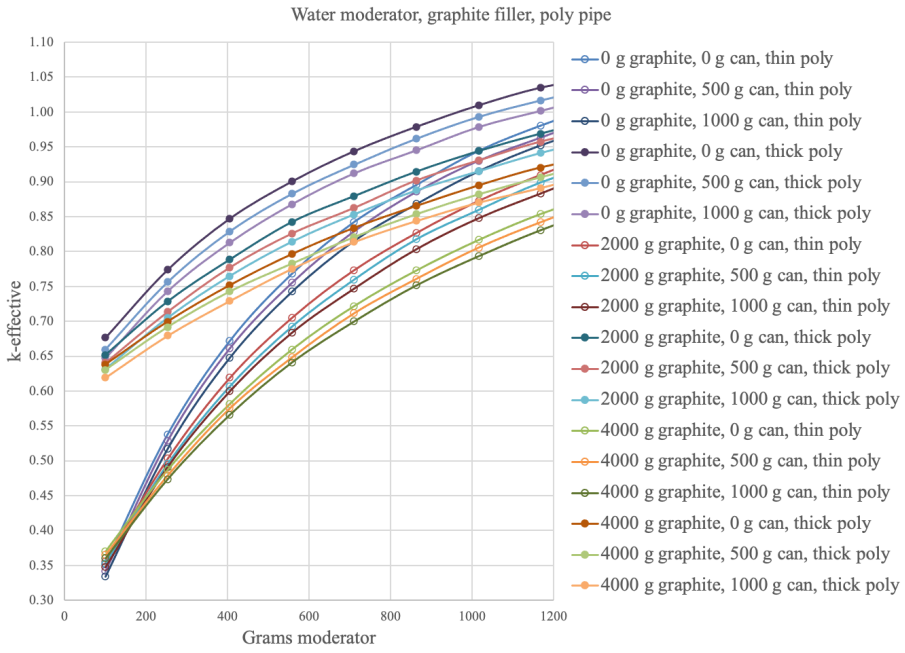

Figure H-4. Set-1-3 cases, water moderator, graphite filler, poly pipe.

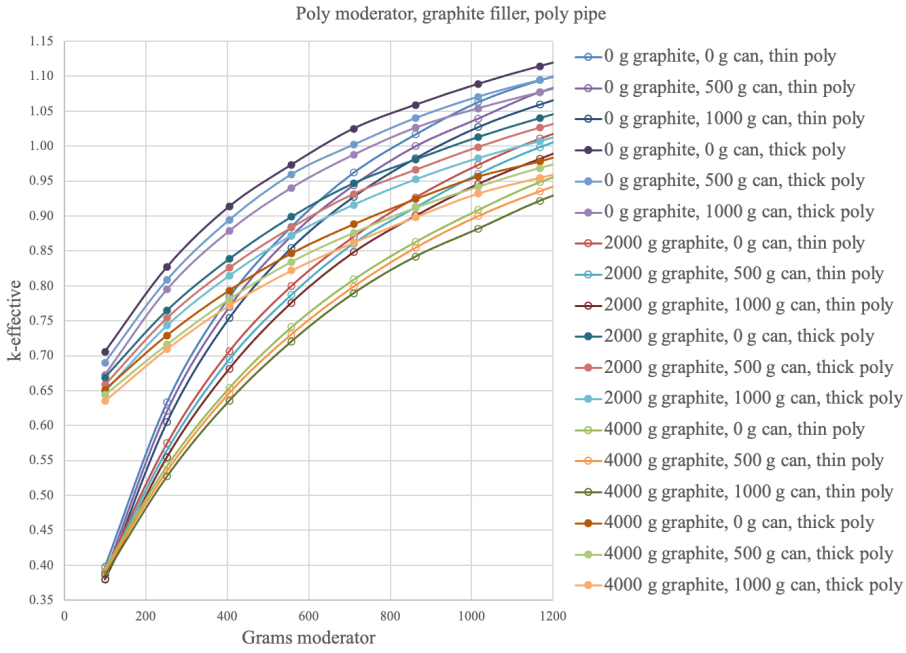

Figure H-5. Set-1-4 cases, poly moderator, graphite filler, poly pipe.

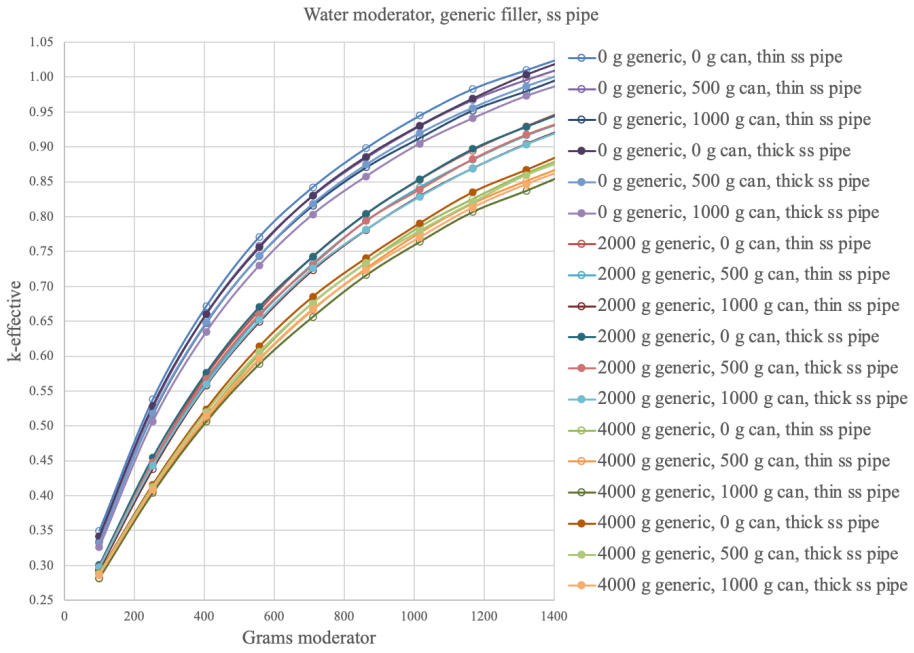

Figure H-6. Set-1-5 cases, water moderator, generic filler, stainless steel pipe.

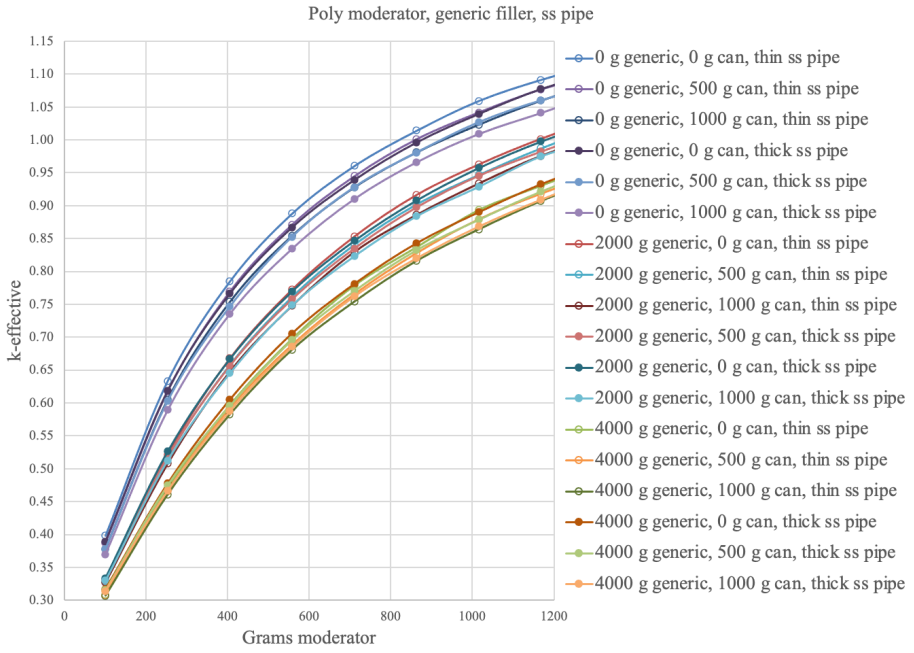

Figure H-7. Set-1-6 cases, poly moderator, generic filler, stainless steel pipe.

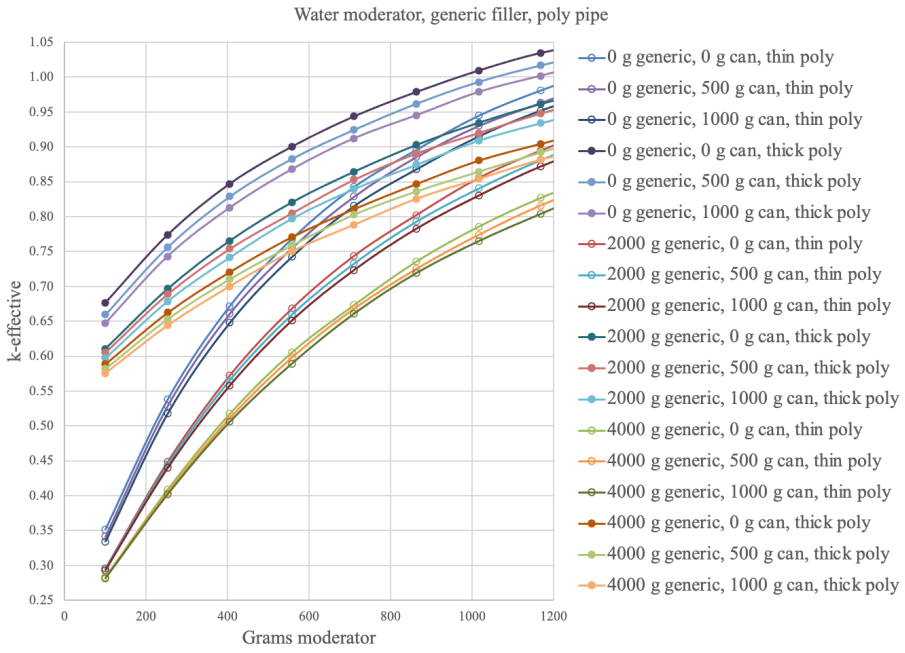

Figure H-8. Set-1-7 cases, water moderator, generic filler, poly pipe.

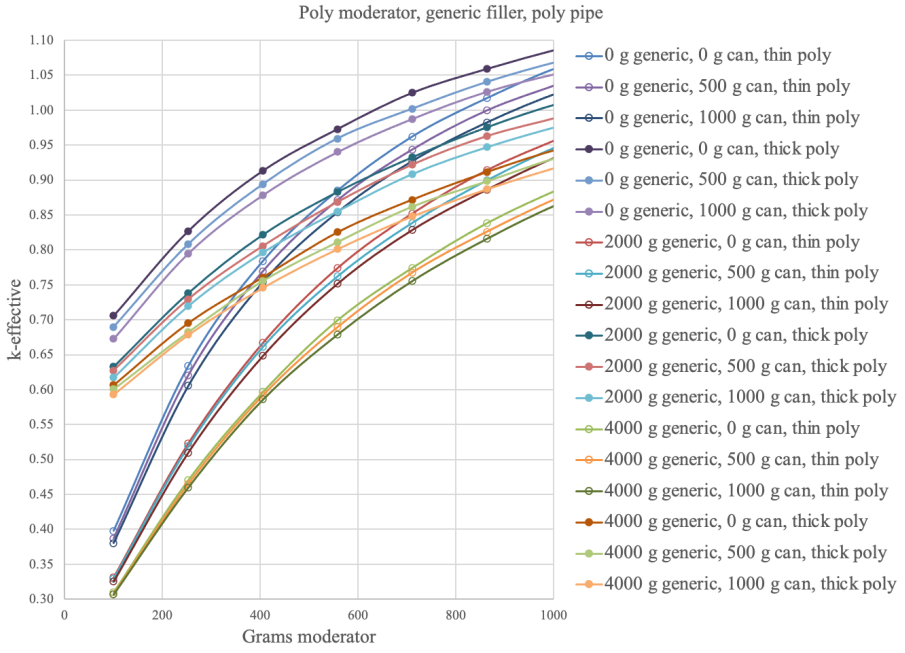

Figure H-9. Set-1-8 cases, poly moderator, generic filler, poly pipe.

Table H-1. Set-1-1 application cases

Case	Short name	Moderator		Filler		Can	Pipe Material	
			grams		grams	grams		cm
set-1-1-uac1_uh_m1_graphite_cyl_ps_1000_yr_para_00657	set-1-1-00657	H_2O	1016	graphite	0	0	ss	0.0010
set-1-1-uac1_uh_m1_graphite_cyl_ps_1000_yr_para_00659	set-1-1-00659					500		0.7112
set-1-1-uac1_uh_m1_graphite_cyl_ps_1000_yr_para_00669	set-1-1-00669				2,000	0		0.0010
set-1-1-uac1_uh_m1_graphite_cyl_ps_1000_yr_para_00671	set-1-1-00671					500		0.7112
With Be								
set-1-1-uac1_uh_m1_graphite_cyl_ps_1000_yr_para_00658	set-1-1-00658	H_2O	1016	graphite	0	0	ss	0.0010
set-1-1-uac1_uh_m1_graphite_cyl_ps_1000_yr_para_00660	set-1-1-00660					500		0.7112
set-1-1-uac1_uh_m1_graphite_cyl_ps_1000_yr_para_00670	set-1-1-00670				2,000	0		0.0010
set-1-1-uac1_uh_m1_graphite_cyl_ps_1000_yr_para_00672	set-1-1-00672					500		0.7112

Table H-2. Set-1-2 application cases

Case	Short name	Moderator		Filler		Can	Pipe Material	
			grams		grams	grams		cm
set-1-2-uac1_uh_m2_graphite_cyl_ps_1000_yr_para_00441	set-1-2-00441	CH_2	710.5	graphite	0	0	ss	0.0010
set-1-2-uac1_uh_m2_graphite_cyl_ps_1000_yr_para_00443	set-1-2-00443					500		0.7112
set-1-2-uac1_uh_m2_graphite_cyl_ps_1000_yr_para_00453	set-1-2-00453				2,000	0		0.0010
set-1-2-uac1_uh_m2_graphite_cyl_ps_1000_yr_para_00455	set-1-2-00455					500		0.7112
With Be								
set-1-2-uac1_uh_m2_graphite_cyl_ps_1000_yr_para_00442	set-1-2-00442	CH_2	710.5	graphite	0	0	ss	0.0010
set-1-2-uac1_uh_m2_graphite_cyl_ps_1000_yr_para_00444	set-1-2-00444					500		0.7112
set-1-2-uac1_uh_m2_graphite_cyl_ps_1000_yr_para_00454	set-1-2-00454				2,000	0		0.0010
set-1-2-uac1_uh_m2_graphite_cyl_ps_1000_yr_para_00456	set-1-2-00456					500		0.7112

Table H-3. Set-1-3 application cases

Case	Short name	Moderator		Filler		Can	Pipe Material	
			grams		grams	grams		cm
set-1-3-uac1_uh_m1_graphite_cyl_pp_1000_yr_para_00441	set-1-3-00441	H_2O	710.5	graphite	0	0	poly	0.0010
set-1-3-uac1_uh_m1_graphite_cyl_pp_1000_yr_para_00443	set-1-3-00443					500		0.7112
set-1-3-uac1_uh_m1_graphite_cyl_pp_1000_yr_para_00453	set-1-3-00453				2,000	0		0.0010
set-1-3-uac1_uh_m1_graphite_cyl_pp_1000_yr_para_00455	set-1-3-00455					500		0.7112
With Be								
set-1-3-uac1_uh_m1_graphite_cyl_pp_1000_yr_para_00442	set-1-3-00442	H_2O	710.5	graphite	0	0	poly	0.0010
set-1-3-uac1_uh_m1_graphite_cyl_pp_1000_yr_para_00444	set-1-3-00444					500		0.7112
set-1-3-uac1_uh_m1_graphite_cyl_pp_1000_yr_para_00454	set-1-3-00454				2,000	0		0.0010
set-1-3-uac1_uh_m1_graphite_cyl_pp_1000_yr_para_00456	set-1-3-00456					500		0.7112

Table H-4. Set-1-4 application cases

Case	Short name	Moderator		Filler		Can	Pipe Material	
			grams		grams	grams		cm
set-1-4-uac1_uh_m2_graphite_cyl_pp_1000_yr_para_00333	set-1-4-00333	CH_2	557.9	graphite	0	0	poly	0.0010
set-1-4-uac1_uh_m2_graphite_cyl_pp_1000_yr_para_00335	set-1-4-00335							0.7112
set-1-4-uac1_uh_m2_graphite_cyl_pp_1000_yr_para_00345	set-1-4-00345					500		0.0010
set-1-4-uac1_uh_m2_graphite_cyl_pp_1000_yr_para_00347	set-1-4-00347							0.7112
set-1-4-uac1_uh_m2_graphite_cyl_pp_1000_yr_para_00369	set-1-4-00369				2,000	0		0.0010
set-1-4-uac1_uh_m2_graphite_cyl_pp_1000_yr_para_00371	set-1-4-00371							0.7112
set-1-4-uac1_uh_m2_graphite_cyl_pp_1000_yr_para_00381	set-1-4-00381					500		0.0010
set-1-4-uac1_uh_m2_graphite_cyl_pp_1000_yr_para_00383	set-1-4-00383							0.7112
With Be								
set-1-4-uac1_uh_m2_graphite_cyl_pp_1000_yr_para_00334	set-1-4-00334	CH_2	557.9	graphite	0	0	poly	0.0010
set-1-4-uac1_uh_m2_graphite_cyl_pp_1000_yr_para_00336	set-1-4-00336							0.7112
set-1-4-uac1_uh_m2_graphite_cyl_pp_1000_yr_para_00346	set-1-4-00346					500		0.0010
set-1-4-uac1_uh_m2_graphite_cyl_pp_1000_yr_para_00348	set-1-4-00348							0.7112
set-1-4-uac1_uh_m2_graphite_cyl_pp_1000_yr_para_00370	set-1-4-00370				2,000	0		0.0010
set-1-4-uac1_uh_m2_graphite_cyl_pp_1000_yr_para_00372	set-1-4-00372							0.7112
set-1-4-uac1_uh_m2_graphite_cyl_pp_1000_yr_para_00382	set-1-4-00382					500		0.0010
set-1-4-uac1_uh_m2_graphite_cyl_pp_1000_yr_para_00384	set-1-4-00384							0.7112

Table H-5. Set-1-5 application cases

Case	Short name	Moderator		Filler		Can	Pipe Material	
			grams		grams	grams		cm
set-1-5-uac1_uh_m1_generic_cyl_ps_1000_yr_para_00657	set-1-5-00657	H_2O	1016	generic	0	0	ss	0.0010
set-1-5-uac1_uh_m1_generic_cyl_ps_1000_yr_para_00659	set-1-5-00659							0.7112
set-1-5-uac1_uh_m1_generic_cyl_ps_1000_yr_para_00669	set-1-5-00669					500		0.0010
set-1-5-uac1_uh_m1_generic_cyl_ps_1000_yr_para_00671	set-1-5-00671							0.7112
set-1-5-uac1_uh_m1_generic_cyl_ps_1000_yr_para_00693	set-1-5-00693				2,000	0		0.0010
set-1-5-uac1_uh_m1_generic_cyl_ps_1000_yr_para_00695	set-1-5-00695							0.7112
set-1-5-uac1_uh_m1_generic_cyl_ps_1000_yr_para_00705	set-1-5-00705					500		0.0010
set-1-5-uac1_uh_m1_generic_cyl_ps_1000_yr_para_00707	set-1-5-00707							0.7112
With Be								
set-1-5-uac1_uh_m1_generic_cyl_ps_1000_yr_para_00658	set-1-5-00658	H_2O	1016	generic	0	0	ss	0.0010
set-1-5-uac1_uh_m1_generic_cyl_ps_1000_yr_para_00660	set-1-5-00660							0.7112
set-1-5-uac1_uh_m1_generic_cyl_ps_1000_yr_para_00670	set-1-5-00670					500		0.0010
set-1-5-uac1_uh_m1_generic_cyl_ps_1000_yr_para_00672	set-1-5-00672							0.7112
set-1-5-uac1_uh_m1_generic_cyl_ps_1000_yr_para_00694	set-1-5-00694				2,000	0		0.0010
set-1-5-uac1_uh_m1_generic_cyl_ps_1000_yr_para_00696	set-1-5-00696							0.7112
set-1-5-uac1_uh_m1_generic_cyl_ps_1000_yr_para_00706	set-1-5-00706					500		0.0010
set-1-5-uac1_uh_m1_generic_cyl_ps_1000_yr_para_00708	set-1-5-00708							0.7112

Table H-6. Set-1-6 application cases

Case	Short name	Moderator		Filler		Can	Pipe Material	
			grams		grams	grams		cm
set-1-6-uac1_uh_m2_generic_cyl_ps_1000_yr_para_00441	set-1-6-00441	CH_2	710.5	generic	0	0	ss	0.0010
set-1-6-uac1_uh_m2_generic_cyl_ps_1000_yr_para_00443	set-1-6-00443							0.7112
set-1-6-uac1_uh_m2_generic_cyl_ps_1000_yr_para_00453	set-1-6-00453					500		0.0010
set-1-6-uac1_uh_m2_generic_cyl_ps_1000_yr_para_00455	set-1-6-00455							0.7112
set-1-6-uac1_uh_m2_generic_cyl_ps_1000_yr_para_00477	set-1-6-00477				2,000	0		0.0010
set-1-6-uac1_uh_m2_generic_cyl_ps_1000_yr_para_00479	set-1-6-00479							0.7112
set-1-6-uac1_uh_m2_generic_cyl_ps_1000_yr_para_00489	set-1-6-00489					500		0.0010
set-1-6-uac1_uh_m2_generic_cyl_ps_1000_yr_para_00491	set-1-6-00491							0.7112
With Be								
set-1-6-uac1_uh_m2_generic_cyl_ps_1000_yr_para_00442	set-1-6-00442	CH_2	710.5	generic	0	0	ss	0.0010
set-1-6-uac1_uh_m2_generic_cyl_ps_1000_yr_para_00444	set-1-6-00444							0.7112
set-1-6-uac1_uh_m2_generic_cyl_ps_1000_yr_para_00454	set-1-6-00454					500		0.0010
set-1-6-uac1_uh_m2_generic_cyl_ps_1000_yr_para_00456	set-1-6-00456							0.7112
set-1-6-uac1_uh_m2_generic_cyl_ps_1000_yr_para_00478	set-1-6-00478				2,000	0		0.0010
set-1-6-uac1_uh_m2_generic_cyl_ps_1000_yr_para_00480	set-1-6-00480							0.7112
set-1-6-uac1_uh_m2_generic_cyl_ps_1000_yr_para_00490	set-1-6-00490					500		0.0010
set-1-6-uac1_uh_m2_generic_cyl_ps_1000_yr_para_00492	set-1-6-00492							0.7112

Table H-7. Set-1-7 application cases

Case	Short name	Moderator		Filler		Can	Pipe Material	
			grams		grams	grams		cm
set-1-7-uac1_uh_m1_generic_cyl_pp_1000_yr_para_00441	set-1-7-00441	H_2O	710.5	generic	0	0	poly	0.0010
set-1-7-uac1_uh_m1_generic_cyl_pp_1000_yr_para_00443	set-1-7-00443							0.7112
set-1-7-uac1_uh_m1_generic_cyl_pp_1000_yr_para_00453	set-1-7-00453					500		0.0010
set-1-7-uac1_uh_m1_generic_cyl_pp_1000_yr_para_00455	set-1-7-00455							0.7112
set-1-7-uac1_uh_m1_generic_cyl_pp_1000_yr_para_00477	set-1-7-00477				2,000	0		0.0010
set-1-7-uac1_uh_m1_generic_cyl_pp_1000_yr_para_00479	set-1-7-00479							0.7112
set-1-7-uac1_uh_m1_generic_cyl_pp_1000_yr_para_00489	set-1-7-00489					500		0.0010
set-1-7-uac1_uh_m1_generic_cyl_pp_1000_yr_para_00491	set-1-7-00491							0.7112
With Be								
set-1-7-uac1_uh_m1_generic_cyl_pp_1000_yr_para_00442	set-1-7-00442	H_2O	710.5	generic	0	0	poly	0.0010
set-1-7-uac1_uh_m1_generic_cyl_pp_1000_yr_para_00444	set-1-7-00444							0.7112
set-1-7-uac1_uh_m1_generic_cyl_pp_1000_yr_para_00454	set-1-7-00454					500		0.0010
set-1-7-uac1_uh_m1_generic_cyl_pp_1000_yr_para_00456	set-1-7-00456							0.7112
set-1-7-uac1_uh_m1_generic_cyl_pp_1000_yr_para_00478	set-1-7-00478				2,000	0		0.0010
set-1-7-uac1_uh_m1_generic_cyl_pp_1000_yr_para_00480	set-1-7-00480							0.7112
set-1-7-uac1_uh_m1_generic_cyl_pp_1000_yr_para_00490	set-1-7-00490					500		0.0010
set-1-7-uac1_uh_m1_generic_cyl_pp_1000_yr_para_00492	set-1-7-00492							0.7112

Table H-8. Set-1-8 application cases

Case	Short name	Moderator		Filler		Can	Pipe Material	
			grams		grams	grams		cm
set-1-8-uac1_uh_m2_generic_cyl_pp_1000_yr_para_00333	set-1-8-00333	CH_2	557.9	generic	0	0	poly	0.0010
set-1-8-uac1_uh_m2_generic_cyl_pp_1000_yr_para_00335	set-1-8-00335							0.7112
set-1-8-uac1_uh_m2_generic_cyl_pp_1000_yr_para_00345	set-1-8-00345					500		0.0010
set-1-8-uac1_uh_m2_generic_cyl_pp_1000_yr_para_00347	set-1-8-00347							0.7112
set-1-8-uac1_uh_m2_generic_cyl_pp_1000_yr_para_00369	set-1-8-00369				2,000	0		0.0010
set-1-8-uac1_uh_m2_generic_cyl_pp_1000_yr_para_00371	set-1-8-00371							0.7112
set-1-8-uac1_uh_m2_generic_cyl_pp_1000_yr_para_00381	set-1-8-00381					500		0.0010
set-1-8-uac1_uh_m2_generic_cyl_pp_1000_yr_para_00383	set-1-8-00383							0.7112
With Be								
set-1-8-uac1_uh_m2_generic_cyl_pp_1000_yr_para_00334	set-1-8-00334	CH_2	557.9	generic	0	0	poly	0.0010
set-1-8-uac1_uh_m2_generic_cyl_pp_1000_yr_para_00336	set-1-8-00336							0.7112
set-1-8-uac1_uh_m2_generic_cyl_pp_1000_yr_para_00346	set-1-8-00346					500		0.0010
set-1-8-uac1_uh_m2_generic_cyl_pp_1000_yr_para_00348	set-1-8-00348							0.7112
set-1-8-uac1_uh_m2_generic_cyl_pp_1000_yr_para_00370	set-1-8-00370				2,000	0		0.0010
set-1-8-uac1_uh_m2_generic_cyl_pp_1000_yr_para_00372	set-1-8-00372							0.7112
set-1-8-uac1_uh_m2_generic_cyl_pp_1000_yr_para_00382	set-1-8-00382					500		0.0010
set-1-8-uac1_uh_m2_generic_cyl_pp_1000_yr_para_00384	set-1-8-00384							0.7112

The TSUNAMI-3D sequence was used to generate SDFs for the modified versions of each of the application cases (shortened *y*-dimension with *y*-direction mirror boundaries, as shown in Figure H-1). The KENO-VI sequence was also used to generate k_{eff} values for the modified cases to compare with the original cases, as shown in Tables H-9 through H-16. The respective EALF values are also included for comparison. The nuclides with the highest magnitude sensitivities are listed in Tables H-17 through H-24. The sensitivities were confirmed through direct perturbation calculations.

Table H-9. Set-1-1 k_{eff} values for comparison

Case	Original		Modified		Original	Modified
	k_{eff}	sigma	k_{eff}	sigma	EALF	EALF
set-1-1-00657	0.9445	0.0013	0.9437	0.0001	0.73	0.73
set-1-1-00658	0.9496	0.0015	0.9492	0.0001	0.69	0.69
set-1-1-00659	0.9303	0.0016	0.9323	0.0001	0.72	0.72
set-1-1-00660	0.9380	0.0014	0.9371	0.0001	0.69	0.69
set-1-1-00669	0.9298	0.0013	0.9290	0.0001	0.74	0.74
set-1-1-00670	0.9340	0.0016	0.9335	0.0001	0.71	0.71
set-1-1-00671	0.9194	0.0013	0.9180	0.0001	0.74	0.74
set-1-1-00672	0.9236	0.0015	0.9225	0.0001	0.71	0.71
set-1-1-00693	0.8732	0.0015	0.8724	0.0001	0.72	0.72
set-1-1-00694	0.8717	0.0013	0.8739	0.0001	0.70	0.69
set-1-1-00695	0.8694	0.0012	0.8702	0.0001	0.72	0.71
set-1-1-00696	0.8693	0.0013	0.8721	0.0001	0.68	0.69
set-1-1-00705	0.8590	0.0016	0.8598	0.0001	0.74	0.74
set-1-1-00706	0.8609	0.0012	0.8610	0.0001	0.71	0.71
set-1-1-00707	0.8559	0.0014	0.8580	0.0001	0.73	0.73
set-1-1-00708	0.8592	0.0013	0.8594	0.0001	0.70	0.70

Table H-10. Set-1-2 k_{eff} values for comparison

Case	Original		Modified		Original	Modified
	k_{eff}	sigma	k_{eff}	sigma	EALF	EALF
set-1-2-00441	0.9604	0.0013	0.9606	0.0001	0.88	0.88
set-1-2-00442	0.9653	0.0014	0.9617	0.0001	0.83	0.83
set-1-2-00443	0.9393	0.0013	0.9403	0.0001	0.88	0.88
set-1-2-00444	0.9406	0.0013	0.9418	0.0001	0.83	0.83
set-1-2-00453	0.9448	0.0014	0.9434	0.0001	0.90	0.90
set-1-2-00454	0.9434	0.0015	0.9444	0.0001	0.85	0.85
set-1-2-00455	0.9282	0.0013	0.9243	0.0001	0.90	0.90
set-1-2-00456	0.9234	0.0013	0.9258	0.0001	0.85	0.85
set-1-2-00477	0.8732	0.0013	0.8721	0.0001	0.86	0.87
set-1-2-00478	0.8729	0.0012	0.8725	0.0001	0.83	0.83
set-1-2-00479	0.8667	0.0013	0.8656	0.0001	0.86	0.86
set-1-2-00480	0.8655	0.0014	0.8670	0.0001	0.83	0.82
set-1-2-00489	0.8566	0.0021	0.8585	0.0001	0.89	0.89
set-1-2-00490	0.8589	0.0017	0.8591	0.0001	0.85	0.85
set-1-2-00491	0.8516	0.0013	0.8528	0.0001	0.88	0.88
set-1-2-00492	0.8548	0.0014	0.8542	0.0001	0.84	0.84

Table H-11. Set-1-3 k_{eff} values for comparison

Case	Original		Modified		Original	Modified
	k_{eff}	sigma	k_{eff}	sigma	EALF	EALF
set-1-3-00441	0.8425	0.0013	0.8421	0.0001	1.45	1.45
set-1-3-00442	0.8561	0.0014	0.8555	0.0001	1.31	1.31
set-1-3-00443	0.9437	0.0013	0.9433	0.0001	0.57	0.57
set-1-3-00444	0.9504	0.0014	0.9498	0.0001	0.52	0.52
set-1-3-00453	0.8289	0.0013	0.8280	0.0001	1.48	1.48
set-1-3-00454	0.8399	0.0014	0.8403	0.0001	1.35	1.35
set-1-3-00455	0.9244	0.0013	0.9271	0.0001	0.57	0.57
set-1-3-00456	0.9313	0.0013	0.9333	0.0001	0.52	0.52
set-1-3-00477	0.7732	0.0012	0.7720	0.0001	1.39	1.38
set-1-3-00478	0.7790	0.0012	0.7789	0.0001	1.29	1.29
set-1-3-00479	0.8794	0.0014	0.8799	0.0001	0.49	0.49
set-1-3-00480	0.8819	0.0013	0.8827	0.0001	0.45	0.45
set-1-3-00489	0.7597	0.0012	0.7604	0.0001	1.41	1.41
set-1-3-00490	0.7692	0.0012	0.7671	0.0001	1.32	1.32
set-1-3-00491	0.8624	0.0014	0.8666	0.0001	0.49	0.49
set-1-3-00492	0.8702	0.0016	0.8691	0.0001	0.46	0.46

Table H-12. Set-1-4 k_{eff} values for comparison

Case	Original		Modified		Original	Modified
	k_{eff}	sigma	k_{eff}	sigma	EALF	EALF
set-1-4-00333	0.8848	0.0014	0.8871	0.0001	1.41	1.41
set-1-4-00334	0.8942	0.0013	0.8940	0.0001	1.28	1.28
set-1-4-00335	0.9730	0.0015	0.9742	0.0001	0.59	0.59
set-1-4-00336	0.9785	0.0013	0.9759	0.0001	0.54	0.54
set-1-4-00345	0.8713	0.0013	0.8705	0.0001	1.45	1.44
set-1-4-00346	0.8761	0.0015	0.8765	0.0001	1.31	1.31
set-1-4-00347	0.9594	0.0014	0.9566	0.0001	0.59	0.59
set-1-4-00348	0.9588	0.0013	0.9583	0.0001	0.54	0.54
set-1-4-00369	0.7999	0.0012	0.7999	0.0001	1.35	1.35
set-1-4-00370	0.8056	0.0013	0.8040	0.0001	1.26	1.26
set-1-4-00371	0.8985	0.0013	0.8975	0.0001	0.51	0.50
set-1-4-00372	0.8976	0.0013	0.8983	0.0001	0.47	0.47
set-1-4-00381	0.7870	0.0013	0.7869	0.0001	1.38	1.38
set-1-4-00382	0.7908	0.0013	0.7912	0.0001	1.29	1.29
set-1-4-00383	0.8834	0.0017	0.8835	0.0001	0.51	0.51
set-1-4-00384	0.8836	0.0015	0.8842	0.0001	0.47	0.48

Table H-13. Set-1-5 k_{eff} values for comparison

Case	Original		Modified		Original	Modified
	k_{eff}	sigma	k_{eff}	sigma	EALF	EALF
set-1-5-00657	0.9445	0.0013	0.9437	0.0001	0.73	0.73
set-1-5-00658	0.9496	0.0015	0.9492	0.0001	0.69	0.69
set-1-5-00659	0.9303	0.0016	0.9323	0.0001	0.72	0.72
set-1-5-00660	0.9380	0.0014	0.9371	0.0001	0.69	0.69
set-1-5-00669	0.9298	0.0013	0.9290	0.0001	0.74	0.74
set-1-5-00670	0.9340	0.0016	0.9335	0.0001	0.71	0.71
set-1-5-00671	0.9194	0.0013	0.9180	0.0001	0.74	0.74
set-1-5-00672	0.9236	0.0015	0.9225	0.0001	0.71	0.71
set-1-5-00693	0.8526	0.0015	0.8531	0.0001	0.76	0.76
set-1-5-00694	0.8592	0.0013	0.8589	0.0001	0.73	0.73
set-1-5-00695	0.8535	0.0012	0.8533	0.0001	0.75	0.75
set-1-5-00696	0.8574	0.0014	0.8583	0.0001	0.72	0.72
set-1-5-00705	0.8421	0.0014	0.8414	0.0001	0.78	0.78
set-1-5-00706	0.8465	0.0015	0.8465	0.0001	0.75	0.74
set-1-5-00707	0.8386	0.0012	0.8417	0.0001	0.76	0.77
set-1-5-00708	0.8455	0.0012	0.8464	0.0001	0.74	0.73

Table H-14. Set-1-6 k_{eff} values for comparison

Case	Original		Modified		Original	Modified
	k_{eff}	sigma	k_{eff}	sigma	EALF	EALF
set-1-6-00441	0.9604	0.0013	0.9606	0.0001	0.88	0.88
set-1-6-00442	0.9653	0.0014	0.9617	0.0001	0.83	0.83
set-1-6-00443	0.9393	0.0013	0.9403	0.0001	0.88	0.88
set-1-6-00444	0.9406	0.0013	0.9418	0.0001	0.83	0.83
set-1-6-00453	0.9448	0.0014	0.9434	0.0001	0.90	0.90
set-1-6-00454	0.9434	0.0015	0.9444	0.0001	0.85	0.85
set-1-6-00455	0.9282	0.0013	0.9243	0.0001	0.90	0.90
set-1-6-00456	0.9234	0.0013	0.9258	0.0001	0.85	0.85
set-1-6-00477	0.8532	0.0013	0.8521	0.0001	0.92	0.92
set-1-6-00478	0.8552	0.0013	0.8571	0.0001	0.88	0.88
set-1-6-00479	0.8468	0.0012	0.8482	0.0001	0.91	0.91
set-1-6-00480	0.8537	0.0011	0.8530	0.0001	0.86	0.87
set-1-6-00489	0.8408	0.0012	0.8395	0.0001	0.95	0.94
set-1-6-00490	0.8436	0.0013	0.8440	0.0001	0.90	0.90
set-1-6-00491	0.8350	0.0015	0.8358	0.0001	0.93	0.93
set-1-6-00492	0.8407	0.0013	0.8403	0.0001	0.89	0.88

Table H-15. Set-1-7 k_{eff} values for comparison

Case	Original		Modified		Original	Modified
	k_{eff}	sigma	k_{eff}	sigma	EALF	EALF
set-1-7-00441	0.8425	0.0013	0.8421	0.0001	1.45	1.45
set-1-7-00442	0.8561	0.0014	0.8555	0.0001	1.31	1.31
set-1-7-00443	0.9437	0.0013	0.9433	0.0001	0.57	0.57
set-1-7-00444	0.9504	0.0014	0.9498	0.0001	0.52	0.52
set-1-7-00453	0.8289	0.0013	0.8280	0.0001	1.48	1.48
set-1-7-00454	0.8399	0.0014	0.8403	0.0001	1.35	1.35
set-1-7-00455	0.9244	0.0013	0.9271	0.0001	0.57	0.57
set-1-7-00456	0.9313	0.0013	0.9333	0.0001	0.52	0.52
set-1-7-00477	0.7439	0.0011	0.7439	0.0001	1.53	1.52
set-1-7-00478	0.7577	0.0014	0.7569	0.0001	1.41	1.40
set-1-7-00479	0.8643	0.0013	0.8648	0.0001	0.51	0.51
set-1-7-00480	0.8703	0.0014	0.8717	0.0001	0.47	0.47
set-1-7-00489	0.7332	0.0012	0.7334	0.0001	1.56	1.56
set-1-7-00490	0.7454	0.0012	0.7456	0.0001	1.44	1.44
set-1-7-00491	0.8531	0.0012	0.8522	0.0001	0.52	0.52
set-1-7-00492	0.8598	0.0015	0.8584	0.0001	0.48	0.48
set-1-7-00444	0.9504	0.0014	0.8421	0.0001	1.45	1.45

Table H-16. Set-1-8 k_{eff} values for comparison

Case	Original		Modified		Original	Modified
	k_{eff}	sigma	k_{eff}	sigma	EALF	EALF
set-1-8-00333	0.8848	0.0014	0.8871	0.0001	1.41	1.41
set-1-8-00334	0.8942	0.0013	0.8940	0.0001	1.28	1.28
set-1-8-00335	0.9730	0.0015	0.9742	0.0001	0.59	0.59
set-1-8-00336	0.9785	0.0013	0.9759	0.0001	0.54	0.54
set-1-8-00345	0.8713	0.0013	0.8705	0.0001	1.45	1.44
set-1-8-00346	0.8761	0.0015	0.8765	0.0001	1.31	1.31
set-1-8-00347	0.9594	0.0014	0.9566	0.0001	0.59	0.59
set-1-8-00348	0.9588	0.0013	0.9583	0.0001	0.54	0.54
set-1-8-00369	0.7741	0.0014	0.7733	0.0001	1.48	1.48
set-1-8-00370	0.7823	0.0013	0.7836	0.0001	1.37	1.37
set-1-8-00371	0.8828	0.0014	0.8835	0.0001	0.53	0.53
set-1-8-00372	0.8887	0.0013	0.8885	0.0001	0.49	0.49
set-1-8-00381	0.7621	0.0013	0.7617	0.0001	1.52	1.51
set-1-8-00382	0.7714	0.0013	0.7713	0.0001	1.40	1.40
set-1-8-00383	0.8686	0.0012	0.8701	0.0001	0.54	0.53
set-1-8-00384	0.8755	0.0013	0.8747	0.0001	0.50	0.50

Table H-17. Nuclides with the highest sensitivities for set-1-1 cases

Case Number	Nuclide	Mixture	Sensitivity coefficient	Total data-induced uncertainty % Δk/k	Case Number	Nuclide	Mixture	Sensitivity coefficient	Total data-induced uncertainty % Δk/k
					With Be				
657	h-1	waste	0.5017	0.6705	658	h-1	waste	0.4628	0.6287
	pu-239	waste	0.0932			pu-239	waste	0.0985	
	o-16	waste	0.0405			be	waste	0.0720	
	cl-35	MgO/NaCl	-0.0134			o-16	waste	0.0322	
						cl-35	MgO/NaCl	-0.0201	
659	h-1	waste	0.4727	0.6627	660	h-1	waste	0.4439	0.6313
	pu-239	waste	0.1057			pu-239	waste	0.1081	
	o-16	waste	0.0315			be	waste	0.0607	
	fe-56	ss pipe	0.0220			o-16	waste	0.0256	
	cl-35	MgO/NaCl	-0.0161			cl-35	MgO/NaCl	-0.0216	
						fe-56	ss pipe	0.0206	
669	h-1	waste	0.4986	0.6685	670	h-1	waste	0.4609	0.6268
	pu-239	waste	0.1030			pu-239	waste	0.1093	
	o-16	waste	0.0388			be	waste	0.0696	
	cl-35	MgO/NaCl	-0.0147			o-16	waste	0.0309	
						cl-35	MgO/NaCl	-0.0216	
671	h-1	waste	0.4745	0.6698	672	h-1	waste	0.4450	0.6397
	pu-239	waste	0.1128			pu-239	waste	0.1162	
	o-16	waste	0.0304			be	waste	0.0592	
	fe-56	ss pipe	0.0219			o-16	waste	0.0250	
	cl-35	MgO/NaCl	-0.0172			cl-35	MgO/NaCl	-0.0228	
						fe-56	ss pipe	0.0205	
693	h-1	waste	0.4726	0.6481	694	h-1	waste	0.4483	0.6224
	pu-239	waste	0.1205			pu-239	waste	0.1266	
	c-graphite	waste	0.0876			c-graphite	waste	0.0758	
	cl-35	MgO/NaCl	-0.0361			be	waste	0.0529	
	o-16	waste	0.0255			cl-35	MgO/NaCl	-0.0435	
						o-16	waste	0.0221	
						mg-24	MgO/NaCl	0.0093	
695	h-1	waste	0.4524	0.6513	696	h-1	waste	0.4331	0.6319
	pu-239	waste	0.1278			pu-239	waste	0.1315	
	c-graphite	waste	0.0737			c-graphite	waste	0.0649	
	cl-35	MgO/NaCl	-0.0349			be	waste	0.0466	
	fe-56	ss pipe	0.0225			cl-35	MgO/NaCl	-0.0407	
	o-16	waste	0.0212			fe-56	ss pipe	0.0223	
						o-16	waste	0.0187	
705	h-1	waste	0.4726	0.6464	706	h-1	waste	0.4476	0.6215
	pu-239	waste	0.1294			pu-239	waste	0.1365	
	c-graphite	waste	0.0857			c-graphite	waste	0.0743	
	cl-35	MgO/NaCl	-0.0377			be	waste	0.0517	
	o-16	waste	0.0249			cl-35	MgO/NaCl	-0.0449	
						o-16	waste	0.0217	
						mg-24	MgO/NaCl	0.0092	
707	h-1	waste	0.4545	0.6585	708	h-1	waste	0.4326	0.6404
	pu-239	waste	0.1351			pu-239	waste	0.1411	
	c-graphite	waste	0.0724			c-graphite	waste	0.0637	
	cl-35	MgO/NaCl	-0.0362			be	waste	0.0457	
	fe-56	ss pipe	0.0226			cl-35	MgO/NaCl	-0.0419	
	o-16	waste	0.0207			fe-56	ss pipe	0.0222	
						o-16	waste	0.0183	

Table H-18. Nuclides with the highest sensitivities for set-1-2 cases

Case Number	Nuclide	Mixture	Sensitivity coefficient	Total data-induced uncertainty % Δk/k	Case Number	Nuclide	Mixture	Sensitivity coefficient	Total data-induced uncertainty % Δk/k
					With Be				
441	h-poly	waste	0.4969	0.6674	442	h-poly	waste	0.4555	0.6236
	pu-239	waste	0.0890			pu-239	waste	0.0941	
	c	waste	0.0505			be	waste	0.0830	
						c	waste	0.0386	
						cl-35	MgO/NaCl	-0.0137	
443	h-poly	waste	0.4720	0.6623	444	h-poly	waste	0.4368	0.6280
	pu-239	waste	0.1002			pu-239	waste	0.1062	
	c	waste	0.0388			be	waste	0.0688	
	fe-56	ss pipe	0.0231			c	waste	0.0306	
	cl-35	MgO/NaCl	-0.0110			fe-56	ss pipe	0.0208	
						cl-35	MgO/NaCl	-0.0165	
453	h-poly	waste	0.4948	0.6632	454	h-poly	waste	0.4556	0.6233
	pu-239	waste	0.0988			pu-239	waste	0.1033	
	c	waste	0.0482			be	waste	0.0801	
	cl-35	MgO/NaCl	-0.0089			c	waste	0.0372	
						cl-35	MgO/NaCl	-0.0152	
455	h-poly	waste	0.4714	0.6671	456	h-poly	waste	0.4374	0.6371
	pu-239	waste	0.1095			pu-239	waste	0.1152	
	c	waste	0.0373			be	waste	0.0671	
	fe-56	ss pipe	0.0226			c	waste	0.0298	
	cl-35	MgO/NaCl	-0.0122			fe-56	ss pipe	0.0207	
						cl-35	MgO/NaCl	-0.0176	
477	h-poly	waste	0.4686	0.6475	478	h-poly	waste	0.4417	0.6201
	pu-239	waste	0.1160			pu-239	waste	0.1229	
	c-graphite	waste	0.1006			c-graphite	waste	0.0858	
	c	waste	0.0309			be	waste	0.0588	
	cl-35	MgO/NaCl	-0.0296			cl-35	MgO/NaCl	-0.0373	
	mg-24	MgO/NaCl	0.0081			c	waste	0.0264	
						mg-24	MgO/NaCl	0.0085	
479	h-poly	waste	0.4492	0.6501	480	h-poly	waste	0.4277	0.6306
	pu-239	waste	0.1251			pu-239	waste	0.1288	
	c-graphite	waste	0.0839			c-graphite	waste	0.0729	
	cl-35	MgO/NaCl	-0.0298			be	waste	0.0516	
	c	waste	0.0258			cl-35	MgO/NaCl	-0.0360	
	fe-56	ss pipe	0.0226			c	waste	0.0224	
						fe-56	ss pipe	0.0221	
489	h-poly	waste	0.4669	0.6451	490	h-poly	waste	0.4428	0.6198
	pu-239	waste	0.1261			pu-239	waste	0.1309	
	c-graphite	waste	0.0976			c-graphite	waste	0.0839	
	cl-35	MgO/NaCl	-0.0313			be	waste	0.0575	
	c	waste	0.0300			cl-35	MgO/NaCl	-0.0389	
	mg-24	MgO/NaCl	0.0083			c	waste	0.0258	
						mg-24	MgO/NaCl	0.0089	
491	h-poly	waste	0.4470	0.6574	492	h-poly	waste	0.4279	0.6384
	pu-239	waste	0.1358			pu-239	waste	0.1379	
	c-graphite	waste	0.0818			c-graphite	waste	0.0714	
	cl-35	MgO/NaCl	-0.0311			be	waste	0.0506	
	c	waste	0.0252			cl-35	MgO/NaCl	-0.0374	
	fe-56	ss pipe	0.0225			c	waste	0.0220	
						fe-56	ss pipe	0.0219	

Table H-19. Nuclides with the highest sensitivities for set-1-3 cases

Case Number	Nuclide	Mixture	Sensitivity coefficient	Total data-induced uncertainty % Δk/k	Case Number	Nuclide	Mixture	Sensitivity coefficient	Total data-induced uncertainty % Δk/k
					With Be				
441	h-1	waste	0.5632	0.6797	442	h-1	waste	0.5026	0.6258
	pu-239	waste	0.1138			pu-239	waste	0.1185	
	o-16	waste	0.0456			be	waste	0.1039	
	na-23	NaCl walls	0.0109			o-16	waste	0.0349	
						cl-35	MgO/NaCl	-0.0159	
443	h-1	waste	0.3487	0.6489	444	h-1	waste	0.3135	0.6067
	h-poly	poly pipe	0.1051			h-poly	poly pipe	0.0961	
	pu-239	waste	0.0809			pu-239	waste	0.0834	
	o-16	waste	0.0303			be	waste	0.0703	
	c	poly pipe	0.0199			o-16	waste	0.0229	
	cl-35	MgO/NaCl	-0.0107			c	poly pipe	0.0179	
						cl-35	MgO/NaCl	-0.0161	
453	h-1	waste	0.5562	0.6718	454	h-1	waste	0.5001	0.6231
	pu-239	waste	0.1250			pu-239	waste	0.1289	
	o-16	waste	0.0432			be	waste	0.0997	
	na-23	NaCl walls	0.0104			o-16	waste	0.0335	
	cl-35	MgO/NaCl	-0.0101			cl-35	MgO/NaCl	-0.0174	
455	h-1	waste	0.3459	0.6446	456	h-1	waste	0.3133	0.6077
	h-poly	poly pipe	0.1043			h-poly	poly pipe	0.0954	
	pu-239	waste	0.0904			pu-239	waste	0.0916	
	o-16	waste	0.0288			be	waste	0.0680	
	c	poly pipe	0.0195			o-16	waste	0.0221	
	cl-35	MgO/NaCl	-0.0118			c	poly pipe	0.0177	
						cl-35	MgO/NaCl	-0.0172	
477	h-1	waste	0.5083	0.6503	478	h-1	waste	0.4728	0.6175
	pu-239	waste	0.1425			pu-239	waste	0.1477	
	c-graphite	waste	0.1258			c-graphite	waste	0.1063	
	cl-35	MgO/NaCl	-0.0345			be	waste	0.0719	
	o-16	waste	0.0263			cl-35	MgO/NaCl	-0.0433	
	mg-24	MgO/NaCl	0.0103			o-16	waste	0.0223	
						mg-24	MgO/NaCl	0.0109	
479	h-1	waste	0.3016	0.6249	480	h-1	waste	0.2819	0.6009
	h-poly	poly pipe	0.1030			pu-239	waste	0.0996	
	pu-239	waste	0.0967			h-poly	poly pipe	0.0975	
	c-graphite	waste	0.0776			c-graphite	waste	0.0648	
	cl-35	MgO/NaCl	-0.0286			be	waste	0.0467	
	c	poly pipe	0.0172			cl-35	MgO/NaCl	-0.0341	
	o-16	waste	0.0166			c	poly pipe	0.0165	
						o-16	waste	0.0139	
489	h-1	waste	0.5048	0.6483	490	h-1	waste	0.4703	0.6175
	pu-239	waste	0.1530			pu-239	waste	0.1580	
	c-graphite	waste	0.1218			c-graphite	waste	0.1036	
	cl-35	MgO/NaCl	-0.0364			be	waste	0.0702	
	o-16	waste	0.0255			cl-35	MgO/NaCl	-0.0449	
	mg-24	MgO/NaCl	0.0104			o-16	waste	0.0217	
						mg-24	MgO/NaCl	0.0112	
491	h-1	waste	0.3001	0.6241	492	h-1	waste	0.2809	0.6023
	pu-239	waste	0.1069			pu-239	waste	0.1094	
	h-poly	poly pipe	0.1013			h-poly	poly pipe	0.0963	
	c-graphite	waste	0.0753			c-graphite	waste	0.0634	
	cl-35	MgO/NaCl	-0.0298			be	waste	0.0457	
	c	poly pipe	0.0171			cl-35	MgO/NaCl	-0.0352	
	o-16	waste	0.0160			c	poly pipe	0.0163	
						o-16	waste	0.0135	

Table H-20. Nuclides with the highest sensitivities for set-1-4 cases

Case Number	Nuclide	Mixture	Sensitivity coefficient	Total data-induced uncertainty % Δk/k	Case Number	Nuclide	Mixture	Sensitivity coefficient	Total data-induced uncertainty % Δk/k
					With Be				
333	h-poly	waste	0.5361	0.6703	334	h-poly	waste	0.4854	0.6217
	pu-239	waste	0.1074			pu-239	waste	0.1071	
	c	waste	0.0527			be	waste	0.1058	
						c	waste	0.0394	
						cl-35	MgO/NaCl	-0.0119	
335	h-poly	waste	0.3436	0.6535	336	h-poly	waste	0.3096	0.6124
	h-poly	poly pipe	0.0990			h-poly	poly pipe	0.0901	
	pu-239	waste	0.0773			pu-239	waste	0.0797	
	c	waste	0.0349			be	waste	0.0729	
	c	poly pipe	0.0201			c	waste	0.0261	
	cl-35	MgO/NaCl	-0.0081			c	poly pipe	0.0179	
						cl-35	MgO/NaCl	-0.0131	
345	h-poly	waste	0.5331	0.6648	346	h-poly	waste	0.4835	0.6197
	pu-239	waste	0.1164			pu-239	waste	0.1179	
	c	waste	0.0501			be	waste	0.1017	
						c	waste	0.0378	
						cl-35	MgO/NaCl	-0.0134	
347	h-poly	waste	0.3418	0.6491	348	h-poly	waste	0.3088	0.6112
	h-poly	poly pipe	0.0978			pu-239	waste	0.0889	
	pu-239	waste	0.0861			h-poly	poly pipe	0.0877	
	c	waste	0.0332			be	waste	0.0700	
	c	poly pipe	0.0196			c	waste	0.0250	
						c	poly pipe	0.0176	
						cl-35	MgO/NaCl	-0.0142	
369	h-poly	waste	0.4910	0.6484	370	h-poly	waste	0.4581	0.6157
	pu-239	waste	0.1350			pu-239	waste	0.1400	
	c-graphite	waste	0.1273			c-graphite	waste	0.1067	
	c	waste	0.0307			be	waste	0.0719	
	cl-35	MgO/NaCl	-0.0292			cl-35	MgO/NaCl	-0.0379	
						c	waste	0.0257	
371	h-poly	waste	0.3002	0.6307	372	h-poly	waste	0.2799	0.6061
	h-poly	poly pipe	0.0954			pu-239	waste	0.0974	
	pu-239	waste	0.0937			h-poly	poly pipe	0.0899	
	c-graphite	waste	0.0812			c-graphite	waste	0.0675	
	cl-35	MgO/NaCl	-0.0252			be	waste	0.0480	
	c	waste	0.0197			cl-35	MgO/NaCl	-0.0307	
	c	poly pipe	0.0171			c	waste	0.0164	
						c	poly pipe	0.0162	
381	h-poly	waste	0.4923	0.6458	382	h-poly	waste	0.4596	0.6162
	pu-239	waste	0.1422			pu-239	waste	0.1476	
	c-graphite	waste	0.1238			c-graphite	waste	0.1048	
	cl-35	MgO/NaCl	-0.0312			be	waste	0.0705	
	c	waste	0.0299			cl-35	MgO/NaCl	-0.0396	
						c	waste	0.0253	
						mg-24	MgO/NaCl	0.0100	
383	h-poly	waste	0.2979	0.6311	384	h-poly	waste	0.2797	0.6071
	pu-239	waste	0.1048			pu-239	waste	0.1063	
	h-poly	poly pipe	0.0947			h-poly	poly pipe	0.0884	
	c-graphite	waste	0.0788			c-graphite	waste	0.0659	
	cl-35	MgO/NaCl	-0.0263			be	waste	0.0469	
	c	waste	0.0191			cl-35	MgO/NaCl	-0.0318	
	c	poly pipe	0.0169			c	poly pipe	0.0162	
						c	waste	0.0160	

Table H-21. Nuclides with the highest sensitivities for set-1-5 cases

Case Number	Nuclide	Mixture	Sensitivity coefficient	Total data-induced uncertainty % Δk/k	Case Number	Nuclide	Mixture	Sensitivity coefficient	Total data-induced uncertainty % Δk/k
					With Be				
657	h-1	waste	0.5017	0.6705	658	h-1	waste	0.4628	0.6287
	pu-239	waste	0.0932			pu-239	waste	0.0985	
	o-16	waste	0.0405			be	waste	0.0720	
	cl-35	MgO/NaCl	-0.0134			o-16	waste	0.0322	
	na-23	NaCl walls	0.0080			cl-35	MgO/NaCl	-0.0201	
659	h-1	waste	0.4727	0.6627	660	h-1	waste	0.4439	0.6313
	pu-239	waste	0.1057			pu-239	waste	0.1081	
	o-16	waste	0.0315			be	waste	0.0607	
	fe-56	ss pipe	0.0220			o-16	waste	0.0256	
	cl-35	MgO/NaCl	-0.0161			cl-35	MgO/NaCl	-0.0216	
						fe-56	ss pipe	0.0206	
669	h-1	waste	0.4986	0.6685	670	h-1	waste	0.4609	0.6268
	pu-239	waste	0.1030			pu-239	waste	0.1093	
	o-16	waste	0.0388			be	waste	0.0696	
	cl-35	MgO/NaCl	-0.0147			o-16	waste	0.0309	
						cl-35	MgO/NaCl	-0.0216	
671	h-1	waste	0.4745	0.6698	672	h-1	waste	0.4450	0.6397
	pu-239	waste	0.1128			pu-239	waste	0.1162	
	o-16	waste	0.0304			be	waste	0.0592	
	fe-56	ss pipe	0.0219			o-16	waste	0.0250	
	cl-35	MgO/NaCl	-0.0172			cl-35	MgO/NaCl	-0.0228	
						fe-56	ss pipe	0.0205	
693	h-1	waste	0.5104	0.6626	694	h-1	waste	0.4798	0.6324
	pu-239	waste	0.1245			pu-239	waste	0.1298	
	o-16	waste	0.0562			be	waste	0.0584	
	cl-35	MgO/NaCl	-0.0345			o-16	waste	0.0484	
	mg-24	MgO/NaCl	0.0093			cl-35	MgO/NaCl	-0.0419	
	na-23	MgO/NaCl	0.0083			mg-24	MgO/NaCl	0.0101	
	na-23	NaCl walls	0.0080			na-23	MgO/NaCl	0.0081	
695	h-1	waste	0.4876	0.6624	696	h-1	waste	0.4594	0.6387
	pu-239	waste	0.1298			pu-239	waste	0.1360	
	o-16	waste	0.0464			be	waste	0.0508	
	cl-35	MgO/NaCl	-0.0335			o-16	waste	0.0404	
	fe-56	ss pipe	0.0241			cl-35	MgO/NaCl	-0.0394	
						fe-56	ss pipe	0.0232	
705	h-1	waste	0.5061	0.6616	706	h-1	waste	0.4785	0.6305
	pu-239	waste	0.1354			pu-239	waste	0.1394	
	o-16	waste	0.0546			be	waste	0.0570	
	cl-35	MgO/NaCl	-0.0359			o-16	waste	0.0471	
	mg-24	MgO/NaCl	0.0094			cl-35	MgO/NaCl	-0.0434	
	na-23	MgO/NaCl	0.0082			mg-24	MgO/NaCl	0.0101	
						na-23	MgO/NaCl	0.0080	
707	h-1	waste	0.4844	0.6688	708	h-1	waste	0.4601	0.6488
	pu-239	waste	0.1404			pu-239	waste	0.1437	
	o-16	waste	0.0451			be	waste	0.0500	
	cl-35	MgO/NaCl	-0.0347			cl-35	MgO/NaCl	-0.0408	
	fe-56	ss pipe	0.0239			o-16	waste	0.0396	
						fe-56	ss pipe	0.0233	

Table H-22. Nuclides with the highest sensitivities for set-1-6 cases

Case Number	Nuclide	Mixture	Sensitivity coefficient	Total data-induced uncertainty % Δk/k	Case Number	Nuclide	Mixture	Sensitivity coefficient	Total data-induced uncertainty % Δk/k
					With Be				
441	h-poly	waste	0.4969	0.6674	442	h-poly	waste	0.4555	0.6236
	pu-239	waste	0.0890			pu-239	waste	0.0941	
	c	waste	0.0505			be	waste	0.0830	
						c	waste	0.0386	
						cl-35	MgO/NaCl	-0.0137	
443	h-poly	waste	0.4720	0.6623	444	h-poly	waste	0.4368	0.6280
	pu-239	waste	0.1002			pu-239	waste	0.1062	
	c	waste	0.0388			be	waste	0.0688	
	fe-56	ss pipe	0.0231			c	waste	0.0306	
	cl-35	MgO/NaCl	-0.0110			fe-56	ss pipe	0.0208	
						cl-35	MgO/NaCl	-0.0165	
453	h-poly	waste	0.4948	0.6632	454	h-poly	waste	0.4556	0.6233
	pu-239	waste	0.0988			pu-239	waste	0.1033	
	c	waste	0.0482			be	waste	0.0801	
	cl-35	MgO/NaCl	-0.0089			c	waste	0.0372	
						cl-35	MgO/NaCl	-0.0152	
455	h-poly	waste	0.4714	0.6671	456	h-poly	waste	0.4374	0.6371
	pu-239	waste	0.1095			pu-239	waste	0.1152	
	c	waste	0.0373			be	waste	0.0671	
	fe-56	ss pipe	0.0226			c	waste	0.0298	
	cl-35	MgO/NaCl	-0.0122			fe-56	ss pipe	0.0207	
						cl-35	MgO/NaCl	-0.0176	
477	h-poly	waste	0.5068	0.6564	478	h-poly	waste	0.4717	0.6273
	pu-239	waste	0.1223			pu-239	waste	0.1287	
	o-16	waste	0.0361			be	waste	0.0652	
	c	waste	0.0349			cl-35	MgO/NaCl	-0.0353	
	cl-35	MgO/NaCl	-0.0278			o-16	waste	0.0304	
	mg-24	MgO/NaCl	0.0084			c	waste	0.0292	
	na-23	NaCl walls	0.0083			mg-24	MgO/NaCl	0.0092	
	si-28	waste	0.0081						
479	h-poly	waste	0.4841	0.6583	480	h-poly	waste	0.4565	0.6349
	pu-239	waste	0.1293			pu-239	waste	0.1328	
	o-16	waste	0.0295			be	waste	0.0566	
	c	waste	0.0289			cl-35	MgO/NaCl	-0.0345	
	cl-35	MgO/NaCl	-0.0283			o-16	waste	0.0253	
	fe-56	ss pipe	0.0240			c	waste	0.0246	
						fe-56	ss pipe	0.0232	
489	h-poly	waste	0.5059	0.6548	490	h-poly	waste	0.4733	0.6251
	pu-239	waste	0.1307			pu-239	waste	0.1365	
	o-16	waste	0.0352			be	waste	0.0635	
	c	waste	0.0339			cl-35	MgO/NaCl	-0.0371	
	cl-35	MgO/NaCl	-0.0292			o-16	waste	0.0296	
	mg-24	MgO/NaCl	0.0086			c	waste	0.0285	
	na-23	NaCl walls	0.0081			mg-24	MgO/NaCl	0.0093	
491	h-poly	waste	0.4837	0.6672	492	h-poly	waste	0.4560	0.6432
	pu-239	waste	0.1379			pu-239	waste	0.1421	
	cl-35	MgO/NaCl	-0.0295			be	waste	0.0555	
	o-16	waste	0.0288			cl-35	MgO/NaCl	-0.0359	
	c	waste	0.0282			o-16	waste	0.0248	
	fe-56	ss pipe	0.0241			c	waste	0.0241	
						fe-56	ss pipe	0.0231	

Table H-23. Nuclides with the highest sensitivities for set-1-7 cases

Case Number	Nuclide	Mixture	Sensitivity coefficient	Total data-induced uncertainty % Δk/k	Case Number	Nuclide	Mixture	Sensitivity coefficient	Total data-induced uncertainty % Δk/k
					With Be				
441	h-1	waste	0.5632	0.6797	442	h-1	waste	0.5026	0.6258
	pu-239	waste	0.1138			pu-239	waste	0.1185	
	o-16	waste	0.0456			be	waste	0.1039	
	na-23	NaCl walls	0.0109			o-16	waste	0.0349	
						cl-35	MgO/NaCl	-0.0159	
443	h-1	waste	0.3487	0.6489	444	h-1	waste	0.3135	0.6067
	h-poly	poly pipe	0.1051			h-poly	poly pipe	0.0961	
	pu-239	waste	0.0809			pu-239	waste	0.0834	
	o-16	waste	0.0303			be	waste	0.0703	
	c	poly pipe	0.0199			o-16	waste	0.0229	
	cl-35	MgO/NaCl	-0.0107			c	poly pipe	0.0179	
						cl-35	MgO/NaCl	-0.0161	
453	h-1	waste	0.5562	0.6718	454	h-1	waste	0.5001	0.6231
	pu-239	waste	0.1250			pu-239	waste	0.1289	
	o-16	waste	0.0432			be	waste	0.0997	
	na-23	NaCl walls	0.0104			o-16	waste	0.0335	
	cl-35	MgO/NaCl	-0.0101			cl-35	MgO/NaCl	-0.0174	
455	h-1	waste	0.3459	0.6446	456	h-1	waste	0.3133	0.6077
	h-poly	poly pipe	0.1043			h-poly	poly pipe	0.0954	
	pu-239	waste	0.0904			pu-239	waste	0.0916	
	o-16	waste	0.0288			be	waste	0.0680	
	c	poly pipe	0.0195			o-16	waste	0.0221	
	cl-35	MgO/NaCl	-0.0118			c	poly pipe	0.0177	
						cl-35	MgO/NaCl	-0.0172	
477	h-1	waste	0.5583	0.6719	478	h-1	waste	0.5148	0.6325
	pu-239	waste	0.1534			pu-239	waste	0.1550	
	o-16	waste	0.0705			be	waste	0.0807	
	cl-35	MgO/NaCl	-0.0326			o-16	waste	0.0592	
	na-23	NaCl walls	0.0111			cl-35	MgO/NaCl	-0.0414	
	mg-24	MgO/NaCl	0.0109			mg-24	MgO/NaCl	0.0119	
	si-28	waste	0.0099			na-23	MgO/NaCl	0.0100	
	na-23	MgO/NaCl	0.0097						
479	h-1	waste	0.3218	0.6348	480	h-1	waste	0.2971	0.6068
	h-poly	poly pipe	0.1128			pu-239	waste	0.1037	
	pu-239	waste	0.1014			h-poly	poly pipe	0.1036	
	o-16	waste	0.0435			be	waste	0.0512	
	cl-35	MgO/NaCl	-0.0271			o-16	waste	0.0359	
	c	poly pipe	0.0180			cl-35	MgO/NaCl	-0.0326	
						c	poly pipe	0.0171	
489	h-1	waste	0.5568	0.6701	490	h-1	waste	0.5111	0.6313
	pu-239	waste	0.1608			pu-239	waste	0.1656	
	o-16	waste	0.0684			be	waste	0.0784	
	cl-35	MgO/NaCl	-0.0343			o-16	waste	0.0575	
	na-23	NaCl walls	0.0112			cl-35	MgO/NaCl	-0.0433	
	mg-24	MgO/NaCl	0.0111			mg-24	MgO/NaCl	0.0120	
	na-23	MgO/NaCl	0.0099			na-23	MgO/NaCl	0.0103	
	si-28	waste	0.0095						
491	h-1	waste	0.3195	0.6337	492	h-1	waste	0.2969	0.6078
	h-poly	poly pipe	0.1115			pu-239	waste	0.1122	
	pu-239	waste	0.1112			h-poly	poly pipe	0.1052	
	o-16	waste	0.0419			be	waste	0.0500	
	cl-35	MgO/NaCl	-0.0283			o-16	waste	0.0350	
	c	poly pipe	0.0178			cl-35	MgO/NaCl	-0.0339	
						c	poly pipe	0.0170	

Table H-24. Nuclides with the highest sensitivities for set-1-8 cases

Case Number	Nuclide	Mixture	Sensitivity coefficient	Total data-induced uncertainty % Δk/k	Case Number	Nuclide	Mixture	Sensitivity coefficient	Total data-induced uncertainty % Δk/k
					With Be				
333	h-poly	waste	0.5361	0.6703	334	h-poly	waste	0.4854	0.6217
	pu-239	waste	0.1074			pu-239	waste	0.1071	
	c	waste	0.0527			be	waste	0.1058	
	na-23	NaCl walls	0.0097			c	waste	0.0394	
						cl-35	MgO/NaCl	-0.0119	
335	h-poly	waste	0.3436	0.6535	336	h-poly	waste	0.3096	0.6124
	h-poly	poly pipe	0.0990			h-poly	poly pipe	0.0901	
	pu-239	waste	0.0773			pu-239	waste	0.0797	
	c	waste	0.0349			be	waste	0.0729	
	c	poly pipe	0.0201			c	waste	0.0261	
						c	poly pipe	0.0179	
						cl-35	MgO/NaCl	-0.0131	
345	h-poly	waste	0.5331	0.6648	346	h-poly	waste	0.4835	0.6197
	pu-239	waste	0.1164			pu-239	waste	0.1179	
	c	waste	0.0501			be	waste	0.1017	
	na-23	NaCl walls	0.0094			c	waste	0.0378	
						cl-35	MgO/NaCl	-0.0134	
347	h-poly	waste	0.3418	0.6491	348	h-poly	waste	0.3088	0.6112
	h-poly	poly pipe	0.0978			pu-239	waste	0.0889	
	pu-239	waste	0.0861			h-poly	poly pipe	0.0877	
	c	waste	0.0332			be	waste	0.0700	
	c	poly pipe	0.0196			c	waste	0.0250	
	cl-35	MgO/NaCl	-0.0091			c	poly pipe	0.0176	
						cl-35	MgO/NaCl	-0.0142	
369	h-poly	waste	0.5404	0.6607	370	h-poly	waste	0.4998	0.6261
	pu-239	waste	0.1442			pu-239	waste	0.1454	
	o-16	waste	0.0461			be	waste	0.0811	
	c	waste	0.0351			o-16	waste	0.0385	
	cl-35	MgO/NaCl	-0.0272			cl-35	MgO/NaCl	-0.0359	
	na-23	NaCl walls	0.0105			c	waste	0.0291	
	si-28	waste	0.0103			mg-24	MgO/NaCl	0.0104	
371	h-poly	waste	0.3198	0.6394	372	h-poly	waste	0.2966	0.6107
	h-poly	poly pipe	0.1048			pu-239	waste	0.0992	
	pu-239	waste	0.0986			h-poly	poly pipe	0.0970	
	o-16	waste	0.0293			be	waste	0.0528	
	cl-35	MgO/NaCl	-0.0236			cl-35	MgO/NaCl	-0.0292	
	c	waste	0.0220			o-16	waste	0.0242	
	c	poly pipe	0.0180			c	waste	0.0180	
						c	poly pipe	0.0169	
381	h-poly	waste	0.5389	0.6594	382	h-poly	waste	0.4963	0.6240
	pu-239	waste	0.1520			pu-239	waste	0.1561	
	o-16	waste	0.0445			be	waste	0.0785	
	c	waste	0.0341			cl-35	MgO/NaCl	-0.0376	
	cl-35	MgO/NaCl	-0.0289			o-16	waste	0.0371	
	na-23	NaCl walls	0.0103			c	waste	0.0281	
	si-28	waste	0.0099			mg-24	MgO/NaCl	0.0105	
383	h-poly	waste	0.3184	0.6382	384	h-poly	waste	0.2954	0.6106
	pu-239	waste	0.1079			pu-239	waste	0.1096	
	h-poly	poly pipe	0.1040			h-poly	poly pipe	0.0977	
	o-16	waste	0.0283			be	waste	0.0514	
	cl-35	MgO/NaCl	-0.0248			cl-35	MgO/NaCl	-0.0305	
	c	waste	0.0213			o-16	waste	0.0234	
	c	poly pipe	0.0178			c	waste	0.0175	
						c	poly pipe	0.0168	

H.3 SIMILARITY ASSESSMENT

A subset of the critical experiments from *The SCALE Verified, Archived Library of Inputs and Data—VALID* [39] was used with TSUNAMI-IP to identify potentially applicable experiments for k_{eff} validation. Results from all of the chosen experiments are also included in the *International Handbook of Evaluated Criticality Safety Benchmark Experiments* [36]. The set of experiments includes 81 experiments from the Pu-solution-thermal category (PST), 49 from the mixed-composition-thermal category (MCT), and 10 from the mixed-solution-thermal category (MST), for a total of 140 experiments. The EALF range of the benchmarks is from 0.04 to 0.95 eV, with the majority being on the lower end of the spectrum. The EALF range from Tables H-9 through H-16 is 0.45 to 1.56 eV. Finding benchmarks with EALFs in the energy range of ~0.7 to 2 eV is a known challenge. The experiments are similar to the applications in the ^{239}Pu content, with an average of > 95% ^{239}Pu in the Pu content. The Pu solution experiments are water moderated and are in the thermal energy region. The mixed composition and mixed solution experiment systems cover mostly the upper thermal into intermediate energy regions.

As discussed above, c_k values are calculated by comparing the select applications to each of the benchmark cases. None of the benchmarks achieved the desired c_k value of 0.8 or higher. This prompted consideration of experiments with smaller c_k values, as well as the need for an additional margin because highly applicable benchmarks were lacking. Tables H-25 through H-32 list the numbers of benchmarks, with c_k values in each range listed for each application case. Case specifics (e.g., moderator type, filler type) are also included for reference.

Table H-25. c_k values for set-1-1 cases

Case	Moderator		Filler		Can	Pipe material	Be	$c_k > 0.7$	$c_k > 0.6$	$c_k > 0.5$
		grams		grams	grams	cm	grams			
set-1-1-00657	H_2O	1016	graphite	0	0	0.0010	0	20	88	135
set-1-1-00658							585	0	88	138
set-1-1-00659						0.7112	0	34	89	139
set-1-1-00660							585	4	88	139
set-1-1-00669					500	0.0010	0	20	88	136
set-1-1-00670							585	0	88	138
set-1-1-00671						0.7112	0	26	89	138
set-1-1-00672							585	3	88	139
set-1-1-00693				2,000	0	0.0010	0	0	65	102
set-1-1-00694							585	0	29	100
set-1-1-00695						0.7112	0	0	87	133
set-1-1-00696							585	0	72	132
set-1-1-00705					500	0.0010	0	0	64	102
set-1-1-00706							585	0	27	98
set-1-1-00707						0.7112	0	0	85	122
set-1-1-00708							585	0	62	118

Table H-26. c_k values for set-1-2 cases

Case	Moderator		Filler		Can	Pipe material		Be	$c_k > 0.7$	$c_k > 0.6$	$c_k > 0.5$
		grams		grams	grams		cm	grams			
set-1-2-00441	CH_2	710.5	graphite	0	0	ss	0.0010	0	0	87	105
set-1-2-00442								585	0	50	105
set-1-2-00443							0.7112	0	3	88	127
set-1-2-00444								585	0	68	131
set-1-2-00453					500		0.0010	0	0	87	105
set-1-2-00454								585	0	46	104
set-1-2-00455							0.7112	0	0	88	105
set-1-2-00456								585	0	53	106
set-1-2-00477				2,000	0		0.0010	0	0	19	90
set-1-2-00478								585	0	3	92
set-1-2-00479							0.7112	0	0	40	92
set-1-2-00480								585	0	16	92
set-1-2-00489					500		0.0010	0	0	19	90
set-1-2-00490								585	0	3	92
set-1-2-00491							0.7112	0	0	31	92
set-1-2-00492								585	0	9	92

Table H-27. c_k values for set-1-3 cases

Case	Moderator		Filler		Can	Pipe material		Be	$c_k > 0.7$	$c_k > 0.6$	$c_k > 0.5$
		grams		grams	grams		cm	grams			
set-1-3-00441	H_2O	710.5	graphite	0	0	poly	0.0010	0	5	87	101
set-1-3-00442								585	0	59	99
set-1-3-00443							0.7112	0	87	96	140
set-1-3-00444								585	37	95	140
set-1-3-00453					500		0.0010	0	4	87	100
set-1-3-00454								585	0	55	99
set-1-3-00455							0.7112	0	86	96	140
set-1-3-00456								585	35	93	140
set-1-3-00477				2,000	0		0.0010	0	0	20	89
set-1-3-00478								585	0	3	89
set-1-3-00479							0.7112	0	9	88	140
set-1-3-00480								585	0	88	140
set-1-3-00489					500		0.0010	0	0	20	89
set-1-3-00490								585	0	3	89
set-1-3-00491							0.7112	0	7	88	140
set-1-3-00492								585	0	89	140

Table H-28. c_k values for set-1-4 cases

Case	Moderator		Filler		Can	Pipe material		Be	$c_k > 0.7$	$c_k > 0.6$	$c_k > 0.5$
		grams		grams	grams		cm	grams			
set-1-4-00333	CH_2	557.9	graphite	0	0	poly	0.0010	0	0	62	90
set-1-4-00334								585	0	19	92
set-1-4-00335							0.7112	0	38	90	140
set-1-4-00336								585	3	91	140
set-1-4-00345					500		0.0010	0	0	61	90
set-1-4-00346								585	0	19	92
set-1-4-00347							0.7112	0	36	90	140
set-1-4-00348								585	1	91	140
set-1-4-00369				2,000	0		0.0010	0	0	3	88
set-1-4-00370								585	0	0	88
set-1-4-00371							0.7112	0	0	88	138
set-1-4-00372								585	0	88	140
set-1-4-00381					500		0.0010	0	0	3	88
set-1-4-00382								585	0	0	88
set-1-4-00383							0.7112	0	0	88	139
set-1-4-00384								585	0	88	140

Table H-29. c_k values for set-1-5 cases

Case	Moderator		Filler		Can	Pipe material		Be	$c_k > 0.7$	$c_k > 0.6$	$c_k > 0.5$
		grams		grams	grams		cm	grams			
set-1-5-00657	H_2O	1016	generic	0	0	ss	0.0010	0	20	88	135
set-1-5-00658								585	0	88	138
set-1-5-00659							0.7112	0	34	89	139
set-1-5-00660								585	4	88	139
set-1-5-00669					500		0.0010	0	20	88	136
set-1-5-00670								585	0	88	138
set-1-5-00671							0.7112	0	26	89	138
set-1-5-00672								585	3	88	139
set-1-5-00693				2,000	0		0.0010	0	0	56	96
set-1-5-00694								585	0	29	98
set-1-5-00695							0.7112	0	0	87	105
set-1-5-00696								585	0	72	128
set-1-5-00705					500		0.0010	0	0	60	96
set-1-5-00706								585	0	26	98
set-1-5-00707							0.7112	0	0	84	103
set-1-5-00708								585	0	61	104

Table H-30. c_k values for set-1-6 cases

Case	Moderator		Filler		Can	Pipe material		Be	$c_k > 0.7$	$c_k > 0.6$	$c_k > 0.5$
		grams		grams	grams		cm	grams			
set-1-6-00441	CH_2	710.5	generic	0	0	ss	0.0010	0	0	87	105
set-1-6-00442								585	0	50	105
set-1-6-00443							0.7112	0	3	88	127
set-1-6-00444								585	0	68	131
set-1-6-00453					500		0.0010	0	0	87	105
set-1-6-00454								585	0	46	104
set-1-6-00455							0.7112	0	0	88	105
set-1-6-00456								585	0	53	106
set-1-6-00477				2,000	0		0.0010	0	0	19	90
set-1-6-00478								585	0	3	91
set-1-6-00479							0.7112	0	0	43	92
set-1-6-00480								585	0	17	92
set-1-6-00489					500		0.0010	0	0	19	90
set-1-6-00490								585	0	3	90
set-1-6-00491							0.7112	0	0	36	92
set-1-6-00492								585	0	14	92

Table H-31. c_k values for set-1-7 cases

Case	Moderator		Filler		Can	Pipe material		Be	$c_k > 0.7$	$c_k > 0.6$	$c_k > 0.5$
		grams		grams	grams		cm	grams			
set-1-7-00441	H_2O	710.5	generic	0	0	poly	0.0010	0	5	87	101
set-1-7-00442								585	0	59	99
set-1-7-00443							0.7112	0	87	96	140
set-1-7-00444								585	37	95	140
set-1-7-00453					500		0.0010	0	4	87	100
set-1-7-00454								585	0	55	99
set-1-7-00455							0.7112	0	86	96	140
set-1-7-00456								585	35	93	140
set-1-7-00477				2,000	0		0.0010	0	0	17	88
set-1-7-00478								585	0	2	88
set-1-7-00479							0.7112	0	7	88	139
set-1-7-00480								585	0	88	140
set-1-7-00489					500		0.0010	0	0	17	88
set-1-7-00490								585	0	2	88
set-1-7-00491							0.7112	0	7	88	139
set-1-7-00492								585	0	88	140

Table H-32. c_k values for set-1-8 cases

Case	Moderator		Filler		Can	Pipe material		Be	$c_k > 0.7$	$c_k > 0.6$	$c_k > 0.5$
		grams		grams	grams		cm	grams			
set-1-8-00333	CH_2	557.9	generic	0	0	poly	0.0010	0	0	62	90
set-1-8-00334								585	0	19	92
set-1-8-00335							0.7112	0	38	90	140
set-1-8-00336								585	3	91	140
set-1-8-00345					500		0.0010	0	0	61	90
set-1-8-00346								585	0	19	92
set-1-8-00347							0.7112	0	36	90	140
set-1-8-00348								585	1	91	140
set-1-8-00369				2,000	0		0.0010	0	0	3	88
set-1-8-00370								585	0	0	87
set-1-8-00371							0.7112	0	0	88	137
set-1-8-00372								585	0	88	140
set-1-8-00381					500		0.0010	0	0	3	88
set-1-8-00382								585	0	0	87
set-1-8-00383							0.7112	0	0	88	137
set-1-8-00384								585	0	88	140

H.4 BIAS AND BIAS UNCERTAINTY DETERMINATION

Using the available c_k data, the USLSTATS program was implemented to determine bias and bias uncertainty by trending on the c_k value. Tables H-33 through H-40 list the results by c_k threshold value. For cases in which there were less than 20 experiments, bias and bias uncertainty are not listed, because there are not enough data points to determine a reliable value. There is a minimum of 26 experiments for each case with a c_k value > 0.5, but there are no data to support using c_k values in this range. The bias and bias uncertainty values with c_k values > 0.5 are smaller than the bias and bias uncertainty values with c_k values > 0.6. Even though there more are smaller similarity values (c_k values < 0.6), the bias and bias uncertainty values should be larger due to the smaller degree of similarity.

S/U techniques provide tools for generating a quantitative, defensible estimate of what an appropriate margin might be. Examining the nuclides and reactions that contribute significantly to data-induced uncertainty will indicate the important processes to be validated. Elements such as Be and chlorine might be entirely absent from the validation set or only poorly represented. For these nuclides, the data-induced uncertainty provides an estimate for the magnitude of the bias that could occur in the application. This approach has been used in several other applications [40, 41, 42].

H.5 ADDITIONAL VALIDATION MARGINS

The magnitude of the data-induced uncertainty in the application also bounds the expected magnitude of the bias if there are no applicable benchmarks. Using this value might be more efficient than investing effort in developing and defending a lower additional margin. A demonstration that the data-induced uncertainty bounds the bias manifested for the most fast or thermal spectrum benchmark systems is provided in Section 3.2.5 of Scaglione et al. [43]. It is not clear if the bias of intermediate spectrum systems is also bounded by the nuclear data–induced uncertainty in k_{eff}. It is likely that the most applicable benchmark experiments would be used to develop a bias and bias uncertainty, and this additional margin would be added to ensure sufficient conservatism in the USL.

For set-1-1, case number 657, the total data-induced uncertainty is 0.6705 %$\Delta k/k$. Given the system k_{eff} value of 0.9437 (for the modified case), the absolute data-induced uncertainty is 0.6327 %Δk, which would be combined with the bias and bias uncertainty and any other applicable additional margins to determine the maximum subcritical k_{eff} value. Tables H-33 through H-40 also include the total data-induced uncertainty and the absolute data-induced uncertainty for each case.

A more complex approach could be to justify an additional margin based on the fact that the available benchmarks provide validation for some incident neutron energies. This approach could be useful for important nuclides that are present in the validation suite but that have energy-dependent sensitivity profiles that differ significantly from the application model. These profiles can be reviewed to determine whether validation exists for an energy range or perhaps multiple energy ranges. For example, it might be evident that high-energy cross sections are validated because fission neutrons are born at high energies in all systems. Thermal cross sections are generally well validated due to the many available thermal benchmark experiments. Therefore, an estimate of the unvalidated portion of the profile may be generated and used to estimate the magnitude of the remaining potential bias in the application in the energy ranges with weaker validation. In some cases, an energy range in the application might have significantly less sensitivity than that present in relevant benchmarks. An additional margin for these situations would not likely be needed because the low sensitivity directly indicates a low potential for bias.

Table H-33. Bias, bias uncertainty, and data-induced uncertainty for set-1-1 cases

Case	ck > 0.7 bias and bias uncertainty	ck > 0.6 bias and bias uncertainty	ck > 0.5 bias and bias uncertainty	Modified k_{eff}	Total data-induced uncertainty	Absolute data-induced uncertainty
set-1-1-00657	0.0822	0.0178	0.0108	0.9437	0.006705	0.006327
set-1-1-00658		0.0216	0.0114	0.9492	0.006287	0.005968
set-1-1-00659	0.0406	0.0168	0.0108	0.9323	0.006627	0.006178
set-1-1-00660		0.0211	0.0113	0.9371	0.006313	0.005916
set-1-1-00669	0.0832	0.0179	0.0108	0.9290	0.006685	0.006211
set-1-1-00670		0.0220	0.0114	0.9335	0.006268	0.005851
set-1-1-00671	0.0574	0.0172	0.0108	0.9180	0.006698	0.006148
set-1-1-00672		0.0214	0.0114	0.9225	0.006397	0.005901
set-1-1-00693		0.0316	0.0145	0.8724	0.006481	0.005654
set-1-1-00694		0.0854	0.0173	0.8739	0.006224	0.005439
set-1-1-00695		0.0226	0.0114	0.8702	0.006513	0.005668
set-1-1-00696		0.0315	0.0122	0.8721	0.006319	0.005511
set-1-1-00705		0.0325	0.0145	0.8598	0.006464	0.005558
set-1-1-00706		0.0913	0.0183	0.8610	0.006215	0.005351
set-1-1-00707		0.0236	0.0119	0.8580	0.006585	0.005650
set-1-1-00708		0.0370	0.0132	0.8594	0.006404	0.005503

Table H-34. Bias, bias uncertainty, and data-induced uncertainty for set-1-2 cases

Case	ck > 0.7 bias and bias uncertainty	ck > 0.6 bias and bias uncertainty	ck > 0.5 bias and bias uncertainty	Modified k_{eff}	Total data-induced uncertainty	Absolute data-induced uncertainty
set-1-2-00441		0.0199	0.0128	0.9606	0.006674	0.006411
set-1-2-00442		0.0415	0.0149	0.9617	0.006236	0.005998
set-1-2-00443		0.0194	0.0113	0.9403	0.006623	0.006228
set-1-2-00444		0.0290	0.0121	0.9418	0.006280	0.005914
set-1-2-00453		0.0202	0.0128	0.9434	0.006632	0.006256
set-1-2-00454		0.0432	0.0152	0.9444	0.006233	0.005886
set-1-2-00455		0.0199	0.0129	0.9243	0.006671	0.006166
set-1-2-00456		0.0362	0.0146	0.9258	0.006371	0.005898
set-1-2-00477		0.1258	0.0234	0.8721	0.006475	0.005647
set-1-2-00478			0.0260	0.8725	0.006201	0.005411
set-1-2-00479		0.0477	0.0206	0.8656	0.006501	0.005628
set-1-2-00480			0.0246	0.8670	0.006306	0.005468
set-1-2-00489			0.0237	0.8585	0.006451	0.005538
set-1-2-00490			0.0262	0.8591	0.006198	0.005325
set-1-2-00491		0.0652	0.0211	0.8528	0.006574	0.005606
set-1-2-00492			0.0250	0.8542	0.006384	0.005453

Table H-35. Bias, bias uncertainty, and data-induced uncertainty for set-1-3 cases

Case	ck > 0.7 bias and bias uncertainty	ck > 0.6 bias and bias uncertainty	ck > 0.5 bias and bias uncertainty	Modified k_{eff}	Total data-induced uncertainty	Absolute data-induced uncertainty
set-1-3-00441		0.0177	0.0125	0.8421	0.006797	0.005724
set-1-3-00442		0.0308	0.0151	0.8555	0.006258	0.005354
set-1-3-00443	0.0174	0.0127	0.0106	0.9433	0.006489	0.006121
set-1-3-00444	0.0572	0.0159	0.0112	0.9498	0.006067	0.005762
set-1-3-00453		0.0180	0.0128	0.8280	0.006718	0.005562
set-1-3-00454		0.0335	0.0152	0.8403	0.006231	0.005235
set-1-3-00455	0.0179	0.0128	0.0106	0.9271	0.006446	0.005976
set-1-3-00456	0.0587	0.0171	0.0112	0.9333	0.006077	0.005672
set-1-3-00477		0.1054	0.0219	0.7720	0.006503	0.005020
set-1-3-00478			0.0257	0.7789	0.006175	0.004809
set-1-3-00479		0.0238	0.0112	0.8799	0.006249	0.005499
set-1-3-00480		0.0303	0.0119	0.8827	0.006009	0.005304
set-1-3-00489		0.1070	0.0222	0.7604	0.006483	0.004930
set-1-3-00490			0.0259	0.7671	0.006175	0.004737
set-1-3-00491		0.0242	0.0112	0.8666	0.006241	0.005409
set-1-3-00492		0.0284	0.0119	0.8691	0.006023	0.005234

Table H-36. Bias, bias uncertainty, and data-induced uncertainty for set-1-4 cases

Case	ck > 0.7 bias and bias uncertainty	ck > 0.6 bias and bias uncertainty	ck > 0.5 bias and bias uncertainty	Modified k_{eff}	Total data-induced uncertainty	Absolute data-induced uncertainty
set-1-4-00333		0.0267	0.0185	0.8871	0.006703	0.005946
set-1-4-00334			0.0214	0.8940	0.006217	0.005557
set-1-4-00335	0.0449	0.0175	0.0108	0.9742	0.006535	0.006366
set-1-4-00336		0.0226	0.0116	0.9759	0.006124	0.005976
set-1-4-00345		0.0277	0.0188	0.8705	0.006648	0.005787
set-1-4-00346			0.0216	0.8765	0.006197	0.005432
set-1-4-00347		0.0178	0.0109	0.9566	0.006491	0.006209
set-1-4-00348		0.0229	0.0116	0.9583	0.006112	0.005857
set-1-4-00369			0.0252	0.7999	0.006484	0.005186
set-1-4-00370			0.0292	0.8040	0.006157	0.004950
set-1-4-00371		0.0260	0.0114	0.8975	0.006307	0.005660
set-1-4-00372		0.0325	0.0123	0.8983	0.006061	0.005444
set-1-4-00381			0.0255	0.7869	0.006458	0.005082
set-1-4-00382			0.0292	0.7912	0.006162	0.004876
set-1-4-00383		0.0262	0.0114	0.8835	0.006311	0.005576
set-1-4-00384		0.0325	0.0123	0.8842	0.006071	0.005368

Table H-37. Bias, bias uncertainty, and data-induced uncertainty for set-1-5 cases

Case	ck > 0.7 bias and bias uncertainty	ck > 0.6 bias and bias uncertainty	ck > 0.5 bias and bias uncertainty	Modified k_{eff}	Total data-induced uncertainty	Absolute data-induced uncertainty
set-1-5-00657	0.0822	0.0178	0.0108	0.9437	0.006705	0.006327
set-1-5-00658		0.0216	0.0114	0.9492	0.006287	0.005968
set-1-5-00659	0.0406	0.0168	0.0108	0.9323	0.006627	0.006178
set-1-5-00660		0.0211	0.0113	0.9371	0.006313	0.005916
set-1-5-00669		0.0179	0.0108	0.9290	0.006685	0.006211
set-1-5-00670		0.0220	0.0114	0.9335	0.006268	0.005851
set-1-5-00671	0.0574	0.0172	0.0108	0.9180	0.006698	0.006148
set-1-5-00672		0.0214	0.0114	0.9225	0.006397	0.005901
set-1-5-00693		0.0361	0.0160	0.8531	0.006626	0.005653
set-1-5-00694		0.0858	0.0177	0.8589	0.006324	0.005432
set-1-5-00695		0.0219	0.0132	0.8533	0.006624	0.005652
set-1-5-00696		0.0308	0.0122	0.8583	0.006387	0.005481
set-1-5-00705		0.0342	0.0160	0.8414	0.006616	0.005567
set-1-5-00706		0.0968	0.0179	0.8465	0.006305	0.005337
set-1-5-00707		0.0234	0.0138	0.8417	0.006688	0.005629
set-1-5-00708		0.0367	0.0150	0.8464	0.006488	0.005492

Table H-38. Bias, bias uncertainty, and data-induced uncertainty for set-1-6 cases

Case	ck > 0.7 bias and bias uncertainty	ck > 0.6 bias and bias uncertainty	ck > 0.5 bias and bias uncertainty	Modified k_{eff}	Total data-induced uncertainty	Absolute data-induced uncertainty
set-1-6-00441		0.0199	0.0128	0.9606	0.006674	0.006411
set-1-6-00442		0.0415	0.0149	0.9617	0.006236	0.005998
set-1-6-00443		0.0194	0.0113	0.9403	0.006623	0.006228
set-1-6-00444		0.0290	0.0121	0.9418	0.006280	0.005914
set-1-6-00453		0.0202	0.0128	0.9434	0.006632	0.006256
set-1-6-00454		0.0432	0.0152	0.9444	0.006233	0.005886
set-1-6-00455		0.0199	0.0129	0.9243	0.006671	0.006166
set-1-6-00456		0.0362	0.0146	0.9258	0.006371	0.005898
set-1-6-00477			0.0225	0.8521	0.006564	0.005594
set-1-6-00478			0.0254	0.8571	0.006273	0.005376
set-1-6-00479		0.0438	0.0195	0.8482	0.006583	0.005584
set-1-6-00480			0.0236	0.8530	0.006349	0.005415
set-1-6-00489			0.0227	0.8395	0.006548	0.005498
set-1-6-00490			0.0267	0.8440	0.006251	0.005276
set-1-6-00491		0.0549	0.0198	0.8358	0.006672	0.005576
set-1-6-00492			0.0239	0.8403	0.006432	0.005405

Table H-39. Bias, bias uncertainty, and data-induced uncertainty for set-1-7 cases

Case	ck > 0.7 bias and bias uncertainty	ck > 0.6 bias and bias uncertainty	ck > 0.5 bias and bias uncertainty	Modified k_{eff}	Total data-induced uncertainty	Absolute data-induced uncertainty
set-1-7-00441		0.0177	0.0125	0.8421	0.006797	0.005724
set-1-7-00442		0.0308	0.0151	0.8555	0.006258	0.005354
set-1-7-00443	0.0174	0.0127	0.0106	0.9433	0.006489	0.006121
set-1-7-00444	0.0572	0.0159	0.0112	0.9498	0.006067	0.005762
set-1-7-00453		0.0180	0.0128	0.8280	0.006718	0.005562
set-1-7-00454		0.0335	0.0152	0.8403	0.006231	0.005235
set-1-7-00455	0.0179	0.0128	0.0106	0.9271	0.006446	0.005976
set-1-7-00456	0.0587	0.0171	0.0112	0.9333	0.006077	0.005672
set-1-7-00477			0.0227	0.7439	0.006719	0.004998
set-1-7-00478			0.0262	0.7569	0.006325	0.004787
set-1-7-00479		0.0227	0.0111	0.8648	0.006348	0.005489
set-1-7-00480		0.0290	0.0118	0.8717	0.006068	0.005290
set-1-7-00489			0.0228	0.7334	0.006701	0.004914
set-1-7-00490			0.0264	0.7456	0.006313	0.004707
set-1-7-00491		0.0231	0.0111	0.8522	0.006337	0.005401
set-1-7-00492		0.0289	0.0118	0.8584	0.006078	0.005217

Table H-40. Bias, bias uncertainty, and data-induced uncertainty for set-1-8 cases

Case	ck > 0.7 bias and bias uncertainty	ck > 0.6 bias and bias uncertainty	ck > 0.5 bias and bias uncertainty	Modified k_{eff}	Total data-induced uncertainty	Absolute data-induced uncertainty
set-1-8-00333		0.0267	0.0185	0.8871	0.006703	0.005946
set-1-8-00334			0.0214	0.8940	0.006217	0.005557
set-1-8-00335	0.0449	0.0175	0.0108	0.9742	0.006535	0.006366
set-1-8-00336		0.0226	0.0116	0.9759	0.006124	0.005976
set-1-8-00345		0.0277	0.0188	0.8705	0.006648	0.005787
set-1-8-00346			0.0216	0.8765	0.006197	0.005432
set-1-8-00347	0.0461	0.0178	0.0109	0.9566	0.006491	0.006209
set-1-8-00348		0.0229	0.0116	0.9583	0.006112	0.005857
set-1-8-00369			0.0246	0.7733	0.006607	0.005109
set-1-8-00370			0.0285	0.7836	0.006261	0.004907
set-1-8-00371		0.0244	0.0114	0.8835	0.006394	0.005649
set-1-8-00372		0.0306	0.0122	0.8885	0.006107	0.005426
set-1-8-00381			0.0247	0.7617	0.006594	0.005023
set-1-8-00382			0.0288	0.7713	0.006240	0.004813
set-1-8-00383		0.0248	0.0114	0.8701	0.006382	0.005553
set-1-8-00384		0.0310	0.0122	0.8747	0.006106	0.005341

APPENDIX I. SET-3a: RESULTS OF THE SIX-HIGH UNIFORM ARRAY WITH ALTERNATIVE SPACING CALCULATIONS

This page is intentionally blank

APPENDIX I. SET-3A: RESULTS OF THE SIX-HIGH UNIFORM ARRAY WITH BOUNDING SPACING CALCULATIONS

The analysis methodology for the uniform arrays is discussed in detail in Section 6.2 of the main report.

This appendix serves as a repository of those results for the set-3a calculations.

The complete results for all SAMPLER sweeps are provided in Addendum 1.

The analysis model use for the calculations in this appendix is shown in Figure I-1 below.

The SAMPLER case sweeps presented in this appendix are summarized in Table I-1 below.

LIST OF FIGURES

LIST OF TABLES

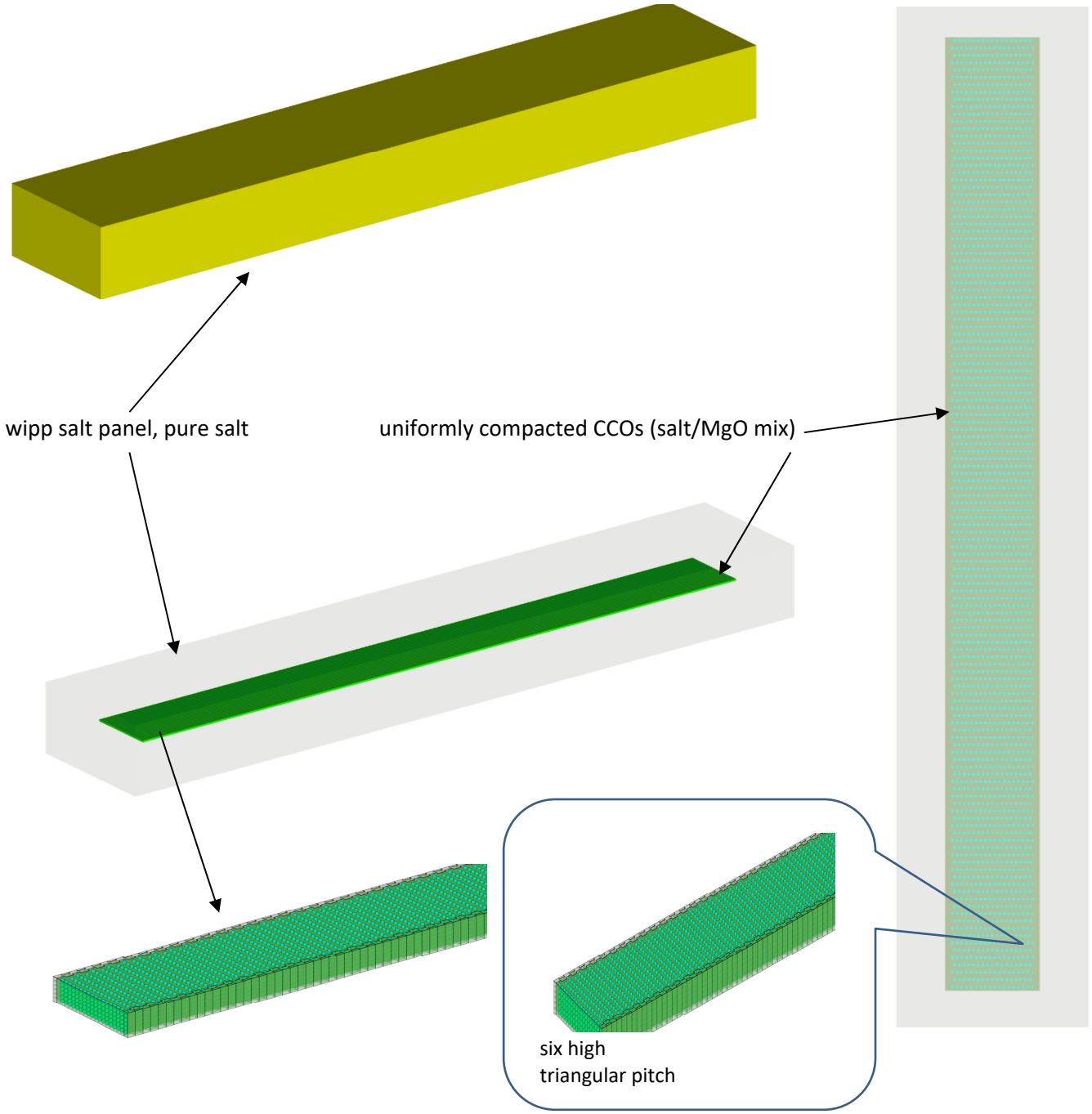

Figure I-1. Diagram of the uniform array six-high model.

Table I-1. Summary of cases for set-3a

Case	Model type	Waste form shape	Waste form moderator	Filler material (0, 2,000, 4,000 g)	Metal in filler	Discrete reflector (thin 0.001 and thick 0.7112 cm)	be (g)	Subcase
Set-3a	Uniform array stacked six high with CCO pitch reduction x = 25%, y = 10%, z = no space	Cylinder (radius range 4.8, 6, 7.7 and height defined by total volume of mass)	water	c12	SS from can (0, 500, 1,000 g)	steel	0 to 585	set-3a-1
			poly	c12		steel		set-3a-2
			water	c12		poly		set-3a-3
			poly	c12		poly		set-3a-4
			water	generic		steel		set-3a-5
			poly	generic		steel		set-3a-6
			water	generic		poly		set-3a-7
			poly	generic		poly		set-3a-8
		Sphere (radius defined by total volume of mass)	water	c12		steel		set-3a-9
			poly	c12		steel		set-3a-10
			water	c12		poly		set-3a-11
			poly	c12		poly		set-3a-12
			water	generic		steel		set-3a-13
			poly	generic		steel		set-3a-14
			water	generic		poly		set-3a-15
			poly	generic		poly		set-3a-16
		Cylinder (radius range 4.8, 6, 7.7 and height defined by total volume of mass) with 25 g B_4C	poly	c12		poly		set-3a-17
		Sphere (radius defined by total volume of mass) with 25 g B_4C	poly	c12		poly		set-3a-18

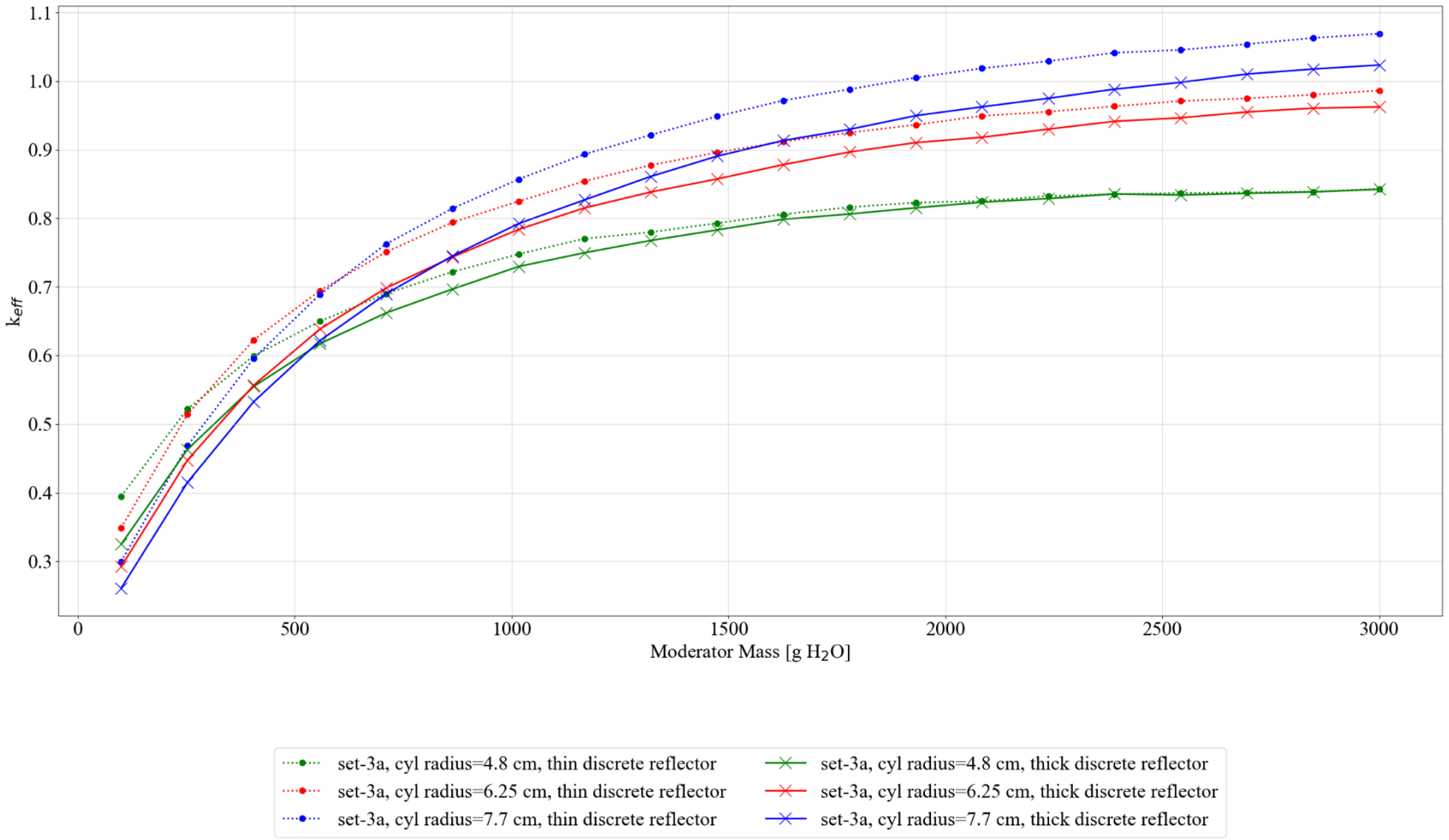

Figure I-2. Set-3a results, plot 1: reactivity effect of cylinder radius, pipe steel, no filler, no Be, water moderated.

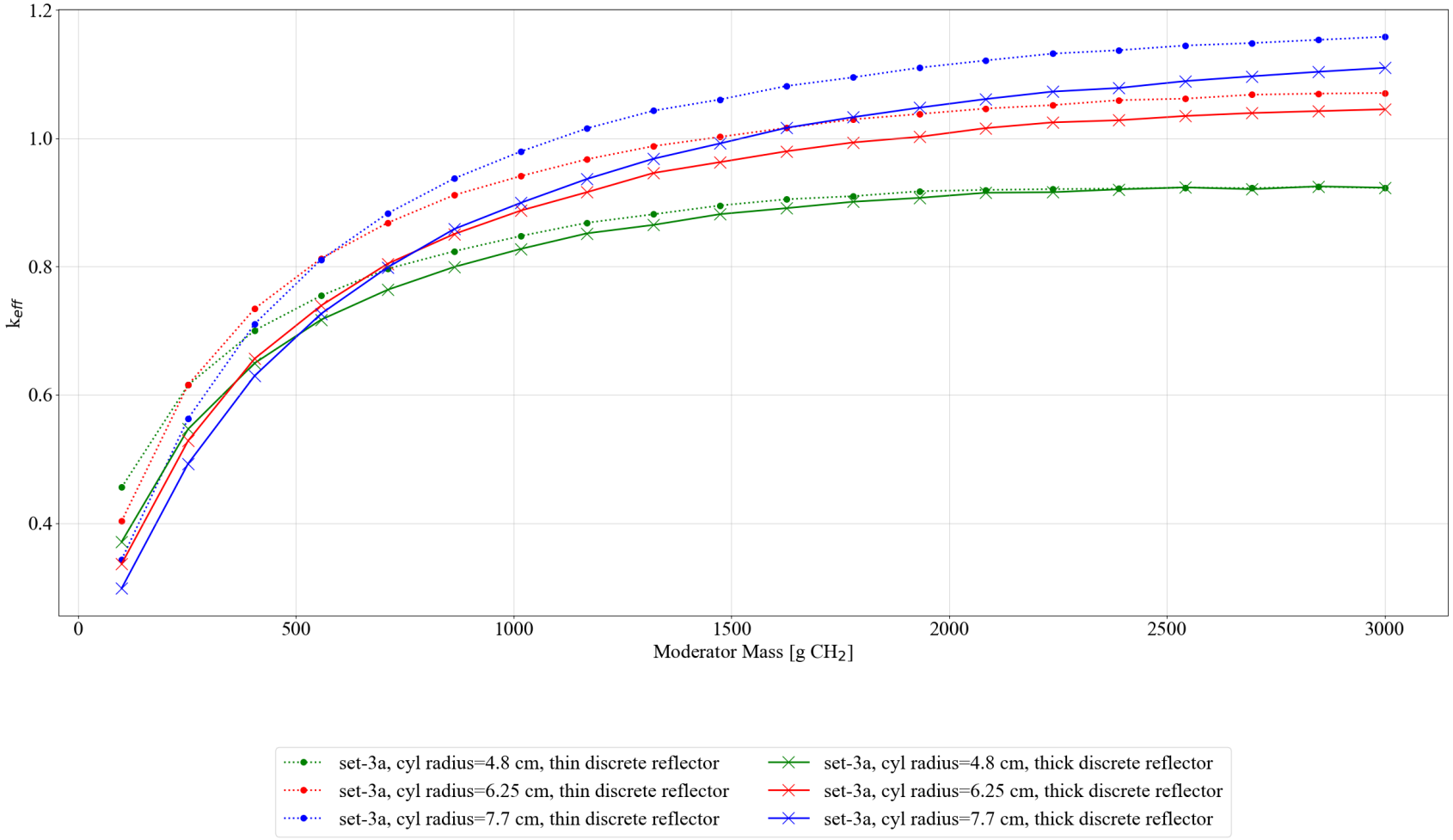

Figure I-3. Set-3a results, plot 2: reactivity effect of cylinder radius, pipe steel, no filler, no Be, poly moderated.

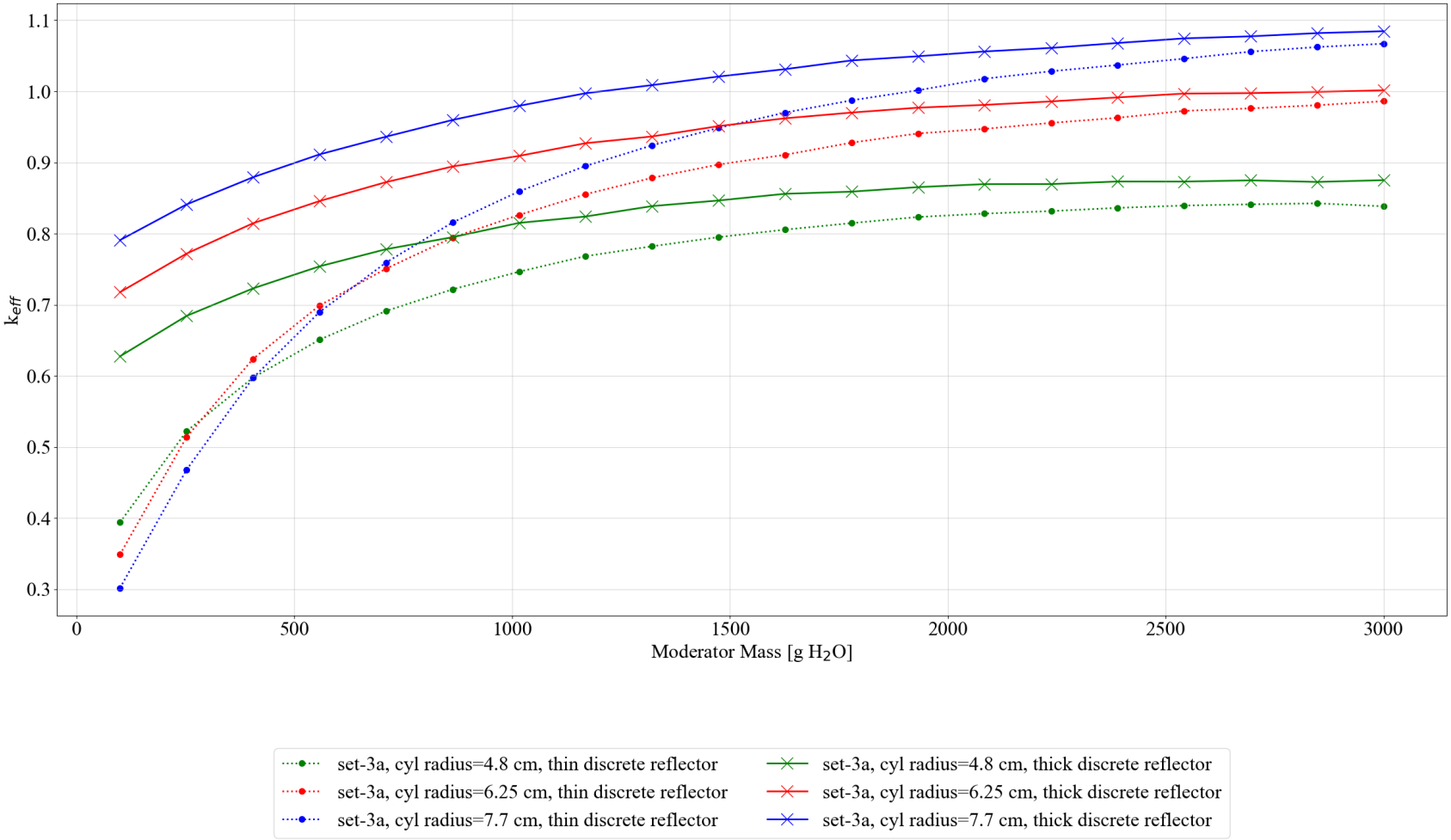

Figure I-4. Set-3a results, plot 3: reactivity effect of cylinder radius, pipe poly, no filler, no Be, water moderated.

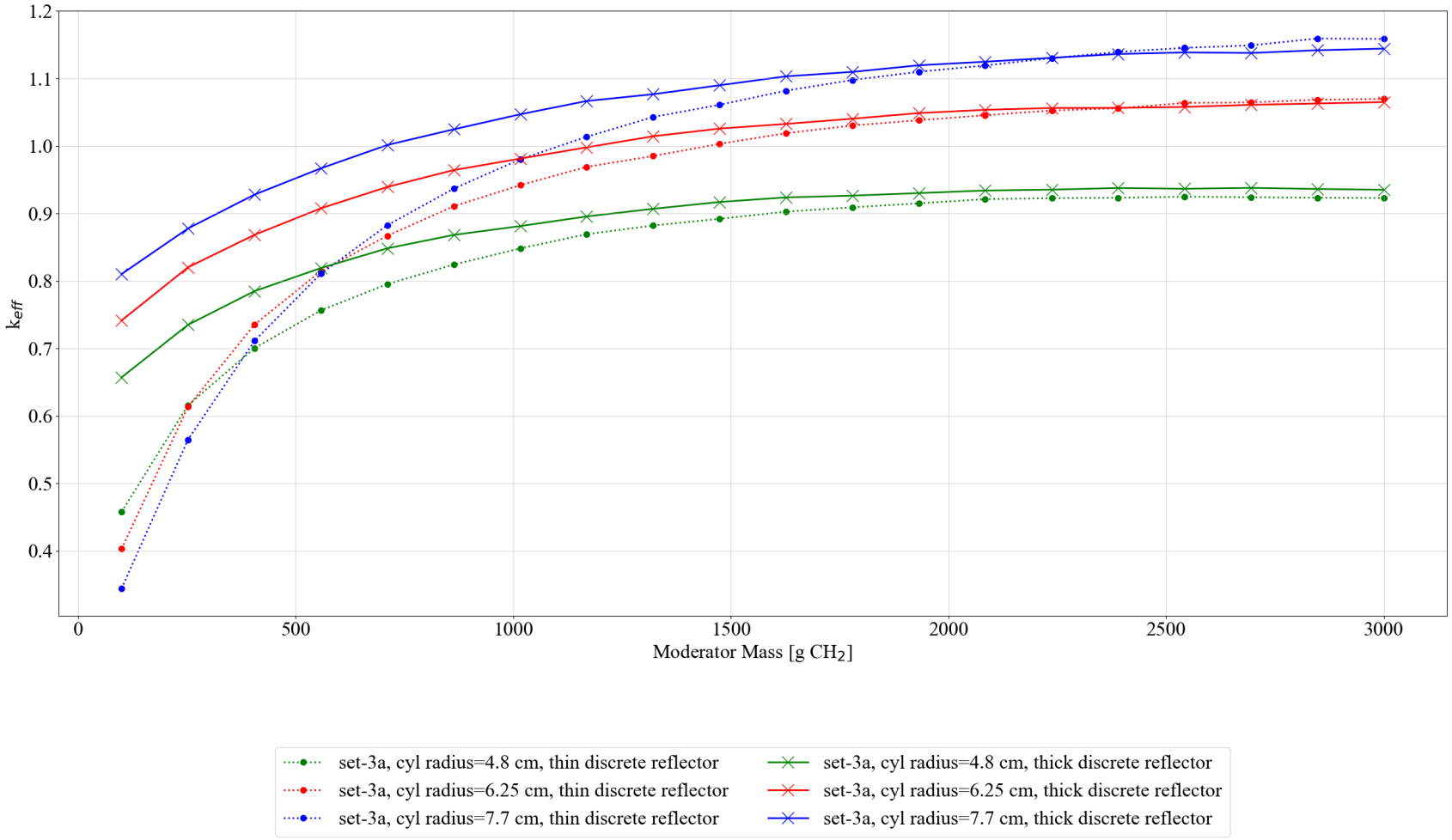

Figure I-5. Set-3a results, plot 4: reactivity effect of cylinder radius, pipe poly, no filler, no Be, poly moderated.

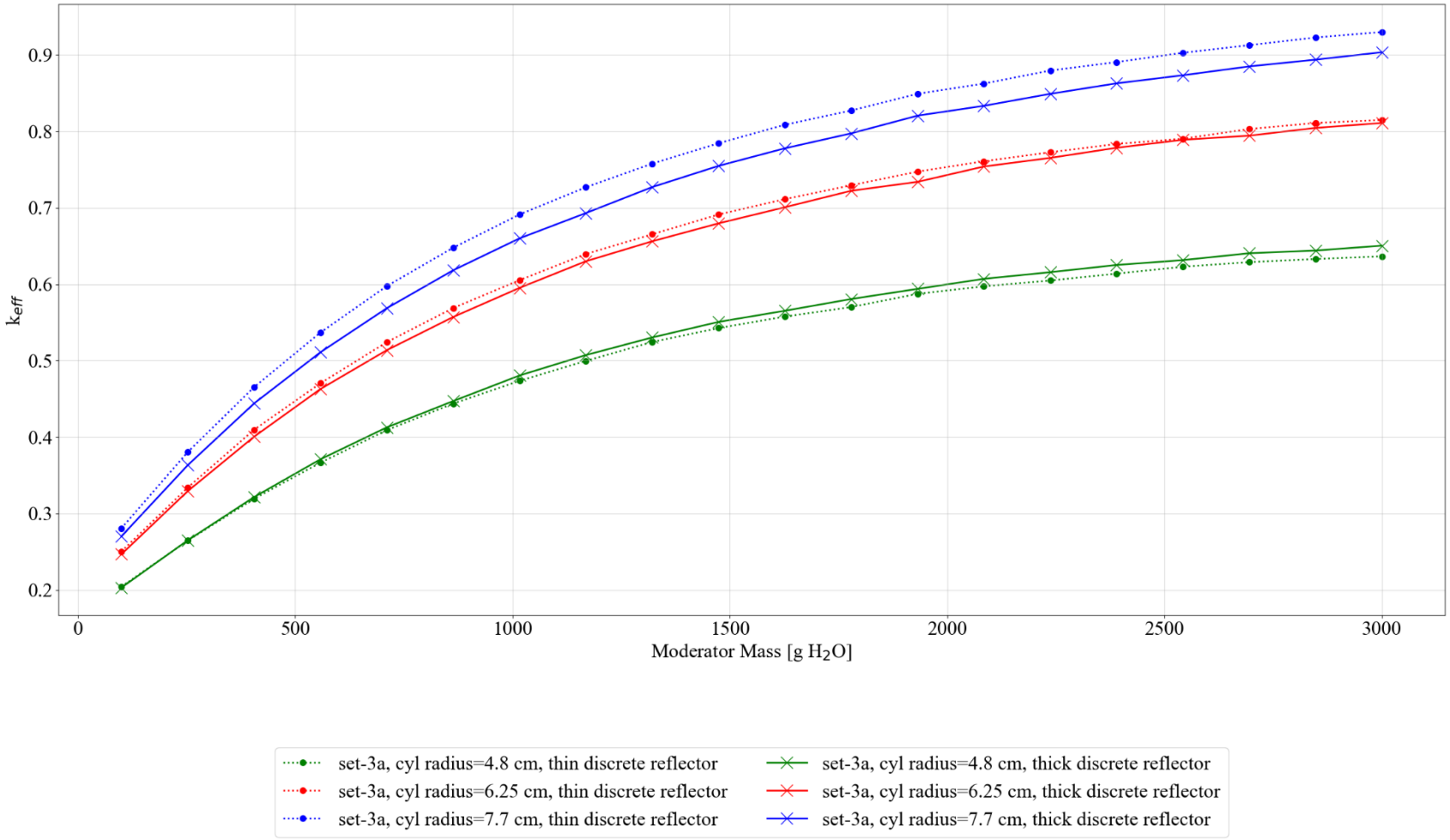

Figure I-6. Set-3a results, plot 5: reactivity effect of cylinder radius, pipe steel, 5 kg graphite/can, no Be, water moderated.

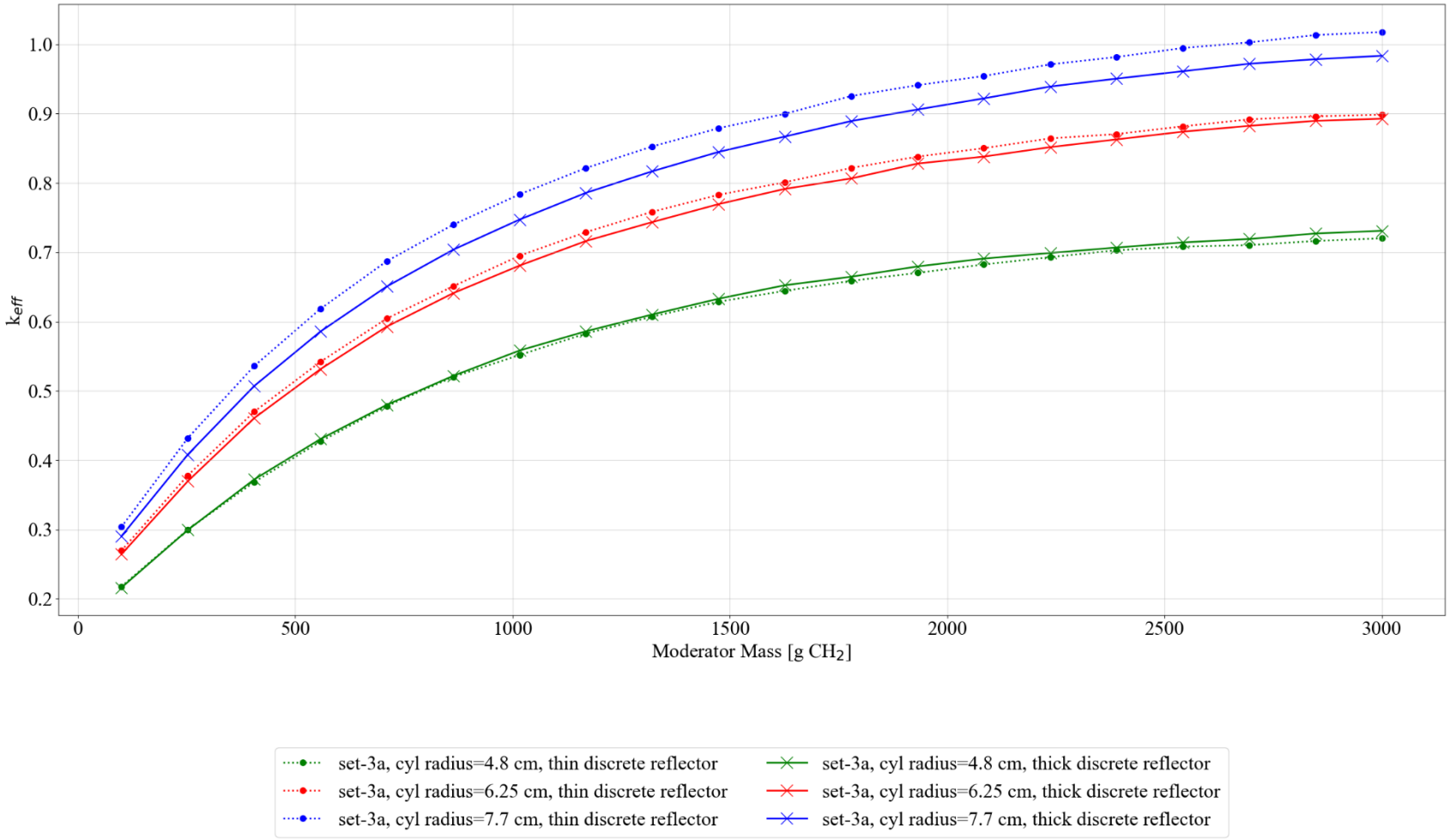

Figure I-7. Set-3a results, plot 6: reactivity effect of cylinder radius, pipe steel, 5 kg graphite/can, no Be, poly moderated.

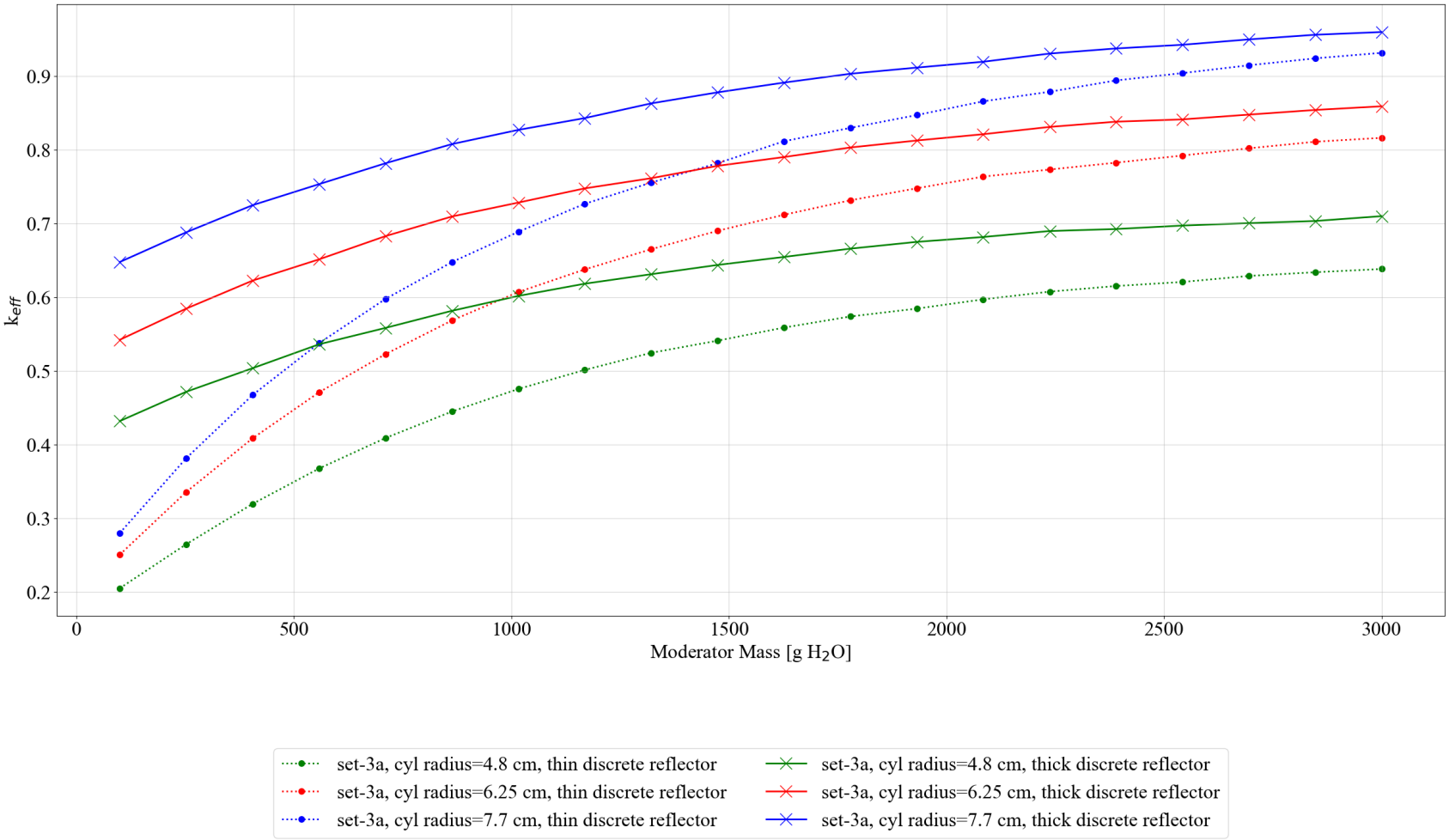

Figure I-8. Set-3a results, plot 7: reactivity effect of cylinder radius, pipe poly, 5 kg graphite/can, no Be, water moderated.

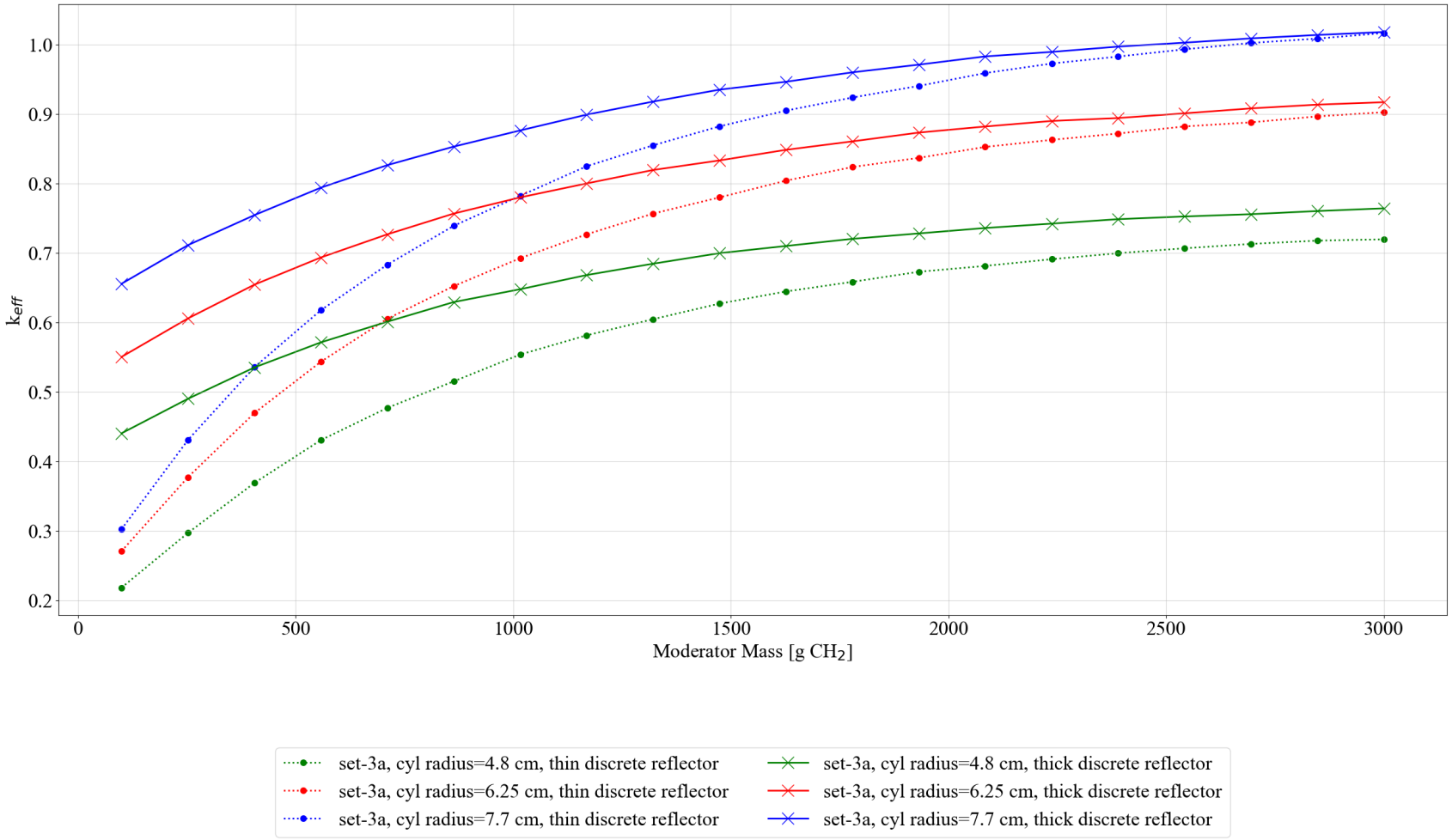

Figure I-9. Set-3a results, plot 8: reactivity effect of cylinder radius, pipe poly, 5 kg graphite/can, no Be, poly moderated.

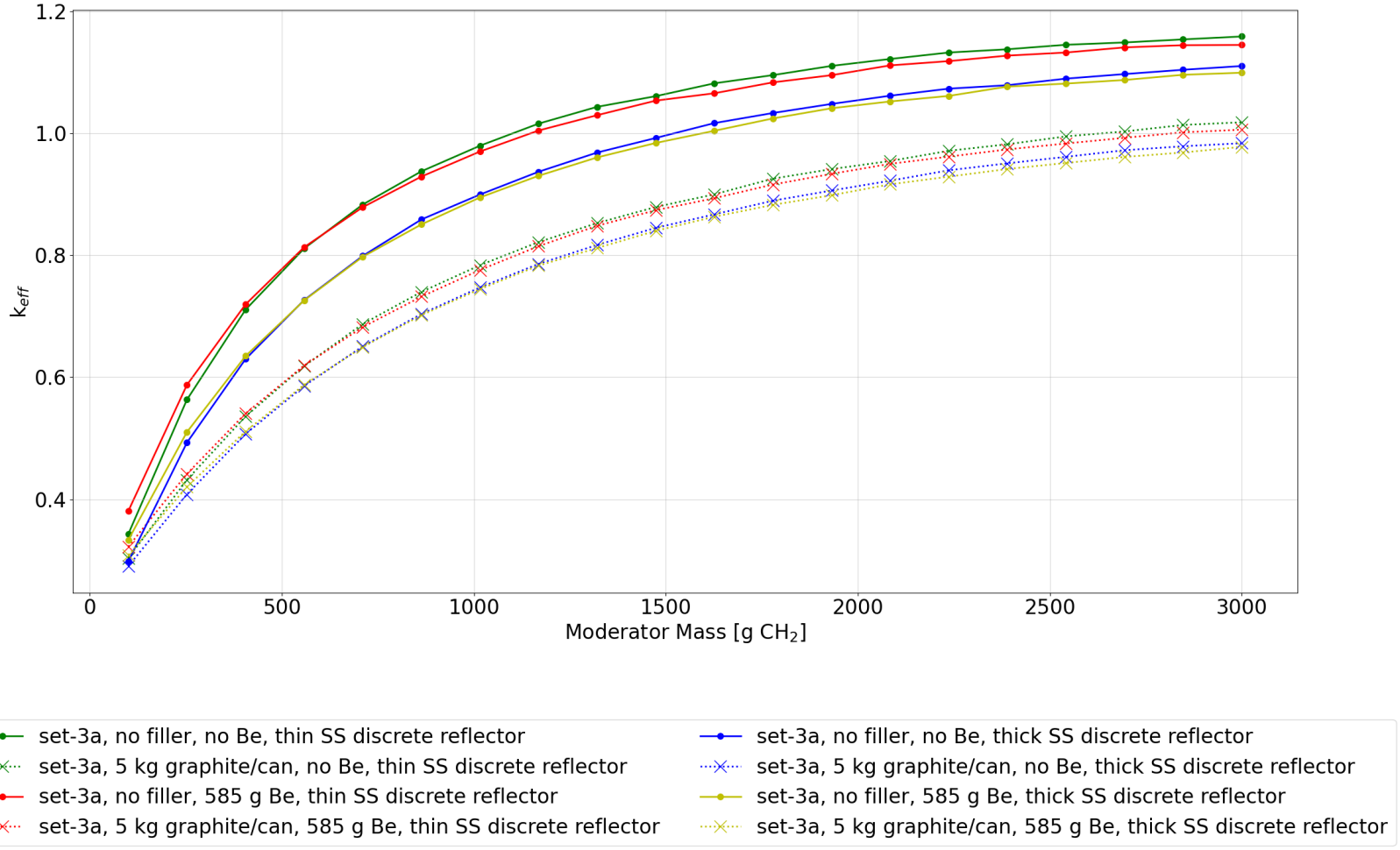

Figure I-10. Set-3a results, plot 9: reactivity effect of various parameters with 7.7 cm cylinder radius, graphite filler, poly moderated.

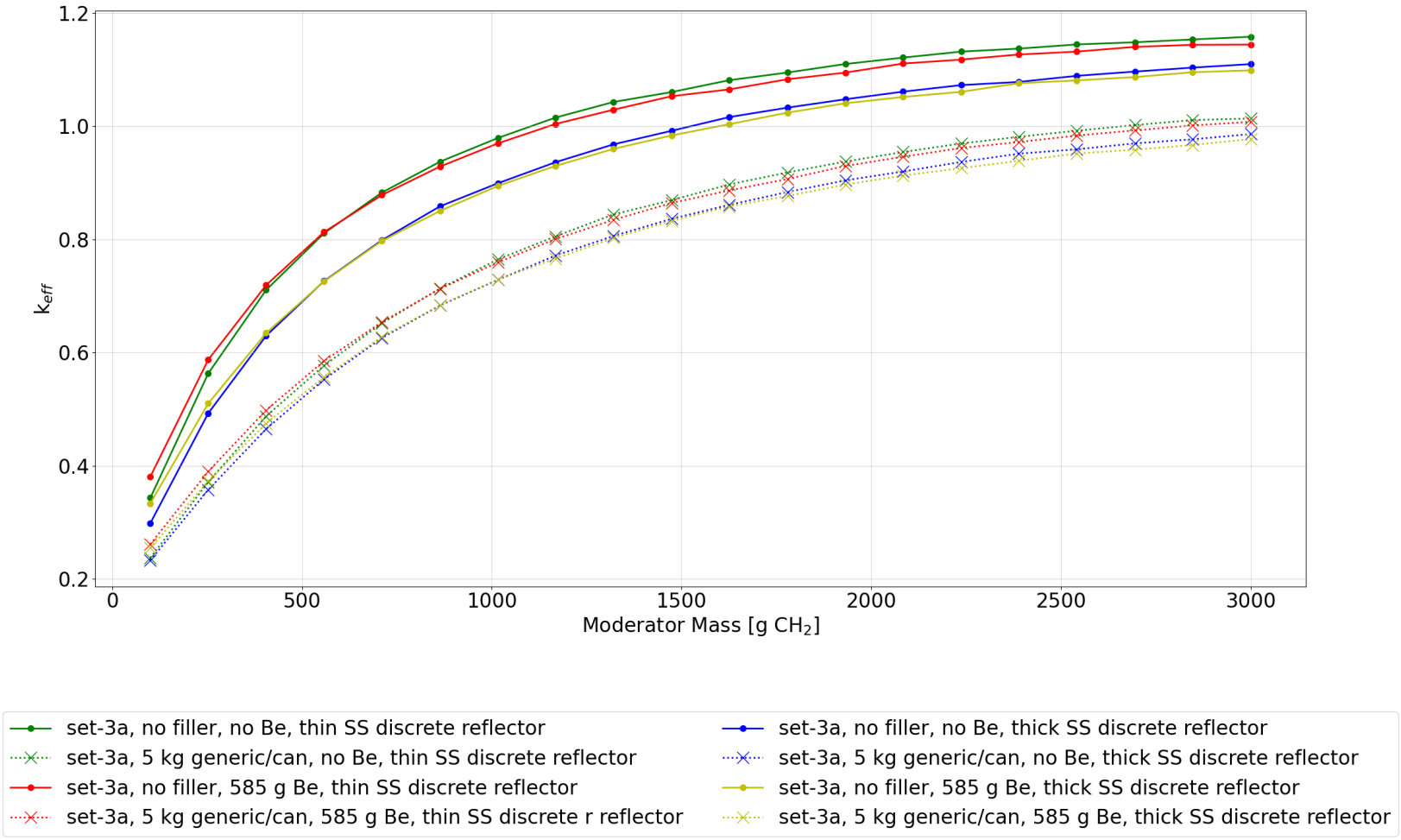

Figure I-11. Set-3a results, plot 10: reactivity effect of various parameters with 7.7 cm cylinder radius, generic filler, poly moderated.

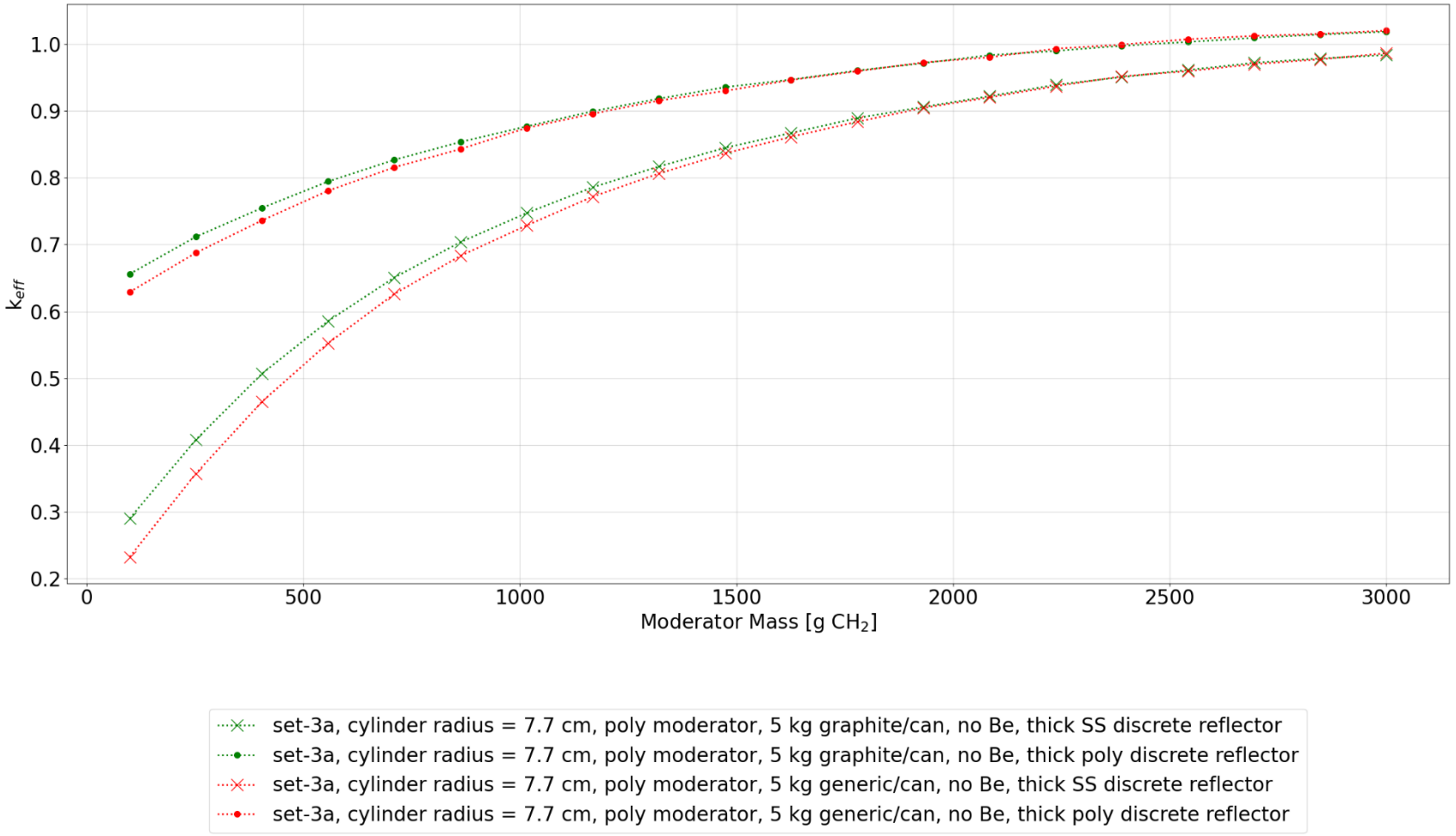

Figure I-12. Set-3a results, plot 11: comparison of graphite and generic filler with 7.7 cm cylinder radius, no Be, poly moderated, thick discrete reflector.

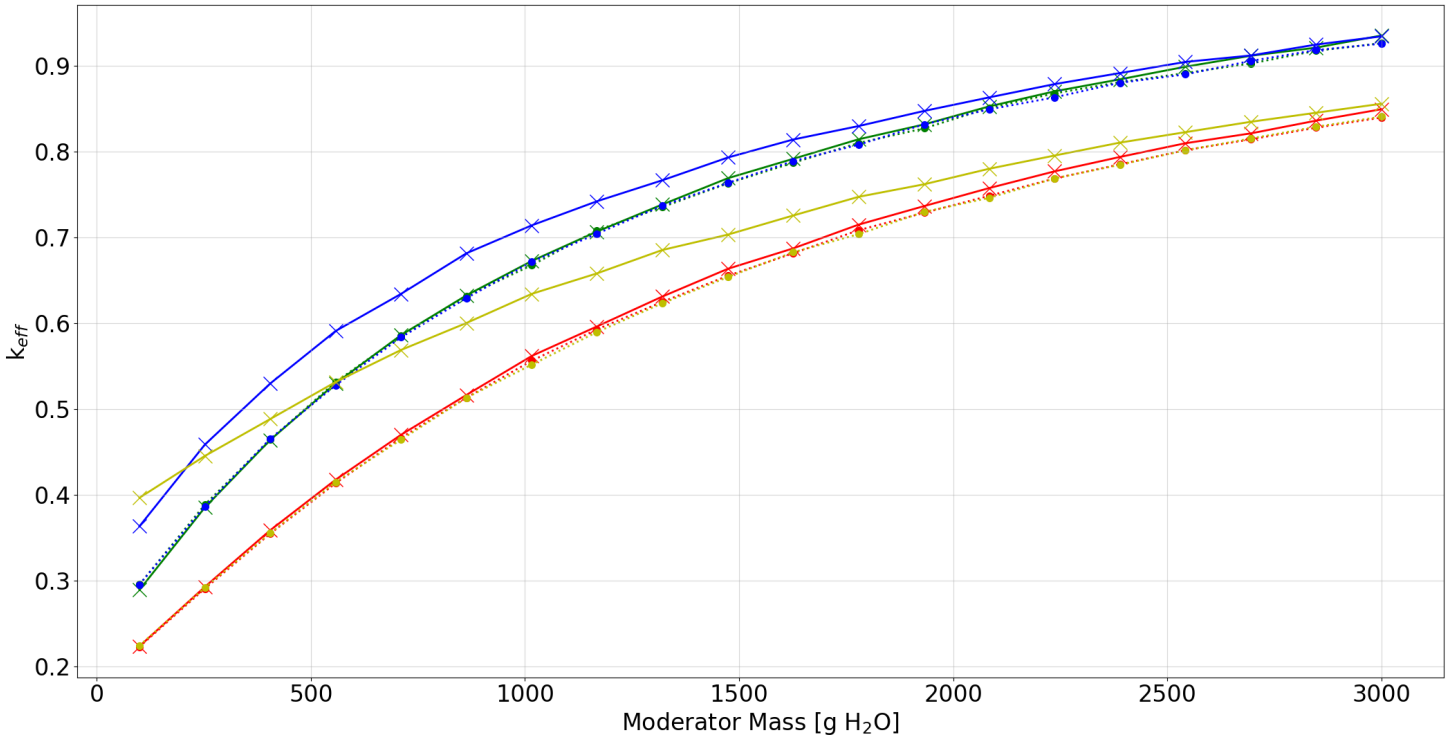

Figure I-13. Set-3a results, plot 12: reactivity effect of various parameters with spherical waste form geometry, graphite filler, water moderated.

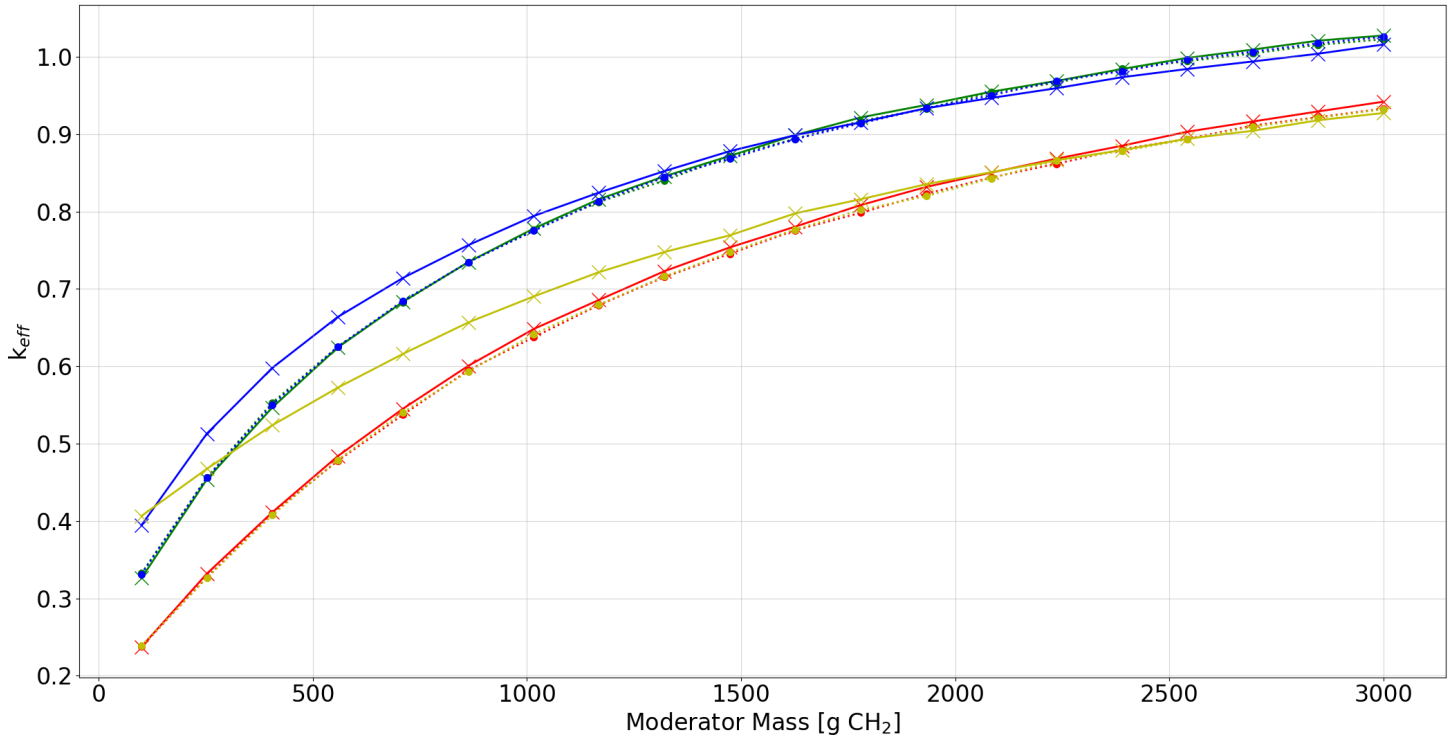

Figure I-14. Set-3a results, plot 13: reactivity effect of various parameters with spherical waste form geometry, graphite filler, poly moderated.

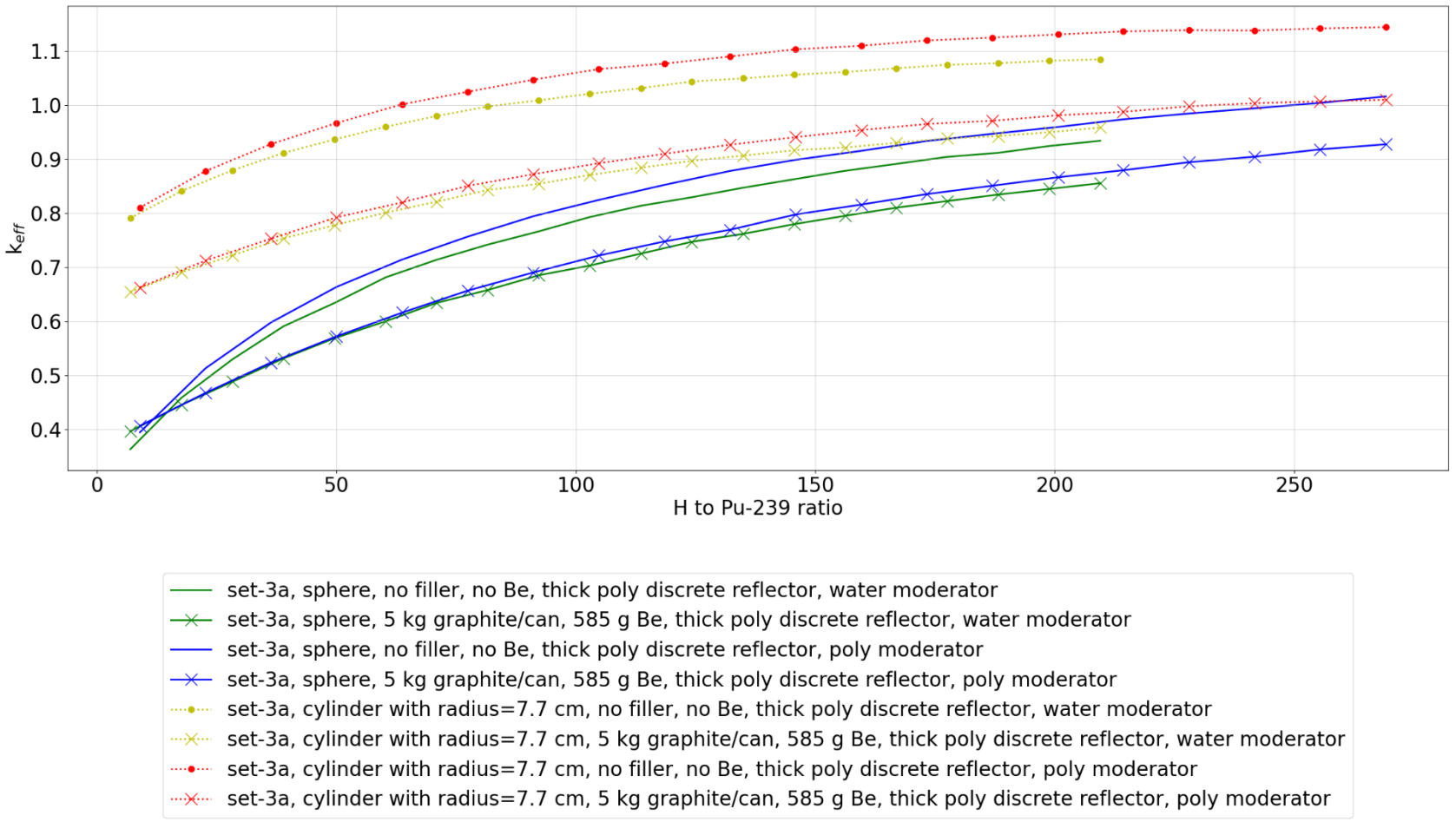

Figure I-15. Set-3a results, plot 14: comparison of spherical and cylindrical geometries (h/x).

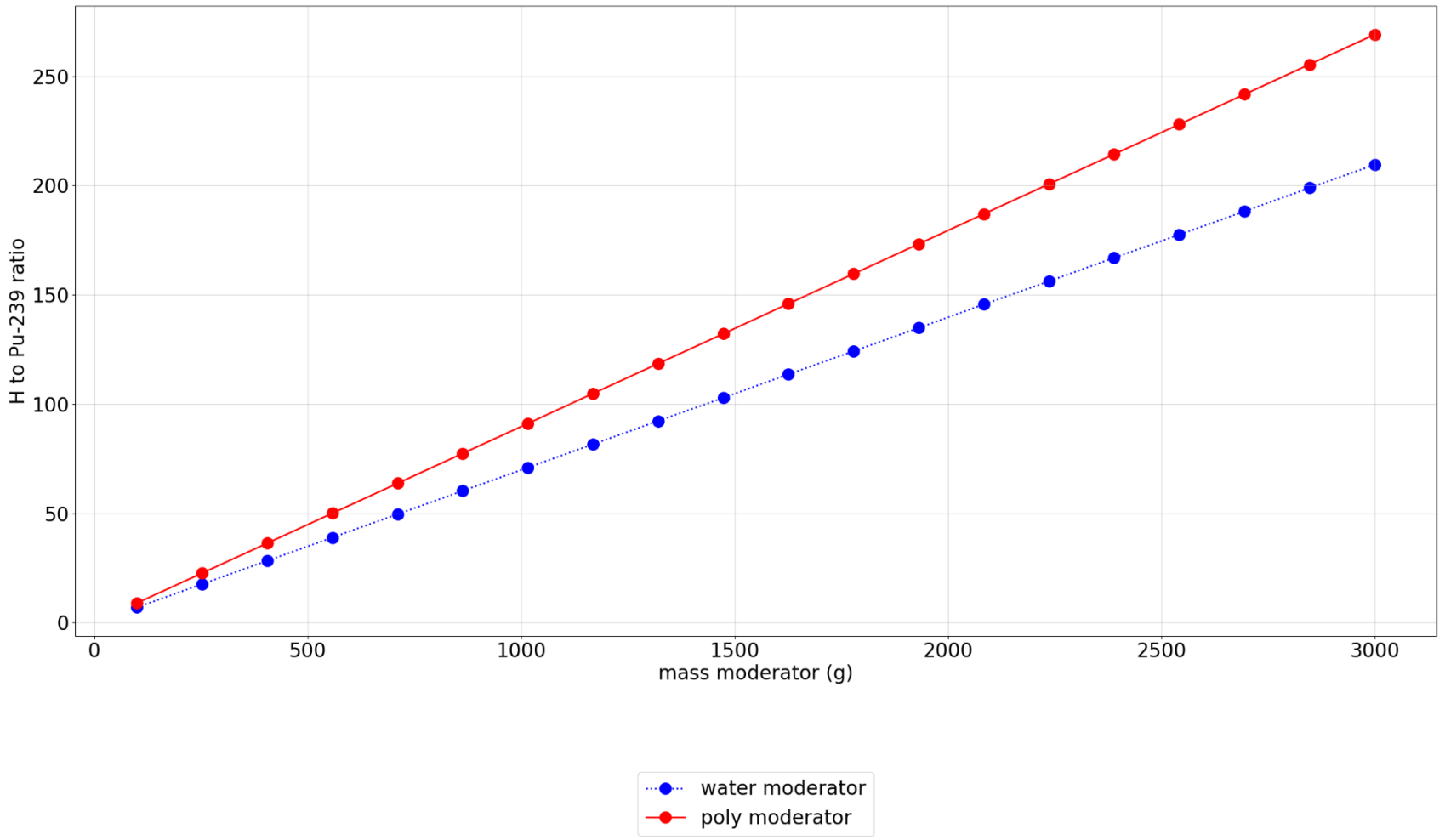

Figure I-16. Set-3a results, plot 15: comparison of water and poly h/x.

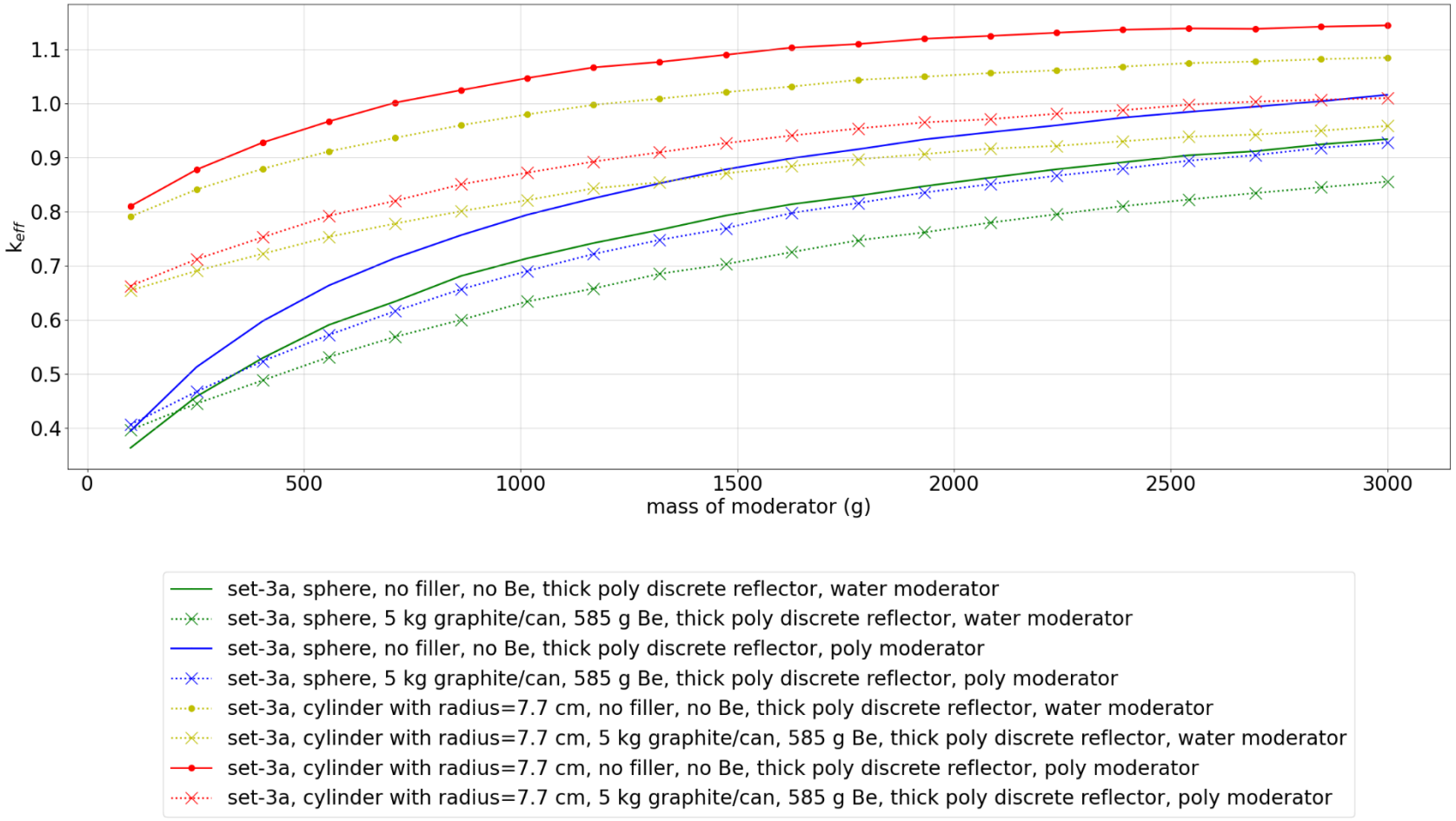

Figure I-17. Set-3a results, plot 16: comparison of spherical and cylindrical geometries (mod mass).

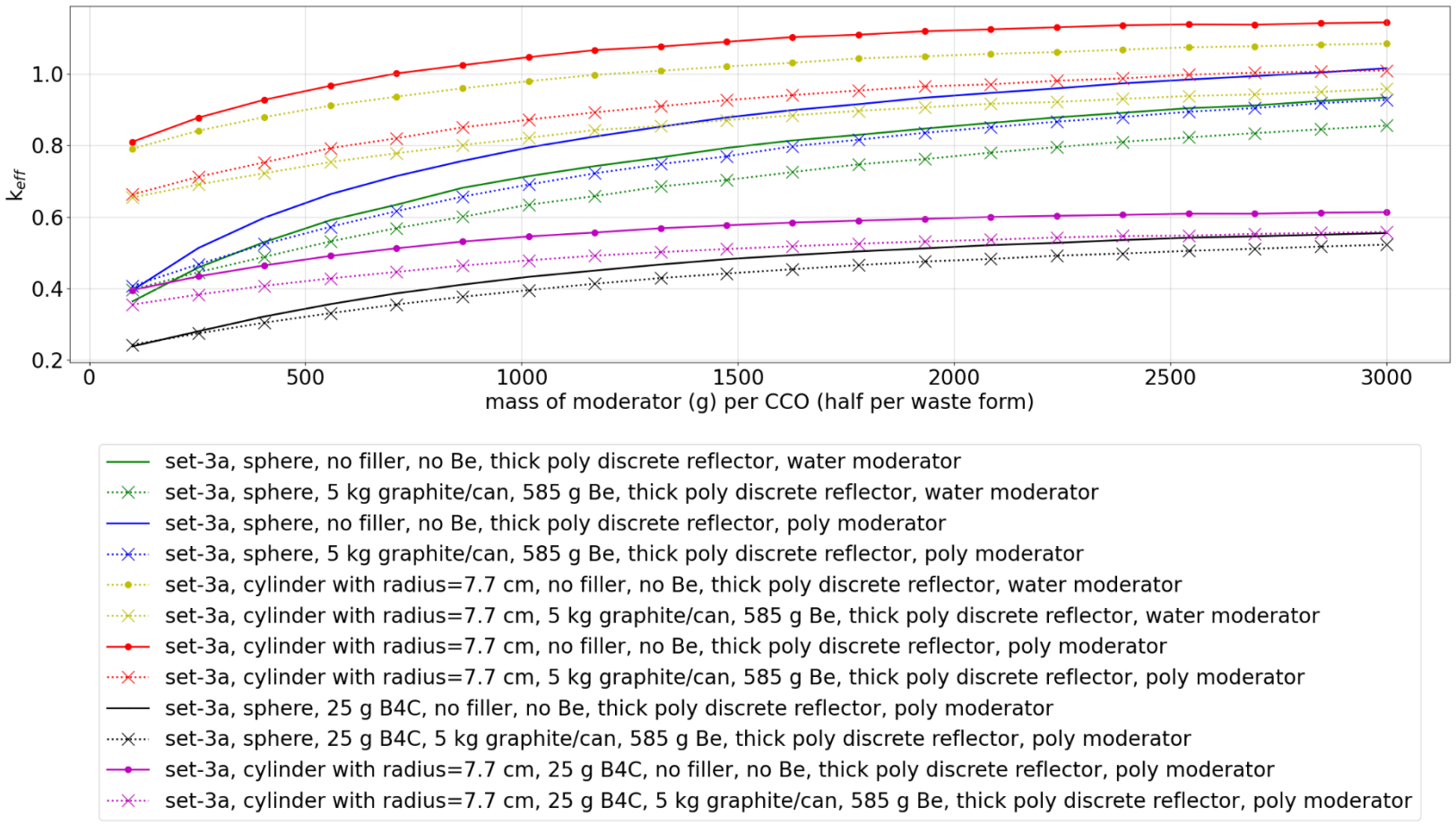

Figure I-18**. Set-3a results, plot 17: Reactivity effect of 25 g B_4C per waste form (2 per CCO)**

This page is intentionally blank

APPENDIX J. SET-4: RESULTS OF HETEROGENOUS WASTE FORM MIXING STUDIES

This page is intentionally blank

APPENDIX J: SET-4: RESULTS OF HETEROGENOUS WASTE FORM MIXING STUDIES

LIST OF FIGURES

LIST OF TABLES

The purpose of this appendix is to evaluate the validity of the assumption that the PuO_2 is uniformly mixed within the waste form. This evaluation examines the effect of locally increased fissile concentration in the waste from in terms of k_{eff}. This appendix is not intended to address all possible heterogeneous configurations, but only a selection of cases that correspond to the analyses performed and which cover a range of sizes which would allow larger particle sizes within a mixture to be acceptable.

This appendix evaluates the assumption that a uniform mixture for the waste form is acceptable by evaluating a unit cylindrical waste form (with set-2-uh subset 2-4 parameters, i.e., polyethylene waste form moderator, polyethylene discrete reflector and graphite filler material) with variations in the number, size, and location of pure PuO_2 spheres (heterogenous spheres) embedded in a mixture of filler and PuO_2. Spheres are used because the neutron leakage is bounding compared to similar sized chunks of FGE.

The mass limit of 380 FGE is maintained for all cases. The PuO_2 sphere size diameter is parametrically swept over the range of 0.1 to 1.0 in. so that the mass of PuO_2 in each heterogenous sphere is dictated by the diameter for each sweep. For each sweep of moderator content, every heterogenous sphere has the same size. The total mass of pure PuO_2 in the heterogenous spheres does not exceed the overall 380 FGE limit. Therefore, to conserve mass, the remainder of PuO_2 that is not contained in the heterogenous spheres is uniformly mixed with filler.

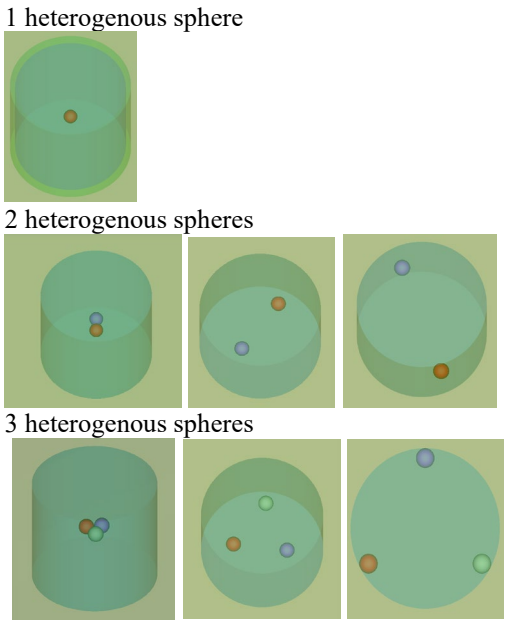

Figure J-1. Diagram of the various heterogenous sphere cases and spacings.

The number of heterogenous spheres ranges from 1 to 3 in the configurations evaluated. Two additional cases are considered with uniform mixtures as baselines against which to compare the heterogenous sphere cases: one with a cylindrical waste form shape and one with a spherical waste form shape.

The location of the spheres within the cylindrical waste form also is also evaluated as: centrally located, located midway between the center, or located at the edges, as shown in Figure J-1. A full listing of parameters evaluated for the study are listed in Table J-1.

To represent the interstitial reflector material used in the analysis, the waste form is embedded in a cube of "50/50" MgO + NaCl mixture with an edge length of 200 cm centered on the waste form. This itself is placed in the cube of NaCl with edge length of 800 cm to represent the WIPP repository, also consistent with the analysis. See Figure J-2. The boundaries are vacuum. Therefore, this study specifically evaluates changes in k_{eff} and is not directly comparable to other evaluations in this analysis. The heterogeneous study most closely resembles set two because the cylinders are not in contact with other cylinders. No attempt is made with this study to evaluate neutron interactions between waste forms since the main impact of the uniform versus heterogenous mixing system is localized.

Table J-1. Parameters varied in the heterogenous study.

Parameter symbol	Description	Values
fge_mass	Mass of PuO_2 in waste form (both uniformly mixed and lumped masses)	Total is fixed at 380 per waste form; heterogenous spheres varies by size
n_hetro	Number of PuO_2 lumped masses in waste form	0, 1, 2, 3
sph/cyl	Shape of waste form	cyl
puo2_het1_diameter	Diameters (in.) of PuO_2 masses when n_hetro>0	0.1, 0.425, 0.75
radial_factor	Fraction of distance from innermost position (0.0) to outermost position (1.0), tangent to cylinder. This defines the position of the sphere when n_hetro>1	0.0, 0.5, 1.0
can_mass	Mass of stainless 304 can material mixed with uniform portion of waste form	0, 500, 1000
thk_pipe		0.7112, 0.001
ch2_mass	Mass of polyethylene (g)	100.0, 252.6, 405.3, 557.9, 710.5, 863.2, 1016.0, 1168.0, 1321.0, 1474.0, 1626.0, 1779.0, 1932.0, 2084.0, 2237.0, 2389.0, 2542.0, 2695.0, 2847.0, 3000.0
graphite_mass	Mass of graphite filler (g)	0, 1500, 3000
be_mass	Mass of Be (g)	585, 0
r_cyl	Waste form radius	7.7

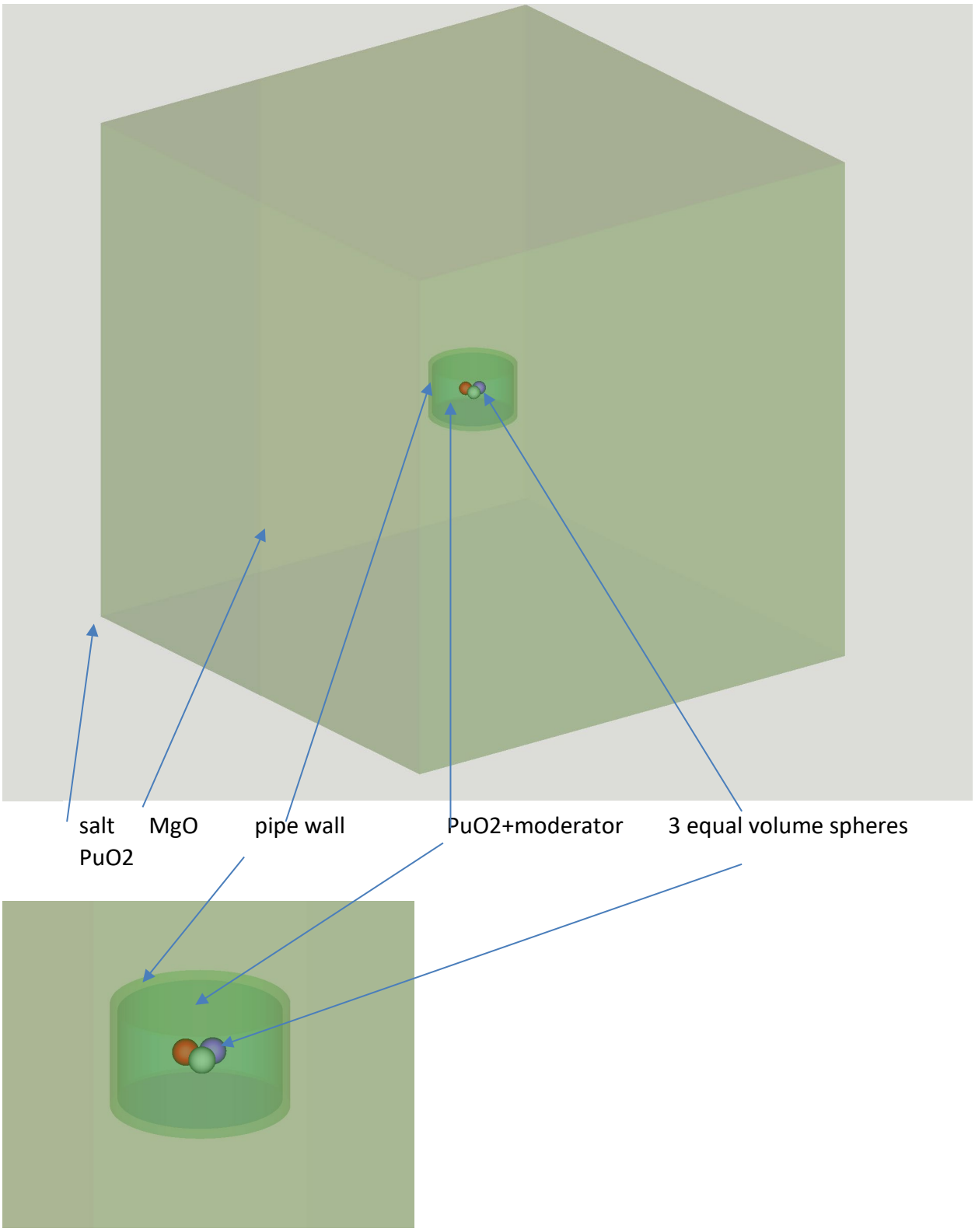

Figure J-2. Geometry diagram for a three-sphere case with spheres in centermost position.

Discussion of Results

The reactivity of the various cases for heterogeneity are shown as k_{eff} comparisons in Figures J-3, Figure J-5, and Figure J-7, which respectively compare 1-sphere, 2-sphere, and three-sphere (heterogenous spheres) to the uniform cylindrical case. In the cases plotted in Figure J-3 through Figure J-10, the waste forms being considered are cylinders with a radius of 7.7 cm. Each heterogenous sphere case is selected to be the worst case for various sphere radii and radial factors that corresponds to a uniform case. The upper envelope of the uniform cases and the heterogenous sphere cases appear to be identical, except at low moderator. Regardless, the difference does not appear to substantially alter k_{eff}. The differences in delta- k_{eff} between cases are more clearly seen in Figures J-4, Figure J-6, and Figure J-8. The cases with the largest increases in k_{eff} due to heterogeneity are at low moderator with a thin polyethylene discrete reflector. This suggests that the heterogeneity is not directly responsible for the change in k_{eff}, but rather the change in reflection may be changing k_{eff} for cases with low moderator masses, or higher fissile concentrations.

The effect of reflection is also seen by examining which heterogeneous configurations are producing the worst case increases in k_{eff}. This is seen in Figures J-9 and J-10 which are scatter plots where darker points indicate a higher frequency of that combination. Figure J-9 shows the number of times a given sphere radius produces the worst delta-k vs a corresponding uniform case for a given moderator mass. To produce the figure, the heterogeneous cases are matched to the non-heterogeneous cases on every parameter except for sphere radius and radial factor. For sphere radius and radial factor, the combination producing the highest k_{eff} is selected, and the radius is plotted on Figure J-9. Figure J-10 is similar, except it shows the number of times a given radial factor produces the worst delta-k. For the three-sphere case, clear trends were only observable at low moderator, and they occurred when all three spheres were large and in contact at the center of the cylinder.

Three large spheres concentrated in the center of a disk-shaped waste from producing the largest jump in delta-k vs a uniformly mixed case is unsurprising. The cylinder configuration at low moderation has a very large leakage, so concentrating mass together in the center of the cylinder reduces the neutron leakage probability. In Figure 6-15 of the main text, similar behavior can be observed when changing between the cylindrical and spherical waste forms at low moderator. While the spherical waste form of Figure 6-15 is uniformly mixed and the configurations here consist of concentrated Pu in the center of a cylindrical waste form, the trend toward decreased leakage is the same in both cases. The worst cases in this section in Figure J-8 results in a delta-k increase of approximately 0.1 when concentrating the majority of the Pu is concentrated at the center of the waste form vs it being uniformly distributed in a disk shaped cylinder. Similarly, in Figure 6-15 of the main text also shows a similar delta-k of approximately 0.1 when transitioning from a cylindrical waste form to a spherical waste form at low moderator. Both times the delta-k correspond to a thin discrete reflector. When a thick discrete reflector is used, delta-k is reduced by about half in both figure 6-15 and J-8. Therefore it is suspected that the behavior being observed has more to do with leakage than non-homogeneity.

Finally, as a means to provide a fuller comparison of the vacuum boundary conditons in this appendix to the remainder of the report, k_{eff} for various cylinder radii are shown in Figure J-11. Comparing Figure J-11 to Figure C-5 for the set-2-uh cases, it is seen that the vacuum boundary conditions result in lower k_{eff}. The vacuum boundary condition cases appear to have slightly exagerated trends vs Figure C-5. The k_{eff} values for spherical waste forms are shown in Figure J-12, and comparing to Figure C-13 for the set-2-uh cases also shows that the vaccum boundary conditions result in lower values of k_{eff}. At a high level trends for set-2-uh and the baseline cases for set-4 appear to be similar overall with set-4 having lower k_{eff} values than set-2-uh.

Various cases were compared to a continous energy baseline to deomonstrate that the cell data card and the multigroup approximation does not substantially alter the trends observed because it is on the order of the Monte Carlo uncertainty. This is shown in Figure J-13.

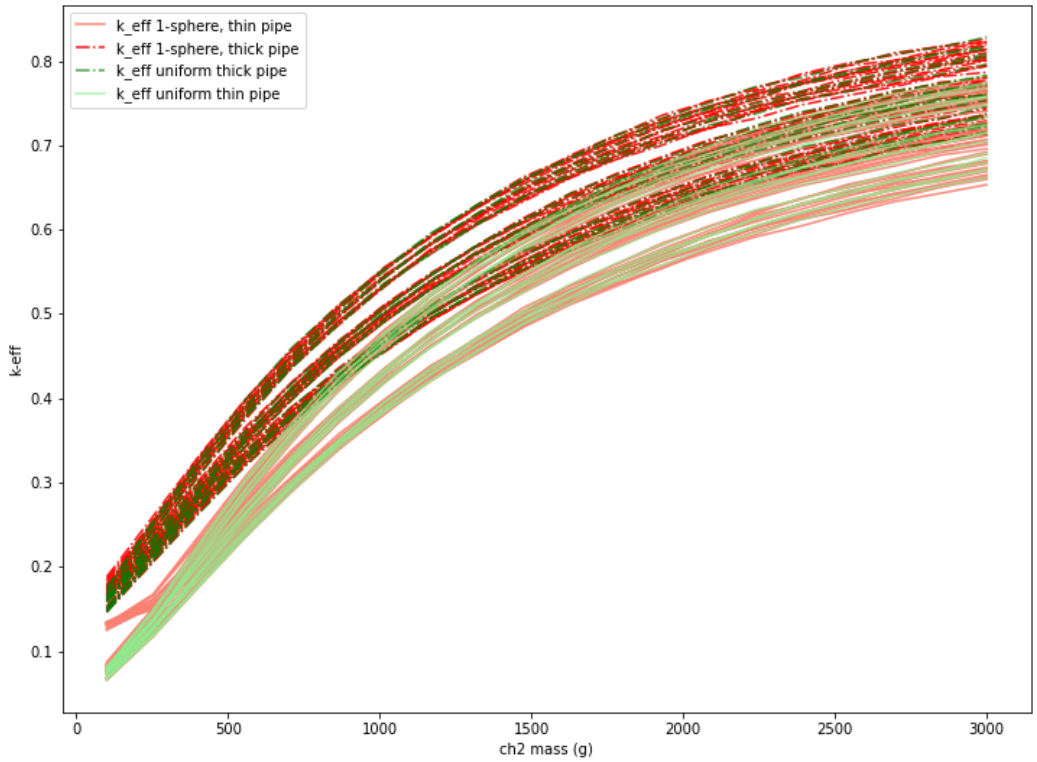

Figure J-3. Comparison of 1-sphere k_{eff} to uniform k_{eff} for cylinderical wasteforms of 7.7 cm diameter.

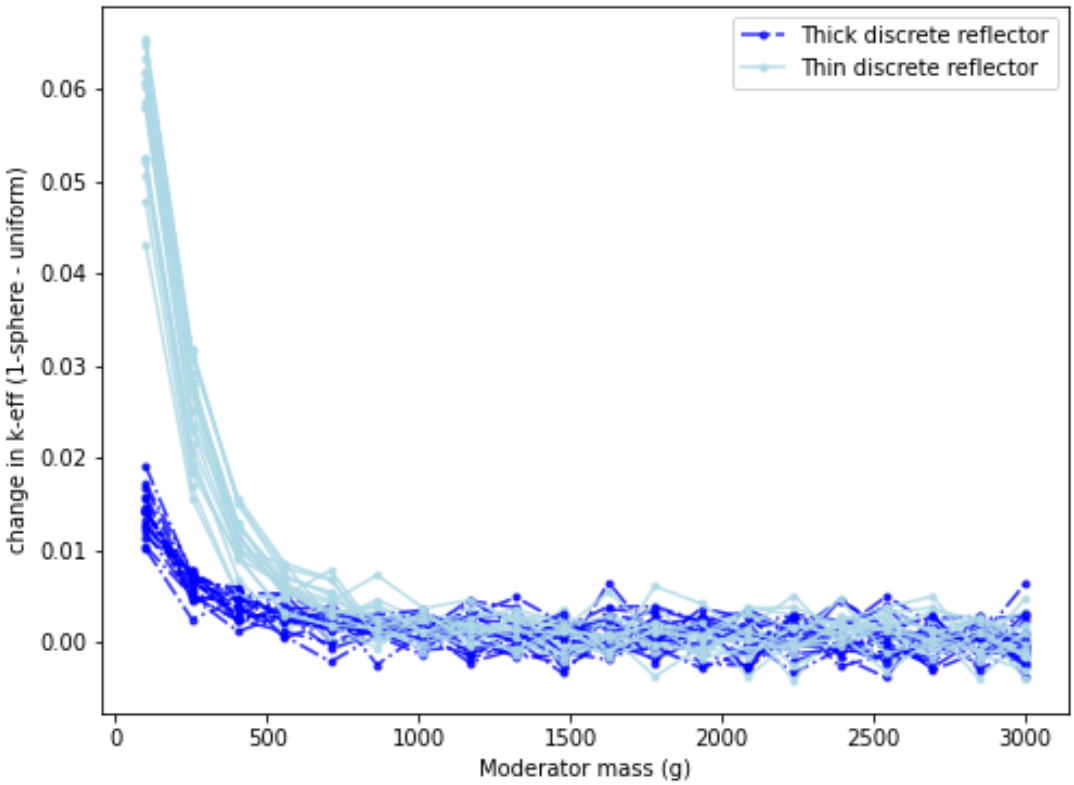

Figure J-4. Delta-k_eff when comparing highest reactivity 1 sphere case to a uniform case (positive values correspond to cases where the highest reactivity 1-sphere configuration has higher keff than uniform configuration.

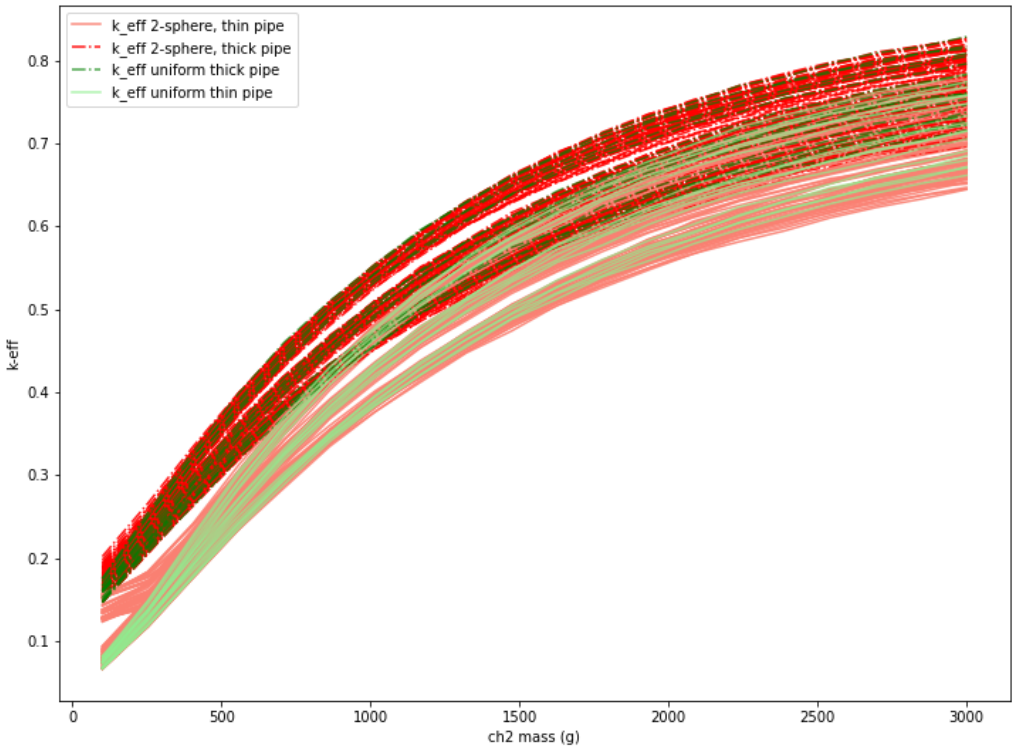

Figure J-5. Comparison of 2-sphere k_{eff} to uniform k_{eff} for cylinderical wasteforms of 7.7 cm diameter.

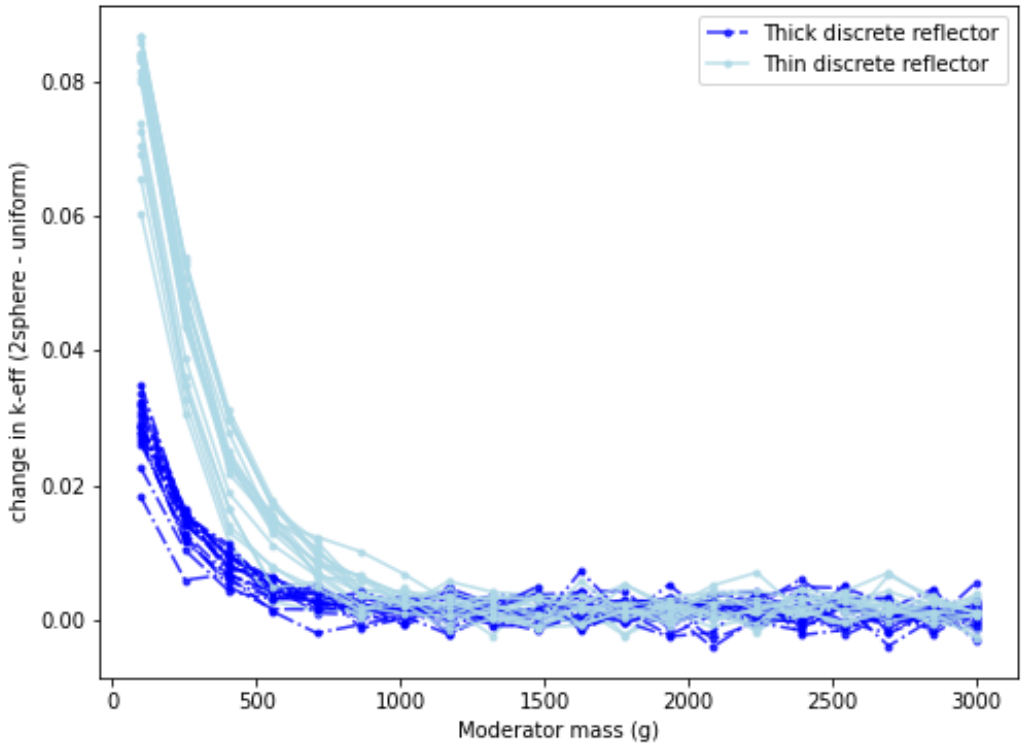

Figure J-6 Delta-k_eff when comparing highest reactivity 2-sphere case to a uniform case (positive values correspond to cases where the highest reactivity 2-sphere configuration has higher k_{eff} than uniform configuration.

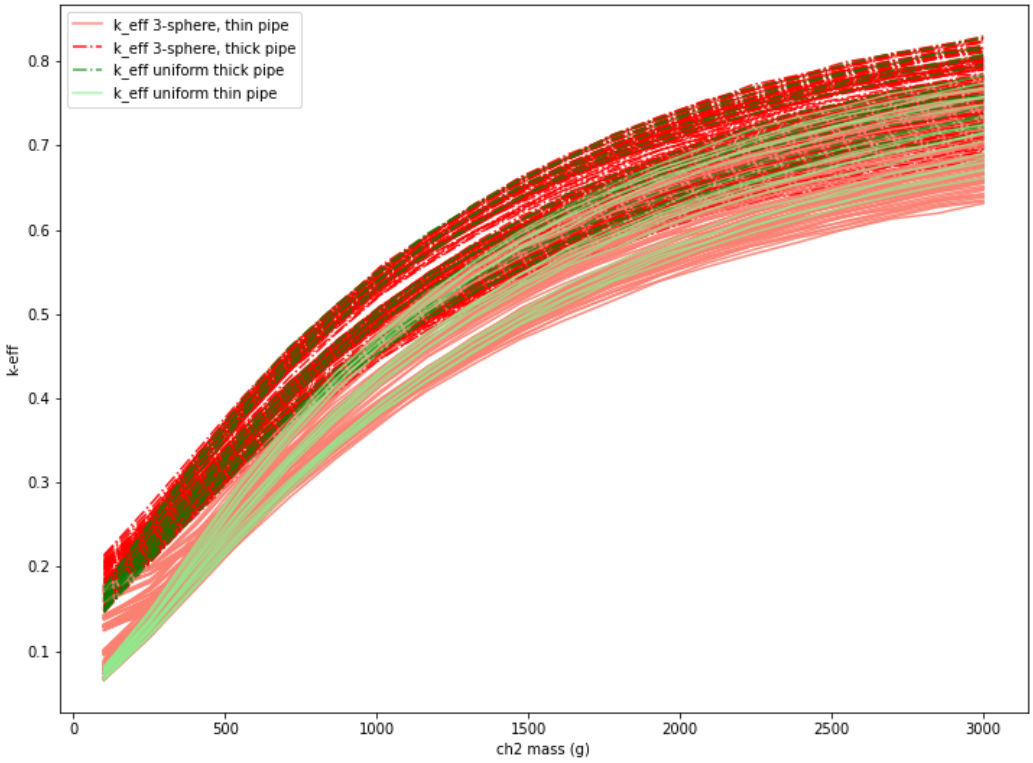

Figure J-7. Comparison of three-sphere k_{eff} to uniform k_{eff} for cylinderical wasteforms of 7.7 cm diameter.

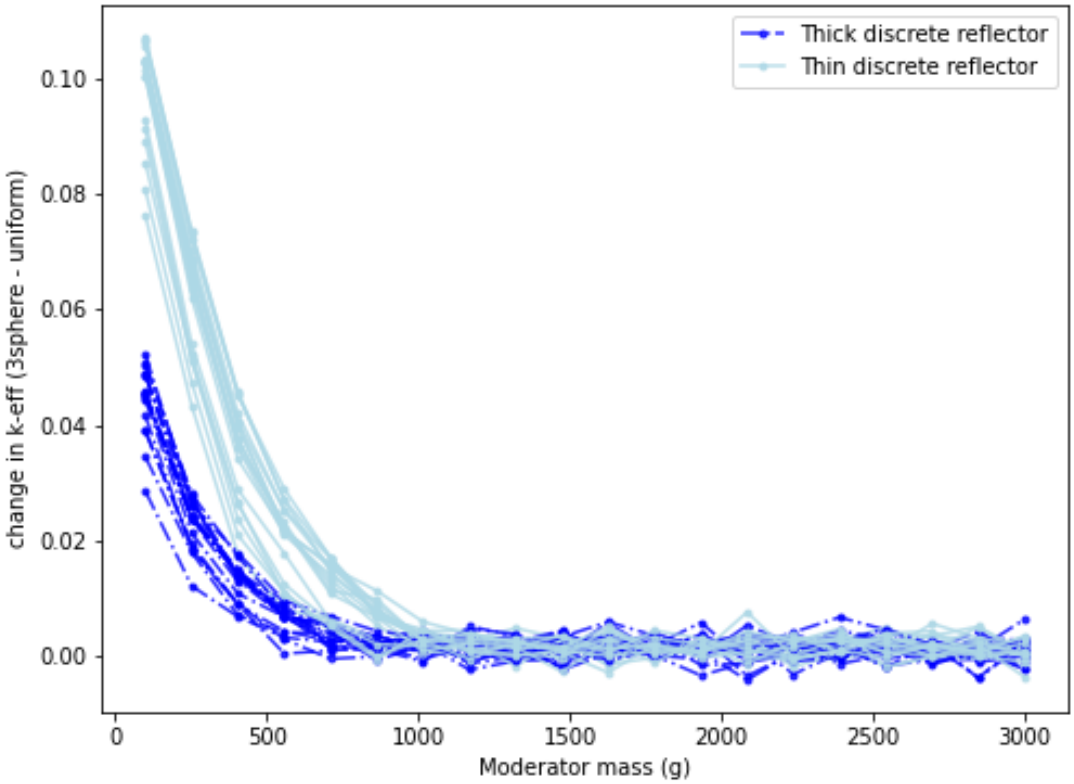

Figure J-8 Delta-k_{eff} when comparing highest reactivity three-sphere case to a uniform case (positive values correspond to cases where the highest reactivity three-sphere configuration has higher k_{eff} than uniform configuration.

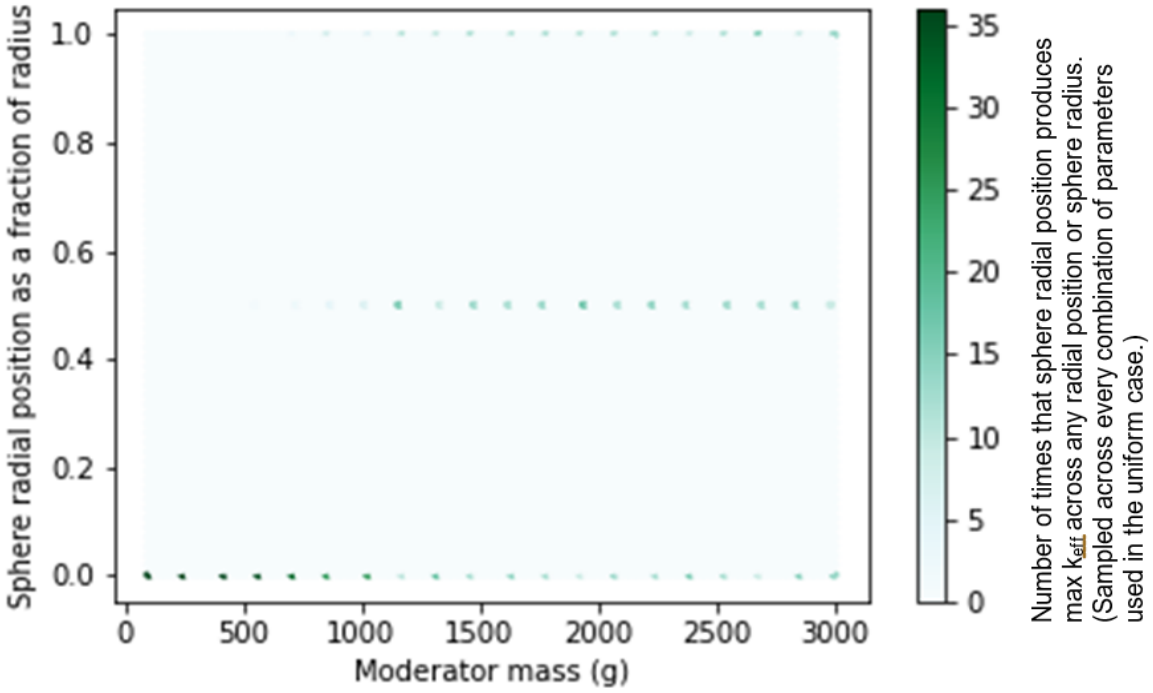

Figure J-9. Plot showing frequency of each radial position factor producing worst k-eff plotted for a given uniform case, plotted against moderator mass. Three sphere case. (Darker dots indicate higher frequency).

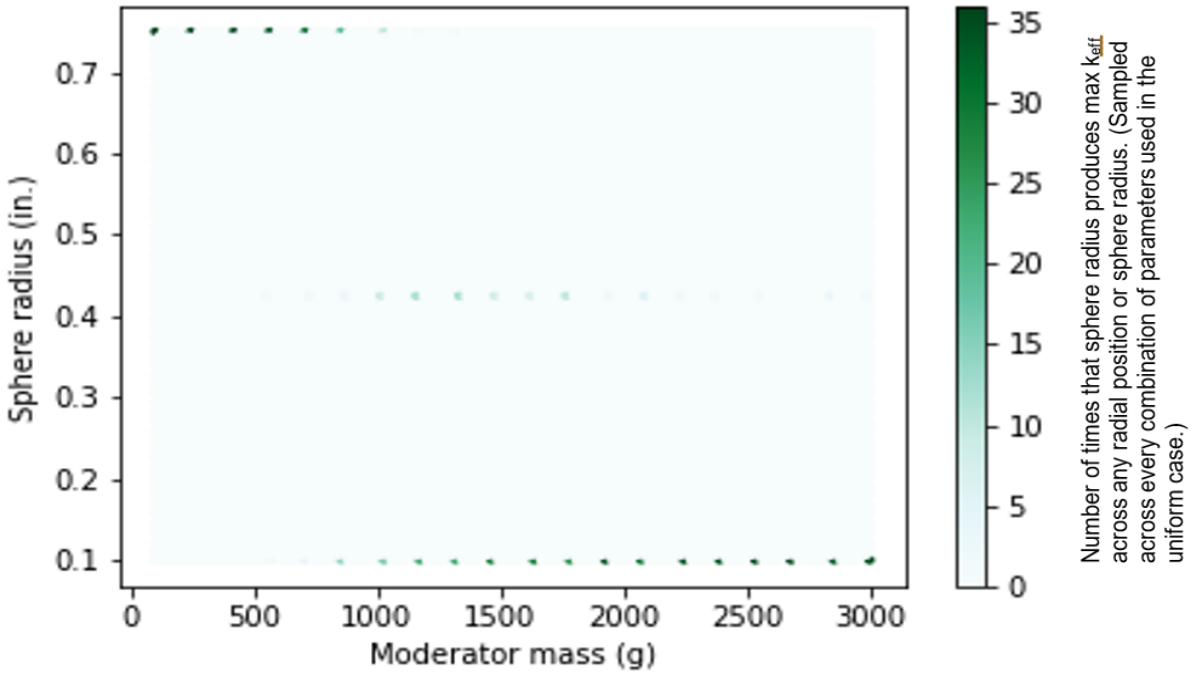

Figure J-10. Plot showing frequency of each sphere radius producing worst k-eff plotted for a given uniform case, plotted against moderator mass. Three sphere case. (Darker dots indicate higher frequency).

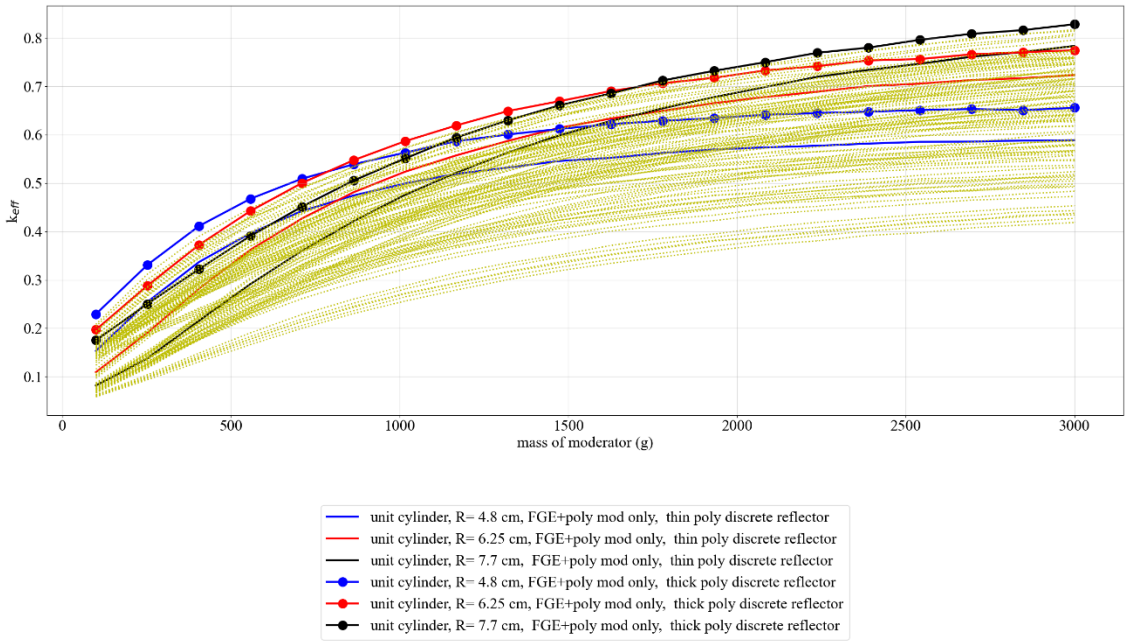

Figure J-11. Plot showing upper values of k_{eff} for various cylinder radii and polyethylene reflector combinations.

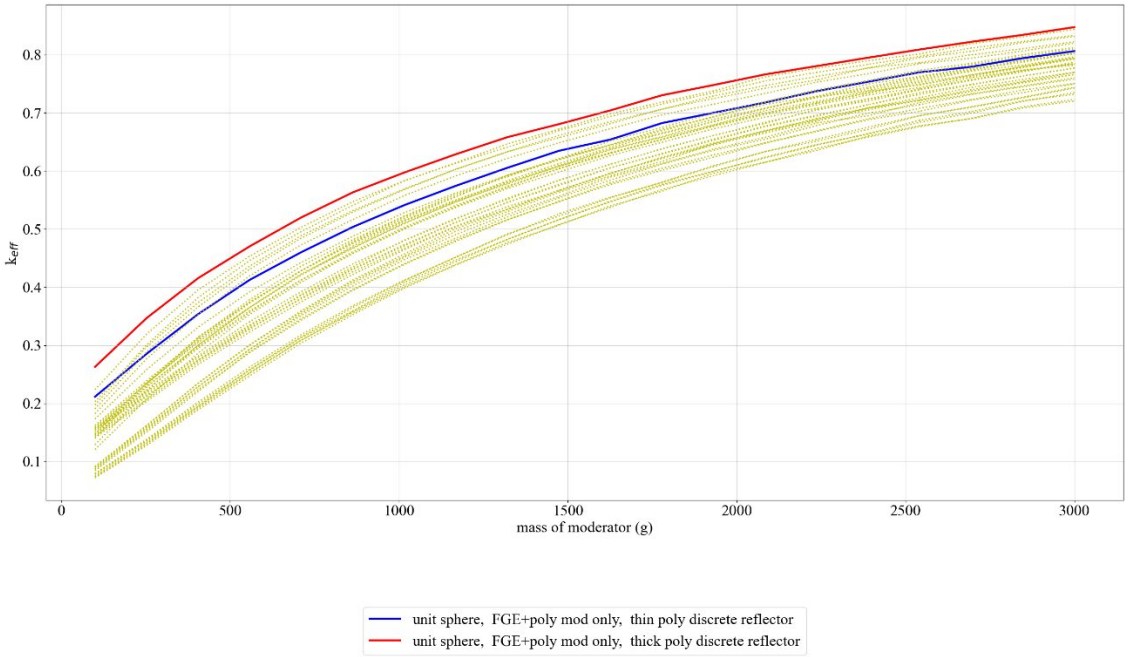

Figure J-12. Plot showing upper values of k_{eff} for spheres with different polyethylene reflector thicknesses.

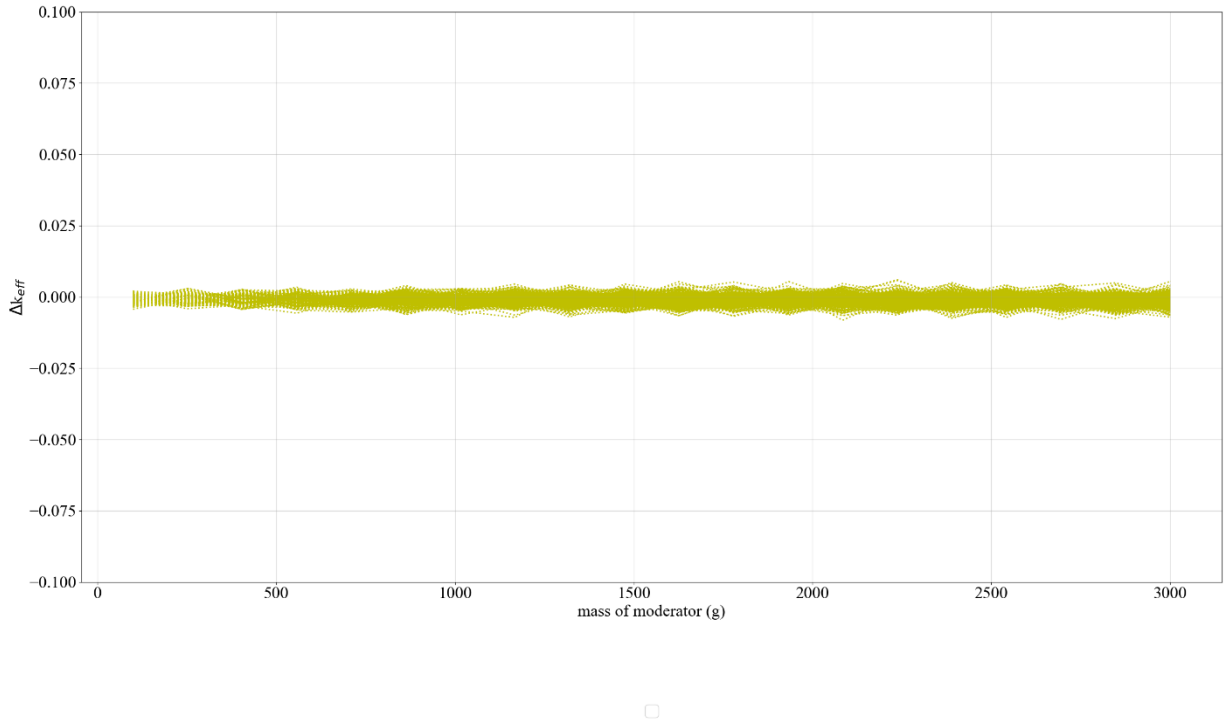

Figure J-13. Comparing k_{eff} computed using multigroup and continuous energy.

This page is intentionally blank

APPENDIX K. EVALUATION OF NEUTRON TRANSPORT FROM A CCO IN 50%MGO 50% NACL MIXTURE

This page is intentionally blank

APPENDIX K. EVALUATION OF NEUTRON TRANSPORT FROM A CCO IN 50%MGO 50% NACL MIXTURE

LIST OF FIGURES

LIST OF TABLES

This appendix documents a study related to neutron transport in the analysis interstitial mixtures of MGO and NaCl.

Shielding model of media surrounding a Pu fission source in a spherical CCC

An exercise to determine the sphere of influence of a CCO was performed using the parameters in Table K-1 for a spherical approximation. The CCO itself is not of particular importance, because the primary concern is the rate at which neutron flux tapers in the salt/MgO mixture. This exercise uses the MAVRIC shielding sequence in SCALE. The MAVRIC sequence uses the same input geometry and materials definition formats as KENO. For this calculation, the automated variance reduction feature was not needed and not used. Because the source was already simulating neutrons from fission of ^{239}Pu, fission was turned off in the model. Continuous energy ENDF-7.1 cross sections were used, and tallies were taken using the 27-group energy structure used for some Scale cross section libraries.

Table K-1. Parameters of the CCO modeled.

Parameter	Value
ch2_mass	252.6 g
graphite_mass	0 g
can_mass	0 g
thk_pipe	0.7112 cm
be_mass	0 g
h/x	22.66

Figure K-1 shows the assumed MAVRIC geometry, which is based on the KENO input set-1-12-uac1_uh_m2_graphite_sph_pp_1000_yr_para_00039_single.inp, with characteristics listed in Table K-1. In Figure K-1, green corresponds to the interstitial reflector (typically a combination of salt and MgO). The blue dot corresponds to the spherical waste form. The cuboid of salt has 600 cm edges with vacuum boundary conditions. A small point source is placed in the center of the sphere. This source is an arbitrary strength ^{239}Pu fission source having a Watt neutron energy spectrum.

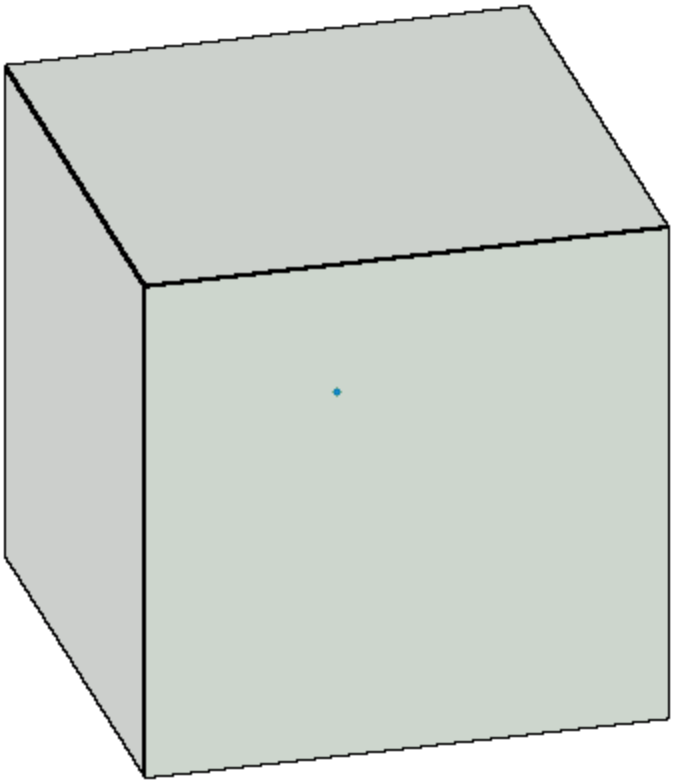

Figure K-1. Geometry of MAVRIC model with vacuum boundary conditions.

Figure K-2 shows neutron fluxes per source particle at varous distances from the source.

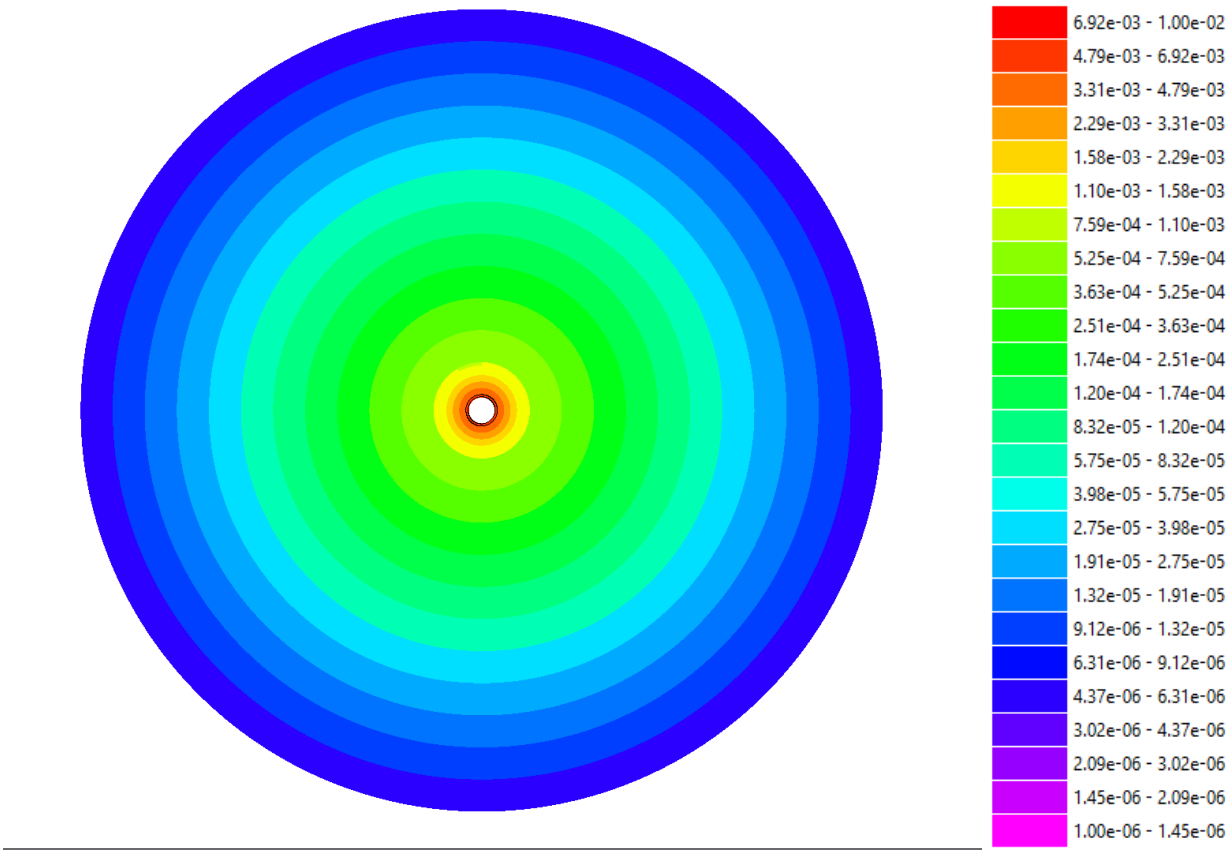

Figure K-2. Neutron flux tallies at locations in 50/50 NaCl/MgO mixture. Values in neutrons/cm^2-s per source particle.

Figure K-3 show the neutron intensities at various distances for various types of interstitial reflector media. Each tally volume is a 30 degree azimuthal sector 10 cm in radial thickness. The innermost radial sector has an inner edge at a radius of 5 cm, and an outer radius of 15 cm. The outermost sector has an inner edge at a radius of 115 cm and an outer radius of 125 cm. After leaving the CCO, the neutron intensity decreases exponentially, consistent with the solution to the diffusion equation for a point source in nonmultiplying media [15]. Table K-2 tabulates the values found in Figure K-3 and K-4. Note that the waste form is assumed to be approximately 10 cm in diameter, but that value will vary in reality.

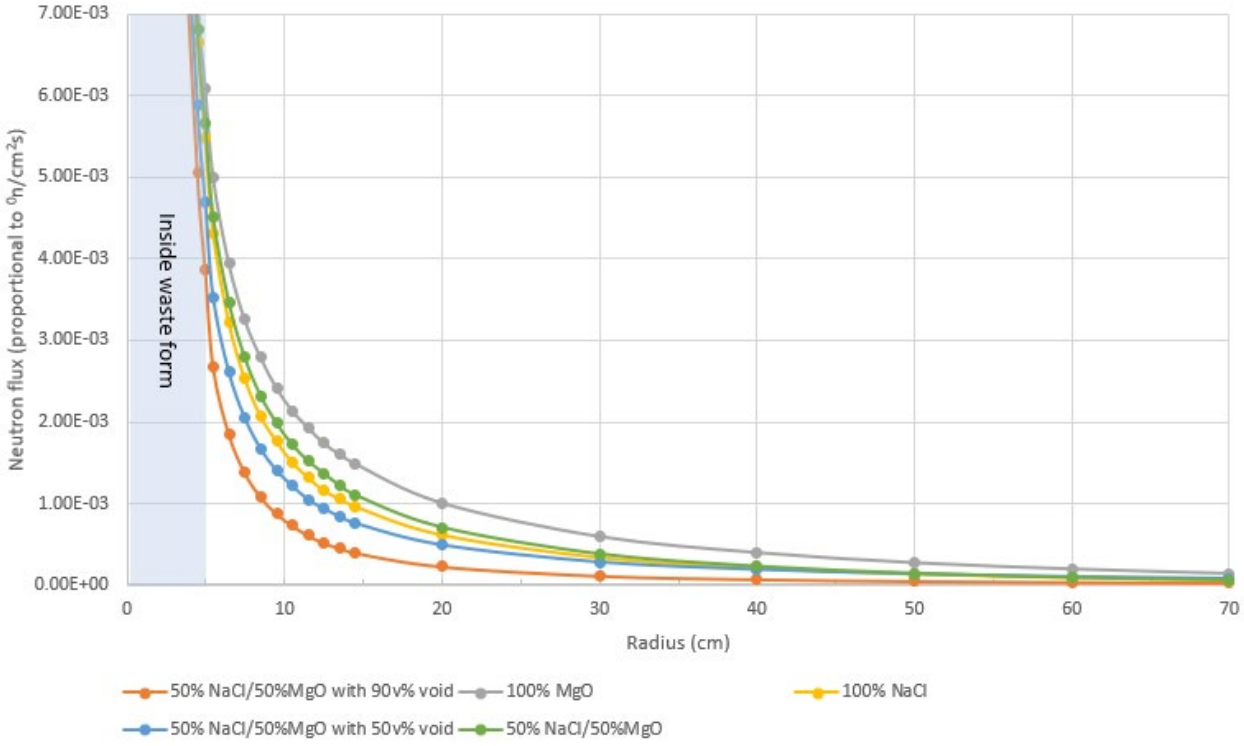

Figure K-3. Flux per source particle at various distances in the salt form the source (linear scale).

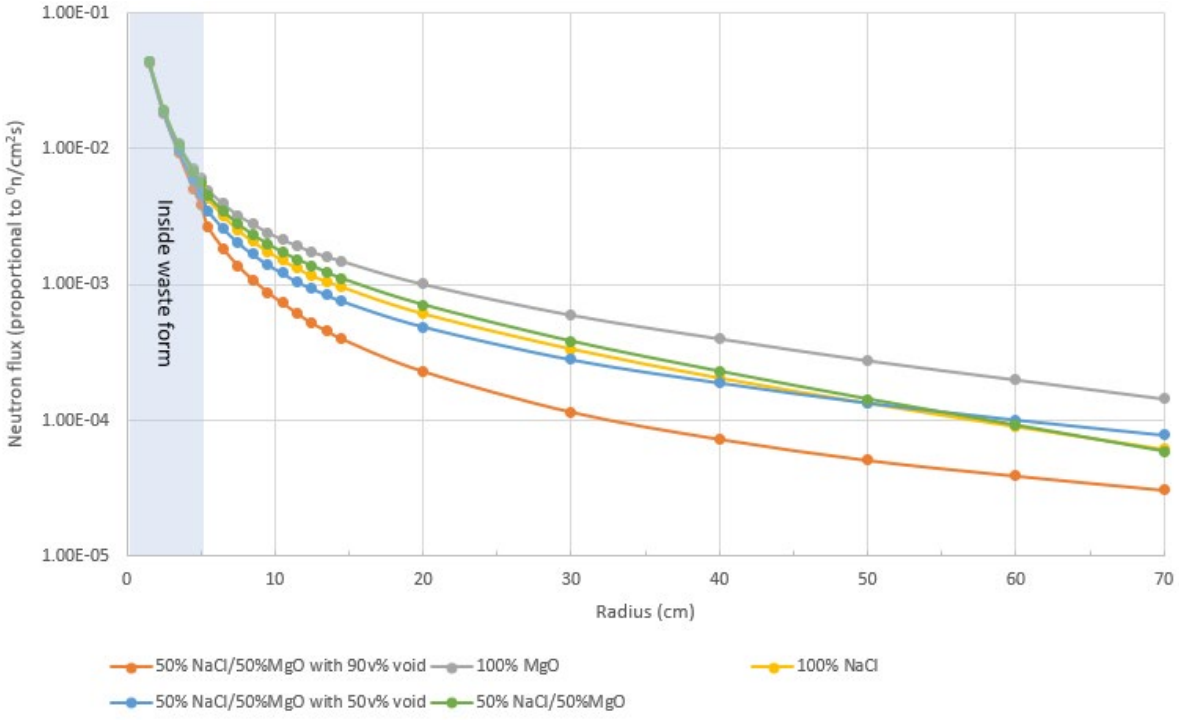

Figure K-4. Flux per source particle at various distances in the salt form the source (log scale).

Figure K-5 shows energy spectra of the neutron flux at various distances from the source. Within 10 cm of sphere, the neutron flux is mostly fast. This is a low moderator case, so fast flux near the fission source is expected because there is no moderator to slow the fast flux down. Any thermal flux is attenuated by about 4 orders of magnitude between 10 cm and 50 cm, with fluxes between 10 eV and 1 MeV penetrating farthest through the NaCl/MgO mixture.

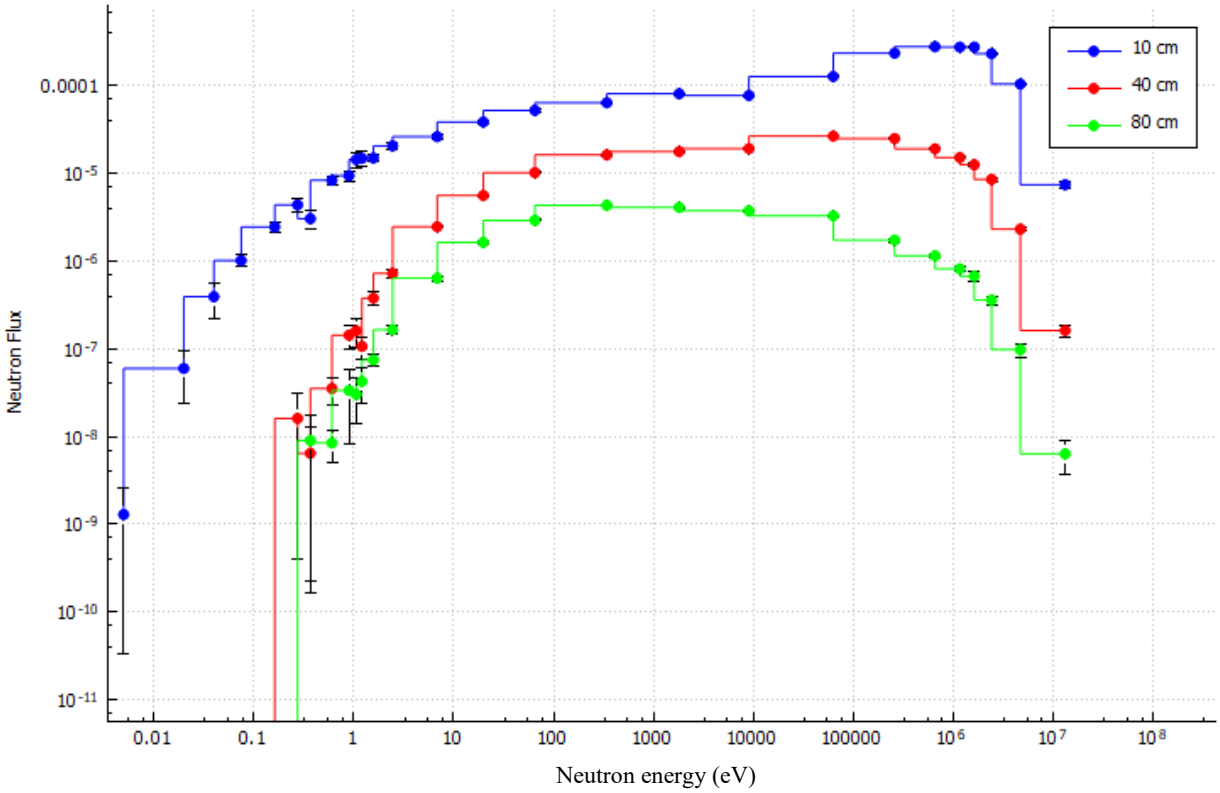

Figure K-5. Flux spectra (n/cm^{2}s per source particle) at 10 cm from source (blue), 50 cm from source (red) and 100 cm from source (green).

Table K-2. Flux per source particle (^{0}n/cm^{2}s) at various distances in the salt form the source

Radius	50% NaCl/50%MgO with 90v% void	Uncertainty	100% MgO	Uncertainty	100% NaCl	Uncertainty	50% NaCl/50%MgO with 50v% void	Uncertainty	50% NaCl/50%MgO	Uncertainty
1.5	4.30E-02	1.13E-04	4.43E-02	1.14E-04	4.41E-02	1.66E-04	4.37E-02	7.98E-05	4.42E-02	1.55E-04
2.5	1.82E-02	6.14E-05	1.94E-02	6.57E-05	1.93E-02	8.85E-05	1.87E-02	5.06E-05	1.93E-02	6.27E-05
3.5	9.31E-03	3.32E-05	1.09E-02	4.31E-05	1.06E-02	4.29E-05	9.89E-03	2.61E-05	1.06E-02	3.82E-05
4.5	5.06E-03	3.03E-05	7.19E-03	3.35E-05	6.65E-03	3.39E-05	5.87E-03	2.82E-05	6.82E-03	2.93E-05
5	3.87E-03	2.41E-05	6.09E-03	3.42E-05	5.48E-03	2.87E-05	4.70E-03	2.43E-05	5.66E-03	2.45E-05
5.5	2.67E-03	1.57E-05	4.99E-03	3.49E-05	4.30E-03	2.24E-05	3.53E-03	1.97E-05	4.51E-03	1.86E-05
6.5	1.85E-03	9.80E-06	3.94E-03	1.96E-05	3.22E-03	2.21E-05	2.61E-03	1.15E-05	3.47E-03	1.72E-05
7.5	1.38E-03	8.60E-06	3.25E-03	1.77E-05	2.53E-03	1.61E-05	2.05E-03	1.14E-05	2.79E-03	1.62E-05
8.5	1.09E-03	8.54E-06	2.79E-03	1.48E-05	2.07E-03	1.28E-05	1.67E-03	1.17E-05	2.32E-03	1.29E-05
9.5	8.80E-04	6.97E-06	2.42E-03	1.09E-05	1.76E-03	1.16E-05	1.40E-03	9.45E-06	1.99E-03	1.14E-05
10.5	7.32E-04	5.60E-06	2.14E-03	1.41E-05	1.51E-03	1.06E-05	1.22E-03	8.73E-06	1.72E-03	1.08E-05
11.5	6.14E-04	5.15E-06	1.93E-03	1.27E-05	1.32E-03	7.44E-06	1.05E-03	8.11E-06	1.52E-03	9.41E-06
12.5	5.19E-04	4.41E-06	1.74E-03	9.18E-06	1.16E-03	6.51E-06	9.34E-04	9.32E-06	1.37E-03	9.91E-06
13.5	4.56E-04	4.06E-06	1.60E-03	1.11E-05	1.06E-03	8.03E-06	8.36E-04	5.42E-06	1.22E-03	8.59E-06
14.5	3.98E-04	4.22E-06	1.49E-03	9.71E-06	9.61E-04	6.67E-06	7.56E-04	5.99E-06	1.10E-03	8.14E-06
20	2.29E-04	1.39E-06	1.01E-03	3.53E-06	6.12E-04	3.27E-06	4.89E-04	1.84E-06	7.07E-04	2.42E-06
30	1.15E-04	8.83E-07	5.97E-04	2.23E-06	3.37E-04	1.30E-06	2.79E-04	1.67E-06	3.80E-04	1.42E-06
40	7.25E-05	6.90E-07	4.00E-04	1.80E-06	2.06E-04	1.27E-06	1.88E-04	1.08E-06	2.28E-04	1.40E-06
50	5.07E-05	5.07E-07	2.76E-04	1.48E-06	1.35E-04	1.12E-06	1.34E-04	9.35E-07	1.43E-04	1.12E-06
60	3.89E-05	5.88E-07	1.99E-04	9.41E-07	9.04E-05	6.80E-07	1.00E-04	6.44E-07	9.14E-05	8.03E-07
70	3.06E-05	3.88E-07	1.44E-04	8.90E-07	6.15E-05	3.95E-07	7.77E-05	3.93E-07	5.87E-05	4.86E-07

This page is intentionally blank

APPENDIX L. SET-5: RESULTS OF THE NONUNIFORM ARRAY FOR THE UPPER HORIZON CALCULATIONS WITH ALTERNATIVE INTERSTITIAL REFLECTOR MATERIALS

This page is intentionally blank

APPENDIX L. SET-5: RESULTS OF THE NONUNIFORM ARRAY FOR THE UPPER HORIZON CALCULATIONS WITH ALTERNATIVE INTERSTITIAL REFLECTOR MATERIALS

The purpose of this Appendix is to document the studies performed to evaluate the reactivity effect of various interstitial material assumptions for the material density of the MgO and salt interstitial material as well as the reactivity effect of a brine intrusion. Since the important parameter being evaluated is the interstitial material the model is modified in some cases to include more interstitial material by moving the location of the y-direction reflective boundary conditions by 50 cm (see also Appendix E). The full summary of the cases evaluated in this Appendix are shown in Table L-1.

The analysis model for the studies in this appendix is based on the set-2-uh nonuniform array model discussed in Section 6.3. For each of the cases listed in Table L-1 the full set of parametric sweeps is provided in Table L-2. For the case with the brine intrusion into the waste form mixture itself (case 5h), the brine mixture replaces the filler mass (graphite is replaced by brine).

LIST OF FIGURES

LIST OF TABLES

Table L-1. Summary of cases for set-5.

Case	Purpose	Interstitial material mixture	Interstitial material density	External salt box material	y-direction reflective boundary condition location	Waste form filler material
Set-5 base case	Same as set-2-uh but with alternative reflective boundary condition location	Mgo+salt	Full density	Pure salt	+ 50 cm	Graphite
Set-5a	Evaluates the assumption that full density is appropriate	50% Mgo 50% salt	Half density	Pure salt	+ 50 cm	Graphite
Set-5b	Evaluates the assumption that full density is appropriate	Void	0 density	Pure salt	+ 50 cm	Graphite
Set-5c	Evaluates the assumption that MgO in the mixture is appropriate	100% salt	Full density	Pure salt	+ 50 cm	Graphite
Set-5d	Shows the reactivity effect of brine without MgO	100% brine (no Mgo)	Full density	Pure salt	+ 50 cm	Graphite
Set-5e	Shows the reactivity effect of brine with MgO	100% brine (no Mgo)	Full density	Pure salt	+ 0 cm	Graphite
Set-5f	Shows the reactivity effect of including brine in the outer salt box	100% brine (no Mgo)	Full density	Brine	+ 0 cm	Graphite
Set-5g	Shows the reactivity effect of including MgO in the brine	50% brine 50% MgO	Full density	Brine	+ 0 cm	Graphite
Set-5h	Shows the reactivity effect of including brine in the waste form	50% brine 50% MgO	Full density	Brine	+ 0 cm	50% brine 50% MgO

Table L-2. Summary of parametric sweeps for set-5 (applicable to set-5 and versions a through h[9])

Case	Model type	Waste form shape	Waste form moderator	Filler material (0, 2,000, 4,000 g)	Metal in filler	Discrete reflector (thin 0.001 and thick 0.7112 cm)	be (g)	Subcase
Set-5	Uniform array stacked six high with CCO pitch reduction x = 25%, y = 10%, z = no space	Cylinder (radius range 4.8, 6, 7.7 and height defined by total volume of mass)	water	c12	SS from can (0, 500, 1,000 g)	steel	0 to 585	set-5-1
			poly	c12		steel		set-5-2
			water	c12		poly		set-5-3
			poly	c12		poly		set-5-4
			water	generic		steel		set-5-5
			poly	generic		steel		set-5-6
			water	generic		poly		set-5-7
			poly	generic		poly		set-5-8
		Sphere (radius defined by total volume of mass)	water	c12		steel		set-5-9
			poly	c12		steel		set-5-10
			water	c12		poly		set-5-11
			poly	c12		poly		set-5-12
			water	generic		steel		set-5-13
			poly	generic		steel		set-5-14
			water	generic		poly		set-5-15
			poly	generic		poly		set-5-16
		Cylinder (radius range 4.8, 6, 7.7 and height defined by total volume of mass) with 25 g B_4C	poly	c12		poly		set-5-17
		Sphere (radius defined by total volume of mass) with 25 g B_4C	poly	c12		poly		set-5-18

[9] set-5h does not include sub-cases 17 or 18 with B_4C.

Summary of Results

- Figure L-1: The delta-k between set-2 and set-5 shows that adding 50 cm of interstitial material between the waste forms and the reflective boundary conditions in the y-direction always yields a decrease in k_{eff}. However, the reactivity effect is relatively small, typically less than 5% delta-k and typically less than 2.5% delta-k for the representative curves.

- Figure L-2. The delta-k between set-5 base and set-5a shows that reducing the material density by 50% for the interstitial material between the waste forms always yields a moderate decrease in k_{eff}. The reactivity effect is moderate, typically less than 7.5% delta-k overall. These results show that full density interstitial material is appropriate.

- Figure L-3. The delta-k between set-5 base and set-5b shows that reducing the material density by 100% for the interstitial material between the waste forms (void) typically yields a significant decrease in k_{eff}. The reactivity effect is significant for under moderated cases, typically less than 22% delta-k overall. These results show that the trend seen for the half density set-5a cases continues and that full density interstitial material is appropriate.

- Figure L-4: The delta-k between set-5 base and set-5c shows that removing the MgO from the interstitial material between the waste forms always yields a decrease in k_{eff}. However, the reactivity effect is relatively small, typically less than 6% delta-k and typically less than 4% delta-k for the representative curves. These results show that the assumption of using MgO is appropriate but not overly conservative because the overall impact is relatively small.

- Figure L-5: The delta-k between set-5 base and set-5d shows that the reactivity effect of the brine in the interstitial material between the waste forms is highly dependent upon whether the waste form is under moderated or over moderated. For cases where the waste form is under moderated, up to about 0.9 kg of moderator, the brine can provide additional moderation and thus increases k_{eff} moderately. Otherwise, when the waste form is not under moderated, the brine reduces reactivity. However, cases in set-2 under 1 kg of moderator are well below subcritical.

- Figure L-6: The plot provides k_{eff} curves for set-5d results compared to a set-2 representative curve. The results shown in Figure L-5 and Figure L-6 show that while for under moderated waste form cases the brine may increase reactivity slightly, the slight increase in reactivity remains well subcritical.

- Figure L-7: The delta-k between set-2 and set-5e shows that the reactivity effect of the brine in the interstitial material between the waste forms is dependent upon the amount of moderator in the waste form. This effect is increased when the amount of brine is decreased (the additional 50 cm of interstitial material in the y-direction is removed). For cases where the waste form is under moderated, up to about 1.5 kg of moderator, the brine can provide additional moderation and thus increases k_{eff} moderately. Otherwise, when the waste form is not under moderated, the brine reduces reactivity.

- Figure L-8: The plot provides k_{eff} curves for set-5e results compared to a set-2 representative curve. The results shown in Figure L-7 and Figure L-8 show that while for under moderated waste form cases the brine may increase reactivity slightly, the slight increase in reactivity remains well subcritical.

- Figure L-9: The delta-k between set-2 and set-5f shows that, similar to set-5e, in which the brine is in the interstitial material between the waste forms, and it is also included in the exterior salt box, the effect of the additional brine is negligible compared to when it is not included (Figure L-7).

- Figure L-10: The delta-k between set-2 and set-5g shows an impact that is similar to that of set-5e, but when the brine in the interstitial material between the waste forms is a 50% mixture with MgO, the positive reactivity effect of the brine is reduced for under moderated cases.

- Figure L-11: The delta-k between set-2 and set-5h shows that when the brine and MgO mixture replaces the graphite filler material in waste form there is a significant positive reactivity effect for under moderated cases.

- Figure L-12: The plot provides k_{eff} curves for set-5h results compared to a set-2 representative curve. The results shown in Figure L-11 and Figure L-12 show that while for under moderated waste form cases the brine and MgO mixture replacing the graphite filler may increase reactivity significantly, the increase in reactivity remains well subcritical.

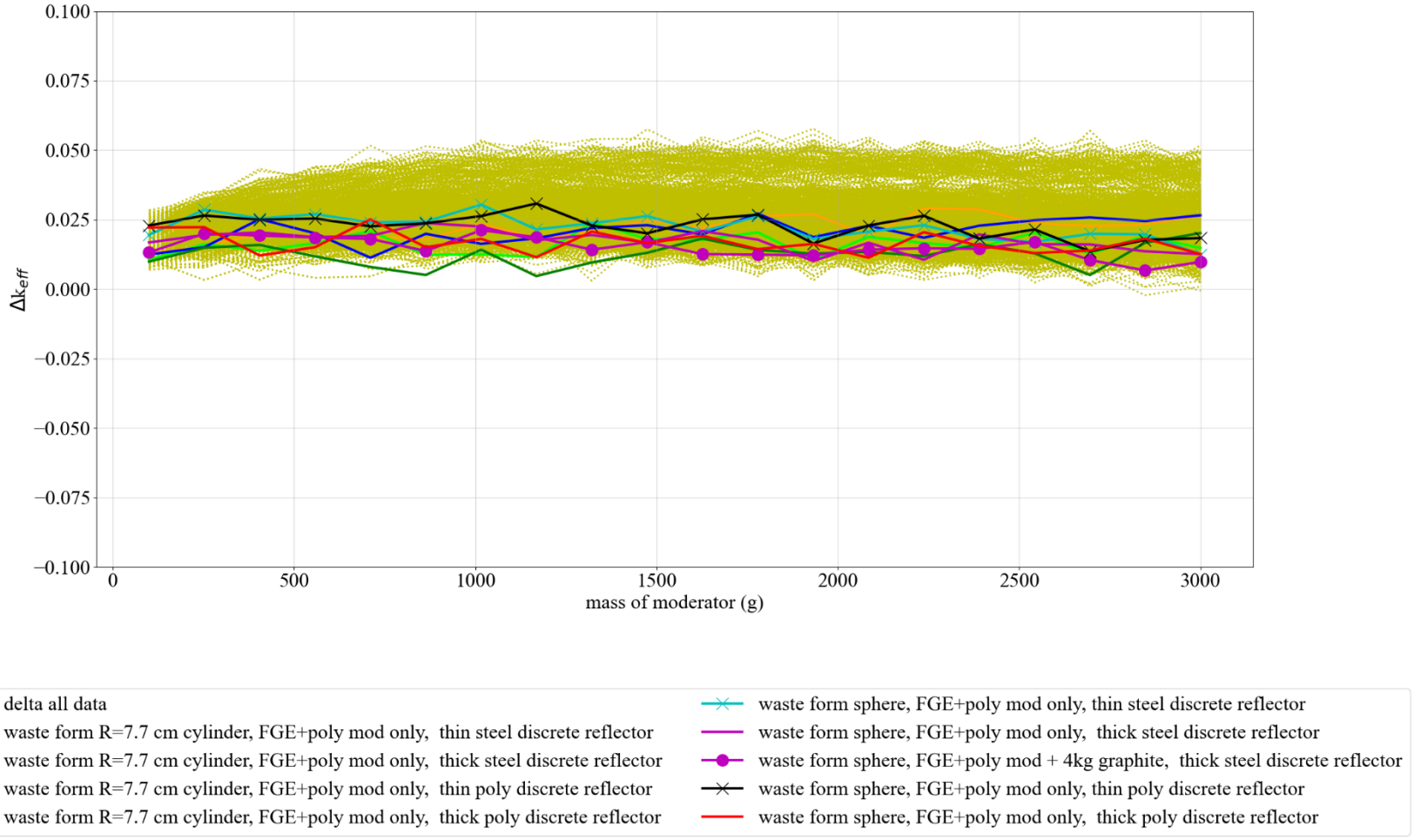

Figure L-1. Delta-k between set-2 and set-5 base case (set-2 minus set-5) to evaluate location of reflective boundary conditions.

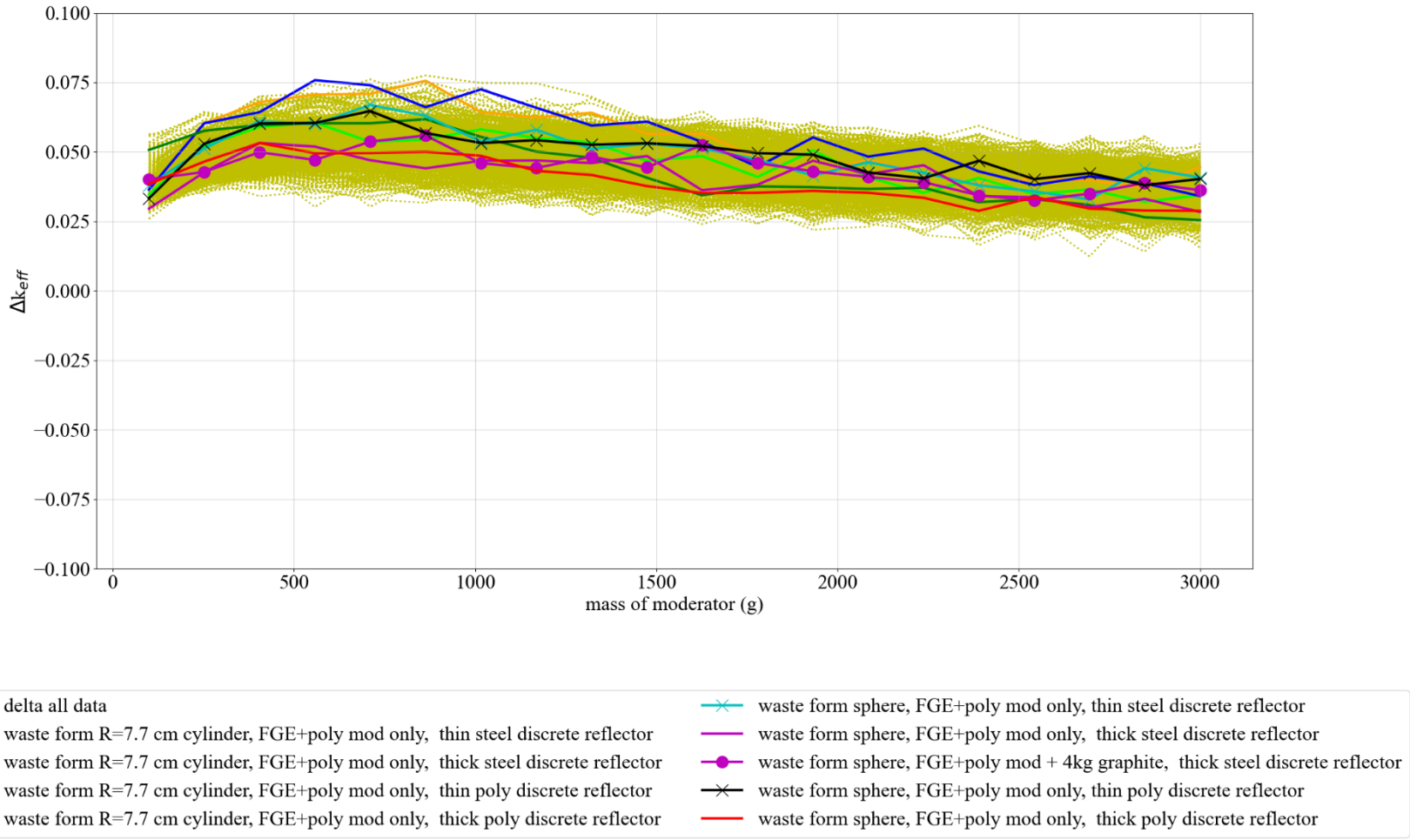

Figure L-2. Delta-k between set-5 base case and set-5a (set-5 minus set-5a) to evaluate the effect of half density interstitial reflective material.

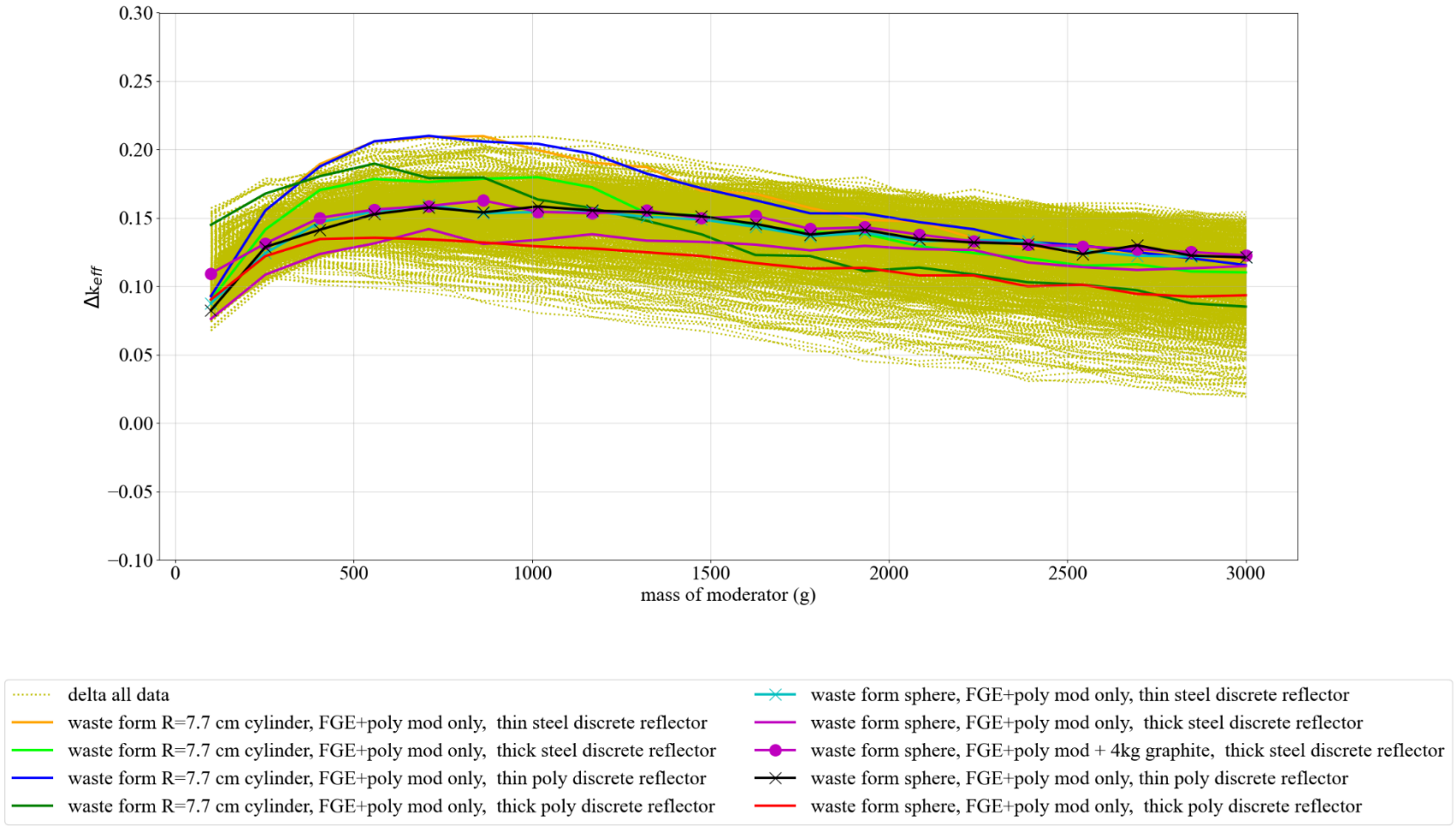

Figure L-3. Delta-k between set-5 base case and set-5b (set-5 minus set-5b) to evaluate the effect of zero density (void) interstitial reflective material.

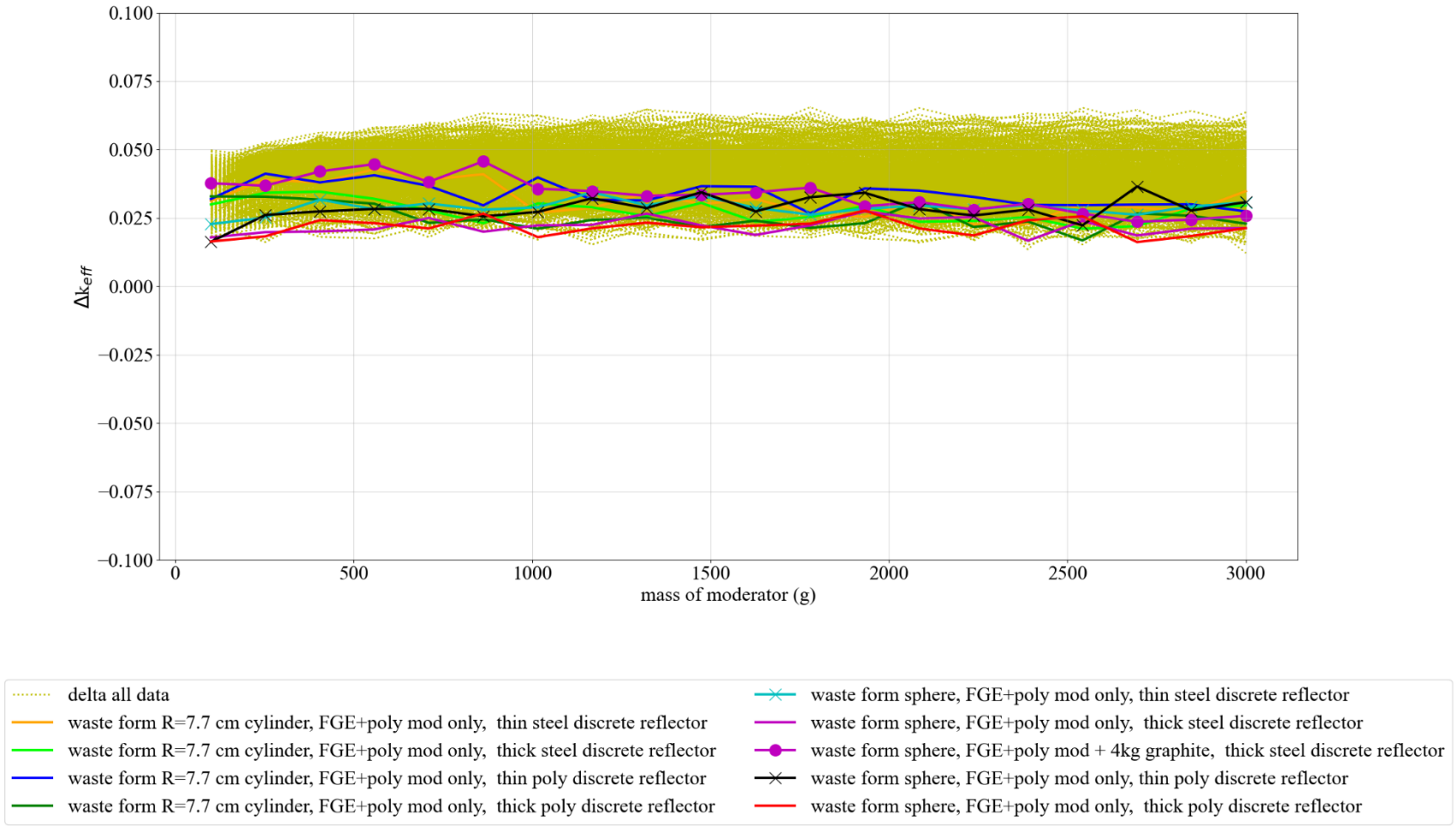

Figure L-4. Delta-k between set-5 base case and set-5c to evaluate the effect of pure salt as interstitial reflective material.

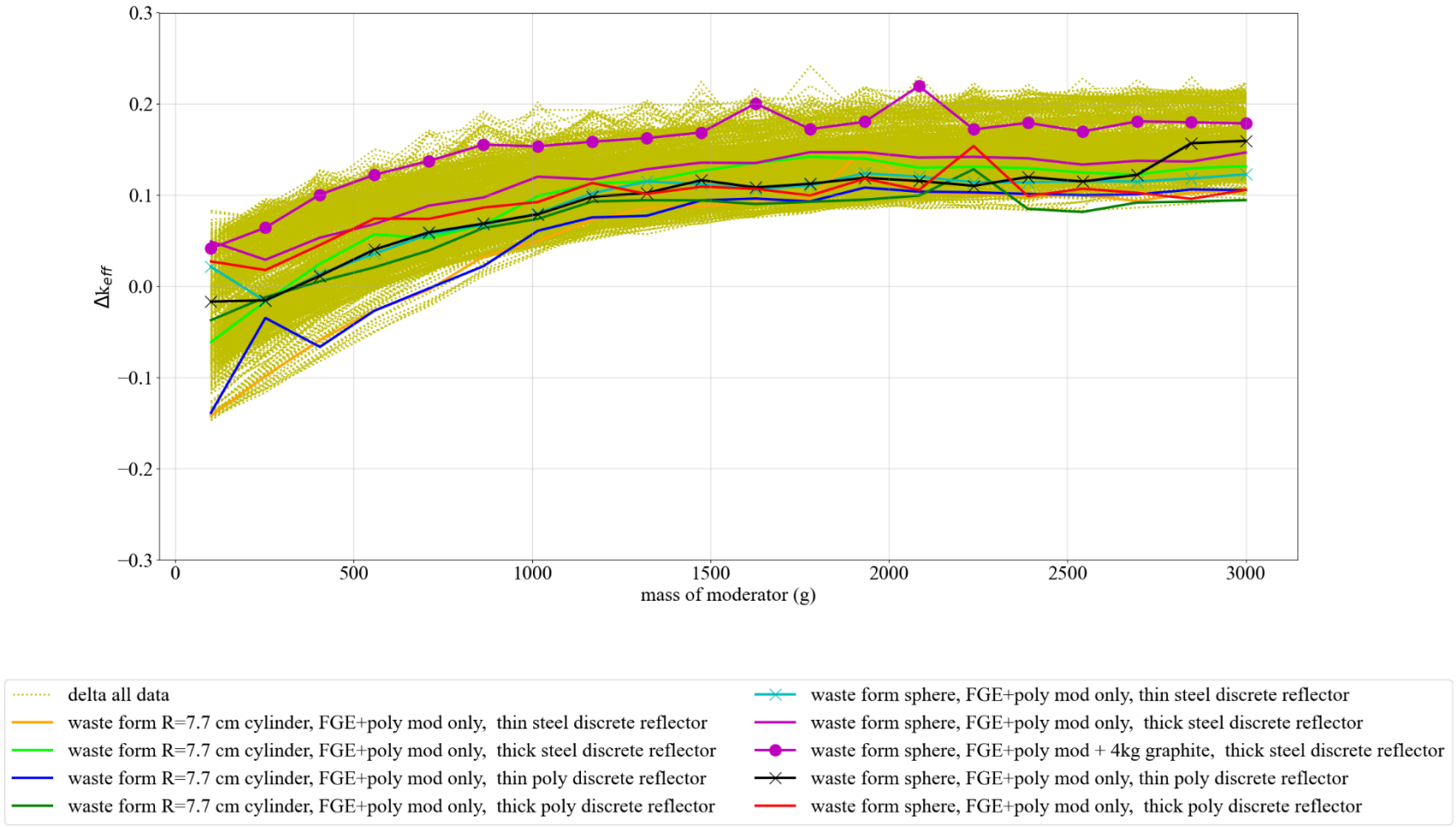

Figure L-5. Delta-k between set-5 base case and set-5d to evaluate the effect of brine (no MgO) as interstitial reflective material.

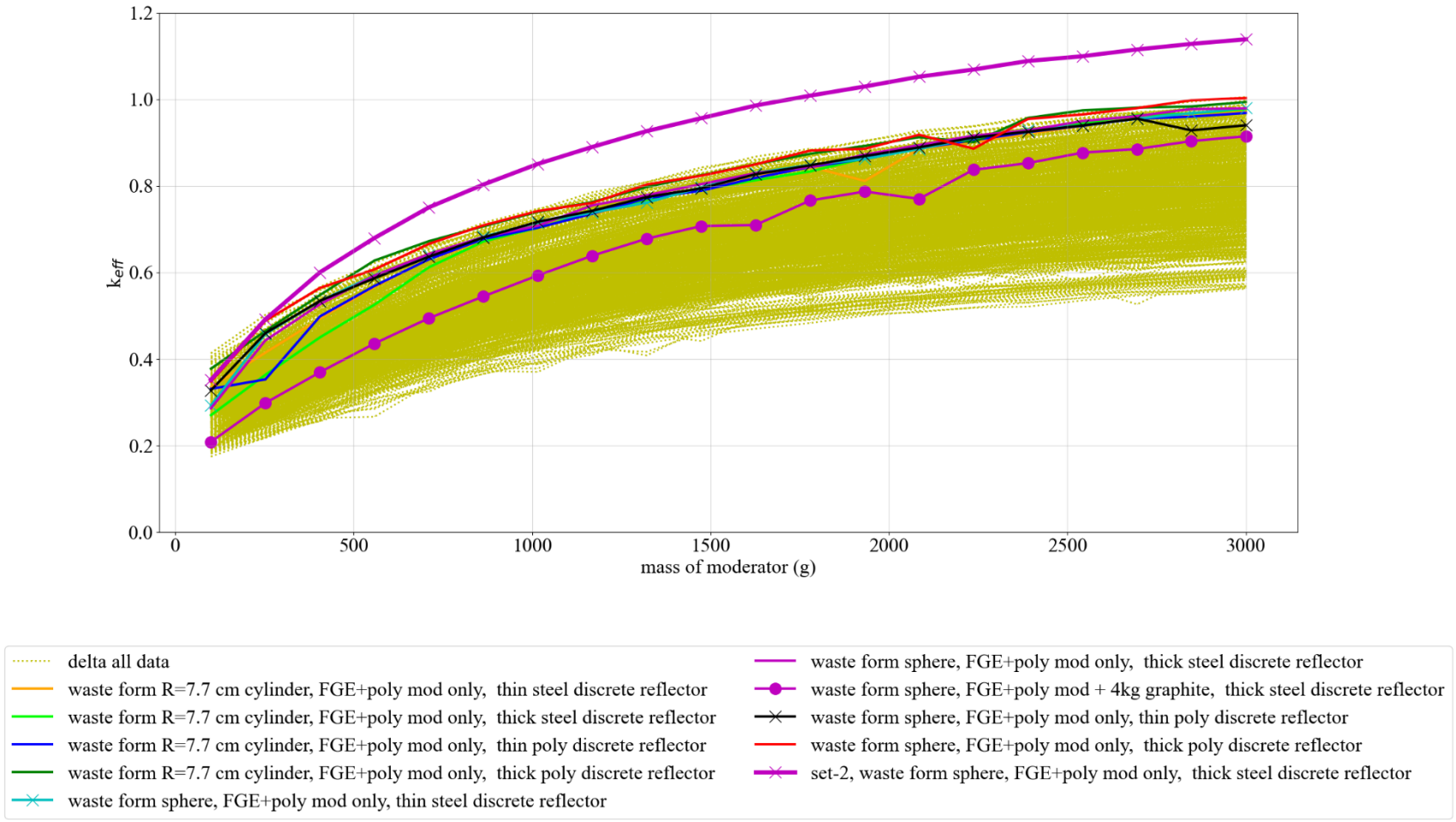

Figure L-6. Reactivity of set-5d compared to a single set-2 representative curve to evaluate the effect of brine (no MgO) as interstitial reflective material.

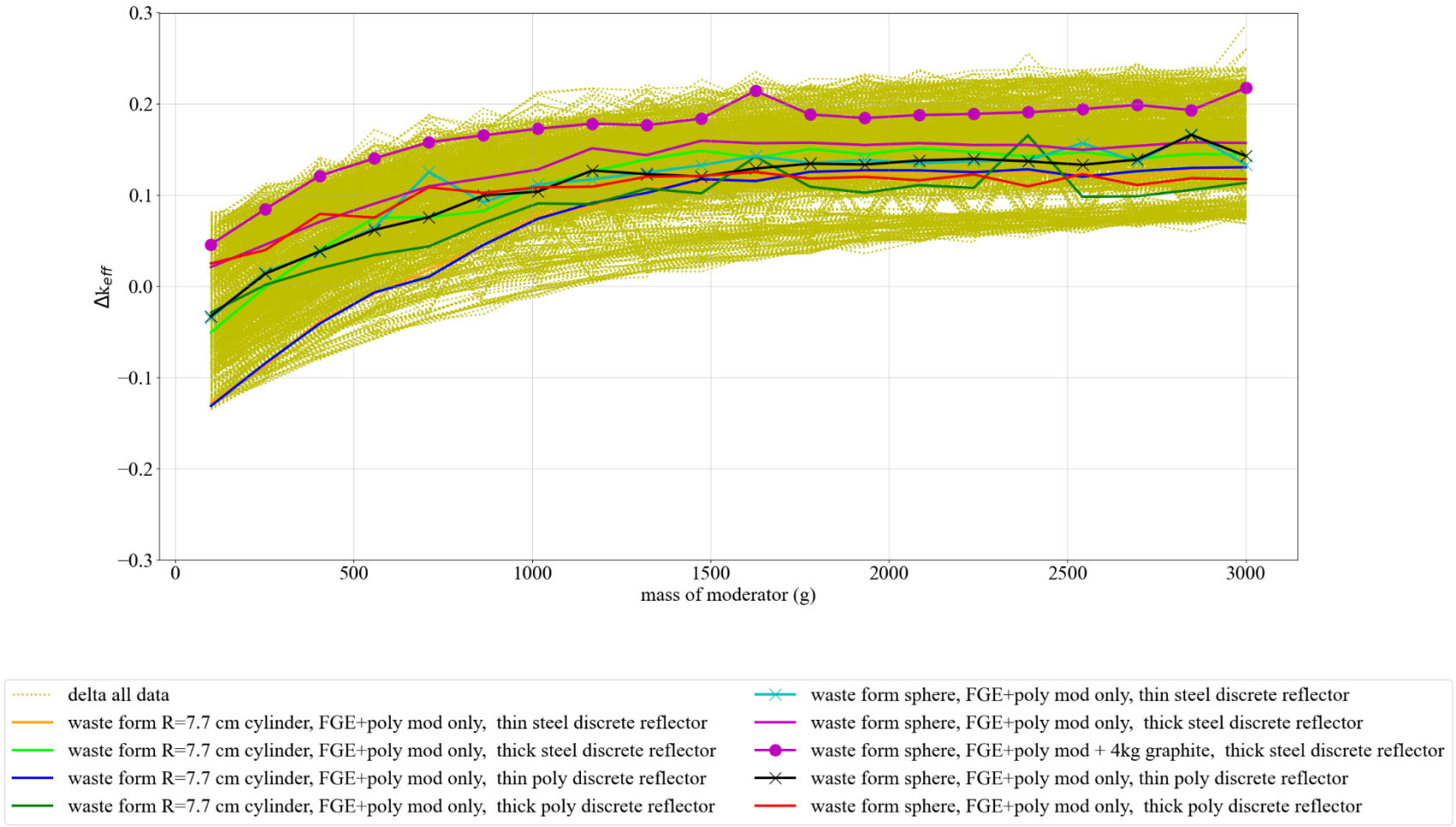

Figure L-7. Delta-k between set-2 and set-5e to evaluate the effect of brine (no MgO) as interstitial reflective material but with the additional 50 cm of space to locate the y-direction reflective boundary conditions removed (similar to set-2).

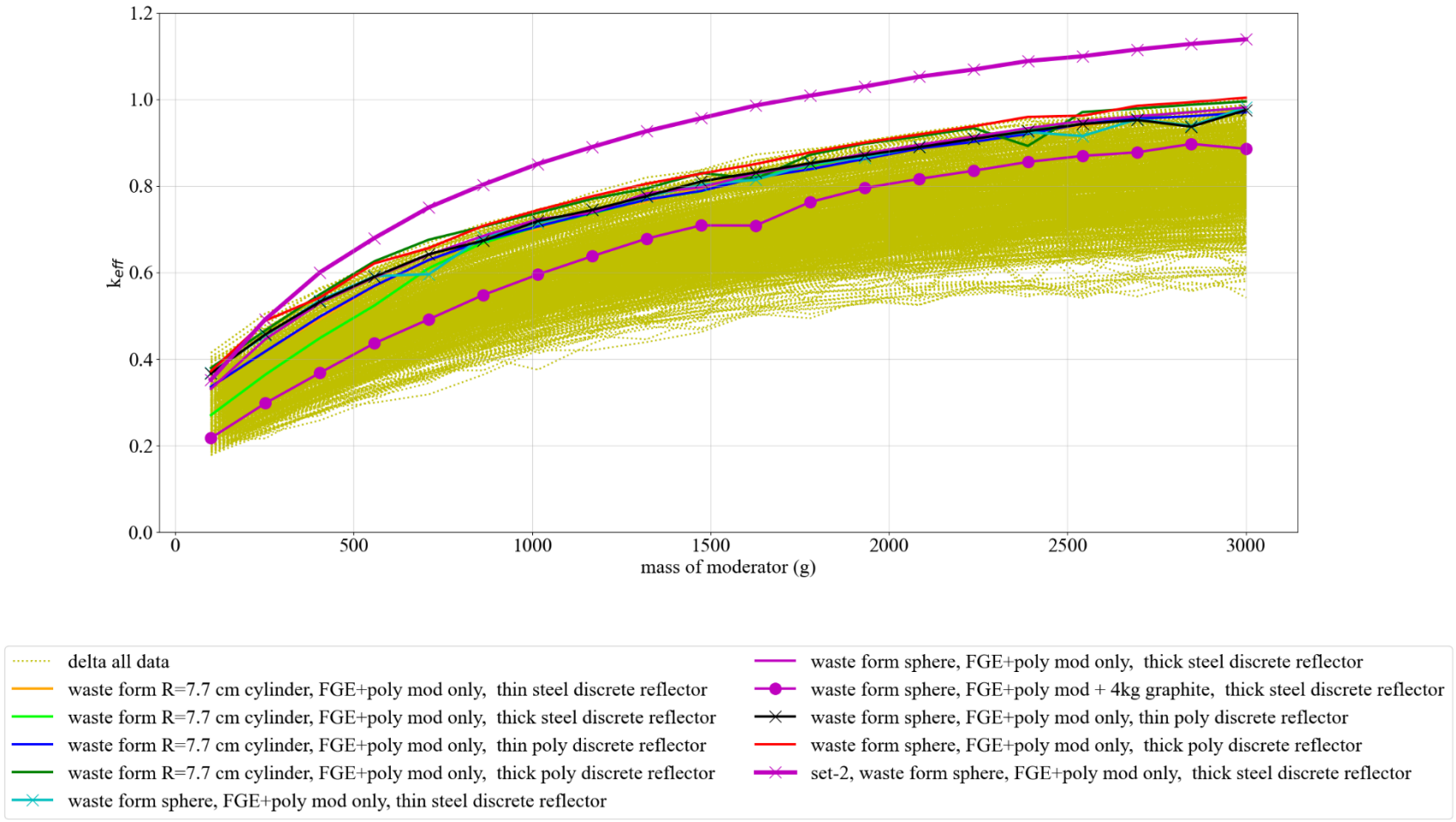

Figure L-8. Reactivity of set-5e compared to a single set-2 representative curve to evaluate the effect of brine (no MgO) as interstitial reflective material but with the additional 50 cm of space to locate the y-direction reflective boundary conditions removed (similar to set-2).

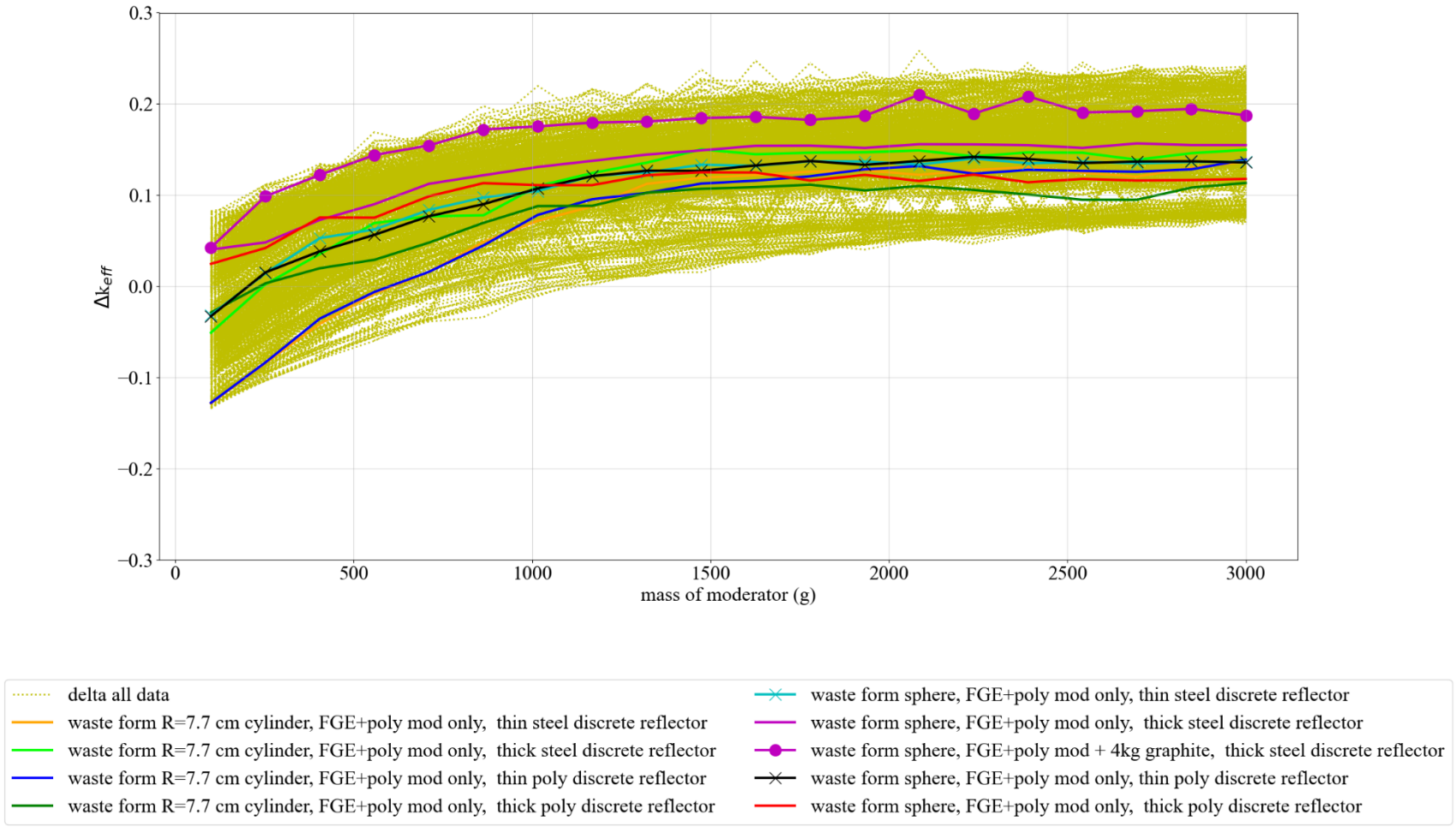

Figure L-9. Delta-k between set-2 and set-5f to evaluate the effect of brine (no MgO) as interstitial reflective material but with the additional 50 cm of space to locate the y-direction reflective boundary conditions removed (similar to set-2) and brine in the external salt box.

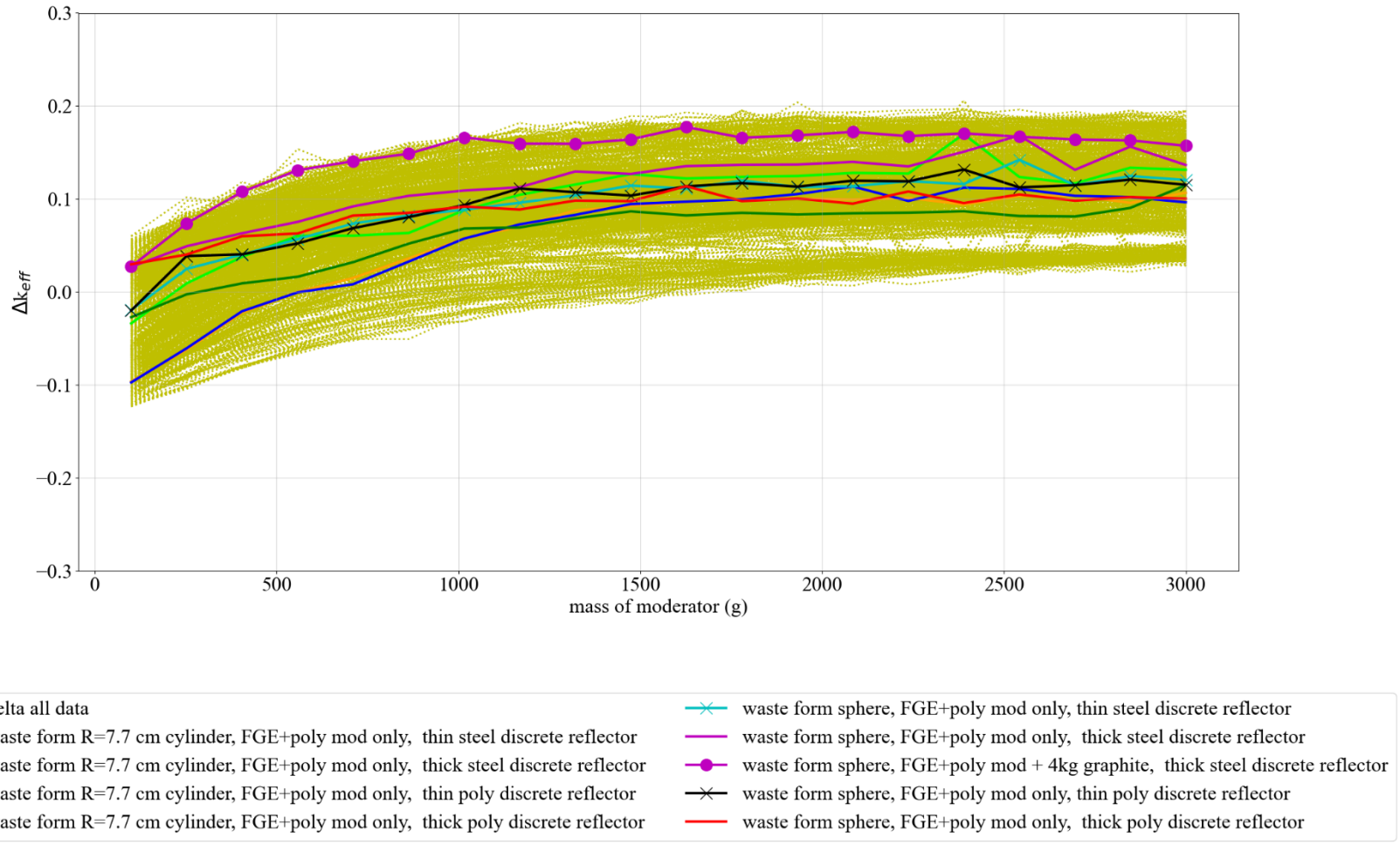

Figure L-10. Delta-k between set-2 and set-5g to evaluate the effect of brine in a 50% mixture with MgO as interstitial reflective material but with the additional 50 cm of space to locate the y-direction reflective boundary conditions removed (similar to set-2) and brine in the external salt box.

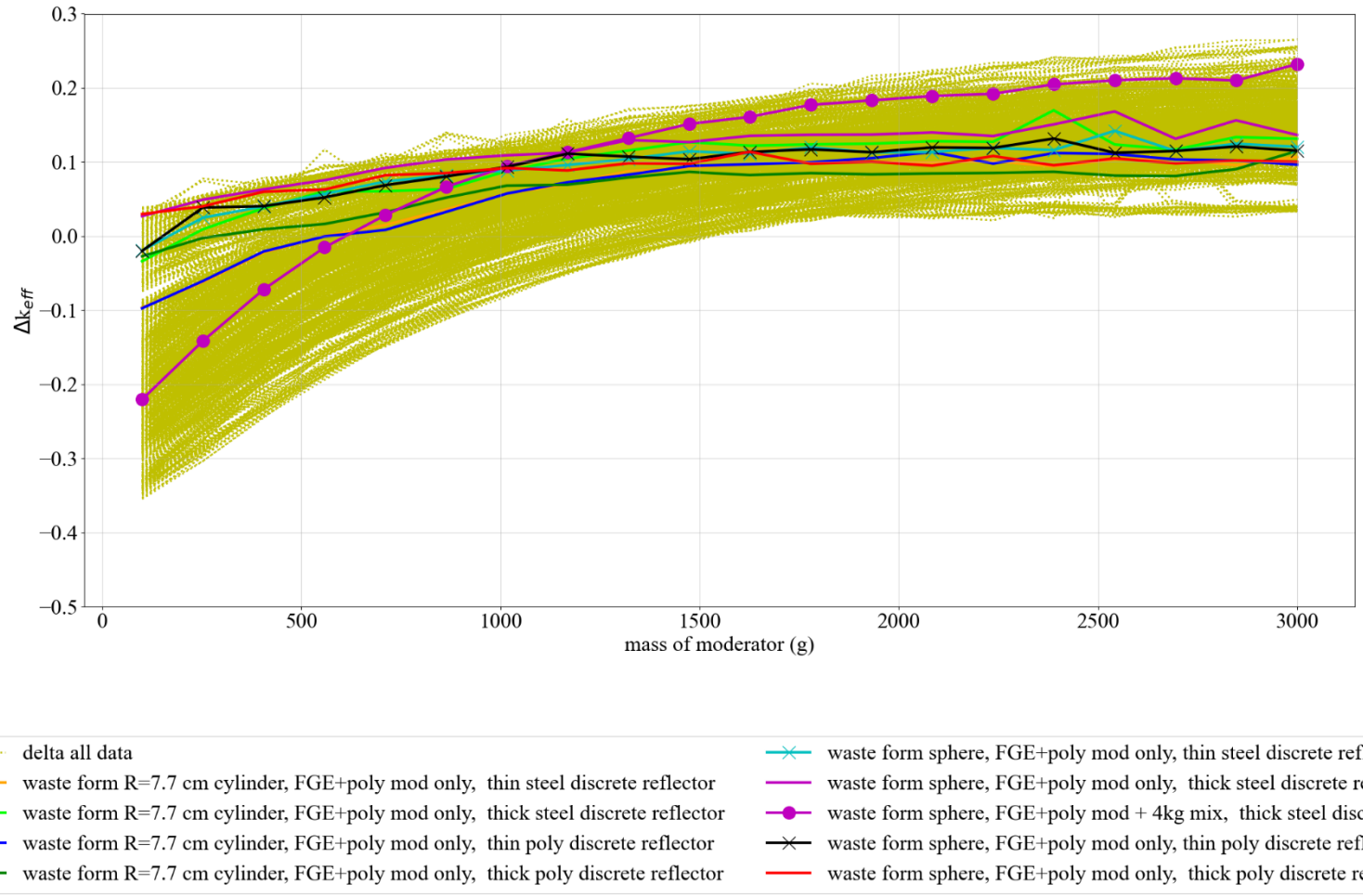

Figure L-11. Delta-k between set-2 and set-5h to evaluate the effect of brine in a 50% mixture with MgO as interstitial reflective material but with the additional 50 cm of space to locate the y-direction reflective boundary conditions removed (similar to set-2) and brine in the external salt box. The graphite filler, when present, is replaced by an equivalent mass of brine in a 50% mixture with MgO.

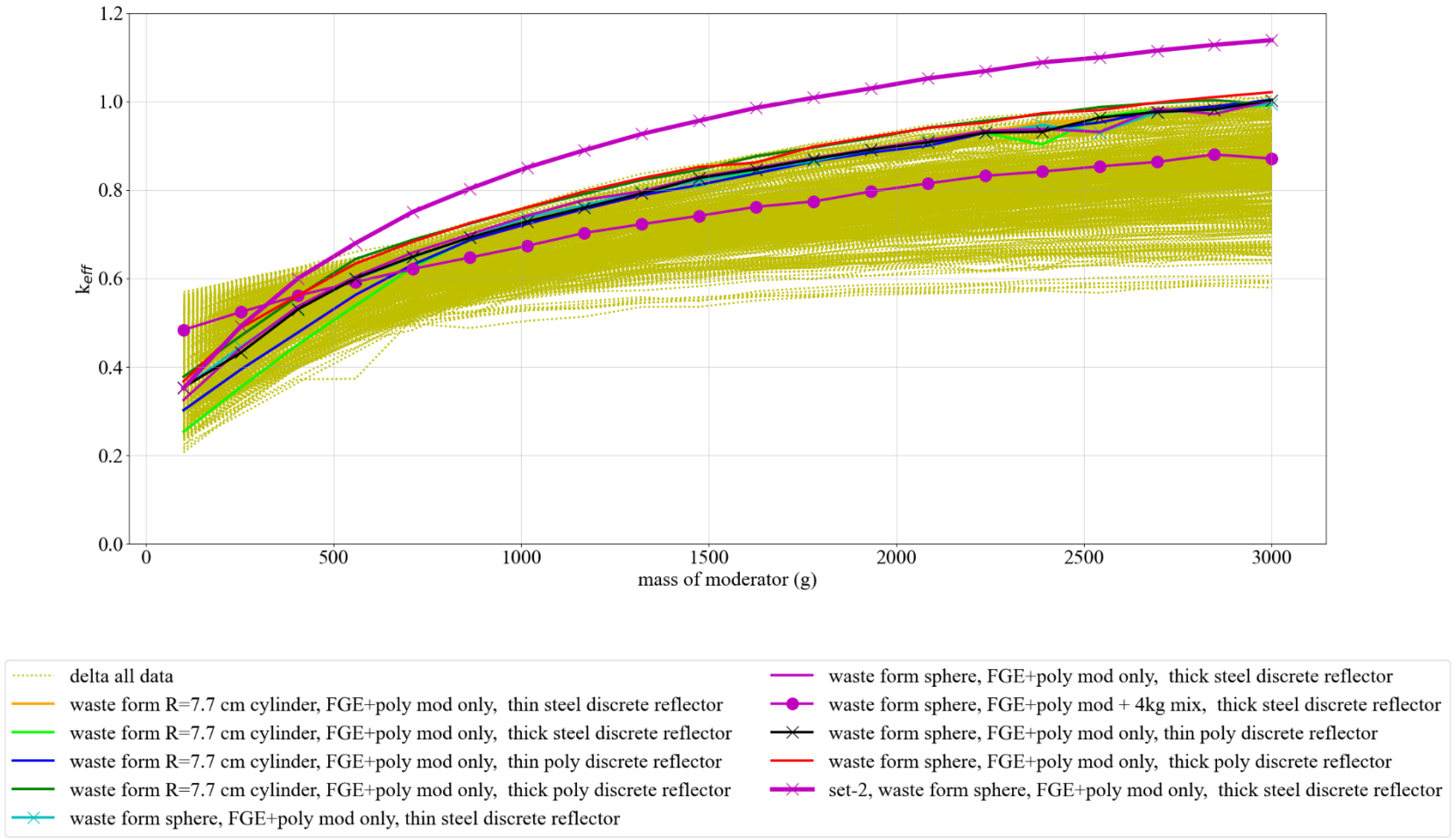

Figure L-12. k_{eff} of set-5h compared to a single set-2 representative curve to evaluate the effect of brine in a 50% mixture with MgO as interstitial reflective material but with the additional 50 cm of space to locate the y-direction reflective boundary conditions removed (similar to set-2) and brine in the external salt box. The graphite filler, when present, is replaced by an equivalent mass of brine in a 50% mixture with MgO.

APPENDIX M. SET-6: RESULTS OF THE TRIANGULAR PITCHED CCO NONUNIFORM ARRAY CENTROID LOCATION STUDIES AND THE POP HEXAGONAL AND TRIANGULAR PITCHED NONUNIFORM ARRAY CENTROID LOCATION STUDIES.

This page intentionally blank.

APPENDIX M. SET-6: RESULTS OF THE TRIANGULAR PITCHED CCO NONUNIFORM ARRAY CENTROID LOCATION STUDIES AND THE POP HEXAGONAL AND TRIANGULAR PITCHED NONUNIFORM ARRAY CENTROID LOCATION STUDIES.

This appendix serves as a repository of the results for the triangular pitched Criticality Control Overpack (CCO) nonuniform array centroid location studies and the Standard Pipe Overpack (POP) hexagonal and triangular pitched nonuniform array centroid location studies. POP containers were evaluated in Brickner [4]; however, in this appendix, they are treated in the same manner as the CCO (same parametric sweeps) with the exception of the FGE limit, which is 200 g.

The analysis models used in this appendix for set-6 are based on the set-2 models discussed in detail in Appendix C and Appendix D. The model changes to the calculations provided in this appendix compared to Appendix C and Appendix D are related to the centroid locations, which changed based on new data provided by Sandia National Laboratory (SNL) [46] including six new centroid location datasets. The SNL data also provide centroid locations for simulations that begin as a triangular pitch rather than a hexagonal pitch (like Appendix C and Appendix D) for both the CCO and POP containers, as well as new hexagonal pitch information for the POP containers. The SNL data are for both lower horizon and upper horizon simulations. For all datasets, the models are constructed in the same fashion as the set-2 models, including the additional centroids for the triangular pitch data, and cases are also added with mirror boundary conditions as well as the periodic boundary conditions, as considered in Appendix C and Appendix D (the mirror boundary conditions are also evaluated in Appendix E).

This appendix (1) expands the studies from the other appendices with new datasets to provide additional technical support of the conclusions in the main report, (2) shows the reactivity trend for additional containers like POP that also have a FGE limit of 200 g, and (3) shows the reactivity trend associated with the boundary condition in a comprehensive manner.

The cases in this appendix are summarized in Table N-1. Note that although six new centroid datasets are evaluated in this appendix, the parametric sweeps are consistent and therefore the subcases are the same for each dataset.

The data provided in Reedlunn and Bean [46] used in this appendix for the 12 new datasets are presented in Table M-1 for the CCO in the lower horizon and upper horizon in a triangular pitched array (two datasets); Table M-2 for the 6 in. POP in the upper horizon in a triangular pitched array and the lower horizon in a hexagonal pitched array (two datasets); and Table M-3 for the 12 in. POP in the upper horizon in a triangular pitched array and the lower horizon in a hexagonal pitched array (two datasets).

For all the datasets, both 0 year and 1,000 year data are provided and used. A summary of the calculations is presented in Table M-5. Figure M-1 through Figure M-6 compare container arrangement (hexagonal vs. triangular pitched) and boundary conditions (periodic vs. mirror) for CCO containers. Figure M-7 through M-12 present the k_{eff} results for 6 in. POP containers, whereas Figure M-13 through Figure M-15 compare container arrangement (hexagonal vs. triangular pitched) and boundary conditions (periodic vs. mirror) for 6 in. POP containers. Figure M-16 through Figure M-19 present the k_{eff} results for 12 in. POP containers, whereas Figure M-20 through Figure M-22 compare container arrangement (hexagonal vs. triangular pitched) and boundary conditions (periodic vs. mirror) for 6 in. POP containers. Figure M-23 displays the maximum occurring k_{eff} given the moderator for each of the evaluated container configurations when in storage for 1,000 years. Figure M-24 through Figure M-39 display the maximum occurring k_{eff} of each subset given the moderator for each of the evaluated container configurations with the maximum occurring k_{eff} for all subsets of set-2-uh for comparison.

Additional calculations were run with the datasets to create flux map plots that can be used to illustrate the most reactive regions of the model. As seen in Appendix E—in which flux maps were provided for the cylindrical waste form models from set-2-uh calculations (Appendix C)—the flux in the model is a function of multiple competing parameters (see discussion in Section 6.4 of the main report). Moreover, when the room is essentially divided in half by the very low reactivity region in the center of the model, the maximum reactivity on either side can be very close to the maximum reactivity on the other side—but as the criticality calculation proceeds in KENO, the code eventually focuses on the region with the highest value. The flux maps created to illustrate the maximum reactivity regions in these models are presented in Figure M-40 to M-47.

LIST OF FIGURES

LIST OF TABLES

Table M-1. Summary of cases for all set-6 models.

Case	Model type	Waste form shape	Waste form moderator	Filler material (0, 2,000, 4,000 g)	Metal in filler	Discrete reflector (thin 0.001 cm and thick 0.7112 cm)	Be (g)	Subcase
Set-6	Models similar to set-2	Cylinder (radius range 4.8, 6, 7.7 and height defined by total volume of mass)	water	c12	SS from can (0, 500, 1,000 g)	steel	0 to 585	set-6-1
			poly	c12		steel		set-6-2
			water	c12		poly		set-6-3
			poly	c12		poly		set-6 -4
			water	generic		steel		set-6-5
			poly	generic		steel		set-6-6
			water	generic		poly		set-6-7
			poly	generic		poly		set-6-8
		Sphere (radius defined by total volume of mass)	water	c12		steel		set-6-9
			poly	c12		steel		set-6-10
			water	c12		poly		set-6-11
			poly	c12		poly		set-6-12
			water	generic		steel		set-6-13
			poly	generic		steel		set-6-14
			water	generic		poly		set-6-15
			poly	generic		poly		set-6-16

Table M-2. Centroid locations from [46] for the CCO containers in a triangular pitch.

CCO containers												
Centroid	Lower horizon triangular with triangular pitch array						Upper horizon triangular with triangular pitch array					
	t = 0 year			t = 1,000 years			t = 0 year			t = 1,000 years		
	x (m)	y (m)	z (m)	x (m)	y (m)	z (m)	x (m)	y (m)	z (m)	x (m)	y (m)	z (m)
0	−3.910681	−0.752791	−5.965605	−2.90163	−0.91488	−5.36427	−3.91082	−0.75279	−3.53563	−3.03254	−0.37986	−3.05446
1	−3.911674	−0.752792	−5.139917	−2.83411	−0.75901	−5.5154	−3.9117	−0.75279	−2.70994	−3.03983	−0.87336	−2.87072
2	−3.912668	−0.752795	−4.314184	−2.91043	−0.78327	−4.91443	−3.91257	−0.7528	−1.88421	−3.18882	−0.83341	−2.2964
3	−3.331431	−0.752792	−5.965029	−2.09153	−0.84417	−5.66998	−3.33159	−0.75279	−3.53513	−2.4117	−0.71271	−3.07672
4	−3.332166	−0.752792	−5.139339	−2.70562	−0.68503	−5.53604	−3.33218	−0.75279	−2.70944	−2.98234	−0.9332	−2.92463
5	−3.332899	−0.752794	−4.313606	−2.81508	−0.63186	−5.11287	−3.33277	−0.75279	−1.88371	−3.0758	−0.69539	−2.46973
6	−2.752036	−0.75279	−5.964558	−1.71718	−0.58932	−5.6277	−2.75221	−0.75279	−3.53476	−1.92937	−0.66768	−3.09643
7	−2.75265	−0.752792	−5.13887	−2.34186	−0.87558	−5.43192	−2.75266	−0.75279	−2.70907	−2.53207	−0.94059	−3.02164
8	−2.753264	−0.752795	−4.313135	−2.59381	−0.45859	−5.22233	−2.75312	−0.75279	−1.88334	−2.86678	−0.6792	−2.59926
9	−2.172671	−0.752791	−5.964178	−1.34539	−0.6985	−5.62668	−2.17281	−0.75279	−3.53448	−1.50153	−0.93716	−3.09943
10	−2.17315	−0.752792	−5.138488	−1.96158	−0.92523	−5.50984	−2.17315	−0.75279	−2.7088	−2.15002	−0.86723	−2.85505
11	−2.173628	−0.752794	−4.312755	−2.55639	−0.71459	−5.3019	−2.1735	−0.7528	−1.88306	−2.71353	−0.69317	−2.689
12	−1.59327	−0.75279	−5.963884	−0.91533	−0.68409	−5.69717	−1.59341	−0.75279	−3.53428	−1.24346	−0.88506	−3.02233
13	−1.593633	−0.752792	−5.138194	−1.53364	−0.92069	−5.49581	−1.59364	−0.75279	−2.7086	−1.91845	−0.69897	−2.94898
14	−1.593999	−0.752796	−4.312461	−2.2069	−0.86025	−5.20043	−1.59388	−0.75279	−1.88286	−2.57222	−0.77731	−2.86477
15	−1.013915	−0.752792	−5.963681	−0.37342	−0.59707	−5.74613	−1.01399	−0.75279	−3.53415	−0.88569	−0.77434	−3.12777
16	−1.014137	−0.752792	−5.13799	−1.06297	−0.94637	−5.58051	−1.01414	−0.75279	−2.70846	−1.58704	−0.79807	−2.84665
17	−1.014358	−0.752794	−4.312257	−1.75793	−0.74029	−5.37522	−1.01428	−0.7528	−1.88273	−2.23934	−0.94098	−2.73115
18	−0.434519	−0.75279	−5.963566	0.013811	−0.57371	−5.53996	−0.43457	−0.75279	−3.53408	−0.47188	−0.87367	−3.16148
19	−0.434623	−0.752792	−5.137877	−0.59212	−0.81901	−5.49691	−0.43463	−0.75279	−2.70839	−0.58075	−0.67582	−3.00091
20	−0.43473	−0.752795	−4.312143	−1.29909	−0.64262	−5.4346	−0.43469	−0.7528	−1.88265	0.346985	−0.70783	−3.00543
21	0.144834	−0.752791	−5.963544	0.411219	−0.53124	−5.52756	0.14485	−0.75279	−3.53406	−0.34495	−0.888	−3.05578
22	0.144872	−0.752792	−5.137854	−0.07078	−0.92379	−5.64527	0.144873	−0.75279	−2.70837	0.476231	−0.53544	−3.02281
23	0.144911	−0.752794	−4.31212	−0.55154	−0.48765	−5.5025	0.144898	−0.75279	−1.88264	1.229786	−0.60485	−2.89042
24	0.724228	−0.75279	−5.963611	0.506316	−0.7523	−5.52825	0.724281	−0.75279	−3.5341	0.445383	−0.80163	−3.06482

Table M-2. Centroid locations from [46] for the CCO containers in a triangular pitch (continued).

CCO containers												
Centroid	Lower horizon triangular with triangular pitch array						Upper horizon triangular with triangular pitch array					
	t = 0 year			t = 1,000 years			t = 0 year			t = 1,000 years		
	x (m)	y (m)	z (m)	x (m)	y (m)	z (m)	x (m)	y (m)	z (m)	x (m)	y (m)	z (m)
25	0.724386	−0.752792	−5.137922	1.266119	−0.94356	−5.5341	0.724384	−0.75279	−2.70842	1.095588	−0.85754	−2.9138
26	0.724539	−0.752795	−4.312189	0.702078	−0.61499	−5.54147	0.724484	−0.75279	−1.88268	1.771318	−0.92091	−2.79517
27	1.303584	−0.752792	−5.963771	0.983463	−0.75424	−5.68954	1.303694	−0.75279	−3.53421	0.906266	−0.66142	−3.16066
28	1.303882	−0.752792	−5.13808	1.658848	−0.68004	−5.40967	1.303885	−0.75279	−2.70852	1.570999	−0.86082	−2.9473
29	1.30418	−0.752794	−4.312347	2.150832	−0.89539	−5.26032	1.30408	−0.7528	−1.88279	2.235273	−0.59693	−2.79569
30	1.882982	−0.75279	−5.964019	1.30921	−0.89122	−5.65918	1.883112	−0.75279	−3.53438	1.410753	−0.77626	−3.14802
31	1.883399	−0.752791	−5.13833	1.943917	−0.92092	−5.51457	1.883398	−0.75279	−2.70869	2.026407	−0.94765	−2.98119
32	1.88381	−0.752796	−4.312598	2.494824	−0.67201	−5.37577	1.883682	−0.75279	−1.88295	2.568517	−0.71637	−2.65583
33	2.462347	−0.752792	−5.964358	1.522499	−0.73278	−5.63065	2.462522	−0.75279	−3.53461	1.853539	−0.89701	−3.09003
34	2.462897	−0.752792	−5.138668	2.153964	−0.9297	−5.46098	2.462913	−0.75279	−2.70892	2.440916	−0.6837	−2.81359
35	2.463446	−0.752794	−4.312934	2.624686	−0.77956	−5.18251	2.463299	−0.7528	−1.88319	2.89419	−0.72366	−2.55665
36	3.041741	−0.75279	−5.964781	1.881795	−0.62726	−5.67045	3.041886	−0.75279	−3.53493	2.165982	−0.57386	−3.07024
37	3.042408	−0.752791	−5.139093	2.531813	−0.92494	−5.62109	3.042417	−0.75279	−2.70924	2.737982	−0.84306	−2.85454
38	3.043068	−0.752795	−4.313359	2.76334	−0.80368	−5.10918	3.042953	−0.7528	−1.88351	2.993375	−0.89953	−2.4846
39	3.621093	−0.752792	−5.965302	2.569047	−0.58884	−5.58595	3.621253	−0.75279	−3.53536	2.736165	−0.88471	−2.91345
40	3.621922	−0.752791	−5.139613	2.872611	−0.9546	−5.3911	3.621934	−0.75279	−2.70967	3.076498	−0.77613	−2.87468
41	3.622749	−0.752794	−4.31388	2.939747	−0.60464	−5.00139	3.622611	−0.75279	−1.88393	3.122722	−0.60842	−2.40351
42	−3.621093	−0.250931	−5.965302	−2.27593	−0.36609	−5.60556	−3.62125	−0.25093	−3.53536	−2.60278	−0.14046	−3.02947
43	−3.621922	−0.250931	−5.139612	−2.90453	−0.50545	−5.50074	−3.62193	−0.25093	−2.70967	−2.98984	−0.46938	−2.88682
44	−3.622749	−0.250931	−4.313879	−2.91594	−0.26364	−4.9536	−3.62261	−0.25093	−1.88393	−3.1574	−0.28211	−2.40037
45	−3.041746	−0.250931	−5.964781	−1.86056	−0.0217	−5.64067	−3.04189	−0.25093	−3.53493	−2.06814	−0.36996	−3.08149
46	−3.042408	−0.250931	−5.139092	−2.45227	−0.32864	−5.5006	−3.04242	−0.25093	−2.70924	−2.68489	−0.47516	−3.03338
47	−3.043065	−0.250931	−4.313358	−2.84788	−0.13519	−5.1589	−3.04295	−0.25093	−1.88351	−2.97401	−0.32629	−2.54036
48	−2.462347	−0.250931	−5.964358	−1.5614	−0.15471	−5.61835	−2.46253	−0.25093	−3.53461	−1.69963	−0.09423	−3.10173
49	−2.462898	−0.250931	−5.138667	−2.19708	−0.34489	−5.49944	−2.46291	−0.25093	−2.70892	−2.37075	−0.13276	−2.99957
50	−2.463445	−0.25093	−4.312934	−2.762	−0.04692	−5.24929	−2.4633	−0.25093	−1.88319	−2.78173	−0.43965	−2.61629

Table M-2. Centroid locations from [46] for the CCO containers in a triangular pitch (continued).

CCO containers												
Centroid	Lower horizon triangular with triangular pitch array						Upper horizon triangular with triangular pitch array					
	t = 0 year			t = 1,000 years			t = 0 year			t = 1,000 years		
	x (m)	y (m)	z (m)	x (m)	y (m)	z (m)	x (m)	y (m)	z (m)	x (m)	y (m)	z (m)
51	−1.882987	−0.250931	−5.964019	−1.17337	−0.38888	−5.71742	−1.88311	−0.25093	−3.53438	−1.3274	−0.15707	−3.0605
52	−1.883399	−0.250931	−5.138329	−1.84055	−0.45972	−5.47792	−1.8834	−0.25093	−2.70869	−2.01178	−0.21326	−2.84592
53	−1.883807	−0.250931	−4.312596	−2.42057	−0.23672	−5.23784	−1.88368	−0.25093	−1.88295	−2.66954	−0.20023	−2.74259
54	−1.303584	−0.250931	−5.963771	−0.71945	−0.24618	−5.72996	−1.30369	−0.25093	−3.53421	−1.04843	−0.14959	−3.06315
55	−1.303882	−0.250931	−5.138081	−1.39634	−0.13213	−5.58268	−1.30388	−0.25093	−2.70852	−1.6725	−0.41786	−2.97043
56	−1.304179	−0.250931	−4.312347	−2.04033	−0.18782	−5.32498	−1.30408	−0.25093	−1.88279	−2.29255	−0.42989	−2.83326
57	−0.724234	−0.250931	−5.963611	−0.26265	−0.12615	−5.7231	−0.72428	−0.25093	−3.5341	−0.91177	−0.23761	−3.05195
58	−0.724387	−0.250931	−5.137921	−0.91377	−0.35643	−5.59889	−0.72438	−0.25093	−2.70842	−1.19835	−0.52436	−2.95329
59	−0.724537	−0.250931	−4.312188	−1.5855	−0.41856	−5.46494	−0.72449	−0.25093	−1.88268	−1.95467	−0.45514	−2.7943
60	−0.144833	−0.250931	−5.963544	0.141201	−0.29516	−5.53718	−0.14485	−0.25093	−3.53406	−0.57928	−0.42216	−3.12582
61	−0.144873	−0.250931	−5.137853	−0.51291	−0.0586	−5.49902	−0.14487	−0.25093	−2.70837	0.350669	−0.26969	−2.95735
62	−0.14491	−0.25093	−4.312119	−1.20347	−0.20346	−5.44826	−0.1449	−0.25093	−1.88264	1.081882	−0.13426	−2.90276
63	0.434514	−0.250931	−5.963566	0.305451	0.006486	−5.66397	0.434566	−0.25093	−3.53408	0.164447	−0.17345	−3.11892
64	0.434622	−0.250931	−5.137876	0.911019	−0.5681	−5.62184	0.434626	−0.25093	−2.70839	0.807891	−0.22681	−3.12133
65	0.434732	−0.250931	−4.312142	0.524582	0.064025	−5.55876	0.434692	−0.25093	−1.88265	1.459983	−0.01117	−2.99928
66	1.013915	−0.250931	−5.963681	0.888984	−0.19572	−5.56381	1.013989	−0.25093	−3.53415	0.687277	−0.28919	−3.18503
67	1.014137	−0.250931	−5.13799	1.455011	−0.49211	−5.41555	1.014136	−0.25093	−2.70846	1.348835	−0.4377	−2.90366
68	1.014358	−0.250931	−4.312256	2.096351	−0.33026	−5.27875	1.014284	−0.25093	−1.88273	2.052539	−0.40291	−2.79158
69	1.593265	−0.250931	−5.963883	1.160565	−0.27796	−5.58742	1.593405	−0.25093	−3.53428	1.154792	−0.2581	−3.16166
70	1.593632	−0.250931	−5.138193	1.813709	−0.50842	−5.53922	1.593642	−0.25093	−2.70859	1.809401	−0.21587	−2.9116
71	1.594002	−0.250931	−4.31246	2.426963	−0.22124	−5.39324	1.593876	−0.25093	−1.88286	2.434813	−0.09709	−2.84374
72	2.172672	−0.250931	−5.964178	1.35735	−0.23775	−5.58942	2.172813	−0.25093	−3.53448	1.608329	−0.20359	−3.04232
73	2.17315	−0.250931	−5.138487	2.005729	−0.48909	−5.56268	2.173153	−0.25093	−2.70879	2.253144	−0.40133	−2.88652
74	2.173628	−0.250931	−4.312754	2.59934	−0.3406	−5.22988	2.173496	−0.25093	−1.88306	2.740789	−0.12856	−2.75294
75	2.75203	−0.250931	−5.964558	1.650364	−0.14252	−5.67396	2.752209	−0.25093	−3.53476	2.031273	−0.11501	−3.07677
76	2.752648	−0.250931	−5.138869	2.336199	−0.2915	−5.51217	2.752663	−0.25093	−2.70907	2.635922	−0.44175	−2.87558

Table M-2. Centroid locations from [46] for the CCO containers in a triangular pitch (continued).

CCO containers												
Centroid	Lower horizon triangular with triangular pitch array						Upper horizon triangular with triangular pitch array					
	t = 0 year			t = 1,000 years			t = 0 year			t = 1,000 years		
	x (m)	y (m)	z (m)	x (m)	y (m)	z (m)	x (m)	y (m)	z (m)	x (m)	y (m)	z (m)
77	2.753268	−0.250931	−4.313134	2.693863	−0.55599	−5.20362	2.753114	−0.25093	−1.88334	2.862431	−0.19575	−2.67176
78	3.331432	−0.250931	−5.965029	2.047828	−0.05314	−5.64528	3.331588	−0.25093	−3.53513	2.380388	−0.41047	−3.09083
79	3.332166	−0.250931	−5.139338	2.717821	−0.13859	−5.52119	3.332182	−0.25093	−2.70944	2.974955	−0.59153	−2.97979
80	3.332899	−0.250931	−4.313605	2.827418	−0.35186	−5.10162	3.332773	−0.25093	−1.88371	2.99987	−0.22719	−2.51851
81	3.910678	−0.250931	−5.965605	2.610284	0.047978	−5.54154	3.910824	−0.25093	−3.53563	3.063602	0.142025	−3.03179
82	3.911673	−0.250931	−5.139918	2.87013	−0.3224	−5.49971	3.911694	−0.25093	−2.70994	3.046717	−0.49012	−2.85716
83	3.912668	−0.250931	−4.314184	2.930382	−0.23711	−4.95818	3.912568	−0.25093	−1.88421	3.148911	−0.29648	−2.37315
84	−3.910679	0.250931	−5.965605	−2.69741	0.034009	−5.57097	−3.91082	0.250931	−3.53563	−2.94076	0.481496	−2.85572
85	−3.911673	0.250931	−5.139918	−2.93088	0.561359	−5.43104	−3.9117	0.250931	−2.70994	−2.93797	−0.17431	−2.88276
86	−3.912667	0.250931	−4.314184	−2.88907	0.156537	−4.9902	−3.91257	0.250931	−1.88421	−3.15322	0.055127	−2.40987
87	−3.331432	0.250931	−5.965029	−2.11592	0.440845	−5.63841	−3.33159	0.250931	−3.53513	−2.49249	0.474328	−3.01817
88	−3.332166	0.250931	−5.139339	−2.63405	0.037576	−5.53679	−3.33218	0.250931	−2.70944	−2.76523	0.049542	−3.02146
89	−3.332899	0.250931	−4.313605	−2.76871	0.21948	−5.17274	−3.33277	0.250931	−1.88371	−3.00916	0.050994	−2.54658
90	−2.75203	0.250931	−5.964558	−1.81793	0.409623	−5.62059	−2.75221	0.250931	−3.53476	−1.88166	0.20788	−3.07979
91	−2.752648	0.250931	−5.138869	−2.35768	−0.00131	−5.45509	−2.75266	0.250931	−2.70907	−2.51015	0.18157	−3.02103
92	−2.753268	0.250931	−4.313134	−2.67789	0.466532	−5.22112	−2.75311	0.250931	−1.88334	−2.79387	0.017696	−2.56154
93	−2.172672	0.250931	−5.964178	−1.37832	0.368461	−5.72034	−2.17281	0.250931	−3.53448	−1.57249	0.316793	−3.02845
94	−2.17315	0.250931	−5.138487	−1.97761	0.154697	−5.42129	−2.17315	0.250931	−2.70879	−2.23891	0.272387	−2.96523
95	−2.173628	0.250931	−4.312754	−2.55302	0.316112	−5.35602	−2.1735	0.250931	−1.88306	−2.69363	0.272768	−2.7115
96	−1.593265	0.250931	−5.963883	−0.94791	0.365318	−5.61155	−1.59341	0.250931	−3.53428	−1.13312	0.22839	−3.09005
97	−1.593632	0.250931	−5.138193	−1.57916	0.312935	−5.4969	−1.59364	0.250931	−2.70859	−1.78776	0.358452	−2.82966
98	−1.594002	0.250931	−4.31246	−2.22389	0.31015	−5.25762	−1.59388	0.250931	−1.88286	−2.46216	0.339946	−2.74376
99	−1.013915	0.250931	−5.963681	−0.51968	0.196313	−5.7111	−1.01399	0.250931	−3.53415	−0.70116	0.289163	−3.00472
100	−1.014136	0.250931	−5.13799	−1.21737	0.178976	−5.5188	−1.01414	0.250931	−2.70846	−1.3371	0.158978	−2.89355
101	−1.014358	0.250931	−4.312256	−1.79514	0.451472	−5.32575	−1.01428	0.250931	−1.88273	−2.10767	0.061665	−2.79626
102	−0.434514	0.250931	−5.963566	−0.0992	0.241545	−5.64028	−0.43457	0.250931	−3.53408	−0.3187	0.174023	−3.01928

Table M-2. Centroid locations from [46] for the CCO containers in a triangular pitch (continued).

CCO containers												
Centroid	Lower horizon triangular with triangular pitch array						Upper horizon triangular with triangular pitch array					
	t = 0 year			t = 1,000 years			t = 0 year			t = 1,000 years		
	x (m)	y (m)	z (m)	x (m)	y (m)	z (m)	x (m)	y (m)	z (m)	x (m)	y (m)	z (m)
103	−0.434622	0.250931	−5.137876	−0.75593	0.091724	−5.51233	−0.43463	0.250931	−2.70839	−0.98941	0.009907	−2.96817
104	−0.434732	0.250931	−4.312142	−1.50217	0.025454	−5.43357	−0.43469	0.250931	−1.88265	0.77203	0.109828	−2.93362
105	0.144833	0.250931	−5.963544	0.312724	0.278738	−5.61426	0.14485	0.250931	−3.53406	−0.01906	0.288524	−3.07031
106	0.144873	0.250931	−5.137853	−0.35417	0.43779	−5.52382	0.144873	0.250931	−2.70837	0.603315	0.022482	−3.13293
107	0.14491	0.250931	−4.312119	−1.0672	0.388367	−5.44826	0.144898	0.250931	−1.88264	1.207432	0.452809	−2.93661
108	0.724234	0.250931	−5.963611	0.703202	0.319221	−5.57559	0.724282	0.250931	−3.5341	0.414521	0.341257	−3.06594
109	0.724387	0.250931	−5.137921	0.968222	0.02463	−5.5126	0.724384	0.250931	−2.70842	1.077825	0.315685	−3.00488
110	0.724536	0.250931	−4.312188	1.669049	0.129907	−5.38472	0.724485	0.250931	−1.88268	1.779156	0.316164	−2.80221
111	1.303584	0.250931	−5.963771	0.904639	0.34647	−5.54455	1.303691	0.250931	−3.53421	0.917503	0.271858	−3.18671
112	1.303883	0.250931	−5.138081	1.483856	0.207134	−5.44857	1.303884	0.250931	−2.70852	1.620341	0.418823	−3.01763
113	1.304179	0.250931	−4.312347	2.025226	0.17975	−5.36093	1.304082	0.250931	−1.88279	2.154816	0.136642	−2.79648
114	1.882987	0.250931	−5.964019	1.23055	0.239141	−5.69719	1.883112	0.250931	−3.53438	1.428994	0.166618	−3.09898
115	1.883399	0.250931	−5.138329	1.86977	−0.03532	−5.52962	1.883398	0.250931	−2.70869	2.07848	0.389502	−2.95697
116	1.883807	0.250931	−4.312596	2.46334	0.147153	−5.2166	1.883683	0.250931	−1.88295	2.605636	0.295323	−2.81093
117	2.462347	0.250931	−5.964358	1.44848	0.388578	−5.63721	2.462528	0.250931	−3.53461	1.894424	0.069549	−3.05378
118	2.462897	0.250931	−5.138667	2.111696	0.229082	−5.48866	2.462914	0.250931	−2.70892	2.560842	0.171722	−2.97675
119	2.463445	0.250931	−4.312934	2.665974	0.080124	−5.19768	2.463296	0.250931	−1.88319	2.814673	0.12854	−2.61904
120	3.041746	0.250931	−5.964781	1.758802	0.530698	−5.55004	3.041886	0.250931	−3.53493	2.207336	0.392462	−2.91714
121	3.042408	0.250931	−5.139092	2.430604	0.351202	−5.47465	3.042418	0.250931	−2.70924	2.787861	0.403343	−3.03886
122	3.043065	0.250931	−4.313358	2.80301	−0.06078	−5.15664	3.042953	0.250931	−1.88351	2.974685	0.006764	−2.61813
123	3.621093	0.250931	−5.965301	2.208283	0.542522	−5.6183	3.621254	0.250931	−3.53536	2.820667	0.068947	−3.02552
124	3.621922	0.250931	−5.139612	2.779644	0.323879	−5.46967	3.621933	0.250931	−2.70967	2.907405	0.44998	−2.84936
125	3.622749	0.250931	−4.313879	2.914363	0.006705	−5.0095	3.622611	0.250931	−1.88393	3.097351	0.122288	−2.47876
126	−3.621093	0.752792	−5.965302	−2.58063	0.581499	−5.56683	−3.62125	0.752791	−3.53536	−3.06648	0.933946	−2.9091
127	−3.621922	0.752792	−5.139612	−2.96656	0.818151	−5.39721	−3.62193	0.752792	−2.70967	−2.72483	0.682488	−2.86591
128	−3.622748	0.752794	−4.31388	−2.87284	0.543105	−5.03024	−3.62261	0.752794	−1.88393	−3.13054	0.409741	−2.43082

Table M-2. Centroid locations from [46] for the CCO containers in a triangular pitch (continued).

CCO containers												
Centroid	Lower horizon triangular with triangular pitch array						Upper horizon triangular with triangular pitch array					
	t = 0 year			t = 1,000 years			t = 0 year			t = 1,000 years		
	x (m)	y (m)	z (m)	x (m)	y (m)	z (m)	x (m)	y (m)	z (m)	x (m)	y (m)	z (m)
129	−3.041741	0.75279	−5.964781	−2.06969	0.827013	−5.66061	−3.04189	0.752791	−3.53493	−2.27169	0.922325	−3.08952
130	−3.042408	0.752792	−5.139093	−2.66728	0.89082	−5.58258	−3.04242	0.752792	−2.70924	−2.87725	0.913511	−2.8763
131	−3.043068	0.752795	−4.313359	−2.71212	0.817717	−5.16005	−3.04295	0.752794	−1.88351	−3.00616	0.520713	−2.55933
132	−2.462347	0.752792	−5.964358	−1.66973	0.86551	−5.63689	−2.46252	0.75279	−3.53461	−1.93197	0.665972	−3.05803
133	−2.462897	0.752792	−5.138668	−2.27298	0.667151	−5.43572	−2.46291	0.752792	−2.70892	−2.44092	0.945383	−2.87202
134	−2.463446	0.752794	−4.312934	−2.65095	0.980043	−5.19575	−2.4633	0.752795	−1.88319	−2.75865	0.662173	−2.57971
135	−1.882981	0.75279	−5.96402	−1.23994	0.863263	−5.65156	−1.88311	0.752791	−3.53438	−1.51664	0.476365	−3.01618
136	−1.883398	0.752791	−5.13833	−1.90459	0.905378	−5.47272	−1.8834	0.752792	−2.70869	−2.02709	0.936722	−2.8438
137	−1.88381	0.752796	−4.312597	−2.48232	0.605465	−5.3613	−1.88368	0.752794	−1.88295	−2.55016	0.662086	−2.68255
138	−1.303584	0.752792	−5.963771	−0.83369	0.734503	−5.70986	−1.30369	0.75279	−3.53421	−0.99908	0.618354	−3.11922
139	−1.303882	0.752792	−5.13808	−1.46874	0.925826	−5.47908	−1.30389	0.752792	−2.70852	−1.61179	0.841436	−3.01353
140	−1.30418	0.752794	−4.312347	−2.1379	0.92774	−5.26097	−1.30408	0.752795	−1.88279	−2.19449	0.565108	−2.89942
141	−0.724228	0.75279	−5.963611	−0.22874	0.804903	−5.74547	−0.72428	0.752791	−3.5341	−0.83732	0.779193	−3.06881
142	−0.724386	0.752792	−5.137922	−0.96491	0.622604	−5.67835	−0.72438	0.752792	−2.70842	−1.19275	0.599147	−2.91593
143	−0.72454	0.752795	−4.312189	−1.62593	0.62544	−5.39074	−0.72449	0.752795	−1.88268	−1.8605	0.780675	−2.80682
144	−0.144834	0.752792	−5.963544	0.22644	0.788729	−5.63729	−0.14485	0.752791	−3.53406	−0.42508	0.745575	−3.04563
145	−0.144873	0.752792	−5.137854	−0.42404	0.938576	−5.53113	−0.14487	0.752792	−2.70837	0.253248	0.493745	−3.00516
146	−0.144911	0.752794	−4.31212	−1.13341	0.801822	−5.43238	−0.1449	0.752794	−1.88264	0.921231	0.73219	−2.91944
147	0.434519	0.75279	−5.963566	0.548746	0.626162	−5.65255	0.434566	0.752791	−3.53408	0.204115	0.780457	−3.03954
148	0.434623	0.752792	−5.137877	0.063484	0.833442	−5.51176	0.434627	0.752792	−2.70839	0.778168	0.924761	−3.02625
149	0.43473	0.752795	−4.312143	−0.62143	0.622957	−5.48109	0.434691	0.752795	−1.88265	1.448677	0.752576	−2.84628
150	1.013914	0.752791	−5.963681	0.709884	0.822319	−5.58049	1.01399	0.752791	−3.53415	0.591139	0.688836	−3.17378
151	1.014136	0.752792	−5.13799	1.262835	0.594437	−5.44393	1.014136	0.752792	−2.70846	1.291674	0.711607	−2.9916
152	1.014359	0.752794	−4.312257	1.803017	0.495589	−5.36065	1.014284	0.752795	−1.88273	1.924553	0.745502	−2.78298
153	1.59327	0.75279	−5.963884	1.143655	0.652482	−5.51145	1.593405	0.752791	−3.53428	1.125323	0.785728	−3.17257
154	1.593633	0.752791	−5.138194	1.698649	0.871221	−5.36652	1.593643	0.752792	−2.70859	1.774273	0.702412	−2.9515

Table M-2. Centroid locations from [46] for the CCO containers in a triangular pitch (continued).

CCO containers												
Centroid	Lower horizon triangular with triangular pitch array						Upper horizon triangular with triangular pitch array					
	t = 0 year			t = 1,000 years			t = 0 year			t = 1,000 years		
	x (m)	y (m)	z (m)	x (m)	y (m)	z (m)	x (m)	y (m)	z (m)	x (m)	y (m)	z (m)
155	1.593999	0.752796	−4.312461	2.31254	0.53717	−5.32034	1.593876	0.752795	−1.88286	2.401345	0.889491	−2.7084
156	2.172671	0.752791	−5.964178	1.385721	0.796297	−5.6133	2.172814	0.752791	−3.53448	1.693158	0.902982	−3.06847
157	2.17315	0.752792	−5.138488	2.033557	0.823406	−5.53022	2.173152	0.752792	−2.7088	2.215579	0.676911	−2.88669
158	2.173628	0.752795	−4.312755	2.575101	0.776472	−5.10254	2.173495	0.752795	−1.88306	2.775491	0.865881	−2.66968
159	2.752036	0.75279	−5.964558	1.603548	0.853843	−5.68795	2.752208	0.752791	−3.53476	2.024711	0.714694	−3.11053
160	2.752649	0.752792	−5.13887	2.270513	0.92132	−5.40265	2.752663	0.752792	−2.70907	2.668941	0.921929	−2.90293
161	2.753264	0.752795	−4.313135	2.725721	0.541925	−5.16865	2.753115	0.752794	−1.88334	2.737126	0.527551	−2.56726
162	3.331431	0.752792	−5.965029	2.01376	0.684832	−5.63457	3.331588	0.752791	−3.53513	2.475437	0.706887	−3.0388
163	3.332166	0.752792	−5.139339	2.587849	0.950717	−5.40044	3.332182	0.752792	−2.70944	2.951343	0.972697	−2.84771
164	3.332899	0.752794	−4.313606	2.857304	0.344833	−5.15884	3.332773	0.752794	−1.88371	3.013397	0.547619	−2.53693
165	3.910681	0.752791	−5.965605	2.807992	0.428743	−5.53663	3.910824	0.752791	−3.53563	3.059556	0.86021	−2.86028
166	3.911674	0.752792	−5.139917	2.786013	0.965766	−5.29039	3.911695	0.752792	−2.70994	2.845196	0.592625	−2.85096
167	3.912668	0.752795	−4.314184	2.916078	0.536843	−5.05188	3.912567	0.752795	−1.88421	3.083926	0.750927	−2.38355

Table M-3. Centroid locations from [46] for the 6 in. POP containers.

6 in. POP containers												
	Upper horizon triangular array						Lower horizon hexagonal array					
	t = 0 year			t = 1,000 years			t = 0 year			t = 1,000 years		
Centroid	x (m)	y (m)	z (m)	x (m)	y (m)	z (m)	x (m)	y (m)	z (m)	x (m)	y (m)	z (m)
0	−3.91231	−0.75278	−3.58444	−3.12238	−0.74717	−3.10268	−3.42855	−0.7916	−6.01389	−2.73344	−0.65793	−5.56198
1	−3.91319	−0.7528	−2.75915	−2.92592	−0.84039	−2.83478	−2.84898	−0.7916	−6.01341	−2.06434	−0.60245	−5.55401
2	−3.91407	−0.75281	−1.93343	−3.08746	−0.78173	−2.27553	−3.13877	−0.28975	−6.01364	−2.64677	−0.3011	−5.56224
3	−3.33271	−0.75278	−3.58393	−2.80602	−0.78022	−3.04358	−3.71833	−0.28975	−6.01418	−3.00605	−0.28624	−5.56601
4	−3.33334	−0.75281	−2.75865	−2.58945	−0.90328	−2.81877	−4.00811	−0.79161	−6.0145	−3.0308	−0.74871	−5.6152
5	−3.33396	−0.75282	−1.93293	−2.81305	−0.59291	−2.47221	−3.42933	−0.79162	−5.1886	−2.53294	−0.94268	−5.40394
6	−2.75312	−0.75279	−3.58357	−2.39734	−0.80979	−3.00609	−2.84963	−0.79162	−5.18811	−2.31914	−1.0235	−5.34378
7	−2.7536	−0.7528	−2.75828	−2.22995	−0.53351	−2.7915	−3.13948	−0.28975	−5.18834	−2.42802	−0.50178	−5.3435
8	−2.75407	−0.7528	−1.93256	−2.58233	−0.89197	−2.69927	−3.7192	−0.28975	−5.18888	−2.57751	−0.48689	−5.33321
9	−2.17353	−0.75278	−3.58329	−1.99075	−0.77734	−2.99884	−4.00913	−0.79162	−5.1892	−2.77577	−0.69737	−5.28899
10	−2.17388	−0.7528	−2.758	−1.72669	−0.90769	−2.86113	−3.43011	−0.79162	−4.36287	−2.83803	−0.76936	−4.93277
11	−2.17422	−0.75281	−1.93228	−2.34292	−0.83734	−2.77207	−2.85027	−0.79163	−4.36239	−2.42816	−0.72184	−5.35454
12	−1.59392	−0.75278	−3.58309	−1.33588	−0.53457	−3.00016	−3.14018	−0.28975	−4.36262	−2.74406	−0.03926	−5.27082
13	−1.59417	−0.7528	−2.7578	−1.32285	−0.92532	−2.97199	−3.72006	−0.28975	−4.36315	−2.91209	−0.28119	−4.92069
14	−1.59442	−0.75281	−1.93208	−1.71157	−0.55328	−2.95865	−4.01014	−0.79162	−4.36348	−3.04666	−0.76465	−4.77055
15	−1.01432	−0.75279	−3.58295	−0.92224	−0.92262	−3.10214	−2.05722	0	−6.01289	−1.87327	−0.23016	−5.53429
16	−1.01447	−0.75279	−2.75767	−0.79803	−0.52918	−3.10468	−1.47758	0	−6.01261	−1.36327	−0.07286	−5.50711
17	−1.01461	−0.75279	−1.93194	−1.11882	−0.69246	−3.04625	−1.76741	0.501872	−6.01274	−1.77763	0.600827	−5.50232
18	−0.43471	−0.75279	−3.58288	−0.44453	−0.94004	−3.15345	−2.34703	0.501863	−6.01306	−1.82058	0.353039	−5.57899
19	−0.43478	−0.7528	−2.75759	−0.38534	−0.63515	−3.13365	−2.63685	0	−6.01325	−2.28469	0.020458	−5.473
20	−0.43484	−0.75281	−1.93187	−0.77033	−0.75814	−3.0693	−2.34703	−0.50186	−6.01306	−2.19962	−0.52669	−5.41206
21	0.14491	−0.75279	−3.58287	0.190665	−0.58996	−3.09238	−1.76741	−0.50187	−6.01274	−1.79175	−0.50012	−5.60377
22	0.144922	−0.7528	−2.75758	−0.27202	−0.79091	−3.01951	−2.05771	0	−5.18759	−2.43117	−0.18431	−5.36619
23	0.14494	−0.7528	−1.93186	0.218245	−0.86035	−3.06506	−1.47794	−1E−06	−5.18732	−2.04167	−0.18681	−5.39586
24	0.724506	−0.75278	−3.58291	0.692335	−0.58857	−3.07871	−1.76782	0.501855	−5.18744	−1.75529	0.186115	−5.47261
25	0.724624	−0.7528	−2.75762	0.662188	−0.99915	−3.01888	−2.34758	0.501858	−5.18776	−2.4079	0.330124	−5.53825
26	0.724734	−0.75281	−1.9319	1.137311	−0.62432	−3.12435	−2.63744	0	−5.18796	−2.48274	−0.31278	−5.36034
27	1.304122	−0.75278	−3.58301	1.449741	−0.88738	−2.97116	−2.34758	−0.50186	−5.18776	−2.08714	−0.85607	−5.35015
28	1.304321	−0.7528	−2.75773	1.16765	−0.8155	−2.97846	−1.76782	−0.50186	−5.18744	−1.90246	−0.8996	−5.45117

6 in. POP containers												
	Upper horizon triangular array						Lower horizon hexagonal array					
	t = 0 year			t = 1,000 years			t = 0 year			t = 1,000 years		
Centroid	x (m)	y (m)	z (m)	x (m)	y (m)	z (m)	x (m)	y (m)	z (m)	x (m)	y (m)	z (m)
29	1.304517	−0.75281	−1.932	1.919734	−0.87205	−2.95109	−2.05818	0	−4.36187	−2.13097	0.005771	−5.49978

Table M-3. Centroid locations from [46] for the 6 in. POP containers (continued).

6 in. POP containers												
	Upper horizon triangular array						Lower horizon hexagonal array					
	t = 0 year			t = 1,000 years			t = 0 year			t = 1,000 years		
Centroid	x (m)	y (m)	z (m)	x (m)	y (m)	z (m)	x (m)	y (m)	z (m)	x (m)	y (m)	z (m)
30	1.883724	−0.75279	−3.58318	1.528693	−0.91196	−3.07825	−1.47828	−1E−06	−4.36159	−1.57353	0.091387	−5.59896
31	1.884021	−0.75279	−2.75789	2.031372	−0.60465	−3.02527	−1.76823	0.501847	−4.36172	−1.9514	0.644844	−5.49318
32	1.884311	−0.75278	−1.93217	2.13425	−0.94374	−2.87101	−2.34812	0.501859	−4.36204	−2.08441	0.616447	−5.39108
33	2.463326	−0.75278	−3.58342	2.271243	−0.69924	−2.90024	−2.63802	0	−4.36223	−2.42868	0.141489	−5.29792
34	2.463736	−0.7528	−2.75813	2.355915	−1.01578	−2.80514	−2.34812	−0.50186	−4.36204	−2.30251	−0.46659	−5.40993
35	2.464138	−0.75281	−1.93241	2.580745	−0.56984	−2.80446	−1.76823	−0.50185	−4.36172	−1.92642	−0.40247	−5.48779
36	3.042924	−0.75278	−3.58374	2.448614	−0.85634	−2.87116	−0.68574	−0.79161	−6.01238	−0.48572	−0.67719	−5.52085
37	3.043466	−0.7528	−2.75845	2.553397	−0.56051	−2.93605	−0.10609	−0.7916	−6.01232	−0.30927	−0.96884	−5.51524
38	3.044004	−0.75281	−1.93273	2.788536	−0.81337	−2.5901	−0.39592	−0.28975	−6.01234	−0.39051	−0.25103	−5.67276
39	3.622497	−0.75279	−3.58416	2.921292	−0.61877	−3.01878	−0.97559	−0.28975	−6.01245	−1.03638	−0.12206	−5.57677
40	3.623213	−0.7528	−2.75888	2.697535	−0.95396	−2.77041	−1.26542	−0.7916	−6.01254	−1.37693	−1.04304	−5.49382
41	3.623916	−0.75281	−1.93316	3.021178	−0.80224	−2.3924	−0.68592	−0.79162	−5.18708	−1.38897	−0.77131	−5.6358
42	−3.6225	−0.25093	−3.58417	−2.98313	−0.26258	−3.07911	−0.10611	−0.79162	−5.18702	−0.17197	−0.46673	−5.62083
43	−3.62321	−0.25093	−2.75888	−2.91267	−0.45487	−2.78546	−0.39602	−0.28975	−5.18704	−0.79741	−0.33769	−5.57405
44	−3.62391	−0.25094	−1.93316	−2.94319	−0.15813	−2.47429	−0.97583	−0.28975	−5.18715	−1.52988	−0.46639	−5.64155
45	−3.04292	−0.25093	−3.58374	−2.3889	−0.13252	−2.90314	−1.26573	−0.79162	−5.18724	−1.59653	−0.66167	−5.50589
46	−3.04347	−0.25093	−2.75845	−2.66237	−0.46802	−2.90197	−0.68609	−0.79162	−4.36136	−1.00347	−0.93268	−5.60277
47	−3.04401	−0.25093	−1.93273	−2.80021	−0.0466	−2.73862	−0.10614	−0.79163	−4.3613	0.312279	−0.90859	−5.53795
48	−2.46333	−0.25093	−3.58342	−1.93399	−0.18199	−2.82474	−0.39611	−0.28976	−4.36132	−0.2099	−0.27537	−5.64602
49	−2.46374	−0.25094	−2.75813	−2.36825	0.061672	−2.85918	−0.97607	−0.28975	−4.36142	−1.15932	−0.36798	−5.53288
50	−2.46414	−0.25094	−1.93241	−2.6356	−0.32081	−2.8232	−1.26603	−0.79163	−4.36151	−1.62151	−0.76009	−5.37193
51	−1.88373	−0.25093	−3.58318	−1.66677	−0.0039	−2.94066	0.685738	0	−6.01238	0.734495	−0.0022	−5.59357
52	−1.88402	−0.25093	−2.75789	−1.80095	−0.35891	−3.01499	1.265415	0	−6.01253	1.24762	−0.247	−5.48223
53	−1.88432	−0.25094	−1.93217	−2.17594	−0.22472	−2.88616	0.975599	0.501865	−6.01245	0.919442	0.545228	−5.53854
54	−1.30412	−0.25093	−3.58301	−1.29476	−0.13498	−3.03279	0.395916	0.501862	−6.01234	0.355871	0.519446	−5.5878
55	−1.30432	−0.25093	−2.75772	−1.16226	−0.29674	−2.92219	0.106099	0	−6.01232	0.221935	−0.0497	−5.64791
56	−1.30452	−0.25094	−1.932	−1.81983	−0.4075	−2.91278	0.395917	−0.50186	−6.01234	0.274748	−0.76918	−5.51875
57	−0.72451	−0.25093	−3.58291	−0.80939	−0.22833	−3.12002	0.975599	−0.50187	−6.01245	1.041745	−0.52277	−5.54486
58	−0.72462	−0.25093	−2.75762	−0.60867	0.063407	−3.08388	0.68592	0	−5.18708	0.817841	−0.34449	−5.57219

Table M-3. Centroid locations from [46] for the 6 in. POP containers (continued).

6 in. POP containers												
	Upper horizon triangular array						Lower horizon hexagonal array					
	t = 0 year			t = 1,000 years			t = 0 year			t = 1,000 years		
Centroid	x (m)	y (m)	z (m)	x (m)	y (m)	z (m)	x (m)	y (m)	z (m)	x (m)	y (m)	z (m)
59	−0.72472	−0.25093	−1.9319	−0.74958	−0.20289	−3.04183	1.265722	0	−5.18724	1.380338	0.34395	−5.5574
60	−0.14491	−0.25093	−3.58287	0.061575	−0.37365	−3.02039	0.975826	0.501859	−5.18715	1.277287	0.646196	−5.63161
61	−0.14492	−0.25093	−2.75758	−0.0201	0.163553	−3.12378	0.396007	0.501856	−5.18704	0.750051	0.765752	−5.57473
62	−0.14494	−0.25093	−1.93185	−0.40441	−0.21401	−3.0522	0.106107	0	−5.18702	−0.24007	−0.05024	−5.55342
63	0.434708	−0.25093	−3.58288	0.396466	−0.26203	−3.0579	0.396008	−0.50186	−5.18704	0.893084	−0.68576	−5.61648
64	0.434775	−0.25093	−2.75759	0.453635	0.069774	−2.95058	0.975826	−0.50186	−5.18715	0.817638	−0.96957	−5.52519
65	0.434842	−0.25094	−1.93187	0.968699	−0.40806	−3.00029	0.686085	0.000001	−4.36136	1.116529	0.186939	−5.59822
66	1.014321	−0.25093	−3.58296	0.955218	−0.39562	−3.0593	1.266019	−1E−06	−4.36151	1.550795	−0.15555	−5.57089
67	1.01447	−0.25093	−2.75766	1.134386	−0.03174	−3.0524	0.976054	0.501858	−4.36143	1.130051	0.723777	−5.56489
68	1.014619	−0.25093	−1.93194	1.187652	−0.49433	−3.0773	0.396097	0.501851	−4.36132	0.805696	0.455416	−5.64714
69	1.593922	−0.25093	−3.58309	1.661345	−0.34911	−3.00617	0.106125	0	−4.3613	0.2759	−0.27686	−5.59871
70	1.594171	−0.25093	−2.7578	1.459601	−0.30481	−2.89375	0.396097	−0.50185	−4.36132	0.271063	−0.51021	−5.64219
71	1.594413	−0.25094	−1.93208	1.975618	−0.56727	−2.97584	0.976053	−0.50186	−4.36143	1.377869	−0.51622	−5.51581
72	2.173529	−0.25093	−3.58329	2.07904	−0.25428	−3.01806	2.057221	−0.7916	−6.01289	1.906264	−0.93159	−5.49001
73	2.173882	−0.25093	−2.758	1.92805	−0.19733	−2.80325	2.636842	−0.79161	−6.01325	2.145236	−0.96944	−5.48435
74	2.174229	−0.25094	−1.93228	2.378876	−0.18397	−2.76063	2.34703	−0.28975	−6.01306	2.055996	−0.34456	−5.39083
75	2.753123	−0.25093	−3.58357	2.390618	−0.26881	−2.98865	1.767409	−0.28975	−6.01274	1.70538	−0.56577	−5.45305
76	2.753592	−0.25093	−2.75828	2.284355	0.009273	−2.82018	1.477581	−0.79162	−6.01262	1.54453	−0.77671	−5.43455
77	2.75405	−0.25093	−1.93256	2.746802	−0.19985	−2.76533	2.057703	−0.79162	−5.18759	2.350791	−0.54894	−5.57722
78	3.332713	−0.25093	−3.58394	2.722765	0.005382	−3.03041	2.637433	−0.79162	−5.18795	2.540043	−1.00492	−5.37453
79	3.333341	−0.25093	−2.75865	2.633769	−0.301	−2.90781	2.347572	−0.28975	−5.18776	2.184308	−0.01856	−5.52228
80	3.33396	−0.25094	−1.93293	2.87217	−0.2948	−2.5077	1.767828	−0.28975	−5.18744	1.629219	−0.11971	−5.42255
81	3.912311	−0.25093	−3.58444	3.089804	−0.21903	−3.11357	1.477936	−0.79161	−5.18731	1.113931	−0.97708	−5.51156
82	3.913197	−0.25093	−2.75915	2.888612	−0.12156	−2.87294	2.058173	−0.79163	−4.36187	2.172858	−0.89286	−5.41562
83	3.914073	−0.25093	−1.93343	3.065469	−0.25998	−2.2992	2.638024	−0.79162	−4.36223	2.425588	−0.56545	−5.32606
84	−3.91231	0.250928	−3.58444	−3.09741	0.153762	−3.13725	2.348106	−0.28976	−4.36204	2.311724	−0.49401	−5.42057
85	−3.9132	0.250934	−2.75915	−2.96214	0.047263	−2.77815	1.768241	−0.28975	−4.36172	1.928692	−0.56745	−5.4989
86	−3.91407	0.250933	−1.93343	−2.98574	0.326728	−2.4169	1.478282	−0.79161	−4.36159	1.772879	−0.90862	−5.57245
87	−3.33271	0.25093	−3.58394	−2.74687	0.453296	−2.9702	3.428558	0	−6.01389	2.702754	−0.13408	−5.52898

Table M-3. Centroid locations from [46] for the 6 in. POP containers (continued).

6 in. POP containers												
	Upper horizon triangular array						Lower horizon hexagonal array					
	t = 0 year			t = 1,000 years			t = 0 year			t = 1,000 years		
Centroid	x (m)	y (m)	z (m)	x (m)	y (m)	z (m)	x (m)	y (m)	z (m)	x (m)	y (m)	z (m)
88	−3.33334	0.250933	−2.75865	−2.79111	0.05204	−2.93207	4.008103	0	−6.0145	2.989456	0.133445	−5.57923
89	−3.33396	0.250938	−1.93293	−2.78933	0.233862	−2.51239	3.71833	0.501875	−6.01417	2.868203	0.523661	−5.46902
90	−2.75312	0.250926	−3.58357	−2.51373	0.141499	−2.91687	3.138772	0.501857	−6.01364	2.356034	0.544058	−5.53781
91	−2.75359	0.250933	−2.75828	−2.42076	0.503264	−2.80189	2.848975	0	−6.0134	1.899889	0.063451	−5.43051
92	−2.75405	0.250933	−1.93256	−2.76518	0.153695	−2.82515	3.138772	−0.50186	−6.01364	2.498321	−0.47441	−5.39994
93	−2.17353	0.250928	−3.58329	−2.15434	0.38274	−2.99426	3.71833	−0.50188	−6.01417	2.759735	−0.53978	−5.42106
94	−2.17388	0.250934	−2.758	−1.86577	0.381673	−2.91674	3.429327	0	−5.1886	2.557723	0.142509	−5.38022
95	−2.17423	0.250936	−1.93228	−2.32295	0.23251	−2.72767	4.009133	0	−5.18921	2.769696	−0.18676	−5.29701
96	−1.59392	0.250929	−3.58309	−1.56192	0.244654	−3.02778	3.719204	0.501849	−5.18888	2.804169	0.918748	−5.27974
97	−1.59417	0.250934	−2.7578	−1.44921	0.54361	−2.89479	3.13948	0.501864	−5.18834	2.666773	0.779192	−5.39418
98	−1.59441	0.250935	−1.93208	−1.98849	0.159264	−2.887	2.849636	0	−5.18811	2.303499	0.131164	−5.42796
99	−1.01432	0.250931	−3.58296	−0.97123	0.206914	−3.13268	3.13948	−0.50186	−5.18834	2.574044	−0.92715	−5.38173
100	−1.01447	0.25093	−2.75766	−0.79194	0.38867	−2.95236	3.719205	−0.50185	−5.18888	2.701623	−0.97307	−5.30427
101	−1.01462	0.25093	−1.93194	−1.13943	0.382096	−3.08243	3.430097	0	−4.36287	2.768989	−0.25935	−5.02199
102	−0.43471	0.25093	−3.58288	−0.38857	0.327744	−3.11849	4.010144	0	−4.36348	2.971555	0.13224	−4.86498
103	−0.43478	0.250932	−2.75759	−0.10675	0.440043	−3.00446	3.720068	0.501839	−4.36316	2.879486	0.47972	−4.9826
104	−0.43484	0.250939	−1.93187	−0.66671	0.207027	−3.08903	3.140181	0.501867	−4.36262	2.613226	0.327092	−5.29179
105	0.144909	0.25093	−3.58287	0.244752	0.050921	−3.13765	2.85028	0	−4.36239	2.448363	−0.31988	−5.25046
106	0.144924	0.250931	−2.75758	0.366742	0.465772	−2.97776	3.140181	−0.50187	−4.36262	2.6712	−0.46382	−5.26397
107	0.144943	0.250931	−1.93186	0.046161	−0.13398	−3.08397	3.720069	−0.50184	−4.36316	2.792762	−0.52891	−5.02587
108	0.724507	0.250929	−3.58291	0.43689	0.319515	−3.0473	−3.42855	0.791602	−6.01389	−2.66436	0.694983	−5.54963
109	0.724619	0.250932	−2.75762	0.990124	0.169254	−3.02583	−2.84898	0.791603	−6.01341	−2.10607	0.747501	−5.51927
110	0.724725	0.250933	−1.9319	0.810122	0.586188	−2.98012	−4.00811	0.791611	−6.0145	−2.99111	0.737713	−5.55717
111	1.304122	0.250928	−3.58301	1.320439	0.186248	−2.95677	−3.71833	0.289747	−6.01417	−2.87378	0.104276	−5.46149
112	1.304324	0.250933	−2.75772	1.274853	0.387764	−2.91104	−3.13877	0.289748	−6.01364	−2.31996	0.609228	−5.52785
113	1.304523	0.250936	−1.932	1.731657	0.258591	−2.96553	−3.42933	0.791616	−5.1886	−2.41573	0.936345	−5.37868
114	1.883726	0.250928	−3.58318	1.790322	0.040219	−2.99087	−2.84963	0.791618	−5.18811	−1.87918	0.941417	−5.31962
115	1.884023	0.250932	−2.75789	1.807353	0.357946	−2.98153	−4.00913	0.791615	−5.1892	−2.7577	0.873623	−5.28247
116	1.884315	0.250934	−1.93217	2.243284	0.130556	−2.88986	−3.7192	0.289753	−5.18888	−2.67157	0.532796	−5.33969

Table M-3. Centroid locations from [46] for the 6 in. POP containers (continued).

6 in. POP containers												
	Upper horizon triangular array						Lower horizon hexagonal array					
	t = 0 year			t = 1,000 years			t = 0 year			t = 1,000 years		
Centroid	x (m)	y (m)	z (m)	x (m)	y (m)	z (m)	x (m)	y (m)	z (m)	x (m)	y (m)	z (m)
117	2.463326	0.250928	−3.58342	2.267997	0.165975	−3.03259	−3.13948	0.289751	−5.18834	−2.39818	0.122204	−5.4808
118	2.463737	0.250935	−2.75813	2.145541	0.432488	−2.74952	−3.43011	0.791623	−4.36287	−2.78512	0.634907	−4.95416
119	2.464138	0.250938	−1.93241	2.569876	0.291732	−2.83075	−2.85027	0.791625	−4.36239	−2.37159	0.656688	−5.26414
120	3.042924	0.25093	−3.58374	2.495227	0.237684	−2.9286	−4.01014	0.791618	−4.36348	−3.02804	0.900095	−4.74833
121	3.043473	0.250934	−2.75845	2.508612	0.603304	−2.84634	−3.72006	0.289755	−4.36315	−2.92091	0.18129	−4.93766
122	3.044013	0.250933	−1.93273	2.674045	0.199694	−2.68353	−3.14018	0.289751	−4.36262	−2.64401	0.266038	−5.11477
123	3.622498	0.250928	−3.58417	2.807103	0.26227	−3.06795	−0.68574	0.791607	−6.01238	−0.55806	0.951115	−5.57731
124	3.62321	0.250934	−2.75888	2.944939	0.335295	−2.81406	−0.10609	0.791604	−6.01232	0.006759	1.061035	−5.54795
125	3.623908	0.250937	−1.93316	2.939778	0.232438	−2.46151	−1.26542	0.791601	−6.01254	−1.22655	0.846087	−5.61512
126	−3.6225	0.752784	−3.58416	−2.91366	0.654929	−2.98319	−0.97559	0.289747	−6.01245	−1.14163	0.298007	−5.61312
127	−3.62321	0.752799	−2.75888	−2.87503	0.950187	−2.82127	−0.39592	0.289745	−6.01234	−0.4115	0.456737	−5.60561
128	−3.62392	0.752806	−1.93316	−2.9908	0.67995	−2.37742	−0.68592	0.791617	−5.18708	−1.17377	1.028937	−5.52392
129	−3.04292	0.752784	−3.58374	−2.63235	0.692569	−2.92111	−0.10611	0.791619	−5.18702	−0.22967	0.617616	−5.55758
130	−3.04347	0.7528	−2.75845	−2.52328	0.965475	−2.90043	−1.26573	0.791622	−5.18724	−1.59886	0.830601	−5.50241
131	−3.04401	0.752808	−1.93273	−2.78117	0.656755	−2.67289	−0.97583	0.289751	−5.18715	−1.49005	0.499568	−5.50518
132	−2.46333	0.75278	−3.58342	−2.29774	0.693713	−2.99743	−0.39602	0.289751	−5.18704	−0.80984	0.348033	−5.56667
133	−2.46374	0.752801	−2.75813	−2.25443	0.928677	−2.72564	−0.68609	0.791622	−4.36136	−0.8562	0.667061	−5.5831
134	−2.46414	0.752811	−1.93241	−2.52127	0.629617	−2.81537	−0.10614	0.791627	−4.3613	0.349544	0.696358	−5.59788
135	−1.88372	0.752794	−3.58318	−1.92565	0.919216	−2.87973	−1.26603	0.791631	−4.36151	−1.64695	0.549872	−5.45051
136	−1.88402	0.752789	−2.75789	−1.74594	0.616501	−2.942	−0.97606	0.289753	−4.36142	−1.07476	0.25814	−5.55291
137	−1.88431	0.752784	−1.93217	−2.00258	0.80116	−2.8081	−0.39611	0.289755	−4.36132	−0.34896	0.16145	−5.69586
138	−1.30412	0.75278	−3.58301	−1.25906	0.643007	−3.04944	2.057221	0.791599	−6.01289	1.88021	0.648041	−5.47579
139	−1.30432	0.752802	−2.75773	−1.07267	0.899952	−2.92565	2.636842	0.791605	−6.01325	2.252306	0.761214	−5.3851
140	−1.30452	0.752811	−1.932	−1.48643	0.836181	−3.00115	1.477581	0.791617	−6.01262	1.656394	0.942845	−5.50276
141	−0.72451	0.752784	−3.58291	−0.80155	0.800576	−3.08415	1.767409	0.289747	−6.01274	1.540706	0.141387	−5.46951
142	−0.72462	0.752799	−2.75762	−0.28579	0.837456	−3.00761	2.34703	0.289747	−6.01306	1.918346	0.318784	−5.3543
143	−0.72473	0.752809	−1.9319	−0.81185	0.6538	−3.00581	2.057703	0.791622	−5.18759	2.201324	1.029696	−5.33687
144	−0.14491	0.752789	−3.58287	−0.2545	0.656702	−3.13591	2.637434	0.791618	−5.18795	2.532902	1.028219	−5.42864
145	−0.14492	0.752796	−2.75758	0.138265	0.972489	−2.95962	1.477936	0.791609	−5.18731	1.053869	0.904511	−5.47865

Table M-3. Centroid locations from [46] for the 6 in. POP containers (continued).

6 in. POP containers												
	Upper horizon triangular array						Lower horizon hexagonal array					
	t = 0 year			t = 1,000 years			t = 0 year			t = 1,000 years		
Centroid	x (m)	y (m)	z (m)	x (m)	y (m)	z (m)	x (m)	y (m)	z (m)	x (m)	y (m)	z (m)
146	−0.14494	0.7528	−1.93186	−0.03111	0.614136	−3.03327	1.767828	0.289752	−5.18744	1.828943	0.581206	−5.39108
147	0.434711	0.752786	−3.58288	0.242697	0.88485	−3.10876	2.347572	0.289754	−5.18776	2.182465	0.48664	−5.50438
148	0.434775	0.7528	−2.75759	0.700076	0.91009	−3.11373	2.058173	0.79163	−4.36187	2.37724	0.700741	−5.36926
149	0.43484	0.752808	−1.93187	0.429908	0.713551	−3.15746	2.638024	0.791623	−4.36223	2.541214	0.715279	−5.28838
150	1.01432	0.752793	−3.58295	1.060789	0.647593	−2.9845	1.478281	0.791607	−4.36159	1.803836	0.86741	−5.48695
151	1.014468	0.752793	−2.75767	0.982485	0.922335	−2.93716	1.768241	0.289753	−4.36172	2.023802	0.026891	−5.31925
152	1.014611	0.752795	−1.93194	1.38683	0.572603	−2.95819	2.348106	0.289755	−4.36204	2.491562	0.208756	−5.28205
153	1.593922	0.752782	−3.58309	1.572962	0.631092	−3.06307						
154	1.594174	0.752803	−2.7578	1.389791	0.958604	−2.99083						
155	1.594414	0.752815	−1.93208	1.977935	0.598896	−2.98487						
156	2.17353	0.75278	−3.58329	2.04346	0.604497	−3.02278						
157	2.173876	0.752803	−2.758	1.892546	0.931721	−2.90148						
158	2.174221	0.752815	−1.93228	2.235544	0.633227	−2.76293						
159	2.753121	0.752791	−3.58357	2.35051	0.627318	−2.96602						
160	2.753597	0.752797	−2.75828	2.213935	0.927412	−2.83138						
161	2.754067	0.752799	−1.93256	2.585767	0.543909	−2.72115						
162	3.332712	0.752782	−3.58393	2.802007	0.605801	−3.06741						
163	3.333338	0.752806	−2.75865	2.608336	0.940514	−2.88407						
164	3.333956	0.752815	−1.93293	2.841664	0.601991	−2.48087						
165	3.912311	0.752783	−3.58444	3.143062	0.663047	−3.13894						
166	3.913192	0.752801	−2.75915	2.924898	0.887031	−2.81574						
167	3.914066	0.752806	−1.93343	3.096061	0.660652	−2.29168						

Table M-4. Centroid locations from [46] for the 12 in. POP containers.

12 in. POP containers												
	Upper horizon triangular array						Lower horizon hexagonal array					
	t = 0 year			t = 1,000 years			t = 0 year			t = 1,000 years		
Centroid	x (m)	y (m)	z (m)	x (m)	y (m)	z (m)	x (m)	y (m)	z (m)	x (m)	y (m)	z (m)
0	−3.91236	−0.75279	−3.54958	−3.12169	−0.71012	−3.16098	−3.42859	−0.7916	−5.97904	−2.66045	−0.68965	−5.55604
1	−3.91324	−0.7528	−2.72436	−2.99825	−0.8318	−2.69454	−2.84901	−0.7916	−5.97855	−2.24666	−0.83134	−5.50583
2	−3.91412	−0.75281	−1.89864	−3.15569	−0.7681	−2.14626	−3.13881	−0.28975	−5.97878	−2.58226	−0.22898	−5.55122
3	−3.33275	−0.75278	−3.54908	−2.75044	−0.8472	−3.01219	−3.71837	−0.28975	−5.97932	−2.96957	−0.22511	−5.52611
4	−3.33337	−0.75281	−2.72386	−2.74386	−0.74247	−2.57811	−4.00816	−0.79161	−5.97964	−3.00482	−0.71155	−5.56082
5	−3.33399	−0.75282	−1.89814	−3.00213	−0.64228	−2.24189	−3.42938	−0.79162	−5.15381	−2.50618	−0.88691	−5.24357
6	−2.75315	−0.75279	−3.54871	−2.47924	−0.73095	−2.94107	−2.84967	−0.79162	−5.15332	−2.0345	−0.90754	−5.14453
7	−2.75362	−0.7528	−2.72349	−2.50873	−0.9553	−2.71847	−3.13953	−0.28975	−5.15355	−2.44479	−0.47174	−5.28105
8	−2.75408	−0.7528	−1.89777	−2.51791	−0.52181	−2.38147	−3.71926	−0.28975	−5.15409	−2.76608	−0.31557	−5.23787
9	−2.17355	−0.75278	−3.54843	−1.8068	−0.75783	−3.00536	−4.00919	−0.79162	−5.15442	−2.90322	−0.90604	−5.14549
10	−2.17389	−0.75281	−2.72321	−2.19497	−0.90476	−2.85255	−3.43017	−0.79163	−4.32808	−2.79194	−0.67622	−4.84066
11	−2.17424	−0.75281	−1.89749	−2.13737	−0.57462	−2.58547	−2.85032	−0.79163	−4.32759	−2.47377	−0.78015	−4.96441
12	−1.59394	−0.75278	−3.54823	−1.51394	−0.79909	−3.02675	−3.14024	−0.28976	−4.32782	−2.69961	−0.24004	−4.94998
13	−1.59418	−0.75281	−2.72301	−1.90875	−0.5104	−2.72417	−3.72013	−0.28975	−4.32836	−3.0273	−0.22994	−4.72324
14	−1.59443	−0.75282	−1.89729	−1.74514	−0.94518	−2.65205	−4.01021	−0.79162	−4.32868	−3.11598	−0.78125	−4.69722
15	−1.01433	−0.75279	−3.5481	−0.70166	−0.8411	−3.02609	−2.05725	0	−5.97803	−1.87562	0.081334	−5.67356
16	−1.01447	−0.75279	−2.72287	−1.48738	−0.61158	−2.90117	−1.47761	0	−5.97776	−1.30703	−0.02266	−5.60444
17	−1.01463	−0.75279	−1.89715	−1.08577	−0.82782	−2.91834	−1.76744	0.501871	−5.97789	−1.71847	0.58668	−5.6327
18	−0.43471	−0.75279	−3.54802	−0.1907	−0.681	−2.98563	−2.34706	0.501862	−5.97821	−2.0651	0.428444	−5.60533
19	−0.43478	−0.7528	−2.7228	−0.56792	−1.0182	−2.81299	−2.63688	0	−5.9784	−2.10175	0.236863	−5.62588
20	−0.43484	−0.75281	−1.89708	−0.59999	−0.5571	−2.87372	−2.34706	−0.50186	−5.97821	−1.88765	−0.67975	−5.54697
21	0.144913	−0.75279	−3.54801	−0.07548	−0.86744	−3.00907	−1.76744	−0.50187	−5.97789	−1.44588	−0.57458	−5.61589
22	0.144925	−0.7528	−2.72279	0.346023	−0.9468	−2.95021	−2.05773	0	−5.15281	−1.77429	0.169107	−5.31419
23	0.144944	−0.7528	−1.89707	0.235886	−0.53603	−2.91957	−1.47796	0	−5.15253	−1.56743	0.255982	−5.46807
24	0.724511	−0.75278	−3.54805	0.769029	−0.88126	−3.04569	−1.76784	0.501853	−5.15266	−1.73324	0.884671	−5.3121
25	0.724626	−0.7528	−2.72283	1.145881	−0.74476	−2.87735	−2.34761	0.501859	−5.15298	−1.92728	0.868697	−5.24824
26	0.724737	−0.75281	−1.89711	0.660288	−0.61214	−2.90741	−2.63747	−1E−06	−5.15317	−2.29009	−0.14847	−5.43753
27	1.304137	−0.75278	−3.54816	1.222922	−0.6656	−3.00436	−2.34761	−0.50186	−5.15298	−2.06032	−0.29746	−5.3849
28	1.304331	−0.7528	−2.72293	1.382151	−0.93775	−2.67087	−1.76784	−0.50185	−5.15266	−1.85058	−0.18147	−5.38606

12 in. POP containers												
	Upper horizon triangular array						Lower horizon hexagonal array					
	t = 0 year			t = 1,000 years			t = 0 year			t = 1,000 years		
Centroid	x (m)	y (m)	z (m)	x (m)	y (m)	z (m)	x (m)	y (m)	z (m)	x (m)	y (m)	z (m)
29	1.304527	−0.75281	−1.89721	1.674747	−0.70761	−2.66778	−2.0582	0.000002	−4.32707	−2.13539	0.033748	−5.14946

Table M-4. Centroid locations from [46] for the 12 in. POP containers (continued).

12 in. POP containers												
	Upper horizon triangular array						Lower horizon hexagonal array					
	t = 0 year			t = 1,000 years			t = 0 year			t = 1,000 years		
Centroid	x (m)	y (m)	z (m)	x (m)	y (m)	z (m)	x (m)	y (m)	z (m)	x (m)	y (m)	z (m)
30	1.883742	−0.7528	−3.54832	1.655704	−0.80199	−2.8387	−1.4783	0	−4.3268	−1.40413	−0.23416	−5.32997
31	1.884033	−0.75279	−2.7231	2.202358	−0.79516	−3.08576	−1.76825	0.501843	−4.32692	−1.79956	0.470528	−5.26112
32	1.884326	−0.75279	−1.89738	2.031082	−0.87263	−2.62744	−2.34815	0.501857	−4.32724	−2.32389	0.379396	−5.12191
33	2.463347	−0.75278	−3.54856	2.458787	−0.64892	−3.06956	−2.63807	−1E−06	−4.32744	−2.48341	0.057502	−5.02471
34	2.463752	−0.75281	−2.72334	2.433864	−0.91434	−2.67755	−2.34815	−0.50186	−4.32724	−2.28974	−0.47604	−5.08747
35	2.464159	−0.75281	−1.89762	2.351707	−0.67635	−2.49462	−1.76825	−0.50184	−4.32692	−1.76574	−0.62318	−5.30671
36	3.042958	−0.75278	−3.54888	2.689908	−0.68311	−2.97788	−0.68576	−0.79161	−5.97753	−0.45825	−0.79518	−5.50834
37	3.04349	−0.7528	−2.72366	2.626242	−0.89515	−2.5278	−0.1061	−0.7916	−5.97747	0.150351	−0.8071	−5.51402
38	3.04403	−0.75281	−1.89794	2.841625	−0.60094	−2.32349	−0.39593	−0.28975	−5.97749	−0.36206	−0.18277	−5.52576
39	3.622536	−0.75279	−3.54931	2.884299	−0.85956	−2.99822	−0.97562	−0.28975	−5.9776	−0.73587	−0.30114	−5.53523
40	3.623245	−0.7528	−2.72409	3.021945	−0.83256	−2.71156	−1.26544	−0.7916	−5.97768	−1.13303	−0.6503	−5.47088
41	3.623956	−0.75281	−1.89837	3.101355	−0.74449	−2.19215	−0.68593	−0.79162	−5.1523	−0.97315	−0.99921	−5.39529
42	−3.62254	−0.25093	−3.54931	−3.13444	−0.25795	−3.12413	−0.10611	−0.79162	−5.15223	−0.03671	−0.41183	−5.55513
43	−3.62324	−0.25094	−2.72409	−2.9341	−0.34883	−2.68619	−0.39602	−0.28975	−5.15225	−0.79066	0.080148	−5.45667
44	−3.62396	−0.25094	−1.89837	−3.14288	−0.23275	−2.25546	−0.97584	−0.28975	−5.15236	−1.18374	0.043004	−5.52197
45	−3.04296	−0.25093	−3.54888	−2.69708	−0.24813	−3.01024	−1.26574	−0.79162	−5.15245	−1.56277	−1.00868	−5.40384
46	−3.0435	−0.25094	−2.72366	−2.74096	−0.33767	−2.67301	−0.68609	−0.79162	−4.32656	−0.84886	−0.62399	−5.4537
47	−3.04404	−0.25094	−1.89794	−2.74047	−0.20051	−2.34344	−0.10613	−0.79163	−4.3265	−0.26762	−0.92926	−5.50626
48	−2.46335	−0.25093	−3.54856	−2.19243	−0.25933	−3.08078	−0.39611	−0.28976	−4.32652	−0.4489	−0.4941	−5.39689
49	−2.46375	−0.25094	−2.72334	−2.49327	−0.56007	−2.84673	−0.97607	−0.28976	−4.32663	−1.11058	−0.36349	−5.44978
50	−2.46416	−0.25094	−1.89762	−2.35697	−0.15481	−2.56562	−1.26603	−0.79164	−4.32672	−1.36177	−0.57358	−5.31442
51	−1.88374	−0.25093	−3.54832	−1.55336	−0.17829	−2.91606	0.685749	0	−5.97753	0.416251	0.181325	−5.49574
52	−1.88404	−0.25094	−2.7231	−2.06299	−0.34837	−2.95411	1.265441	0	−5.97768	1.31229	0.017544	−5.64537
53	−1.88433	−0.25094	−1.89738	−1.98919	−0.17968	−2.66378	0.975621	0.501866	−5.97759	1.112264	0.625149	−5.49708
54	−1.30414	−0.25093	−3.54816	−1.02879	−0.11062	−3.04091	0.395924	0.501866	−5.97749	0.43624	0.646254	−5.49063
55	−1.30433	−0.25093	−2.72293	−1.53873	−0.12729	−2.87457	0.106103	0	−5.97746	0.060221	0.116966	−5.65622
56	−1.30453	−0.25093	−1.89721	−1.5639	−0.33488	−2.61102	0.395924	−0.50187	−5.97749	0.486118	−0.73141	−5.61383
57	−0.72451	−0.25093	−3.54806	−0.57698	−0.12899	−2.95595	0.975621	−0.50187	−5.97759	0.920857	−0.53434	−5.4854
58	−0.72462	−0.25093	−2.72283	−0.96251	−0.53479	−2.98338	0.685928	0	−5.1523	1.085968	−0.13843	−5.53514

Table M-4. Centroid locations from [46] for the 12 in. POP containers (continued).

12 in. POP containers												
	Upper horizon triangular array						Lower horizon hexagonal array					
	t = 0 year			t = 1,000 years			t = 0 year			t = 1,000 years		
Centroid	x (m)	y (m)	z (m)	x (m)	y (m)	z (m)	x (m)	y (m)	z (m)	x (m)	y (m)	z (m)
59	−0.72473	−0.25093	−1.89711	−0.92115	−0.18269	−2.77471	1.265732	0	−5.15245	1.516822	−0.3412	−5.32357
60	−0.14491	−0.25093	−3.54801	−0.01599	−0.40295	−2.93399	0.975833	0.501856	−5.15236	1.298201	0.280059	−5.40016
61	−0.14493	−0.25093	−2.72279	−0.45526	−0.35477	−2.82364	0.396009	0.501852	−5.15225	0.902006	0.801115	−5.53241
62	−0.14495	−0.25093	−1.89707	0.026034	−0.08748	−2.87611	0.106108	0	−5.15224	0.330125	−0.27696	−5.52664
63	0.434713	−0.25093	−3.54803	0.472103	−0.4282	−3.05045	0.396007	−0.50185	−5.15225	0.904208	−0.95483	−5.43665
64	0.434781	−0.25093	−2.7228	0.204102	−0.20198	−2.81096	0.975832	−0.50186	−5.15236	1.361483	−0.6685	−5.25979
65	0.434846	−0.25093	−1.89708	0.644938	−0.14819	−2.87681	0.686086	0.000001	−4.32656	0.717916	0.064012	−5.47077
66	1.014332	−0.25093	−3.5481	0.931435	−0.31768	−2.88799	1.266025	0	−4.32672	1.202849	0.019799	−5.26197
67	1.014479	−0.25093	−2.72287	1.022021	−0.09249	−2.67501	0.976057	0.501852	−4.32663	0.901535	0.427393	−5.36124
68	1.014629	−0.25093	−1.89715	1.617822	−0.19747	−2.75382	0.396093	0.501847	−4.32652	0.242528	0.495601	−5.50702
69	1.593937	−0.25093	−3.54823	1.156296	−0.3287	−2.86236	0.106126	0	−4.3265	0.001143	0.180805	−5.46508
70	1.594179	−0.25093	−2.72301	1.797167	−0.34679	−2.94253	0.396093	−0.50185	−4.32652	0.420438	−0.39856	−5.51768
71	1.594423	−0.25094	−1.89729	1.936065	−0.47257	−2.53365	0.976058	−0.50185	−4.32663	0.737592	−0.33634	−5.47857
72	2.173551	−0.25093	−3.54844	1.955452	−0.11432	−3.04477	2.057251	−0.7916	−5.97804	1.713645	−0.84601	−5.56193
73	2.173895	−0.25093	−2.72321	2.458473	−0.42627	−2.89281	2.636879	−0.79161	−5.9784	2.323647	−0.49468	−5.51515
74	2.174241	−0.25094	−1.89749	2.163383	−0.34681	−2.60979	2.347062	−0.28975	−5.97821	1.947333	−0.48105	−5.61581
75	2.753148	−0.25093	−3.54871	2.48637	−0.08547	−2.9734	1.767441	−0.28975	−5.97789	1.473046	−0.34578	−5.57099
76	2.753612	−0.25094	−2.72349	2.690075	−0.13212	−2.65433	1.47761	−0.79162	−5.97776	1.250347	−0.80572	−5.49017
77	2.754078	−0.25094	−1.89777	2.492678	−0.39595	−2.45262	2.057727	−0.79162	−5.15281	2.200328	−0.88027	−5.5208
78	3.332748	−0.25093	−3.54908	2.781039	−0.35136	−3.03727	2.63747	−0.79162	−5.15317	2.443994	−0.98587	−5.44012
79	3.333368	−0.25094	−2.72386	2.774961	−0.15828	−2.65351	2.347604	−0.28976	−5.15298	2.064545	−0.17242	−5.35263
80	3.333992	−0.25094	−1.89814	2.970317	−0.27416	−2.25546	1.76785	−0.28975	−5.15266	1.878651	−0.54812	−5.39788
81	3.912359	−0.25093	−3.54958	3.077755	−0.00885	−3.13467	1.477952	−0.79161	−5.15253	1.709485	−0.96984	−5.28554
82	3.913238	−0.25094	−2.72436	3.050907	−0.26484	−2.76841	2.058201	−0.79164	−4.32707	2.018609	−0.75137	−5.15254
83	3.91412	−0.25094	−1.89864	3.172256	−0.25688	−2.1575	2.638068	−0.79163	−4.32744	2.448851	−0.77692	−5.03867
84	−3.91236	0.250928	−3.54958	−3.06125	0.192525	−3.18749	2.348141	−0.28976	−4.32724	2.279582	−0.50433	−5.06519
85	−3.91324	0.250936	−2.72436	−3.08003	0.177958	−2.75432	1.768262	−0.28976	−4.32692	1.761915	−0.18123	−5.24418
86	−3.91412	0.250935	−1.89864	−3.13211	0.264656	−2.21189	1.478297	−0.7916	−4.3268	1.557701	−0.55173	−5.15323
87	−3.33275	0.250927	−3.54908	−2.78157	0.477429	−2.97214	3.428595	0	−5.97904	2.682308	0.022021	−5.54087

Table M-4. Centroid locations from [46] for the 12 in. POP containers (continued).

12 in. POP containers												
	Upper horizon triangular array						Lower horizon hexagonal array					
	t = 0 year			t = 1,000 years			t = 0 year			t = 1,000 years		
Centroid	x (m)	y (m)	z (m)	x (m)	y (m)	z (m)	x (m)	y (m)	z (m)	x (m)	y (m)	z (m)
88	−3.33337	0.250936	−2.72386	−2.84419	−0.0031	−2.71586	4.008152	0	−5.97964	2.985804	0.019081	−5.5332
89	−3.33399	0.250935	−1.89814	−2.91229	0.297618	−2.40701	3.718369	0.501866	−5.97932	2.905028	0.490525	−5.45706
90	−2.75315	0.250928	−3.54871	−2.47819	0.468301	−2.93111	3.138808	0.501857	−5.97878	2.625752	0.380749	−5.45023
91	−2.75361	0.250937	−2.72349	−2.60457	0.006326	−2.77111	2.84901	0	−5.97855	2.359	0.036794	−5.57522
92	−2.75408	0.250936	−1.89777	−2.54882	0.394392	−2.51488	3.138808	−0.50186	−5.97878	2.510952	−0.33055	−5.4542
93	−2.17355	0.250928	−3.54844	−1.96009	0.523689	−2.92498	3.71837	−0.50187	−5.97932	2.865059	−0.40524	−5.47591
94	−2.17389	0.250934	−2.72321	−2.34122	−0.06433	−2.95736	3.429376	0	−5.15381	2.513751	−0.08001	−5.22955
95	−2.17424	0.250937	−1.89749	−2.16515	0.273794	−2.6583	4.009198	0	−5.15442	2.880893	−0.05623	−5.1763
96	−1.59394	0.250929	−3.54823	−1.3454	0.329858	−3.00747	3.719264	0.501852	−5.15409	2.78676	0.898975	−5.16707
97	−1.59418	0.250933	−2.72301	−1.66665	0.392476	−2.9834	3.139526	0.501866	−5.15355	2.460111	0.505793	−5.15004
98	−1.59442	0.250936	−1.89729	−1.90679	0.134361	−2.69866	2.849679	0	−5.15333	2.163522	0.036029	−5.27461
99	−1.01433	0.250931	−3.5481	−1.0053	0.514422	−3.01902	3.139527	−0.50187	−5.15355	2.599956	−0.80871	−5.33163
100	−1.01448	0.250934	−2.72287	−1.1105	0.107577	−2.8037	3.719264	−0.50185	−5.15409	2.865276	−0.88881	−5.19225
101	−1.01463	0.25093	−1.89715	−1.57207	0.194376	−2.67222	3.430157	0	−4.32808	2.780665	0.110989	−4.85741
102	−0.43471	0.250929	−3.54803	−0.4469	0.265057	−3.10278	4.010225	0	−4.32869	3.076107	0.053241	−4.71186
103	−0.43478	0.250933	−2.7228	−0.85219	0.239825	−2.83585	3.720149	0.501845	−4.32836	3.018568	0.595085	−4.74759
104	−0.43485	0.250932	−1.89708	−0.30745	0.228736	−2.88357	3.14024	0.501871	−4.32782	2.800643	0.470171	−4.93066
105	0.144913	0.25093	−3.54801	0.413574	0.073732	−3.00712	2.850333	0	−4.32759	2.547663	0.02674	−4.92595
106	0.144928	0.250933	−2.72279	−0.16472	0.236572	−2.97996	3.14024	−0.50187	−4.32782	2.650004	−0.40801	−4.97136
107	0.144946	0.25093	−1.89707	0.200818	0.369639	−2.95904	3.720149	−0.50184	−4.32836	2.962743	−0.4677	−4.81178
108	0.724511	0.250928	−3.54806	0.90383	0.083363	−2.95174	−3.42859	0.791604	−5.97904	−2.67989	0.706953	−5.56056
109	0.72462	0.250933	−2.72283	0.506805	0.393262	−2.87103	−2.84901	0.791603	−5.97855	−2.26555	0.712144	−5.56036
110	0.724731	0.250933	−1.89711	1.096664	0.408727	−2.8506	−4.00816	0.791609	−5.97964	−2.9979	0.761044	−5.55994
111	1.304136	0.250928	−3.54816	1.158867	0.088853	−3.00701	−3.71837	0.28975	−5.97932	−2.79418	0.122936	−5.61837
112	1.304334	0.250934	−2.72293	1.613132	0.26578	−3.08628	−3.13881	0.289749	−5.97878	−2.48544	0.454814	−5.50527
113	1.304529	0.250934	−1.89721	1.468625	0.232186	−2.78717	−3.42938	0.79162	−5.15381	−2.5568	0.9558	−5.25929
114	1.883744	0.250929	−3.54832	1.961509	0.421396	−2.92237	−2.84967	0.791619	−5.15332	−2.19968	0.939638	−5.22101
115	1.884034	0.250936	−2.7231	1.931244	−0.12489	−2.72712	−4.00919	0.791617	−5.15442	−2.92093	0.771261	−5.15947
116	1.884328	0.250934	−1.89738	1.913564	0.381098	−2.67499	−3.71926	0.28975	−5.15409	−2.93933	0.337345	−5.16316

Table M-4. Centroid locations from [46] for the 12 in. POP containers (continued).

12 in. POP containers												
	Upper horizon triangular array						Lower horizon hexagonal array					
	t = 0 year			t = 1,000 years			t = 0 year			t = 1,000 years		
Centroid	x (m)	y (m)	z (m)	x (m)	y (m)	z (m)	x (m)	y (m)	z (m)	x (m)	y (m)	z (m)
117	2.463349	0.250926	−3.54856	2.318782	0.246136	−2.88479	−3.13953	0.289752	−5.15355	−2.51551	0.138164	−5.36313
118	2.46375	0.250936	−2.72334	2.383524	0.477025	−2.59156	−3.43017	0.791629	−4.32808	−2.72783	0.781352	−4.85486
119	2.464155	0.250937	−1.89762	2.292436	0.020472	−2.52188	−2.85032	0.791631	−4.32759	−2.54323	0.673603	−4.99949
120	3.042958	0.250928	−3.54888	2.548386	0.189475	−2.90063	−4.01021	0.79162	−4.32869	−3.12577	0.786447	−4.6859
121	3.043501	0.250935	−2.72366	2.725856	0.369299	−2.60705	−3.72014	0.289753	−4.32836	−3.05758	0.298216	−4.6684
122	3.044037	0.250935	−1.89794	2.791171	0.247124	−2.30777	−3.14024	0.289755	−4.32782	−2.69927	0.314759	−4.94159
123	3.622539	0.250928	−3.54931	2.93996	0.432671	−3.14074	−0.68576	0.791606	−5.97753	−0.44113	0.857951	−5.53853
124	3.623244	0.250937	−2.72409	2.974567	0.240715	−2.69751	−0.1061	0.791604	−5.97747	0.137899	0.811433	−5.55086
125	3.623955	0.250938	−1.89837	3.138872	0.230508	−2.19455	−1.26544	0.7916	−5.97768	−1.21591	0.644822	−5.57744
126	−3.62254	0.752787	−3.54931	−2.94433	0.878782	−2.98235	−0.97562	0.289747	−5.9776	−0.82325	0.53944	−5.61371
127	−3.62325	0.752805	−2.72409	−3.05533	0.768002	−2.67605	−0.39593	0.289749	−5.97749	−0.28066	0.192112	−5.64104
128	−3.62396	0.75281	−1.89837	−3.0664	0.718952	−2.13976	−0.68593	0.791616	−5.1523	−0.9837	1.018876	−5.41533
129	−3.04296	0.752784	−3.54888	−2.80371	0.710526	−2.93403	−0.10611	0.791621	−5.15224	0.016602	0.470308	−5.52827
130	−3.04349	0.752804	−2.72366	−2.70575	0.966254	−2.55358	−1.26574	0.791623	−5.15245	−1.44785	1.025177	−5.42478
131	−3.04403	0.752811	−1.89794	−2.75601	0.644666	−2.36602	−0.97584	0.289753	−5.15236	−1.45987	0.362982	−5.50702
132	−2.46335	0.752778	−3.54856	−2.16419	0.83137	−2.96171	−0.39602	0.289753	−5.15225	−0.56769	0.64082	−5.46128
133	−2.46375	0.752805	−2.72334	−2.55196	0.839225	−2.9262	−0.68609	0.791623	−4.32656	−0.83994	0.624155	−5.37588
134	−2.46416	0.752813	−1.89762	−2.4081	0.74881	−2.50917	−0.10613	0.791629	−4.3265	−0.25699	0.922007	−5.46696
135	−1.88374	0.752795	−3.54832	−1.45613	0.801935	−2.84946	−1.26603	0.791635	−4.32672	−1.27999	0.521797	−5.27569
136	−1.88403	0.752787	−2.7231	−2.03785	0.879039	−2.83202	−0.97607	0.289756	−4.32663	−0.97758	0.296017	−5.41937
137	−1.88433	0.752788	−1.89738	−2.11082	0.648579	−2.60179	−0.39611	0.289758	−4.32652	−0.3762	0.189984	−5.36535
138	−1.30414	0.752782	−3.54816	−1.14308	0.849718	−2.89256	2.057251	0.7916	−5.97804	1.701194	0.835923	−5.60037
139	−1.30433	0.752803	−2.72293	−1.5001	0.853414	−2.68016	2.636878	0.791606	−5.9784	2.322519	0.676432	−5.56328
140	−1.30453	0.752809	−1.89721	−1.75672	0.526568	−2.73674	1.47761	0.791615	−5.97776	1.280974	0.786964	−5.58466
141	−0.72451	0.752784	−3.54805	−0.74747	0.885863	−2.92984	1.767441	0.28975	−5.97789	1.529722	0.21706	−5.49019
142	−0.72463	0.752802	−2.72283	−1.04079	0.561187	−2.74413	2.347062	0.289747	−5.97821	1.687639	0.315408	−5.48318
143	−0.72474	0.75281	−1.89711	−0.57742	0.734919	−2.82557	2.057727	0.791624	−5.15281	2.229523	0.916176	−5.55109
144	−0.14491	0.75279	−3.54801	−0.22229	0.600576	−3.05275	2.637471	0.791619	−5.15317	2.605339	0.961959	−5.37441
145	−0.14493	0.752798	−2.72279	−0.19661	0.95655	−2.91029	1.477952	0.791607	−5.15253	1.752532	0.948267	−5.35006

Table M-4. Centroid locations from [46] for the 12 in. POP containers (continued).

12 in. POP containers												
	Upper horizon triangular array						Lower horizon hexagonal array					
	t = 0 year			t = 1,000 years			t = 0 year			t = 1,000 years		
Centroid	x (m)	y (m)	z (m)	x (m)	y (m)	z (m)	x (m)	y (m)	z (m)	x (m)	y (m)	z (m)
146	−0.14494	0.752802	−1.89707	−0.36098	0.513449	−2.84643	1.767849	0.289754	−5.15266	1.788434	0.602688	−5.26204
147	0.434714	0.752787	−3.54802	0.483656	0.835606	−3.038	2.347604	0.289755	−5.15298	2.171804	0.483955	−5.52161
148	0.434777	0.7528	−2.7228	0.073481	0.77627	−2.91596	2.058201	0.791635	−4.32707	2.010708	0.802043	−5.19885
149	0.434843	0.752806	−1.89708	0.636502	0.773352	−2.84094	2.638068	0.791628	−4.32744	2.394844	0.776964	−5.04736
150	1.01433	0.752793	−3.5481	1.03232	0.76913	−3.02287	1.478296	0.791604	−4.3268	1.273444	0.764656	−5.27997
151	1.014474	0.752793	−2.72287	0.896123	0.815816	−2.73602	1.768262	0.289756	−4.32692	1.767326	0.111603	−5.18417
152	1.014626	0.752793	−1.89715	1.382086	0.698374	−2.74872	2.348141	0.289758	−4.32724	2.186319	0.34296	−5.08883
153	1.593935	0.75278	−3.54823	1.454874	0.767377	−2.97204						
154	1.594184	0.752806	−2.72301	1.862781	0.845661	−3.06569						
155	1.594431	0.752815	−1.89729	1.759203	0.632823	−2.72129						
156	2.173551	0.75278	−3.54843	2.233855	0.695485	−2.95875						
157	2.173893	0.752807	−2.72321	2.031724	0.909775	−2.72813						
158	2.174238	0.752814	−1.89749	2.149959	0.648437	−2.55292						
159	2.753147	0.752792	−3.54871	2.415224	0.809595	−2.89912						
160	2.753617	0.752794	−2.72349	2.50545	0.897433	−2.56129						
161	2.754082	0.752797	−1.89777	2.633536	0.625728	−2.38836						
162	3.332746	0.752779	−3.54908	2.578598	0.867686	−2.9613						
163	3.333366	0.752808	−2.72386	2.787421	0.692669	−2.68058						
164	3.333987	0.752815	−1.89814	2.969734	0.764581	−2.30927						
165	3.912361	0.752786	−3.54958	3.039836	0.663804	−3.15321						
166	3.913236	0.752804	−2.72436	3.04233	0.835564	−2.71542						
167	3.914116	0.752811	−1.89864	3.158888	0.735983	−2.17246						

Table M-5. Summary of the calculations in this appendix.

Set	Condition at the *y*-axis boundary	Horizon	Container	Arrangement	Mass of FGE (g)	Time of compaction (years)
set6-lhpop12-hp	Mirror	lower	12 in. pop	Hexagonal pitch	200	0, 1,000
set6a-lhpop12-hp	Periodic					
set6-uhpop12-tp	Mirror	upper		Triangular pitch		
set6a-uhpop12-tp	Periodic					
set6-lhpop6-hp	Mirror	lower	6 in. pop	Hexagonal pitch		
set6a-lhpop6-hp	Periodic					
set6-uhpop6-tp	Mirror	upper		Triangular pitch		
set6a-uhpop6-tp	Periodic					
set6-lh-tp	Mirror	lower	COC	Triangular pitch	380	
set6a-lh-tp	Periodic					
set6-uh-tp	Mirror	upper		Triangular pitch		
set6a-uh-tp	Periodic					

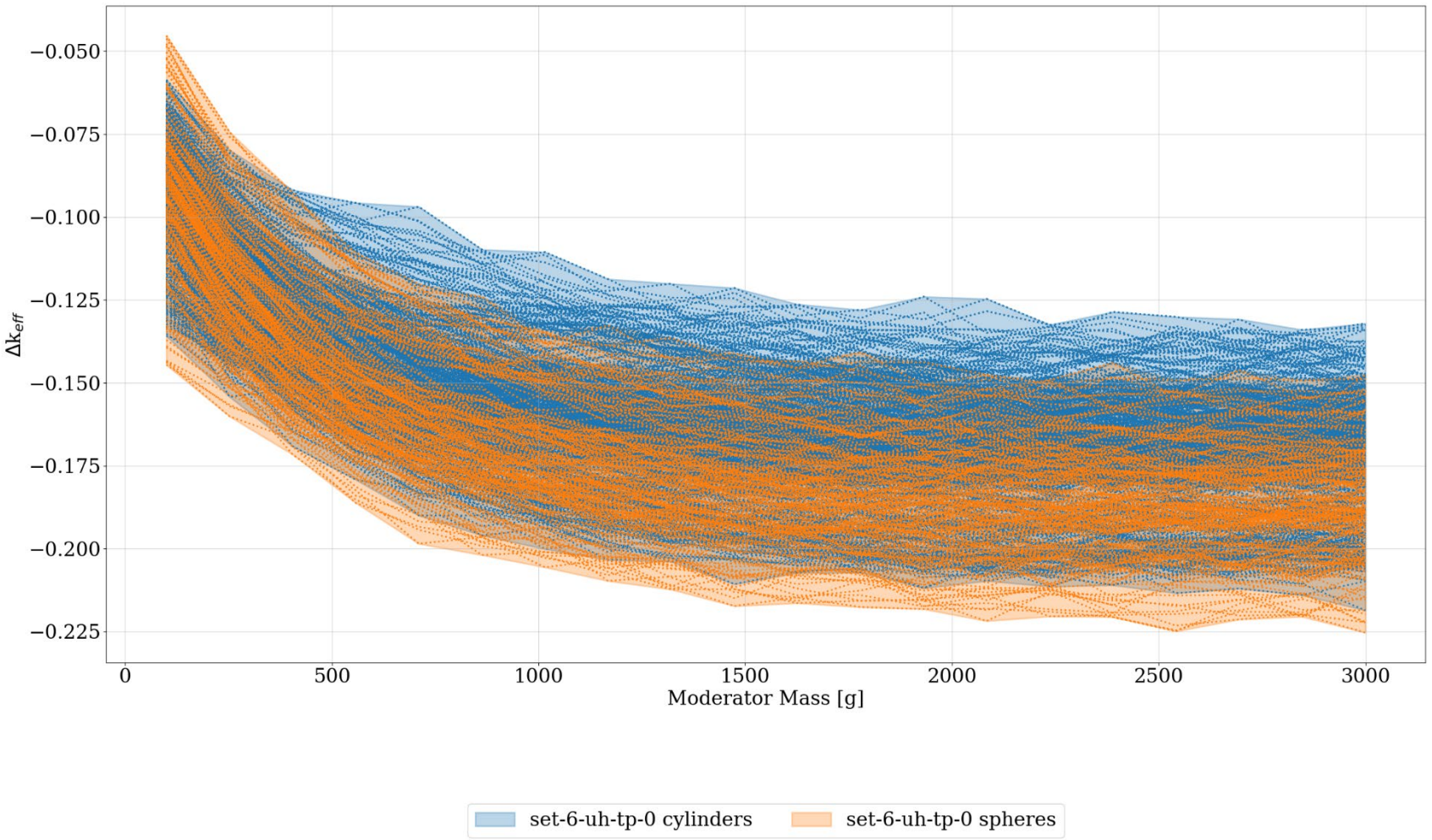

Figure M-1. Comparison of CCO upper horizon datasets, set-2-uh hexagonal pitch results (mirror boundary conditions) with set-6-uh-tp triangular pitch results (mirror boundary conditions) as delta-k_{eff} vs. moderator mass, time = 0 years.

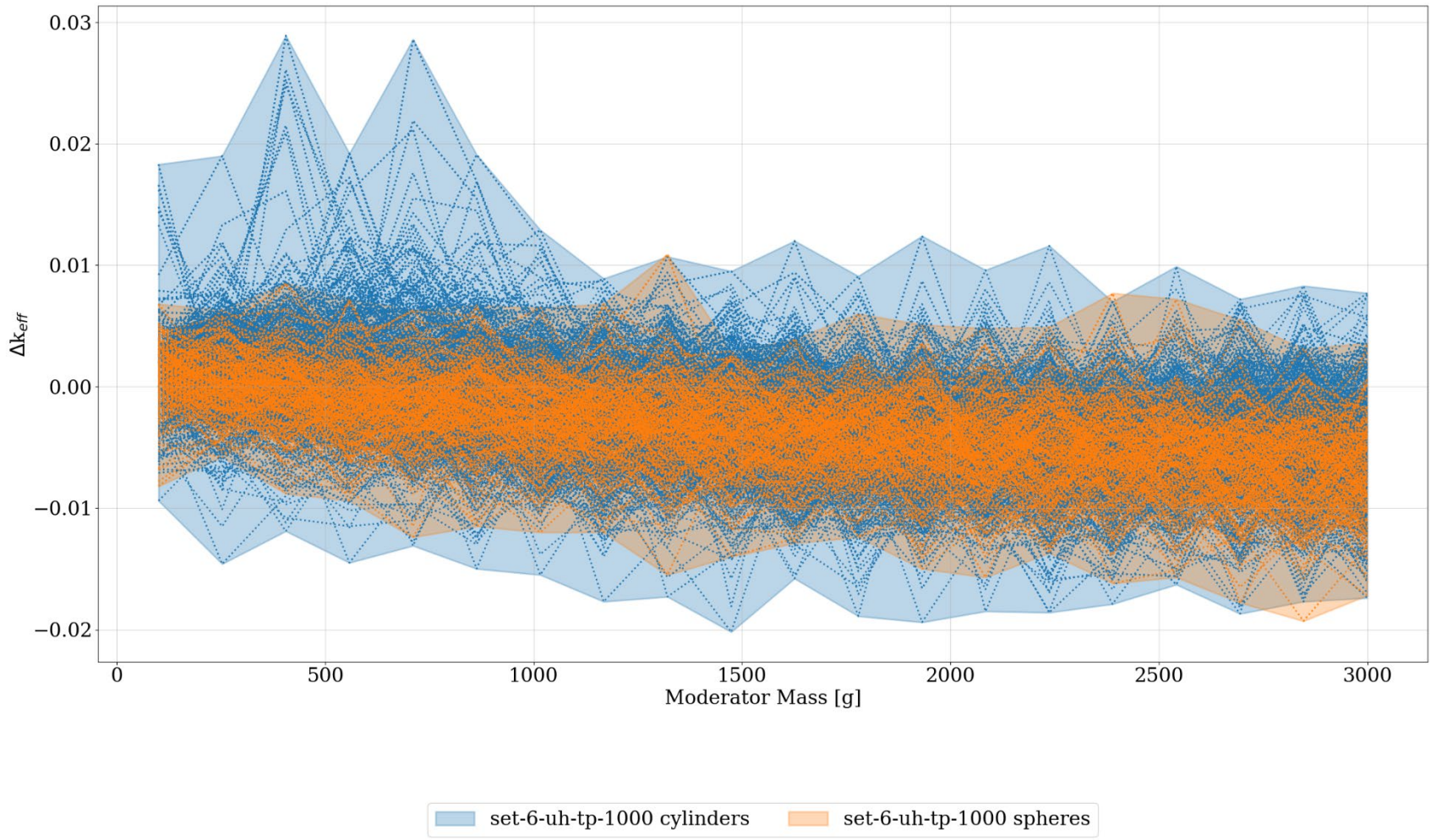

Figure M-2. Comparison of CCO upper horizon datasets, set-2-uh hexagonal pitch results (mirror boundary conditions) with set-6-uh-tp triangular pitch results (mirror boundary conditions) as delta-k_{eff} vs. moderator mass, time = 1,000 years.

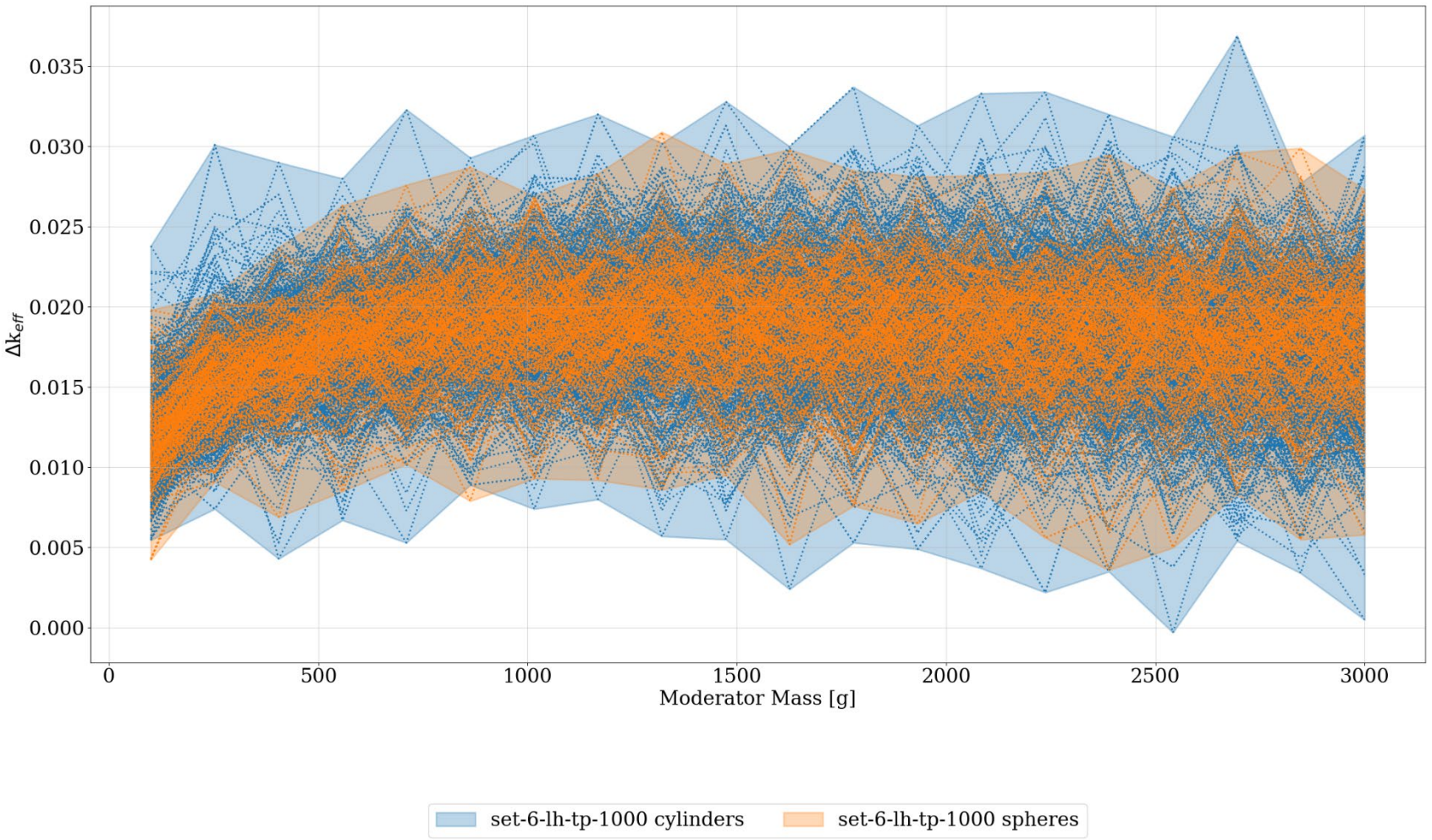

Figure M-3. Comparison of CCO lower horizon datasets, set-2-lh hexagonal pitch results (mirror boundary conditions) with set-6-lh-tp triangular pitch results (mirror boundary conditions) as delta-k_{eff} vs. moderator mass, time = 1,000 years.

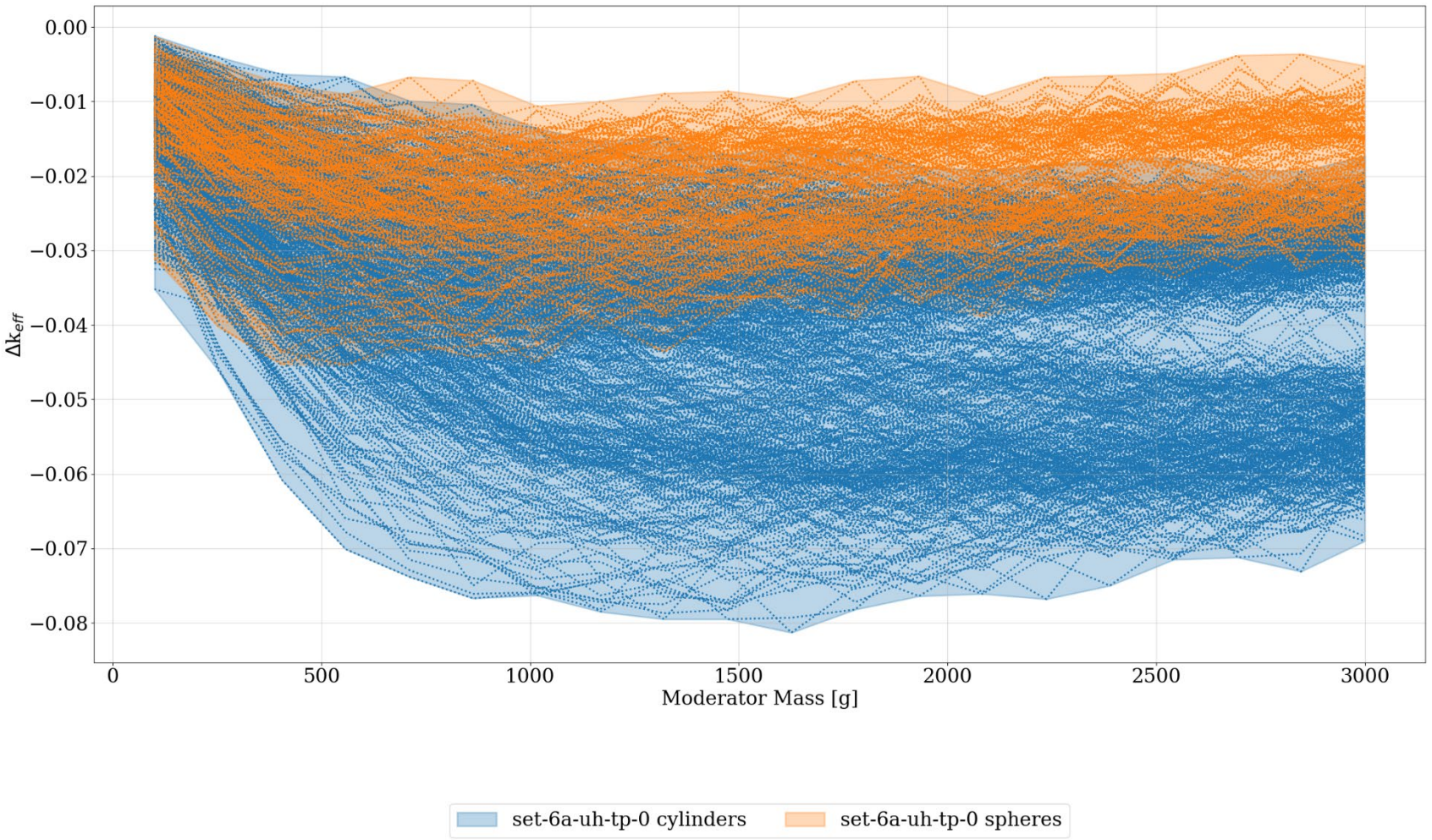

Figure M-4. Comparison of CCO upper horizon datasets, set6-uh-tp triangular pitch results (mirror boundary conditions) results with set6a-uh-tp triangular pitch results (periodic boundary conditions) as delta-k_{eff} vs. moderator mass, time = 0 years.

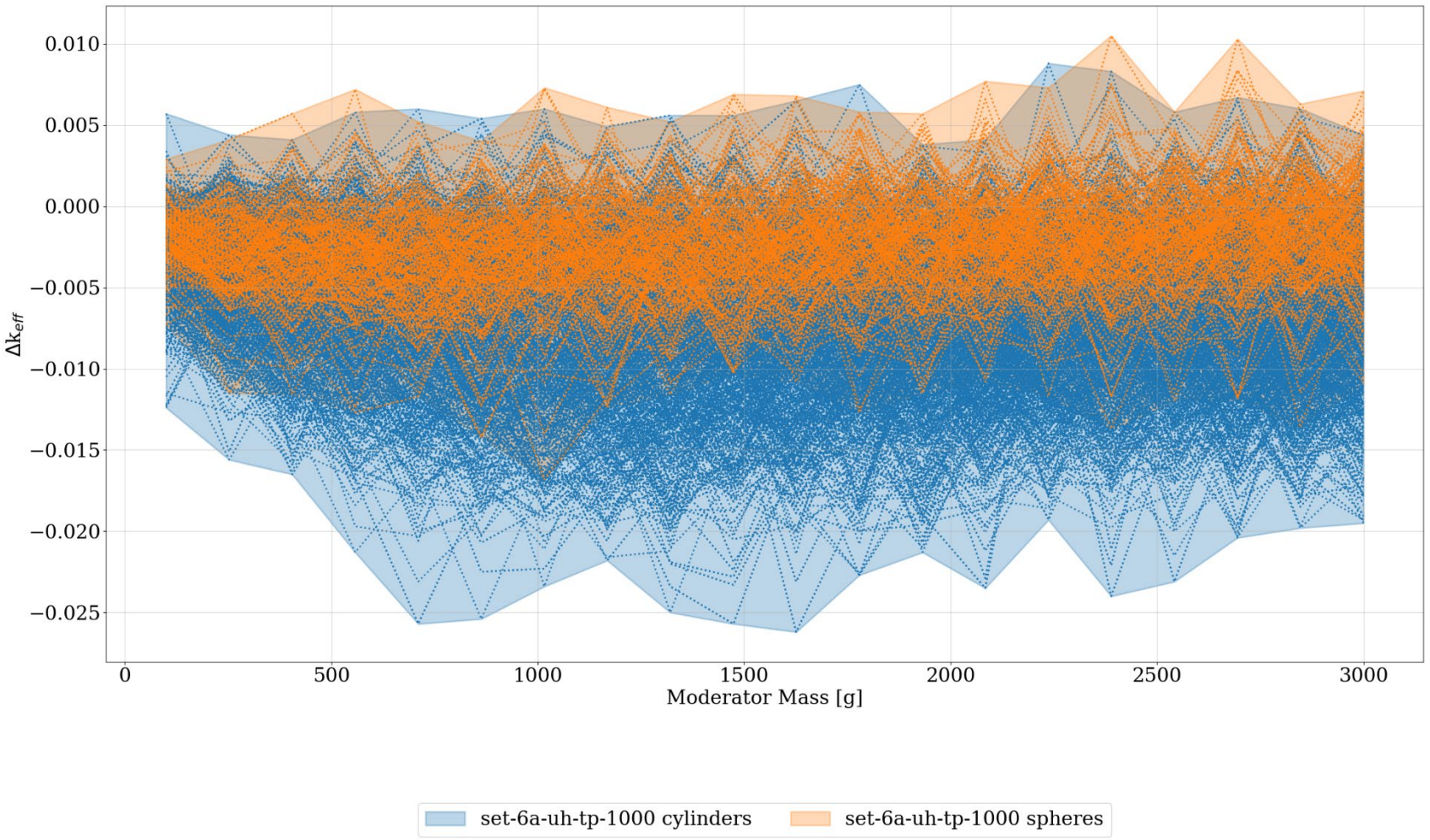

Figure M-5. Comparison of CCO upper horizon datasets, set6-uh-tp triangular pitch results (mirror boundary conditions) results with set6a-uh-tp triangular pitch results (periodic boundary conditions) as delta-k_{eff} vs. moderator mass, time = 1,000 years.

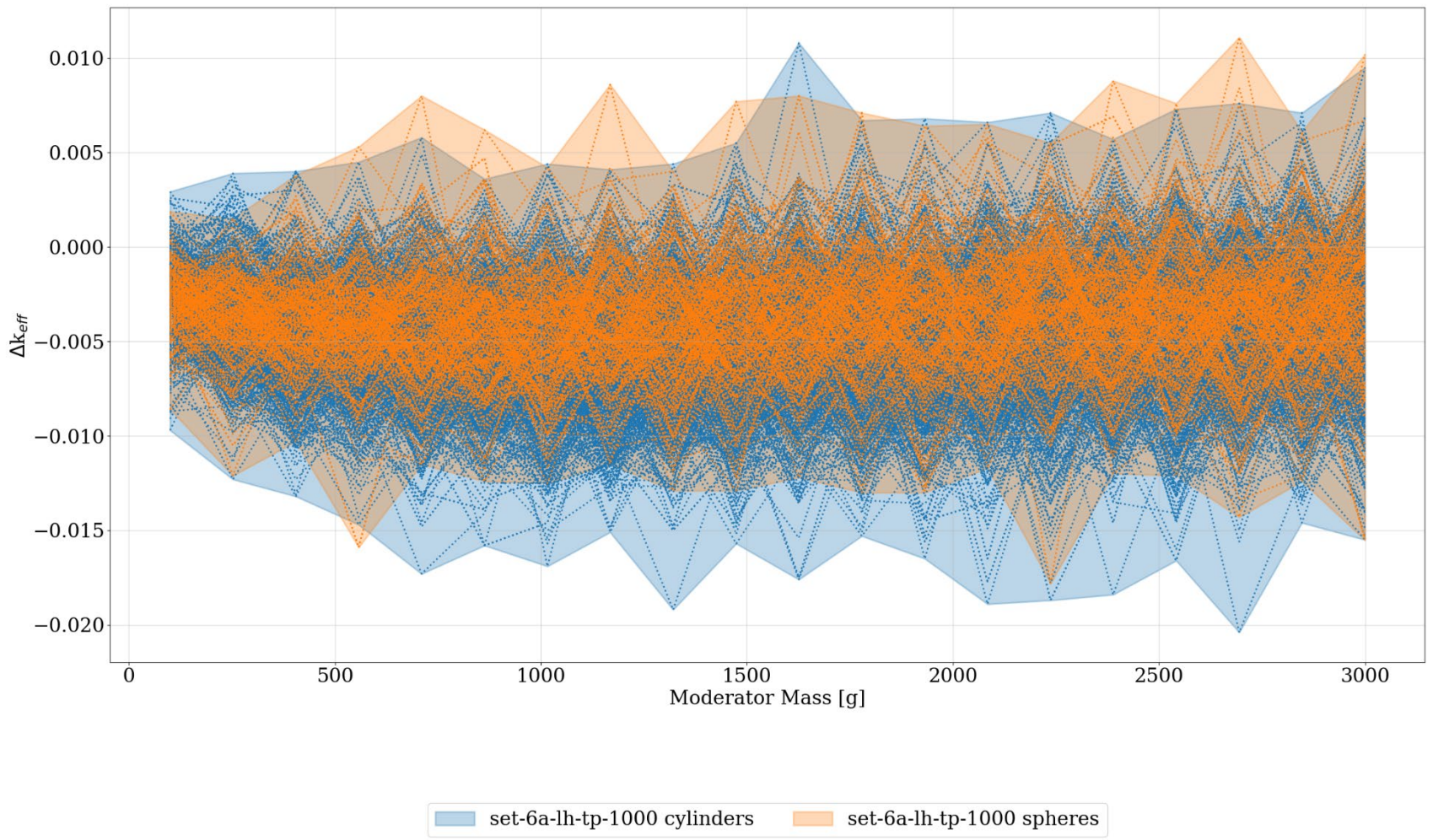

Figure M-6. Comparison of CCO lower horizon datasets, set6-lh-tp triangular pitch results (mirror boundary conditions) results with set6a-lh-tp triangular pitch results (periodic boundary conditions) as delta-k_{eff} vs. moderator mass, 1,000 years.

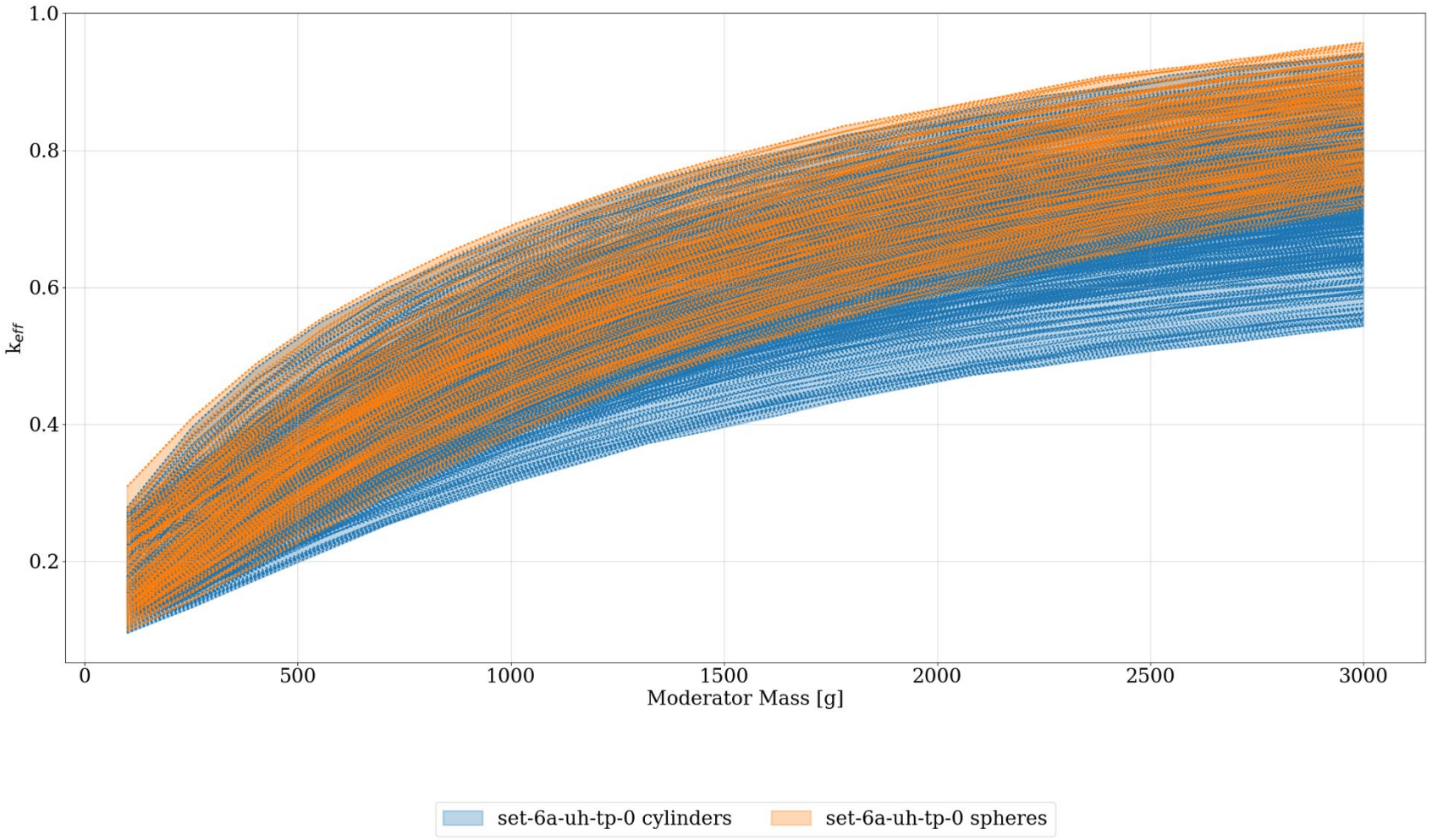

Figure M-7. Summary of CCO upper horizon datasets, set6a-uh-tp triangular pitch results (periodic boundary conditions) as k_{eff} vs. moderator mass, time = 0 years.

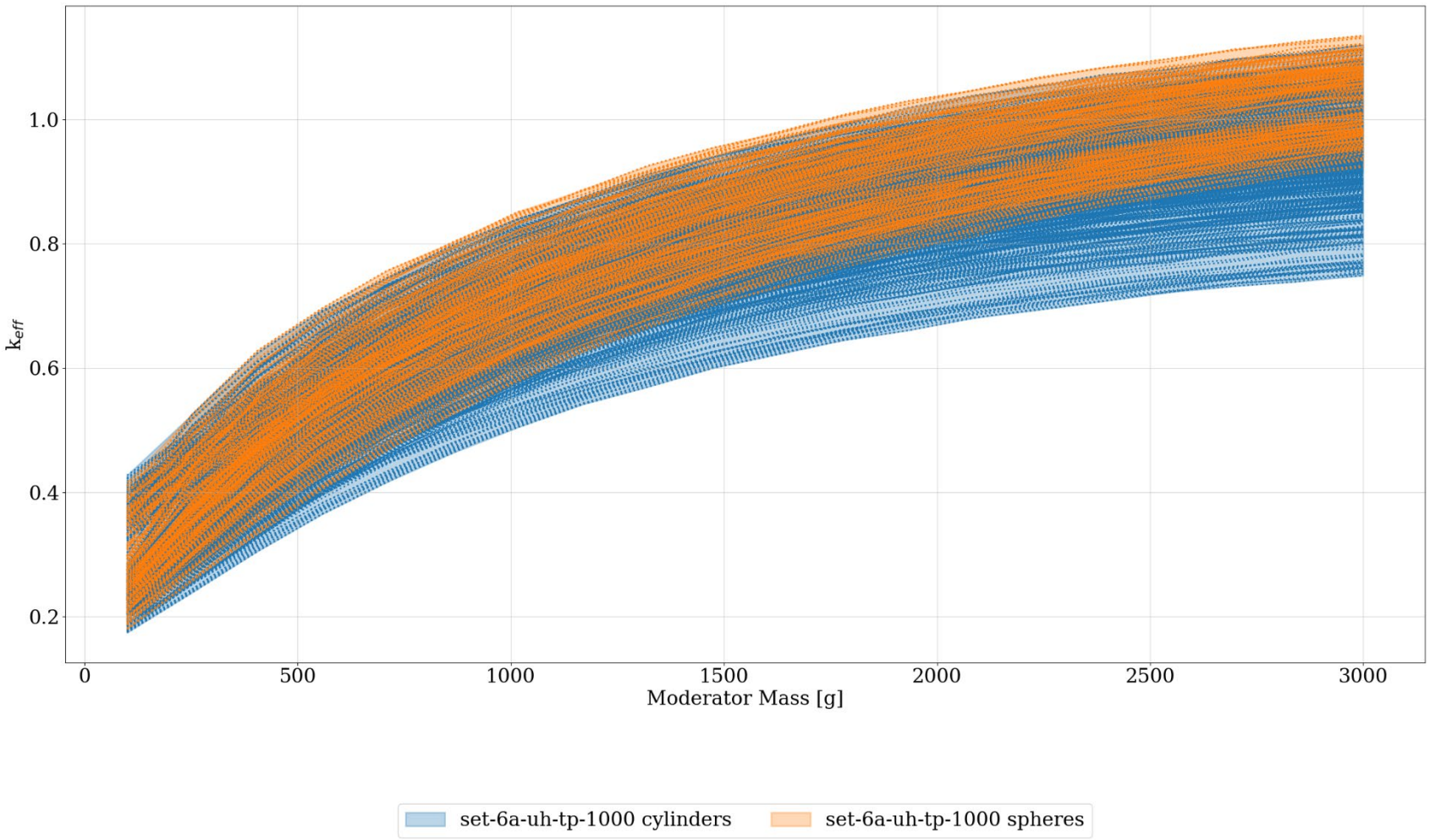

Figure M-8. Summary of CCO upper horizon datasets, set6a-uh-tp triangular pitch results (periodic boundary conditions) as k_{eff} vs. moderator mass, time = 1,000 years.

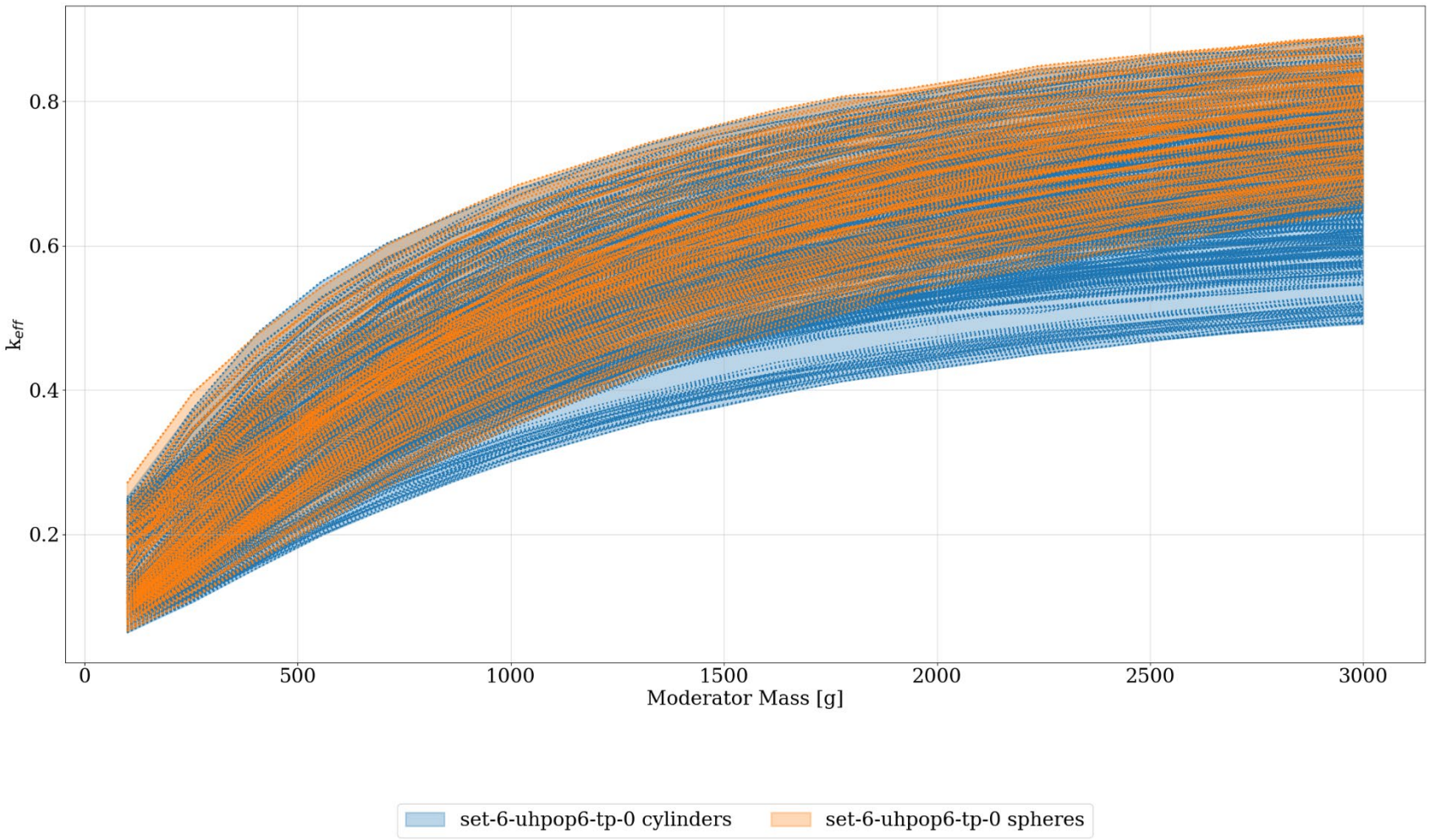

Figure M-9. Summary of 6 in. POP upper horizon datasets, set6-uhpop6-tp triangular pitch results (mirror boundary conditions) as k_{eff} vs. moderator mass, time = 0 years.

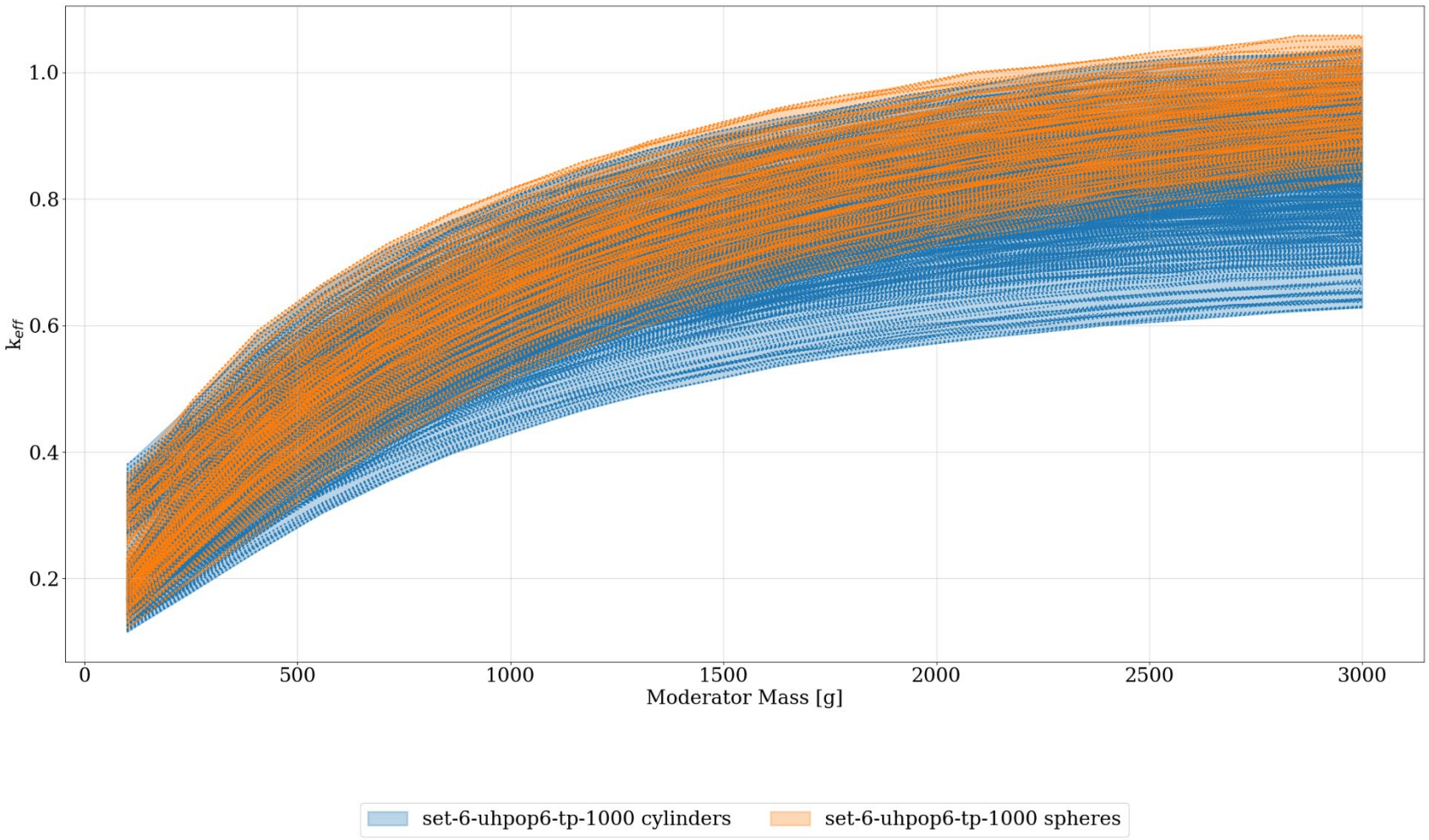

Figure M-10. Summary of 6 in. POP upper horizon datasets, set6-uhpop6-tp triangular pitch results (mirror boundary conditions) as k_{eff} vs. moderator mass, time = 1,000 years.

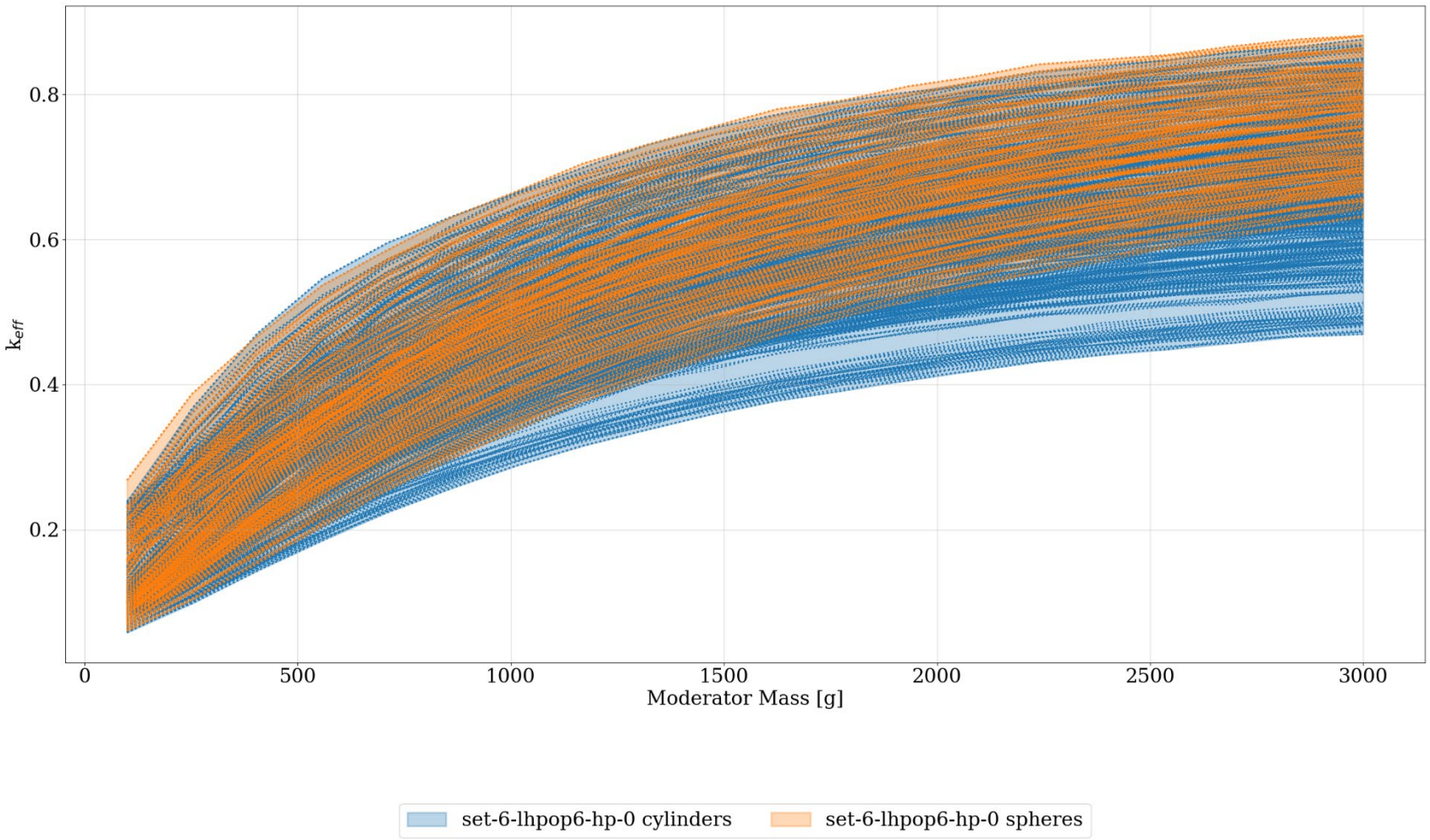

Figure M-11. Summary of 6 in. POP lower horizon datasets, set6-lhpop6-hp hexagonal pitch results (mirror boundary conditions) as k_{eff} vs. moderator mass, time = 0 years.

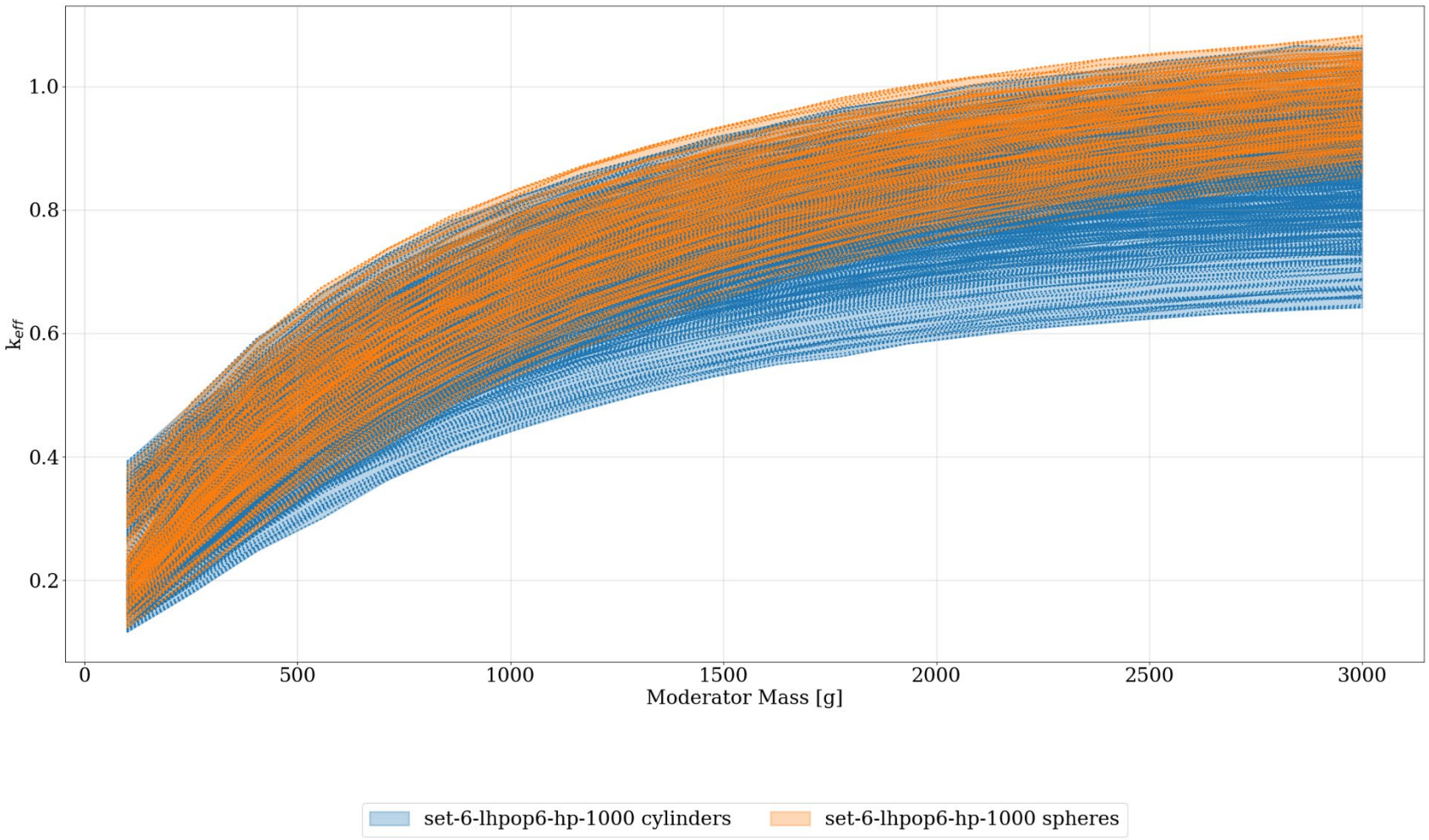

Figure M-12. Summary of 6 in. POP lower horizon datasets, set6-lhpop6-hp hexagonal pitch results (mirror boundary conditions) as k_{eff} vs. moderator mass, time = 1,000 years.

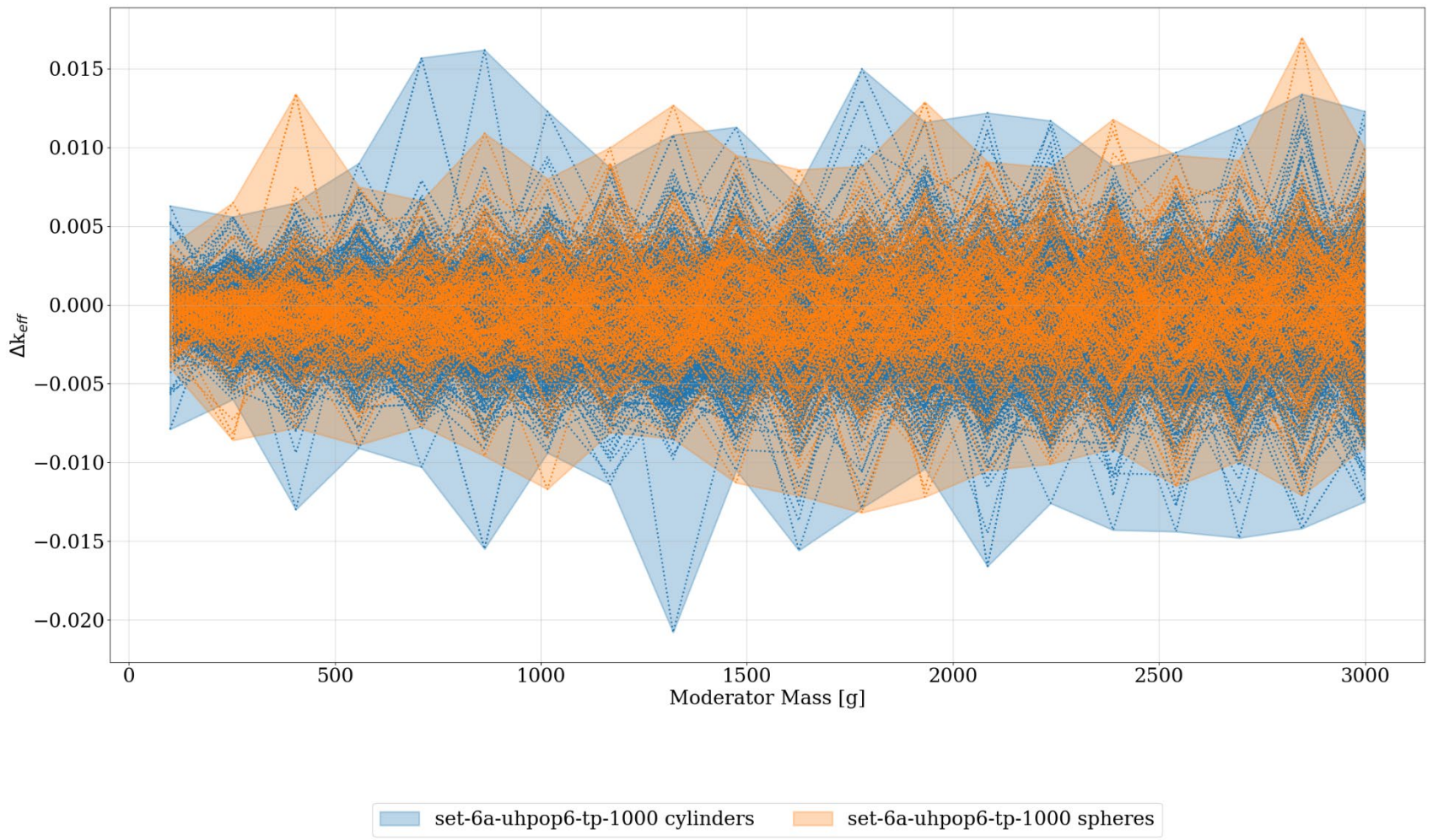

Figure M-13. Comparison of 6 in. POP upper horizon datasets set6-uhpop6-tp triangular pitch results (mirror boundary conditions) results with set6a-uhpop6-tp triangular pitch results (periodic boundary conditions) as delta-k_{eff} vs. moderator mass, time = 1,000 years.

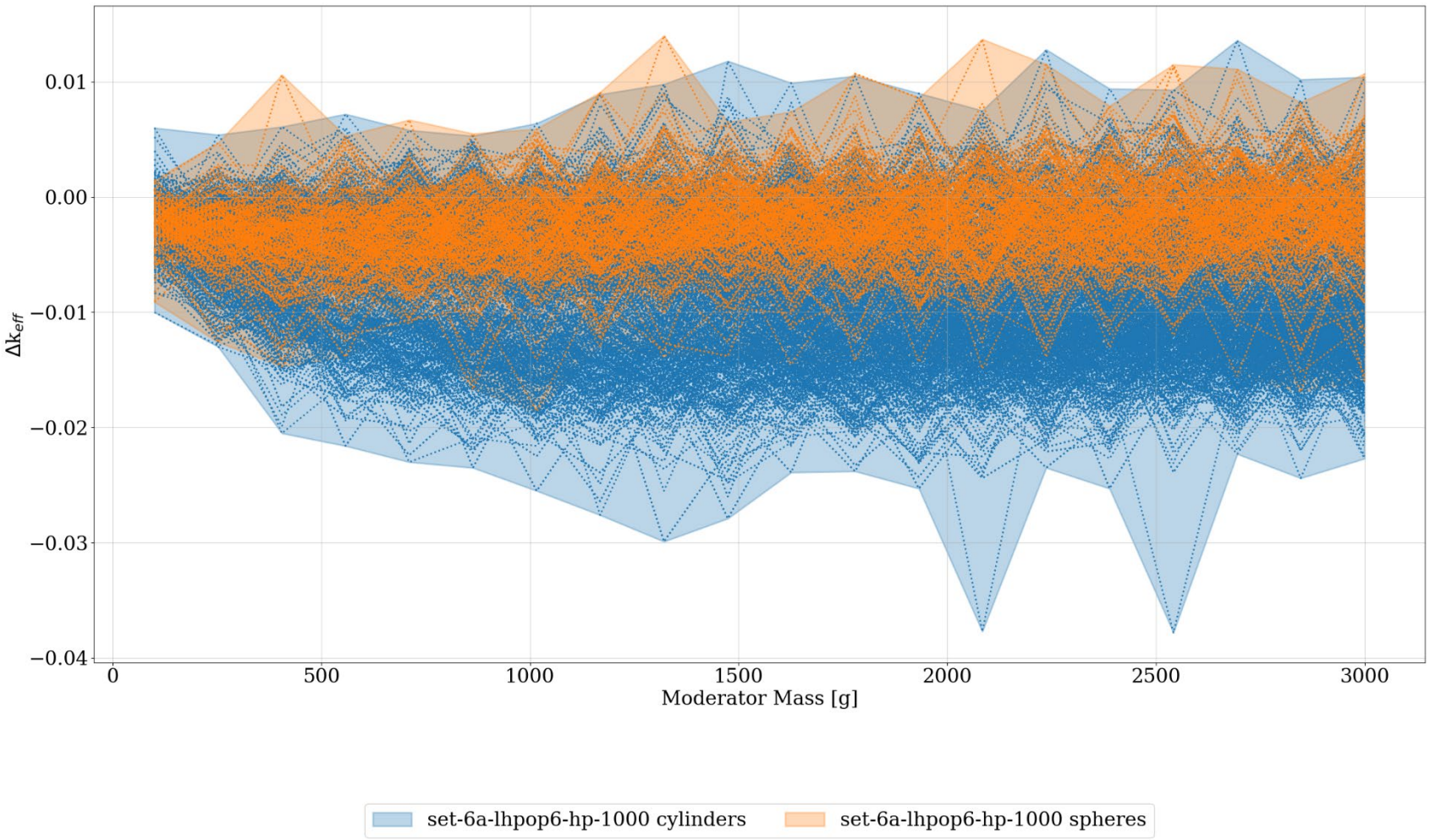

Figure M-14. Comparison of 6 in. POP lower horizon datasets set6-lhpop6-hp hexagonal pitch results (mirror boundary conditions) results with set6a-lhpop6-hp hexagonal pitch results (periodic boundary conditions) as delta-k_{eff} vs. moderator mass, time = 1,000 years.

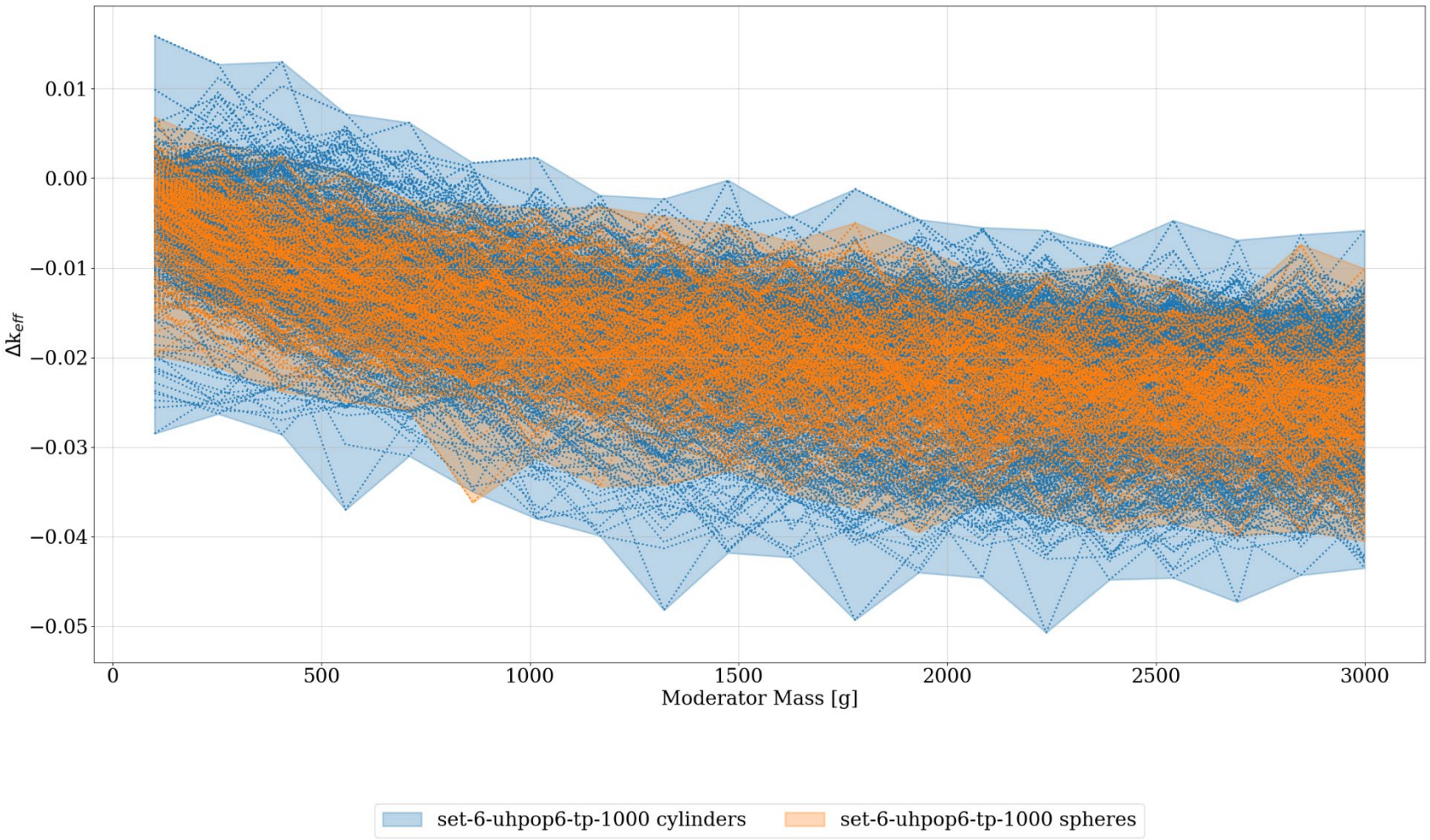

Figure M-15. Comparison of 6 in. POP lower horizon datasets set6-lhpop6-hp hexagonal pitch results (mirror boundary conditions) results with upper horizon set6-uhpop6-tp triangular pitch results (mirror boundary conditions) as delta-k_{eff} vs. moderator mass, time = 1,000 years.

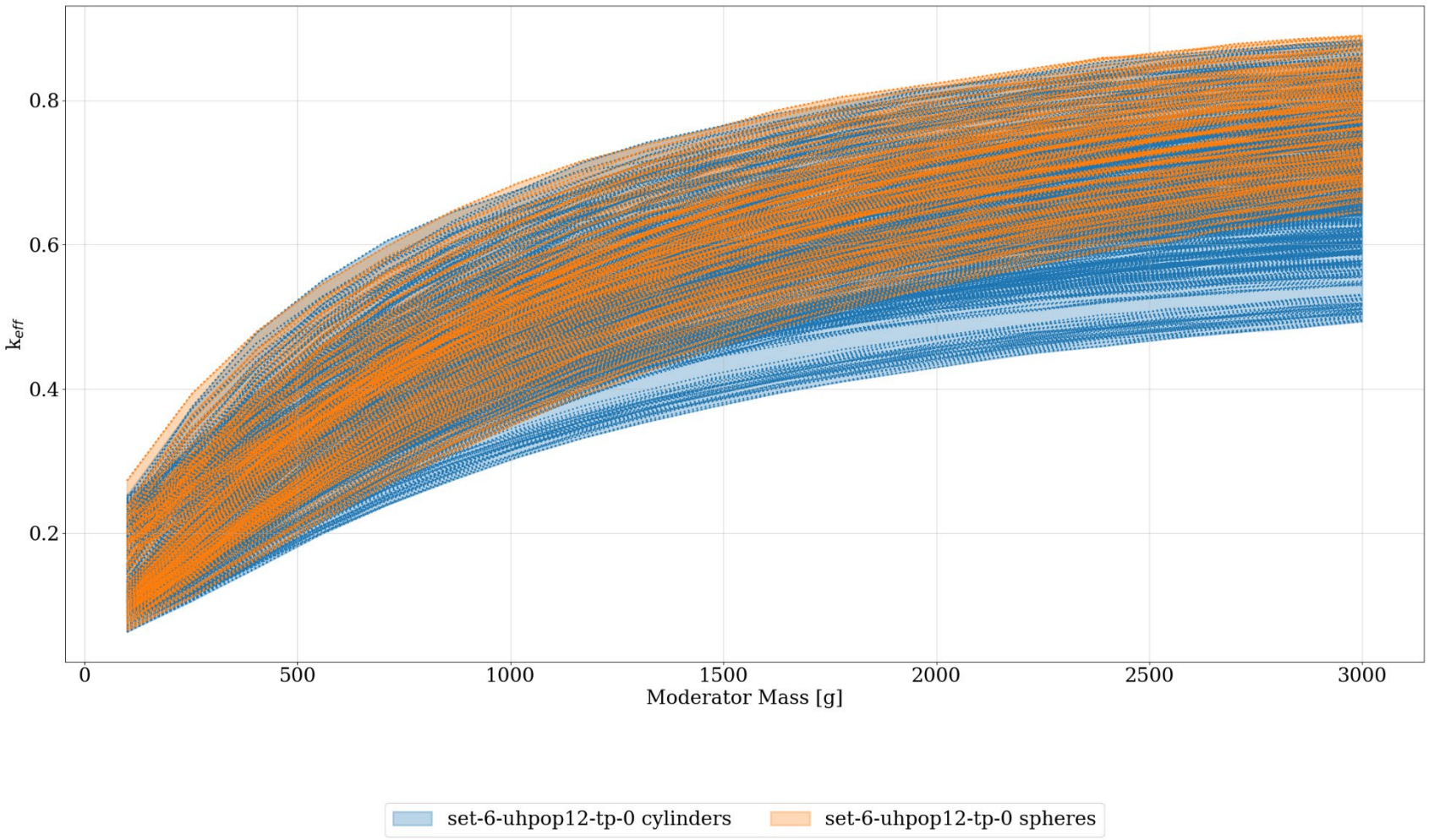

Figure M-16. Summary of 12 in. POP upper horizon datasets, set6-uhpop12-tp triangular pitch results (mirror boundary conditions) as k_{eff} vs. moderator mass, time = 0 years.

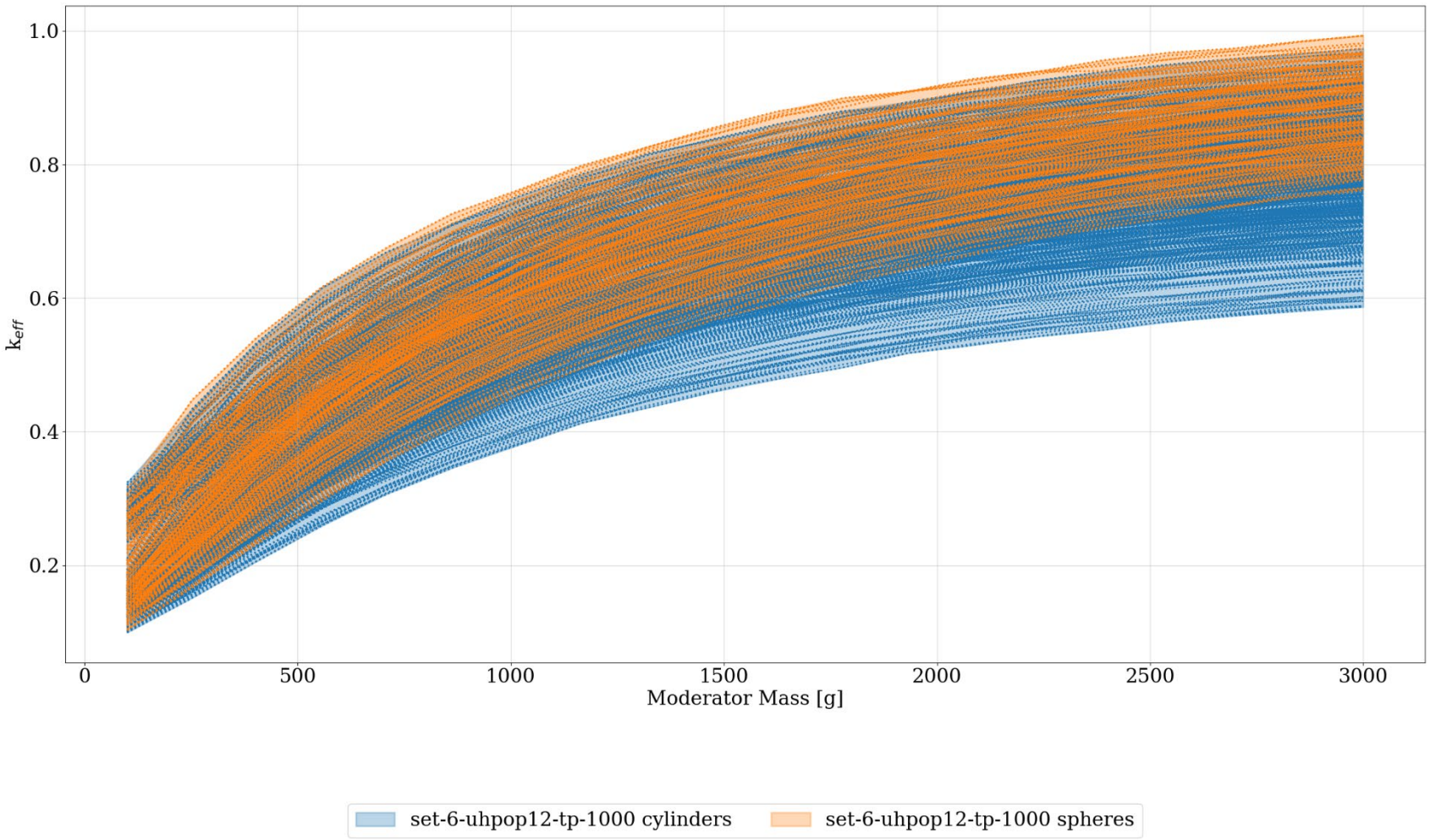

Figure M-17. Summary of 12 in. POP upper horizon datasets, set6-uhpop12-tp triangular pitch results (mirror boundary conditions) as k_{eff} vs. moderator mass, time = 1,000 years.

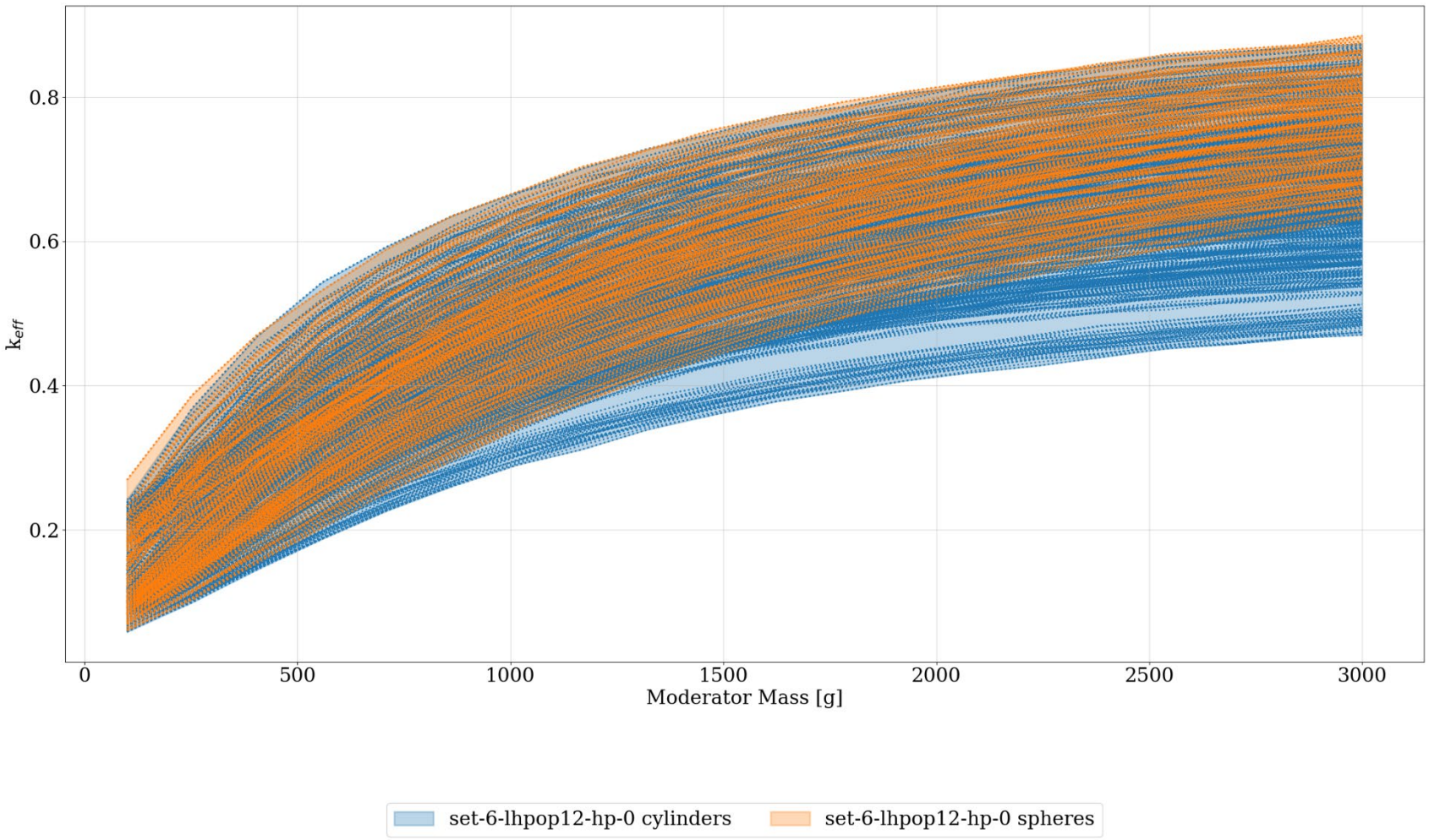

Figure M-18. Summary of 12 in. POP lower horizon datasets, set6-lhpop12-hp hexagonal pitch results (mirror boundary conditions) as k_{eff} vs. moderator mass, time = 0 years.

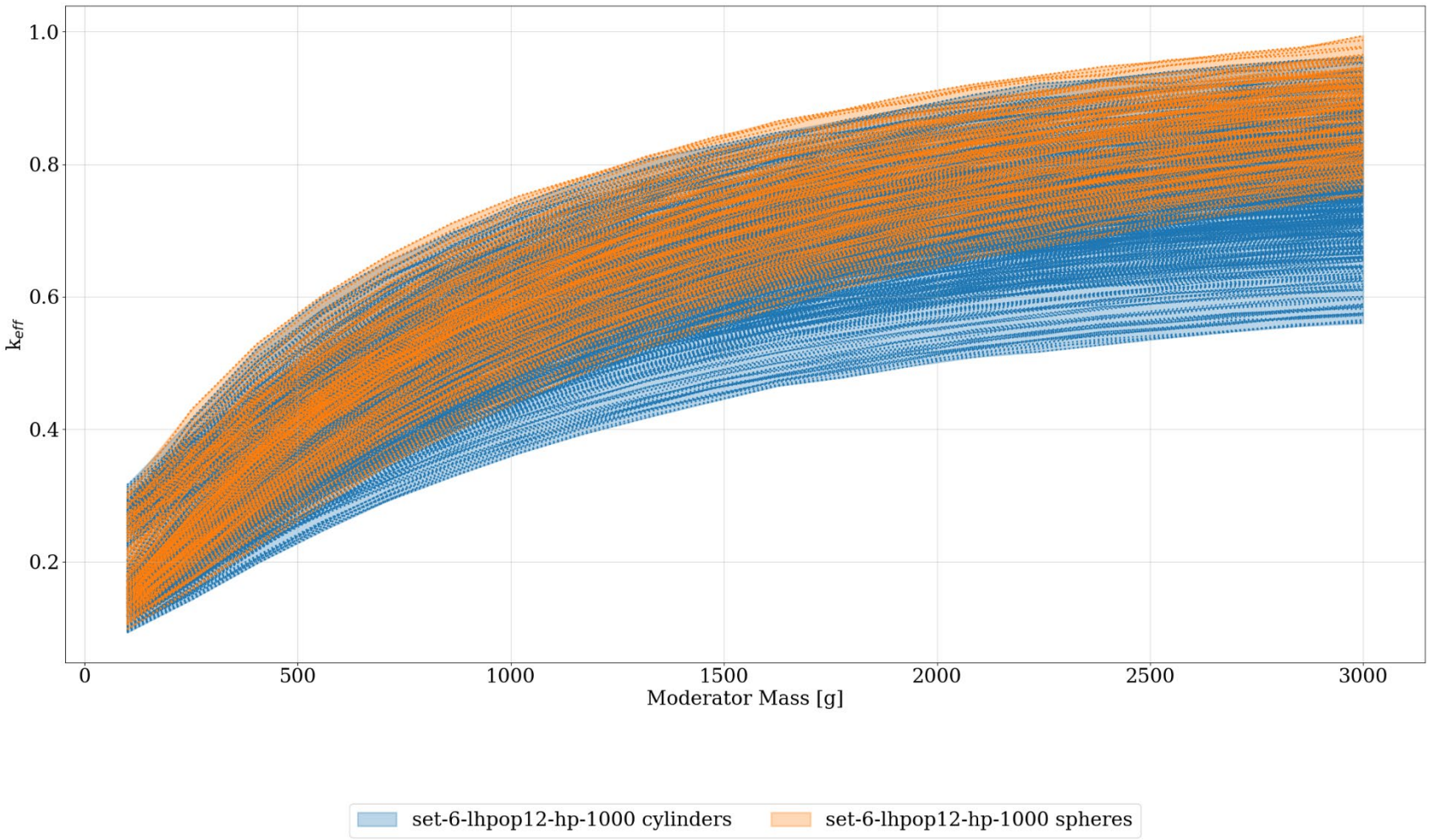

Figure M-19. Summary of 12 in. POP lower horizon datasets, set6-lhpop12-hp hexagonal pitch results (mirror boundary conditions) as k_{eff} vs. moderator mass, time = 1,000 years.

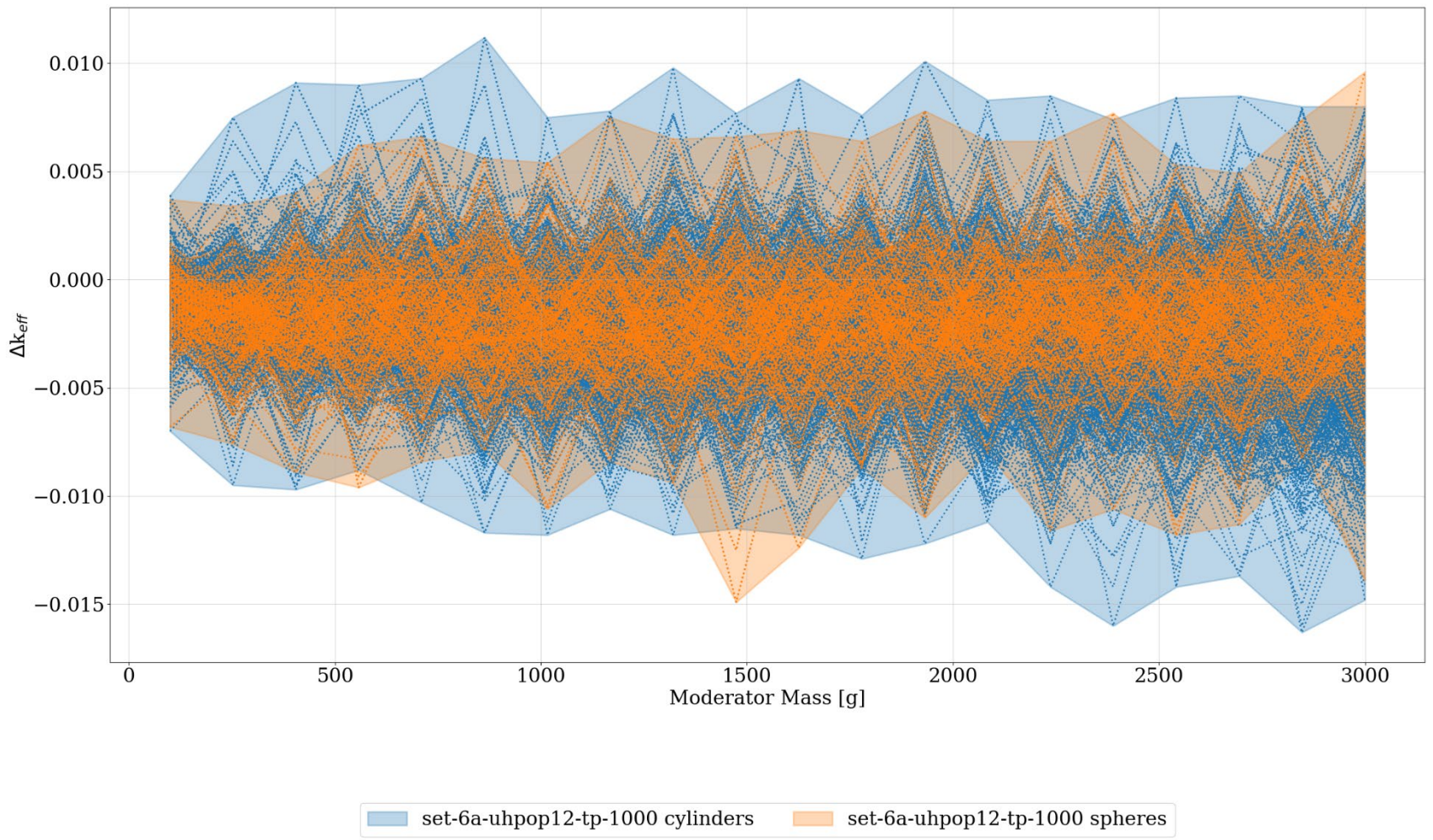

Figure M-20. Comparison of 12 in. POP upper horizon datasets set6-uhpop12-tp triangular pitch results (mirror boundary conditions) results with set6a-uhpop12-tp triangular pitch results (periodic boundary conditions) as delta-k_{eff} vs. moderator mass, time = 1,000 years.

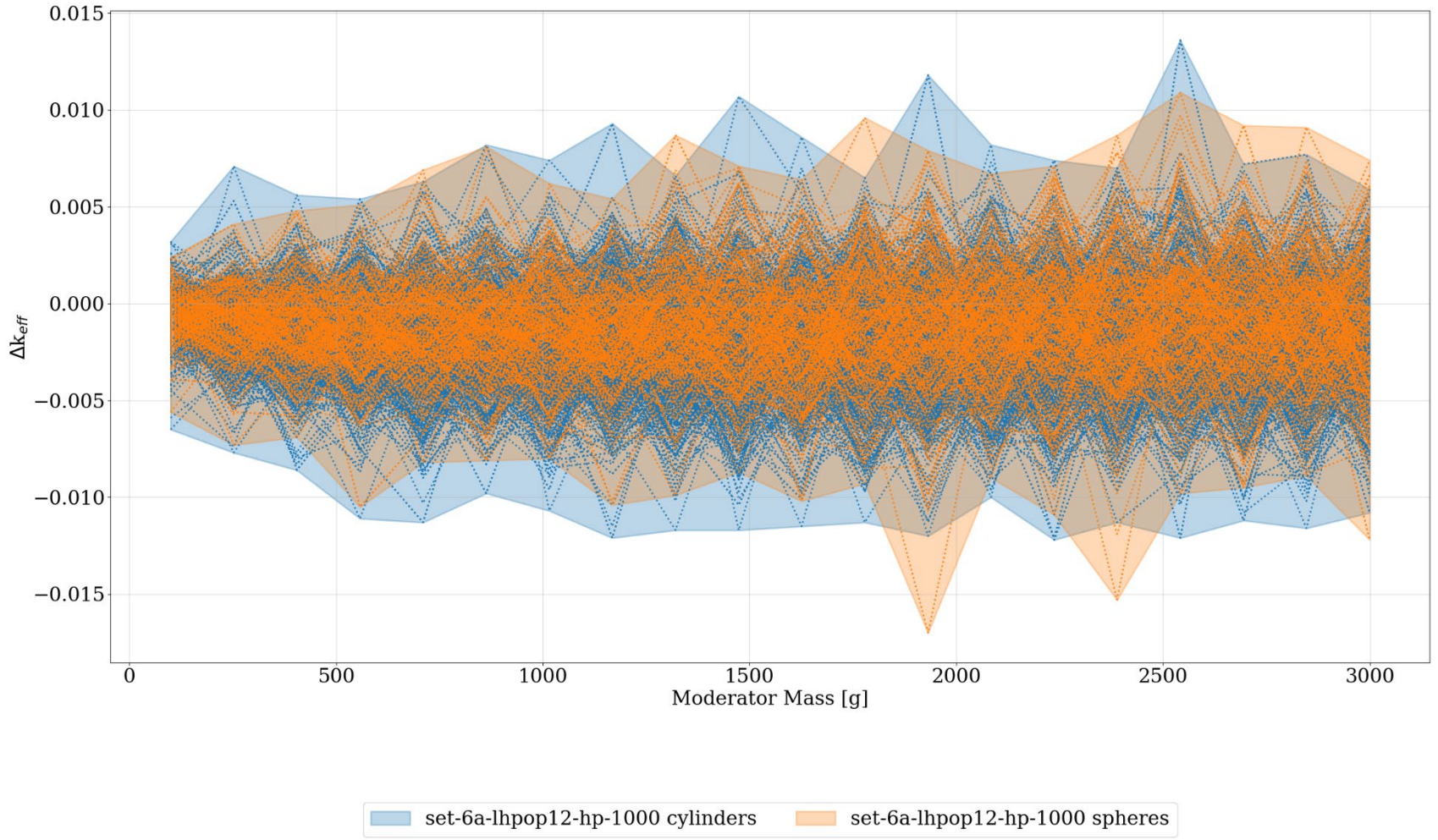

Figure M-21. Comparison of 12 in. POP lower horizon datasets set6-lhpop12-hp hexagonal pitch results (mirror boundary conditions) results with set6a-lhpop12-hp hexagonal pitch results (periodic boundary conditions) as delta-k_{eff} vs. moderator mass, time = 1,000 years.

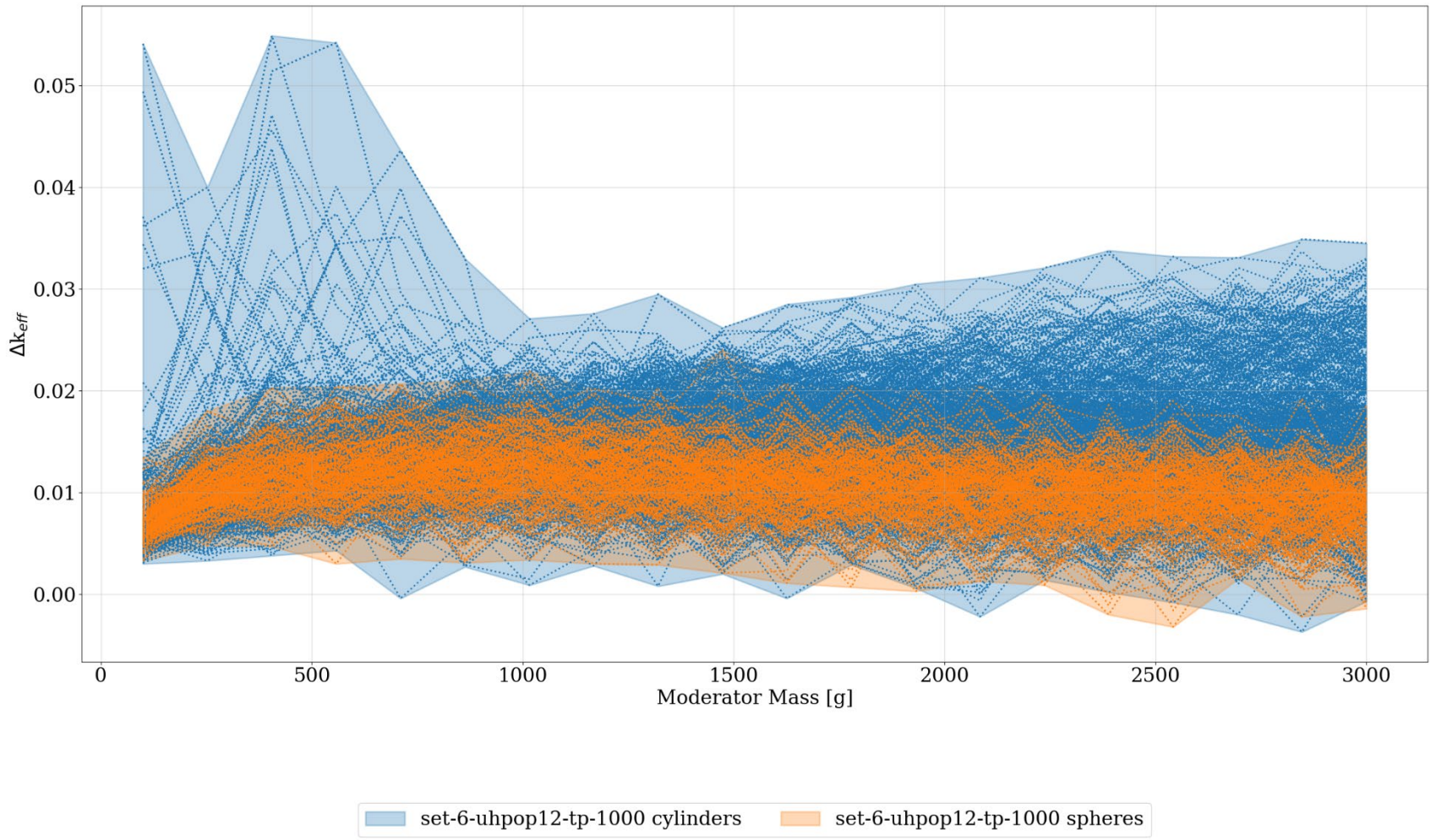

Figure M-22. Comparison of 12 in. POP lower horizon datasets set6-lhpop12-hp hexagonal pitch results (mirror boundary conditions) results with upper horizon set6-uhpop12-tp triangular pitch results (mirror boundary conditions) as delta-k_{eff} vs. moderator mass, time = 1,000 years.

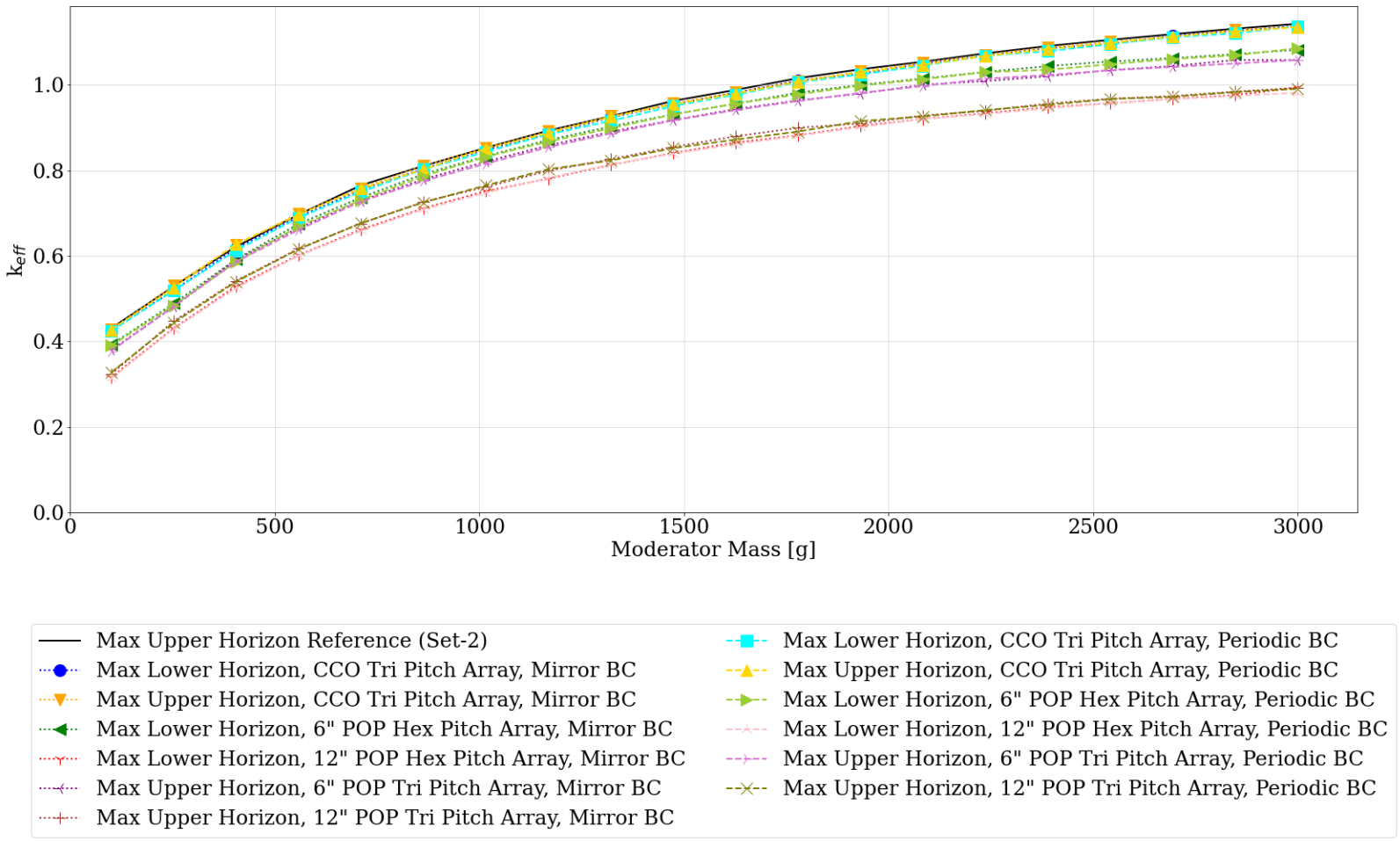

Figure M-23. Max k_{eff} of all subsets of all CCO and POP centroid configurations at time = 1,000 years compared with max k_{eff} of all subsets of set-2-uh hexagonal pitch (mirror boundary conditions) as k_{eff} vs. moderator mass, time = 1,000 years.

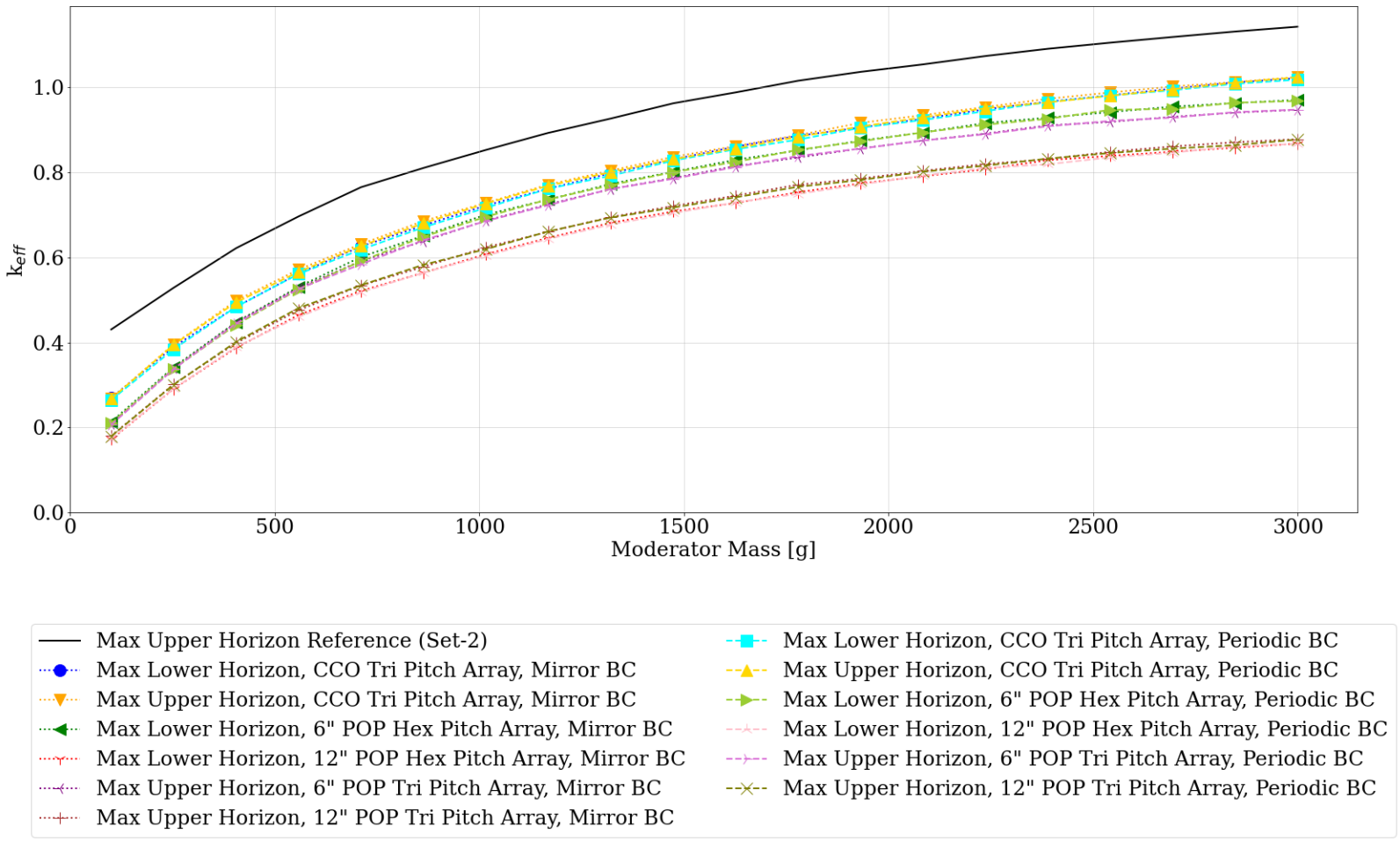

Figure M-24. Max k_{eff} of all subcase-1 of all CCO and POP centroid configurations at time = 1,000 years compared with max k_{eff} of all subsets of set-2-uh hexagonal pitch (mirror boundary conditions) as k_{eff} vs. moderator mass, time = 1,000 years.

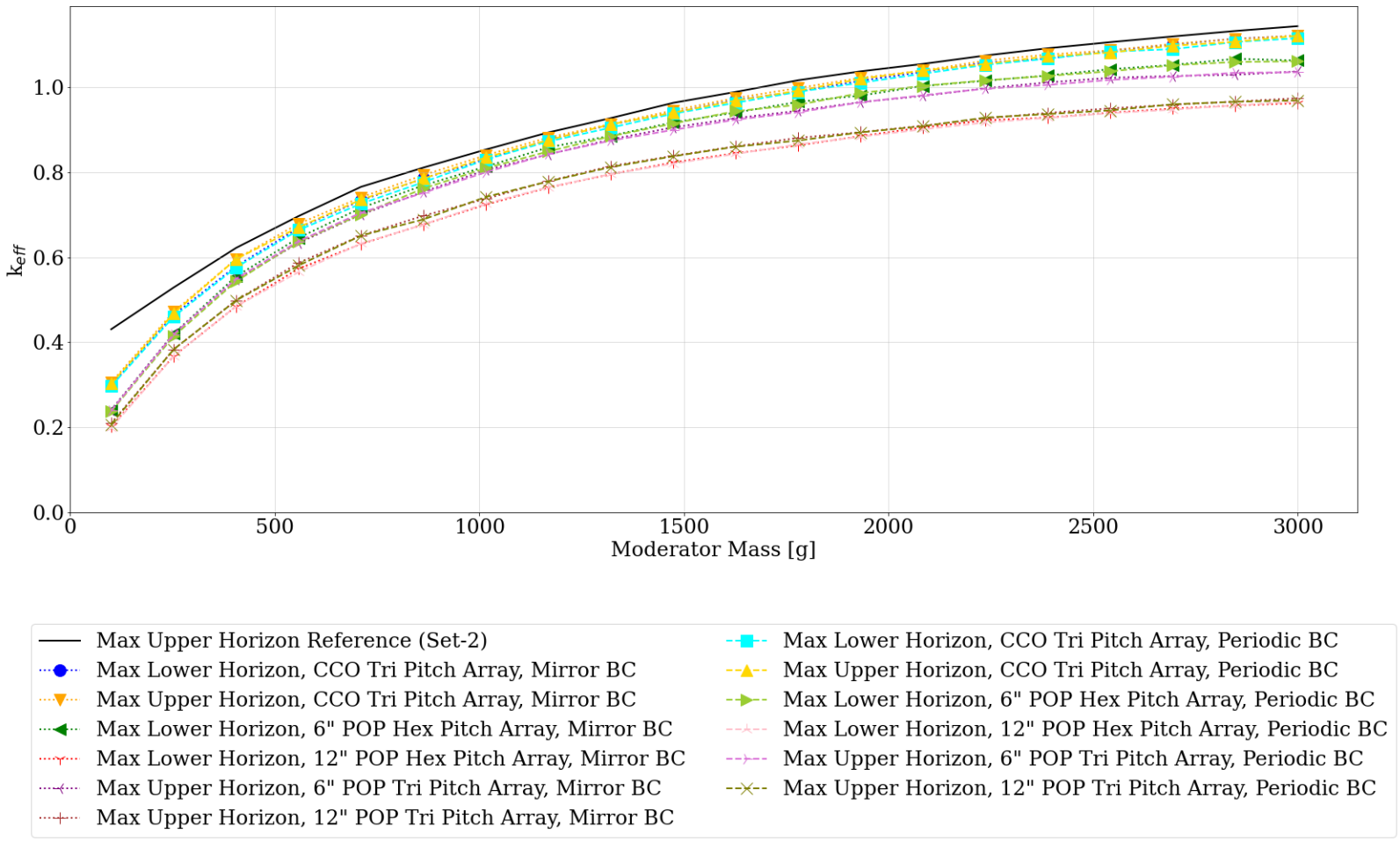

Figure M-25. Max k_{eff} of all subcase-2 of all CCO and POP centroid configurations at time = 1,000 years compared with max k_{eff} of all subsets of set-2-uh hexagonal pitch (mirror boundary conditions) as k_{eff} vs. moderator mass, time = 1,000 years.

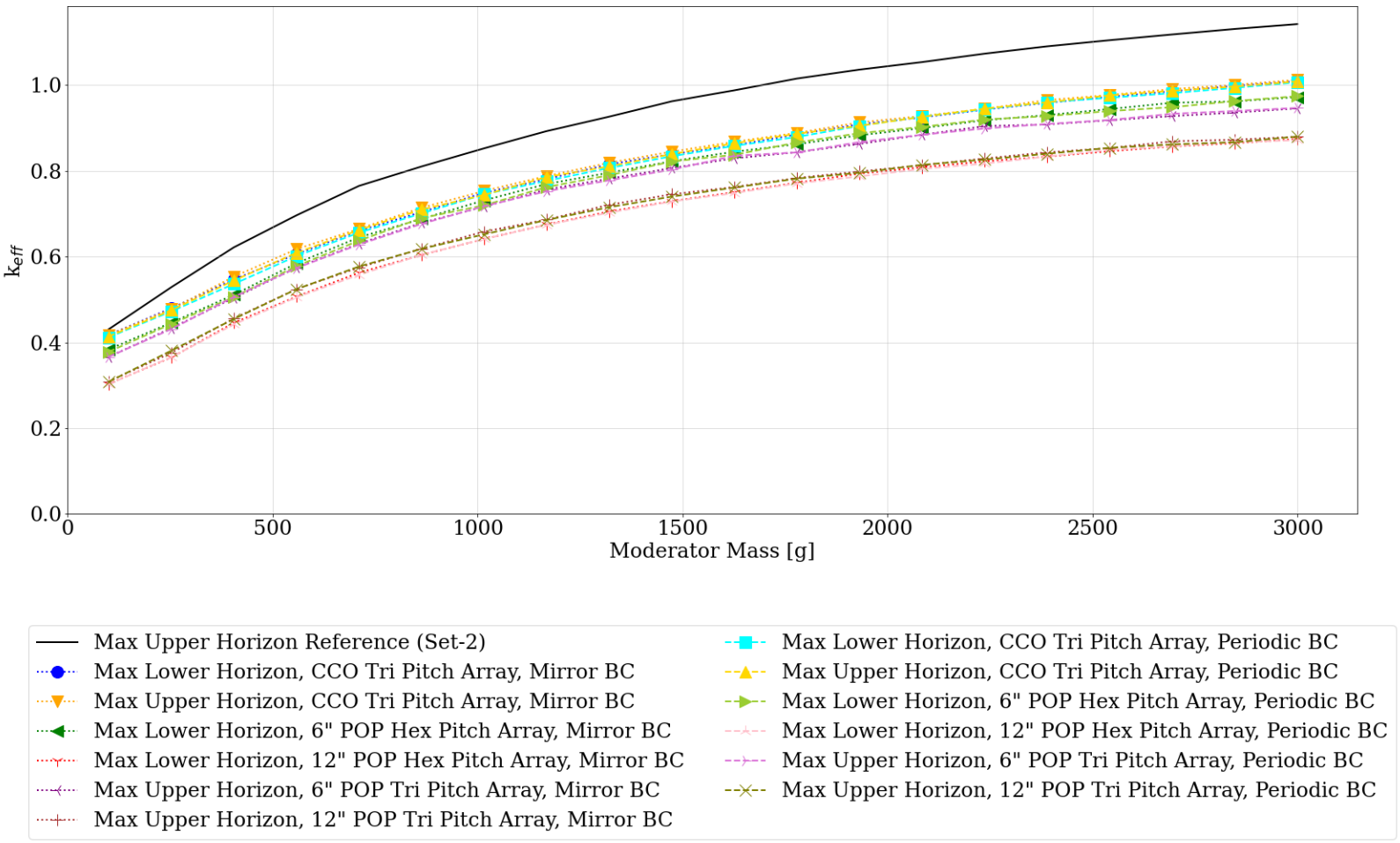

Figure M-26. Max k_{eff} of all subcase-3 of all CCO and POP centroid configurations at time = 1,000 years compared with max k_{eff} of all subsets of set-2-uh hexagonal pitch (mirror boundary conditions) as k_{eff} vs. moderator mass, time = 1,000 years.

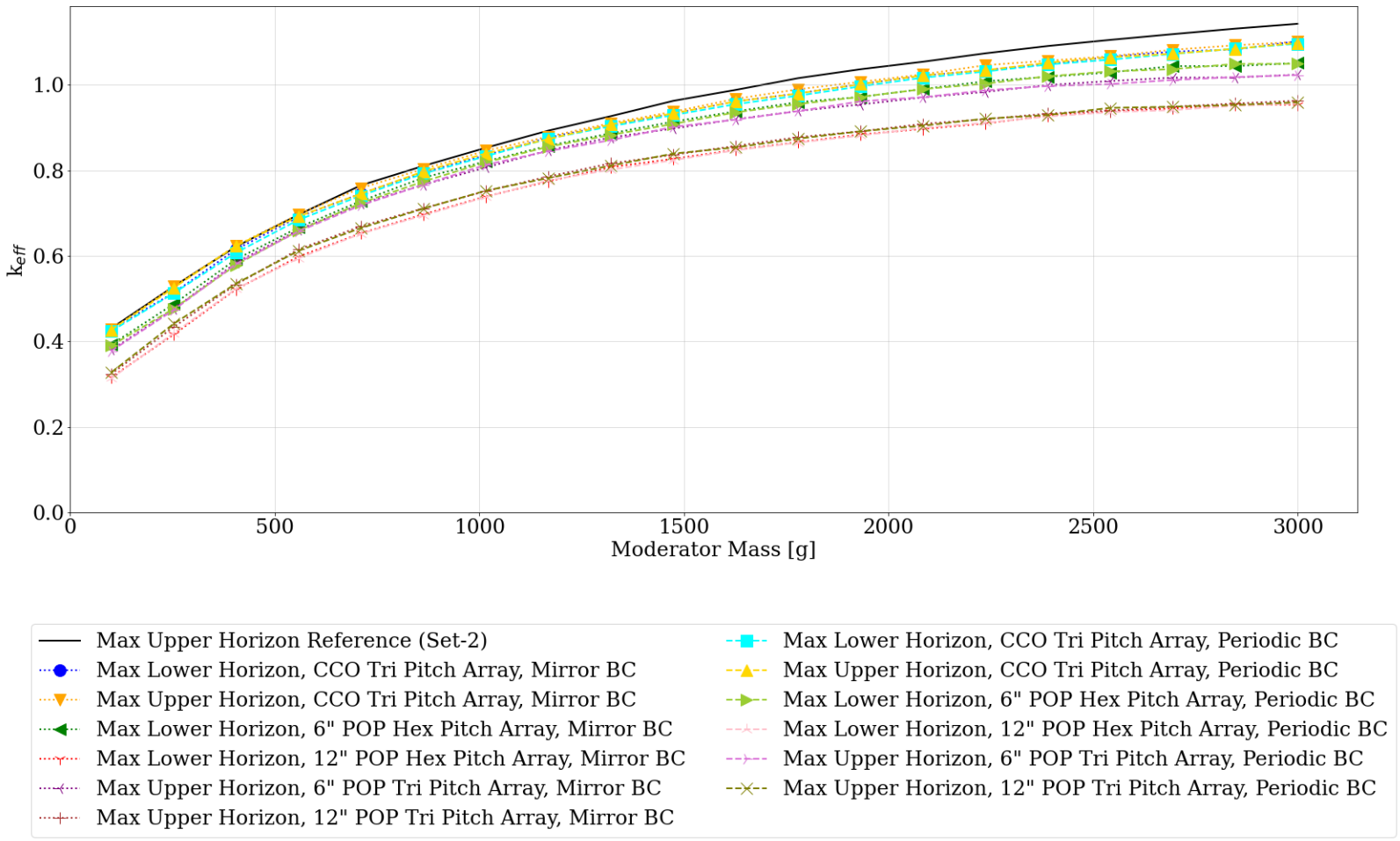

Figure M-27. Max k_{eff} of all subcase-4 of all CCO and POP centroid configurations at time = 1,000 years compared with max k_{eff} of all subsets of set-2-uh hexagonal pitch (mirror boundary conditions) as k_{eff} vs. moderator mass, time = 1,000 years.

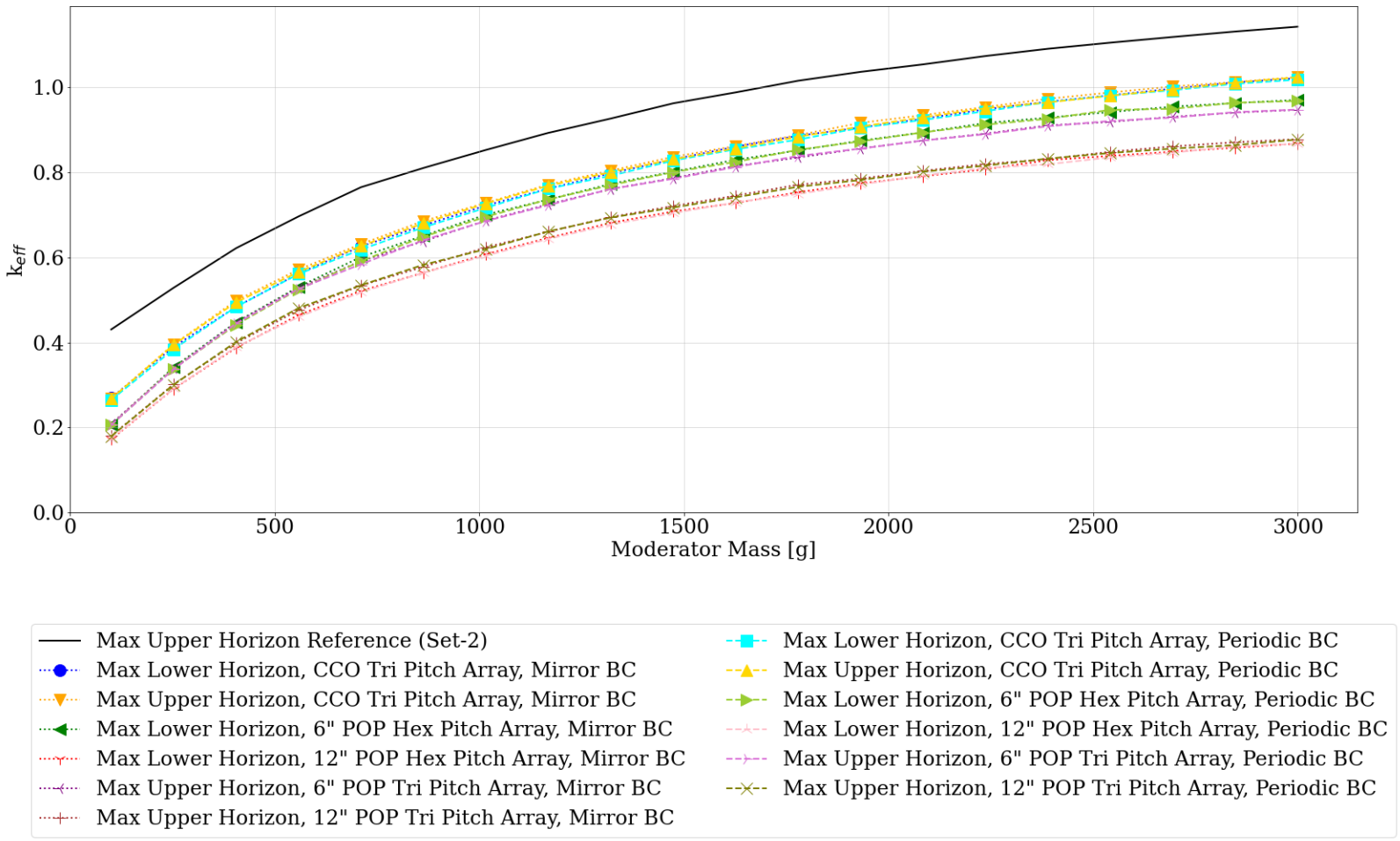

Figure M-28. Max k_{eff} of all subcase-5 of all CCO and POP centroid configurations at time = 1,000 years compared with max k_{eff} of all subsets of set-2-uh hexagonal pitch (mirror boundary conditions) as k_{eff} vs. moderator mass, time = 1,000 years.

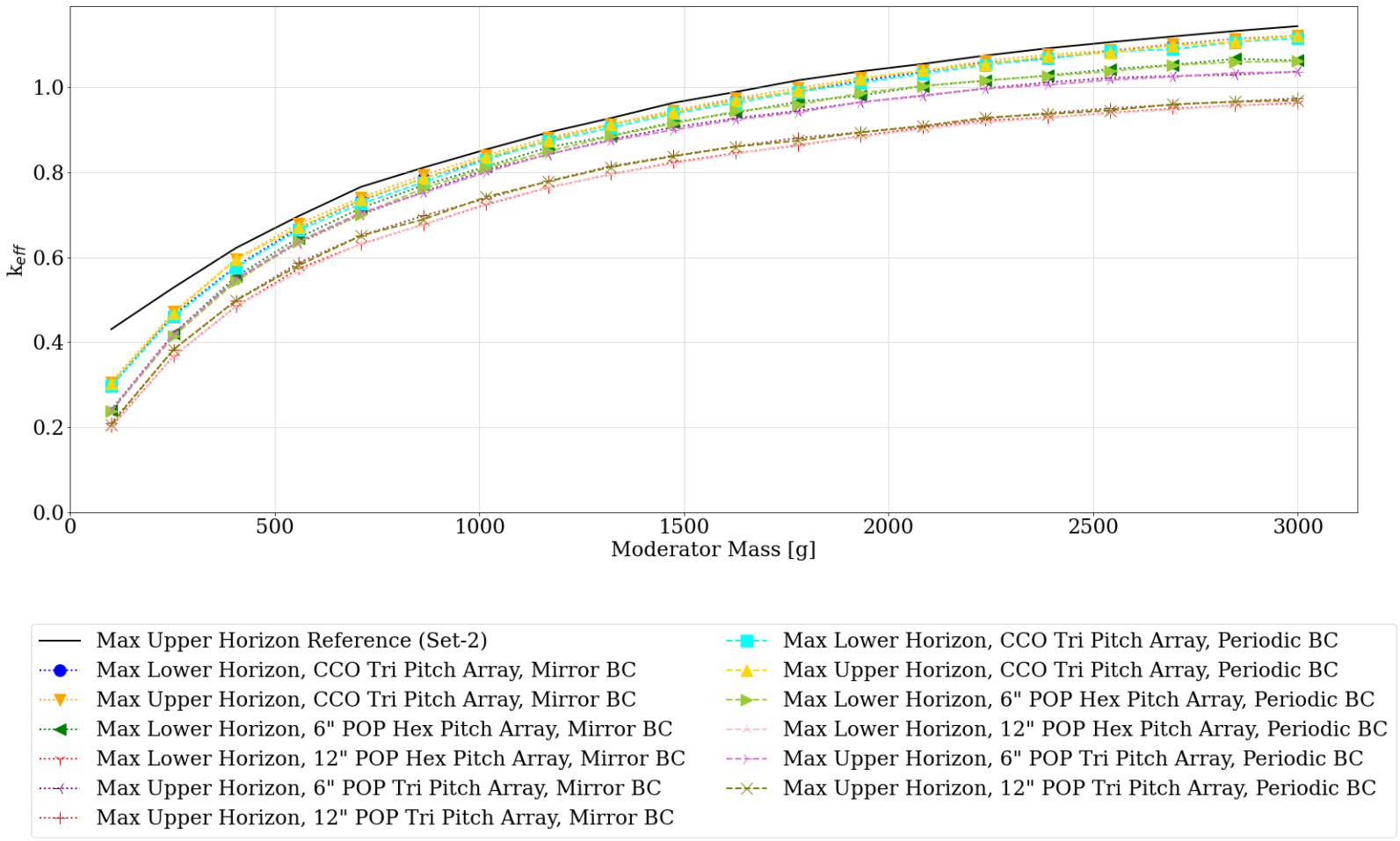

Figure M-29. Max k_{eff} of all subcase-6 of all CCO and POP centroid configurations at time = 1,000 years compared with max k_{eff} of all subsets of set-2-uh hexagonal pitch (mirror boundary conditions) as k_{eff} vs. moderator mass, time = 1,000 years.

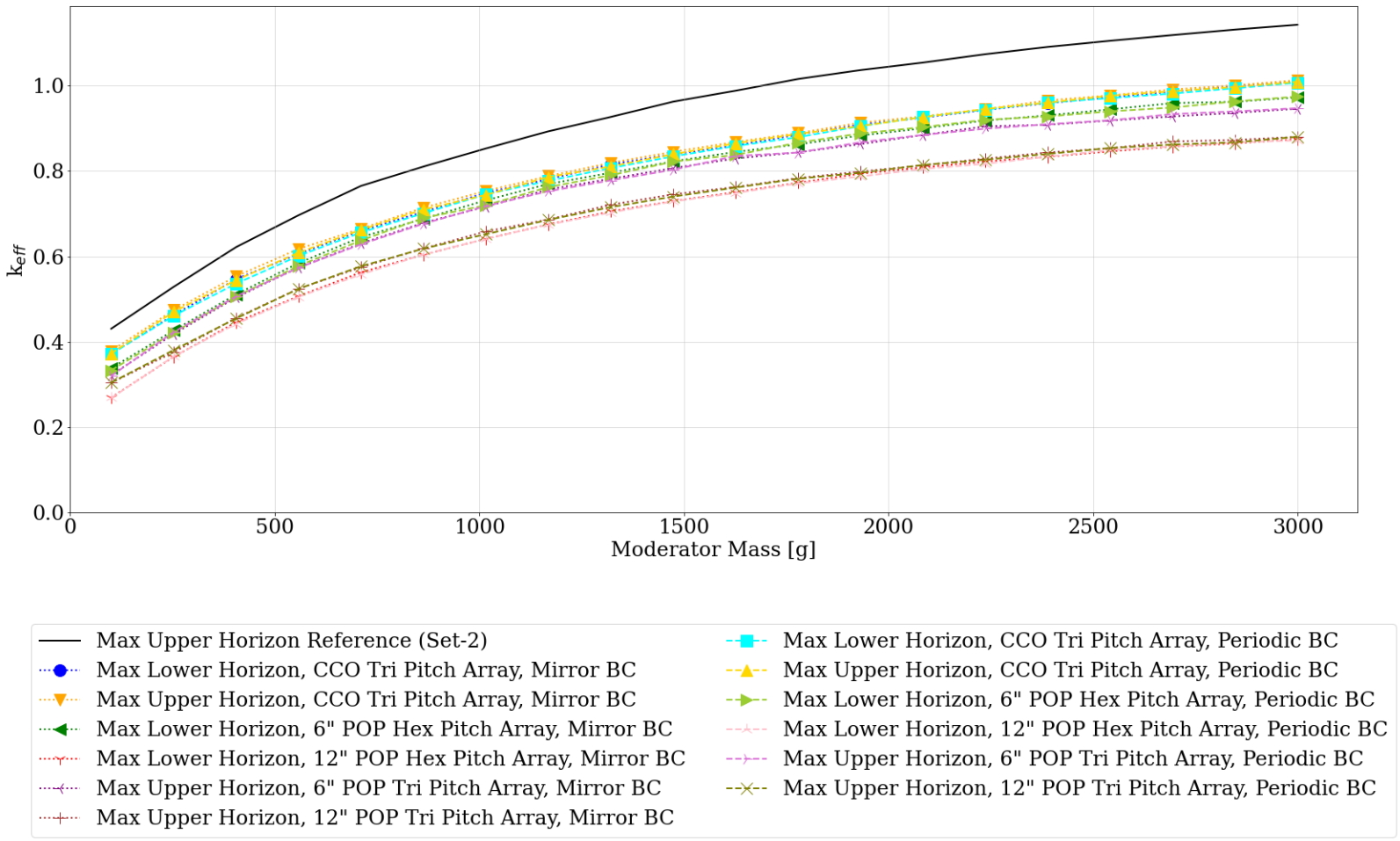

Figure M-30. Max k_{eff} of all subcase-7 of all CCO and POP centroid configurations at time = 1,000 years compared with max k_{eff} of all subsets of set-2-uh hexagonal pitch (mirror boundary conditions) as k_{eff} vs. moderator mass, time = 1,000 years.

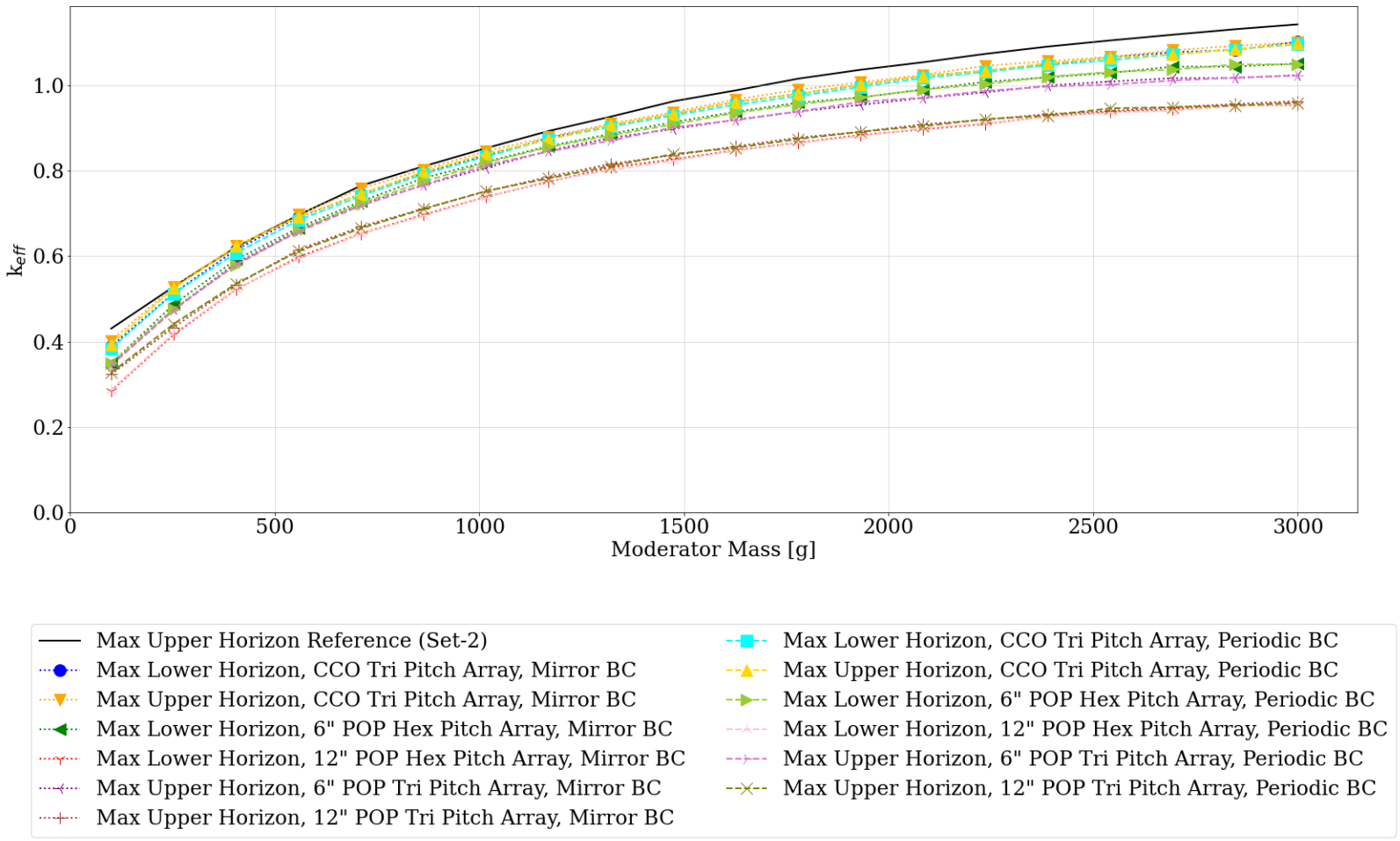

Figure M-31. Max k_{eff} of all subcase-8 of all CCO and POP centroid configurations at time = 1,000 years compared with max k_{eff} of all subsets of set-2-uh hexagonal pitch (mirror boundary conditions) as k_{eff} vs. moderator mass, time = 1,000 years.

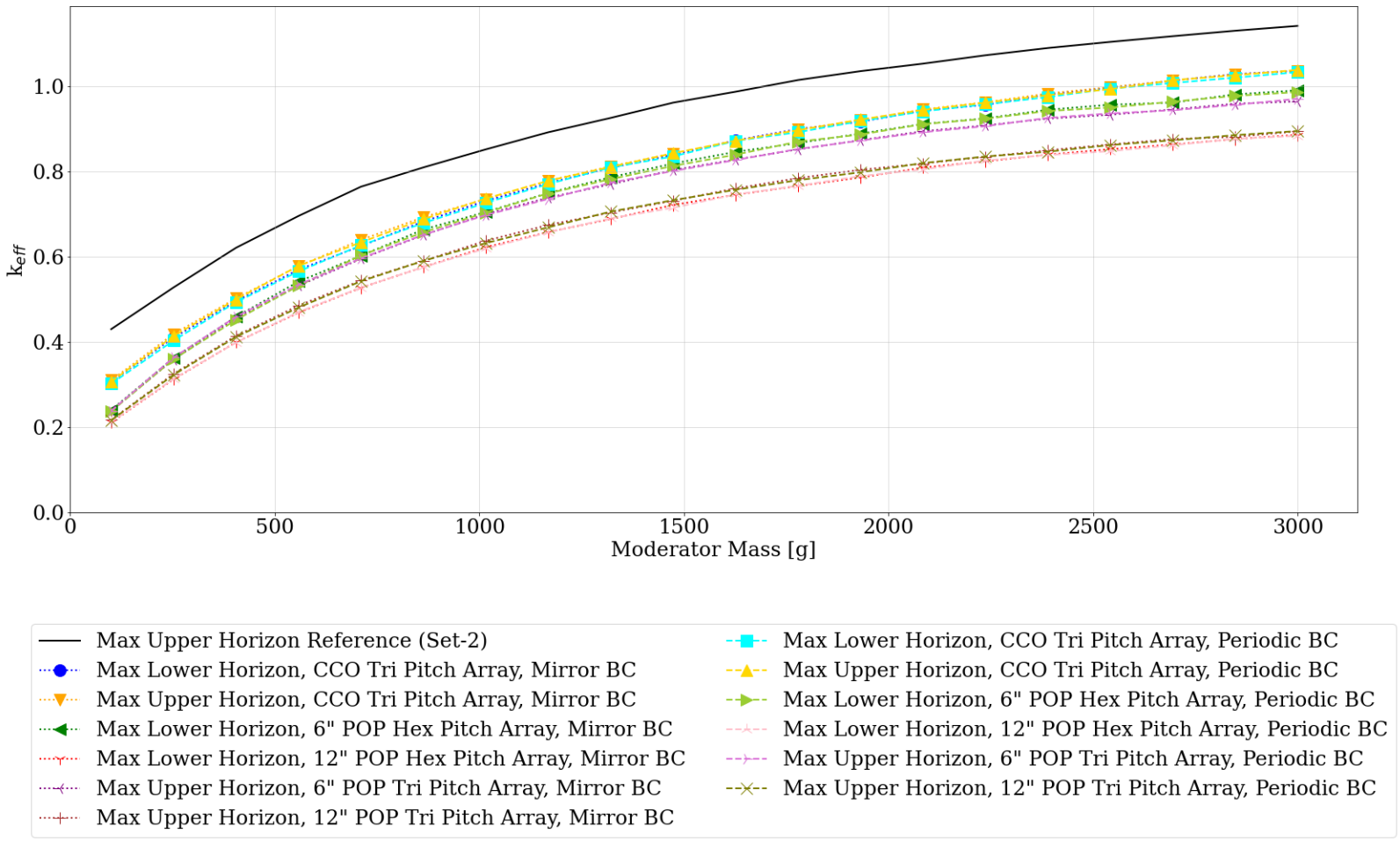

Figure M-32. Max k_{eff} of all subcase-9 of all CCO and POP centroid configurations at time = 1,000 years compared with max k_{eff} of all subsets of set-2-uh hexagonal pitch (mirror boundary conditions) as k_{eff} vs. moderator mass, time = 1,000 years.

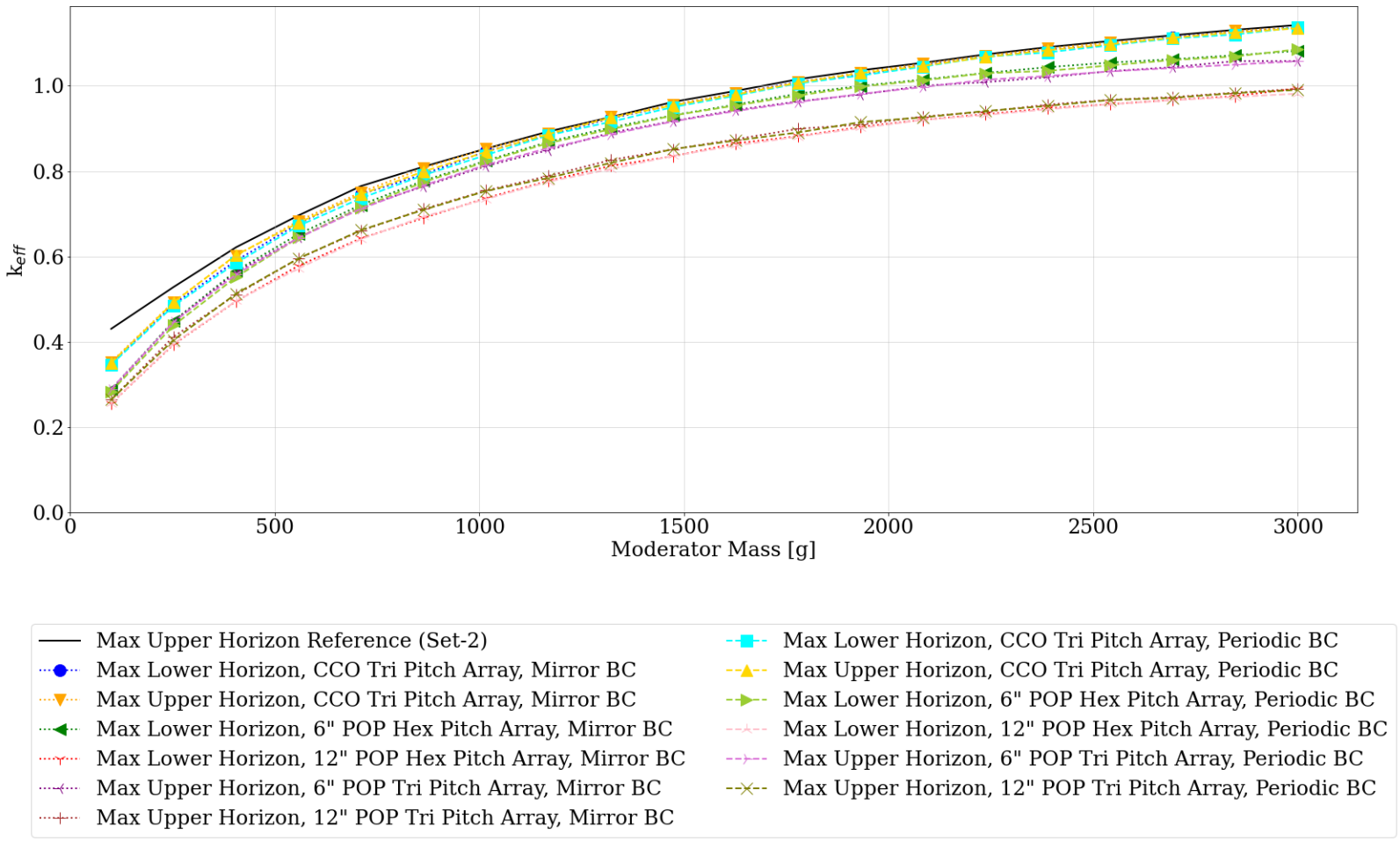

Figure M-33. Max k_{eff} of all subcase-10 of all CCO and POP centroid configurations at time = 1,000 years compared with max k_{eff} of all subsets of set-2-uh hexagonal pitch (mirror boundary conditions) as k_{eff} vs. moderator mass, time = 1,000 years.

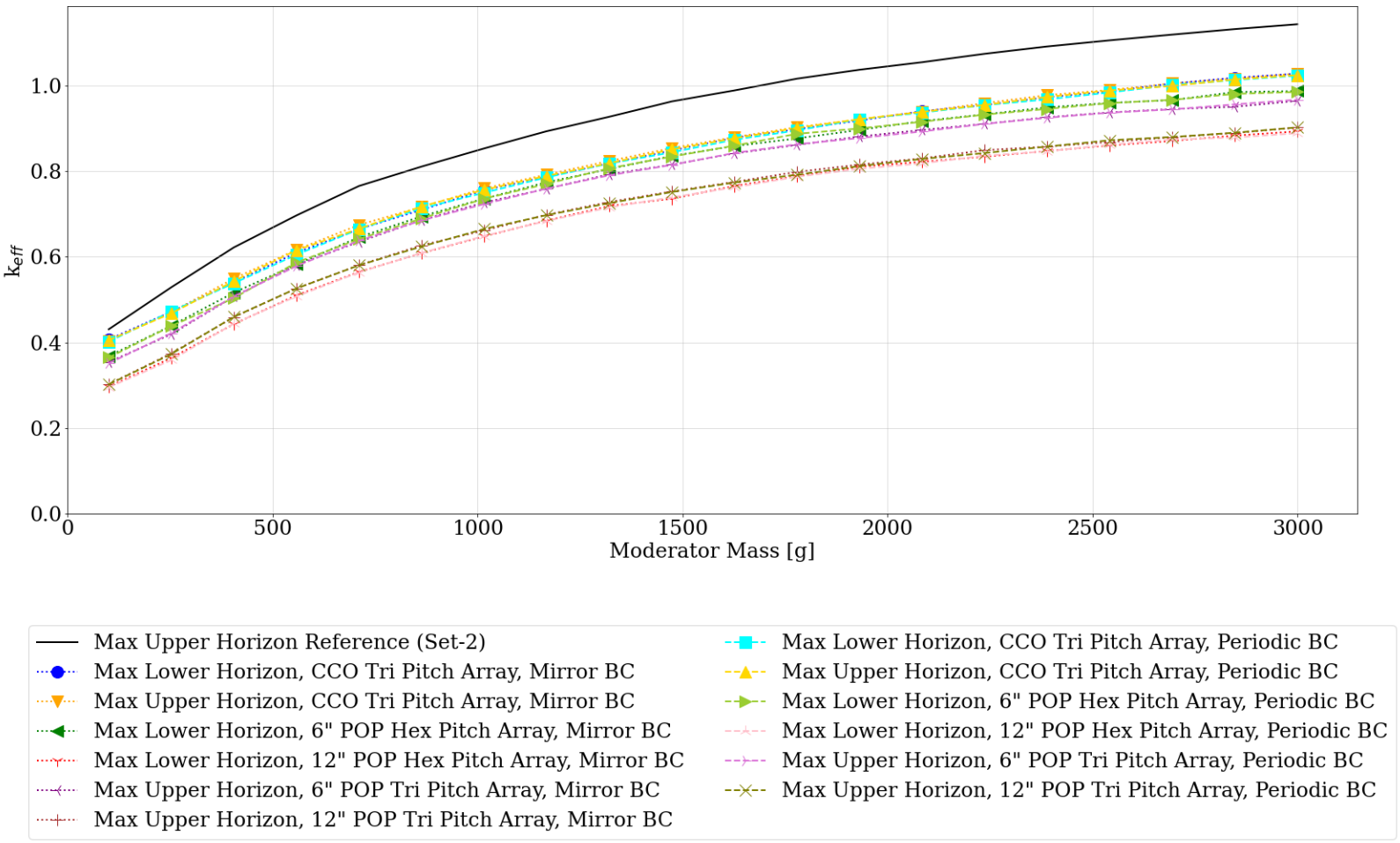

Figure M-34. Max k_{eff} of all subcase-11 of all CCO and POP centroid configurations at time = 1,000 years compared with max k_{eff} of all subsets of set-2-uh hexagonal pitch (mirror boundary conditions) as k_{eff} vs. moderator mass, time = 1,000 years.

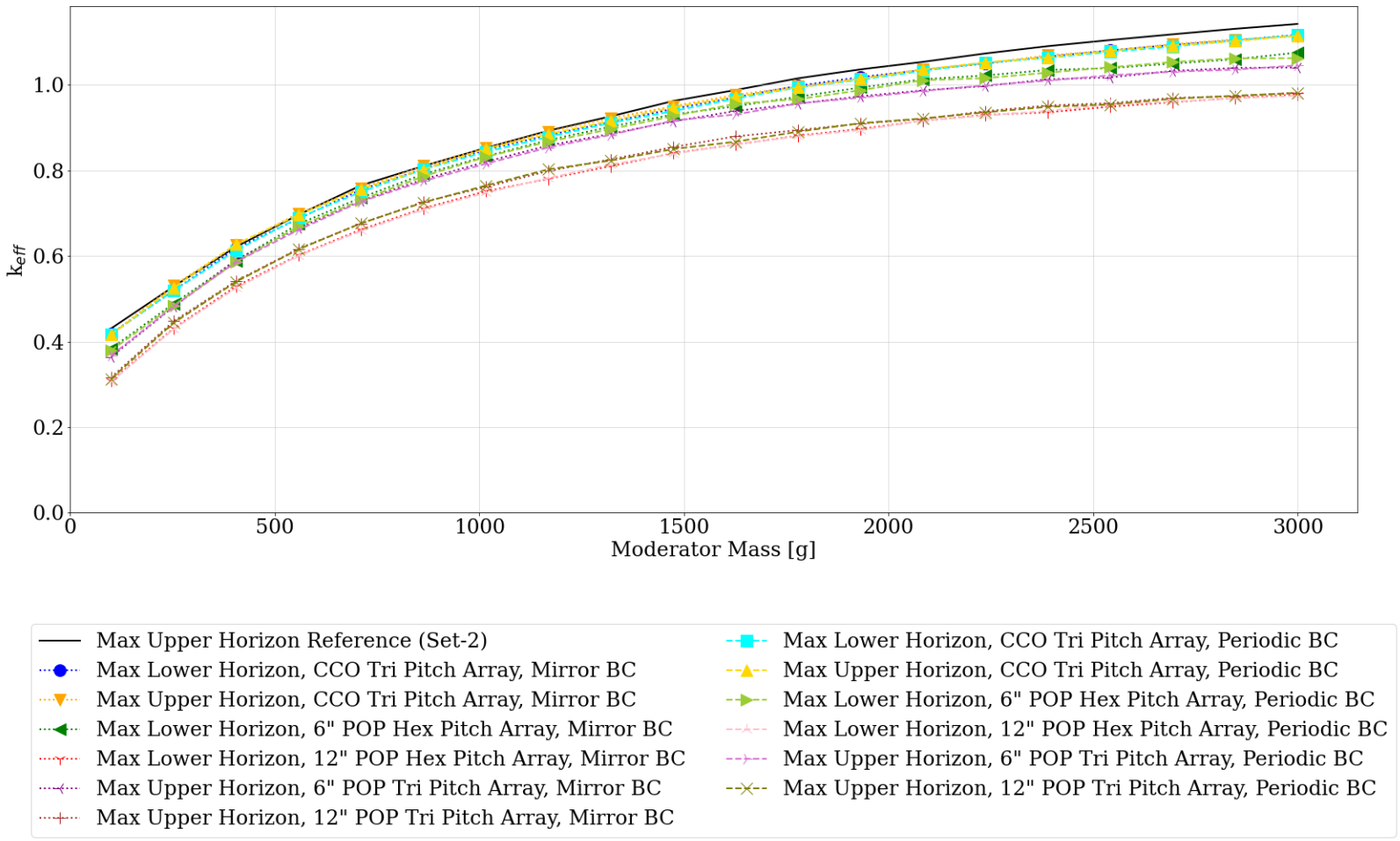

Figure M-35. Max k_{eff} of all subcase-12 of all CCO and POP centroid configurations at time = 1,000 years compared with max k_{eff} of all subsets of set-2-uh hexagonal pitch (mirror boundary conditions) as k_{eff} vs. moderator mass, time = 1,000 years.

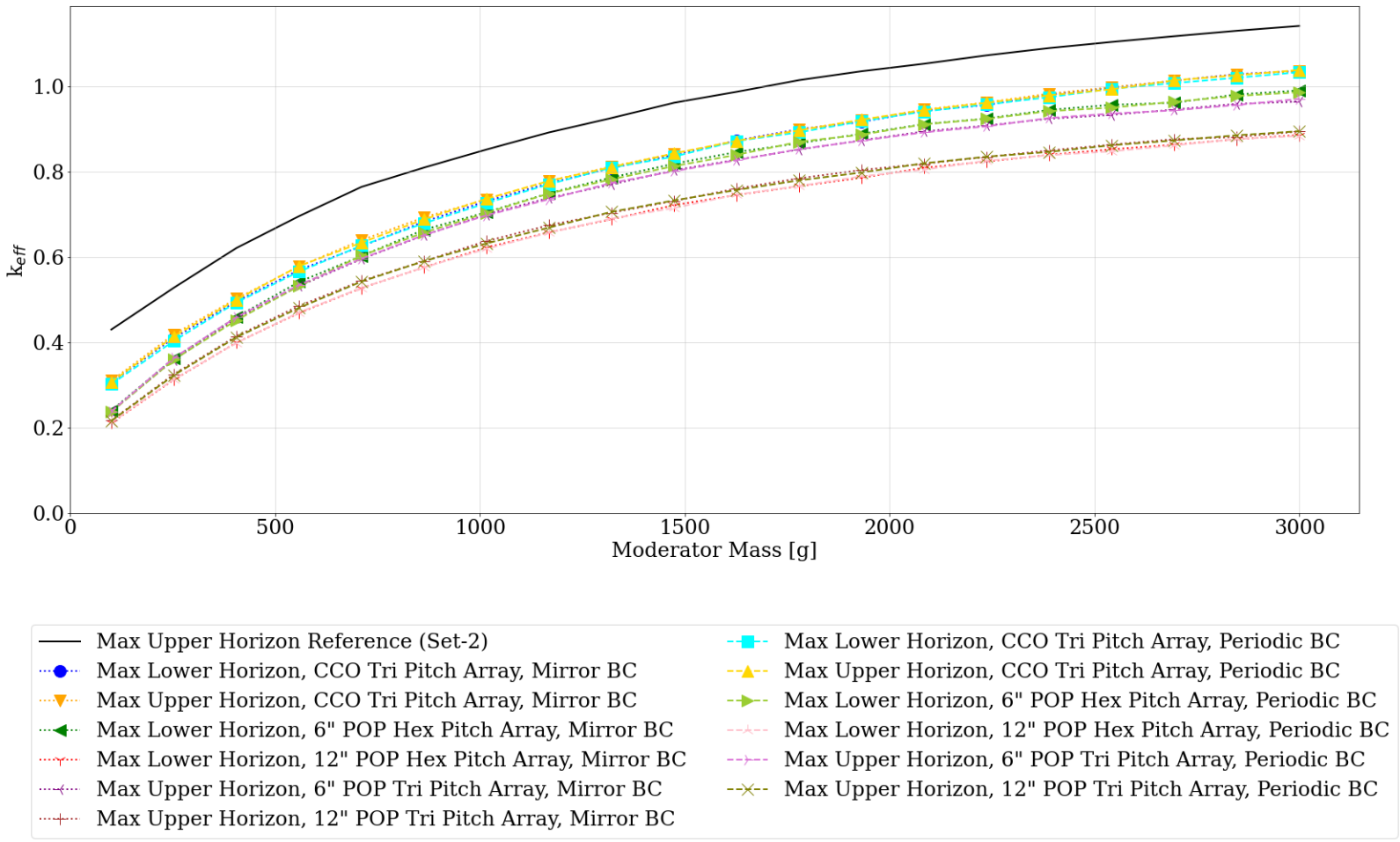

Figure M-36. Max k_{eff} of all subcase-13 of all CCO and POP centroid configurations at time = 1,000 years compared with max k_{eff} of all subsets of set-2-uh hexagonal pitch (mirror boundary conditions) as k_{eff} vs. moderator mass, time = 1,000 years.

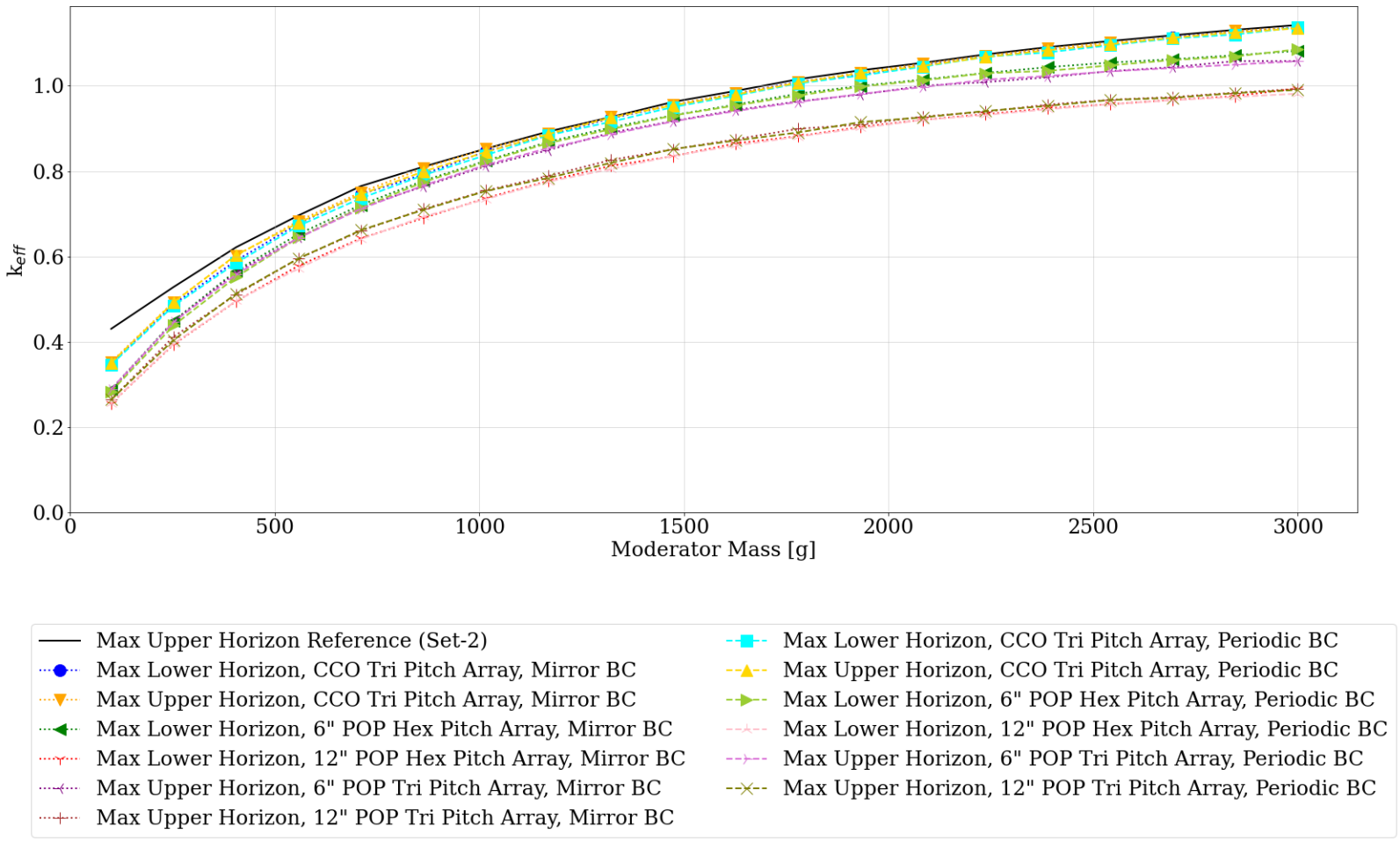

Figure M-37. Max k_{eff} of all subcase-14 of all CCO and POP centroid configurations at time = 1,000 years compared with max k_{eff} of all subsets of set-2-uh hexagonal pitch (mirror boundary conditions) as k_{eff} vs. moderator mass, time = 1,000 years.

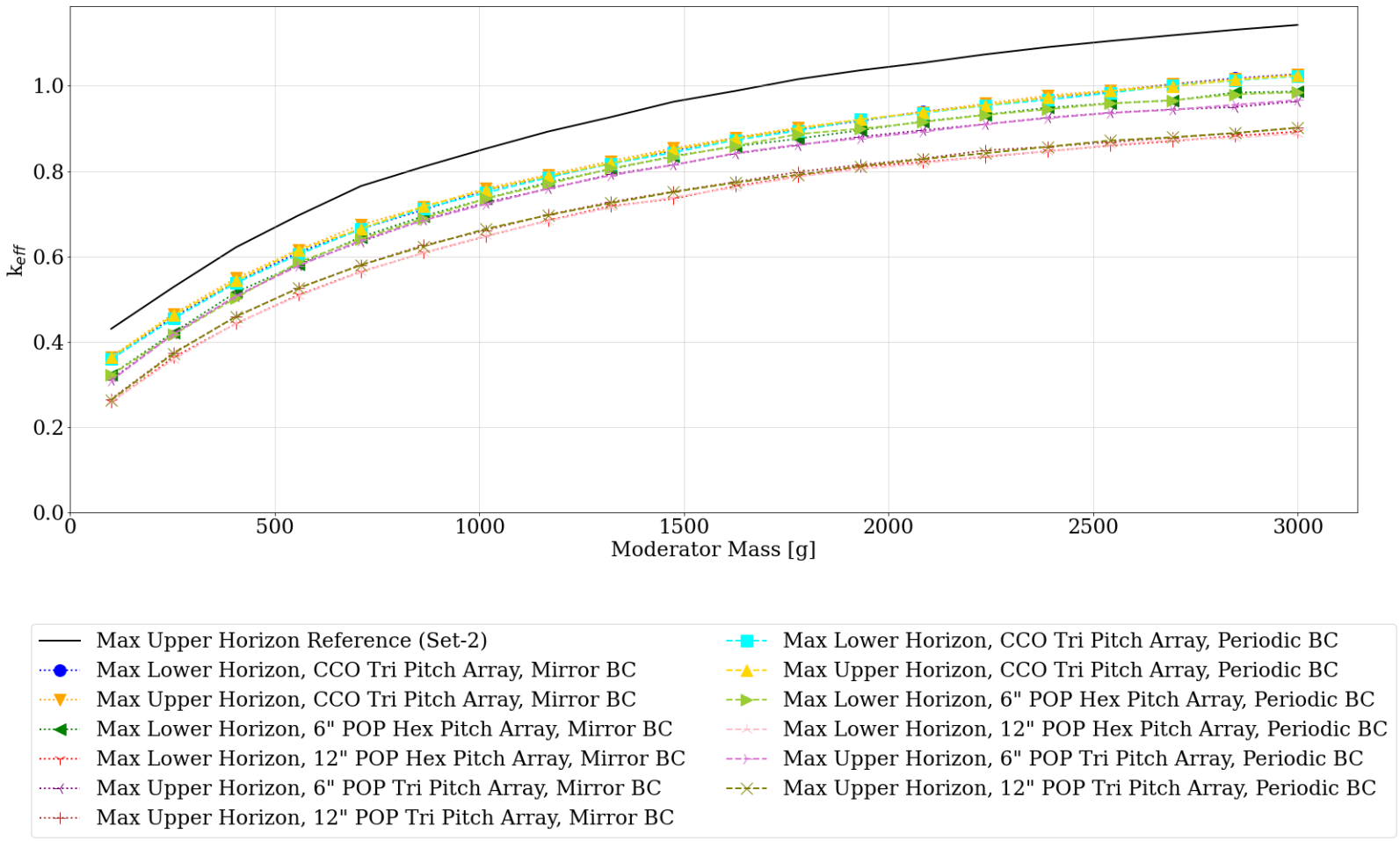

Figure M-38. Max k_{eff} of all subcase-15 of all CCO and POP centroid configurations at time = 1,000 years compared with max k_{eff} of all subsets of set-2-uh hexagonal pitch (mirror boundary conditions) as k_{eff} vs. moderator mass, time = 1,000 years.

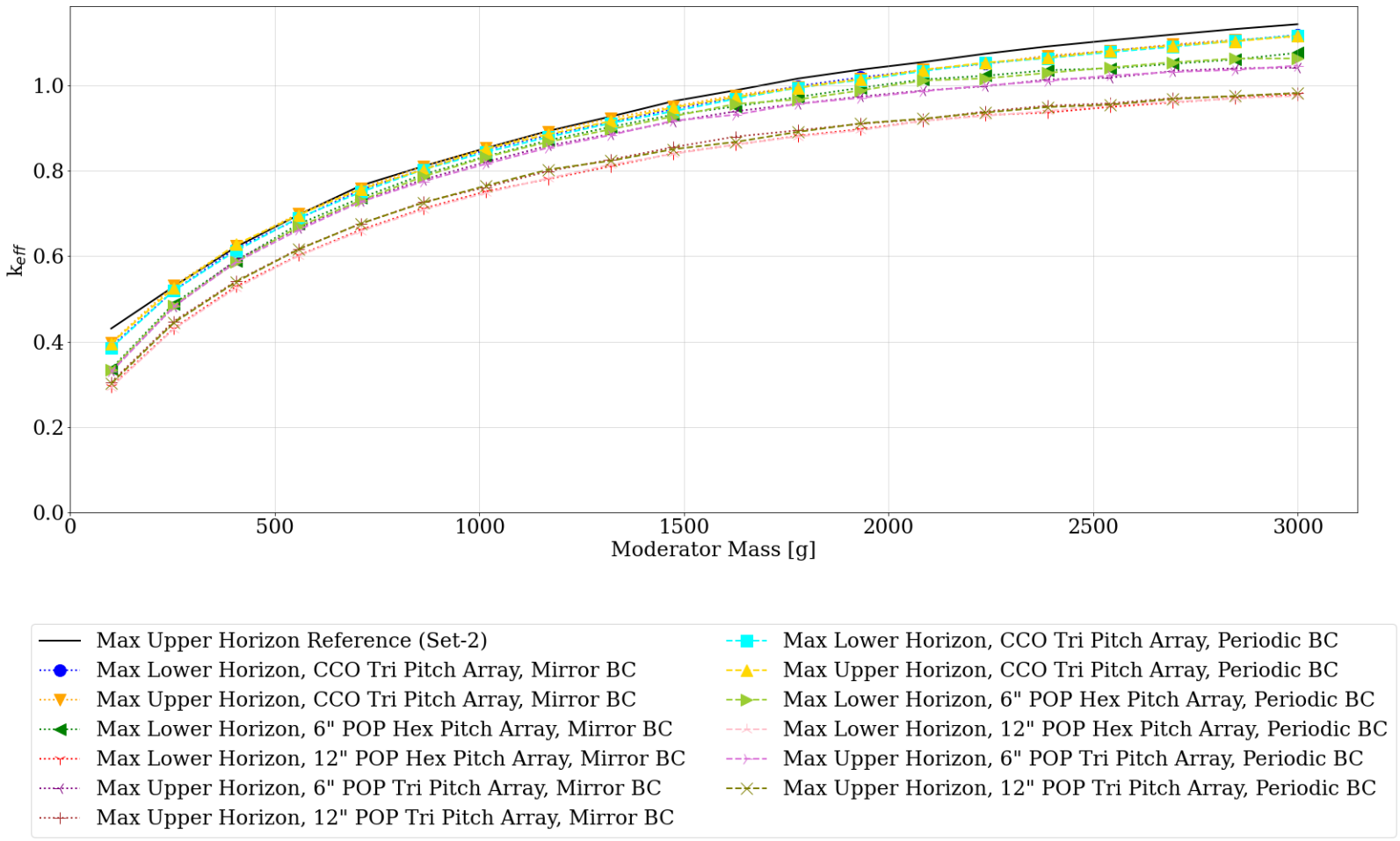

Figure M-39. Max k_{eff} of all subcase-16 of all CCO and POP centroid configurations at time = 1,000 years compared with max k_{eff} of all subsets of set-2-uh hexagonal pitch (mirror boundary conditions) as k_{eff} vs. moderator mass, time = 1,000 years.

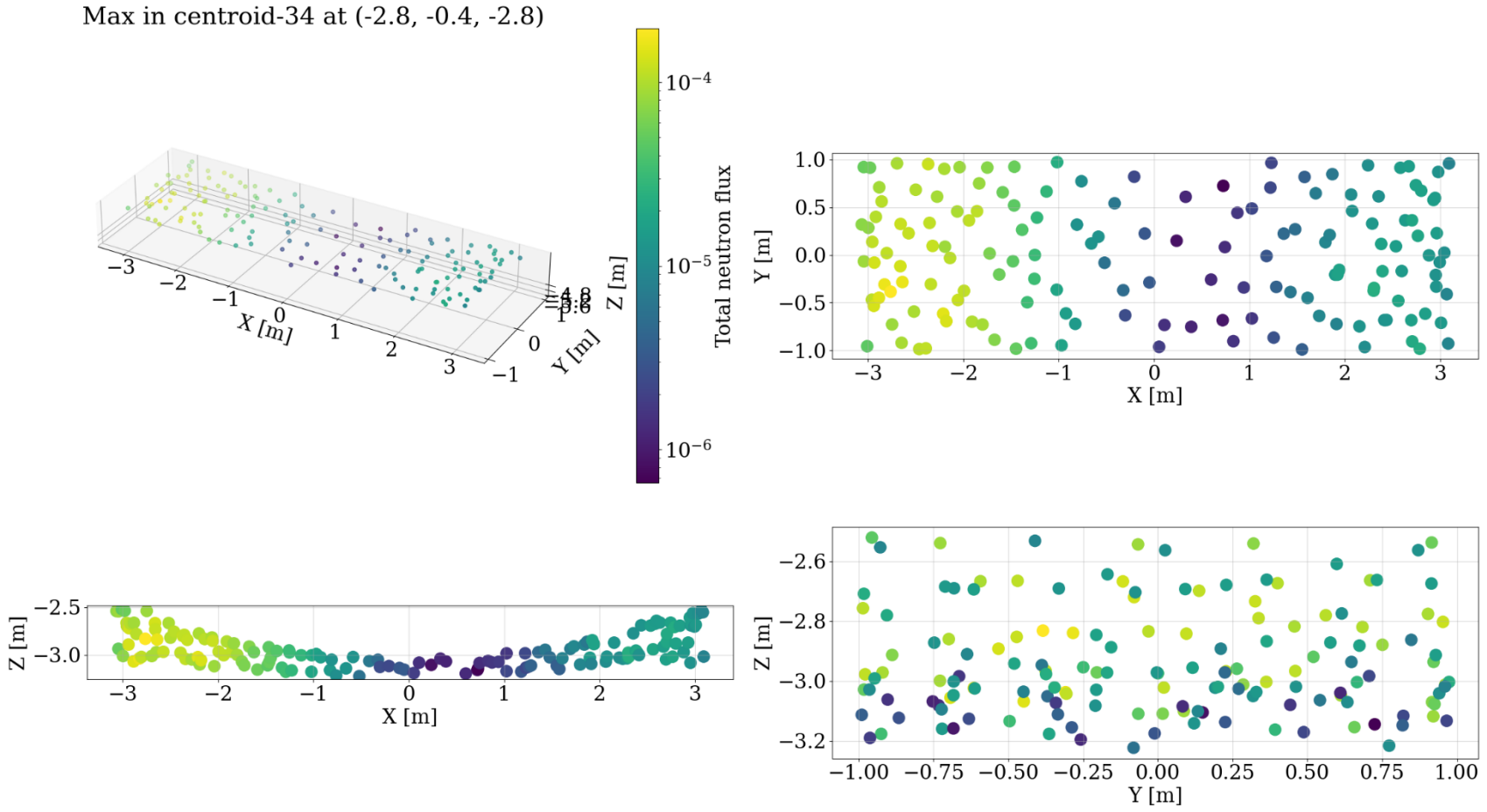

Figure M-40. Diagram of the neutron flux for subcase-10 in the CCO with no filler material and thin SS discrete reflector (sweep 470), upper horizon with hexagonal pitch (set-2-uh) with a maximum k_{eff} of 1.0134 and moderator mass of 2,084 g, comparable to Figure 29 in [46].

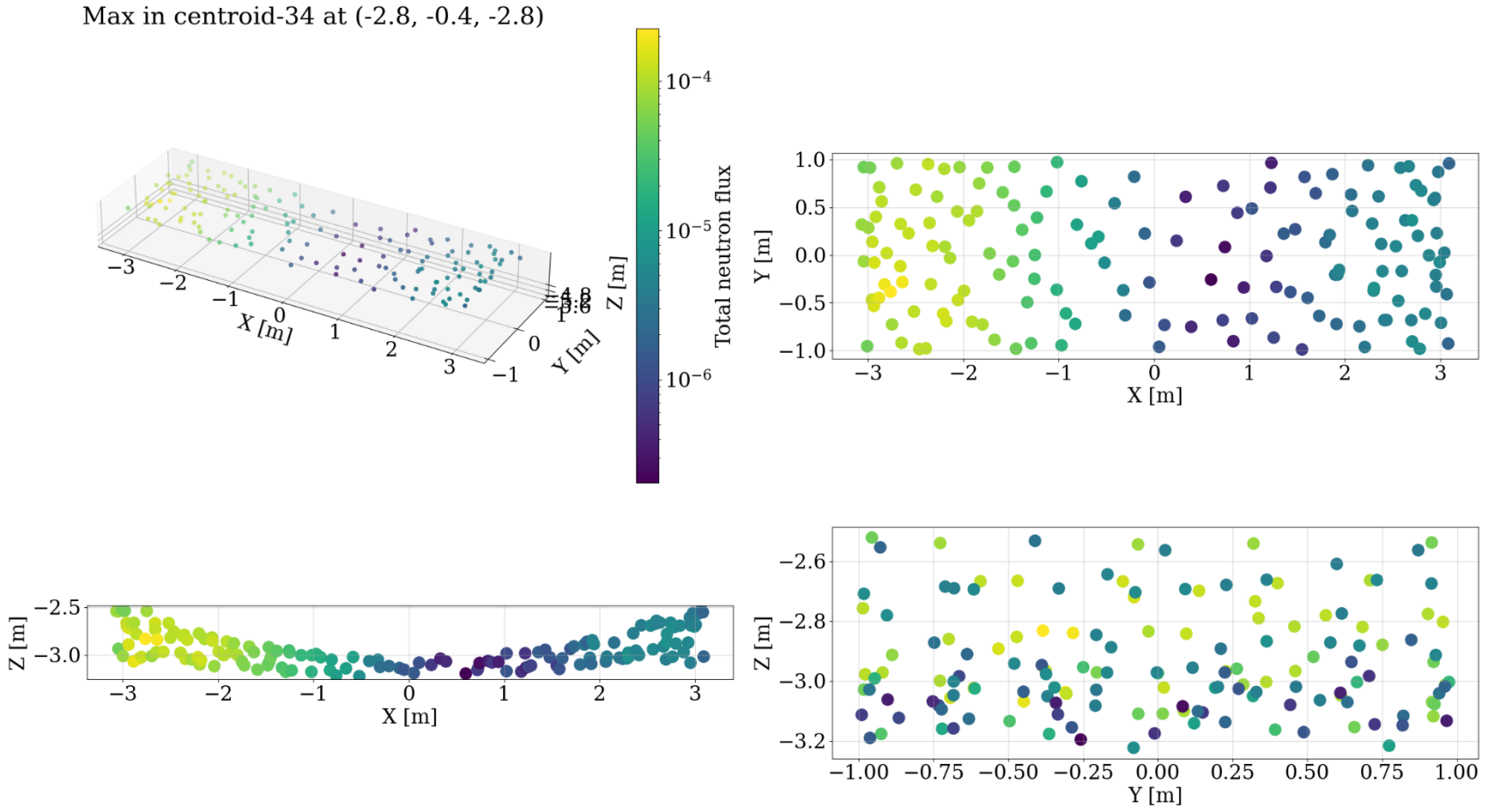

Figure M-41. Diagram of the neutron flux for subcase-10 in the CCO with 4 kg graphite filler material and thin SS discrete reflector (sweep 494), upper horizon with hexagonal pitch (set-2-uh) with a maximum k_{eff} of 0.9649 and moderator mass of 2,084 g, comparable to Figure 29 in [46].

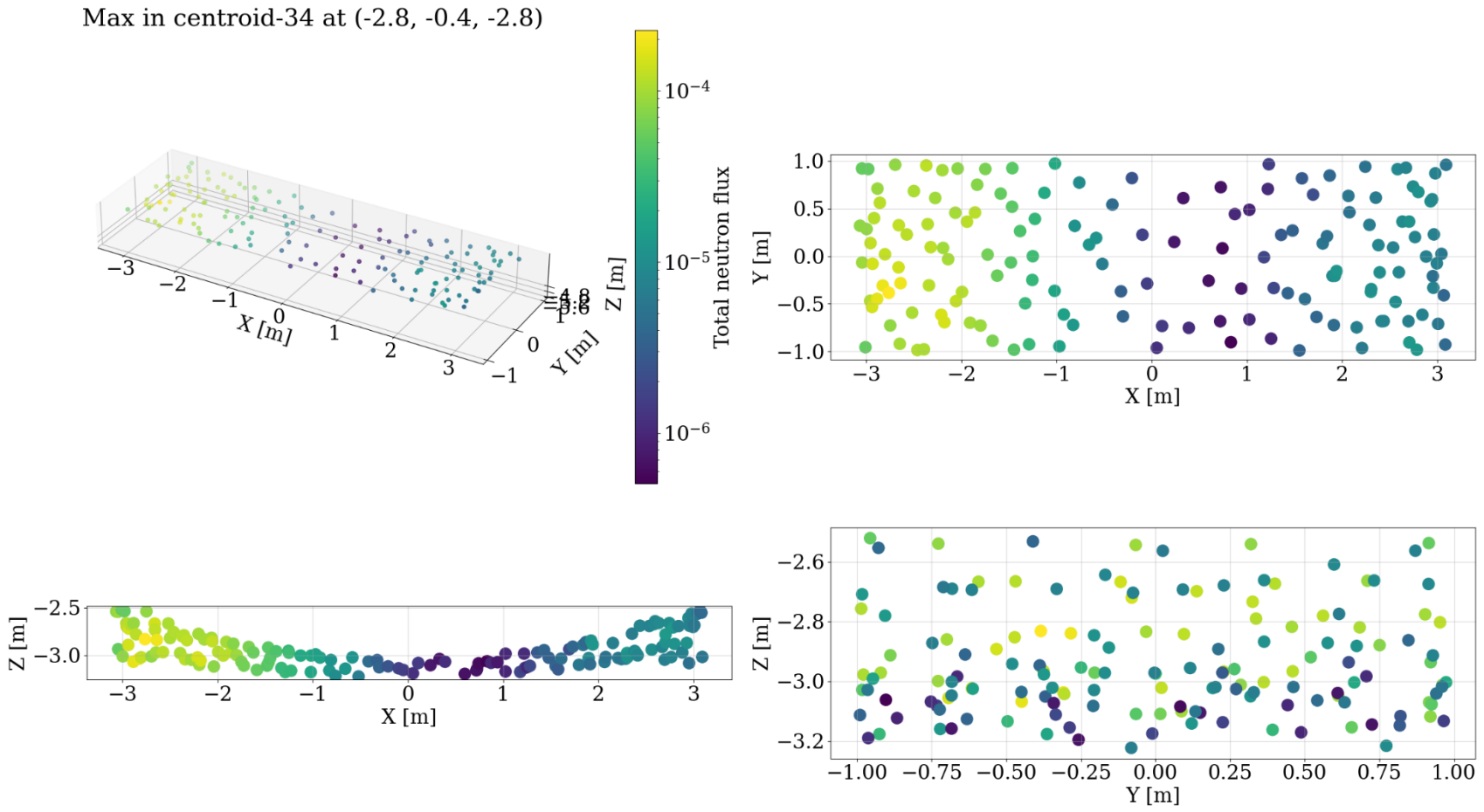

Figure M-42. Diagram of the neutron flux for subcase-10 in the CCO with no filler material and thick SS discrete reflector (sweep 472), upper horizon with hexagonal pitch (set-2-uh) with a maximum k_{eff} of 1.047 and moderator mass of 2,084 g, comparable to Figure 29 in [46].

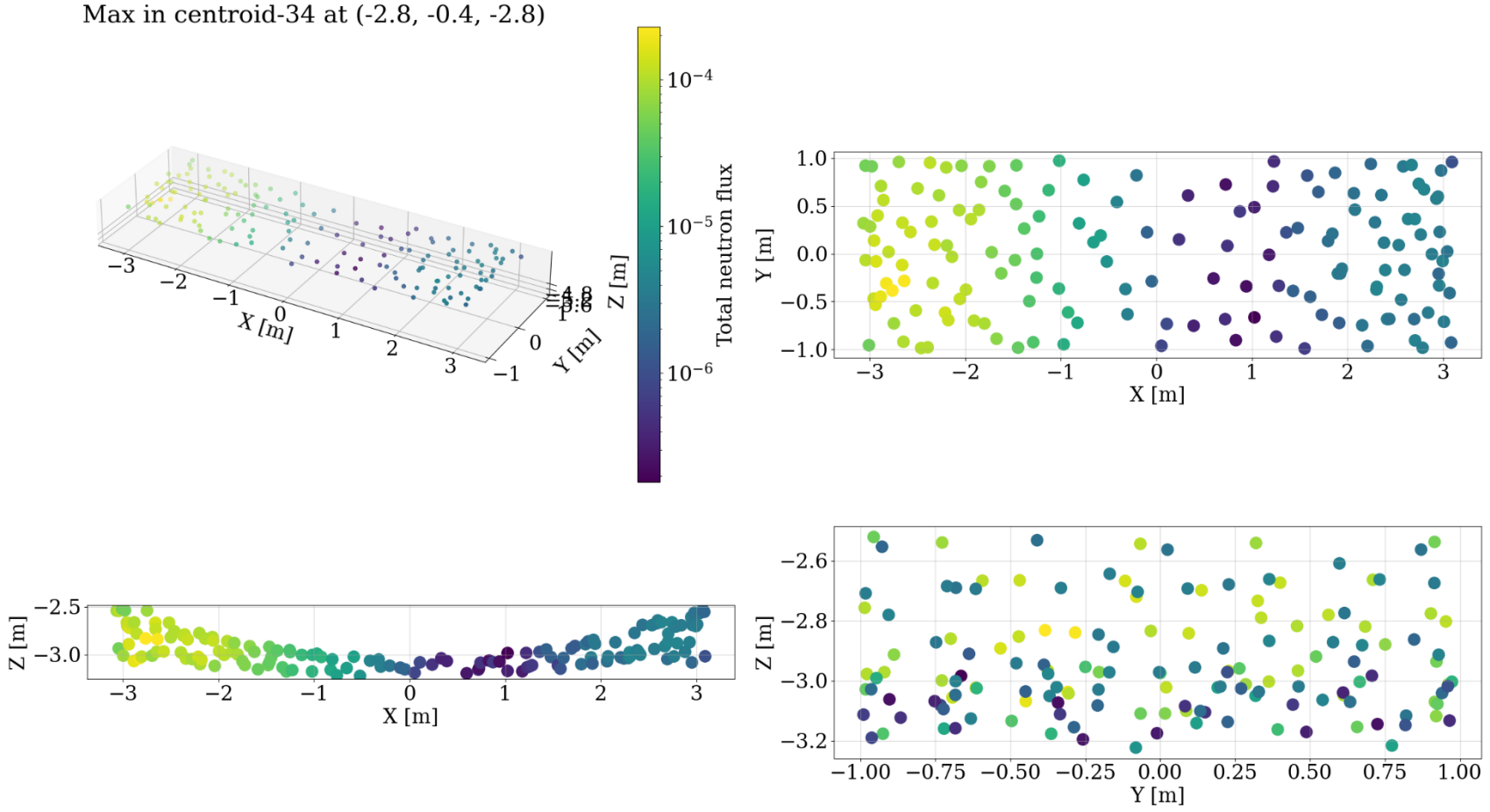

Figure M-43. Diagram of the neutron flux for subcase-10 in the CCO with 4 kg graphite filler material and thick SS discrete reflector (sweep 496), upper horizon with hexagonal pitch (set-2-uh) with a maximum k_{eff} of 1.047 and moderator mass of 2,084 g, comparable to Figure 29 in [46].

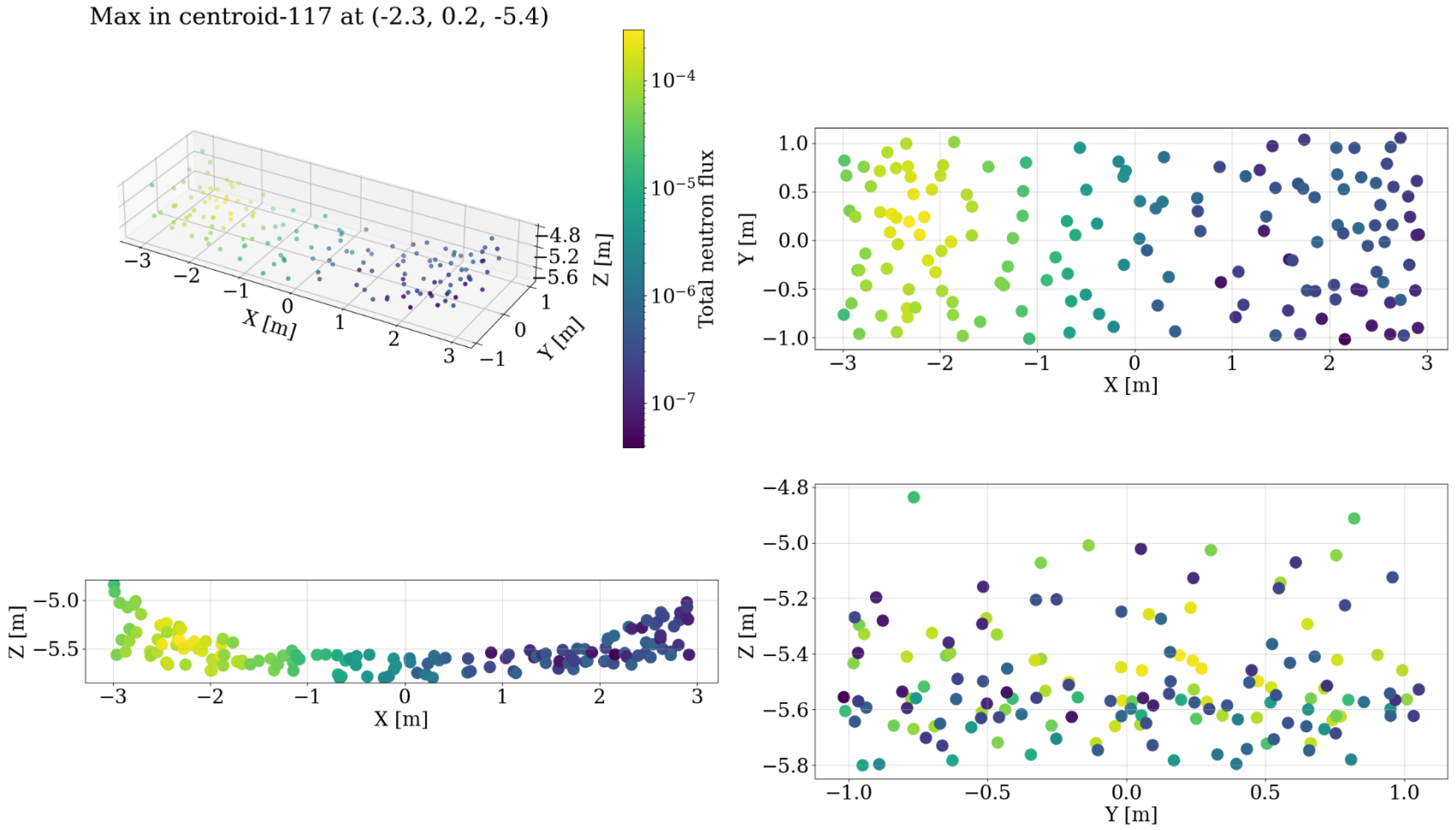

Figure M-44. Diagram of the neutron flux for subcase-10 in the CCO with no filler material and thin SS discrete reflector (sweep 470), lower horizon with hexagonal pitch (set-2-lh) with a maximum k_{eff} of 1.0428 and moderator mass of 2,084 g, comparable to Figure 27 in [46].

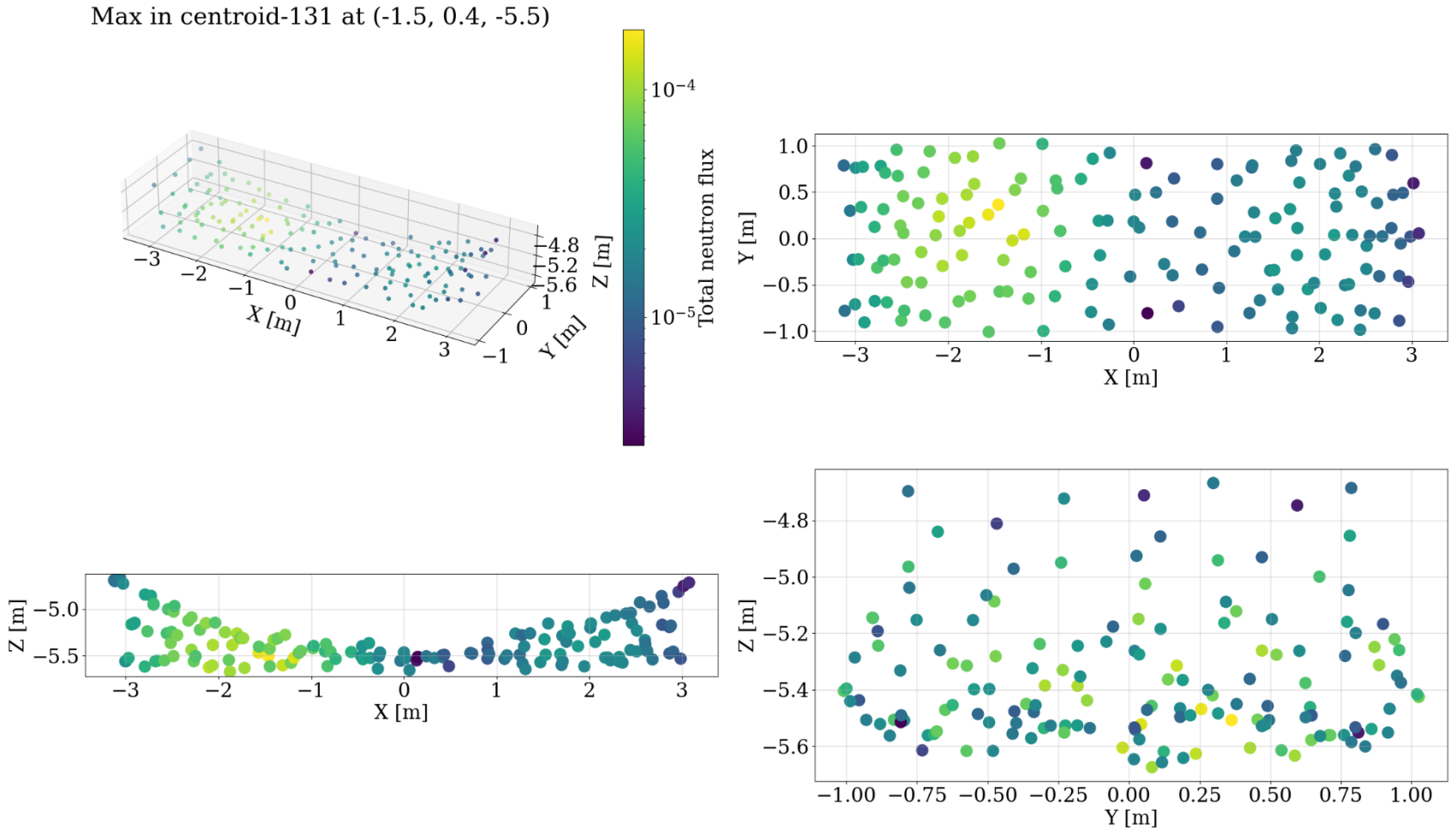

Figure M-45. Diagram of the neutron flux for subcase-10 in the 12 in. POP with no filler material and thick SS discrete reflector (sweep 688), lower horizon with hexagonal pitch with a maximum k_{eff} of 0.9816 and moderator mass of 3,000 g, comparable to Figure 37 in [46].

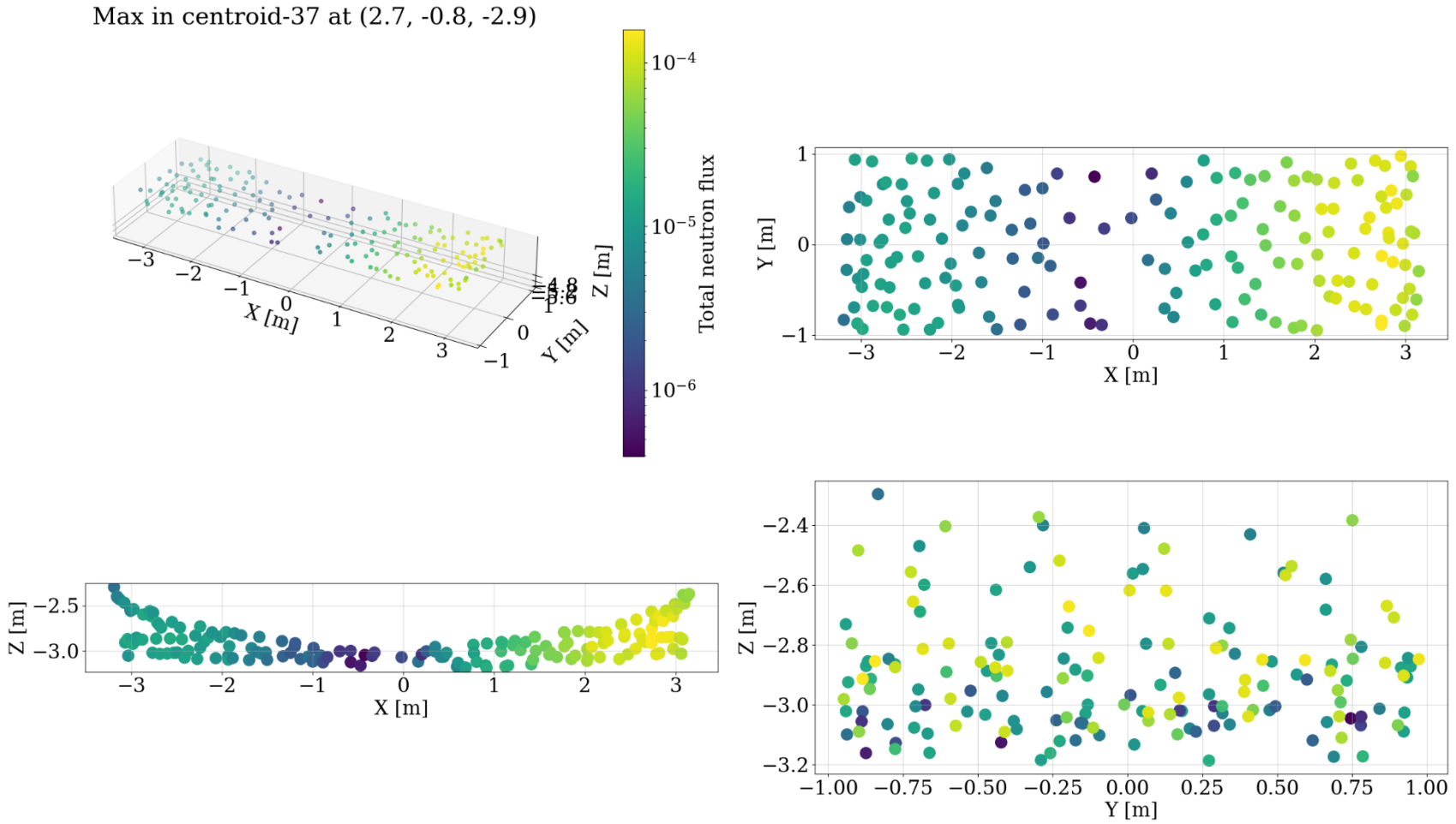

Figure M-46. Diagram of the neutron flux for subcase-10 in the CCO with no filler material and thin SS discrete reflector (sweep 470), lower horizon with triagonal pitch with a maximum k_{eff} of 1.0227 and moderator mass of 2,084 g, comparable to Figure 33 in [46].

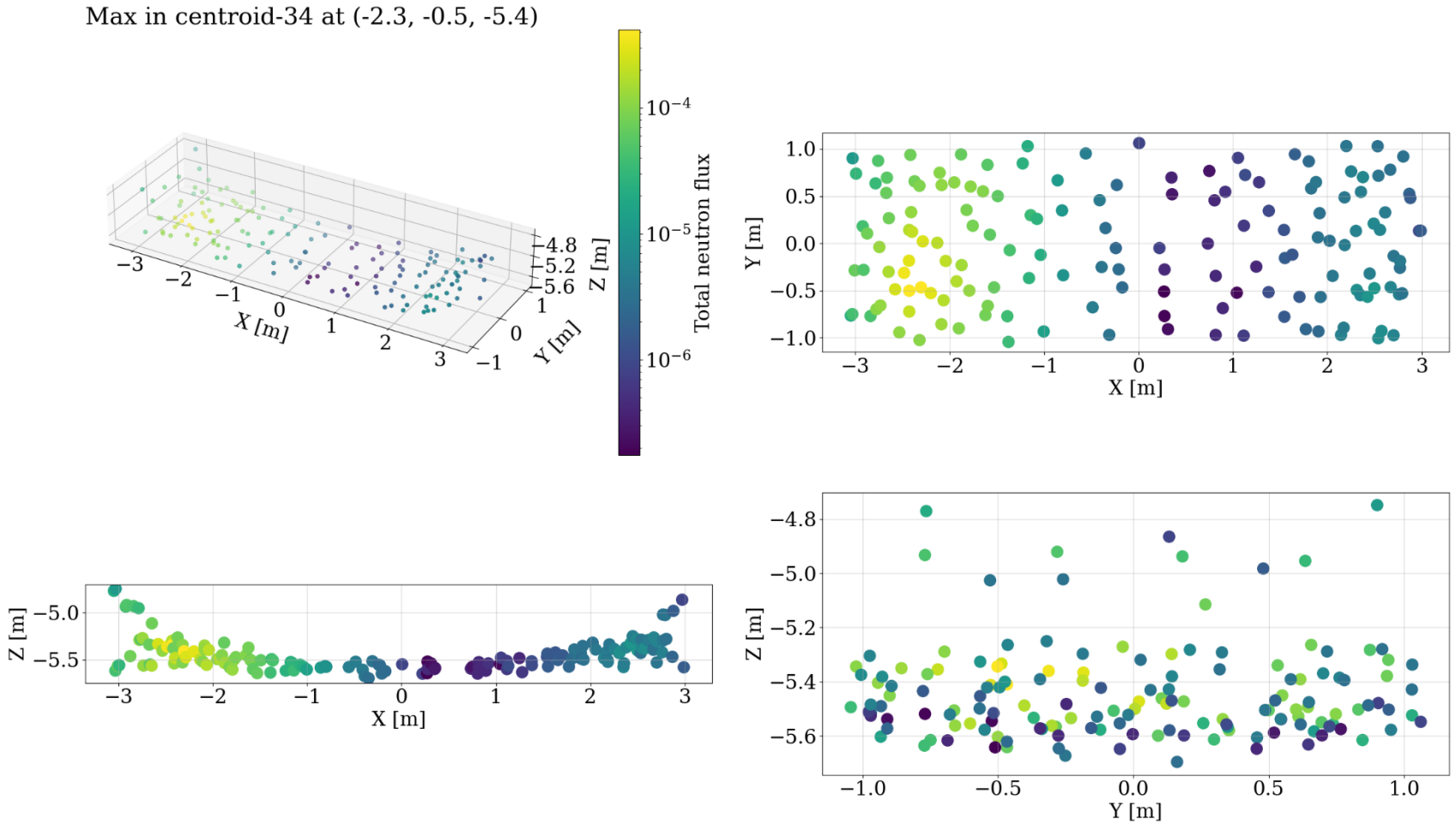

Figure M-47. Diagram of the neutron flux for subcase-10 in the 6 in. POP with no filler material and thin SS discrete reflector (sweep 470), lower horizon with hexagonal pitch with a maximum k_{eff} of 1.0227 and moderator mass of 2,084 g, comparable to Figure 35 in [46].

This page is intentionally blank

APPENDIX N. SET-7: RESULTS OF THE CALCULATIONS TO SHOW THE REACTIVITY EFFECT OF VARIOUS AMOUNTS OF B_4C UNIFORMLY MIXED IN THE WASTE FORM

This page intentionally blank.

APPENDIX N. SET-7: RESULTS OF THE CALCULATIONS TO SHOW THE REACTIVITY EFFECT OF VARIOUS AMOUNTS OF B_4C UNIFORMLY MIXED IN THE WASTE FORM.

This appendix serves as a repository of the results for additional B_4C calculations to provide technical support for the use of B_4C as a control.

The analysis models used in this appendix for set-7a are the same as the set-1 models discussed in detail in Appendix A, the analysis models used for set-7b are the same as the set-3 models discussed in detail in Appendix F, and the analysis models used for set-7c are the same as the set-2-uh models discussed in detail in Appendix C. The model changes to the calculations provided in this appendix compared with Appendices A, F, and C are related to changes made to include the addition of various amounts of B_4C uniformly mixed in the waste form and to increase the total amount of moderator mass in the waste form up to 6 kg (subcase-10 only) (Tables N-1, N-2, and N-3).

The purpose of this appendix is to (1) expand the studies from the other appendices to the full set of subcases with B_4C uniformly mixed in the waste form because only a small set of subcases was previously evaluated, (2) show the reactivity trend for additional lower masses of B_4C because only 50 g were previously evaluated, and (3) provide sufficient detail to support technical justification for a potential $B_4C < 50$ g control by specifically using subcase-10 parametric sweeps only (Tables N-1, N-2, and N-3).

The cases in this appendix are summarized in Tables N-1, N-2, and N-3 for set-7a, set-7b, and set-7c, respectively.

The results for the first two stated purposes—showing the complete dataset (i.e., all parametric sweeps) reactivity trends as a delta k_{eff} to their reference case (set-1 for set-7a, set-3 for set-7b, and set-2-uh for set-7c) as a function of waste form moderator mass when including 10, 30, or 50 g of B_4C—are provided in Figures N-1, N-2, and N-3 for set-7a, set-7b, and set-7c, respectively. The results shown for the reactivity trends associated with all subsets of parametric sweeps show similar reactivity trends, as expected, because of how the ^{10}B neutron absorption affects the system. Additionally, the same set of results is plotted as k_{eff} as a function of waste form moderator mass, as provided in Figures N-4, N-5, and N-6 for set-7a, set-7b, and set-7c, respectively, and as k_{eff} as a function of B_4C mass, as provided in Figures N-7, N-8, and N-9. As expected, the results show that the reactivity effect of the ^{10}B decreases with decreasing mass. Depending on the model, the system can remain subcritical with only the addition of uniformly mixed B_4C within the waste. The summary of these results is provided in Table N-4.

However, because of the current lack of moderator mass limits on the CCO transportation requirements (2 kg plastic limit, no water limit), additional studies are required to provide more robust technical justification for a single minimum B_4C mass limit (significantly less than 50 g) with no restriction on moderator mass. This appendix presents a study to provide this additional technical justification.

The results for the third aforementioned purpose—showing the subcase-10 parametric sweeps with additional B_4C masses and additional moderator masses to show the peak reactivity mass conclusively—are shown as k_{eff} as a function of moderator mass in Figures N-10, N-11, and N-12 for set-7a, set-7b, and set-7c, respectively, and as k_{eff} as a function of B_4C mass in Figures N-13, N-14, and N-15 for set-7a, set-7b, and set-7c, respectively. The results show that although k_{eff} continues to increase with additional moderator, this trend tapers with increasing B_4C mass. Reviewing additional quantities of B_4C within the waste material (i.e., 15, 20, and 25 g B_4C) also demonstrates that even though adding B_4C is not a linear trend, a linear trend would be conservative. Based on these results for all of set-7 (i.e., all model designs, all subcases), 30 g of B_4C are considered sufficient as a control with no additional controls (i.e., no moderator mass control).

Additionally, for any waste form limit that is based at least partly on some mass of B_4C uniformly mixed in the waste form, it is important to establish that it is possible (albeit very unlikely) for the ^{10}B to be depleted because of neutron absorption over the lifetime of the repository. The following discussion provides the technical justification related to the possibility of ^{10}B depletion.

Discussion

Criticality can be prevented by adding isotopes that have a large neutron absorption cross section. The absorption of neutrons via neutron capture by the ^{10}B isotope component of B_4C is an example material used as a parasitic neutron absorber. This discussion assumes that the waste stream mixture uses naturally occurring B with the relative abundance of ^{10}B of ~19 atom %. Neutrons are not a significant source of naturally occurring radiation and primarily occur from the interaction of cosmic rays and solar particle events with the atmosphere. Because the system is in a deep repository, there is no neutron source other than nuclear reactions within the waste. In this system, the neutron production within the waste can occur from either the spontaneous fission of the fissile material or the α-Be reactions in which the alpha particles are emitted from the natural decay of Pu (the assumption is that all fissile material are Pu). Essentially, fissile material will always decay via α-decay, so spontaneous fission is not a credible neutron source. Therefore, the discussion focuses on the secondary reaction of α-Be reactions.

The quantity of alpha-emitting isotopes is evaluated to show the number of alpha decays needed to deplete all B in the package, assuming that all neutrons are absorbed by B. The assumption that all neutrons emitted via α-Be reactions is grossly conservative because the probability of an alpha produced from decay interacting with Be is low, and most neutrons produced from this reaction will leak from the waste form.

In this discussion, the PuBe source was engineered to maximize neutron production efficiency from Pu. The PuBe source produces only 2×10^6 neutrons/s per curie of ^{238}Pu [44]. Because all Pu isotopes also produce alphas with similar energies between 5 and 6 MeV [45], this number is likely sufficient for all Pu isotopes. However, for conservatism, an alpha-to-neutron conversion efficiency of 10^7 neutrons/s per Curie is assumed. This is five times worse than the PuBe system engineered for neutron production. Applying the definition of a Curie as 3.7×10^{10} decays per second per Curie, the conversion efficiency of Be in a PuBe source is 2.7×10^{-4} neutrons per alpha. Assuming that every neutron produced is absorbed by ^{10}B, 3,700 times more Pu nuclei would be needed than ^{10}B nuclei to deplete all the ^{10}B. Because of Pu's large mass, the Pu mass must be roughly 88,000 times larger than the ^{10}B mass. Given that each package has at most 380 g of Pu, 0.0043 g of ^{10}B would be depleted if all the Pu decays over all time interact ideally with Be to produce neutrons, all of which are then absorbed by ^{10}B.

For perspective, 10 g of B_4C contains 7.8 g of B, 19.65% (1.53 g) of which is ^{10}B, and only 0.28% of this would be depleted by neutrons from (α,n) interactions under the grossly conservative assumptions used in this discussion. Therefore, the likelihood of ^{10}B being depleted beyond what is needed to perform the function as evaluated is considered unrealistic.

LIST OF FIGURES

LIST OF TABLES

Table N-1. Summary of cases for set-7a for the three-high uniform array model.

Case	Model type	Waste form shape	Waste form moderator	Filler material (0, 2,000, 4,000 g)	Metal in filler	Discrete reflector (thin 0.001 cm and thick 0.7112 cm)	Be (g)	B_4C (g)	Subcase
Set-7a	Models from set-1	Cylinder (radius range 4.8, 6, and 7.7, and height defined by total volume of mass)	Water	c12	SS from can (0, 500, 1,000 g)	Steel	0–585	10, 30, 50	set-7a-1
			Poly	c12		Steel			set-7a-2
			Water	c12		Poly			set-7a-3
			Poly	c12		Poly			set-7a -4
			Water	Generic		Steel			set-7a -5
			Poly	Generic		Steel			set-7a -6
			Water	Generic		Poly			set-7a -7
			Poly	Generic		Poly			set-7a -8
		Sphere (radius defined by total volume of mass)	Water	c12		Steel			set-7a -9
			Poly	c12		Steel			set-7a -10
			Water	c12		Poly			set-7a -11
			Poly	c12		Poly			set-7a -12
			Water	Generic		Steel			set-7a -13
			Poly	Generic		Steel			set-7a -14
			Water	Generic		Poly			set-7a -15
			Poly	Generic		Poly			set-7a -16

Table N-2. Summary of cases for set-7b for the six-high uniform array model.

Case	Model type	Waste form shape	Waste form moderator	Filler material (0, 2,000, 4,000 g)	Metal in filler	Discrete reflector (thin 0.001 cm and thick 0.7112 cm)	Be (g)	B_4C (g)	Subcase
Set-7b	Models from set-3	Cylinder (radius range 4.8, 6, and 7.7, and height defined by total volume of mass)	Water	c12	SS from can (0, 500, 1,000 g)	Steel	0–585	10, 30, 50	set-7b-1
			Poly	c12		Steel			set-7b-2
			Water	c12		Poly			set-7b-3
			Poly	c12		Poly			set-7b -4
			Water	Generic		Steel			set-7b -5
			Poly	Generic		Steel			set-7b -6
			Water	Generic		Poly			set-7b -7
			Poly	Generic		Poly			set-7b -8
		Sphere (radius defined by total volume of mass)	Water	c12		Steel			set-7b -9
			Poly	c12		Steel			set-7b -10
			Water	c12		Poly			set-7b -11
			Poly	c12		Poly			set-7b -12
			Water	Generic		Steel			set-7b -13
			Poly	Generic		Steel			set-7b -14
			Water	Generic		Poly			set-7b -15
			Poly	Generic		Poly			set-7b -16

Table N-3. Summary of cases for set-7c for the nonuniform array model.

Case	Model type	Waste form shape	Waste form moderator	Filler material (0, 2,000, 4,000 g)	Metal in filler	Discrete reflector (thin 0.001 cm and thick 0.7112 cm)	Be (g)	B_4C (g)	Subcase
Set-7c	Models from set-2-uh	Cylinder (radius range 4.8, 6, and 7.7, and height defined by total volume of mass)	Water	c12	SS from can (0, 500, 1,000 g)	Steel	0–585	10, 30, 50	set-7c-1
			Poly	c12		Steel			set-7c-2
			Water	c12		Poly			set-7c-3
			Poly	c12		Poly			set-7c -4
			Water	Generic		Steel			set-7c -5
			Poly	Generic		Steel			set-7c -6
			Water	Generic		Poly			set-7c -7
			Poly	Generic		Poly			set-7c -8
		Sphere (radius defined by total volume of mass)	Water	c12		Steel			set-7c -9
			Poly	c12		Steel			set-7c -10
			Water	c12		Poly			set-7c -11
			Poly	c12		Poly			set-7c -12
			Water	Generic		Steel			set-7c -13
			Poly	Generic		Steel			set-7c -14
			Water	Generic		Poly			set-7c -15
			Poly	Generic		Poly			set-7c -16

Table N-4. Summary of results for the addition of 10, 30, or 50 g of B_4C with a waste form moderator mass up to 3 kg for all subcases.

Model	Amount of B_4C
Three-high uniform array model (set-1 and set-7a)	30 g B_4C
Six-high uniform array model (set-3 and set-7b)	30 g B_4C
Nonuniform upper-horizon array model (set-2-uh and set-7c)	10 g B_4C

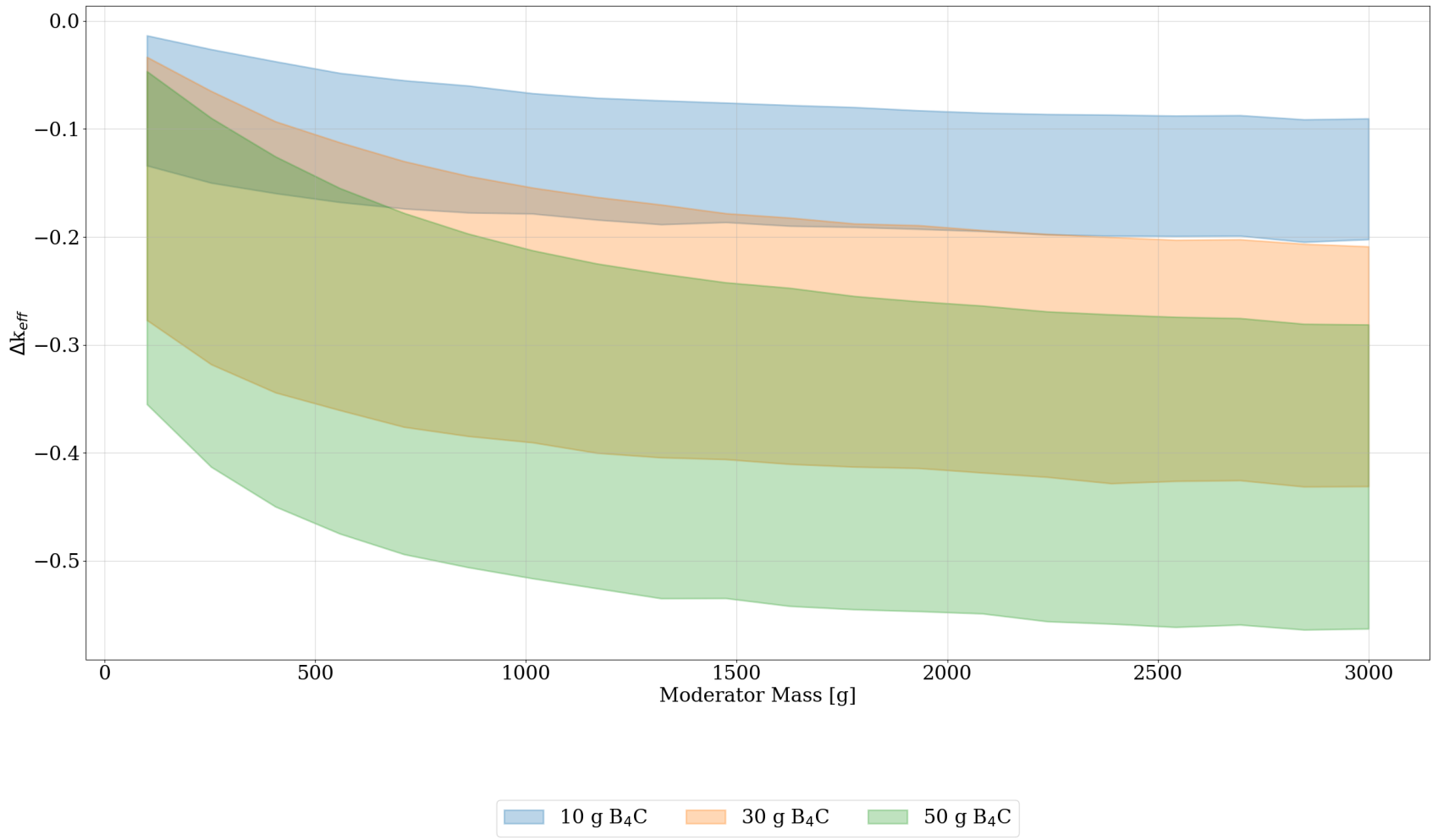

Figure N-1. Set-7a results (three-high uniform array model) for 10, 30, and 50 g of B_4C for all subcases.
Reactivity trends of all subcases as a delta k_{eff} as a function of moderator mass.

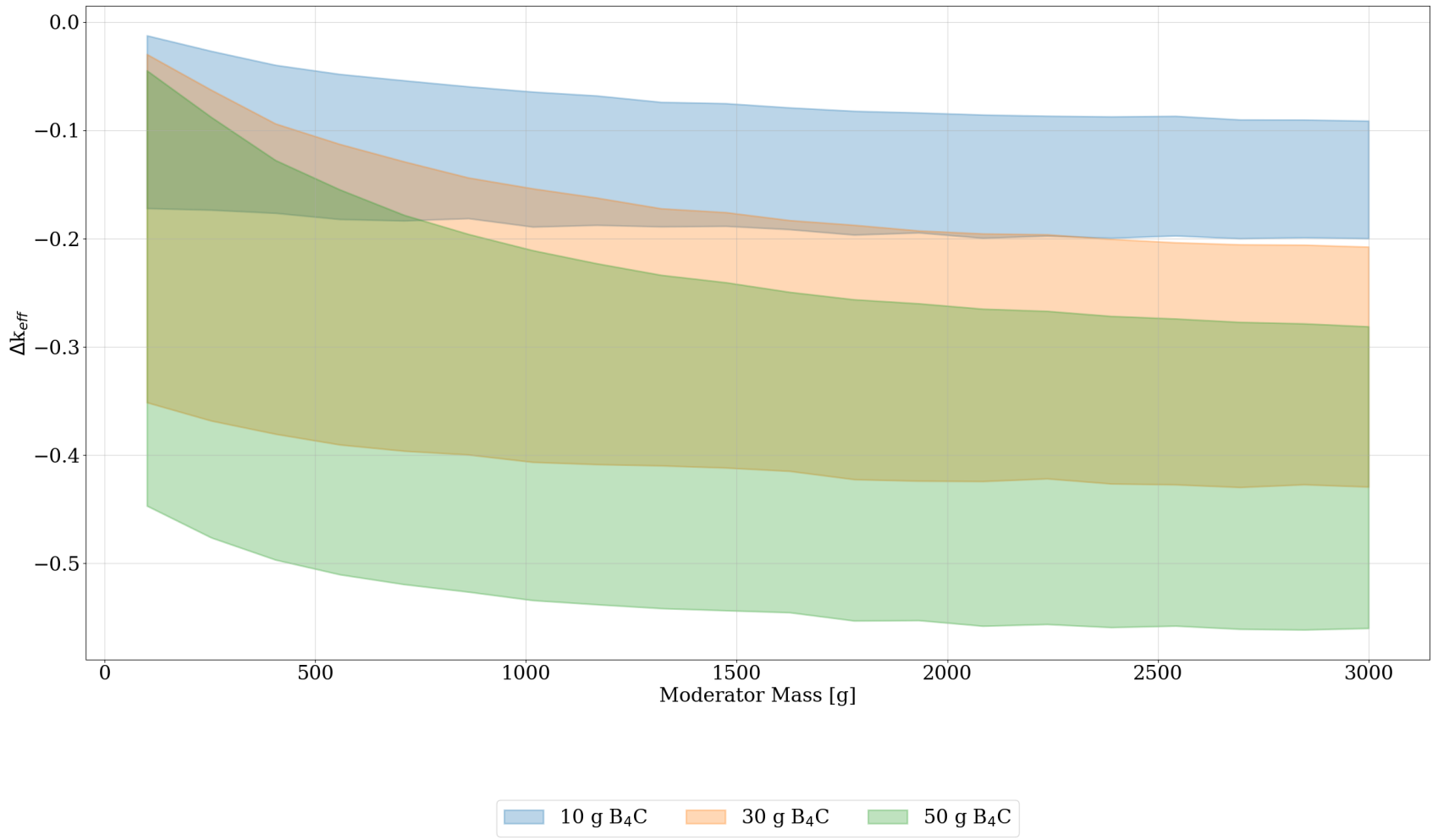

Figure N-2. Set-7b results (six-high uniform array model) for 10, 30, and 50 g of B_4C for all subcases.
Reactivity trends of all subcases as a delta k_{eff} as a function of moderator mass.

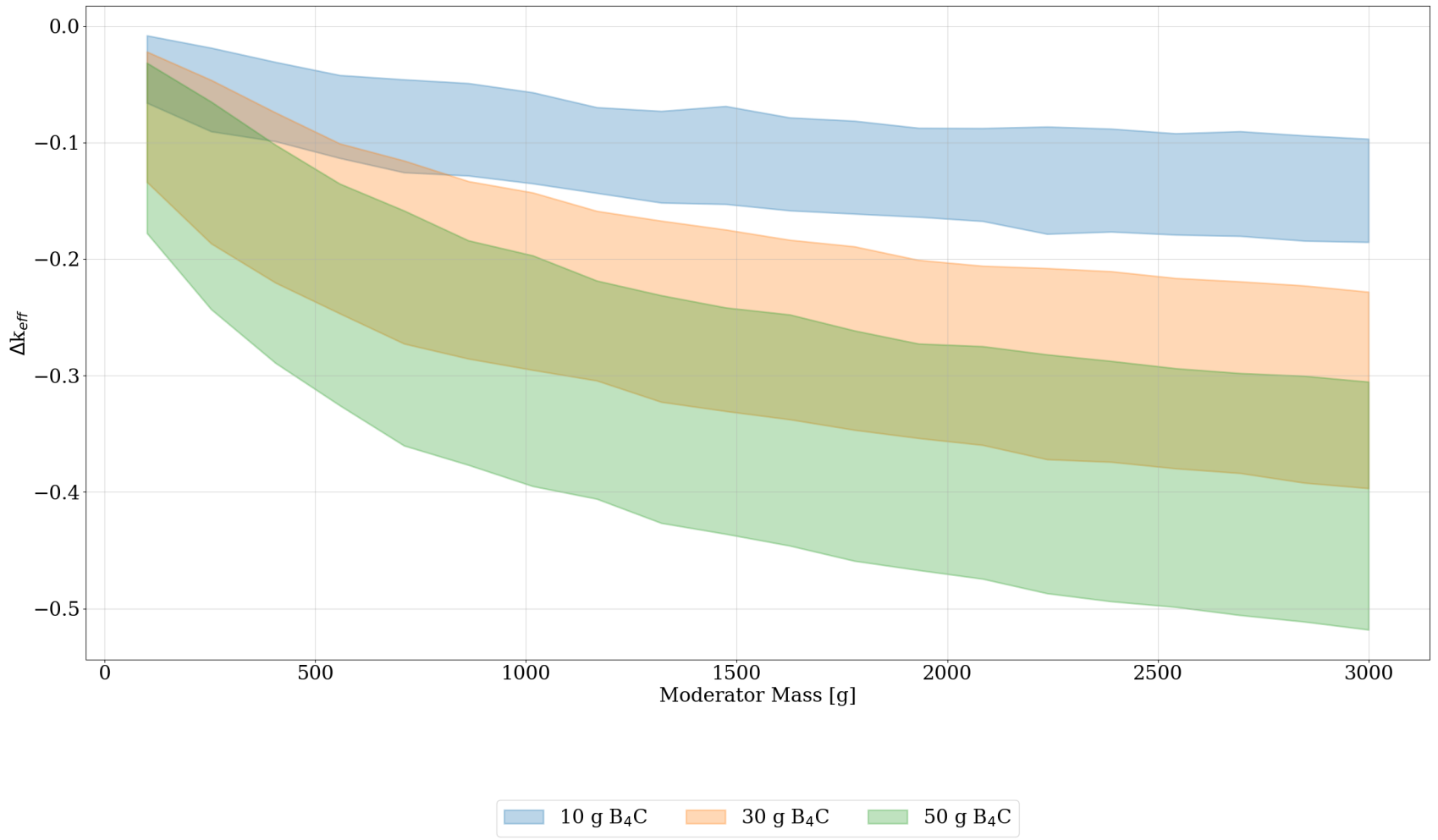

Figure N-3. Set-7c results (three-high uniform array model) for 10, 30, and 50 g of B_4C for all subcases.
Reactivity trends of all subcases as a delta k_{eff} as a function of moderator mass.

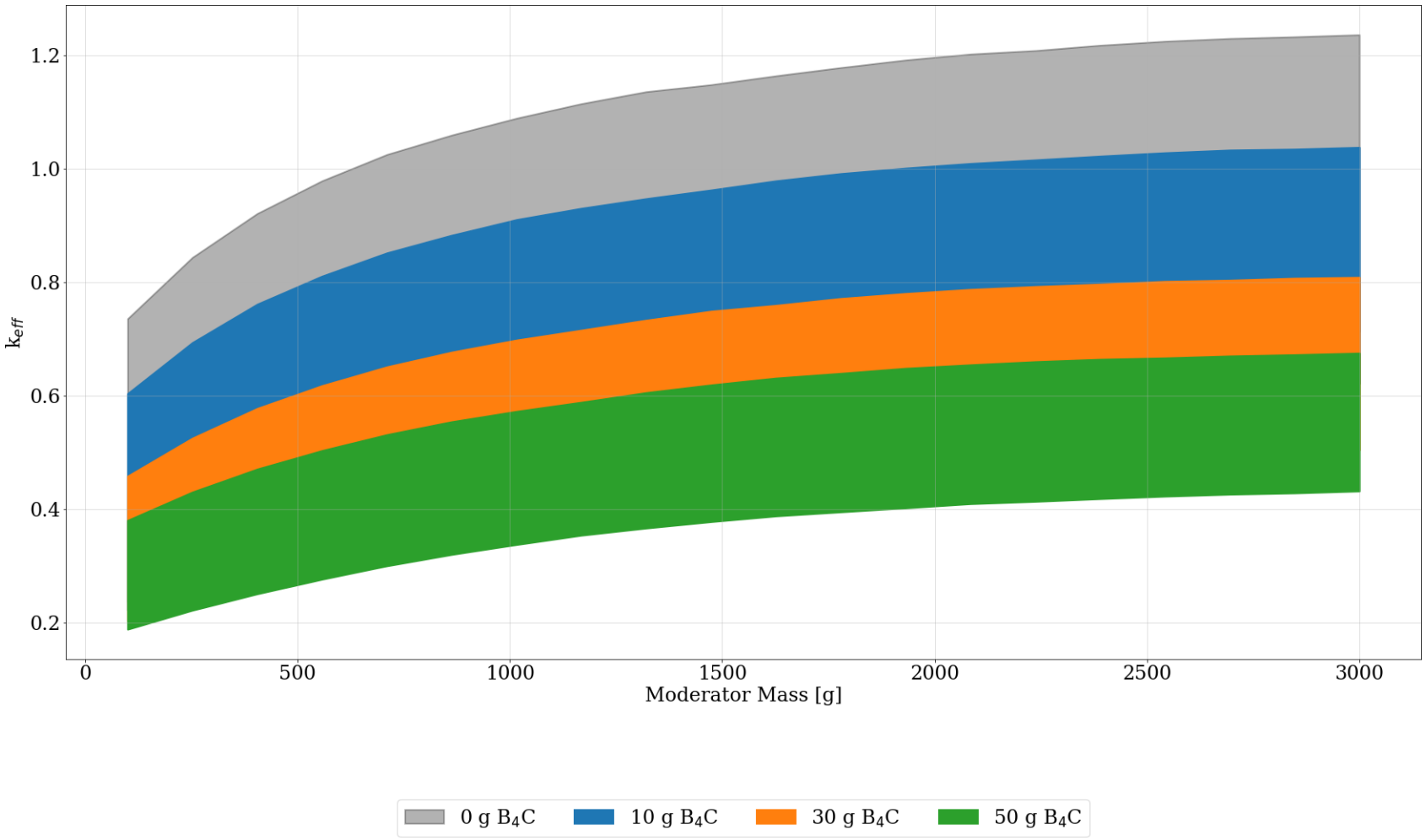

Figure N-4. Set-7a results (three-high uniform array model) for 0, 10, 30, and 50 g of B_4C for all subcases.
Reactivity trends of all subcases as a k_{eff} as a function of moderator mass.

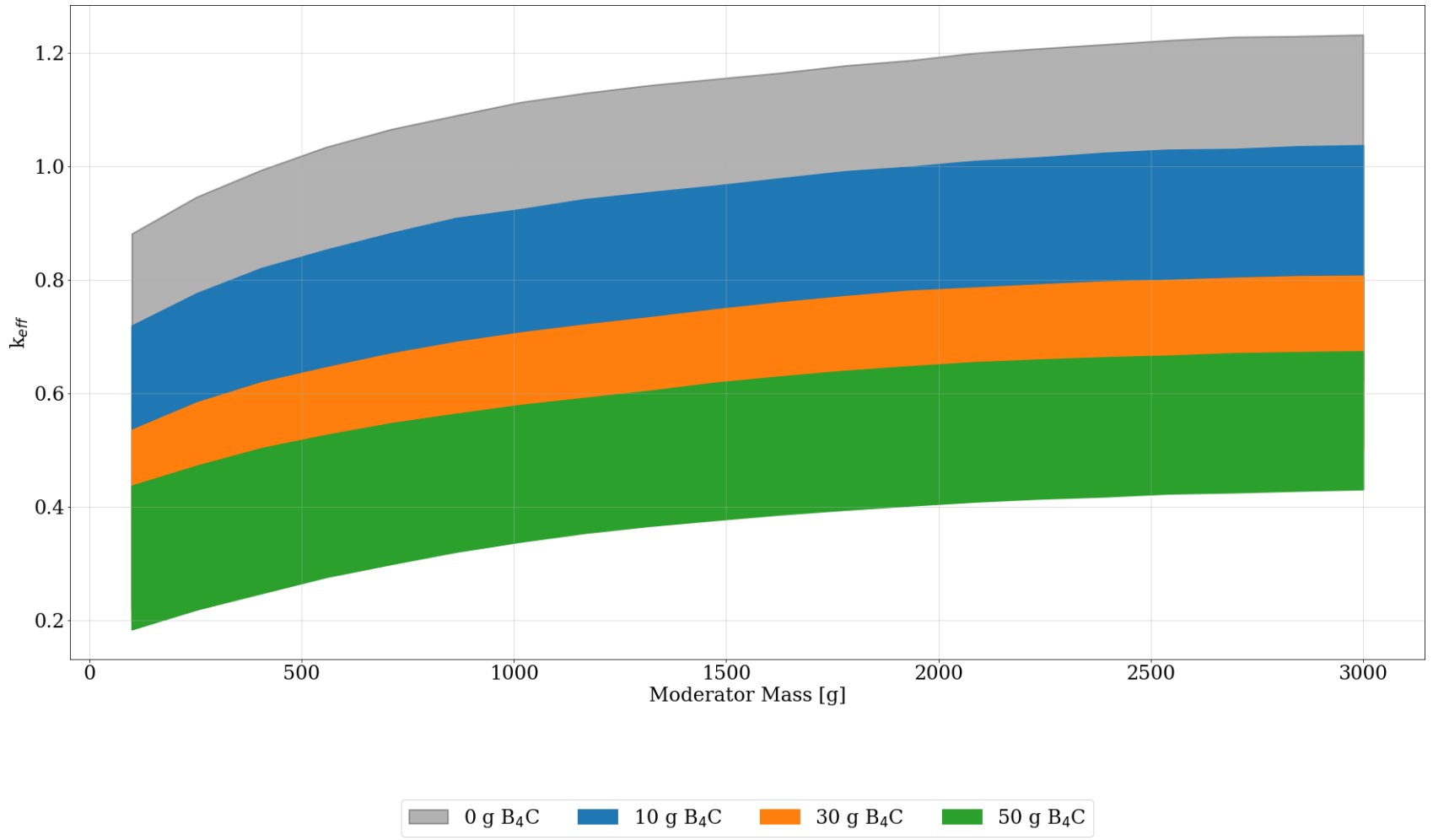

Figure N-5. Set-7b results (six-high uniform array model) for 0,10, 30, and 50 g of B_4C for all subcases.
Reactivity trends of all subcases as k_{eff} as a function of moderator mass.

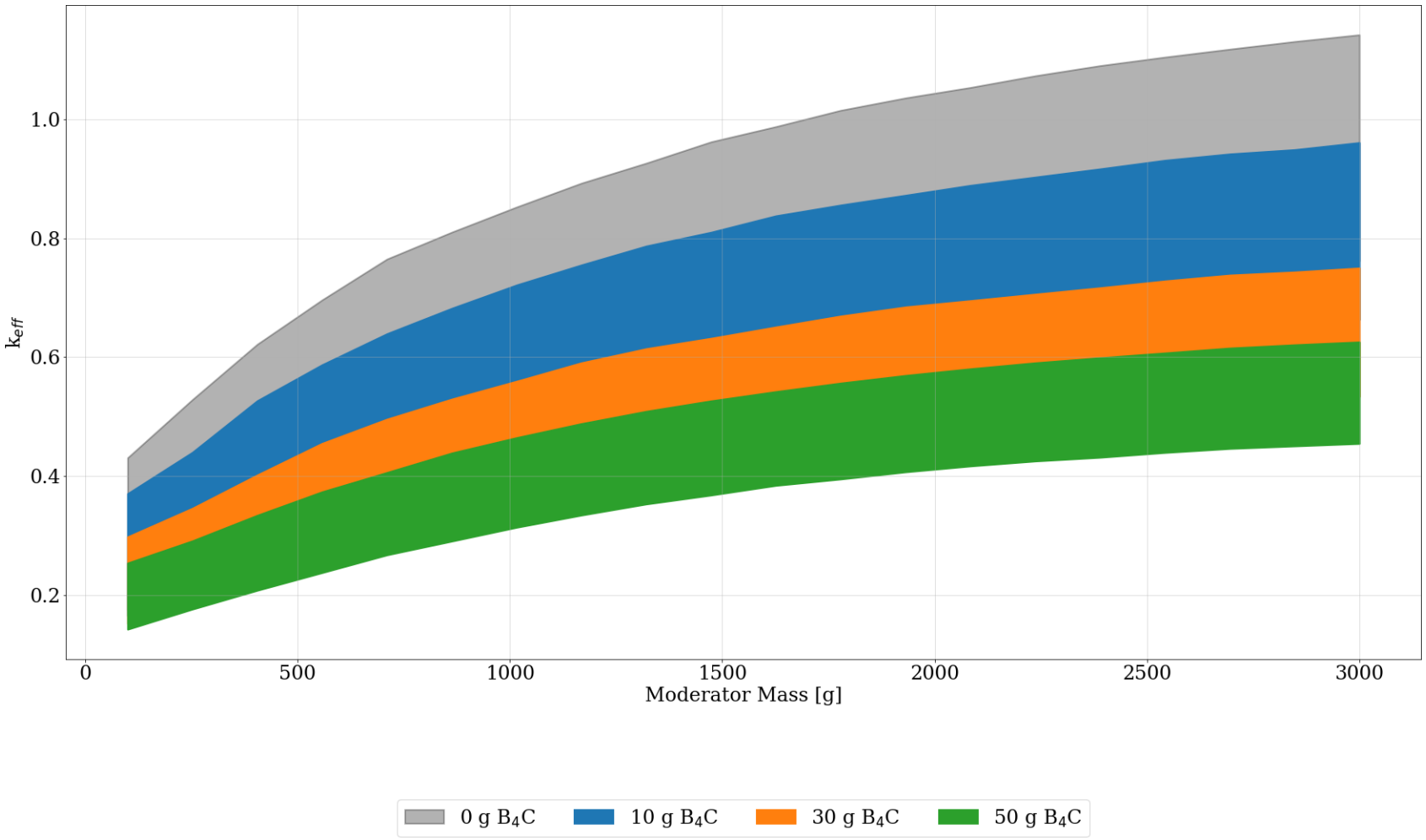

Figure N-6. Set-7c results (nonuniform upper horizon array model) for 0, 10, 30, and 50 g of B_4C for all subcases.
Reactivity trends of all subcases as a delta k_{eff} as a function of moderator mass.

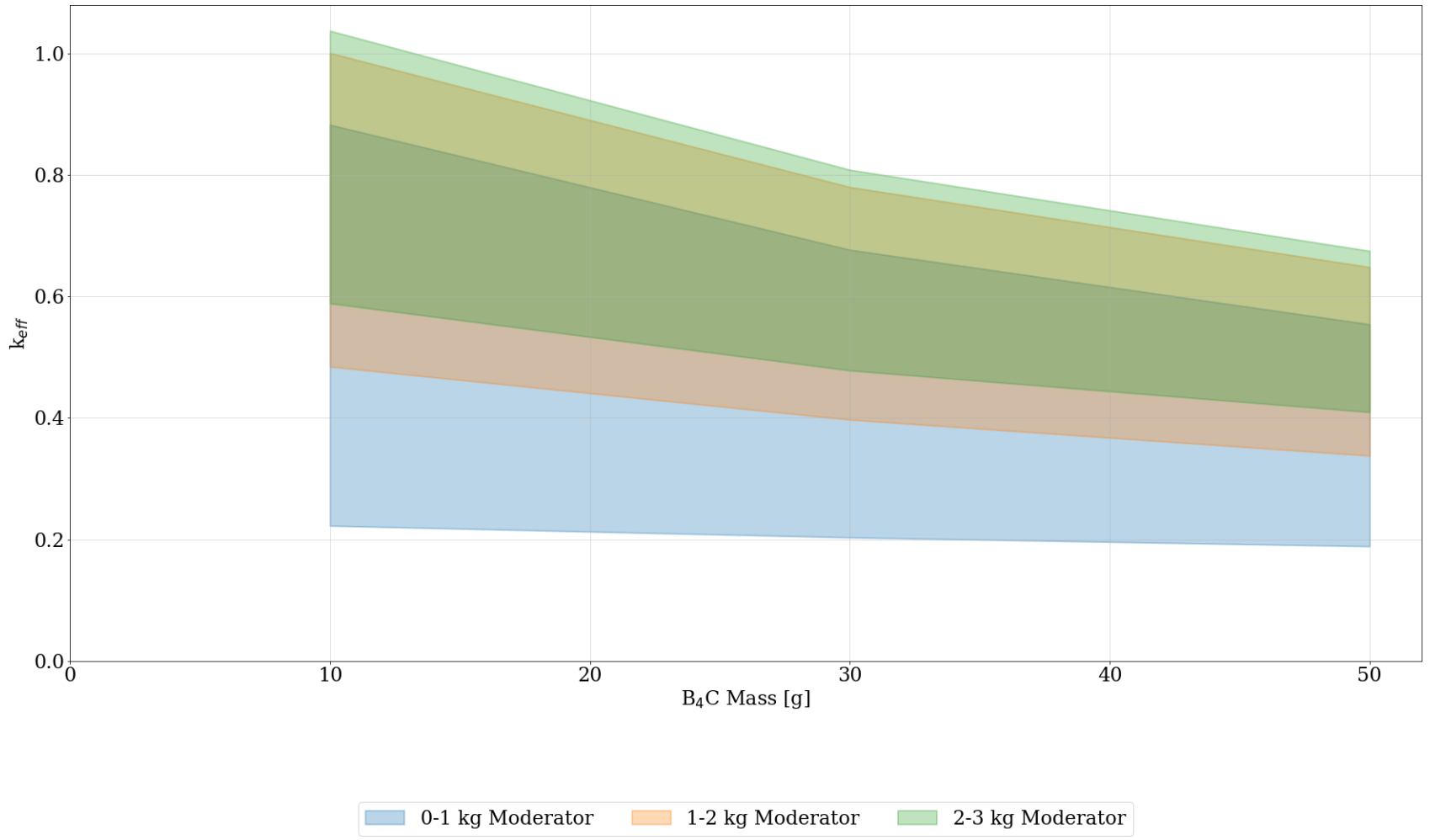

Figure N-7. Set-7a results (three-high uniform array model) for 10, 30, and 50 g of B_4C for all subcases.
Reactivity trends of all subcases as k_{eff} as a function of B_4C mass.

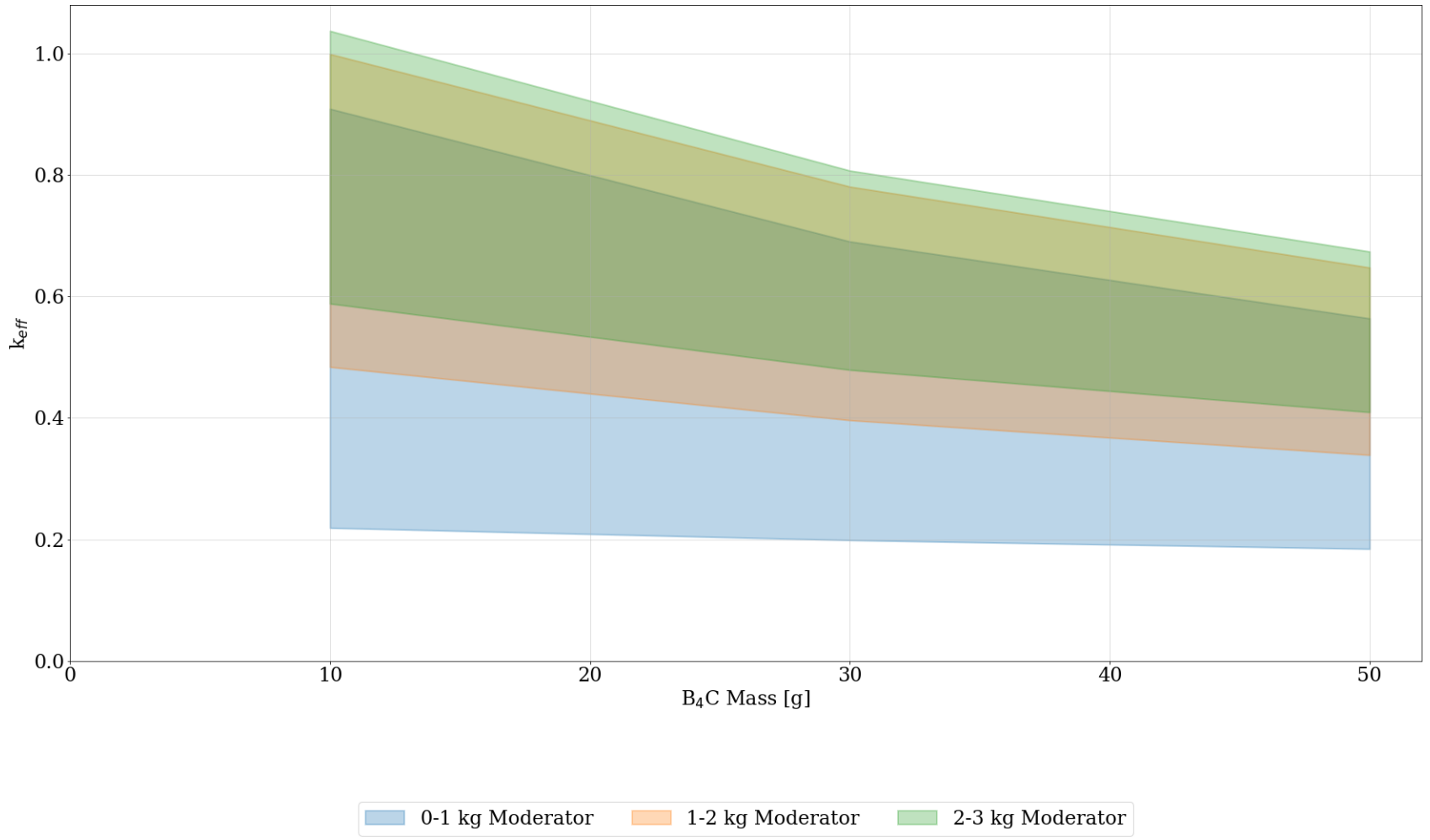

Figure N-8. Set-7b results (six-high uniform array model) for 10, 30, and 50 g of B_4C for all subcases.
Reactivity trends of all subcases as k_{eff} as a function of B_4C mass.

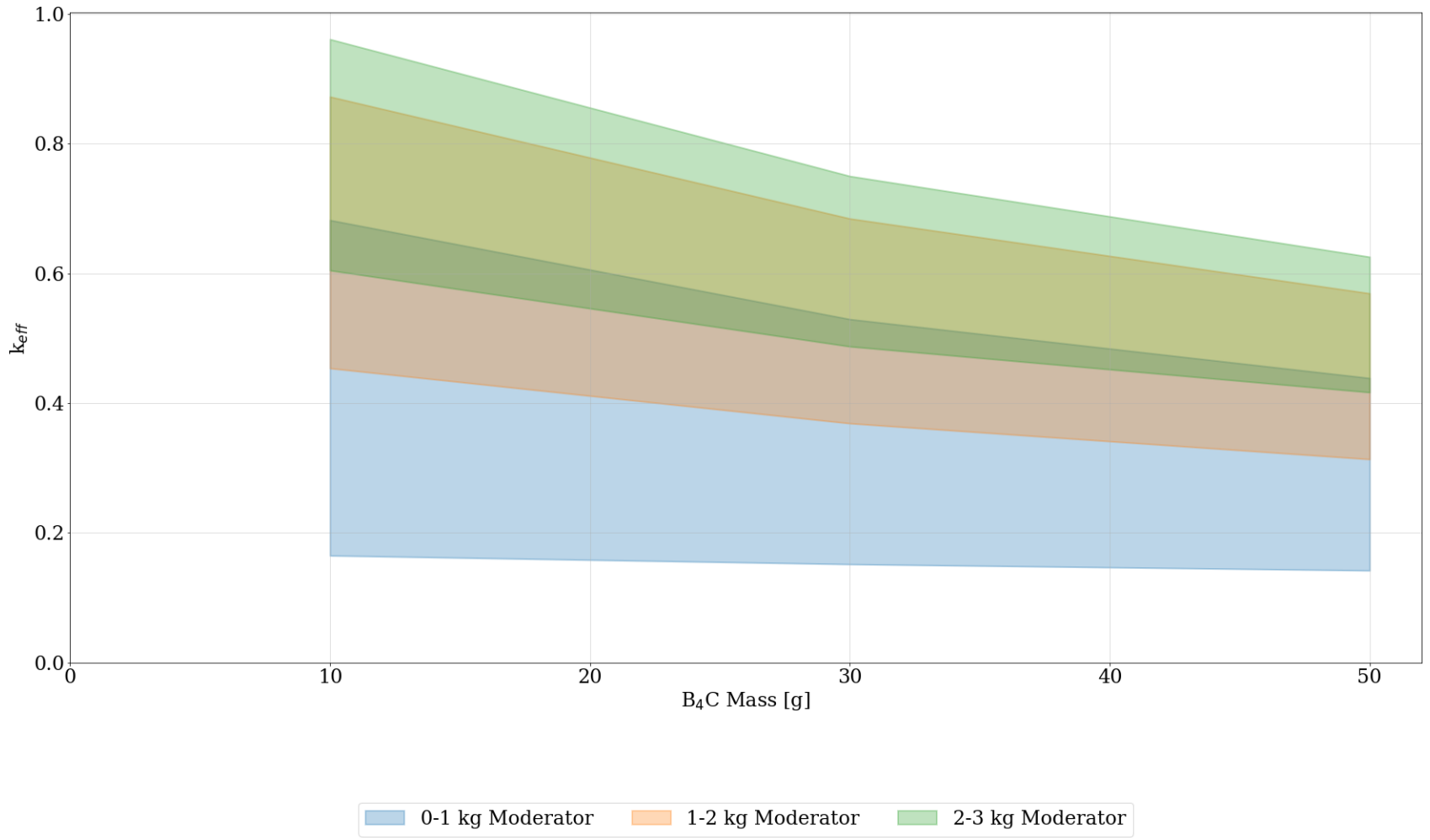

Figure N-9. Set-7c results (nonuniform array model) for 10, 30, and 50 g of B_4C for all subcases.
Reactivity trends of all subcases as k_{eff} as a function of B_4C mass.

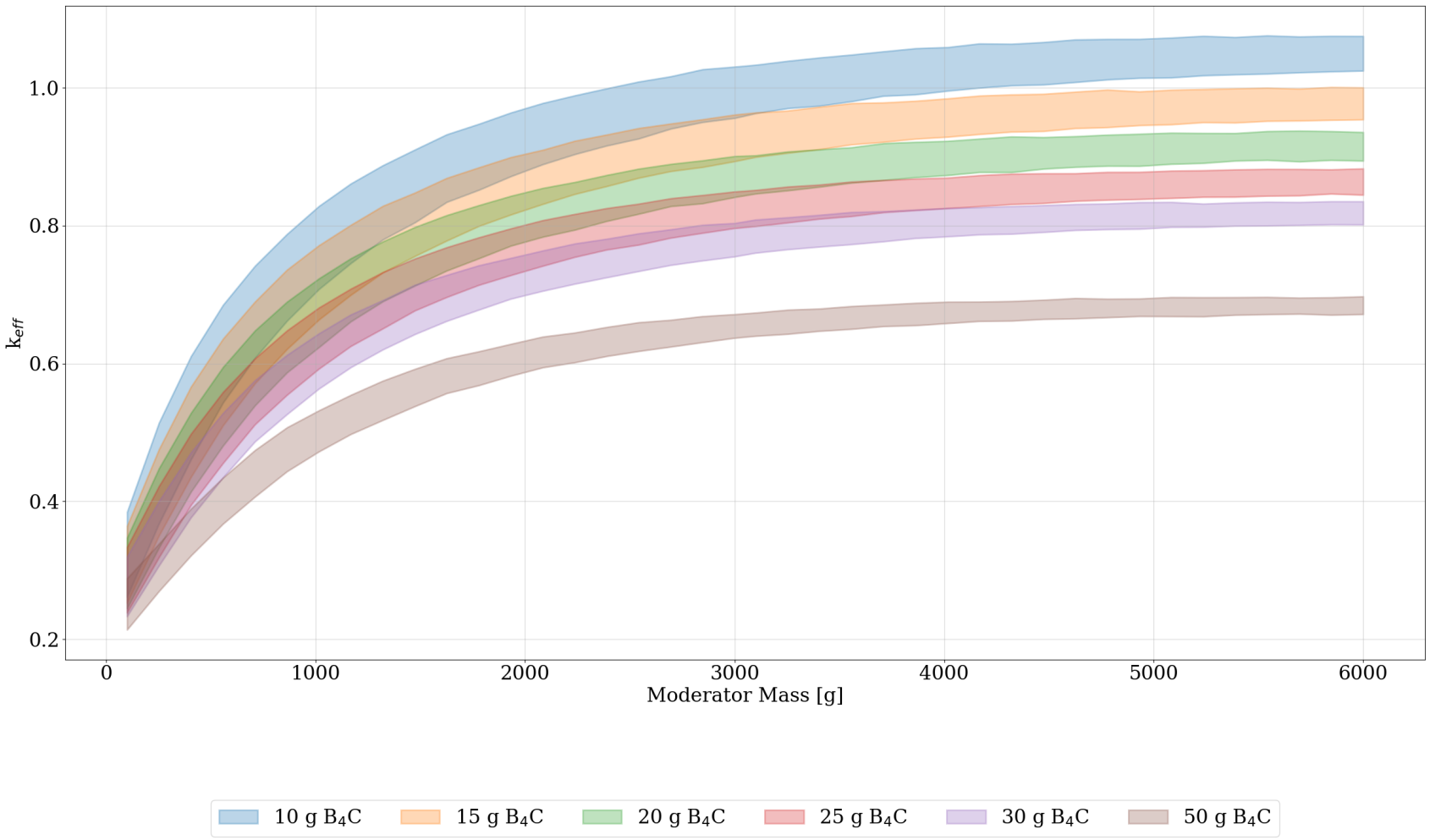

Figure N-10. Set-7a results (three-high uniform array model) for 10, 15, 20, 25, 30, and 50 g of B_4C for subcase-10 only.
Reactivity trends of all subcases as k_{eff} as a function of moderator mass up to 6 kg.

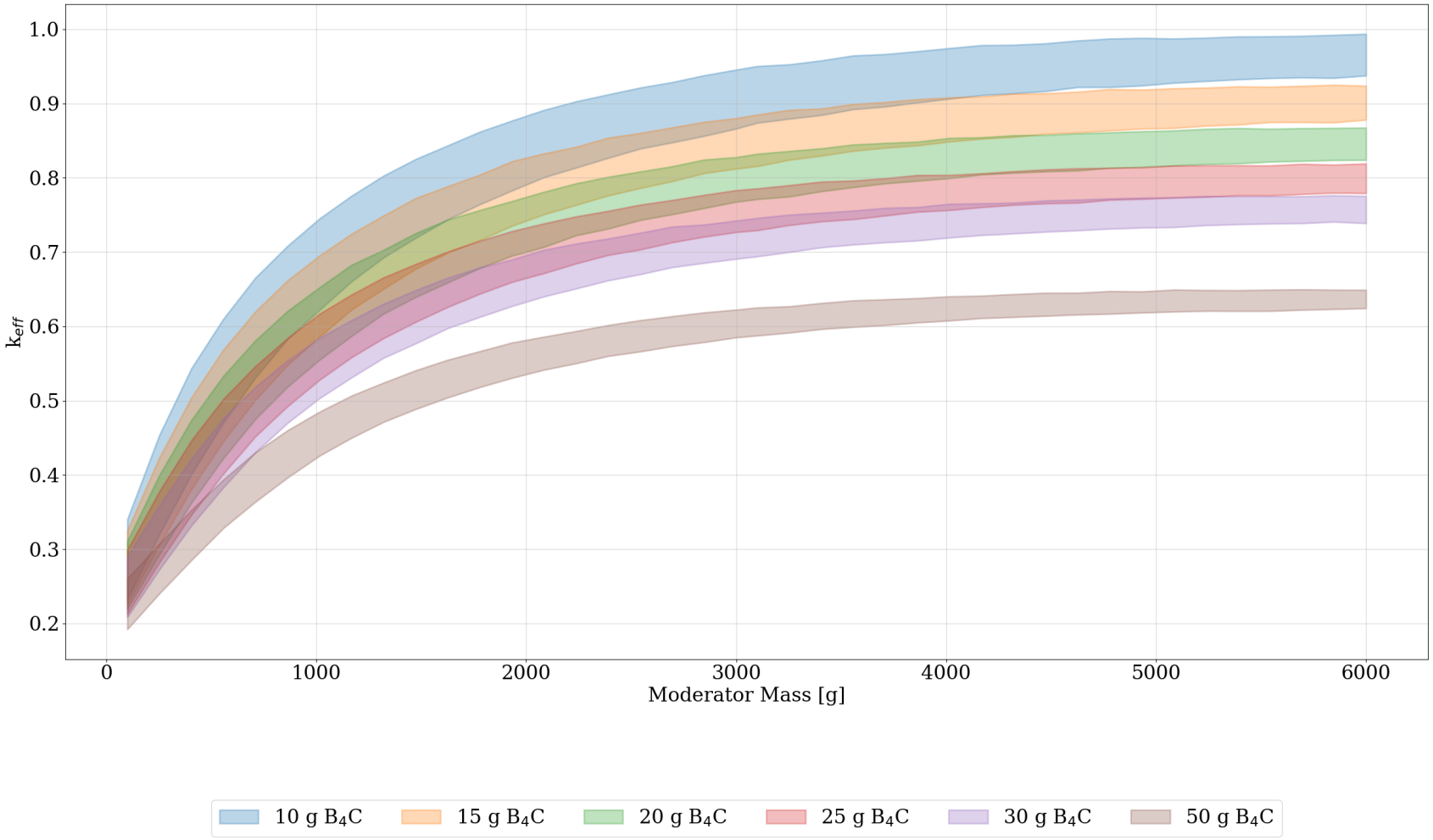

Figure N-11. Set-7b results (six-high uniform array model) for 10, 15, 20, 25, 30, and 50 g of B_4C for subcase-10 only.
Reactivity trends of subcase-10 as k_{eff} as a function of moderator mass up to 6 kg.

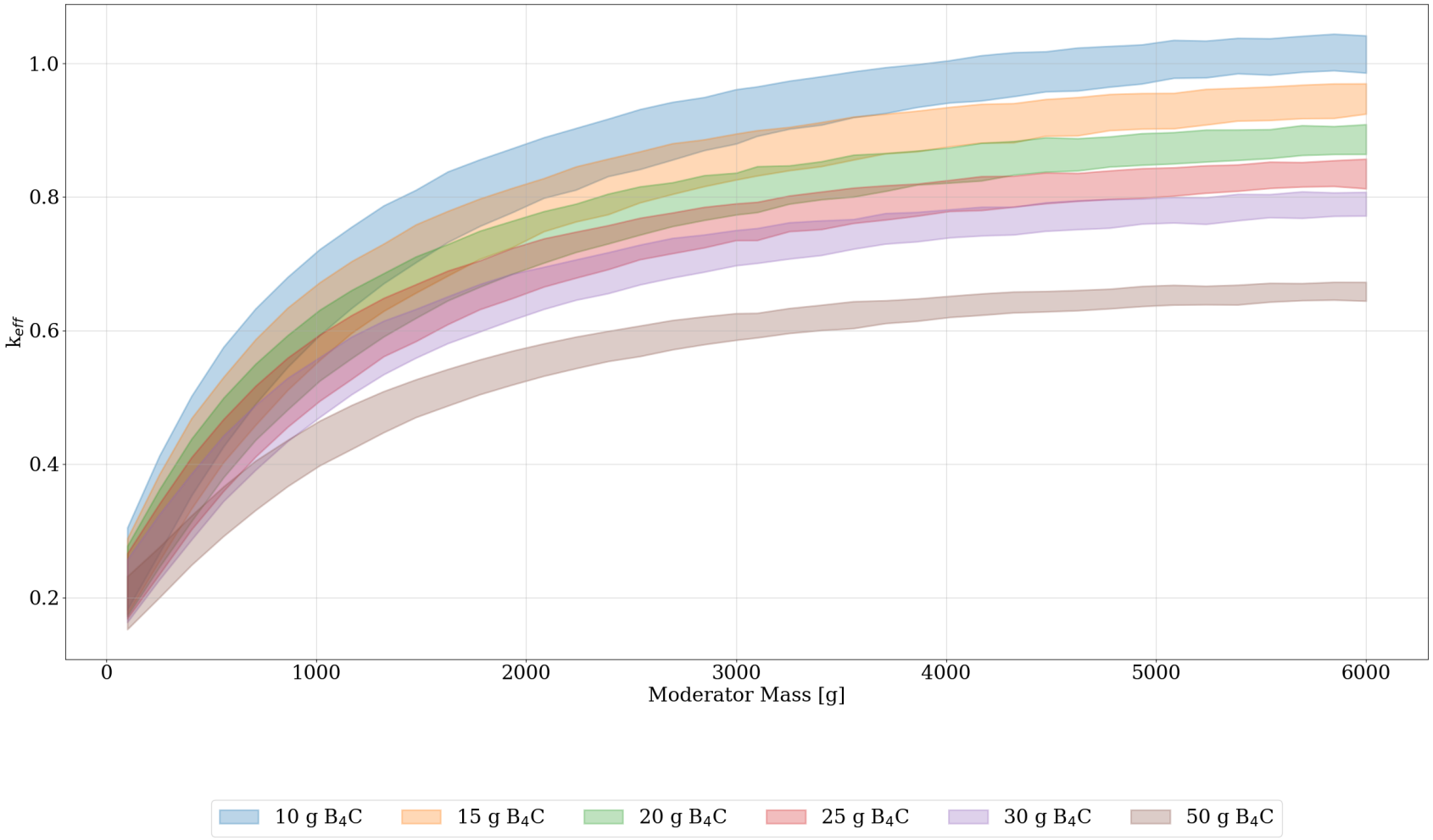

Figure N-12 Set-7c results (nonuniform array model) for 10, 15, 20, 25, 30, and 50 g of B_4C for subcase-10 only.
Reactivity trends of subcase-10 as k_{eff} as a function of moderator mass up to 6 kg.

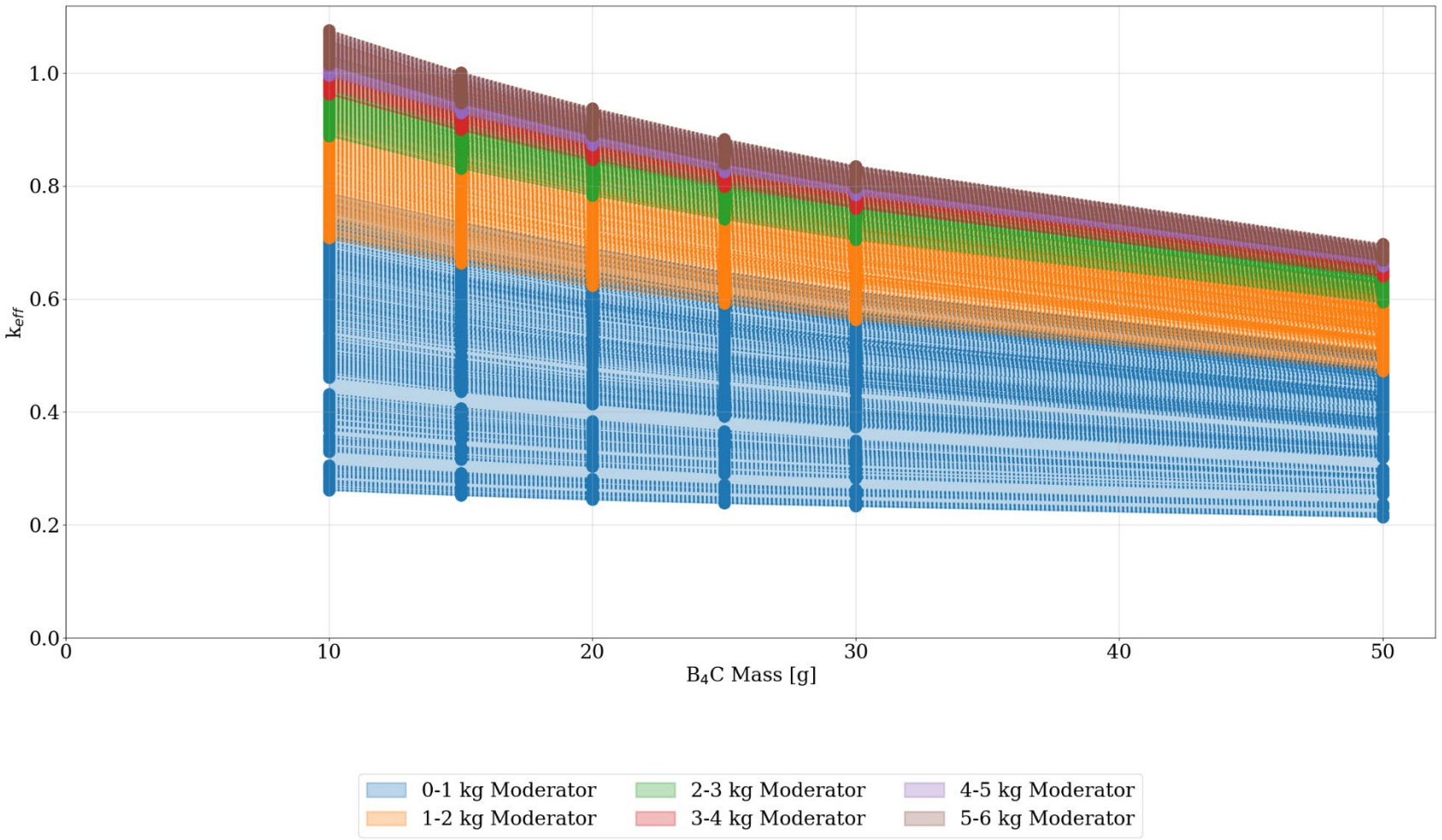

Figure N-13. Set-7a results (three-high uniform array model) for 10, 15, 20, 25, 30, and 50 g of B_4C for all subcases.
Reactivity trends of all subcase-10 as k_{eff} as a function of B_4C mass.

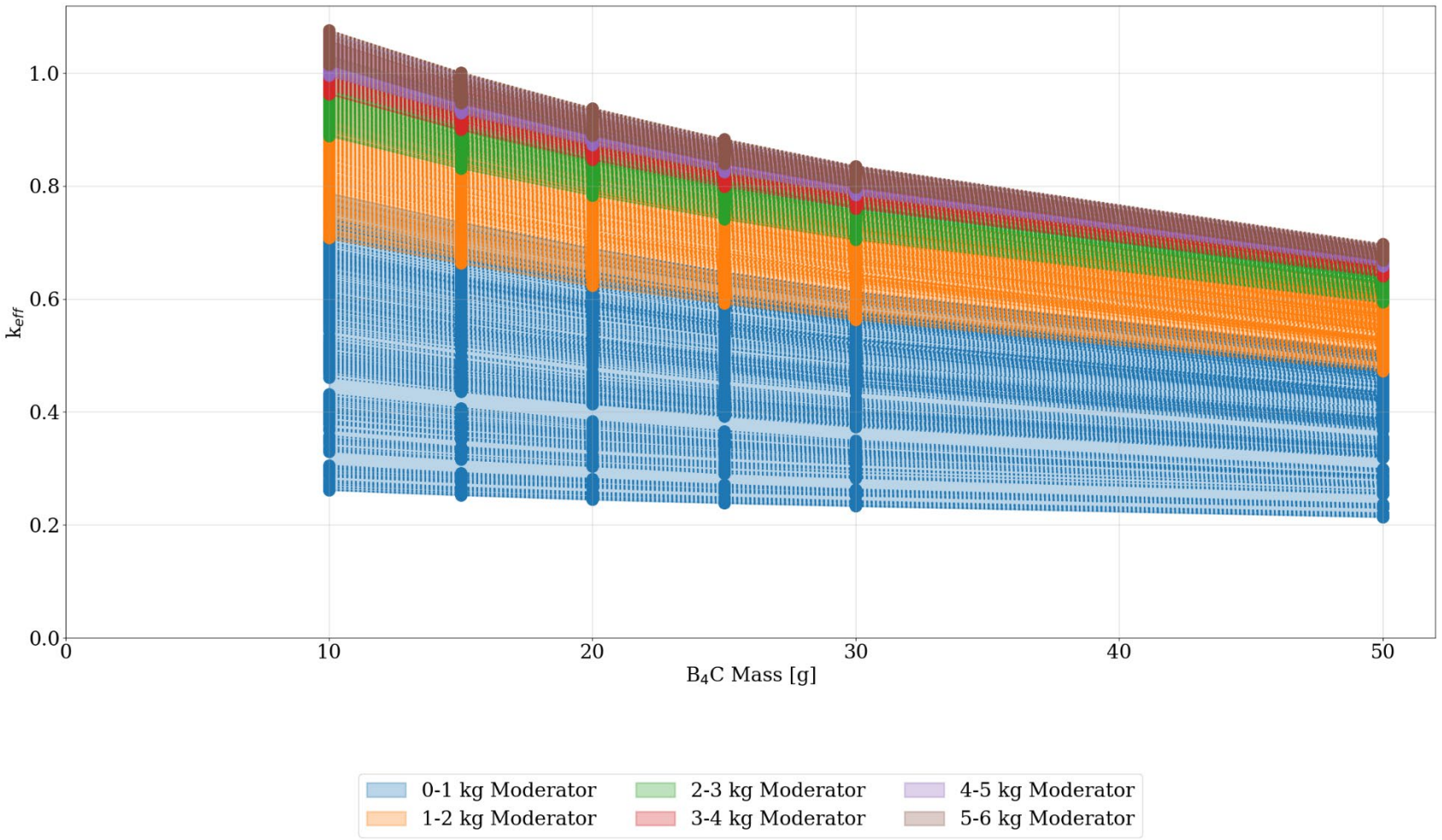

Figure N-14. Set-7b results (six-high uniform array model) for 10, 15, 20, 25, 30, and 50 g of B_4C for all subcases.
Reactivity trends of all subcase-10 as k_{eff} as a function of B_4C mass.

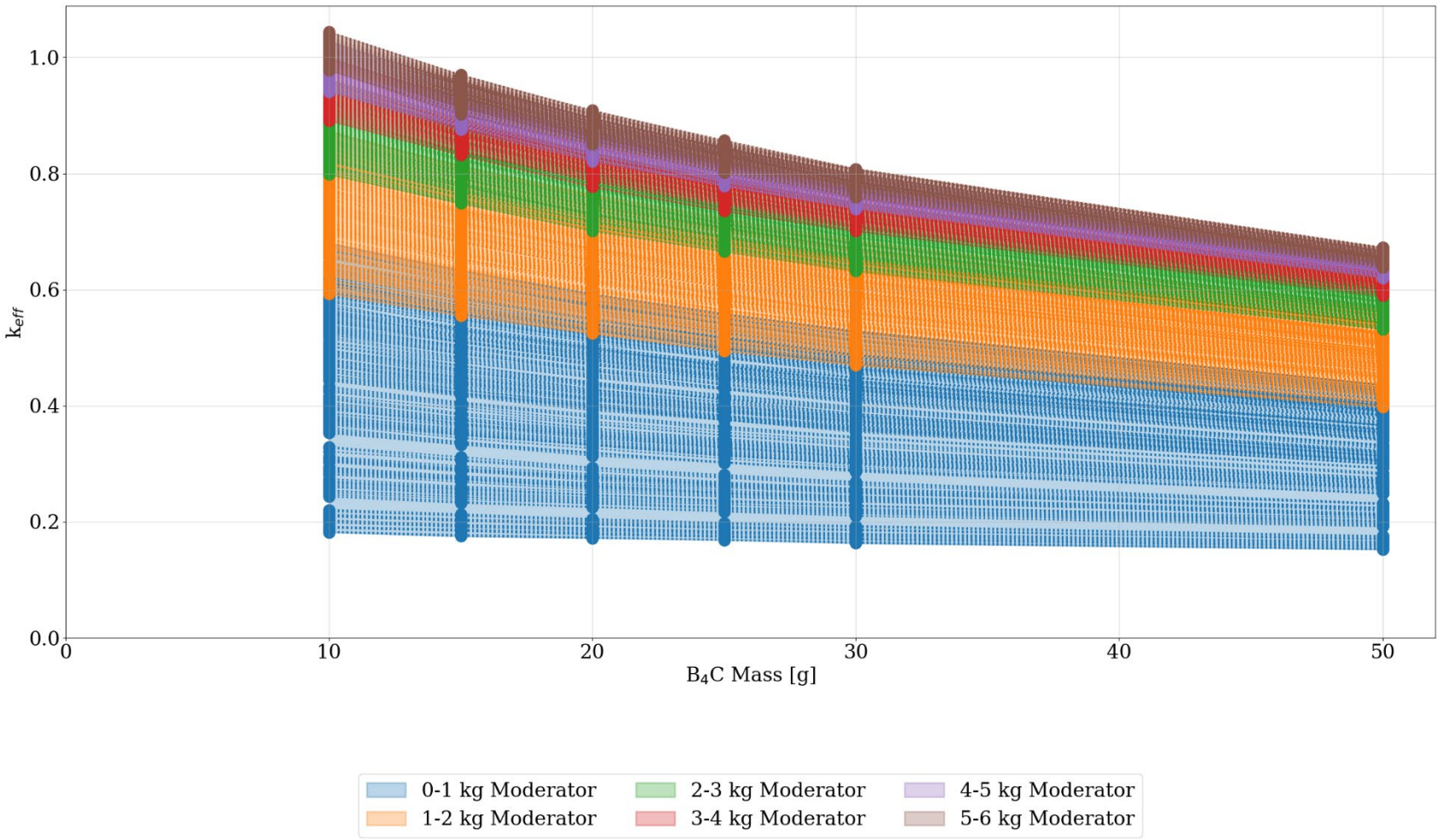

Figure N-15. Set-7c results (nonuniform array model) for 10, 15, 20, 25, 30, and 50 g of B_4C for up to a 6 kg moderator.
Reactivity trends of subcase-10 as k_{eff} as a function of B_4C mass.

This page is intentionally blank

APPENDIX O. SET-8: RESULTS OF THE CALCULATIONS TO SHOW THE REACTIVITY EFFECT OF GREATER THICKNESSES OF THE DISCRETE REFLECTOR MATERIAL AROUND THE WASTE FORM

This page is intentionally blank

APPENDIX O. SET-8: RESULTS OF THE CALCULATIONS TO SHOW THE REACTIVITY EFFECT OF GREATER THICKNESSES OF THE DISCRETE REFLECTOR MATERIAL AROUND THE WASTE FORM

This appendix serves as a repository of the results for additional thicker thicknesses of the discrete reflector material around the waste form.

The analysis models used in this appendix for set-8a are the same as those used for the set-1 models discussed in detail in Appendix A, and those used for set-8b are the same as those used the set-2-uh models discussed in detail in Appendix C. The model changes to the calculations in this appendix compared with Appendix A and Appendix C are for the increase in the discrete reflector thickness around each waste form.

This appendix expands upon how k_{eff} is affected when the thickness of the discrete reflector is increased from what was already evaluated. The source of the discrete reflector material is expected to be mainly steel from the pipes and CCO drums, and although the evaluation already considered in the main report uses a thin and a thick thickness to account for this material, the maximum thickness evaluated is equivalent to the thickness of the inner CCO pipe only. Because additional material is known to exist, additional calculations are considered by increasing the thickness to multiples of the inner CCO pipe thickness of 0.7112: 1.422 and 2.134 cm. Note that for set-8b, the maximum thickness used is limited to 1.422 cm because of the close proximity of the centroids.

The cases in this appendix are summarized in Table O-1 and Table O-2 for set-8a and set-8b, respectively.

The results in this appendix are presented first as a summary of the reactivity trends related to discrete reflector thickness and then as a delta k_{eff} for each sublisting. For the summary evaluations, the results to demonstrate the reactivity effect of the increasing discrete reflector thickness are provided in Figures O-1 through O-5 for set-8a and in Figures O-6 through O-10 for set-8b. Specifically, these results summaries are provided to demonstrate the impact of discrete reflector thickness on the system at its maximum subcritical moderator mass for the two waste form geometries and the two discrete reflector materials considered, or four total combinations.

For each combination of waste form geometry and discrete reflector material composition, the maximum moderator mass over all sublistings was determined for set-1 calculations as follows.

- The maximum subcritical moderator mass for cylindrical waste forms with a poly discrete reflector is a 557.9 g moderator mass.
- The maximum subcritical moderator mass for spherical waste forms with a poly discrete reflector is a 1,016 g moderator.
- The maximum subcritical moderator mass for cylindrical waste forms with a stainless-steel discrete reflector is a 710.5 g moderator.
- The maximum subcritical moderator mass for spherical waste forms with a stainless-steel discrete reflector is a 1,016 g moderator.

For each combination of waste form geometry and discrete reflector material composition, the maximum moderator mass over all sublistings was determined for set-2-uh calculations as follows.

- The maximum subcritical moderator mass for cylindrical waste forms with a poly discrete reflector is a 1,779 g moderator mass.
- The maximum subcritical moderator mass for spherical waste forms with a poly discrete reflector is a 1,779 g moderator.
- The maximum subcritical moderator mass for cylindrical waste forms with a stainless-steel discrete reflector is a 1,626 g moderator.
- The maximum subcritical moderator mass for spherical waste forms with a stainless-steel discrete reflector is a 1,474 g moderator.

The set of parameter sweeps was identified for each of these identified maximum subcritical moderator masses for the discrete reflector thickness of 0.001 cm. Using these same set of parameter sweeps for the 0.001 cm thickness, the datasets for the additional discrete reflector thicknesses were identified so that the only difference in the plotted results is the discrete reflector thickness. These four datasets for each of the four thickness are then plotted against the complete set of data results in Figures O-1 through O-4 for set-1 and set-8a and in Figures O-6 through O-9 for set-2-uh and set-8b. As expected, there is much variation in the results, showing the interdependence of the system parameters on k_{eff}.

Alternatively, the results are also provided as k_{eff} vs. discrete reflector thickness in Figure O-5 for set-1 and set-8a and in Figure O-10 for set-2-uh and set-8b. For these plots, the maximum k_{eff} is provided, regardless of the parameter sweeps that yield the maximum result.

To provide more detailed results that specifically evaluate the reactivity trends seen in the summary figures, additional k_{eff} plots are presented for each sublisting. The sublisting results for the k_{eff} from set-1 to set-8a are presented in Figures O-11 through O-26, and the k_{eff} from set-2-uh to set-8b are presented in Figures O-27 through O-42.

LIST OF FIGURES

LIST OF TABLES

Table O-1. Summary of cases for set-8a for three-high uniform array model.

Case	Model type	Waste form shape	Waste form moderator	Filler material (0, 2,000, 4,000 g)	Metal in filler	Discrete reflector (1.4224cm thick and 2.1336 cm thick)	Be (g)	Sublisting
Set-8a	Models from Set-1	Cylinder (radius range 4.8, 6.25, 7.7 and height defined by total volume of mass)	Water	c12	SS from can (0, 500, 1,000 g)	Steel	0 to 585	set-8a-1
			Poly	c12		Steel		set-8a-2
			Water	c12		Poly		set-8a-3
			Poly	c12		Poly		set-8a -4
			Water	Generic		Steel		set-8a -5
			Poly	Generic		Steel		set-8a -6
			Water	Generic		Poly		set-8a -7
			Poly	Generic		Poly		set-8a -8
		Sphere (radius defined by total volume of mass)	Water	c12		Steel		set-8a -9
			Poly	c12		Steel		set-8a -10
			Water	c12		Poly		set-8a -11
			Poly	c12		Poly		set-8a -12
			Water	Generic		Steel		set-8a -13
			Poly	Generic		Steel		set-8a -14
			Water	Generic		Poly		set-8a -15
			Poly	Generic		Poly		set-8a -16

Table O-2. Summary of cases for set-8b for the nonuniform array model.

Case	Model type	Waste form shape	Waste form moderator	Filler material (0, 2,000, 4,000 g)	Metal in filler	Discrete reflector (1.4224 cm thick)	Be (g)	Sublisting
Set-8b	Models from Set-2-uh	Cylinder (radius range 4.8, 6.25, 7.7 and height defined by total volume of mass)	Water	c12	SS from can (0, 500, 1,000 g)	Steel	0 to 585	set-8b-1
			Poly	c12		Steel		set-8b-2
			Water	c12		Poly		set-8b-3
			Poly	c12		Poly		set-8b-4
			Water	Generic		Steel		set-8b-5
			Poly	Generic		Steel		set-8b-6
			Water	Generic		Poly		set-8b-7
			Poly	Generic		Poly		set-8b-8
		Sphere (radius defined by total volume of mass)	Water	c12		Steel		set-8b-9
			Poly	c12		Steel		set-8b-10
			Water	c12		Poly		set-8b-11
			Poly	c12		Poly		set-8b-12
			Water	Generic		Steel		set-8b-13
			Poly	Generic		Steel		set-8b-14
			Water	Generic		Poly		set-8b-15
			Poly	Generic		Poly		set-8b-16

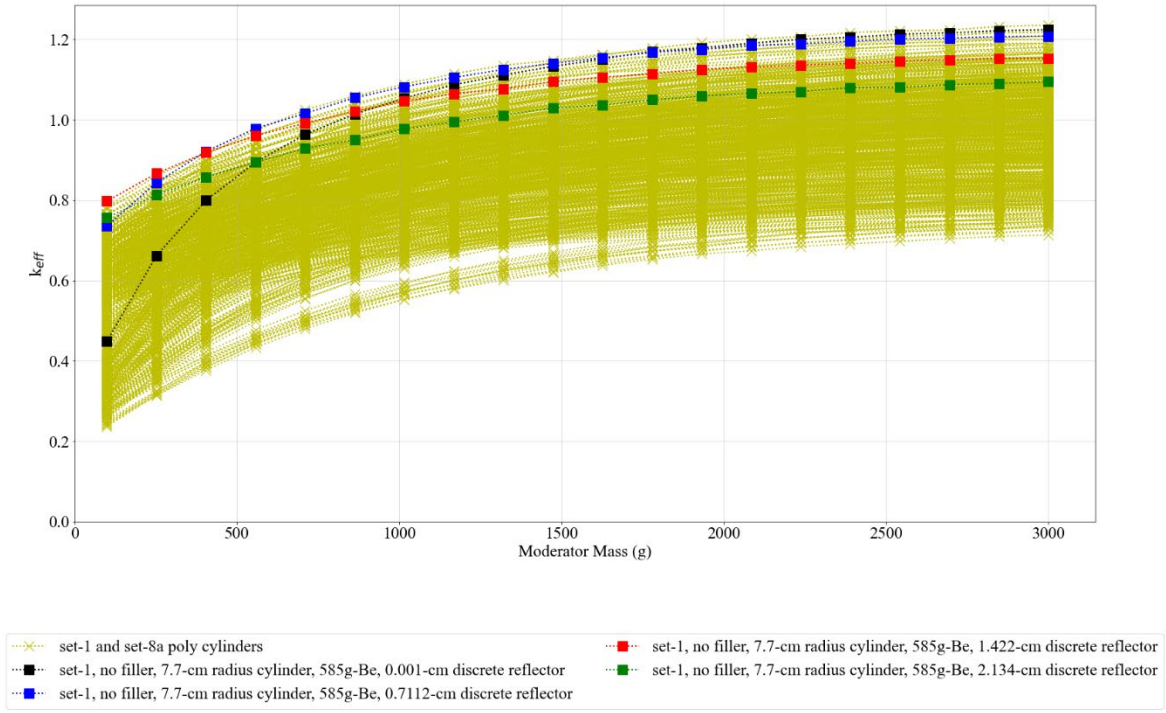

Figure O-1. Set-8a and set-1 k_{eff} results (three-high uniform array model) for the cylindrical waste forms with a poly discrete reflector and a discrete reflector thickness comparison between the sublisting parameters, which yield a maximum subcritical moderator mass for a discrete reflector thickness of 0.001 cm.

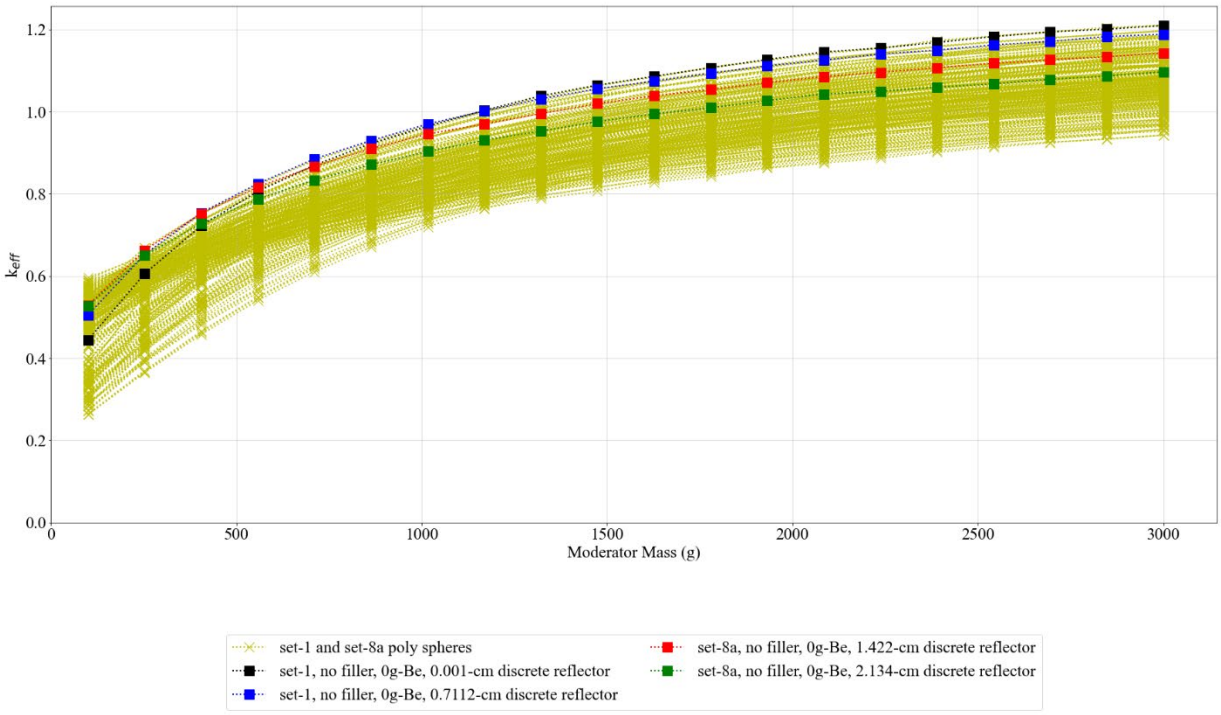

Figure O-2. Set-8a and set-1 k_{eff} results (three-high uniform array model) for the spherical waste forms with a poly discrete reflector, and a discrete reflector thickness comparison between the sublisting parameters, which yield a maximum subcritical moderator mass for a discrete reflector thickness of 0.001 cm.

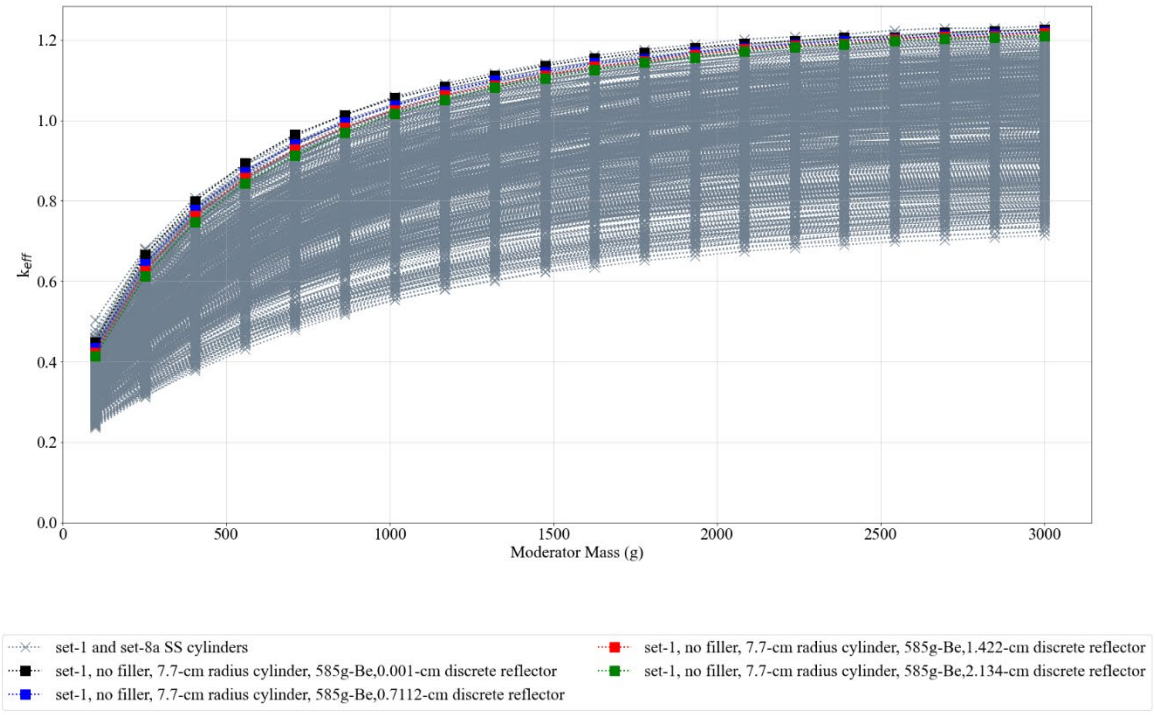

Figure O-3. Set-8a and set-1 k_{eff} results (three-high uniform array model) for the cylindrical waste forms with a stainless-steel discrete reflector and a discrete reflector thickness comparison between the sublisting parameters, which yield a maximum subcritical moderator mass for a discrete reflector thickness of 0.001 cm.

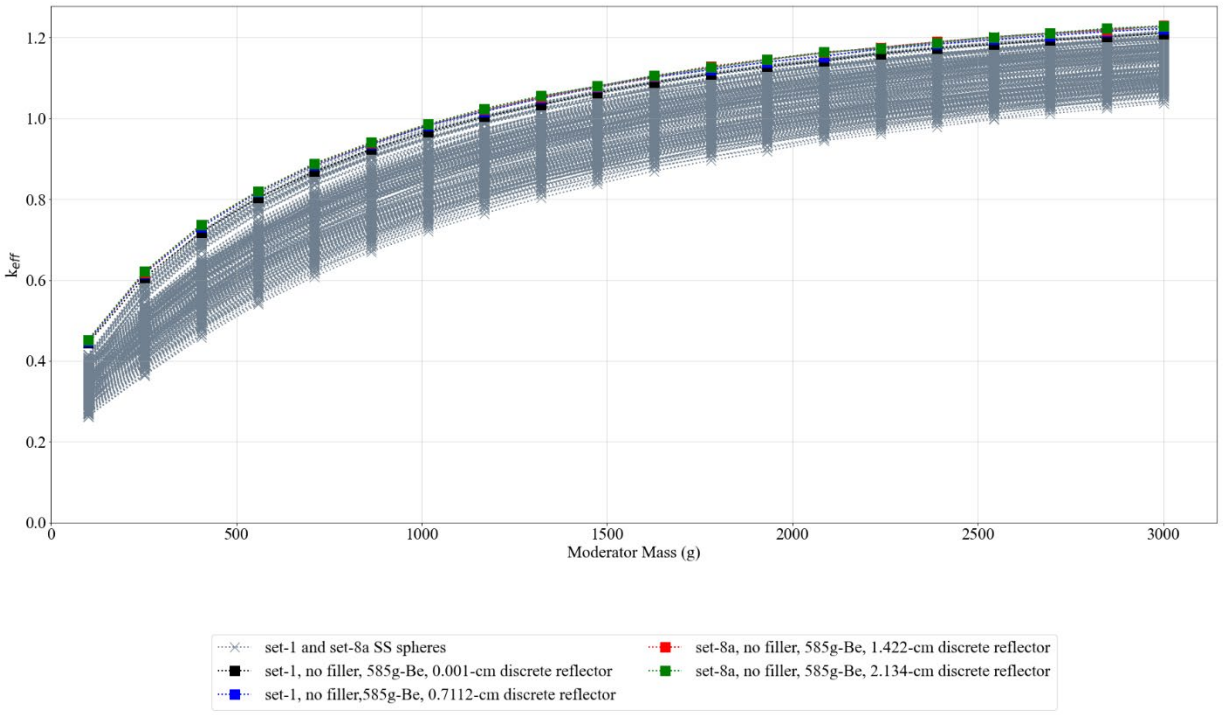

Figure O-4. Set-8a and set-1 k_{eff} results (three-high uniform array model) for the spherical waste forms with a stainless-steel discrete reflector and a discrete reflector thickness comparison between the sublisting parameters, which yield a maximum subcritical moderator mass for a discrete reflector thickness of 0.001 cm.

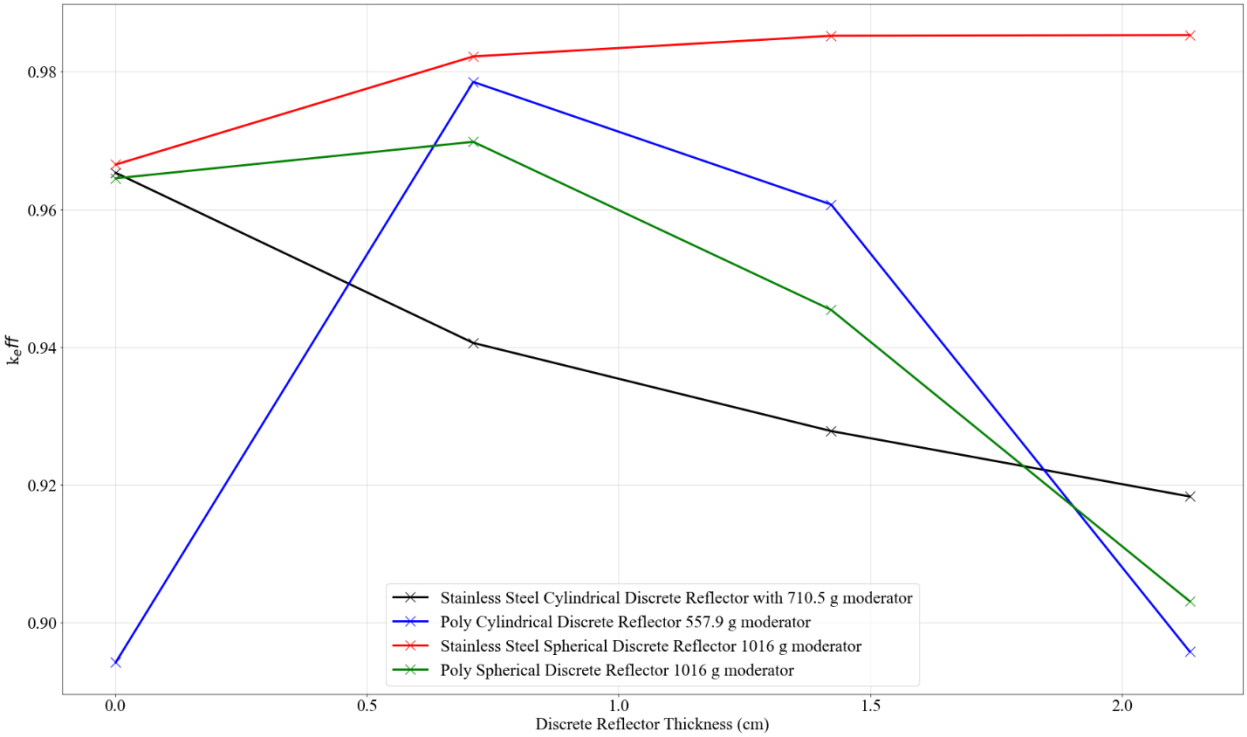

Figure O-5. Set-8a and set-1 maximum k_{eff} results (three-high uniform array model) overall sublistings as a function of discrete reflector thickness.

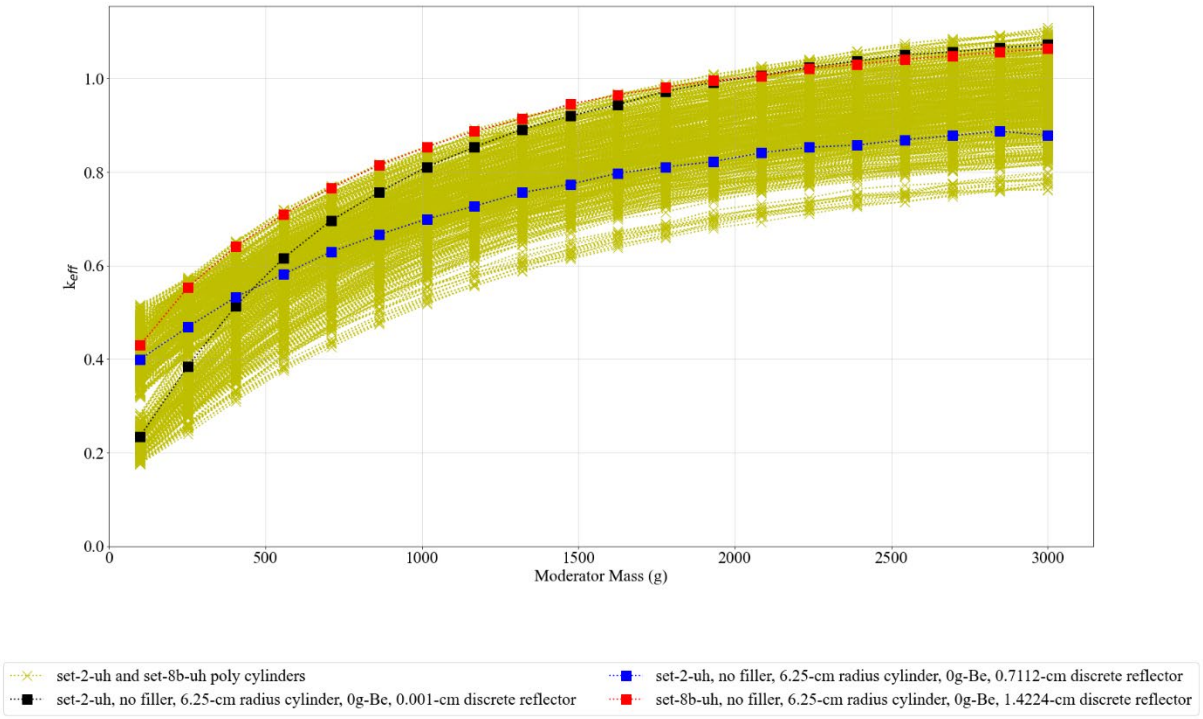

Figure O-6. Set-8b and set-2-uh k_{eff} results (nonuniform array model) for the cylindrical waste forms with a poly discrete reflector and a discrete reflector thickness comparison between the sublisting parameters, which yield a maximum subcritical moderator mass for a discrete reflector thickness of 0.001 cm.

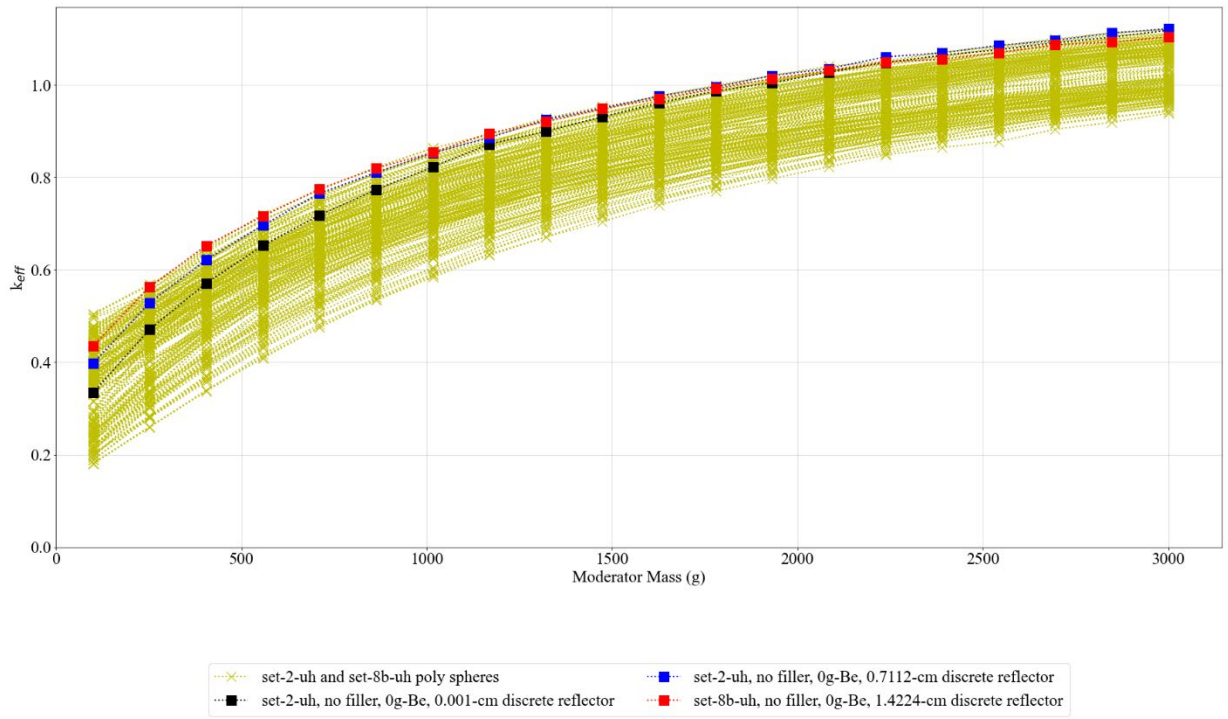

Figure O-7. Set-8b and set-2-uh k_{eff} results (nonuniform array model) for the spherical waste forms with a poly discrete reflector and a discrete reflector thickness comparison between the sublisting parameters, which yield a maximum subcritical moderator mass for a discrete reflector thickness of 0.001 cm.

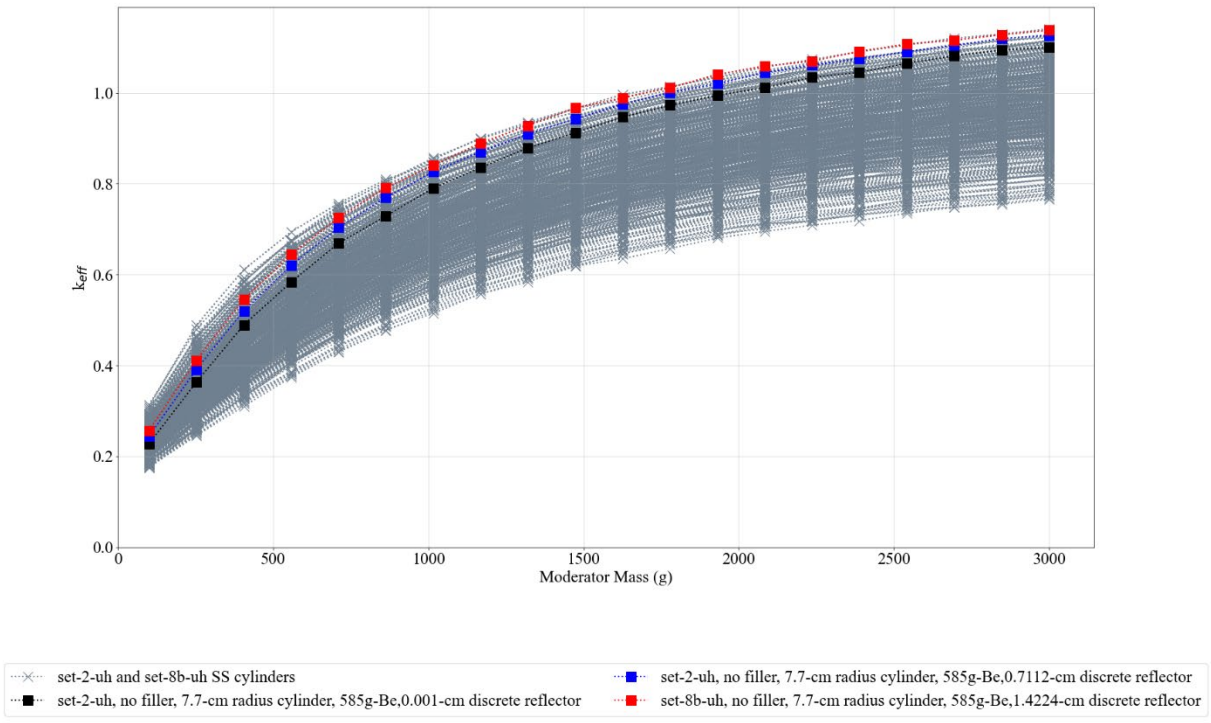

Figure O-8. Set-8b and set-2-uh k_{eff} results (nonuniform array model) for the cylindrical waste forms with a stainless-steel discrete reflector and a discrete reflector thickness comparison between the sublisting parameters, which yield a maximum subcritical moderator mass for a discrete reflector thickness of 0.001 cm.

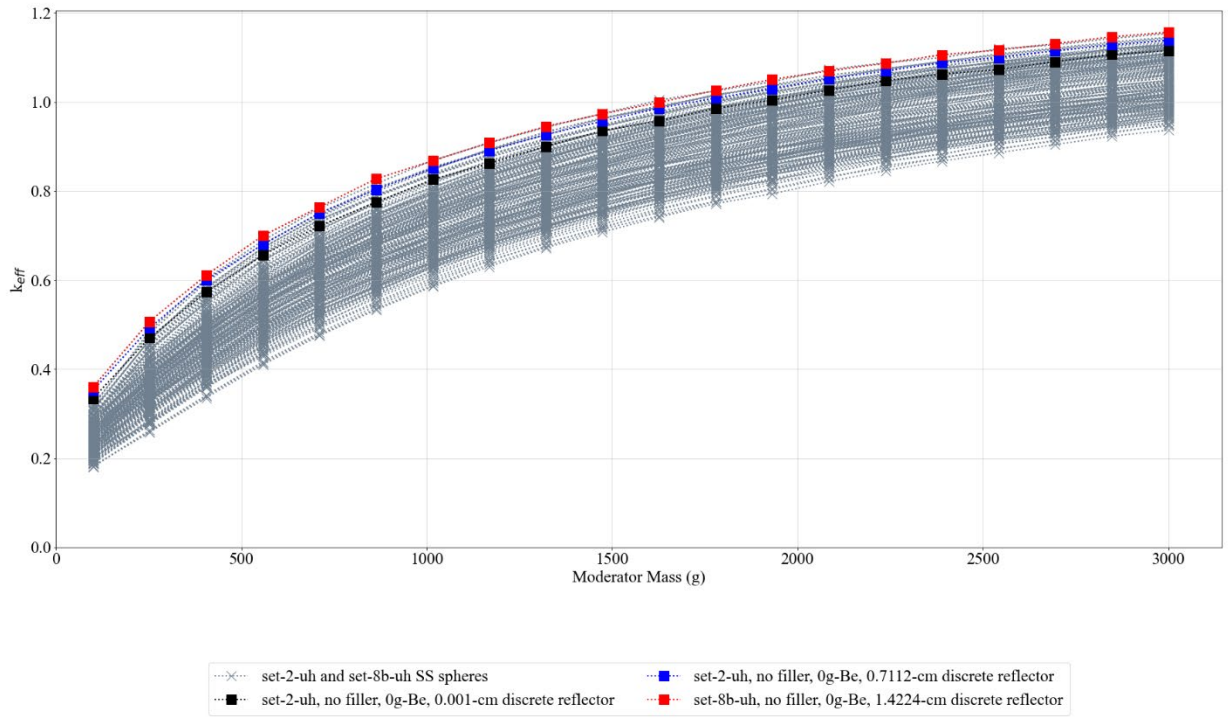

Figure O-9. Set-8b and set-2-uh k_{eff} results (nonuniform array model) for the spherical waste forms with a stainless-steel discrete reflector and a discrete reflector thickness comparison between the sublisting parameters, which yield a maximum subcritical moderator mass for a discrete reflector thickness of 0.001 cm.

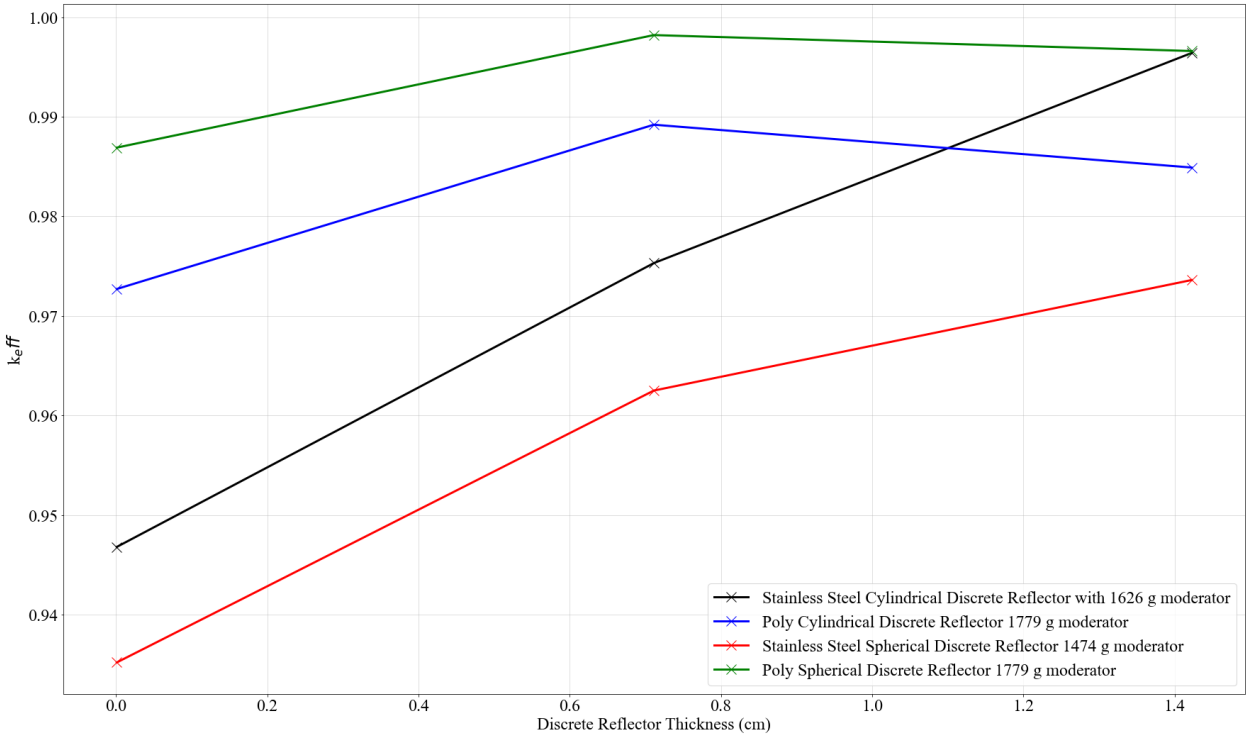

Figure O-10. Set-8b and set-2-uh maximum k_{eff} results (nonuniform array model) overall sublistings as a function of discrete reflector thickness.

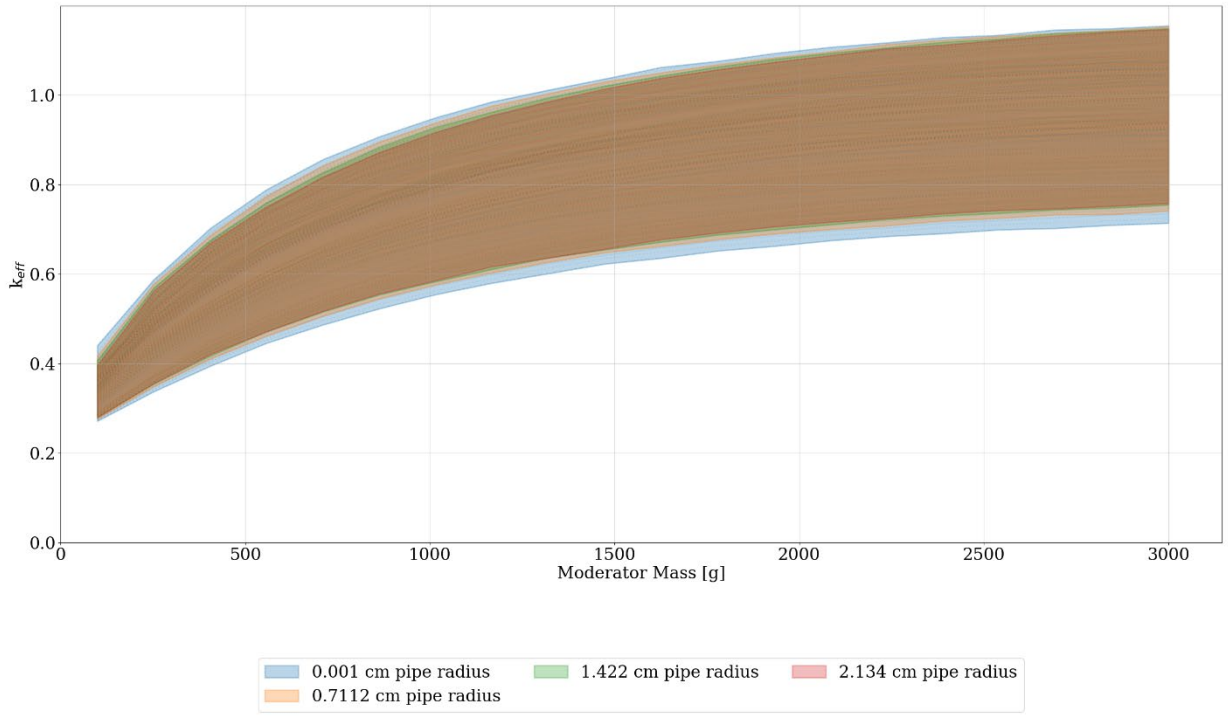

Figure O-11. Set-8a sublisting-1 results (three-high uniform array model): k_{eff} for set-1 and set-8a by discrete reflector thicknesses.

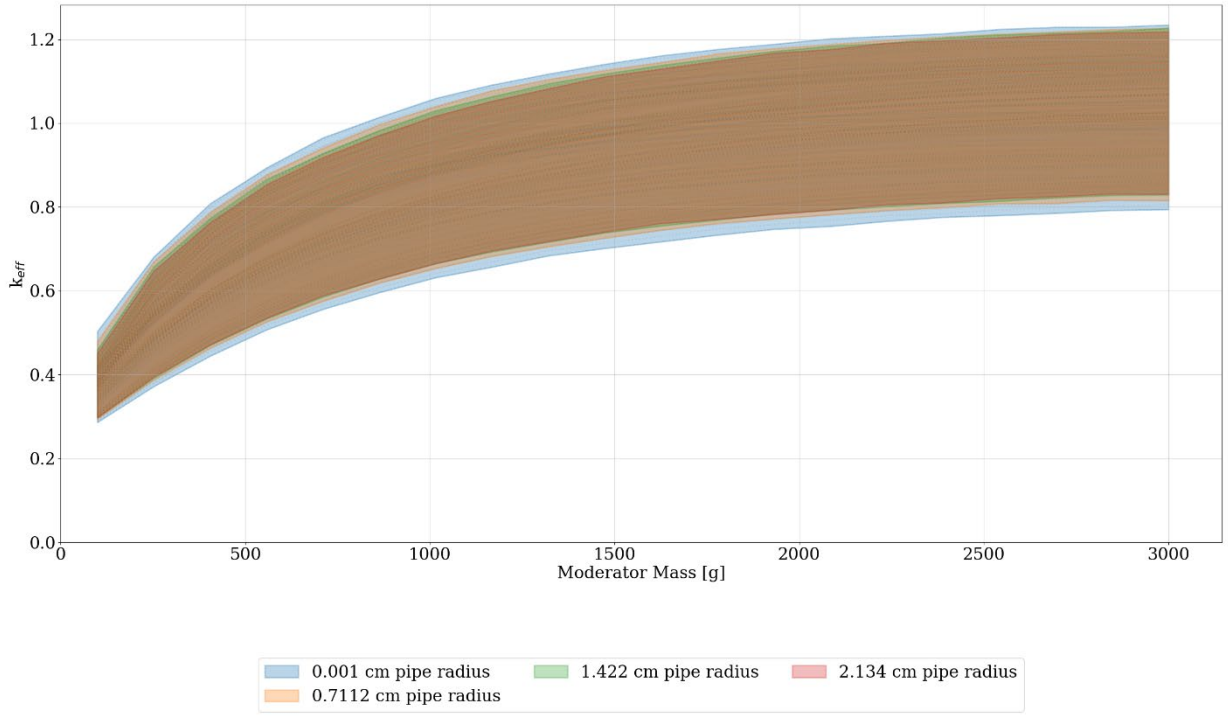

Figure O-12. Set-8a sublisting-2 results (three-high uniform array model): k_{eff} for set-1 and set-8a by discrete reflector thicknesses.

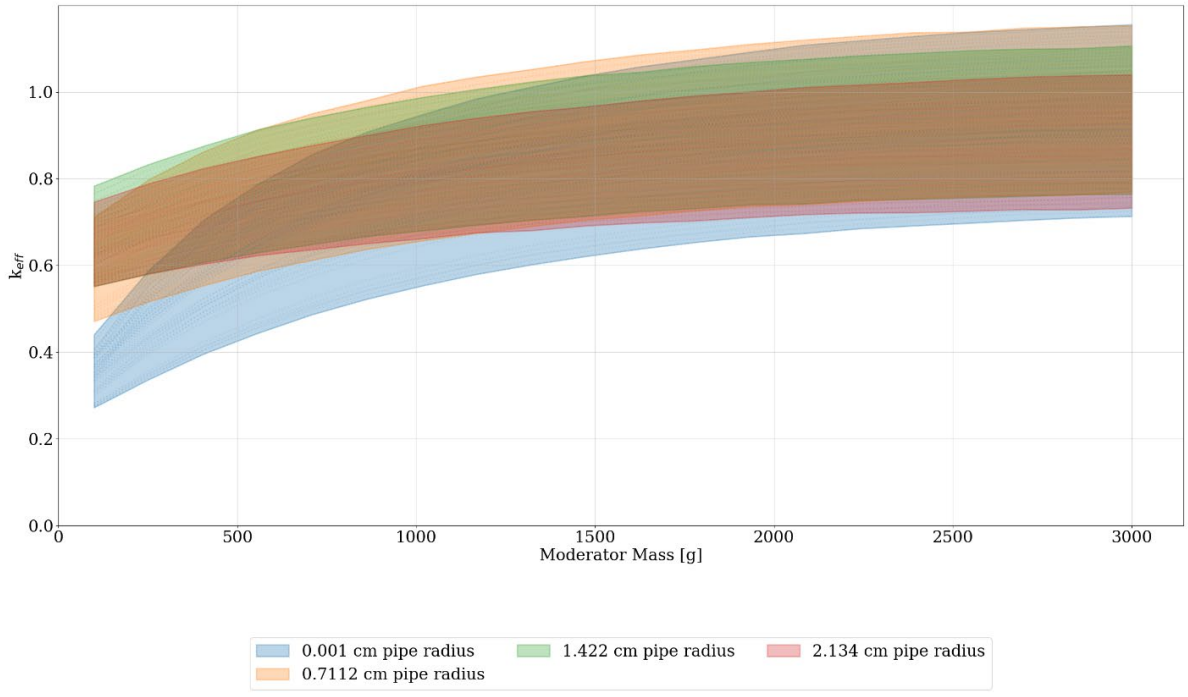

Figure O-13. Set-8a sublisting-3 results (three-high uniform array model):): k_{eff} for set-1 and set-8a by discrete reflector thicknesses.

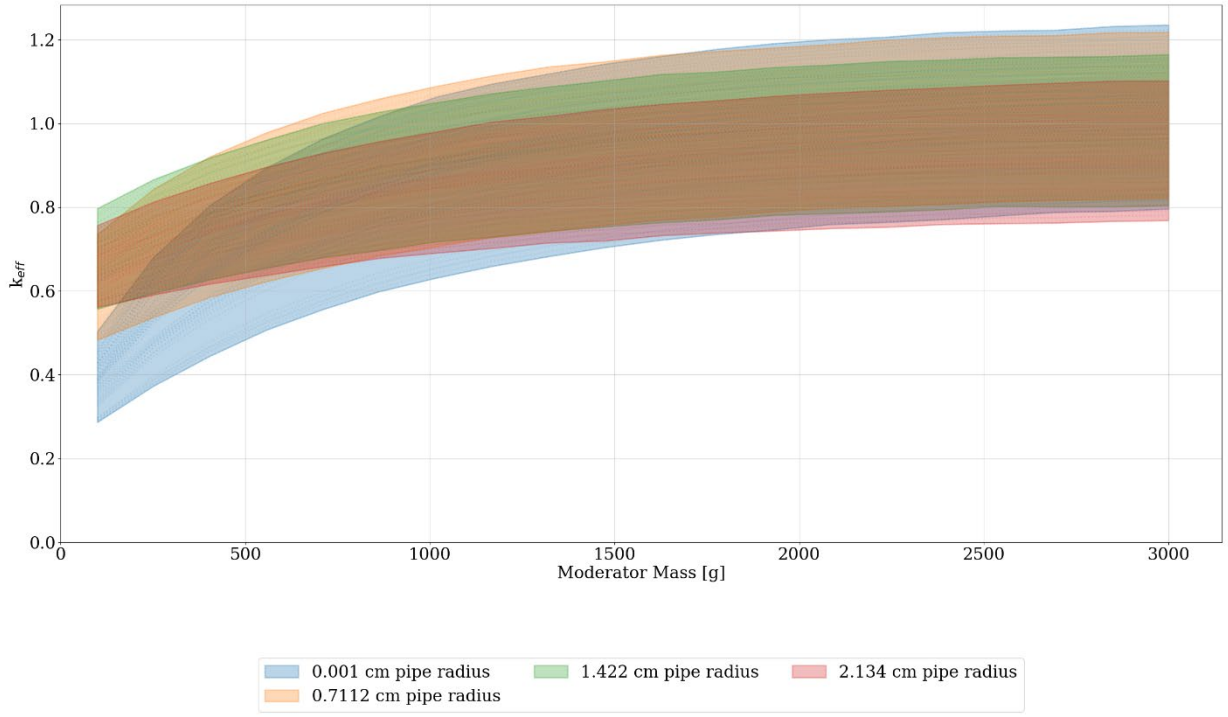

Figure O-14. Set-8a sublisting-4 results (three-high uniform array model): k_{eff} for set-1 and set-8a by discrete reflector thicknesses.

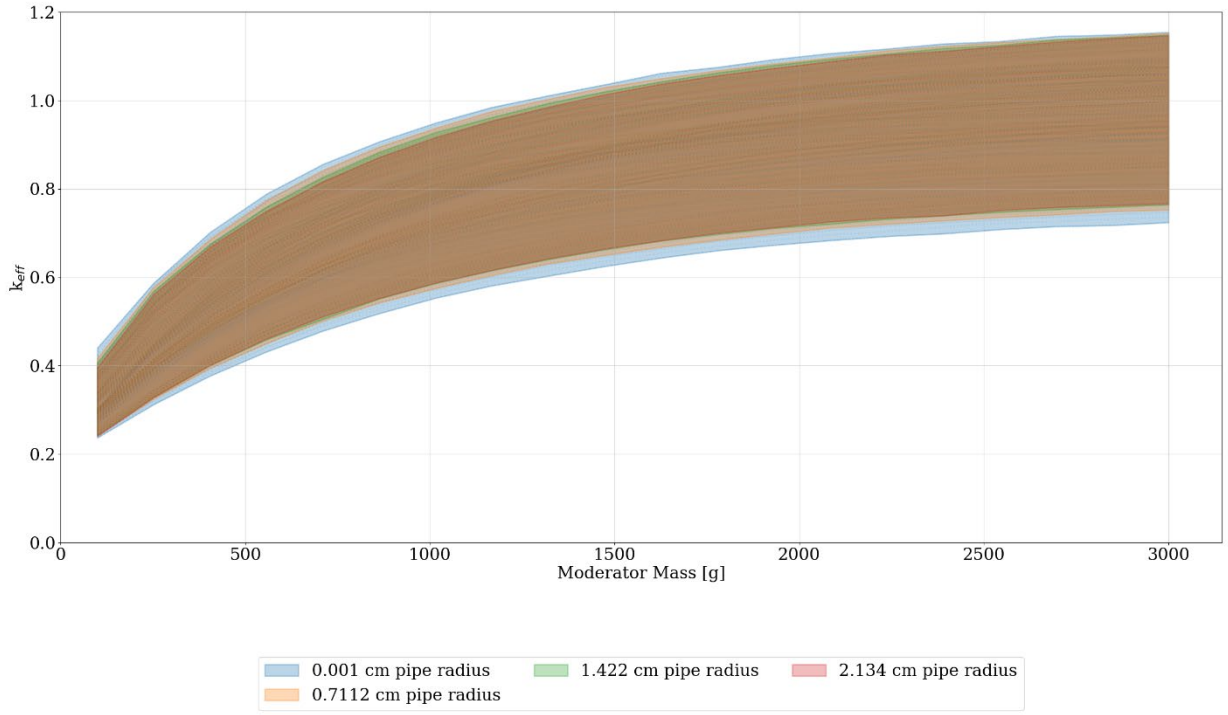

Figure O-15. Set-8a sublisting-5 results (three-high uniform array model): k_{eff} for set-1 and set-8a by discrete reflector thicknesses.

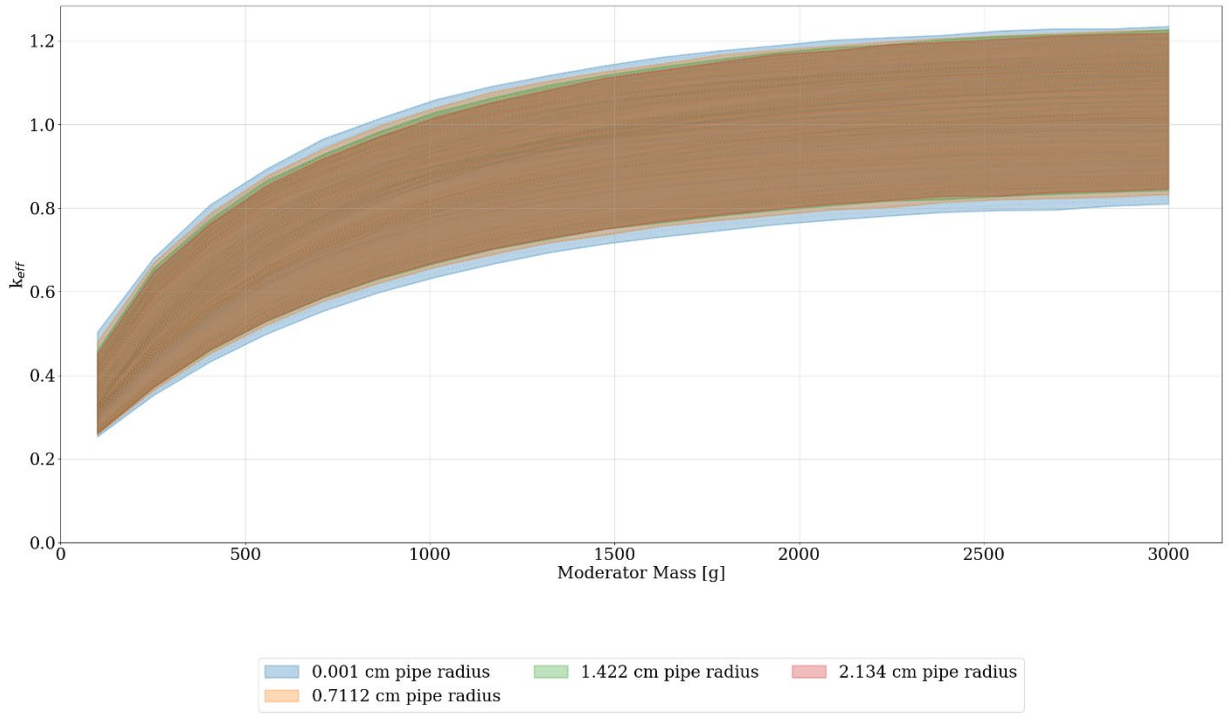

Figure O-16. Set-8a sublisting-6 results (three-high uniform array model): k_{eff} for set-1 and set-8a by discrete reflector thicknesses.

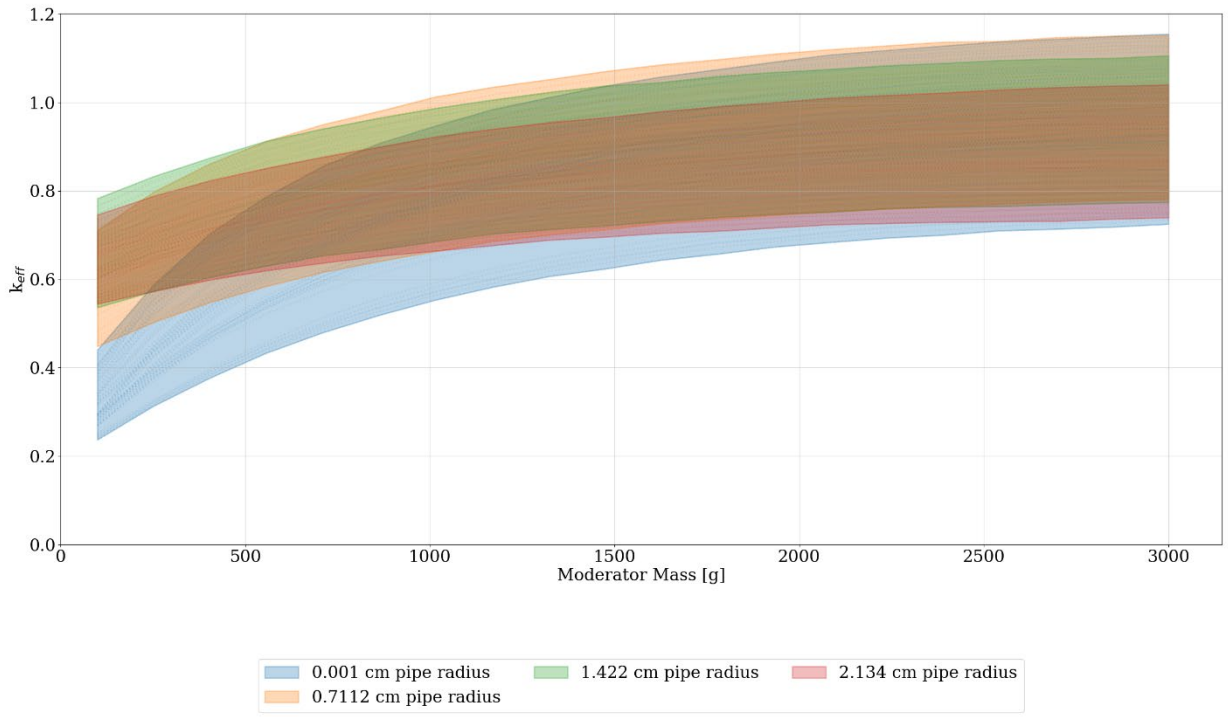

Figure O-17. Set-8a sublisting-7 results (three-high uniform array model): k_{eff} for set-1 and set-8a by discrete reflector thicknesses.

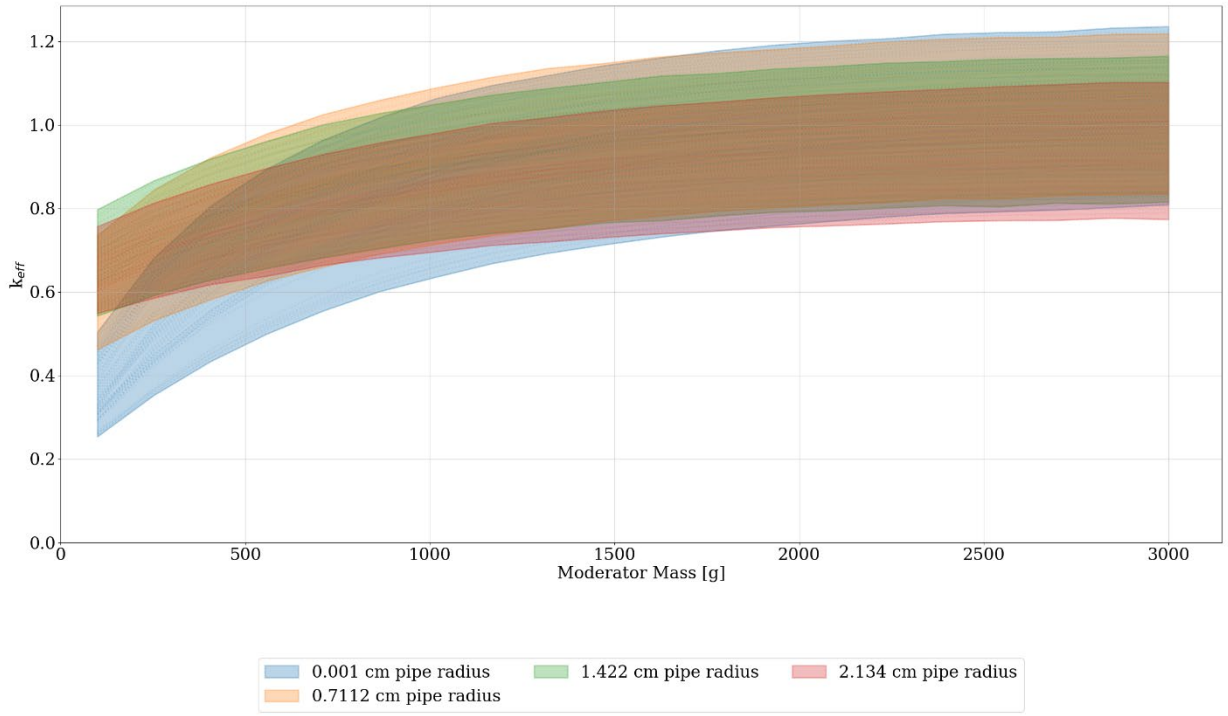

Figure O-18. Set-8a sublisting-8 results (three-high uniform array model): k_{eff} for set-1 and set-8a by discrete reflector thicknesses.

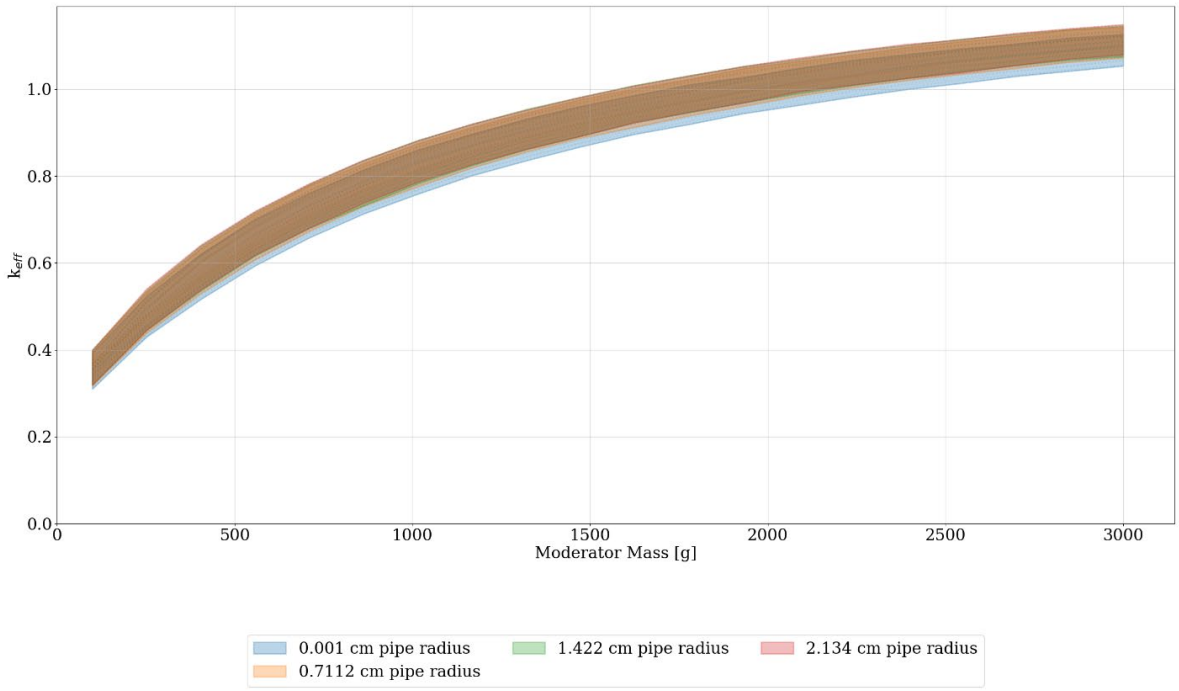

Figure O-19. Set-8a sublisting-9 results (three-high uniform array model): k_{eff} for set-1 and set-8a by discrete reflector thicknesses.

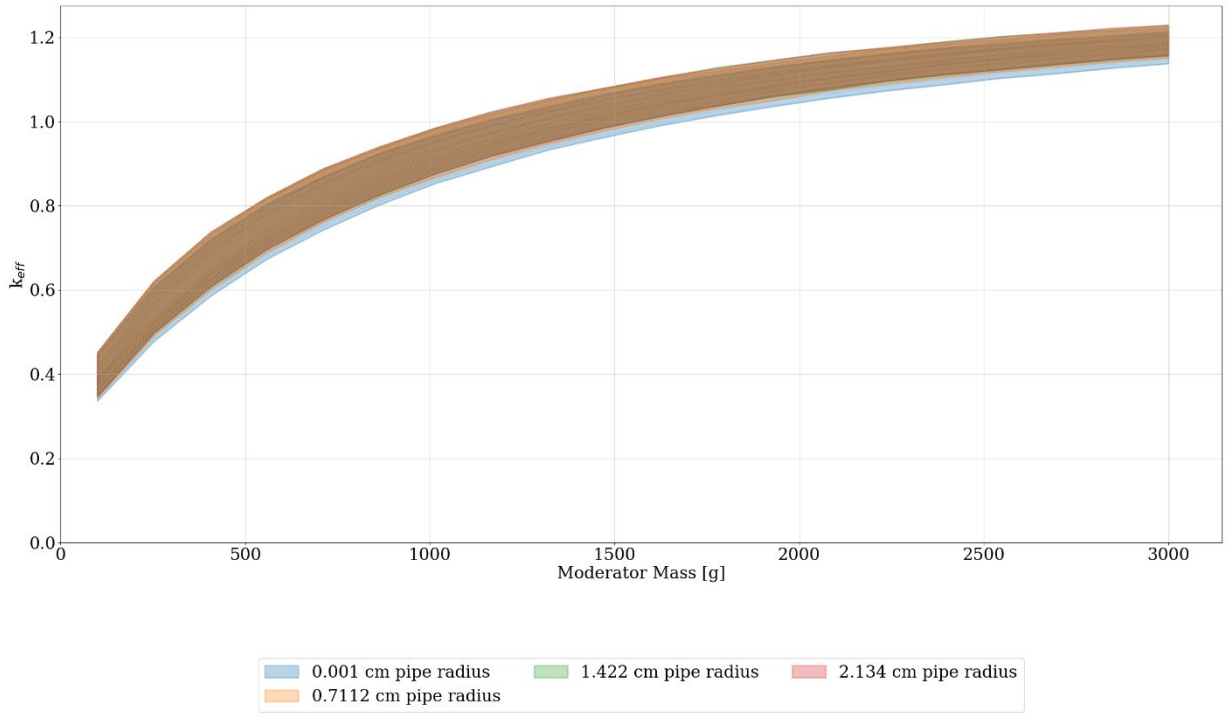

Figure O-20. Set-8a sublisting-10 results (three-high uniform array model): k_{eff} for set-1 and set-8a by discrete reflector thicknesses.

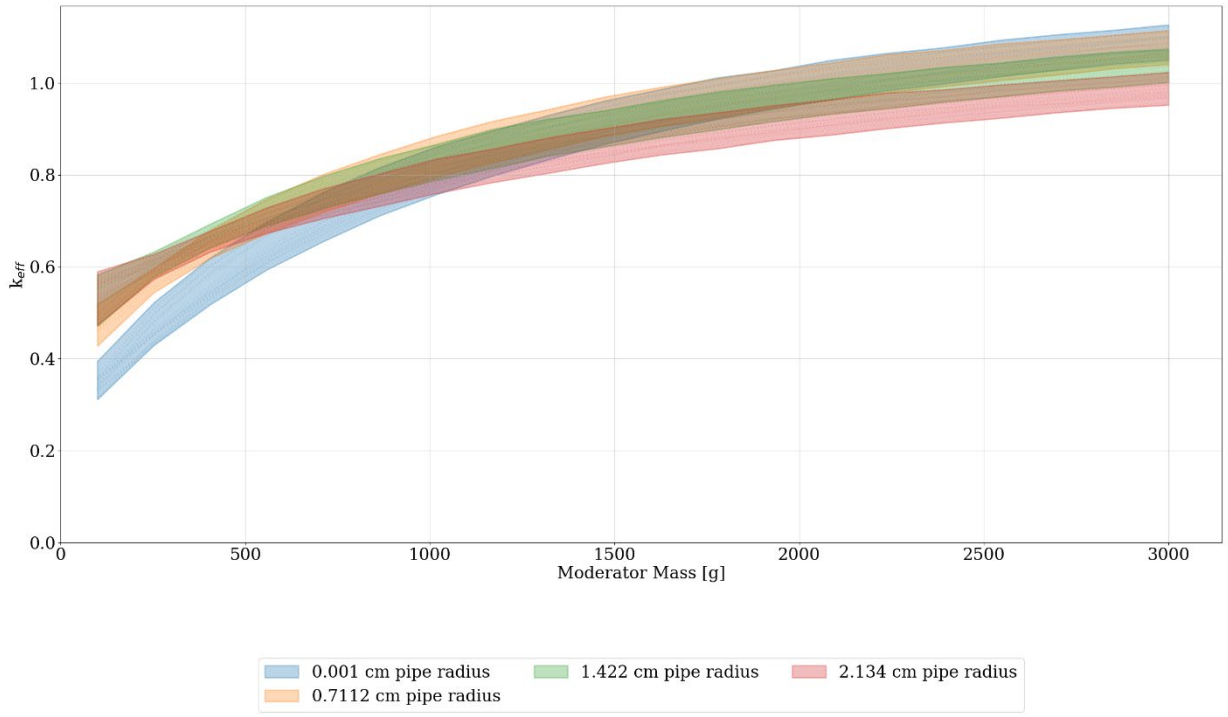

Figure O-21. Set-8a sublisting-11 results (three-high uniform array model): k_{eff} for set-1 and set-8a by discrete reflector thicknesses.

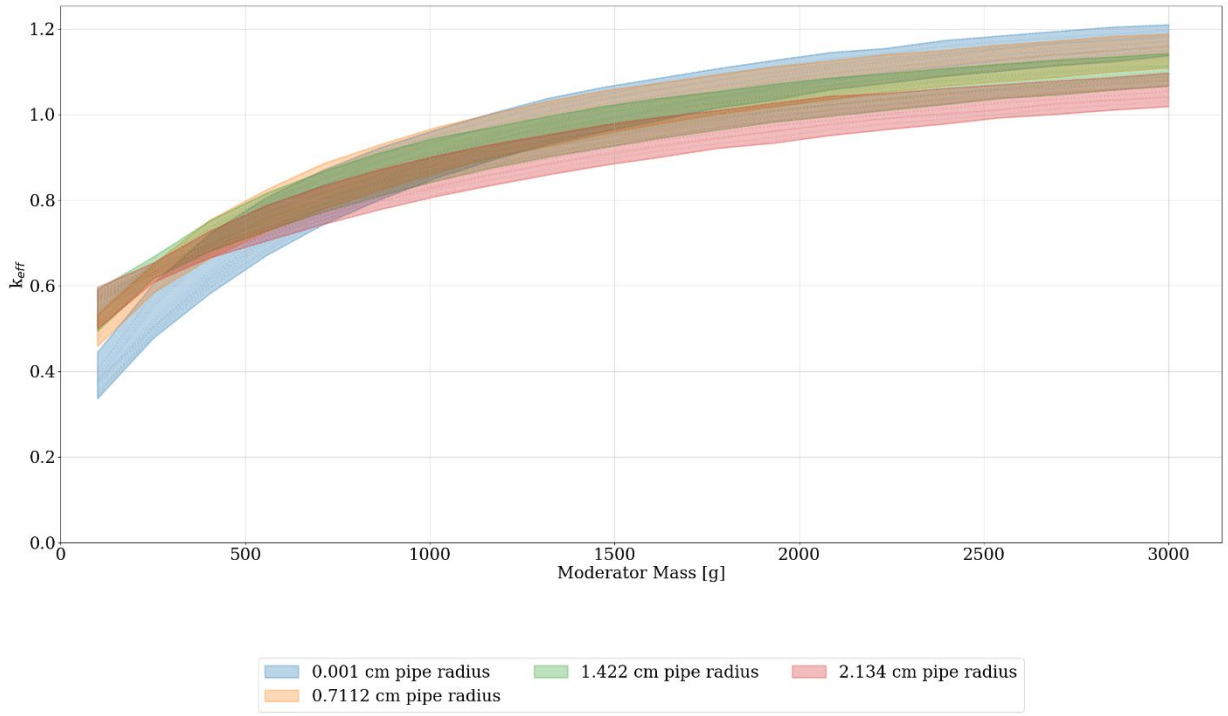

Figure O-22. Set-8a sublisting-12 results (three-high uniform array model): k_{eff} for set-1 and set-8a by discrete reflector thicknesses.

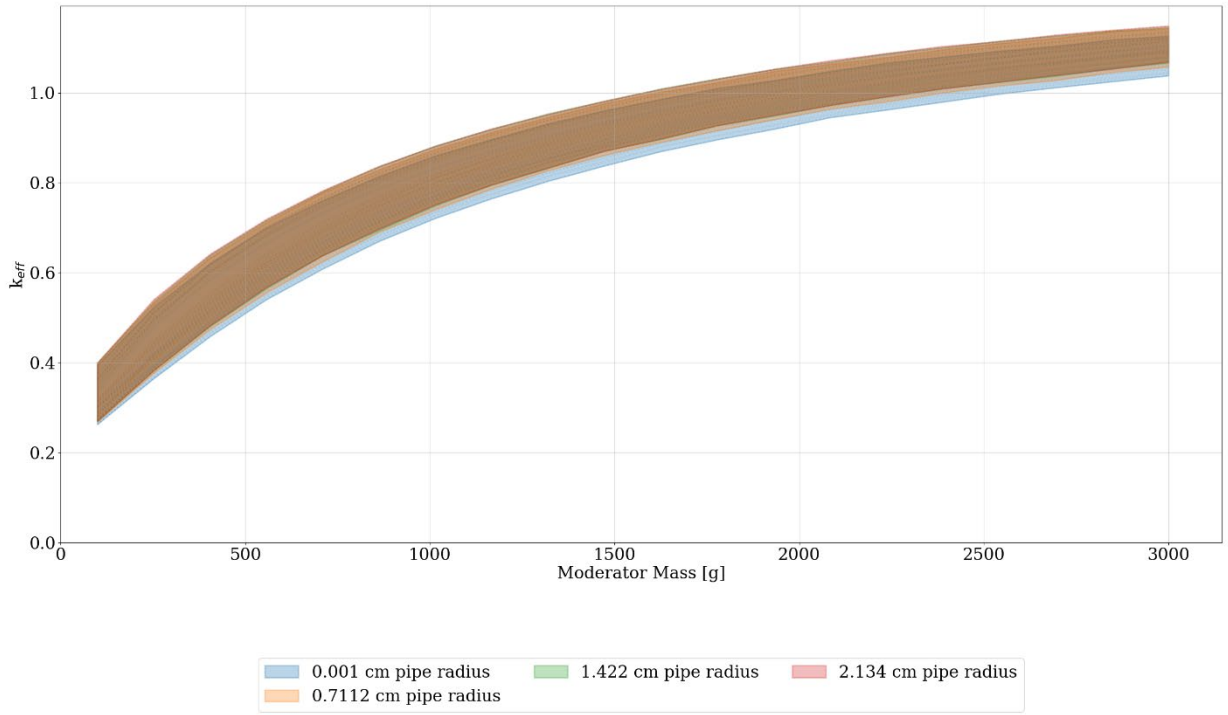

Figure O-23. Set-8a sublisting-13 results (three-high uniform array model): k_{eff} for set-1 and set-8a by discrete reflector thicknesses.

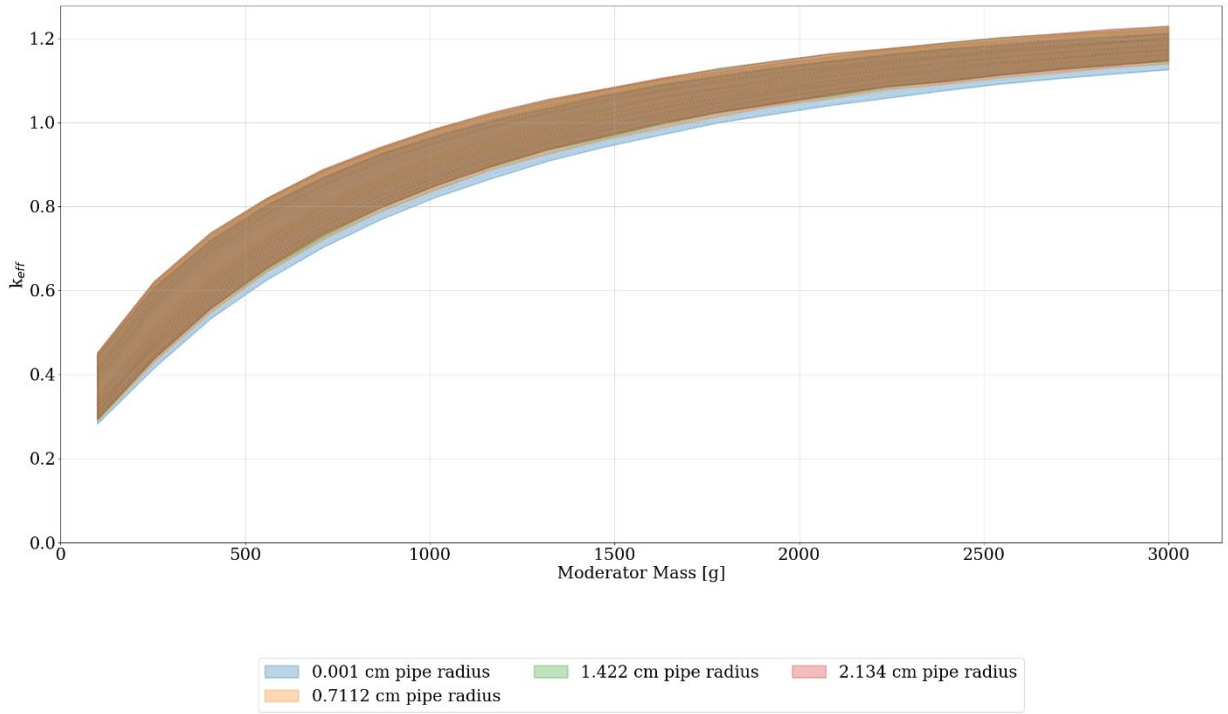

Figure O-24. Set-8a sublisting-14 results (three-high uniform array model): k_{eff} for set-1 and set-8a by discrete reflector thicknesses.

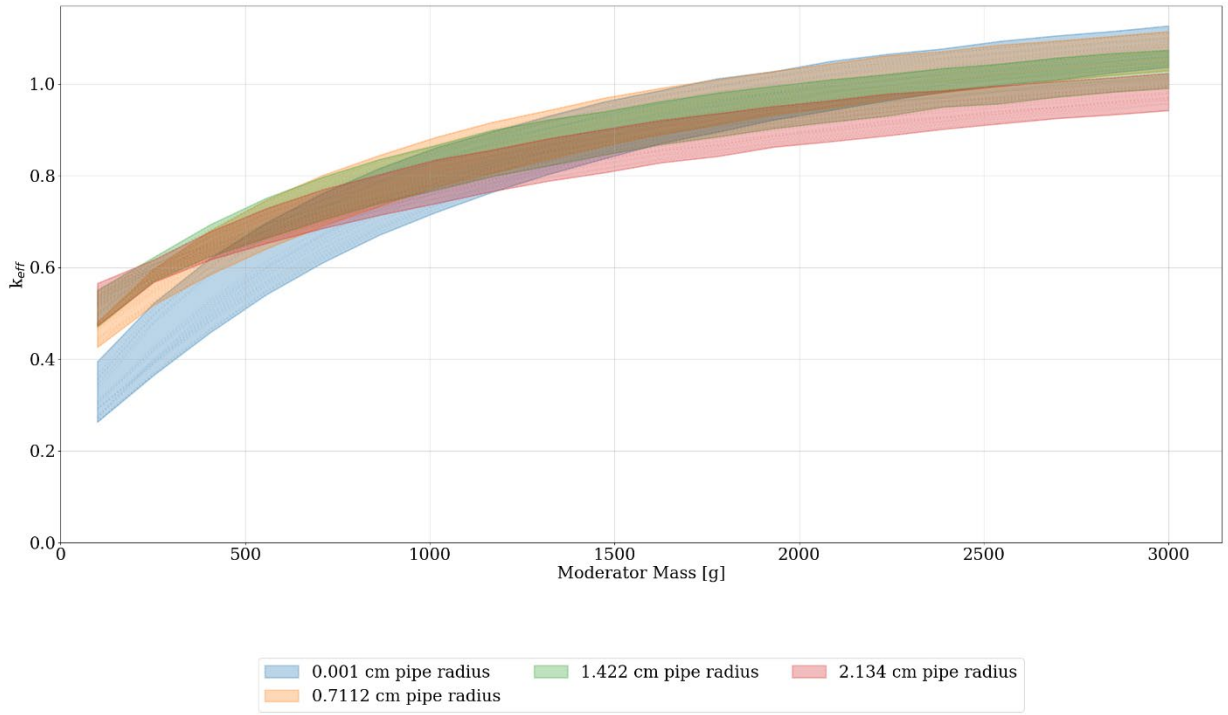

Figure O-25**. Set-8a sublisting-15 results (three-high uniform array model): k_{eff} for set-1 and set-8a by discrete reflector thicknesses.**

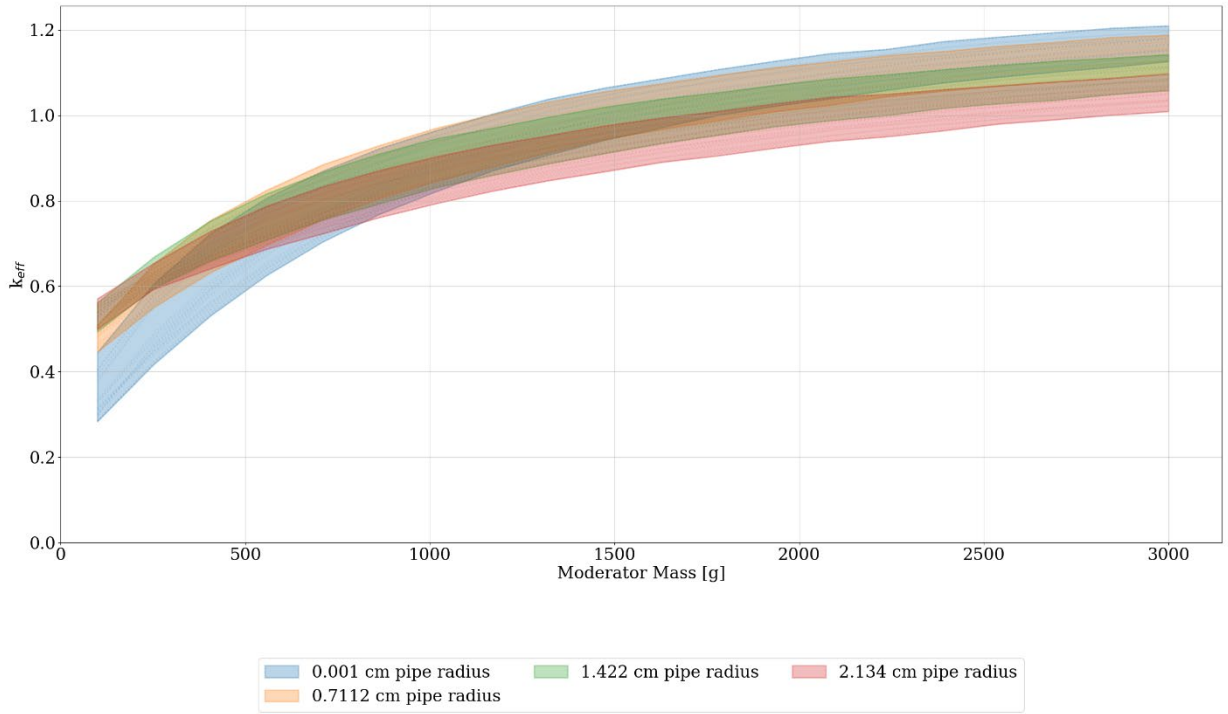

Figure O-26. Set-8a sublisting-16 results (three-high uniform array model): k_{eff} for set-1 and set-8a by discrete reflector thicknesses.

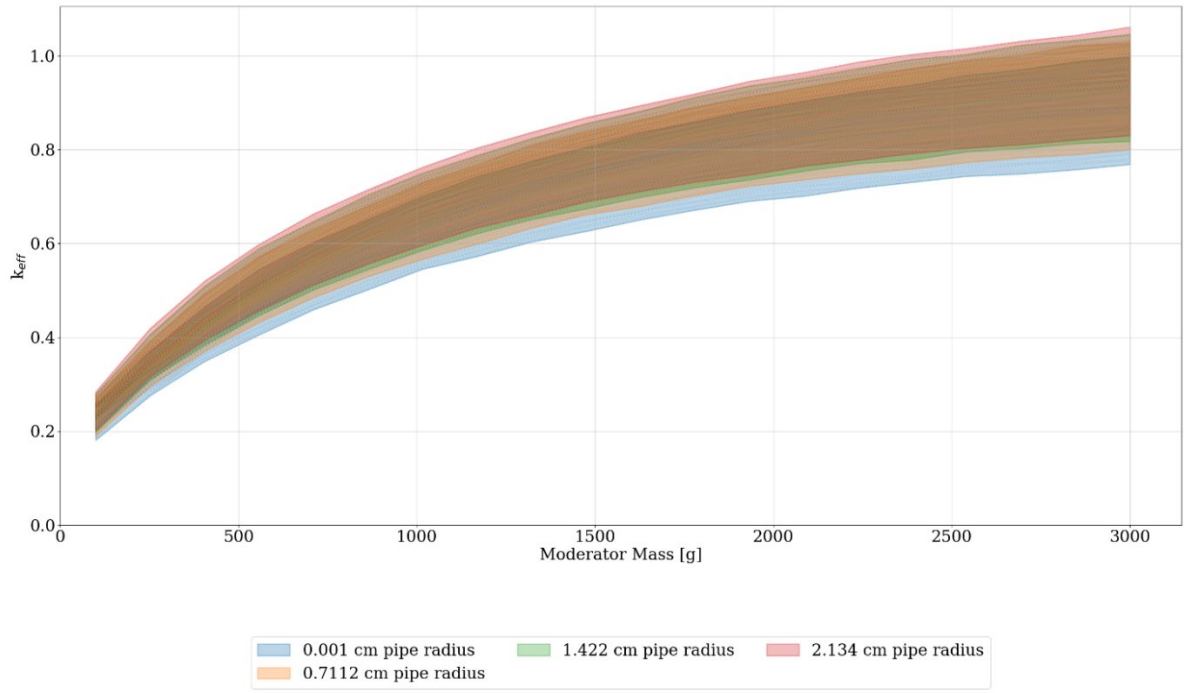

Figure O-27. Set-8b sublisting-1 results (nonuniform array model): k_{eff} for set-2-uh and set-8a by discrete reflector thicknesses.

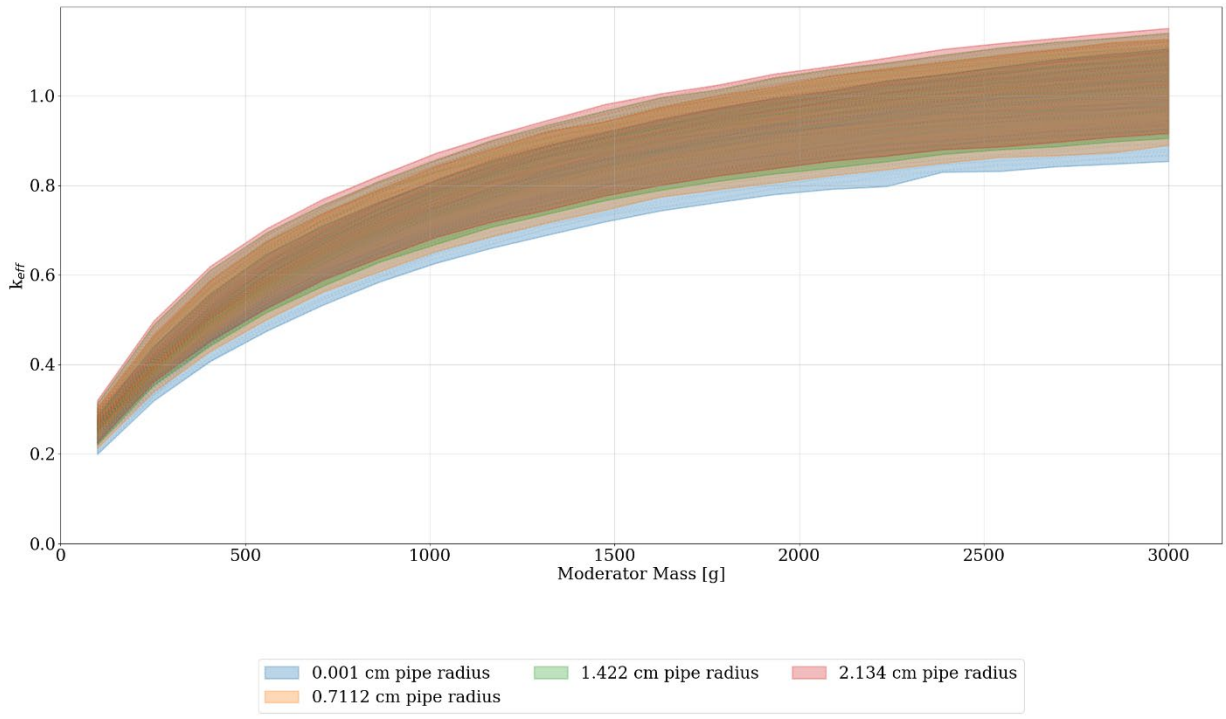

Figure O-28. Set-8b sublisting-2 results (nonuniform array model): k_{eff} for set-2-uh and set-8a by discrete reflector thicknesses.

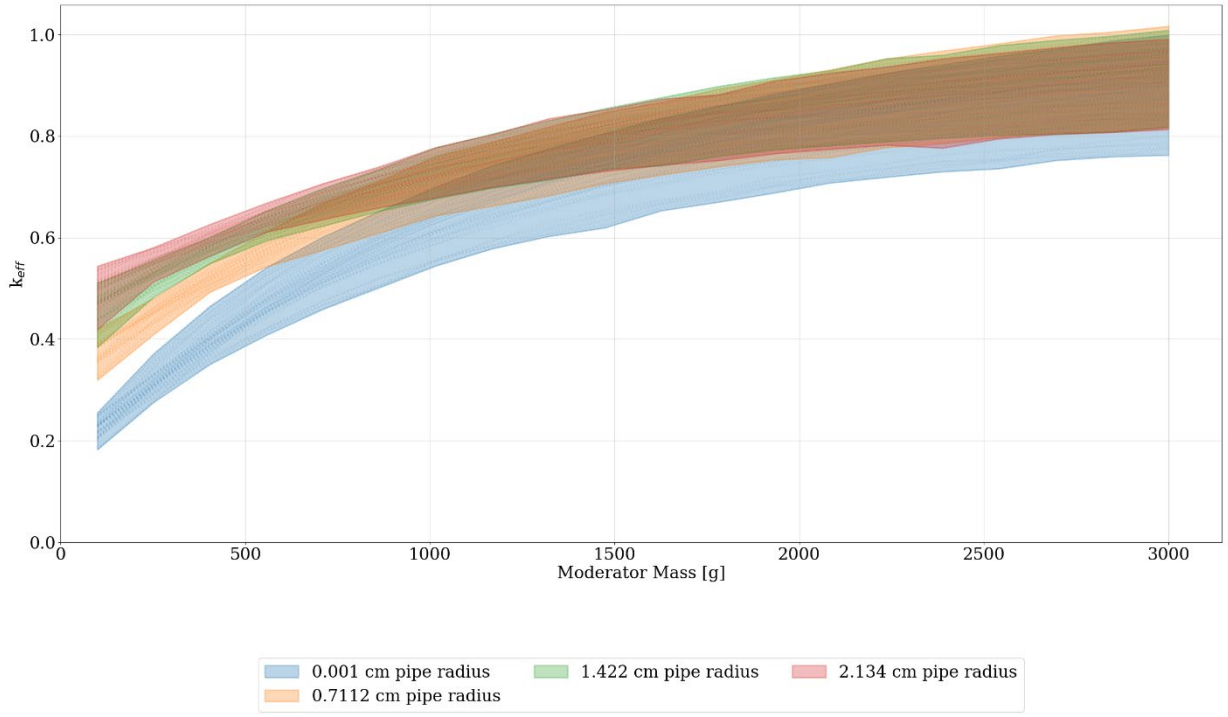

Figure O-29**. Set-8b sublisting-3 results (nonuniform array model): k_{eff} for set-2-uh and set-8a by discrete reflector thicknesses.**

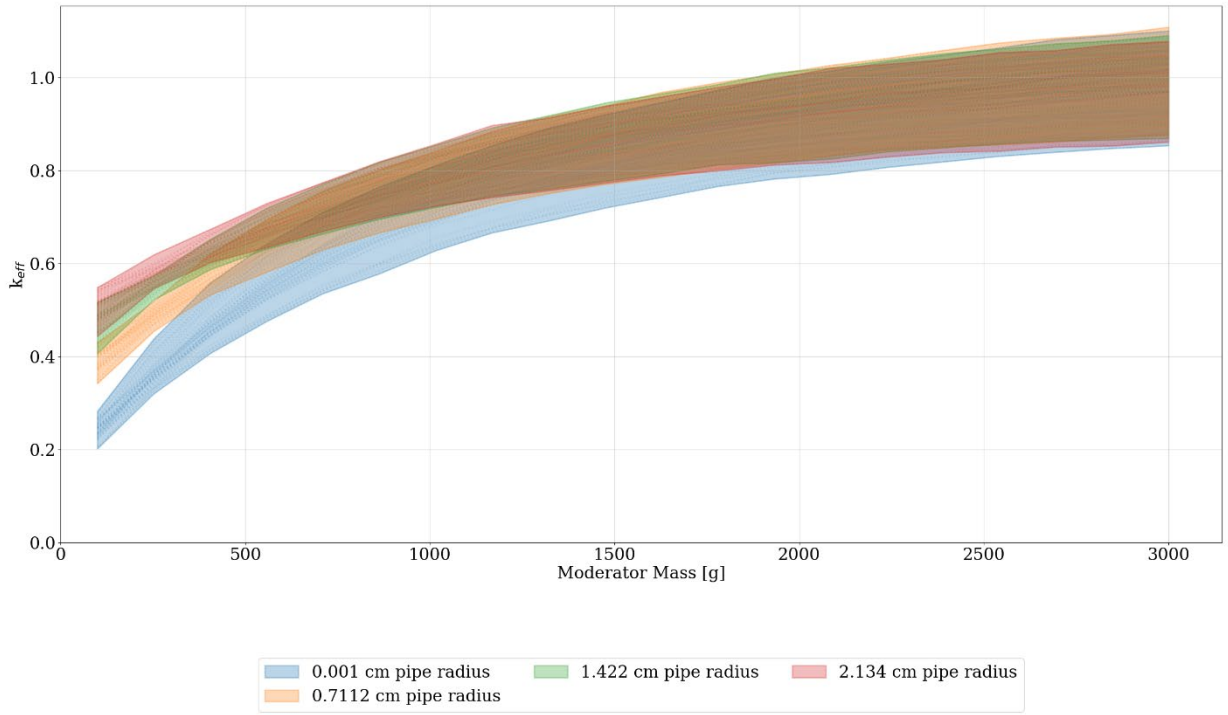

Figure O-30. Set-8b sublisting-4 results (three-high uniform array model): k_{eff} for set-2-uh and set-8a by discrete reflector thicknesses.

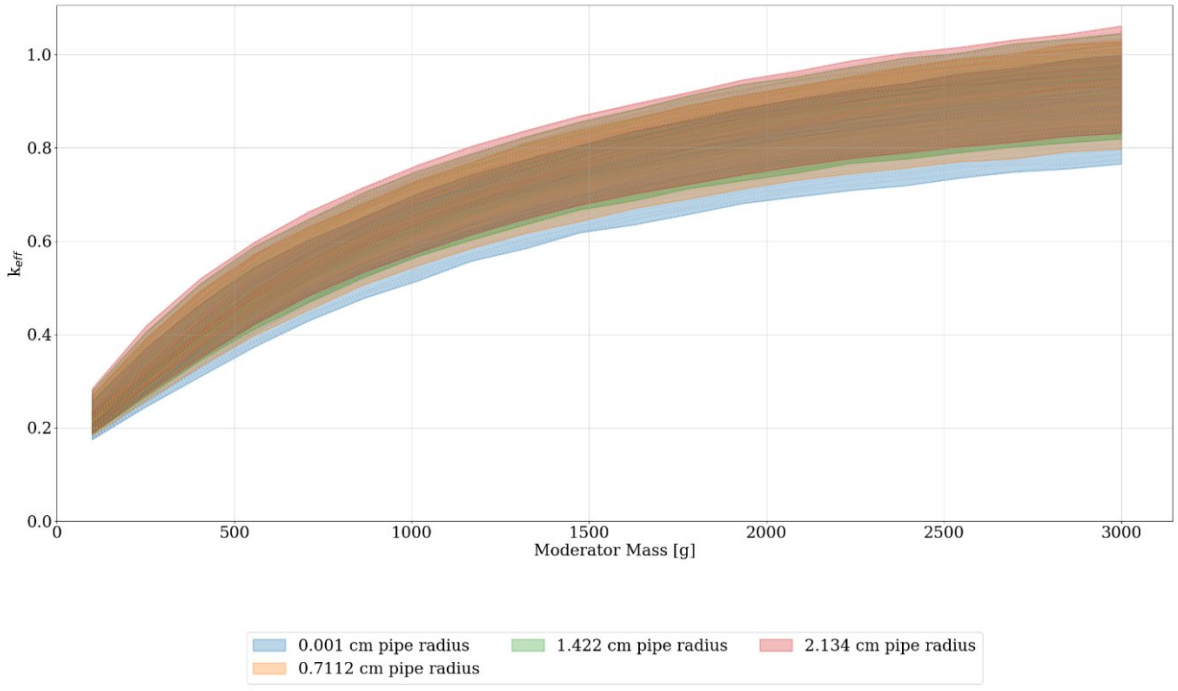

Figure O-31**. Set-8b sublisting-5 results (nonuniform array model): k_{eff} for set-2-uh and set-8a by discrete reflector thicknesses.**

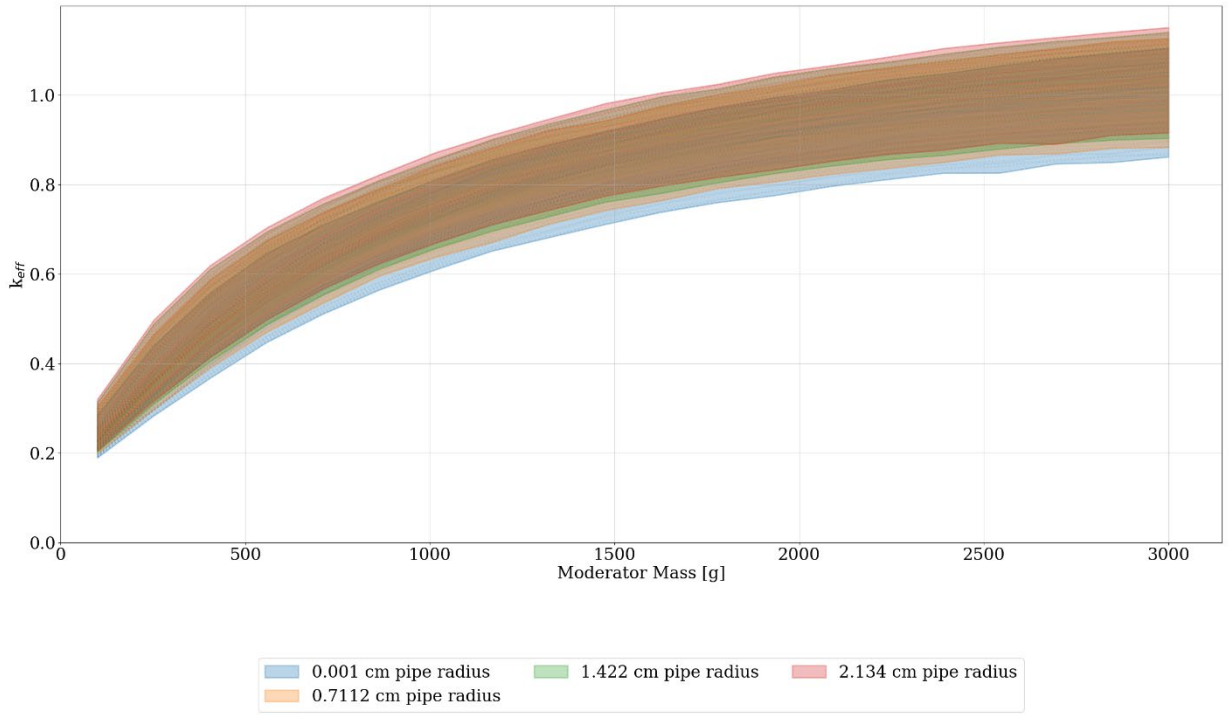

Figure O-32. Set-8b sublisting-6 results (nonuniform array model): k_{eff} for set-2-uh and set-8a by discrete reflector thicknesses.

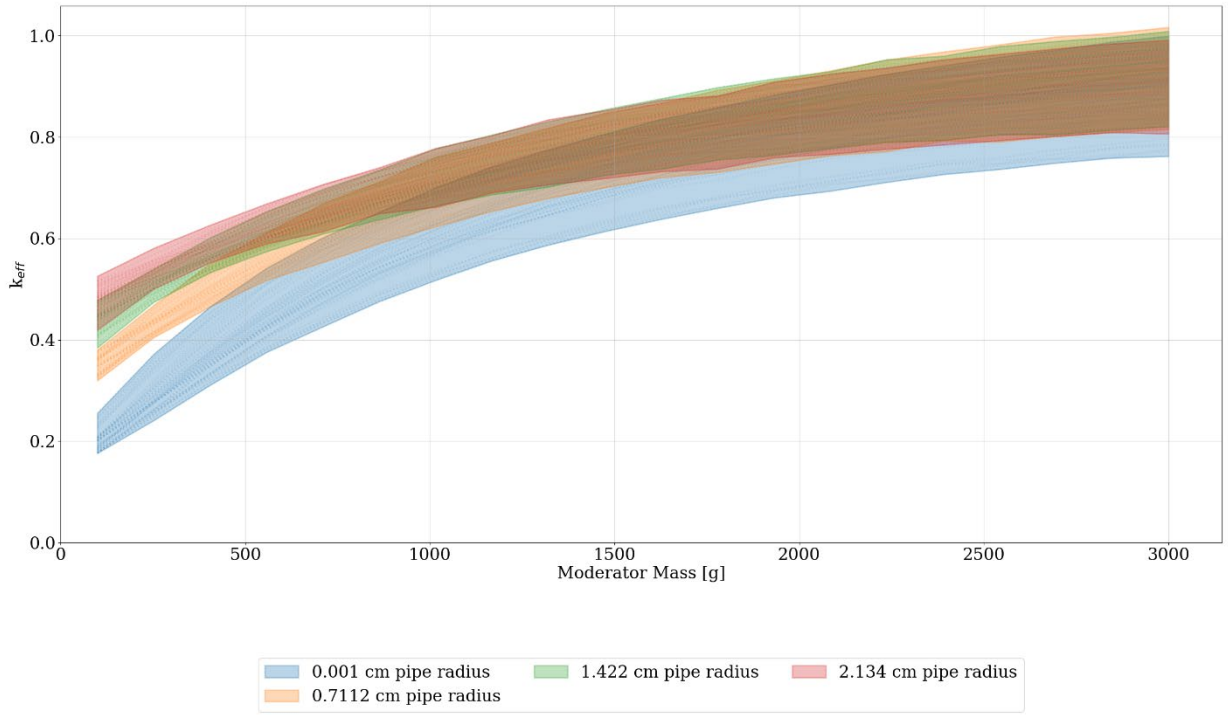

Figure O-33**. Set-8b sublisting-7 results (nonuniform array model): k_{eff} for set-2-uh and set-8a by discrete reflector thicknesses.**

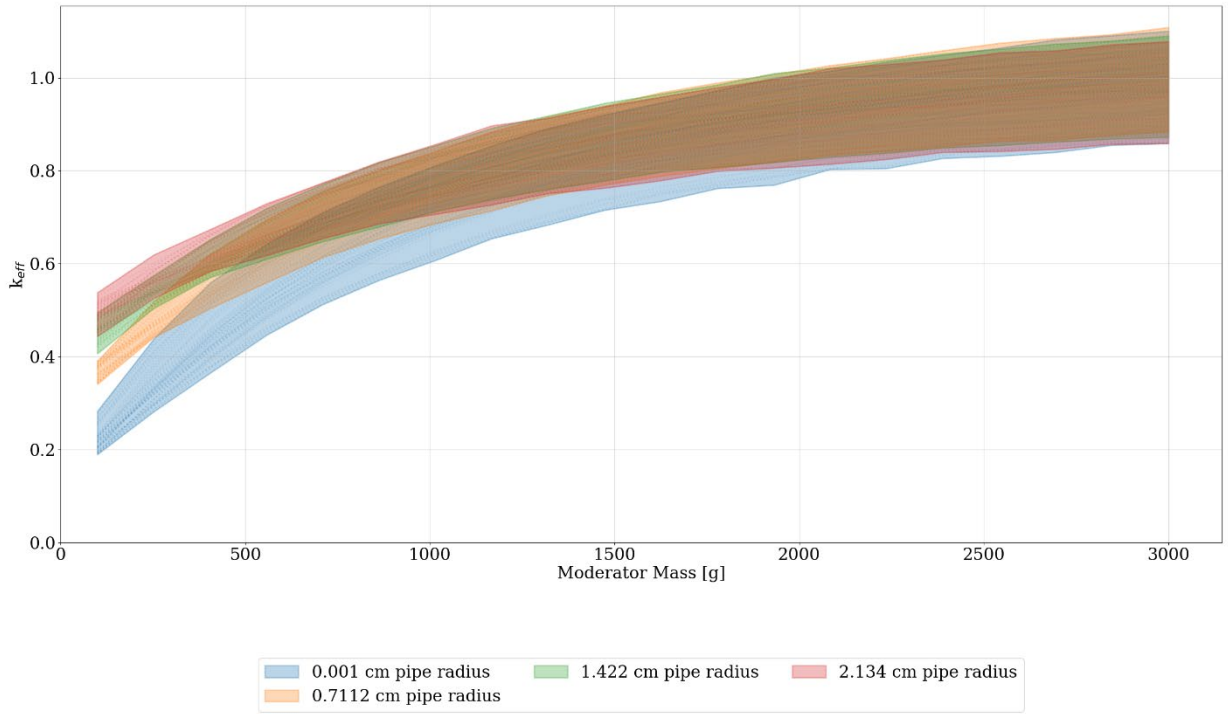

Figure O-34. Set-8b sublisting-8 results (nonuniform array model): k_{eff} for set-2-uh and set-8a by discrete reflector thicknesses.

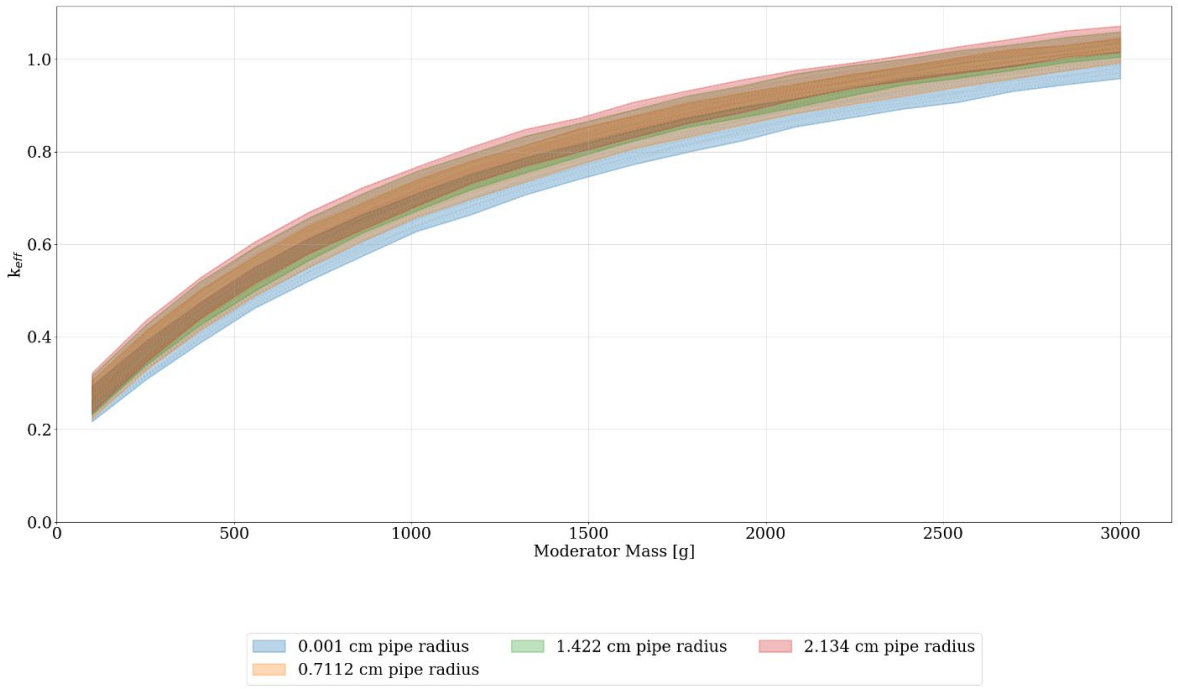

Figure O-35**. Set-8a sublisting-9 results (nonuniform array model): k_{eff} for set-2-uh and set-8a by discrete reflector thicknesses.**

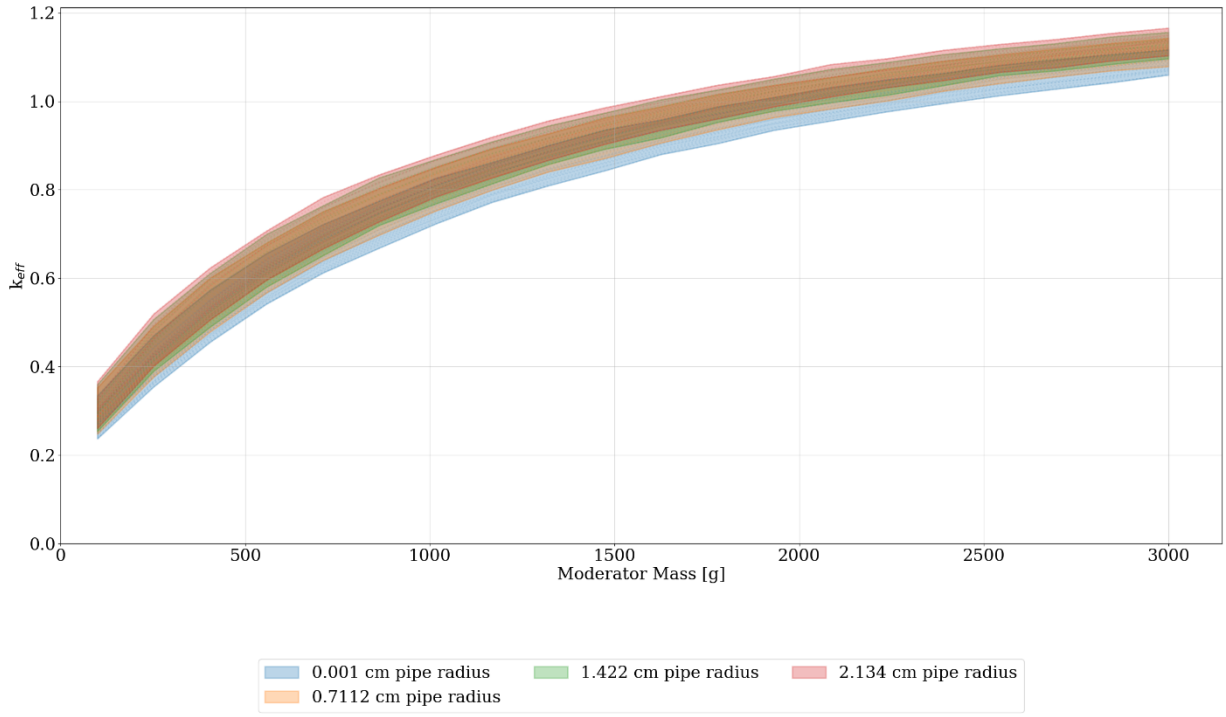

Figure O-36. Set-8a sublisting-10 results (nonuniform array model): k_{eff} for set-2-uh and set-8a by discrete reflector thicknesses.

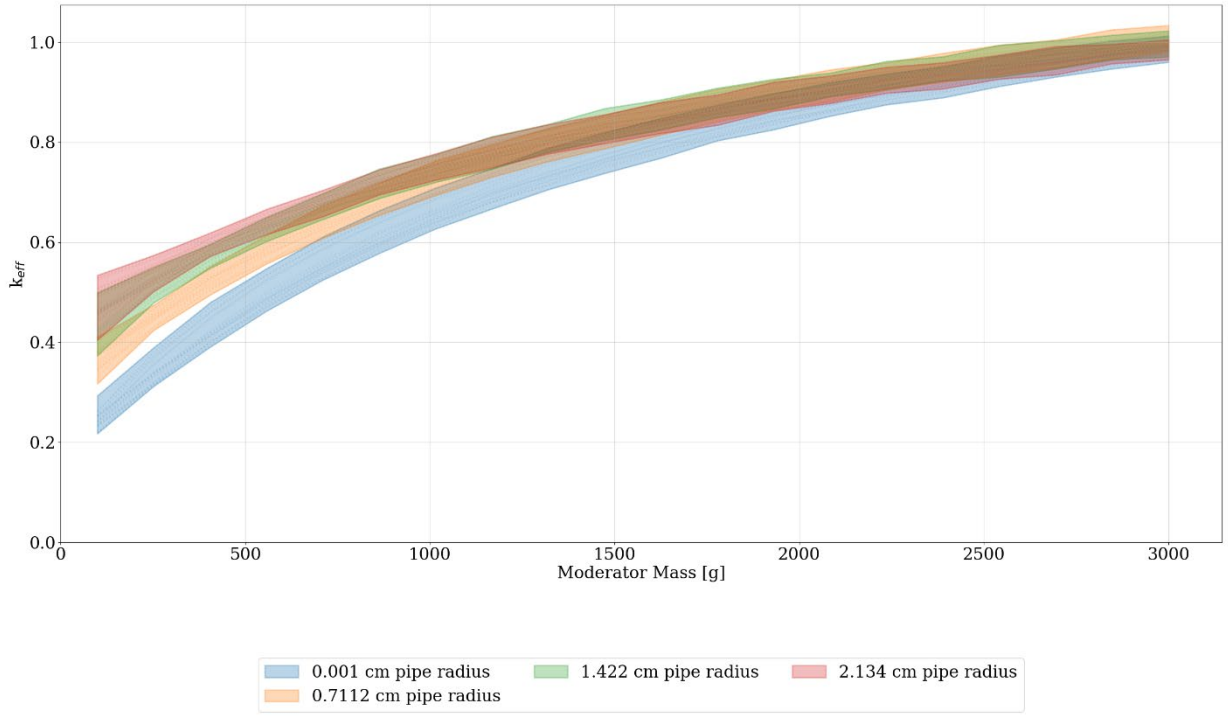

Figure O-37**. Set-8b sublisting-11 results (nonuniform array model): k_{eff} for set-2-uh and set-8a by discrete reflector thicknesses.**

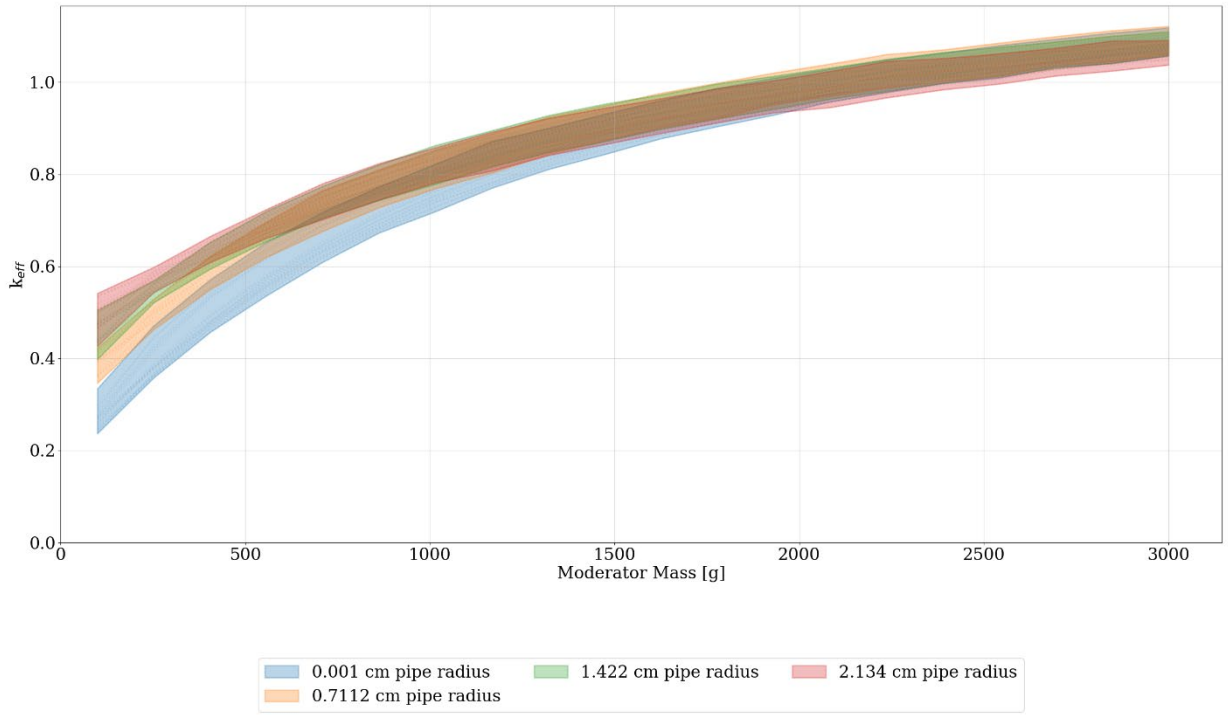

Figure O-38. Set-8b sublisting-12 results (nonuniform array model): k_{eff} for set-2-uh and set-8a by discrete reflector thicknesses.

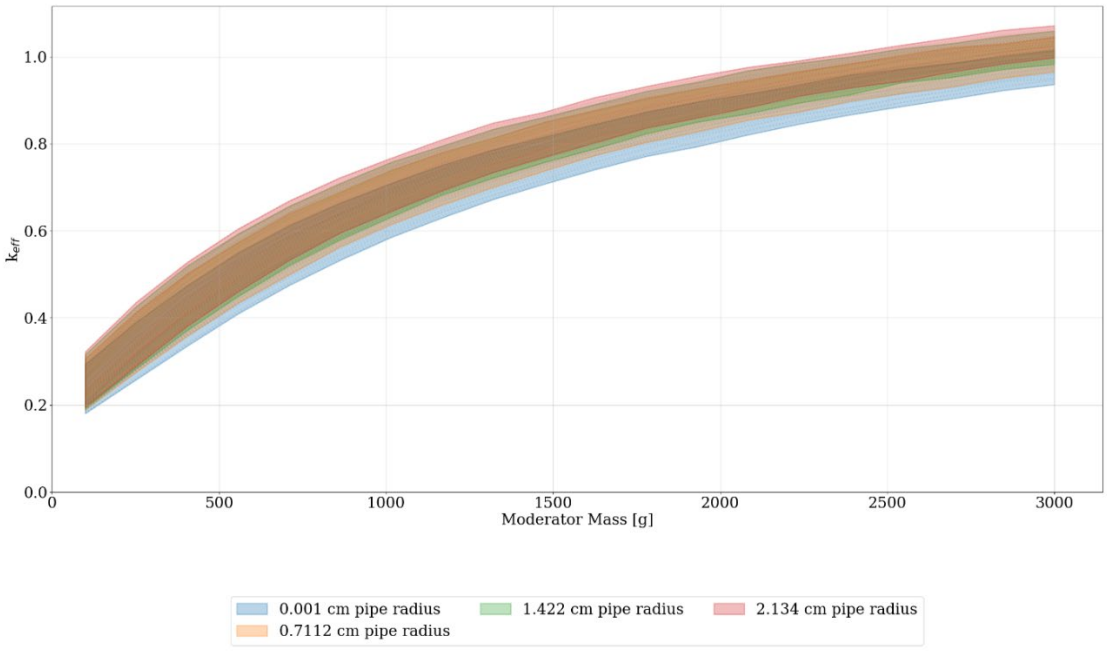

Figure O-39**. Set-8b sublisting-13 results (nonuniform array model): k_{eff} for set-2-uh and set-8a by discrete reflector thicknesses.**

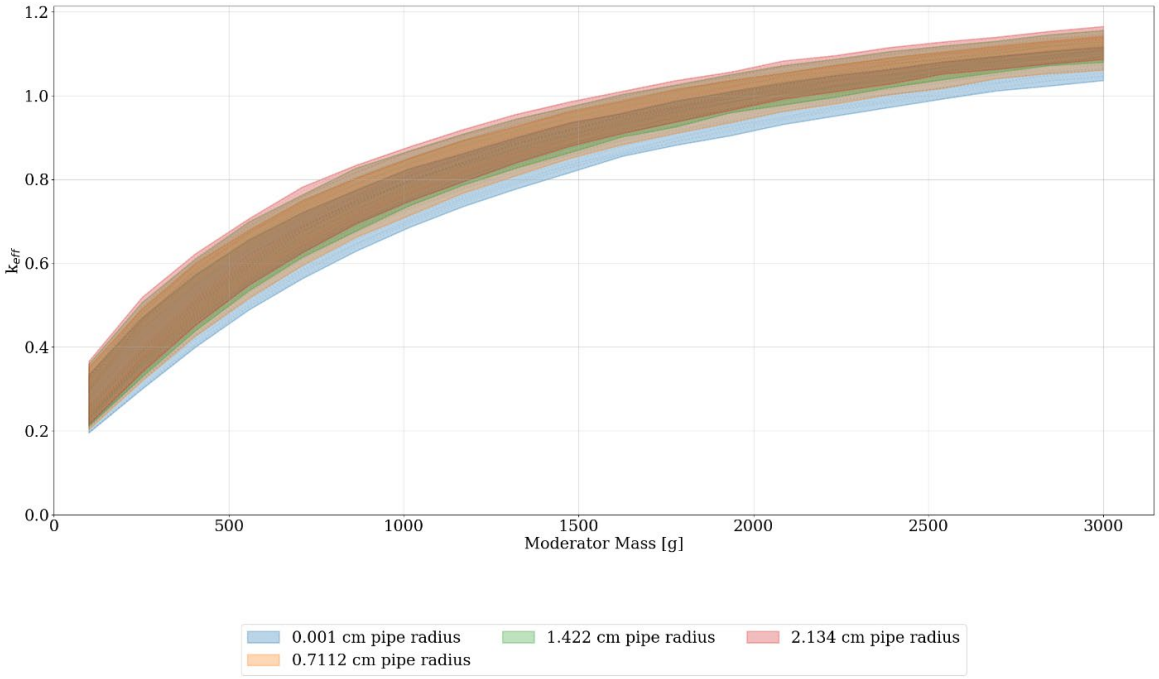

Figure O-40. Set-8b sublisting-14 results (nonuniform array model): k_{eff} for set-2-uh and set-8a by discrete reflector thicknesses.

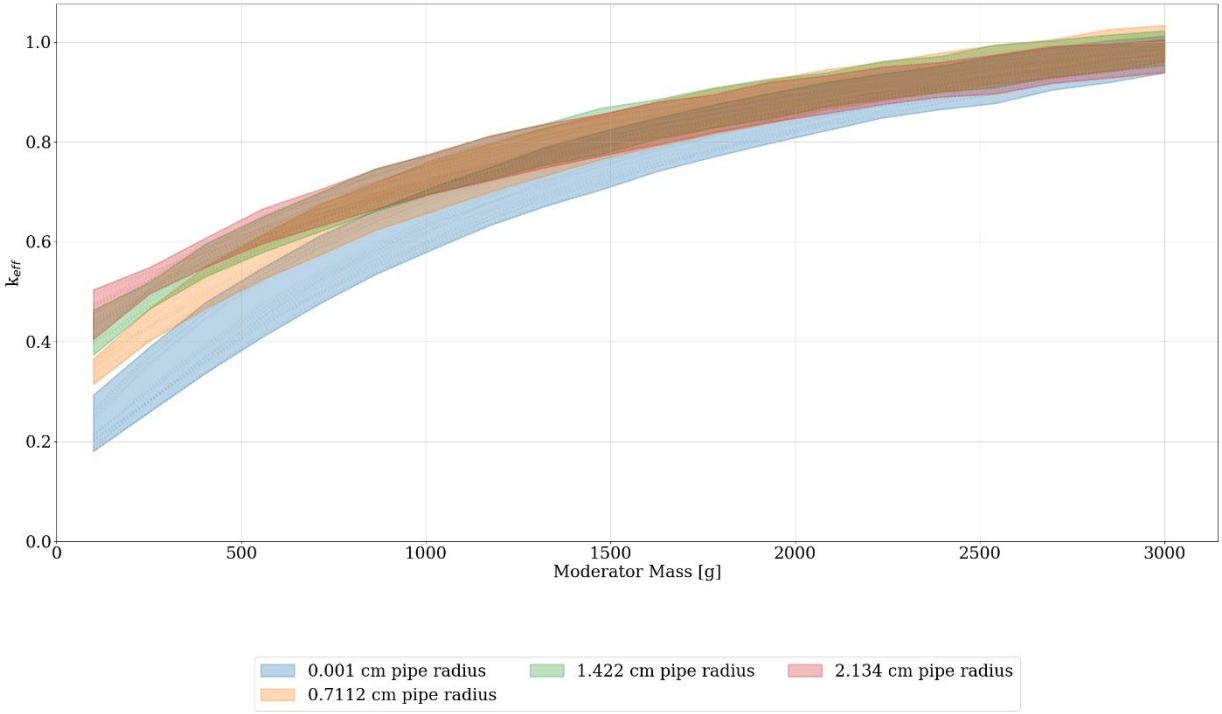

Figure O-41**. Set-8b sublisting-15 results (nonuniform array model): k_{eff} for set-2-uh and set-8a by discrete reflector thicknesses.**

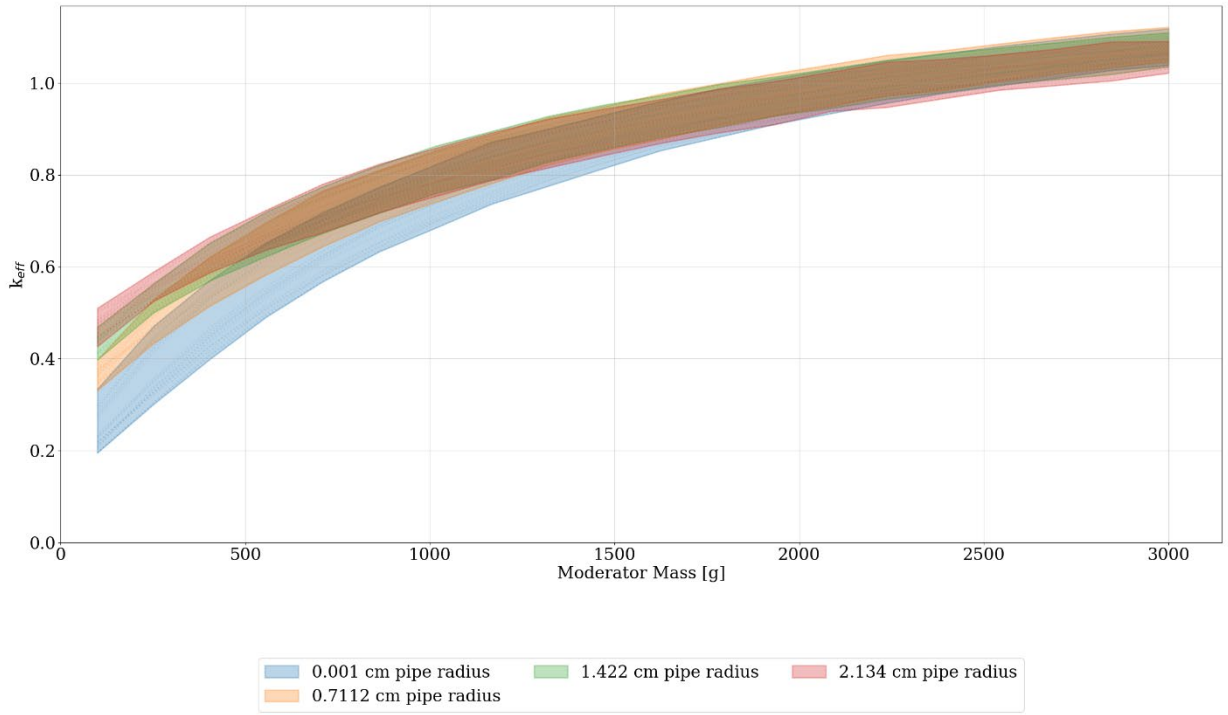

Figure O-42. Set-8b sublisting-16 results (nonuniform array model): k_{eff} for set-2-uh and set-8a by discrete reflector thicknesses.

ADDENDUM 1 SUMMARY OF ANALYSIS RESULTS

This page is intentionally blank

ADDENDUM 1. SUMMARY OF ANALYSIS RESULTS

Addendum 1 is the repository of the full set of analysis results. The analysis results have been postprocessed into various sets of "reorder" files so that the data can be evaluated in various ways. These data files have been placed on the Constellation Portal at ORNL and may be accessed by emailing bricknerbd@ornl.gov for more information.

This page is intentionally blank